NATURAL PRODUCTS FROM MARINE MICROORGANISMS

EDITED BY: Xian-Wen Yang, Bin-Gui Wang and Peter Proksch
PUBLISHED IN: Frontiers in Chemistry

frontiers Research Topics

frontiers

ISSN 1664-8714
ISBN 978-2-88963-358-6
DOI 10.3389/978-2-88963-358-6

About Frontiers

Frontiers is more than just an open-access publisher of scholarly articles: it is a pioneering approach to the world of academia, radically improving the way scholarly research is managed. The grand vision of Frontiers is a world where all people have an equal opportunity to seek, share and generate knowledge. Frontiers provides immediate and permanent online open access to all its publications, but this alone is not enough to realize our grand goals.

Frontiers Journal Series

The Frontiers Journal Series is a multi-tier and interdisciplinary set of open-access, online journals, promising a paradigm shift from the current review, selection and dissemination processes in academic publishing. All Frontiers journals are driven by researchers for researchers; therefore, they constitute a service to the scholarly community. At the same time, the Frontiers Journal Series operates on a revolutionary invention, the tiered publishing system, initially addressing specific communities of scholars, and gradually climbing up to broader public understanding, thus serving the interests of the lay society, too.

Dedication to Quality

Each Frontiers article is a landmark of the highest quality, thanks to genuinely collaborative interactions between authors and review editors, who include some of the world's best academicians. Research must be certified by peers before entering a stream of knowledge that may eventually reach the public - and shape society; therefore, Frontiers only applies the most rigorous and unbiased reviews.
Frontiers revolutionizes research publishing by freely delivering the most outstanding research, evaluated with no bias from both the academic and social point of view. By applying the most advanced information technologies, Frontiers is catapulting scholarly publishing into a new generation.

What are Frontiers Research Topics?

Frontiers Research Topics are very popular trademarks of the Frontiers Journals Series: they are collections of at least ten articles, all centered on a particular subject. With their unique mix of varied contributions from Original Research to Review Articles, Frontiers Research Topics unify the most influential researchers, the latest key findings and historical advances in a hot research area! Find out more on how to host your own Frontiers Research Topic or contribute to one as an author by contacting the Frontiers Editorial Office: researchtopics@frontiersin.org

NATURAL PRODUCTS FROM MARINE MICROORGANISMS

Topic Editors:
Xian-Wen Yang, Third Institute of Oceanography, Ministry of Natural Resources, China
Bin-Gui Wang, Institute of Oceanology, Chinese Academy of Sciences, China
Peter Proksch, Heinrich Heine University of Düsseldorf, Germany

Natural products continue to serve as sources for the development of new medicines. There is currently a revival of interest in the discovery of bioactive compounds with new chemical structures from natural sources, largely due to the fact that synthetic libraries have not yielded the expected number of developmental candidates in the pharmaceutical industry during the last decade. In addition, the emergence of clinically relevant pathogens that are becoming increasingly resistant to currently used medicines strengthens the notion that natural product research is urgently required. Considering the fact that almost 10% of bioactive compounds are of microbial origin, and that marine microorganisms are relatively poorly studied compared to their terrestrial relatives, marine microorganisms are regarded as the most potential-laden resource for drug discovery.

Citation: Yang, X.-W., Wang, B.-G., Proksch, P., eds. (2020). Natural Products From Marine Microorganisms. Lausanne: Frontiers Media SA.
doi: 10.3389/978-2-88963-358-6

Table of Contents

frontiers in Chemistry

ORIGINAL RESEARCH
published: 13 June 2018
doi: 10.3389/fchem.2018.00212

Isolation and Synthesis of Misszrtine A: A Novel Indole Alkaloid From Marine Sponge-Associated *Aspergillus* sp. SCSIO XWS03F03

Rong Zhou, Xiaojian Liao, Hangbin Li, Jing Li, Pengju Feng, BingXin Zhao* and Shihai Xu**

Department of Chemistry, Jinan University, Guangzhou, China

A novel indole alkaloid, misszrtine A (**1**), was isolated from marine sponge-derived fungus *Aspergillus* sp. SCSIO XWS03F03. The planar structure of **1** was assigned by analysis of spectroscopic data, the absolute configuration of which was unambiguously determined by total synthesis. Compound **1** represents the first example of *N*-isopentenyl tryptophan methyl ester with a phenylpropanoic amide arm, which exhibited a potent antagonistic activity on HL60 (IC_{50} = 3.1 μM) and LNCaP (IC_{50} = 4.9 μM) cell lines. Bioactivity evaluation reveals that functional group on indole nitrogen of **1** has a great effect on its cytotoxity, which provides a mean to probe the structure-activity relationships of **1.**

Keywords: indole alkaloid, marine-derived fungi, secondary metabolites, sponge, total synthesis, antagonistic activity

OPEN ACCESS

Edited by:
Xian-Wen Yang,
Third Institute of Oceanography, State Oceanic Administration, China

Reviewed by:
Hyun Lee,
University of Illinois at Chicago, United States
Margherita Brindisi,
University of Siena, Italy

****Correspondence:***
Pengju Feng
pfeng@jnu.edu.cn
BingXin Zhao
zbx840622@163.com
Shihai Xu
txush@jnu.edu.cn

Specialty section:
This article was submitted to Medicinal and Pharmaceutical Chemistry, a section of the journal Frontiers in Chemistry

Received: *27 March 2018*
Accepted: *23 May 2018*
Published: *13 June 2018*

Citation:
Zhou R, Liao X, Li H, Li J, Feng P, Zhao B and Xu S (2018) Isolation and Synthesis of Misszrtine A: A Novel Indole Alkaloid From Marine Sponge-Associated Aspergillus sp. SCSIO XWS03F03. Front. Chem. 6:212. doi: 10.3389/fchem.2018.00212

INTRODUCTION

Marine-derived fungi, a rich source of structurally diverse secondary metabolites, have attracted considerable attention due to their potential for the discovery of pharmaceutically interesting molecules (Attaway and Zaborsky, 1993; Newman and Cragg, 2016). Important drugs, such as Plinabulin, sorbicillactone A, etc., are derived from Marine-derived fungi (Bringmann et al., 2003; Nogueira et al., 2010; Millward et al., 2012). The genus *Aspergillus* (Moniliaceae) which firstly described by Micheli in 1729 was one of the largest and mostly intensively investigated fungal genera (Saleem et al., 2007; Ebrahim et al., 2016). A wide array of bioactive secondary metabolites from marine-derived *Aspergillus* species have been elucidated, including polyketides, terpenoids, alkaloids sterols, and peptides (Debbab et al., 2012), most of which exhibited antibacterial, antioxidant, radical-scavenging, cytotoxic, and anti-inflammatory activities (Li et al., 2004, 2012; Almeida et al., 2010; Lee et al., 2011; Sun et al., 2011).

The secondary metabolites from the sponge-derived fungus *Aspergillus* usually are terpenoids and polyketides. The alkaloids with an indole unit were extremely rare from the isolated structures (Varoglu et al., 1997). Previous investigations into marine sponge-associated fungus *Aspergillus* sp. SCSIO XWS03F03 by our group have resulted in the isolation of three polyketides, aspergchromones A, B, and secalonic acid D, along with other four small molecules (Wang Y. et al., 2016). In the course of our ongoing research on this fungus, a novel indole alkaloid, misszrtine A (**1**), was isolated by further investigation of the less polar fraction of the fungus extract. Compound **1** represents the first example of *N*-isopentenyl tryptophan methyl ester with a phenyl propanoic amide arm (**Figure 1**). Herein, we report the isolation, structural elucidation, plausible biogenetic route, total synthesis, and biological evaluation of **1**.

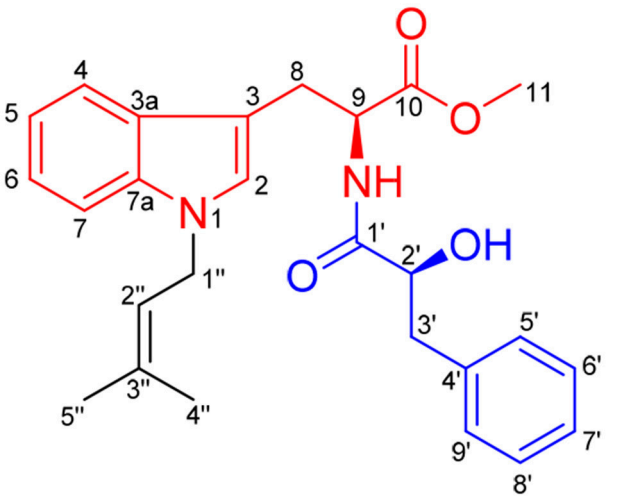

FIGURE 1 | Chemical structure of misszrtine A (**1**).

MATERIALS AND METHODS

General Experimental Procedures

Optical rotations were measured by using Anton Paar MCP-500 polarimeter (Auton Paar, Graz, Austria). UV spectra were recorded on a Shimadzu UV-2600 UV–vis spectrophotometer (Shimadzu, Kyoto, Japan). The NMR spectra were measured on a Bruker Av 300 or 500 MHz NMR spectrometer (Bruker, Fallanden, Switzerland). HR-ESI-MS were recorded on a Bruker micro TOF-QII mass spectrometer (Bruker, Fallanden, Switzerland). CD spectra were measured with a Chirascan circular dichroism spectrometer (JASCO International Co. Ltd., Hachioji, Tokyo, Japan). Size exclusion chromatography was done on Sephadex LH-20 gel (GE Healthcare, Uppsala, Sweden). Semi-preparative reversed-phase HPLC [Rp-C18: 9.4. 250 mm i.d, 5 μm (Cosmosil, Nacalai, Japan)] was performed on an Agilent 1200 series apparatus (Agilent, Palo Alto, American). Column chromatography (CC) was carried out on silica gel (200–300 mesh, Qingdao Marine Chemical Factory, Qingdao, China). Thin layer chromatography was carried out with precoated silica gel plates (GF-254, Jiangyou Silica Gel Development, Inc., Yantai, China).

Fungal Strain

The fungal strain SCSIO XWS03F03 was isolated from a sponge which was collected from the sea area Xuwen County, Guangdong Province, China, in August, 2013. The isolate was stored on MB agar (malt extract 15 g, sea salt 10 g, agar 15 g, distilled water 1,000 mL, pH 7.4∼7.8) slants at 4°C and deposited at CAS Key Laboratory of Tropical Marine Bio-resources and Ecology.

ITS Region Sequence

The strain was cultured in Sabouraud's Dextrose Broth (consisting of 40 g dextrose, 10 g peptone, 2.5 g NaCl, and 1,000 mL distilled water, pH = 5.6) for 1.5 days, and then the mycelia were collected and powdered in a mixer mill after liquid nitrogen was added. DNA was isolated through the Hpure Fungal DNA Kit (Guangzhou Genebase Bioscience Co., Guangzhou, China) according to the manufacturer's protocol. The ITS region of strain SCSIO XWS03F03 was amplified by polymerase chain reaction with the primer pair ITS1-ITS4 (ITS1: 5′-GTA GTC ATA TGC TTG TCT C-3′; ITS4: 5′-TCC GCA GGT TCA CCT ACG GA-3′). The amplified product was purified with a TIANgel mini purification kit (TianGen Biotech, Beijing, China). The recovery pure PCR product was sequenced by a commercial service (Shanghai Majorbio Bio-pharm Technology Co., Ltd., Shanghai, China). Through BLAST-Algorithmus, the derived ITS region sequence was compared against the GenBank database (NCBI). Similarity analysis was performed by using Clustal W program (Nam et al., 2001).

Nucleotide Sequence Accession Number

The nucleotide sequence of the ITS region reported in this article was assigned the GenBank accession number KU975059.

Fermentation, Extraction, and Isolation

Strain SCSIO XWS03F03 stored on MB agar slants at 4°C was cultured on MB agar plates and incubated at 25°C for 7 days. Seed medium (Melt extract 15 g, sea salt 10 g, distilled water 1,000 mL) was inoculated with strain SCSIO XWS03F03 and incubated at 25°C for 48 h on a rotating shaker (180 rpm; 25°C). Large scale fermentation in a solid rice medium of 1,000 mL flasks supplemented with 1% NaCl (rice 200 g, sea salt 2.0 g, distilled water 200 mL) (n = 45) was inoculated with 10 mL of seed solution. Flasks were incubated at 25°C under static condition and fermented for 45 days.

The fungal cultures from 45 flasks were harvested and the mycelia were cut into small pieces and soaked in acetone for 12 h, sonicated (10 min) and filtered, yielding the rice solid medium and water phases. The solid rice medium was extracted with ethyl acetate (EtOAc) (6 × 500 mL) and the water phase was extracted with EtOAc (3×10 L).Both EtOAc extracts were combined and partitioned with petroleum ether (PE) three times to remove the oil, then evaporated under vacuum at 42°C to yield 83 g crude extract, which was subjected to silica gel column chromatography (Φ 11 × 90 cm) eluting with PE/EtOAc in gradient eluent (90:10, 80:20, 70:30, 75:25, 65:35, 60:40, 50:50, 25:75, 0:100), to obtain 5 fractions (Fr. 1-5). Fr.2 (5.21 g) was then purified by silica gel column (PE/EtOAc, 90:10∼0:100) to obtain six subfractions (Fr. 2-1∼Fr. 2-6). Fr. 2-3 (256.3 mg) was further purified by semi preparative reversed-phase HPLC (2 mL/min, MeOH/H_2O = 6/4) to give **1** (15 mg) (t_R = 20.3 min).

Total Synthesis of Misszrtine A (1)

Methyl ((*S*)-2-hydroxy-3-phenylpropanoyl)-L-tryptophanate (**2**)

To a solution of L-3-Phenyllactic acid (4.0 g, 24.0 mmol) in dry degassed DCM (100 mL) was added EDCI (4.56 g, 24.0 mmol), HOBt (3.24 g, 24.0 mmol), and L-tryptophan methyl ester hydrochloride (5.1 g, 20.0 mmol). After stirring for 30 h, the reaction mixture was concentrated and extracted with EtOAc

(20 mL × 2). The combined organic extracts were washed with saturated aqueous $NaHCO_3$ (20 mL × 2), dried over $MgSO_4$, filtered, concentrated, and purified by flash chromatography over 200–400 mesh silica gel (PE/EA= 4:1) to give **2** as a light yellow oil (6.38 g, 87%). ^{1}H NMR (300 MHz, $CDCl_3$) δ 8.96 (s, 1H), 7.53 (d, J = 7.6 Hz, 1H), 7.47 (d, J = 8.1 Hz, 1H), 7.41–7.17 (m, 8H), 6.73 (s, 1H), 5.99 (dd, J = 12.9, 5.2 Hz, 1H), 4.36 (dd, J = 6.2, 3.6 Hz, 1H), 3.93 (brs, 1H), 3.61 (s), 3.36 (dd, J = 14.7, 7.2 Hz, 1H), 3.24–3.10 (m, 2H), 2.91 (dd, J = 13.7, 7.2 Hz, 1H). ^{13}C NMR (75 MHz, $CDCl_3$) δ 173.5, 136.9, 136.0, 129.6, 128.2, 127.1, 126.6, 123.2, 121.8, 119.2, 118.2, 111.4, 108.7, 77.4, 72.3, 52.2, 40.1, 27.5. HRESIMS *m/z* 367.1625 $[M+H]^+$ (calcd for $C_{21}H_{22}N_2O_4$ 367.1652).

Methyl ((*S*)-2-((*tert*-butyldimethylsilyl)oxy)-3-phenylpropanoyl)-L-tryptophanate (**3**)

To a solution of **2** (1.83 g, 5.0 mmol) in dry MeCN (50 mL) was added imidazole (0.14 g, 2.0 mmol) and TBSCl (0.91 g, 6.0 mmol); After stirring for 2 h, the combined organic extracts were washed with saturated aqueous $NaHCO_3$(10 mL×2), dried over $MgSO_4$, filtered, concentrated, and purified by flash chromatography over 200–400 mesh silica gel (PE/EA= 1:1) to give **3** as a yellow gum (2.30 g, 96%). ^{1}H NMR (300 MHz, DMSO-d_6) δ 10.9 (s, 1H), 7.35–7.23 (m, 5H), 7.19–7.12 (m, 2H), 7.05 (td, J = 8.1, 1.1 Hz, 1H), 6.96 (td, J = 8.1, 0.8 Hz, 1H), 6.83 (d, J = 2.3 Hz, 1H), 4.77–4.65 (m, 1H), 4.21 (dd, J = 7.5, 3.7 Hz, 1H), 3.58 (s, 3H), 3.18 (dd, J = 14.6, 5.9 Hz), 2.98 (dd, J = 14.6, 5.4 Hz, 1H), 2.88 (dd, J = 13.4, 3.6 Hz, 1H), 2.70 (dd, J = 13.4, 7.5 Hz, 1H), 0.61 (s, 9H), −0.25 (s, 3H), −0.33 (s, 3H); ^{13}C NMR (75 MHz, DMSO-d_6) δ 172.1, 171.9, 137.7, 136.6, 130.4, 128.3, 127.6, 126.8, 124.1, 121.4, 119.0, 118.4, 111.8, 108.5, 74.3, 52.4, 52.1, 41.4, 27.6, 25.8, 17.9, −5.3, −5.6.

Methyl((*S*)-2-((tert-butyldimethylsilyl)oxy)-3-phenylpropanoyl)-1-(3-methylbut-2-en-1-yl)-L-tryptophanate (**4**)

To a solution of **3** (0.96 g, 1.0 mmol) in dry DMF (50 mL) was added NaH (0.05 g, 2.0 mmol). After stirring for 1 h, 1-bromo-3-methyl-2-butene (0.3 mL, 1.5 mmol) was added dropwise to the reaction mixture. Upon stirring for 4 h, the reaction was quenched with water and extracted with EtOAc (10 mL × 3). The combined organic extracts were washed with saturated aqueous $NaHCO_3$(10 mL × 2), dried over $MgSO_4$, filtered, concentrated, and purified by flash chromatography over 200–400 mesh silica gel (PE/EA= 1:1) to give **4** as a yellow gum (0.99 g, 90%). ^{1}H NMR (300 MHz, DMSO-d_6) δ 7.38–7.20 (m, 6H), 7.20–7.15 (m, 2H), 7.11 (t, J = 7.9 Hz, 1H), 7.00 (t, J = 7.3 Hz, 1H), 6.73 (s, 1H), 5.24 (t, J = 6.7 Hz, 1H), 4.80–4.70 (m, 1H), 4.68–4.60 (m, 2H), 4.23 (dd, J = 7.2, 3.7 Hz, 1H), 3.58 (s, 1H), 3.20 (dd, J = 14.6, 5.8 Hz, 1H), 2.98 (dd, J = 14.6, 5.3 Hz, 1H), 2.88 (dd, J = 13.4, 3.7 Hz, 1H), 2.75 (dd, J = 13.4, 7.4 Hz, 1H), 1.79 (s, 3H), 1.68 (s, 3H), −0.23 (s, 3H), −0.31 (s, 3H).

Methyl-((*S*)-2-hydroxy-3-phenylpropanoyl)-1-(3-methylbut-2-en-1-yl)-L-tryptophanate (**1**)

To a solution of **3** (0.55 g, 1.0 mmol) in dry THF (30 mL) was added dropwise pyridine-HF (2.3 mL, 10.0 mmol). After stirring for 1 h, the reaction mixture was quenched with water and extracted with DCM (10 mL × 3). The crude product was purified by HPLC to give **1** as a white solid (0.40 g, 92%). $[\alpha]_D^{25}$ −5.35 (*c* 2, CH_3OH); UV(MeOH) λ_{max} (log ε) 225 (1.51) nm 275(0.25)nm; ^{1}H NMR (300 MHz, Chloroform-d) δ 7.42 (d, J = 7.9 Hz, 1H), 7.36–7.18 (m, 7H), 7.11

TABLE 1 | ^{1}H and ^{13}C NMR spectral data of **1** (*J* in Hz, in CDCl**3**)[a].

No.	Misszrtine A (1)	
	δ_H	δ_C
2	6.69 (s)	126.1
3	–	108.2
3a	–	128.2
4	7.37 (dd, 7.8, 1.2)	118.7
5	7.06 (ddd, 7.8, 6.9, 1.2)	119.1
6	7.18 (ddd, 7.2, 6.9, 1.2)	121.6
7	7.27	109.6
7a	–	136.2
8	a 3.28 (dd, 14.7,5.4)	27.8
	b 3.17 (dd, 14.7, 5.1)	
9	4.92 (ddd, 8.4, 5.4, 5.1)	52.5
10	–	172.1
11	3.66 (s)	52.3
1′	–	172.2
2′	4.29 (dd,7.8,4.2)	72.7
3′	a 3.13 (dd,13.8,4.2)	40.5
	b 2.83(dd,13.8, 7.8)	
4′	–	136.6
5′	7.23	129.7
6′	7.29	128.7
7′	7.26	127.0
8′	7.29	128.7
9′	7.23	129.7
1″	4.60 (d,6.9)	44.0
2″	5.30 (m)	119.9
3″	–	136.3
4″	1.80 (d, 1.2)	18.0
5″	1.74 (d, 1.2)	25.6
NH	6.95 (d, 8.4)	–

[a]*Overlapped signals are reported without designating multiplicity.*

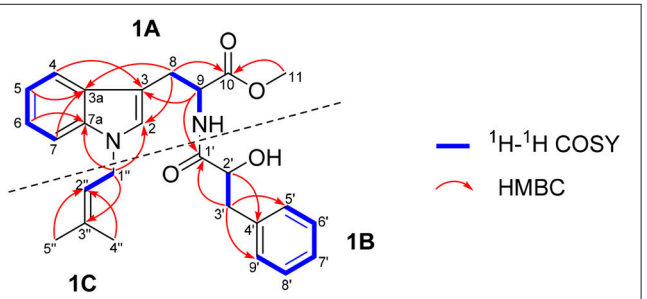

FIGURE 2 | Key ^{1}H-^{1}H COSY and HMBC correlations of **1**.

(d, J = 7.5 Hz, 1H), 7.06 (d, J = 6.8 Hz, 1H), 6.70 (s, 1H), 5.34 (t, J = 6.8 Hz, 1H), 4.97–4.90 (m, 1H), 4.64 (s, 1H), 4.62 (s, 1H), 4.30 (dd, J = 7.7, 4.1 Hz, 1H), 3.30 (dd, J = 14.7, 5.6 Hz, 1H), 3.20–3.10 (m, 2H), 2.88 (d, J = 7.7 Hz, 1H), 2.83 (d, J = 7.7 Hz,1H), 1.84 (s, 3H), 1.78 (s, 3H).^{13}C NMR (75 MHz, Chloroform-d) δ 172.5, 172.2, 136.8, 136.2, 136.2, 129.8, 128.6, 128.2, 126.95, 126.2, 121.6, 119.95, 119.1, 118.7, 109.7, 108.2, 72.6, 52.5, 52.3, 44.1, 40.5, 27.8, 25.7, 18.1.

Evaluation of General Cytotoxicity of Compound 1 and 2

Cytotoxic activity was assessed by using the CCK-8 (Dojindo, Japan) method according to established procedures (Bai et al., 2014). Eight human cancer cell lines (HepG2, HL60, Hela, A375, A549, HT29, SK-BR-3, LNCaP, and MCF-7) were used in the cytotoxicity bioassay. The cells were cultured in RPMI or DMEM medium supplemented with 10% heat-inactivated fetal bovine serum (Gibco, USA) with 5% CO_2 in air at 37°C. A cell viability assay was determined with the CCK-8 (Dojindo, Japan) assay. Cells were seeded at a density of 400–800 cells/well in 384-well plates and treated with various concentrations of compounds or solvent control. After 72 h incubation, CCK-8 reagent was added, and absorbance was measured at 450 nm using an Envision 2104 multilabel reader (PerkinElmer, USA). Dose–response curves were plotted to determine the IC_{50} values by using Prism 5.0 (GraphPad Software Inc., USA).

RESULTS AND DISCUSSION

Identification of (*S, S*)-misszrtine A

Misszrtine A (**1**) was obtained as a light yellow powder, which showed a molecular ion cluster $[M+H]^+$ at 435.2284, revealing a molecular formula $C_{26}H_{30}N_2O_4$, indicating thirteen degrees of unsaturation. The UV absorption maximum at 225 and 290 nm implied the presence of an indole chromophore in **1** (Sangster and Stuart, 1995). The IR bands implied the presence of amino group (3380 cm^{-1}) hydroxyl group (3262 cm^{-1}), carbonyl

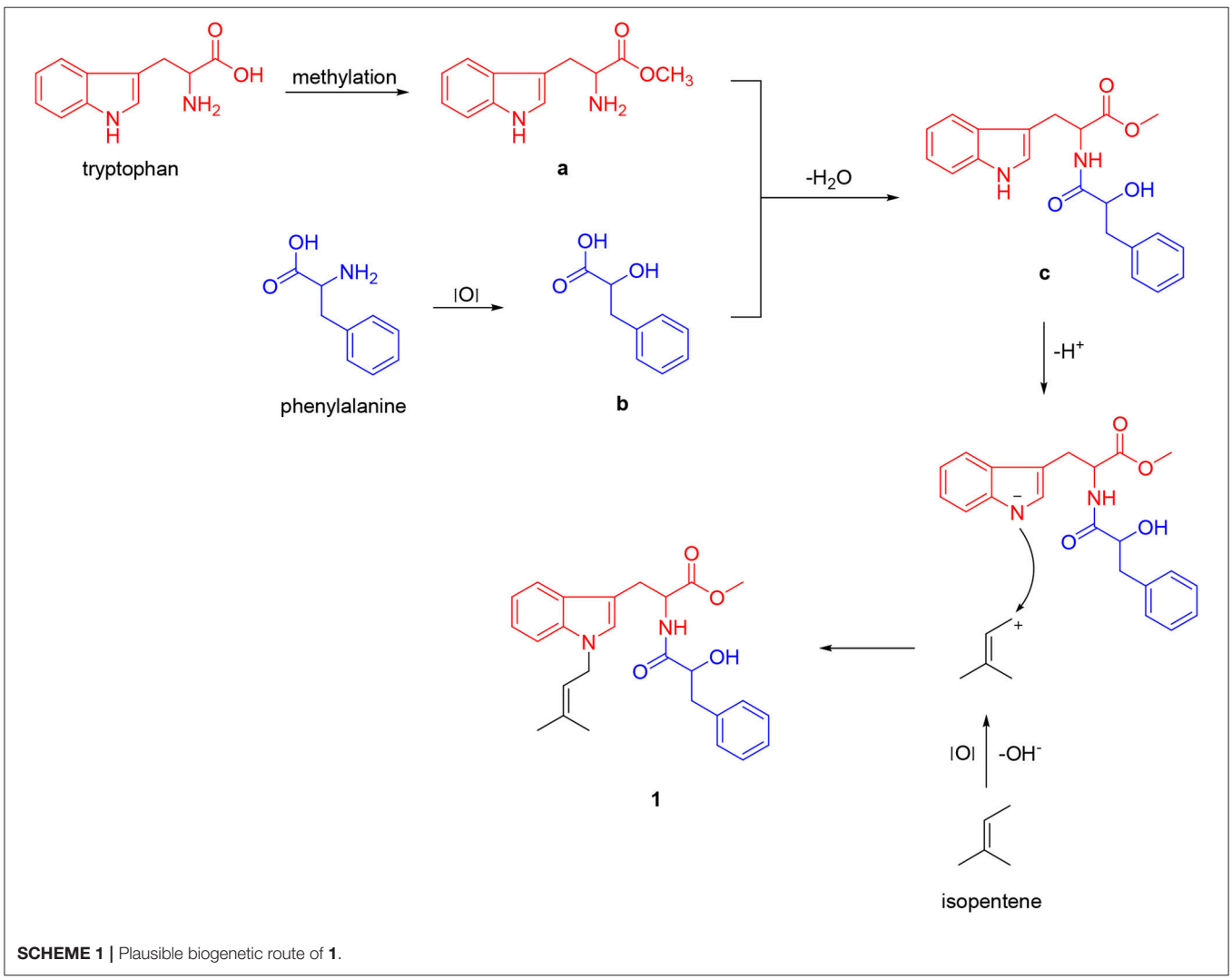

SCHEME 1 | Plausible biogenetic route of **1**.

groups (1745 and 1731 cm^{-1}), and aromatic ring (1645 and 1535 cm^{-1}). The analysis of NMR spectra revealed the presence of two carbonyls (δ_C 172.2 and 172.1), a monosubstituted benzene ring [δ_H 7.29 (2H), 7.26 (1H), and 7.23 (2H); δ_C 136.6, 129.7, 128.7, and 127.0], a disubstituted benzene ring [δ_H 7.37 (1H, dd, J = 7.8, 1.2 Hz), 7.27 (1H), 7.18 (1H, ddd, J = 7.2, 6.9, 1.2 Hz), and 7.06 (1H, ddd, J = 7.8, 6.9, 1.2 Hz); δ_C 136.2, 128.2, 121.6, 119.1, 118.7, and 109.6], two trisubstituted double bonds [δ_H 5.30 (1H, m) and 6.69 (1H, s); δ_C 136.3, 126.1, 119.9, and 108.2), two methines [δ_H 4.92 (1H, ddd, J = 8.4, 5.4, 5.1 Hz) and 4.29 (1H, dd, J = 7.8, 4.2 Hz); δ_C 72.7 and 52.5], three methenes [δ_H 4.60 (2H, d, J = 6.9 Hz), 3.28 (1H, dd, J = 14.7, 5.4 Hz), 3.17 (1H, dd, J = 14.7, 5.1 Hz), 3.13 (1H, dd, J = 13.8, 4.2 Hz), and 2.83 (1H, dd, J = 13.8, 7.8 Hz); δ_C 44.0, 40.5, and 27.8], a methoxyl [δ_H 3.66 (1H, s); δ_C 52.3] and two methyls [δ_H 1.80 (3H, d, J = 1.2Hz) and 1.74 (3H, d, J = 1.2Hz); δ_C 25.6 and 18.0]. The above spectral data suggested that misszrtine A (**1**) might be an indole alkaloid (Estevão et al., 2010; Khalil et al., 2014). A comprehensive analysis of the ^1H-^1H COSY, HSQC, and HMBC spectra allowed the full assignment of all proton and carbon resonances of **1** as shown in **Table 1**.

The ^1H-^1H COSY data of misszrtine A (**1**) revealed the presence of five spin coupling systems in bold as shown in **Figure 2**. In the HMBC spectrum, correlations between H-4/H-9 and C-3, between H-5/H-7/H-8 and C-3a, between H-6 and C-7a, between H-8 and C-2/C-10 as well as between H-11 and C-10 allowed the establishment of tryptophanmethyl ester moiety (**1A**). Furthermore, the HMBC correlations from H-3′ to C-1′/C-5′/C-9′ as well as from H-2′ to C-4′ validated the

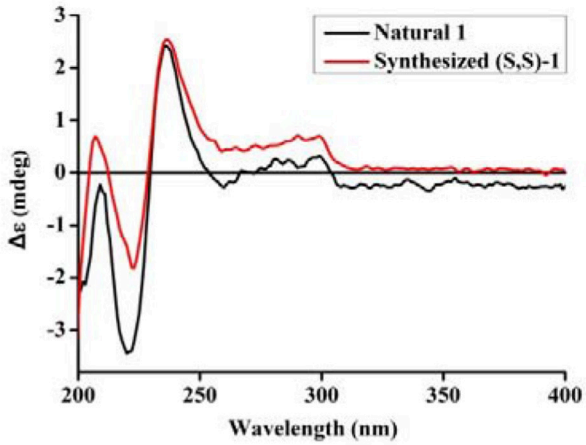

FIGURE 3 | CD spectrum of synthesized (*S*,*S*)-**1** and natural **1**.

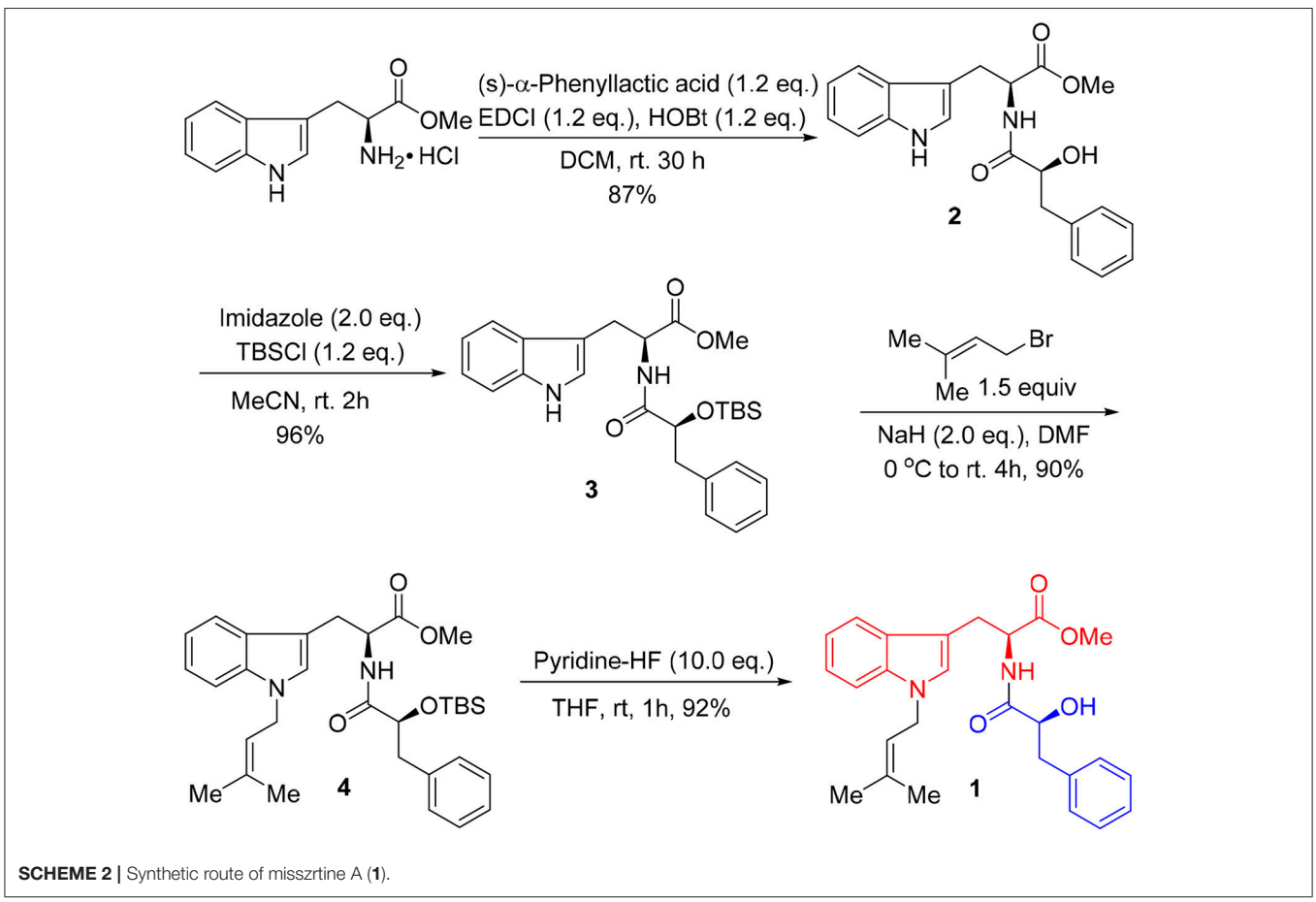

SCHEME 2 | Synthetic route of misszrtine A (**1**).

TABLE 2 | Biological evaluation of misszrtine A (**1**) and compound **2**[a].

Cmpd	Observed IC_{50} (μM)								
	HepG2	HL-60	Hela	A375	A549	HT29	SK-BR-3	LNCap	MCF-7
1	NA	3.12	NA	NA	>30	>30	>30	4.94	>30
2	NA	>30	NA	NA	NA	NA	NA	NA	NA

[a]*Antitumor activities were determined by microdilution method. ">30 μM" means cell survival rate between 70–85%; "NA" means cell survival rate over 85%.*

presence of phenylpropanoic acid unit. Additionally, according to the molecular formula information and the obvious downfield shifts at C-2′, a hydroxyl group should be attached to C-2′. Thus, the structure of α-hydroxy-phenylpropanoic acid residue (**1B**) was deduced. Moreover, the HMBC correlations between H-1″ and C-3″ as well as between H-4″/H-5″ and C-2″ verified the skeleton of isopentene group (**1C**). In addition, the HMBC correlations between H-9 and C-1′ suggested that **1A** and **1B** were connected via N-C-1′ bond. The HMBC correlations from H-1″ to C-2/C-7a indicated that **1C** was linked to N-1. Therefore, the planar structure of **1** was identified (**Figure 2**).

Unfortunately, no helpful NOE correlation was observed in the NOESY spectrum to determine the relative stereochemistry of **1**. However, the biogenetic route of **1** could be proposed, which was plausibly traced back to tryptophan, phenylalanine, and isopentene. First, tryptophan was methylated to form tryptophan methyl ester (**a**). Meanwhile, phenylalanine was oxidized to α-hydroxy-3-phenylpropanoic acid (**b**) (Winitz et al., 1956; Khelifa et al., 1998; Senkpeil et al., 2002; Busto et al., 2014). Intermediates **a** and **b** were dehydrated to give compound **c**, which took a nucleophilic substitution reaction with isopentene to produce **1** (**Scheme 1**). Accordingly, a total synthesis of **1** was carried out to confirm the absolute configurations of C-9 and C-2′ (**Scheme 2**). Since the L configuration of α-amino acids are more common in nature, L-tryptophan methyl ester hydrochloride and (*S*)-α-hydroxy-3-phenylpropanoic acid were selectively chosen as substrates to undergo an amidation coupling, yielding compound **2** (87% yield) with two chiral centers (Airiau et al., 2008). The hydroxyl group was chemo-selectively protected by TBSCl to give compound **3** in 96% yield. After removing N-H proton of **3** with NaH at 0°C, bromo-3-methyl-2-butene was injected to the reaction mixture, furnishing a protected indole **4** in 90% yield without any racemic counterparts (Estevão et al., 2010). Pyridine-HF reagent (Ohshima et al., 2003; Shiozaki et al., 2013) was employed to remove TBS group under slightly acidic condition for delivering compound **1** which was then fully characterized.

The UV spectrum, NMR data, optical rotations, and CD profiles of the natural misszrtine A (**1**) were compared with those of synthesized (*S*, *S*)-**1**. As shown in supporting information, the UV spectrum, ^{1}H and ^{13}C NMR data for natural **1** were essentially identical to those of synthesized (*S*, *S*)-**1**. As for specific optical rotation, the value of natural Misszrtion A ($[\alpha]_D^{25}$-6.13 (C 0.10, CH_3OH)) was in good agreement with that of the synthesized (*S*, *S*)-**1** ($[\alpha]_D^{25}$-5.35 (C 2.0, CH_3OH)), indicating that the absolute configuration at both C-9 and C-2″ of natural misszrtine A (**1**) were *S*. In addition, the results from CD profiles showed that natural misszrtine A (**1**) had identical pattern as that of synthesized (*S, S*)-**1** (**Figure 3**).

Biological Evaluation of Misszrtine A (1) and Compound 2

The synthesized key intermediate **2** and misszrtine A (**1**) were selected for the evaluation of general cytotoxicity toward nine human cancer cell lines (HepG2, HL60, Hela, A375, A549, HT29, SK-BR-3, LNCaP, and MCF-7) (**Table 2**). Misszrtine A (**1**) exhibited cytotoxic activity against HL-60 and LNCap cells with IC_{50} values of 3.1 and 4.9 μM, respectively, but with no cytotoxicity against the rest of tested cell lines. Interestingly, compound **2**, without protecting group on the indole nitrogen, showed a lost cytotoxicity toward HL-60 and LNCap cell lines, indicating that the nitrogen protecting group may be a key factor for tuning biological activities of misszrtine A (**1**) derivatives. Misszrtine A (**1**) was also tested for inhabitation against H3N2 influenza, antituberculous activity, anti-inflammatory activity using COX-1 and COX-2 as molecular targets (Wang J. et al., 2016). However, no positive results were obtained thus far.

CONCLUSION

In summary, a novel indole alkaloid (misszrtine A, **1**), with two chiral centers, was isolated and characterized from the marine sponge-derived *Aspergillus* sp. SCSIO XWS03F03. The planar structure of **1** was assigned by analysis of UV, IR, and NMR spectroscopic data, and its absolute configuration was unambiguously determined by total synthesis and specific optical rotation, CD spectrum comparison. Bioactivity evaluation results showed that compound **1** exhibited a potent antagonistic activity on HL60 (IC_{50} = 3.1 μM) and LNCaP (IC_{50} = 4.9 μM) cell lines, while compound **2** was inactive to those cell lines. The findings indicated that functional group on indole nitrogen of **1** has a great effect on its cytotoxity, which provides a mean to probe the structure-activity relationships of **1**.

AUTHOR CONTRIBUTIONS

RZ and XL contributed equally. RZ was responsible for the isolation and synthesis of misszrtine A. XL did the purification and identification of compound. HL, JL, and BZ are responsible

for the fermentation and extraction of the fungal strain. PF was designed the synthesis. BZ, PF, and SX were prepared the manuscript, and all authors have approved the final version.

ACKNOWLEDGMENTS

This work was financially supported by the National Natural Science Foundation of China [Nos. 21672084, 41376155, and 81302665]; the Science and Technology Planning Project of Guangzhou [Nos. 201704030042 and 201710010088]; the Scientific Research Cultivation and Innovation Fund Research Project of Jinan University [Nos. 21616113 and 21617472].

SUPPLEMENTARY MATERIAL

The Supplementary Material for this article can be found online at: https://www.frontiersin.org/articles/10.3389/fchem.2018.00212/full#supplementary-material

REFERENCES

Airiau, E., Spangenberg, T., Girard, N., Schoenfelder, A., Salvadori, J., Taddei, M., et al. (2008). A general approach to Aza-Heterocycles by means of domino sequences driven by hydroformylation. *Chem. Eur. J.* 14, 10938–10948. doi: 10.1002/chem.200801795

Almeida, A. P., Dethoup, T., Singburaudom, N., Lima, R., Vasconcelos, M. H., Pinto, M., et al. (2010). The *in vitro* anticancer activity of the crude extract of the sponge-associated fungus Eurotium cristatum and its secondary metabolites. *J. Nat. Pharm.* 1, 25–29. doi: 10.4103/2229-5119.73583

Attaway, D. H., and Zaborsky, O. R. (eds). (1993). *Marine Biotechnology. Pharmaceutical and Bioactive Natural Products, Vol. 1*. New York, NY: Plenum Press.

Bai, Z.-Q., Lin, X., Wang, Y., Wang, J., Zhou, X., Yang, B., et al. (2014). New phenyl derivatives from endophytic fungus *Aspergillus flavipes* AIL8 derived of mangrove plant *Acanthus ilicifolius*. *Fitoterapia* 95, 194–202. doi: 10.1016/j.fitote.2014.03.021

Bringmann, G., Lang, G., Muhlbacher, J., Schaumann, K., Steffens, S., Rytik, P. G., et al. (2003). Sorbicillactone A: a structurally unprecedented bioactive novel-type alkaloid from a sponge-derived fungus. *Prog. Mol. Subcell. Biol.* 37, 231–253. doi: 10.1007/978-3-642-55519-0_9

Busto, E., Richter, N., Grischek, B., and Kroutil, W. (2014). Biocontrolled formal inversion or retention of L-α-amino acids to enantiopure (R)- or (S)-hydroxyacids. *Chemistry* 20, 11225–11228. doi: 10.1002/chem.201403195

Debbab, A., Aly, A. H., and Proksch, P. (2012). Endophytes and associated marine derived fungi—ecological and chemical perspectives. *Fungal Divers.* 57, 45–83. doi: 10.1007/s13225-012-0191-8

Ebrahim, W., El-Neketi, M., Lewald, L. I., Orfali, R. S., Lin, W., Rehberg, N., et al. (2016). Metabolites from the fungal endophyte *Aspergillus austroafricanus* in axenic culture and in fungal-bacterial mixed cultures. *J. Nat. Prod.* 79, 914–922. doi: 10.1021/acs.jnatprod.5b00975

Estevão, M., Carvalho, L. C., Ribeiro, D., Couto, D., Freitas, M., Gomes, A., et al. (2010). Antioxidant activity of unexplored indole derivatives: synthesis and screening. *Eur. J. Med. Chem.* 45, 4869–4878. doi: 10.1016/j.ejmech.2010.07.059

Khalil, Z. G., Huang, X.-C., Raju, R., Piggott, A. M., and Capon, R. J. (2014). Shornephine A: structure, chemical stability, and P-glycoprotein inhibitory properties of a rare diketomorpholine from an Australian marine-derived Aspergillus sp. *J. Org. Chem.* 79, 8700–8705. doi: 10.1021/jo501501z

Khelifa, N., Butel, M.-J., and Rimbault, A. (1998). Synthesis of 2-hydroxy acid from 2-amino acid by *Clostridium butyricum*. *Bioorg. Med. Chem. Lett.* 8, 3429–3434. doi: 10.1016/S0960-894X(98)00620-9

Lee, D. S., Jeong, G. S., Li, B., Lee, S. U., Oh, H., and Kim, Y. C. (2011). Asperlin from the marine-derived fungus Aspergillus sp. SF-5044 exerts anti-inflammatory effects through heme oxygenase-1 expression in murine macrophages. *J. Pharmacol. Sci.* 116, 283–295. doi: 10.1254/jphs.10219FP

Li, D., Xu, Y., Shao, C. L., Yang, R. Y., Zheng, C. J., Chen, Y. Y., et al. (2012). Antibacterial bisabolane-type sesquiterpenoids from the sponge-derived fungus Aspergillus sp. *Mar. Drugs* 10, 234–241. doi: 10.3390/md10010234

Li, Y., Li, X. F., Kim, S. K., Kang, J. S., Choi, H. D., Rho, J. R., et al. (2004). Golmaenone, a new diketopiperazine alkaloid from the marine-derived fungus Aspergillus sp. *Chem. Pharm. Bull.* 52, 375–376. doi: 10.1248/cpb.52.375

Millward, M., Mainwaring, P., Mita, A., Federico, K., Lloyd, G. K., Reddinger, N., et al. (2012). Phase 1 study of the novel vascular disrupting agent plinabulin (NPI-2358) and docetaxel. *Invest. New Drugs* 30, 1065–1073. doi: 10.1007/s10637-011-9642-4

Nam, J.-W., Nojiri, H., Yoshida, T., Habe, H., Yamane, H., and Omori, T. (2001). New classification system for oxygenase components involved in ring-hydroxylating oxygenations. *Biosci. Biotechnol. Biochem.* 65, 254–263. doi: 10.1271/bbb.65.254

Newman, D. J., and Cragg, G. M. (2016). Drugs and drug candidates from marine sources: an assessment of the current "State of Play". *Planta Med.* 82, 775–789. doi: 10.1055/s-0042-101353

Nogueira, I., Lobo-da-Cunha, A., Afonso, A., Rivera, S., Azevedo, J., and Monteiro, R. (2010). Toxic effects of domoic acid in the seabream *Sparus aurata*. *Mar. Drugs* 8, 2721–2732. doi: 10.3390/md8102721

Ohshima, T., Gnanadesikan, V., Shibuguchi, T., Fukuta, Y., Nemoto, T., and Shibasaki, M. (2003). Enantioselective syntheses of aeruginosin 298-A and its analogues using a catalytic asymmetric phase-transfer reaction and epoxidation. *J. Am. Chem. Soc.* 125, 11206–11207. doi: 10.1021/ja037290e

Saleem, M., Ali, M. S., Haussain, S., Jabbar, A., Ashraf, M., and Lee, Y. S. (2007). Marine natural products of fungal origin. *Nat. Prod. Rep.* 24, 1142–1152. doi: 10.1039/b607254m

Sangster, A. W., and Stuart, K. L. (1995). Ultraviolet spectra of alkaloids. *Chem. Rev.* 65, 69–130. doi: 10.1021/cr60233a003

Senkpeil, R. F., Pantaleone, D. P., and Taylor, P. P. (2002). *Production of Hydroxyl-Carboxylic Acids Using a Coupled Enzyme System*. Chicago, IL. WO 2002/033110.

Shiozaki, M., Tashiro, T., Koshino, H., Shigeura, T., Watarai, H., Taniguchi, M., et al. (2013). Synthesis and biological activity of hydroxylated analogues of KRN7000 (α-galactosylceramide). *Carbohydr. Res.* 370, 46–66. doi: 10.1016/j.carres.2013.01.010

Sun, H. H., Mao, W. J., Jiao, J. Y., Xu, J. C., Li, H. Y., Chen, Y., et al. (2011). Structural characterization of extracellular polysaccharides produced by the marine fungus Epicoccumnigrum JJY-40 and their antioxidant activities. *Mar. Biotechnol.* 13, 1048–1055. doi: 10.1007/s10126-011-9368-5

Varoglu, M., Corbett, T. H., Valeriote, F. A., and Crews, P. (1997). Asperazine, a selective cytotoxic alkaloid from a sponge-derived culture of *Aspergillus niger*. *J. Org. Chem.* 62, 7078–7079. doi: 10.1021/jo970568z

Wang, J., Wei, X., Qin, X., Tian, X., Liao, L., Li, K., et al. (2016). Antiviral merosesquiterpenoids produced by the antarctic fungus *Aspergillus ochraceopetaliformis* SCSIO 05702. *J. Nat. Prod.* 79, 59–65. doi: 10.1021/acs.jnatprod.5b00650

Wang, Y., Lin, X.-P., Lu, Z.-R., Liao, X.-J., Huang, X.-J., Zhang, C., et al. (2016). Aspergchromones A and B, two new polyketides from the marine sponge-associated fungus Aspergillus sp. SCSIO XWS03F03. *J. Asian Nat. Prod. Res.* 19, 684–690. doi: 10.1080/10286020.2016.1231673

Winitz, M., Frankenthal, L. B., Lzumiya, N., Birnbaum, S. M., Baker, C. G., and Greenstein, J. P. (1956). Studies on diastereoisomeric α-amino acids and corresponding α-hydroxy acids VI.rotatory dispersion of copper complexes. *J. Am. Chem. Soc.* 78, 1602–1605. doi: 10.1021/ja01589a027

Conflict of Interest Statement: The authors declare that the research was conducted in the absence of any commercial or financial relationships that could be construed as a potential conflict of interest.

frontiers in Chemistry

ORIGINAL RESEARCH
published: 14 June 2018
doi: 10.3389/fchem.2018.00226

New Anti-inflammatory Cyclopeptides From a Sponge-Derived Fungus *Aspergillus violaceofuscus*

Jingtang Liu[1†], *Binbin Gu*[1†], *Lianjuan Yang*[2], *Fan Yang*[1*] *and Houwen Lin*[1*]

[1] *Research Center for Marine Drugs, State Key Laboratory of Oncogenes and Related Genes, Department of Pharmacy, Renji Hospital, School of Medicine, Shanghai Jiao Tong University, Shanghai, China,* [2] *The Fungal Reference Laboratory of Shanghai Dermatology Hospital, Shanghai, China*

Three new cyclic peptides including a cyclic tetrapeptide (**1**), an aspochracin-type cyclic tripeptide sclerotiotide L (**2**) and a diketopiperazine dimer (**3**), have been isolated from the ethyl acetate extract of a marine sponge-derived fungus *Aspergillus violaceofuscus*. The structures of all compounds were unambiguously elucidated on the basis of HRESIMS, 1D and 2D NMR spectroscopic data, MS/MS experiments and chemical methods. Compounds **1** and **3** showed anti-inflammatory activity against IL-10 expression of the LPS-induced THP-1 cells with inhibitory rates of 84.3 and 78.1% respectively at concentration of 10 μM.

Keywords: sponge-derived fungus, *Aspergillus violaceofuscus*, cyclic peptides, structural characterization, anti-inflammatory

OPEN ACCESS

Edited by:
Xian-Wen Yang,
Third Institute of Oceanography, State Oceanic Administration, China

Reviewed by:
Hiroshi Noguchi,
Nihon Pharmaceutical University, Japan
Abdul Sadiq,
University of Malakand, Pakistan

***Correspondence:**
Fan Yang
yang-fan@sjtu.edu.cn
Houwen Lin
franklin67@126.com

†These authors have contributed equally to this work.

Specialty section:
This article was submitted to Medicinal and Pharmaceutical Chemistry, a section of the journal Frontiers in Chemistry

Received: *05 March 2018*
Accepted: *31 May 2018*
Published: *14 June 2018*

Citation:
Liu J, Gu B, Yang L, Yang F and Lin H (2018) New Anti-inflammatory Cyclopeptides From a Sponge-Derived Fungus Aspergillus violaceofuscus. Front. Chem. 6:226. doi: 10.3389/fchem.2018.00226

INTRODUCTION

As a class of important metabolites from marine-derived organisms, cyclic peptides are extensively present in marine tunicate (Ireland et al., 1982), sponge (Zhang et al., 2010), algae (Xu et al., 2008), bacteria (Teta et al., 2017), fungi (Bao et al., 2013), etc., and often these cyclopeptides possess rare molecular skeleton (Fukuhara et al., 2015). Moreover, due to versatile biological functions including antineoplastic (Ireland et al., 1982), antimicrobial (Teta et al., 2017), anti-inflammatory (Randazzo et al., 2001), antitubercular (Daletos et al., 2015) and histone deacetylase inhibitory activities (Gu et al., 2007), the cyclic peptides have received enduring attention of organic chemists, biologists and pharmacologists. The structures of cyclic peptides may contain unusual amino acids or be modified by methylation (Jang et al., 2017), acetylation, lipidation (Luo et al., 2014), and sulfuration (Fukuhara et al., 2015). These characteristics are playing a vital role in the interactions with relevant bioactive targets (Sieber and Marahiel, 2005; Raaijmakers et al., 2010).

The sponge-derived fungi have been proven to be a prolific source of cyclic peptides (Amagata et al., 2006; Yu et al., 2008). In previous search for structurally unique cyclic peptides from marine sponge-derived fungus *Nigrospora oryzae* PF18 collected off the Xisha Islands in the South China Sea, we have identified a series of new cyclohexadepsipeptides oryzamides A–C (Ding et al., 2016). As part of our continuing quest for new bioactive molecules, chemical investigation of secondary metabolites of the fungus *Aspergillus violaceofuscus* from the marine sponge *Reniochalina* sp. resulted in the identification of three new cyclopeptides, including a cyclic tetrapeptide violaceotide A (**1**), an aspochracin-type cyclic tripeptide sclerotiotide L (**2**), and a new diketopiperazine dimer (**3**) (**Figure 1**). Herein, the isolation, structure elucidation and anti-inflammatory studies of the three new cyclic peptides were described.

MATERIALS AND METHODS

General Experimental Procedures

Optical rotations were determined on a Rudolph research analytical autopol VI polarimeter with a 1 dm length cell at room temperature. UV spectra were performed on a Persee TU-1950 UV-VIS spectrophotometer. The NMR spectra were recorded on a Bruker AMX-600 instrument. HRESIMS data were obtained on a Waters Xevo G2-XS Q-Tof mass spectrometer. Reversed-phase HPLC was performed on Waters X-Bridge C18 (5 μm) columns with a Waters 1525 separation module equipped with a Waters 2998 photodiode array detector. MPLC was accomplished using a Interchim PuriFlash 450 chromatography system. Silica gel 60 (200–300 mesh; Yantai, China), Sephadex LH-20 (18–110 μm, Pharmacia Co.) and ODS (50 μm, YMC Co.) were used for column chromatography.

Fungal Strain and Fermentation

The fungus *Aspergillus violaceofuscus* was isolated from the inner part of the marine sponge *Reniochalina* sp. collected from the Xisha Islands in the South China Sea. The sample was deposited at the Research Center for Marine Drugs, School of Medicine, Shanghai Jiao Tong University. This strain was identified based on the morphology analyze and ITS gene sequencing (GenBank accession No. FJ491681).

The strain was cultivated on potato dextrose agar at 28°C for 7 days. Large scale fermentation was carried out in 50 erlenmeyer flasks (2 L) each containing 80 g of rice and 120 mL of distilled H_2O with 0.3% (m/v) peptone. Each flask was inoculated with 20 mL of cultured broth and incubated under static conditions at room temperature for 40 days.

Extraction and Isolation

The fermented substrate was exhaustively extracted with ethyl acetate to provide the residue (26.0 g) after removal of the organic solvent under reduced pressure.

The EtOAc extract was fractionated by vacuum liquid chromatography on silica gel (200–300 mesh) using CH_2Cl_2/MeOH gradient elution (500:1–0:1, v/v) to give eleven fractions A–K. Fraction H (6.1 g) was separated by column chromatography (CC) over Sephadex LH-20 eluted with MeOH to afford subfractions H1–H9. Subfraction H3 (1.5 g) was applied to medium pressure liquid chromatography (MPLC) on ODS, eluted with a gradient of 10 to 100% (v/v) MeCN in H_2O, to give H3A–H3F. H3D was subjected to reversed-phase HPLC with an elution of 55% MeOH in H_2O to give **1** (2.0 mL/min, t_R = 23.0 min, 8.6 mg). H3C (31.3 mg) was purified by semi-preparative reversed-phase HPLC eluted with 18% MeCN in H_2O to yield **2** (2.0 mL/min, t_R = 37.7 min, 2.0 mg). Subfraction H2 (1.82 g) was applied to MPLC on ODS, eluted with a gradient of 10 to 100% (v/v) MeCN in H_2O, to give Fr. H2A–H2H. Fraction H2F (169 mg) was then purified by semi-preparative RP-HPLC eluted with 37% MeCN in H_2O resulted in the isolation of **3** (2.0 mL/min, t_R = 30.5 min, 1.8 mg).

Violaceomide A (**1**): white amorphous powder; [α]25 D −230 (*c* 0.6, MeOH); UV (MeOH) λ_{max} (log ε) 220 (3.26), 276 (1.31) nm; HRESIMS m/z 477.2719 $[M + H]^+$ (calcd for $C_{24}H_{37}N_4O_6$, 477.2713); ^1H and ^{13}C NMR data, **Table 1**.

Sclerotiotide L (**2**): pale yellow amorphous powder; [α]25 D −92 (*c* 0.5, MeOH); UV (MeOH) λ_{max} (log ε) 216 (3.84), 258 (3.98) nm; HRESIMS m/z 481.3042 $[M + H]^+$ (calcd for $C_{24}H_{41}N_4O_6$, 481.3026); ^1H and ^{13}C NMR data, **Table 2**.

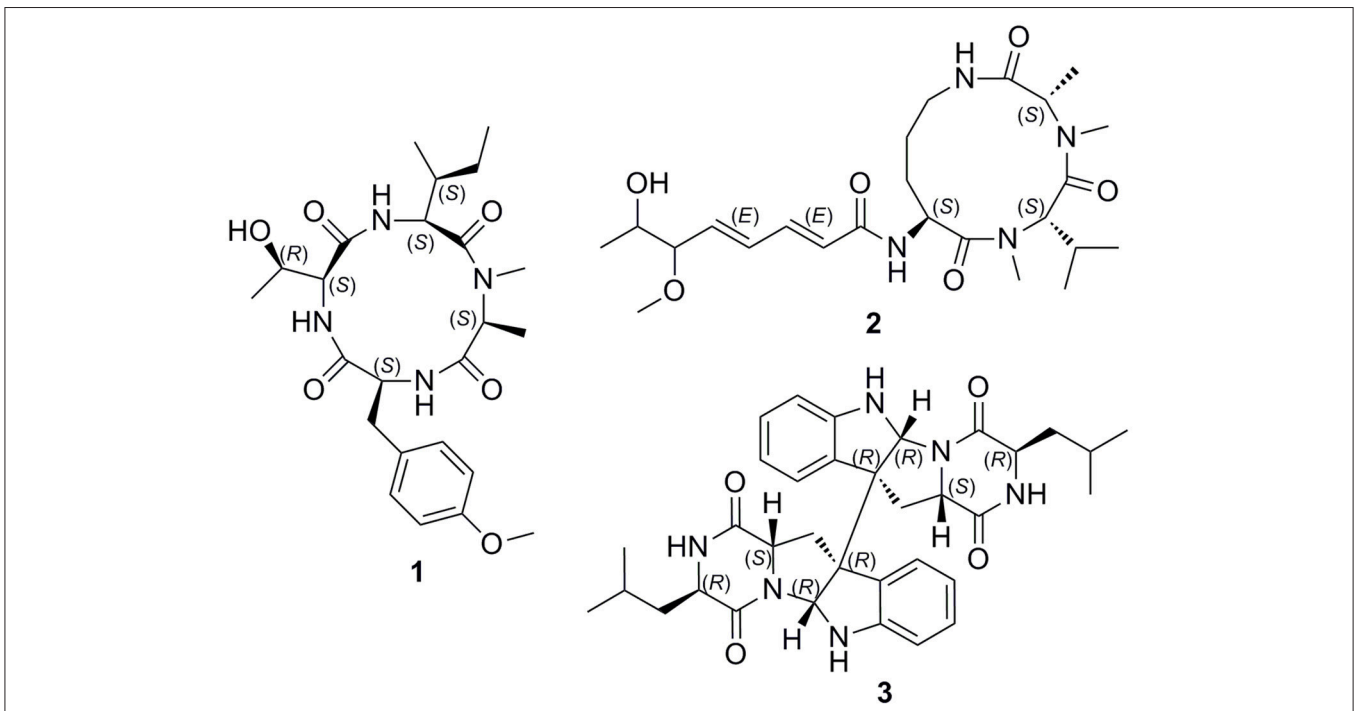

FIGURE 1 | Structures of compounds **1-3**.

Compound (**3**): White powder. [α]25 D +530.0 (*c* 0.3, MeOH); UV (MeOH) λ_{max} (log ε) 239 (3.58), 300 (1.55) nm; HRESIMS m/z 597.3177 $[M + H]^+$ (calc. for $C_{34}H_{41}N_6O_4$ 597.3189). ^1H and ^{13}C NMR data, **Table 3**.

Advanced Marfey's Analysis of Compound 1

Compound **1** (1 mg) were hydrolyzed in HCl (6 M; 1 mL) for 18 h at 110°C. The solutions were then evaporated to dryness and redissolved in H_2O (200 μL). The aqueous hydrolysate was added with 1% (w/v) solution of 1-fluoro-2,4-dinitrophenyl-5-L-leucinamide (L-FDLA, 100 μL) in acetone and 1 M $NaHCO_3$ (40 μL). After treating at 45°C for 90 min, the reactions were quenched by the addition of HCl (1 M, 40 μL). Appropriate amino acid standards were treated with L-FDLA and D-FDLA as described above and yielded the L-FDLA and D-FDLA standards. Marfey's derivatives of **1** was subjected to UPLC-MS selected ion chromatography on a reversed-phase column (Waters ACQUITY HS T3 column; 1.8 μm, 2.1 × 100 mm) with a linear gradient from 10 to 60% aqueous CH_3CN containing 0.1% formic acids over 18 min and their retention times were compared with those from the authentic standard derivatives.

Advanced Marfey's Analysis of Compound 2

Compound **2** (1 mg) were hydrolyzed in HCl (6 M; 1 mL) for 20 h at 110°C. The solutions were then evaporated to dryness and redissolved in H_2O (200 μL). The aqueous hydrolysate was divided into two equal portions. One portion was treated with 1% (w/v) solution of 1-fluoro-2,4-dinitrophenyl-5-D-leucinamide (D-FDLA, 100 μL) in acetone and 1 M $NaHCO_3$ (40 μL). The second portion was treated with a racemic mixture of a 1% (w/v) solution of 1-fluoro-2,4-dinitrophenyl-5-D-leucinamide (D-FDLA, 50 μL) in acetone, 1% (w/v) solution of 1-fluoro-2,4-dinitrophenyl-5-L-leucinamide (L-FDLA, 50 μL) in acetone, and 1 M $NaHCO_3$ (40 μL). Both mixtures were heated at 45°C for 90 min and the reactions were quenched by the addition of HCl (1 M, 40 μL). The aliquots were subjected to HPLC-MS selected ion chromatography on a reversed-phase column (Waters XBridge C18 column; 5 μm, 4.6 × 250 mm; 1.0 mL/min) with a linear gradient from 10 to 80% aqueous CH_3CN containing 0.1% formic acids over 30 min according to the advanced Marfey's method. The retention times and ESIMS product ions (t_R in min, m/z $[M + H]^+$) of the D-FDLA mono-derivatized amino acids in the hydrolysate of the first portion were observed to be Orn (13.1, 427.5), *N*-Me-Ala (20.4, 398.5), and *N*-Me-Val (24.3, 426.4), while the reaction with racemic D/L-FDLA in the second portion gave rise to two peaks for each corresponding amino acid moiety. The retention times and ESIMS product ions (t_{R1}/t_{R2}, min, m/z $[M + H]^+$) were observed to be Orn (13.1/14.1, 427.5), *N*-Me-Ala (20.1/20.4, 398.5), and *N*-Me-Val (22.1/24.3, 426.4). Consequently, the absolute configuration of the amino acids in the hydrolysate of **2** was confirmed as L-Orn, *N*-Me-L-Ala, and *N*-Me-L-Val.

Marfey's Analysis of Compound 3

Compound **3** (0.4 mg) was dissolved in 6 N HCl (1 mL) and heated at 110°C for 24 h. Then, the solvent was evaporated under reduced pressure and resuspended in 50 μL of H_2O. The hydrolysates were treated with 200 μL of 1% (w/v) 1-fluoro-2,4-dinitrophenyl-5-L-leucinamide (FDLA) in acetone and 40 μL of 1.0 N $NaHCO_3$. The reaction mixtures were heated at 45°C for 2 h, cooled to room temperature, and then neutralized with 40 μL of 1 N HCl. Standard D-Leu and D/L-Leu were derivatised in a similar fashion separately. The derivatives of the hydrolysates and the standard amino acids were analyzed by LC-MS selected ion chromatography on a reversed-phase column (Waters XBridge C18 column; 5 μm, 4.6 × 250 mm; 1.0 mL/min) with a linear gradient from 10 to 100% aqueous CH_3CN containing 0.1% formic acids over 30 min. The retention times for FDLA derivatives of standard D-Leu and L-Leu were 21.8 and 18.7 min, respectively, while this for FDLA derivatives of compound **3** were 21.8 min.

Anti-inflammatory Assay

THP-1 (a human acute monocytic leukemia cell line) cells (CCTCC) were maintained in RPMI-1640 supplemented with 10% (v/v) FBS and 0.05 mmol/L 2-mercaptoethanol at 37°C in a 5% CO_2 and humidified environment. THP-1 cells (5×10^5/mL) were differentiated using 160 nmol/L PMA for 36 h. Differentiation of PMA-treated cells was enhanced by removing the PMA-containing media and the cells were incubated in FBS free, fresh RPMI 1640 for a further 12 h, and then stimulated with compounds or/and LPS at the indicated concentrations and time periods.

Cytokines IL-6, IL-10, MCP-1, and TNF-α in the culture media of THP-1 cells treated with 10 μM compounds or/and 0.1 μg/mL LPS were determined by flow cytometry using the Human Inflammation Cytometric Bead Array (CBA) according to the instruction of the manufacturer (BD Biosciences, San Jose, CA, USA). Cytokine levels were measured on a FACSCalibur flow cytometer (BD Biosciences Pharmingen). The concentrations were assessed by using FCAP Array software.

RESULTS AND DISCUSSION

Compound **1** was isolated as a White, amorphous powder, which possessed a molecular formula of $C_{24}H_{36}N_4O_6$ deduced from the pseudomolecular ion peak at m/z 477.2719 $[M + H]^+$ in its HRESIMS (Supplementary Figure 19). The signal distribution pattern observed in the ^1H and ^{13}C NMR spectrum (pyridine-d_5) (Supplementary Figures 1–2), which showed three exchangeable amide NH signals (δ_H 9.30, 8.80, 7.20), four amide carbonyls (δ_C 173.8, 173.6, 173.2, and 171.4), four characteristic α-methine signals ($\delta_{H/C}$ 5.14/55.7, 4.74/55.1, 4.47/55.9, and 4.37/65.3) and one *N*-methyl ($\delta_{H/C}$ 3.32/30.8), indicated the characteristic of a peptide. Combined analysis of the 2D NMR spectra (Supplementary Figures 3–6) revealed the structures of four amino acid residues, including alanine (Ala), isoleucine (Ile), threonine (Thr), and one tyrosine (Tyr). An HMBC correlation from 4-*N*-CH_3 (δ_H 3.32) to Ala C-2 (δ_C 55.1) indicated that the Ala residue was *N*-methylated. The 24-OCH_3 linked to the

TABLE 1 | ^{1}H (600 MHz) and ^{13}C NMR (150 MHz) Data for **1** in Pyridine-d_5.

Position	δ_C	δ_H, mult. (*J* in Hz)	Position	δ_C	δ_H, mult. (*J* in Hz)
N-Me-Ala			12	65.3, CH	4.37, dd (8.9, 2.4)
1	173.6, C		13	68.1, CH	4.78, m
2	55.1, CH	4.74, m	14	22.2, CH_3	1.40, d (6.3)
3	17.0, CH_3	1.46, d (7.1)	12-NH		7.20, brs
4	30.8, CH_3	3.32, s	O-Me-Tyr		
Ile			15	173.8, C	
5	171.4, C		16	55.9, CH	4.47, m, overlapped
6	55.7, CH	5.14, dd (10.0, 7.6)	17	35.7, CH_2	3.81, m; 3.63, m
7	37.6, CH	2.37, m	18	132.7, C	
8	17.6, CH_3	1.16, d (6.5)	19/23	131.9, CH	7.31, d (8.0)
9	25.2, CH_2	2.00, m; 1.42, m	20/22	114.9, CH	7.03, d (8.2)
10	12.4, CH_3	0.94, t (7.4)	21	159.6, C	
6-NH		8.80, brs	24	55.9, CH_3	3.78, s
Thr			16-NH		9.30, brs
11	173.2, C				

TABLE 2 | ^{1}H (600 MHz) and ^{13}C NMR (150 MHz) Data for **2** in $CDCl_3$.

Position	δ_C	δ_H, mult. (*J* in Hz)	Position	δ_C	δ_H, mult. (*J* in Hz)
Ala			10-NH		6.53, d (7.2)
1	171.5, C		11	28.6, CH_2	2.39, m; 1.60, m
2	55.2, CH	4.59, q (7.1)	12	21.9, CH_2	1.66, m; 1.57, m
3	17.0, CH_3	1.51, d (7.1)	13	39.7, CH_2	3.38, m; 3.06, m
N-CH_3	29.9, CH_3	3.06, s	13-NH		5.68, brs
Val			Fatty acid		
4	169.2, C		1′	164.8, C	
5	58.8, CH	5.11, d (10.5)	2′	124.2, CH	5.92, d (15.0)
6	27.0, CH	2.43, m	3′	140.3, CH	7.23, dd (15.0, 10.8)
7	20.0, CH_3	0.92, d (6.3)	4′	132.1, CH	6.36, dd (15.4, 11.0)
8	18.0, CH_3	0.74, d (6.8)	5′	137.7, CH	6.00, dd (15.4, 7.8)
N-CH_3	30.4, CH_3	2.95, s	6′	85.5, CH	3.62, dd (7.8, 3.7)
Orn			7′	69.5, CH	3.90, dd (6.5, 3.7)
9	173.1, C		8′	18.0, CH_3	1.12, d (6.5)
10	49.7, CH	4.98, t (7.2)	9′	57.1, CH_3	3.32, s

TABLE 3 | ^{1}H (600 MHz) and ^{13}C NMR (150 MHz) Data for **3** in $CDCl_3$.

Position	δ_C	δ_H, mult. (*J* in Hz)	Position	δ_C	δ_H, mult. (*J* in Hz)
2/2′	80.5, CH	4.94, s	12/12′	37.2, CH_2	3.18, dd (14.0, 9.1)
3/3′	59.7, C		13/13′	168.5, C	
4/4′	130.0, C		14/14′		5.93, s
5/5′	124.9, CH	7.34, d (7.5)	15/15′	56.3, CH	3.77, m
6/6′	119.9, CH	6.81, t (7.5)	16/16′	168.2, C	
7/7′	129.8, CH	7.15, t (7.6)	17/17′	41.8, CH_2	1.48, m; 2.82, dd (14.0, 8.6)
8/8′	110.3, CH	6.65, d (7.9)	18/18′	24.5, CH	1.64, m
9/9′	148.8, C		19/19′	23.1, CH_3	0.89, d (6.5)
11/11′	55.8, CH	3.99, t (8.8)	20/20′	21.3, CH_3	0.87, d (6.5)

benzene ring at C-21 was supported by the HMBC correlation from H_3-24 (δ_H 3.78) to C-21 (δ_C 159.6). The assignment of the amino acid sequence was carried out by a combination of HMBC, NOESY (**Figure 2**), and MS/MS analysis. The HMBC correlations from *N*MeAla H_3-4 (δ_H 3.32) to Ile C-5 (δ_C 171.4) and from Ile H-6 (δ_H 5.14) to Thr C-11 (δ_C 173.2), suggesting a partial sequence of *N*MeAla-Ile-Thr. The NOESY correlation between *O*MeTyr NH (δ_H 9.30) and *N*MeAla H_3-3 (δ_H 1.46) extended this sequence to *O*MeTyr-*N*MeAla-Ile-Thr. The 9° of unsaturation and the molecular formula suggested that **1** was a cyclic peptide. Therefore, the cyclic tetrapeptide ring was closed between *O*MeTyr and Thr. In addition, the amino acid sequence of **1** was confirmed by mass fragmentation analysis using a quadrupole-time-of-flight (Q-TOF) tandem mass spectrometer (**Figure 3**). Consequently, the planar structure of **1** was elucidated as a cyclic tetrapeptide with the sequence cyclo-(Thr-*O*-MeTyr-*N*-MeAla-Ile).

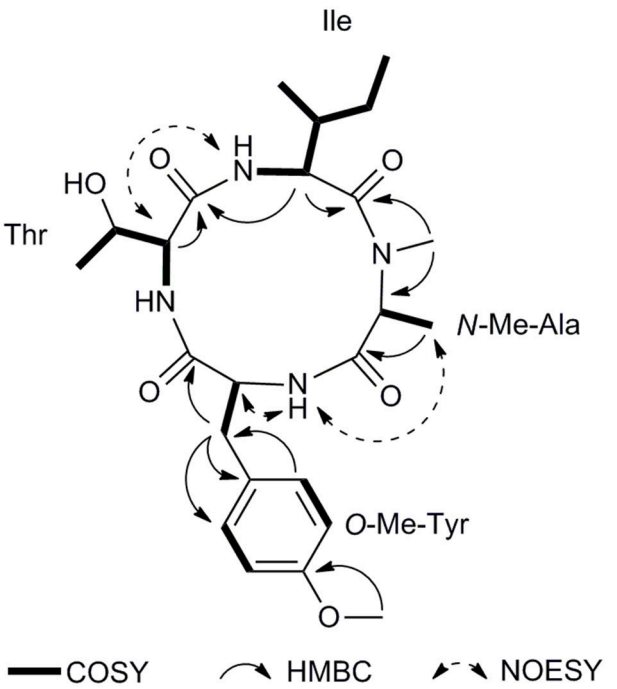

FIGURE 2 | Key COSY, HMBC, and NOESY correlations of **1**.

The absolute configurations of the amino acids were determined by the advanced Marfey's method after acid hydrolysis (Fujii et al., 1997). Compound **1** was hydrolyzed and then derivatized with L-FDLA. The UPLC-MS comparison between Marfey's derivatives of the hydrolysate of **1** and appropriate amino acid standards assigned the L configurations for Thr, Tyr, *N*-Me-Ala, and Ile (Supplementary Figure 23). The final structure of **1** was elucidated as cyclo-[L-Thr–L-*O*-Me-Tyr–L-*N*-Me-Ala–L-Ile] and named as violaceotide A.

Compound **2** was isolated as a pale yellow amorphous powder. The molecular formula can be determined as $C_{24}H_{40}N_4O_6$ by HRESIMS ion peak at m/z 481.3042 $[M + H]^+$ (calcd for $C_{24}H_{41}N_4O_6$, 481.3026) (Supplementary Figure 20). The ^1H NMR spectrum of **2** showed an amide NH proton (δ_H 6.53), two *N*-methyl protons (δ_H 2.95 and 3.06), and three characteristic α-methine signals (δ_H 4.59, 4.98, and 5.11), indicating a tripeptide structure. The ^{13}C NMR spectrum exhibited a total of 24 carbon resonances, including four amide carbonyl carbons, ten methine carbons, three methene carbons, and seven methyl carbons. The obvious difference in the NMR spectra between compound **2** and sclerotiotide H (Zheng et al., 2010) was the appearance of an additional *O*-methyl group at δ_H 3.32 (H-9′) and δ_C 57.1 (C-9′). The HMBC correlations (**Figure 4**) from H_3-9′ to C-6′ (δ_C

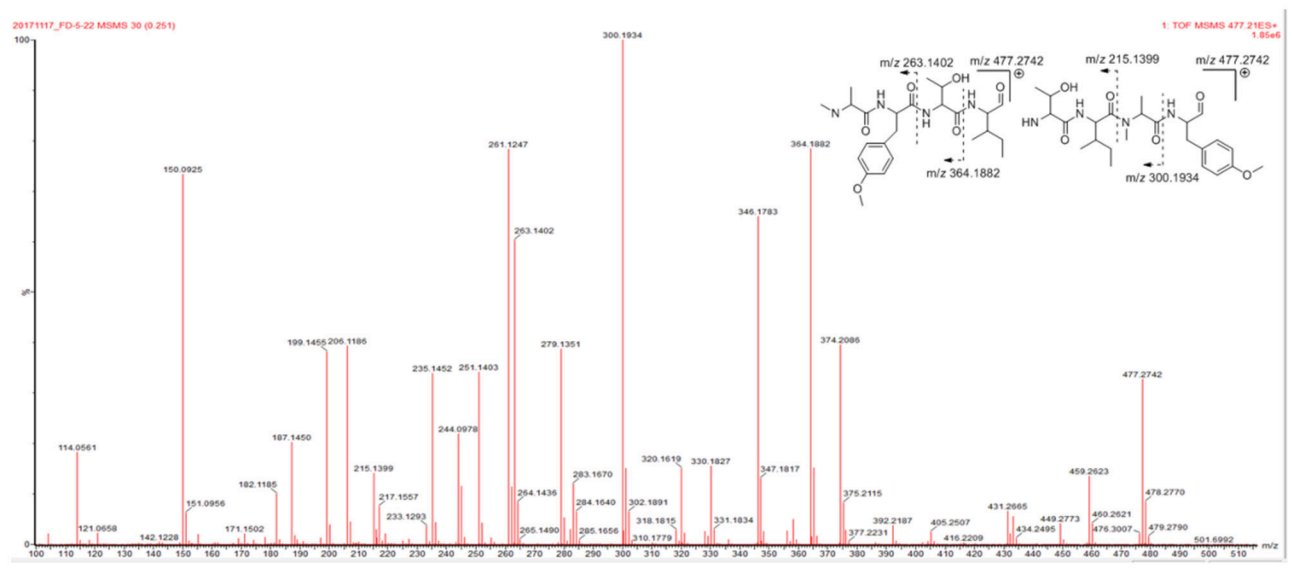

FIGURE 3 | MS/MS spectrum of **1**.

85.5) revealed that the *O*-methyl was linked to fatty acid chain at position 6′ (Supplementary Figures 7–12). The geometries of the $\Delta^{2',3'}$ and $\Delta^{4',5'}$ olefins were identified as 2′*E* and 4′*E*, by the proton spin coupling constants of $J_{H-2',H-3'}$ (15.0 Hz) and $J_{H-4',H-5'}$ (15.4 Hz). In order to determine the absolute configurations of the amino acid residues of **2,** advanced Marfey's method was utilized (Fujii et al., 1997). HPLC-MS analysis of derivatives of the hydrolysates with D-FDLA and D/L-FDLA indicated that the amino acids were *N*Me-L-Ala, *N*Me-L-Val, and L-Orn (Supplementary Figure 24). Thus, compound **2** was elucidated as (2′*E*,4′*E*)-*cyclo*-[(*N*Me-L-Ala)-(*N*Me-L-Val)-(N_α-6′-methoxy-7′-hydroxyocta-2′,4′-dienoyl-L-Orn)] and named as sclerotiotide L.

Compound **3** was isolated as a white amorphous powder. Its molecular formula was determined as $C_{34}H_{40}N_6O_4$ on the basis of the pseudomolecular ion peak at m/z 597.3177 [M + H]$^+$ (calcd for $C_{34}H_{41}N_6O_4$, 597.3189) in the HRESIMS (Supplementary Figure 21), requiring 18 degrees of unsaturation. The NMR spectra of **3** revealed 17 carbon signals, indicating that **3** would be a symmetric homodimer which was further confirmed by its half MS fragment ion peak at m/z 298.2 (Supplementary Figure 22).

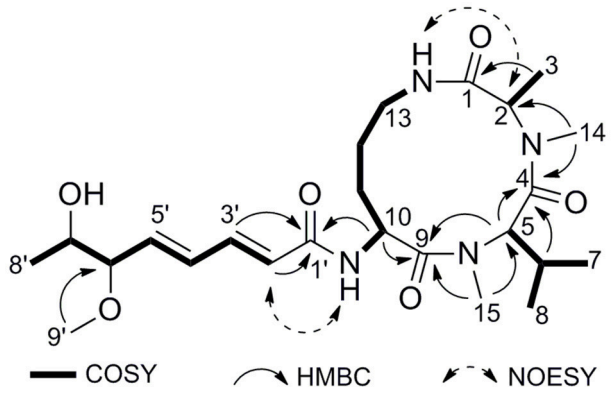

FIGURE 4 | Key COSY, HMBC, and NOESY correlations of **2**.

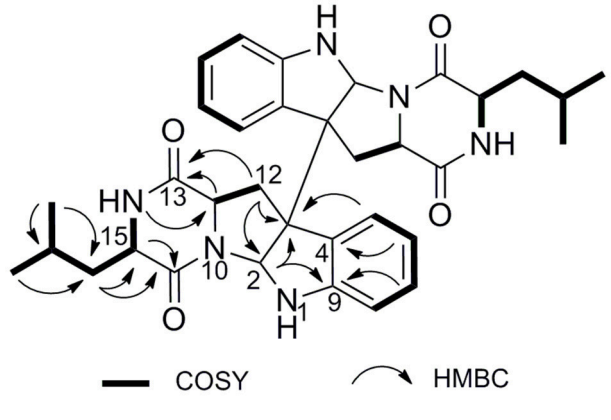

FIGURE 5 | Key HMBC and COSY correlations of **3**.

In the ^{1}H NMR spectrum, four aromatic signals at δ_H 7.34 (d, J = 7.5 Hz, H-5/H-5′), 7.15 (t, J = 7.6 Hz, H-7/H-7′), 6.81 (t, J = 7.5 Hz, H-6/H-6′), and 6.65 (d, J = 7.9 Hz, H-8/H-8′) and a proton at 4.94 (s, ^{1}H, H-2/H-2′) were observed, which suggested a indoline moiety.[16] In addition, two methyl signals were also observed at δ_H 0.89 (d, J = 6.5 Hz, H_3-19/H_3-19′) and 0.87 (d, J = 6.5 Hz, H_3-20/H_3-20′). The ^{13}C NMR spectrum exhibited a total of 17 carbon resonances, including five quaternary carbons, eight methine carbons, two methene carbons, and two methyl carbons. Two ^{13}C NMR resonances at δ 168.5 (C-13/C-13′) and δ 168.2 (C-16/C-16′) were characteristic signals of lactam carbonyls. The HMBC correlations from H-17 (δ_H 1.48) to C-15 (δ_C 56.3), and C-16 (δ_C 168.2) and COSY correlations of H-14 (δ_H 5.93)/H-15 (δ_H 3.77)/H-17/H-18 (δ_H 1.64)/H-19 and H-18/H-20 established a leucine unit (**Figure 5**). A tryptophan moiety can be concluded from the ^{1}H NMR signals and the key HMBC correlations from H-12 (δ_H 3.18) to C-2 (δ_C 80.5), C-3 (δ_C 59.7), C-11 (δ_C 55.8), and C-13, from H-2 to C-3, and C-9 (δ_C 148.8). Ultimately, extensive analysis of the 2D NMR data and comparison of the spectroscopic data with the reported literature (Ovenden et al., 2004) allowed identifying the planar structure of **3** as shown (Supplementary Figures 13–18).

The relative configurations of **3** were deduced from the observed NOESY correlations (**Figure 6**). The key NOESY correlations of H-11/H-17 and H-11/ H-2, indicated that these protons were on the same face. The NOESY correlations of H-5′ with H-11 and H-11 with H-2 suggested *cis*-fused ring junction at C-2 and C-3. Marfey's method (Cho et al., 2018) was employed to determine the absolute configuration at C-15. Compound **3** was hydrolyzed and derivatized with L-FDLA and analyzed by LC-MS to the establishment of absolute configuration of Leu residues.

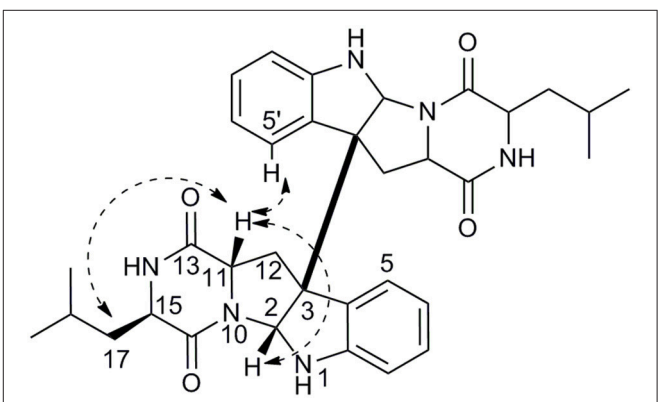

FIGURE 6 | Key NOESY correlations of **3**.

TABLE 4 | The inhibitory rates of compounds **1-3** against the cytokines expression of LPS-induced THP-1 cells at concentration of 10 μM.

Compound	IL-6 (%)	IL-10 (%)	MCP-1 (%)	TNF-α (%)
1	45.9	84.3	32.9	64.2
2	28.0	23.6	40.5	61.5
3	51.2	78.1	40.0	63.1

By comparing the retention times of authentic standards of L- and D- forms of Leu, the hydrolysate was identified to contain a unit of D-Leu (Supplementary Figure 25). Therefore, the absolute configurations of **3** were assigned as 2*R*, 3*R*, 11*S*, 15*R* (**Figure 1**).

To the best of our knowledge, compound **3** has the same planar structure as a unnamed and ambiguous compound without any spectroscopic data or optical rotation published on a patent (Masashi et al., 1995). Our compound possesses the different stereochemistry with it. Therefore, **3** was reported as a new diketopiperazine dimer herein.

Compounds **1–3** were evaluated their inhibitory activities against the production of four cytokines levels in the serum of human acute monocytic leukemia cell line THP-1 by using the human inflammation cytometric bead array (CBA) assay (**Table 4**). The cytokines, including IL-6, IL-10, MCP-1, TNF-α in this study, are pivotal mediators that contribute to inflammation and various related diseases (Liu et al., 2017; Wu et al., 2017). Notably, treatment of THP-1 cells by LPS showed a significant elevation in the secretion of the cytokines ($P < 0.01$). Results showed that the THP-1 cells pretreated with compounds **1** and **3** showed a significant decrease in the LPS-induced expression of IL-10 with inhibitory rates of 84.3 and 78.1% ($P < 0.01$), respectively. These compounds did not show cytotoxicity against THP-1 cells after 24 h treatment.

CONCLUSIONS

From the marine sponge-derived fungus *Aspergillus violaceofuscus*, three new cyclic peptides were obtained. Aspochracin-type cyclic tripeptide sclerotiotide L (**2**) and a diketopiperazine dimer (**3**) showed anti-inflammatory activity against IL-10 expression of the LPS-induced THP-1 cells, which indicated that the marine sponge-derived microorganism are a fertile source of compounds with novel structures and significant bioactivities.

AUTHOR CONTRIBUTIONS

JL, BG, and LY: performed the experiments; JL: identified the structures and analyzed the data; HL and FY: conceived and designed the experiments; JL and FY: wrote the paper. All authors listed have approved the work for publication.

FUNDING

This research was supported by the National Natural Science Fund for Distinguished Young Scholars of China (81225023), the National Natural Science Fund of China (Nos. U1605221, 81741151, and 41476121), Shanghai Municipal Commission of Health and Family Planning (20140388), and the Fund of the Science and Technology Commission of Shanghai Municipality (15431900900).

SUPPLEMENTARY MATERIAL

The Supplementary Material for this article can be found online at: https://www.frontiersin.org/articles/10.3389/fchem.2018.00226/full#supplementary-material

REFERENCES

Amagata, T., Morinaka, B. I., Amagata, A., Tenney, K., Valeriote, F. A., Lobkovsky, E., et al. (2006). A chemical study of cyclic depsipeptides produced by a sponge-derived fungus. *J. Nat. Prod.* 69, 1560–1565. doi: 10.1021/np060178k

Bao, J., Zhang, X.-Y., Xu, X.-Y., He, F., Nong, X.-H., and Qi, S.-H. (2013). New cyclic tetrapeptides and asteltoxins from gorgonian-derived fungus *Aspergillus* sp. SCSGAF 0076. *Tetrahedron* 69, 2113–2117. doi: 10.1016/j.tet.2013.01.021

Cho, K. H., Sohn, J. H., and Oh, H. (2018). Isolation and structure determination of a new diketopiperazine dimer from marine-derived fungus *Aspergillus* sp. SF-5280. *Nat. Prod. Res.* 32, 214–221. doi: 10.1080/14786419.2017.1346642

Daletos, G., Kalscheuer, R., Koliwer-Brandl, H., Hartmann, R., de Voogd, N. J., Wray, V., et al. (2015). Callyaerins from the Marine Sponge *Callyspongia aerizusa*: cyclic peptides with antitubercular activity. *J. Nat. Prod.* 78, 1910–1925. doi: 10.1021/acs.jnatprod.5b00266

Ding, L. J., Yuan, W., Liao, X. J., Han, B. N., Wang, S. P., Li, Z. Y., et al. (2016). Oryzamides A-E, Cyclodepsipeptides from the Sponge-Derived Fungus Nigrospora oryzae PF18. *J. Nat. Prod.* 79, 2045–2052. doi: 10.1021/acs.jnatprod.6b0034

Fujii, K., Ikai, Y., Oka, H., Suzuki, M., and Harada, K.-I. (1997). A nonempirical method using LC/MS for determination of the absolute configuration of constituent Amino Acids in a Peptide: combination of Marfey's method with mass spectrometry and its practical application. *Anal. Chem.* 69, 5146–5151.

Fukuhara, K., Takada, K., Okada, S., and Matsunaga, S. (2015). Nazumazoles A-C, cyclic pentapeptides dimerized through a disulfide bond from the marine sponge Theonella swinhoei. *Org. Lett.* 17, 2646–2648. doi: 10.1021/acs.orglett.5b01020

Gu, W. X., Cueto, M., Jensen, P. R., Fenical, W., and Silverman, R. B. (2007). Microsporins A and B: new histone deacetylase inhibitors from the marine-derived fungus Microsporum cf. gypseum and the solid-phase synthesis of microsporin A. *Tetrahedron* 63, 6535–6541. doi: 10.1016/j.tet.2007.04.025

Ireland, C. M. Jr., Durso, A. R., Newman, R. A., and Hacker, M. P. (1982). Antineoplastic cyclic peptides from the marine tunicate Lissoclinum patella. *J. Org. Chem.* 47, 1807–1811.

Jang, J. P., Nogawa, T., Futamura, Y., Shimizu, T., Hashizume, D., Takahashi, S., et al. (2017). Octaminomycins A and B, Cyclic Octadepsipeptides Active against Plasmodium falciparum. *J. Nat. Prod.* 80, 134–140. doi: 10.1021/acs.jnatprod.6b00758

Liu, J. T., Wu, W., Cao, M. J., Yang, F., and Lin, H. W. (2017). Trienic alpha-pyrone and ochratoxin derivatives from a sponge-derived fungus Aspergillus ochraceopetaliformis. *Nat. Prod. Res.*. doi: 10.1080/14786419.2017.1402325

Luo, S., Krunic, A., Kang, H. S., Chen, W. L., Woodard, J. L., Fuchs, J. R., et al. (2014). Trichormamides A and B with antiproliferative activity from the cultured freshwater Cyanobacterium Trichormus sp. UIC 10339. *J. Nat. Prod.* 77, 1871–1880. doi: 10.1021/np5003548

Masashi, H., Hiroshi, M., Mitsuyoshi, S., Toshie, H., and Hidenor, Y. (1995). *Cholecystokinin B/Gastrin Receptor Antagonist.* Japan patent application JP 1994–119123.

Ovenden, S. P., Sberna, G., Tait, R. M., Wildman, H. G., Patel, R., Li, B., et al. (2004). A diketopiperazine dimer from a marine-derived isolate of *Aspergillus niger*. *J. Nat. Prod.* 67, 2093–2095. doi: 10.1021/np0497494

Raaijmakers, J. M., Bruijn, I.,d., Nybroe, O., and Ongena, M. (2010). Natural functions of lipopeptides from Bacillus and Pseudomonas: more than surfactants and antibiotics. *FEMS Microbiol. Rev.* 34, 1037–1061. doi: 10.1111/j.1574-6976.2010.00221.x

Randazzo, A., Bifulco, G., Giannini, C., Bucci, M., Debitus, C., Cirino, G., et al. (2001). Halipeptins A and B: two novel potent anti-inflammatory cyclic depsipeptides from the Vanuatu marine sponge *Haliclona* species. *J. Am. Chem. Soc.* 123, 10870–10876. doi: 10.1021/ja010015c

Sieber, S. A., and Marahiel, M. A. (2005). Molecular mechanisms underlying nonribosomal peptide synthesis: approaches to new antibiotics. *Chem. Rev.* 105, 715–738. doi: 10.1021/cr0301191

Teta, R., Marteinsson, V. T., Longeon, A., Klonowski, A. M., Groben, R., Bourguet-Kondracki, M. L., et al. (2017). Thermoactinoamide A, an Antibiotic Lipophilic Cyclopeptide from the Icelandic Thermophilic Bacterium Thermoactinomyces vulgaris. *J. Nat. Prod.* 80, 2530–2535. doi: 10.1021/acs.jnatprod.7b00560

Wu, W., Zhen, Z., Niu, T., Zhu, X., Gao, Y., Yan, J., et al. (2017). kappa-Carrageenan Enhances Lipopolysaccharide-Induced Interleukin-8 Secretion by Stimulating the Bcl10-NF-kappaB Pathway in HT-29 Cells and Aggravates C. freundii-Induced Inflammation in Mice. *Med. Inflamm.* 2017:8634865. doi: 10.1155/2017/8634865

Xu, W. J., Liao, X. J., Xu, S. H., Diao, J. Z., Du, B., Zhou, X. L., et al. (2008). Isolation, Structure Determination, and Synthesis of Galaxamide, A Rare Cytotoxic Cyclic Pentapeptide from a Marine Algae *Galaxaura filamentosa*. *Org. Lett.* 10, 4569–4572. doi: 10.1021/ol801799d

Yu, Z., Lang, G., Kajahn, I., Schmaljohann, R., and Imhoff, J. F. (2008). Scopularides A and B, cyclodepsipeptides from a marine sponge-derived fungus, *Scopulariopsis brevicaulis*. *J. Nat. Prod.* 71, 1052–1054. doi: 10.1021/np070580e

Zhang, H. J., Yi, Y. H., Yang, G. J., Hu, M. Y., Cao, G. D., Yang, F., et al. (2010). Proline-containing cyclopeptides from the marine sponge Phakellia fusca. *J. Nat. Prod.* 73, 650–655. doi: 10.1021/np9008267

Zheng, J., Xu, Z., Wang, Y., Hong, K., Liu, P., and Zhu, W. (2010). Cyclic tripeptides from the halotolerant fungus Aspergillus sclerotiorum PT06-1. *J. Nat. Prod.* 73, 1133–1137. doi: 10.1021/np100198h

Conflict of Interest Statement: The authors declare that the research was conducted in the absence of any commercial or financial relationships that could be construed as a potential conflict of interest.

frontiers in Chemistry

ORIGINAL RESEARCH
published: 12 July 2018
doi: 10.3389/fchem.2018.00282

Structurally Diverse Polyketides From the Mangrove-Derived Fungus *Diaporthe* sp. SCSIO 41011 With Their Anti-influenza A Virus Activities

Xiaowei Luo[1,2†], *Jie Yang*[3†], *Feimin Chen*[3], *Xiuping Lin*[1], *Chunmei Chen*[1,2], *Xuefeng Zhou*[1,2*], *Shuwen Liu*[3,4*] *and Yonghong Liu*[1,2*]

[1] CAS Key Laboratory of Tropical Marine Bio-Resources and Ecology, Guangdong Key Laboratory of Marine Materia Medica, South China Sea Institute of Oceanology, Chinese Academy of Sciences, Guangzhou, China, [2] University of Chinese Academy of Sciences, Beijing, China, [3] Guangdong Provincial Key Laboratory of New Drug Screening, Guangzhou Key Laboratory of Drug Research for Emerging Virus Prevention and Treatment, School of Pharmaceutical Sciences, Southern Medical University, Guangzhou, China, [4] State Key Laboratory of Organ Failure Research, Southern Medical University, Guangzhou, China

OPEN ACCESS

Edited by:
Xian-Wen Yang,
Third Institute of Oceanography, State Oceanic Administration, China

Reviewed by:
Christophe Salome,
SpiroChem AG, Switzerland
Rongbiao Pi,
Sun Yat-sen University, China

***Correspondence:**
Xuefeng Zhou
xfzhou@scsio.ac.cn
Shuwen Liu
liusw@smu.edu.cn
Yonghong Liu
yonghongliu@scsio.ac.cn

[†]These authors have contributed equally to this work.

Specialty section:
This article was submitted to Medicinal and Pharmaceutical Chemistry, a section of the journal Frontiers in Chemistry

Received: 07 May 2018
Accepted: 22 June 2018
Published: 12 July 2018

Citation:
Luo X, Yang J, Chen F, Lin X, Chen C, Zhou X, Liu S and Liu Y (2018) Structurally Diverse Polyketides From the Mangrove-Derived Fungus Diaporthe sp. SCSIO 41011 With Their Anti-influenza A Virus Activities. Front. Chem. 6:282. doi: 10.3389/fchem.2018.00282

Influenza A virus (IAV) is a severe worldwide threat to public health and economic development due to its high morbidity and mortality. Marine-derived fungi have been evidenced as a prolific source for the discovery of pharmacologically-active lead compounds. During the course of our search for novel bioactive substances from marine microorganisms, six new polyketides, including two octaketides (**1–2**), one chromone derivative (**13**), two highly substituted phthalides (**17–18**), and one α-pyrone derivative (**21**) along with 22 known congeners were isolated from a mangrove-associated fungus *Diaporthe* sp. SCSIO 41011. Their structures were determined by spectroscopic analysis and by comparison with literature data. And the absolute configurations were established according to the specific rotation or electron circular dichroism method. Antiviral evaluation results revealed that compounds **14**, **15**, **26**, and 5-chloroisorotiorin displayed significant anti-IAV activities against three influenza A virus subtypes, including A/Puerto Rico/8/34 H274Y (H1N1), A/FM-1/1/47 (H1N1), and A/Aichi/2/68 (H3N2), with IC_{50} values in the range of 2.52–39.97 μM. The preliminary structure-activity relationships (SARs) are also discussed. These findings expand the chemical and bioactive diversity of polyketides derived from the genus *Diaporthe*, and also provide a basis for further development and utilization of chromone, xanthone, and chloroazaphilone derivatives as source of potential anti-viral chemotherapy agents.

Keywords: *Diaporthe* sp., polyketides, cytosporones, phthalides, anti-influenza A virus

INTRODUCTION

Polyketides represent an important category of secondary metabolites with great structural diversity from simple aromatics to highly modified complex architectures, such as macrolides, polyphenols, polyethers, polyenes, and enediynes (Fujii, 2010; Zheng et al., 2015). Distributing broadly in microbial origins, they are constructed by combination of iterative polyketide synthases (PKSs) and multifunctional and iterative oxygenases (Hang et al., 2016). In addition,

polyketides play a vital role in modern medicine due to their diverse pharmacological features, such as lovastatin, a well-known fungal polyketide statins functioned as a cholesterol-lowering agent (Crawford and Townsend, 2010). Belonging to the family of octaketides, biosynthetically related cytosporones, dothiorelones and phomopsins are characterized with a di-/tri-hydroxybenzene lactone or a resorcinol scaffold harboring an *n*-heptane substituent, which were mainly encountered in endophytic fungi of several genera, such as *Phomopsis* (Kornsakulkarn et al., 2015; Kongprapan et al., 2017; Tan et al., 2017), *Diaporthe* (Brady et al., 2000; Liu et al., 2018), *Cytospora* (Brady et al., 2000; Abreu et al., 2010), *Pestalotiopsis* (Xu et al., 2009b). Of special note, cytosporone B (**7**) was reported as a nuclear orphan receptor Nur77 agonist as a promising therapeutic drug for cancers and hypoglycemia (Zhan et al., 2008), as well as the transcription factor NR4A1 agonist to control IAV infection and improve pulmonary function in infected mice (Xia et al., 2013; Egarnes et al., 2017), which had aroused a great interest for chemical synthesis study (Von Delius et al., 2017).

Influenza A virus (IAV), a negative sense RNA virus, is one of the main causes of human acute respiratory diseases characterized with high morbidity and mortality, posing a serious threat to public health and economic development (Liu et al., 2017). IAVs repeatedly circulate in many animal hosts, such as humans, birds, horses, dogs, and pigs, which can be subtyped to two envelope proteins: haemagglutinin (HA) and neuraminidase (NA) glycoproteins according to the antigenic properties (Medina and Garcia-Sastre, 2011). In 2009, the pandemic influenza H1N1 virus rapidly spread to 214 countries around the world, causing human infection and acute respiratory illness of more than 17,700 deaths (Bautista et al., 2010). As of 25th April 2018, there have been reported 1625 confirmed cases of human H7N9 infection and 623 deaths since 2013 according to the World Health Organization (http://www.fao.org/ag/againfo/programmes/en/empres/H7N9/situation_update.html). However, two families of antiviral drugs are hitherto currently used to treat human IAV infections, which are NA inhibitors, like zanamivir and oseltamivir, and inhibitors of the viral M2 protein exemplified by amantadine and rimantadine (Medina and Garcia-Sastre, 2011; Song et al., 2015). Due to the emergence of drug-resistant viral strains, there is an urgent development for novel classes of anti-IAV agents with new mode of action.

Marine-derived fungi are reported as a prodigious source of development for new antivirals against different important viruses (Moghadamtousi et al., 2015). In our continuing endeavor to discover biologically active compounds from marine microbes, a series of structurally interesting and biologically active natural products have been described (Luo et al., 2017; Tan et al., 2018). Recently, six new cytotoxic chloroazaphilone derivatives, isochromophilones A–F, have been isolated from the fungus *Diaporthe* sp. SCSIO 41011, an endophytic fungus obtained from the fresh tissue of the marine mangrove plant *Rhizophora stylosa* (Luo et al., 2018). Subsequent chemical investigations on the remaining fractions of the fungus led to the isolation of structurally diverse aromatic polyketides, including octaketides (dothiorelones or cytosporones), phthalides, chromones, xanthones, etc. (**Figure 1**). The structures of these compounds were determined by physicochemical properties and spectral data analysis as well as comparison with those reported in the literature. All the compounds were examined for anti-IAV activities against three influenza A virus subtypes, including A/Puerto Rico/8/34 H274Y (H1N1), A/FM-1/1/47 (H1N1), and A/Aichi/2/68 (H3N2). Details of the isolation, structure elucidation, and biological activity of these compounds, as well as preliminary SARs, are reported herein.

MATERIALS AND METHODS

General Experimental Procedures

Semi-preparative HPLC was performed on a Hitachi Primaide apparatus using an ODS (octadecylsilanized silica) column (YMC-pack ODS-A, YMC Co. Ltd., 10 × 250 mm, 5 μm, 2.5 mL/min). Chiral HPLC separation was performed using CHIRALPAK IC column (250 × 4.6 mm, 5 μm). TLC and column chromatography (CC) were performed on plates precoated with silica gel GF254 (10–40 μm) and over silica gel (200–300 mesh) (Qingdao Marine Chemical Factory), and Sephadex LH-20 (Amersham Biosciences), respectively. Spots were detected on TLC (Qingdao Marine Chemical Factory) under 254 nm UV light. All solvents employed were of analytical grade (Tianjin Fuyu Chemical and Industry Factory). The NMR spectra were obtained on a Bruker Avance spectrometer (Bruker) operating at 500 and 700 MHz for ^{1}HNMR, 125 MHz, and 175 MHz for ^{13}CNMR, using TMS as an internal standard. Optical rotations were acquired using a Perkin Elmer MPC 500 (Waltham) polarimeter. HRESIMS and ESIMS spectra data were recorded on a MaXis quadrupole-time-of-flight mass spectrometer and an amaZon SL ion trap mass spectrometer (Bruker), respectively. UV spectra were recorded on a Shimadzu UV-2600 PC spectrometer (Shimadzu). ECD spectra were performed on a Chirascan circular dichroism spectrometer (Applied Photophysics). IR spectra were measured on an IR Affinity-1 spectrometer (Shimadzu). The artificial sea salt was a commercial product (Guangzhou Haili Aquarium Technology Company).

Fungal Material

The fungus *Diaporthe* sp. SCSIO 41011 had the same origination as that in our recent published paper (Luo et al., 2018). A voucher specimen was deposited in the CAS Key Laboratory of Tropical Marine Bio-resources and Ecology, South China Sea Institute of Oceanology, Chinese Academy of Sciences, Guangzhou, China.

Extraction and Isolation

The fermentation of the strain and the extraction and isolation of its extract was identical to that of our recent published paper (Luo et al., 2018). Briefly, nine fractions was isolated from the EtOAc extract (150 g) by silica gel vacuum liquid chromatography (VLC) using step gradient elution with petroleum ether/CH_2Cl_2 (0–100%). Compounds **23** (40 mg, t_R 30 min) and **25** (4.5 mg, t_R 18 min) were purified from Fr.2 (13 g) by an ODS column (MeOH/H_2O: 10–100%) and followed by semiprep-HPLC with

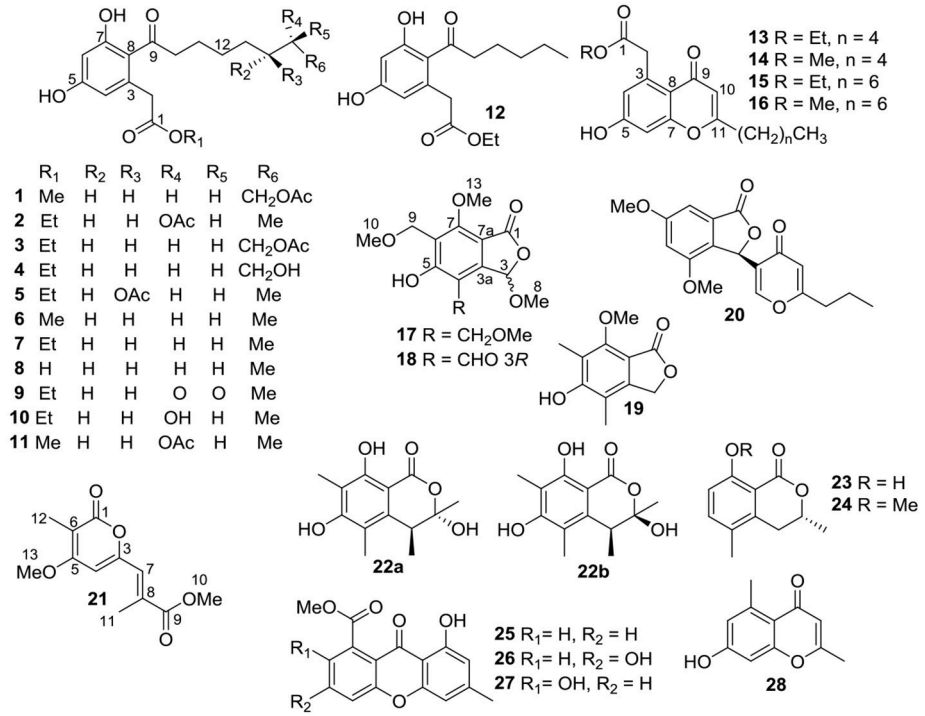

	R_1	R_2	R_3	R_4	R_5	R_6
1	Me	H	H	H	H	CH_2OAc
2	Et	H	H	OAc	H	Me
3	Et	H	H	H	H	CH_2OAc
4	Et	H	H	H	H	CH_2OH
5	Et	H	OAc	H	H	Me
6	Me	H	H	H	H	Me
7	Et	H	H	H	H	Me
8	H	H	H	H	H	Me
9	Et	H	H	O	O	Me
10	Et	H	H	OH	H	Me
11	Me	H	H	OAc	H	Me

FIGURE 1 | Structures of compounds **1**–**28**.

72% (2.5 mL/min) and 50% MeCN (2.3 mL/min) elutions, respectively. Fr.3 (10 g) was purified on Sephadex LH-20 (MeOH), an ODS column ($MeOH/H_2O$: 10–100%) and finally semiprep-HPLC (70% MeCN, 2.3 mL/min) to afford compounds **17** (4.2 mg, t_R 7 min) and **24** (3.5 mg, t_R 9 min). Fraction 4 (12 g) was subjected to Sephadex LH-20 (MeOH) to provide eight subfractions (Frs.4-1∼4-8). Then ten subfractions (Frs.4-3-1∼4-3-10) were obtained from Fr. 4-3 by an ODS column ($MeOH/H_2O$: 10–100%). Compound **18** (150 mg) was isolated from Fr. 4-3-4 by recrystallization. Meanwhile, compounds **20** (7.1 mg, t_R 24 min), **14** (4.3 mg, t_R 15 min) and **6** (141 mg, t_R 25 min) were isolated from Frs. 4-3-6, 4-3-7, 4-3-8 by semiprep-HPLC with 55% MeOH (2.5 mL/min), 50% MeCN (2.3 mL/min), and 68% MeCN (1.4 mL/min) elutions, respectively. Besides, compounds **27** (2 mg, t_R 10 min) and **26** (2.2 mg, t_R 12 min) was purified from Fr.4-4 and Fr. 4-6 by semiprep-HPLC with 80% MeOH (2.5 mL/min) and 60% MeCN (2.3 mL/min) elutions, respectively. Fraction 5 (4 g) was subjected to Sephadex LH-20 (MeOH) to provide five subfractions (Frs.5-1∼5-5). Fr. 5-4 was further purified on semiprep-HPLC by 66% MeCN (2.5 mL/min) to give compounds **8** (77 mg, t_R 9 min), **12** (4 mg, t_R 11.5 min), and **7** (142 mg, t_R 20.6 min). Seven subfractions (Frs.7-1∼7-7) were obtained from Fr. 7 (4 g) by Sephadex LH-20 (MeOH). Then Fr. 7-4 was subjected to an ODS column ($MeOH/H_2O$: 10–100%) to provide thirteen subfractions (Frs.7-4-1∼7-4-13). Fr. 7-4-8 was further purified on semiprep-HPLC by 47% MeCN (2.5 mL/min) to give compounds **4** (2.3 mg, t_R 12 min), **10** (2 mg, t_R 16 min), and **2** (3.8 mg, t_R 39 min), along with one subfraction (Fr. 7-4-8-6). Compounds **11** (4.7 mg, t_R 42 min) and **1** (24 mg, t_R 45 min) were purified from Fr. 7-4-8-6 by semiprep-HPLC by 56% MeOH (2.3 mL/min). Fr. 7-4-12 was subjected to semiprep-HPLC (74%MeOH, 1.8 mL/min) to give compounds **16** (2.6 mg, t_R 14 min) and **15** (3.8 mg, t_R 45 min). Similarly, Fr. 7-5 was subjected to an ODS column ($MeOH/H_2O$: 10–100%) to provide eight subfractions (Frs.7-5-1∼7-5-8). Compounds **19** (5.6 mg, t_R 10.4 min) and **28** (5 mg, t_R 8 min) were purified from Fr.7-5-5 and Fr.7-5-6 by semiprep-HPLC with 50% MeCN (2.5 mL/min) and 47% MeCN (2.5 mL/min) elutions, respectively. Fr. 7-5-7 was subjected to semiprep-HPLC (50%MeCN, 2.5 mL/min) to afford compounds **22** (5 mg, t_R 11.5 min) and **21** (1.5 mg, t_R 15 min). Fr.9 (7 g) was subjected to Sephadex LH-20 (MeOH) and followed by an ODS column ($MeOH/H_2O$: 10–100%) to provide six subfractions (Frs.9-1-1∼9-1-6). Fr. 9-1-4 was purified by semiprep-HPLC (55%MeCN, 2.0 mL/min) to provide compounds **9** (3 mg, t_R 12 min), **5** (3 mg, t_R 25 min), **3** (2 mg, t_R 28 min). Compund **13** (0.8 mg, t_R 10 min) was isolated from Fr.9-1-5 by semiprep-HPLC (78% MeOH, 2.0 mL/min).

Antiviral Activity

All the isolated compounds (**1**–**28**), along with recently reported co-isolated 5-chloroisorotiorin (Luo et al., 2018), were screened for their anti-IAV activities according to the previously reported 3-(4,5-dimethylthiazol-2yl)-2,5-diphenyltetrazolium bromide (MTT) colorimetric assay, using ribavirin as a positive control (Li et al., 2017; Yang et al., 2018). In brief, Madin Derby canine kidney (MDCK) cells were cultured in Dulbecco's modified Eagle's medium (DMEM) supplemented with 10% fetal bovine serum and 1% penicillin/streptomycin. Meanwhile, different

influenza A virus subtypes, including A/Puerto Rico/8/34 H274Y (H1N1), A/FM-1/1/47 (H1N1), and A/Aichi/2/68 (H3N2), were multiplied in 10-day-old chick embryo at 37°C. The cytotoxicity of the compounds was also evaluated by the MTT assay. Briefly, approximately 90% confluent cells in 96-well plates were exposed to the compounds at 2-fold serial dilutions. After 48 h of incubation, 100 μL of MTT solution, which was diluted by the medium to 0.5 mg/mL, was added and retained at 37°C for 4 h. Then the supernatant was removed, followed by the addition of 150 μL of dimethyl sulfoxide (DMSO) to dissolve the formazan product. The optical density for each well was measured on the Tecan Genios Pro microplate reader (Bedford, MA, USA) at 570 nm. To determine the antiviral activities of the compounds, confluent MDCK cells were infected with the virus at multiplicity of infection (MOI) of 0.01 at 37°C for 1 h. The compounds of non-cytotoxic concentrations were then added to the cells after washing away the unabsorbed virus with phosphate-buffered saline (PBS), and the cells were cultured for another 48 h. At the end of the culture, the MTT-based assay as previously described was assessed for the antiviral activity of the isolated compounds.

Statistical Analysis

All statistical analysis of the data were processed by GraphPad Prism. The results are presented as the mean ± standard deviation (SD) from experiments in triplicate. Student's *t*-test was used to analyze the statistical significance between two groups, more groups by one-way ANOVA with or without Tukey–Kramer multiple comparison. A $p < 0.05$ was regarded as statistically significant.

RESULTS AND DISCUSSION

Identification of Compounds

The endophytic fungus *Diaporthe* sp. SCSIO 41011 was cultured on solid rice medium for 60 days. The EtOAc extract (150 g) of the fermentation was separated by continuously silica gel chromatography and semi-preparative HPLC chromatography to yield 28 aromatic polyketides (**1**–**28**). Their chemical structures were determined by comprehensive spectroscopic analyses or comparison with those reported data.

Compound **1** was obtained as colorless oil and had the molecular formula $C_{19}H_{26}O_7$ as determined by a deprotonated ion peak at *m/z* 365.1607 (calcd for $C_{19}H_{25}O_7$, 365.1600) in HRESIMS data. The ^{1}H NMR data (**Table 1**) along with HSQC experiment of **1** displayed two singlet methyls at δ_H 2.01 (3H, s) and 3.65 (3H, s), two aromatic protons at δ_H 6.26 (1H, d, $J = 2.2$ Hz) and 6.19 (1H, d, $J = 2.2$ Hz), along with an array of methylene signals. The ^{13}C NMR spectrum (**Table 1**) showed 19 resonances that were sorted by a distortionless enhancement by polarization transfer (DEPT) experiment, assigned to three carbonyls (δ_C 209.0, 174.0, and 173.1), six aromatic carbons (δ_C 161.8, 160.1, 137.0, 120.9, 112.0, and 102.9), eight methylenes (δ_C 65.7, 45.0, 40.4, 30.3, 30.1, 29.6, 26.8, and 25.4) and two methyls (δ_C 52.3 and 20.8). The aforementioned NMR data showed **1** was closely related structurally to the co-isolated 16-acetoxydothiorelone C (**3**) (Liu et al., 2018). The only difference was the appearance of a methyl group ($\delta_{H/C}$ 3.65/52.3) at C-1′ in **1** instead of an ethyl group in **3**, which was also verified by the HMBC correlation from H_3-1′ to C-1 (**Figure 2**). Thus, the structure of **1** was determined as shown in **Figure 1** and assigned the trivial name dothiorelone O.

Compound **2** was also acquired as colorless oil and was determined to have the molecular formula $C_{20}H_{28}O_7$ from the HRESIMS data. Inspection of the comprehensive spectral data of **2**, including MS, and 1D, 2D-NMR data, indicated that **2** shared the same planer structure with (15S)-acetoxydothiorelone A (Liu et al., 2018). Comparison of the specific rotations between **2** ($[\alpha]_D^{25} = -5.8$ (c 0.10, MeOH)) and (15S)-acetoxydothiorelone A ($[\alpha]_D^{20} = +4.9$ (c 0.25, MeOH)) suggested **2** had the 15R configuration (Izuchi et al., 2011; Beekman and Barrow, 2015; Liu et al., 2018), given that they possessed only one chiral carbon at C-15. Therefore, the structure of **2** was resolved and accordingly named (15R)-acetoxydothiorelone A.

Compound **13** was also isolated as colorless oil and gave a molecular formula of $C_{18}H_{22}O_5$ relied on a deprotonated ion peak at *m/z* 317.1403 (calcd for $C_{18}H_{21}O_5$, 317.1389) in the HRESIMS spectrum. The ^{1}H NMR data (**Table 1**) together with

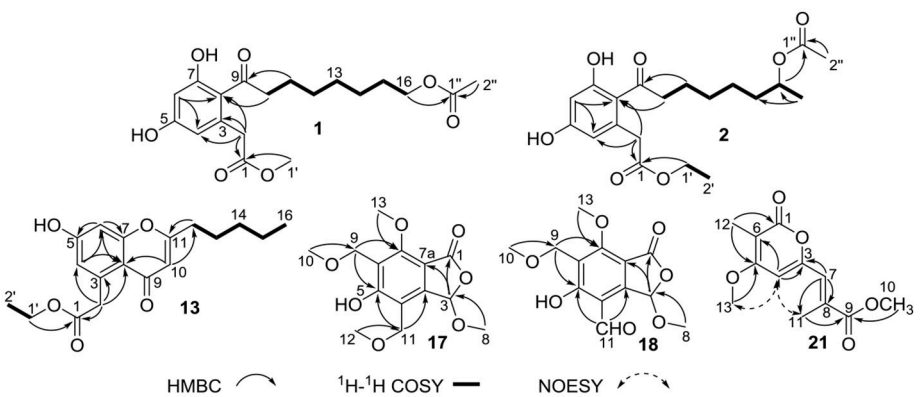

FIGURE 2 | Key HMBC, ^{1}H-^{1}H COSY, and NOESY correlations of compounds **1**–**2**, **13**, **17**–**18**, and **21**.

TABLE 1 | ^{1}H and ^{13}C NMR spectral data of compounds **1**, **2,** and **13** in CD_3OD.

	1		**2**		**13**	
No.	δ_H[a]	δ_C, type[b]	δ_H[c]	δ_C, type[d]	δ_H[c]	δ_C, type[d]
1		174.0, C		173.6, C		173.6, C
2	3.58, s	40.4, CH_2	3.60, s	40.6, CH_2	4.06, s	42.1, CH_2
3		137.0, C		137.1, C		138.5, C
4	6.19, d (2.2)	112.0, CH	6.21, d (2.2)	111.9, CH	6.65, d (2.2)	120.3, CH
5		161.8, C		161.6, C		164.8, C
6	6.26, d (2.2)	102.9, CH	6.28, d (2.2)	102.8, CH	6.73, d (2.2)	103.1, CH
7		160.1, C		160.0, C		161.5, C
8		120.9, C		121.1, C		115.1, C
9		209.0, C		208.9, C		181.4, C
10	2.85, t (7.6)	45.0, CH_2	2.83, t (7.6)	43.3, CH_2	5.98, s	110.3, CH
11	1.61, m	25.4, CH_2	1.62, o	25.3, CH_2		170.3, C
12	1.34, o	30.3, CH_2	1.35, o	30.2, CH_2	2.61, t (7.1)	34.5, CH_2
13	1.34, o	30.1, CH_2	1.35, o	26.3, CH_2	1.73, m	27.6, CH_2
14	1.34, o	26.8, CH_2	1.52, m	36.8, CH_2	1.39, o	32.3, CH_2
15	1.61, m	29.6, CH_2	4.86, o	72.4, CH	1.39, o	23.4, CH_2
16	4.04, t (7.1)	65.7, CH_2	1.22, d (7.1)	20.2, CH_3	0.93, t (7.1)	14.2, CH_3
1′	3.65, s	52.3, CH_2	4.14, q (7.1)	61.8, CH_2	4.13, q (7.1)	61.7, CH_2
2′			1.26, t (7.1)	14.5, CH_3	1.24, t (7.1)	14.5, CH_3
1′′		173.1, C		172.8, C		
2′′	2.01, s	20.8, CH_3	2.02, s	21.2, CH_3		

[a] *In 500 MHz.*
[b] *In 125 MHz.*
[c] *In 700 MHz.*
[d] *In 175 MHz, m, multiplet; o, overlapped.*

HSQC and HMBC spectra of **13** displayed signals indicative of two doublet methyls at δ_H 0.93 (3H, d, J = 7.1 Hz) and 1.24 (3H, d, J = 7.1 Hz), three aromatic protons at δ_H 6.65 (1H, d, J = 2.2 Hz), 6.73 (1H, d, J = 2.2 Hz) and 5.98 (1H, s), along with several methylenes. The ^{13}C NMR spectrum (**Table 1**) showed 18 resonances attributable to two carbonyls (δ_C 173.6 and 181.4), six aromatic carbons (three oxygenated ones), six methylenes (δ_C 61.7, 42.1, 34.5, 32.3, 27.6, and 23.4) and two methyls (δ_C 14.2 and 14.5). The above mentioned spectral characteristics were closely consistent to those of the co-isolated pestalotiopsone F (**14**) (Xu et al., 2009a), but suggested the appearance of an ethyl group ($\delta_{H/C}$ 4.13/61.7 at C-1′ and 1.24/14.5 at C-2′) in **13** rather than a methyl group ($\delta_{H/C}$ 3.66/52.2) at C-1′ in **14**. These changes were also ascertained by the HMBC correlations from H_3-1′ to C-1 and from H_3-2′ to C-1′, as well as the ^{1}H-^{1}H COSY correlation of H_3-2′ and H_2-1′ (**Figure 2**). Based on the above discussion, the structure of **13** was elucidated and the trivial name pestalotiopsone H was assigned.

Compound **17** was obtained as a white solid and its molecular formula was found to be $C_{14}H_{18}O_7$ on the basis of HRESIMS and NMR data. The ^{1}H NMR data (**Table 2**) of **17** revealed four *O*-methyls at δ_H 3.38, 3.38, 3.54, and 3.99, two singlet methylenes at δ_H 4.60 and 4.65, and a hemiketal methine at δ_H 6.29. In addition to the above seven corresponding hydrogen-bearing carbons, seven carbons remained in the ^{13}C NMR spectrum, including one carbonyl (δ_C 169.6), six aromatic carbons [(δ_C 111.4, 119.0, 121.4, 148.9), and two oxygenated ones at δ_C 160.7 and 174.3]. The foregoing spectroscopic data showed great similarity to that of microsphaerophthalide F (Sommart et al., 2012) except that a methyl group ($\delta_{H/C}$ 2.16/8.5) located at C-6 in microsphaerophthalide F was replaced by an ethoxyl group ($\delta_{H/C}$ 4.60/65.3 at C-9 and 3.38/58.1 at C-10) anchored at C-6 in **17**. This deduction was also supported by the HMBC correlations from H_3-10 to C-9 and from H_2-9 to C-5 and C-7. The barely measurable optical rotation value and quite weak Cotton effects in the ECD spectrum suggested **17** was racemic, which was also confirmed by the chiral HPLC analysis with two peaks (peak area ratio: 1:1) in the HPLC profile (Supplementary Materials). However, the quantity of **17** was too little to perform further resolution. Hence, the structure of compound **17** was elucidated and the trivial name (±)-microsphaerophthalide H was assigned.

Compound **18** was obtained as colorless needle crystals and had the molecular formula $C_{13}H_{14}O_7$, as evidenced by HRESIMS ($[M+H]^+$, 283.0809; calcd for $C_{13}H_{15}O_7$, 283.0818) and the NMR data. The highly similar NMR spectroscopic data of **18** to those of **17** indicated that their structures were closely related, except for the presence of an aldehyde group ($\delta_{H/C}$ 10.14/192.5) joined at C-4 in **18**, rather than an ethoxyl group ($\delta_{H/C}$ 4.65/67.2 and 3.38/58.4) anchored at C-4 in **17**. The absolute configuration of C-3 of **18** was mainly determined by comparison of the specific rotations with those reported data, as well as comparison between

TABLE 2 | ^{1}H and ^{13}C NMR spectral data of compounds **17**, **18** and **21** (^{1}H for 700 MHz, ^{13}C for 175 MHz).

	17[a]		**18**[b]		**21**[a]	
No.	δ_H	δ_C, type	δ_H	δ_C, type	δ_H	δ_C, type
1		169.6, C		164.7, C		166.3, C
2						
3	6.29, s	103.1, CH	6.75, s	100.7, CH		158.8, C
3a		148.9, C		151.7, C		
4		119.0, C		112.4, C	6.87, d (1.4)	98.8, CH
5		174.3, C		166.3, C		167.8, C
6		121.4, C		120.9, C		105.6, C
7		160.7, C		163.1, C	6.67, s	120.3, CH
7a		111.4, C		109.6, C		
8	3.54, s	56.1, CH_3	3.60, s	56.9, CH_3		144.5, C
9	4.60, s	65.3, CH_2	4.44, s	61.3, CH_2		168.0, C
10	3.38, s	58.1, CH_3	3.27, s	57.7, CH_3	3.76, s	52.0, CH_3
11	4.65, s	67.2, CH_2	10.14, s	192.5, CH	2.44, d (1.4)	13.6, CH_3
12	3.38, s	58.4, CH_3			1.92, s	8.8, CH_3
13	3.99, s	63.0, CH_3	4.14, s	63.4, CH_3	4.02, s	57.5, CH_3

[a] *In CD_3OD.*
[b] *In DMSO-d_6.*

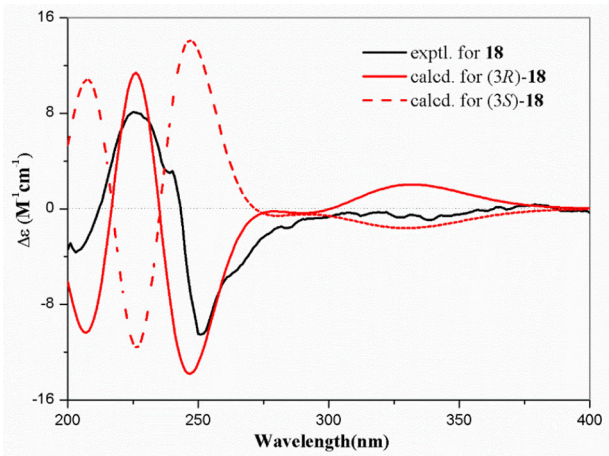

FIGURE 3 | Experimental and calculated ECD spectra of **18**.

the computed and experimental ECD spectra. Among these reported 3-oxygenated phthalides, the 3*S*- and 3*R*- ones generally showed negative and positive specific rotations, respectively (Sommart et al., 2012). Thus, the positive sign of specific rotation $[[\alpha]_D^{25} = +25$ (c 0.10, MeOH)] of **18** led to the deduction of 3*R* configuration in **18**, which was also confirmed from experimental and calculated ECD spectra of **18** as shown in **Figure 3**. Further chiral HPLC analysis confirmed that **18** was single enantiomer. Consequently, the structure of **18** was determined as shown in **Figure 1** and termed microsphaerophthalide I. Notably, the 3-oxygenated phthalides are uncommon in natural sources.

Compound **21** was obtained as a white solid and had the molecular formula $C_{12}H_{14}O_5$, as determined from HRESIMS

TABLE 3 | Inhibition activity of compounds **1**–**28** and 5-chloroisorotiorin against Influenza A Virus strains.

Compounds	**IC_{50} (μM)**[a]		
	A/Puerto Rico/8/34 H274Y (H1N1)	**A/FM-1/1/47 (H1N1)**	**A/Aichi/2/68 (H3N2)**
14	21.80 ± 7.96	6.74 ± 1.26	6.17 ± 1.46
15	2.56 ± 0.32	4.82 ± 1.90	6.76 ± 2.72
26	9.40 ± 1.96	4.80 ± 1.28	5.12 ± 1.49
5-chloroisorotiorin	2.52 ± 0.21	37.97 ± 15.11	10.10 ± 1.84
Remainings	IN[b]	IN	IN

[a] *The samples were tested in triplicate, and the data are presented as the mean ± SD*
[b] *Inactive.*

($[M+H]^+$, 239.0917; calcd for $C_{12}H_{15}O_5$, 239.0919) and the NMR data. Detailed analyses of its NMR spectroscopic features implied that it was closely related structurally to convolvulopyrone (Tsantrizos et al., 1992), but for the presence of an additional *O*-methyl group ($\delta_{H/C}$ 3.76/52.0) at C-10 in **21**, indicating that **21** was a methyl derivative of convolvulopyrone. Besides, compound **21** and convolvulopyrone shared the same relative configuration of 7*E* due to the absence of a NOESY correlation between H-7 and H_3-11. As a result, the structure of **21** was determined and given the trivial name methyl convolvulopyrone. However, compound **21** was likely obtained as an artifact formed in the process of extraction and purification using MeOH as a solvent.

Besides, these co-isolated known congeners were elucidated by comparing their physicochemical properties and spectroscopic data with those reported literature values (Supplementary Materials). They were determined as 16-acetoxydothiorelone C (**3**) (Liu et al., 2018), dothiorelone C (**4**) (Liu et al., 2018),

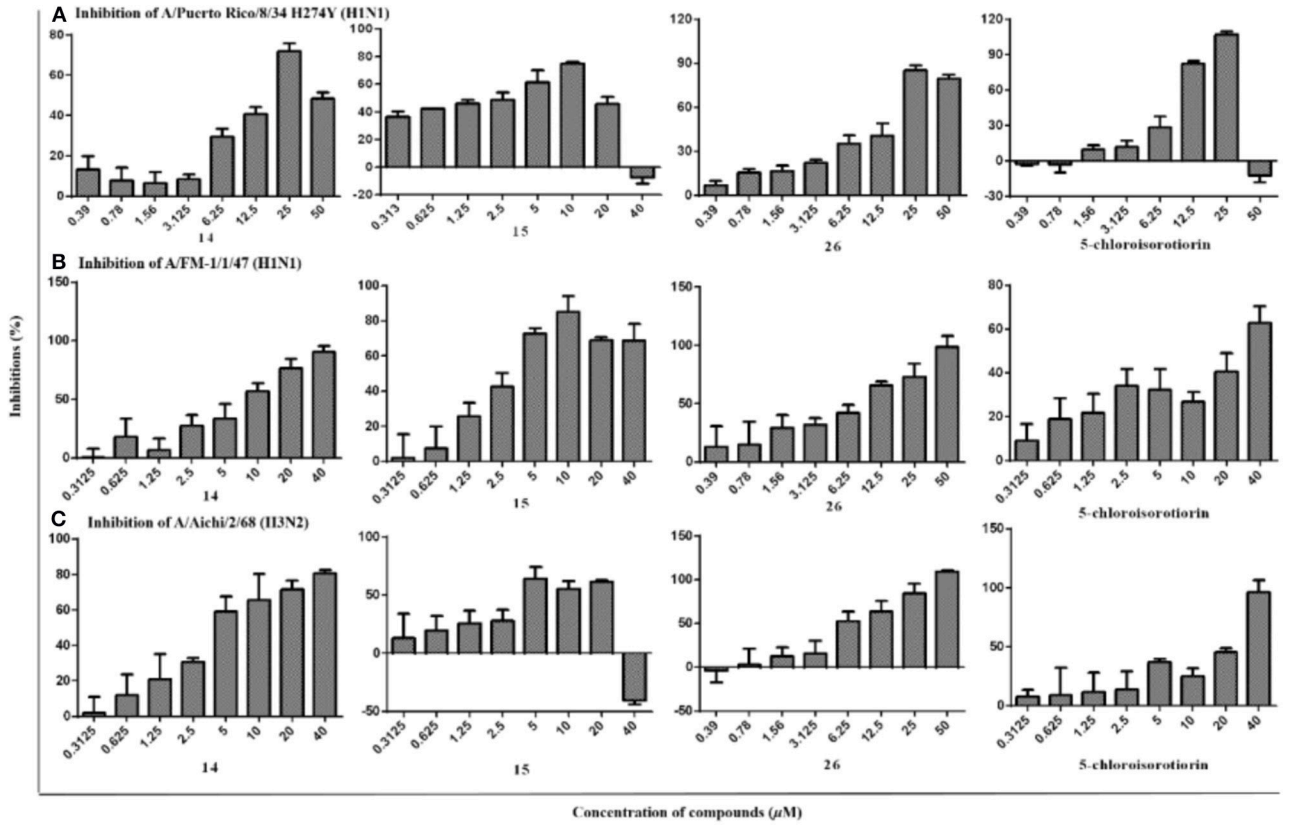

FIGURE 4 | The inhibitory activities of compounds **14**, **15**, **26**, and 5-chloroisorotiorin against influenza A viruses, including A/Puerto Rico/8/34 H274Y (H1N1) (**A**), A/FM-1/1/47 (H1N1) (**B**), and A/Aichi/2/68 (H3N2) (**C**).

(14*R*)-acetoxydothiorelone B (**5**) (Liu et al., 2018), cytosporone N (**6**) (Beekman and Barrow, 2015), cytosporone B (**7**) (Brady et al., 2000), cytosporone A (**8**) (Brady et al., 2000), dothiorelone I (**9**) (Liu et al., 2018), (15*R*)-dothiorelone A (**10**) (Liu et al., 2018), methyl (*R*)-2-(2-(7-acetoxyoctanoyl)-3,5-dihydroxyphenyl)acetate (**11**) (Beekman and Barrow, 2015), secocurvularin (**12**) (Bracher and Krauss, 1998), pestalotiopsone F (**14**) (Xu et al., 2009a), pestalotiopsone B (**15**) (Xu et al., 2009a), pestalotiopsone A (**16**) (Xu et al., 2009a), 5-hydroxy-7-methoxy-4,6-dimethylphthalide (**19**) (Sommart et al., 2012), dihydrovermistatin (**20**) (Komai et al., 2005), sclerotinin A (**22**) (Lai et al., 2013), 3,5-dimethyl-8-hydroxy-3,4-dihydroisocoumarin (**23**) (Kokubun et al., 2003), 3,5-dimethyl-8-methoxy-3,4-dihydroisocoumarin (**24**) (Kokubun et al., 2003), methyl 8-hydroxy-6-methyl-9-oxo-9*H*-xanthene-1-carboxylate (**25**) (Lai et al., 2013), 3,8-dihydroxy-6-methyl-9-oxo-9*H*-xanthene-1-carboxylate (**26**) (Nguyen et al., 2017), pinselin (**27**) (Cui et al., 2016), 7-hydroxy-2,5-dimethylchromone (**28**) (Koenigs et al., 2010). Amongst, methyl (*R*)-2-[2-(7-acetoxyoctanoyl)-3,5-dihydroxyphenyl]acetate (**11**) was isolated as a naturally occurring compound for the first time. While sclerotinin A (**22**) was isolated as a diastereoisomeric mixture which could not be separated by RP-HPLC method (Lai et al., 2013). This research further enriched secondary metabolites in the genus *Diaporthe* and also expanded the chemical diversity of polyketides, such as dothiorelones, cytosporones, phthalides, chromones, etc.

Antiviral Activity

Antiviral effect of the isolated compounds **1**–**28** and 5-chloroisorotiorin against different IAV subtypes, including A/Puerto Rico/8/34 H274Y (H1N1), A/FM-1/1/47 (H1N1), and A/Aichi/2/68 (H3N2), were then evaluated. Those compounds showed nearly no cytotoxicity against MDCK cells (IC_{50} > 200 μM). Compounds **14**, **15**, **26**, and 5-chloroisorotiorin displayed significant anti-IAV activities against the above mentioned subtypes with IC_{50} values in the range of 2.52–39.97 μM (**Table 3**). However, the remaining compounds (**1**–**13**, **16**–**25**, **27**–**28**) were inactive toward the three aforementioned IAV subtypes. Furthermore, pestalotiopsone F (**14**) and 3,8-dihydroxy-6-methyl-9-oxo-9*H*-xanthene-1-carboxylate (**26**) exhibited obvious inhibition effect on A/FM-1/1/47 (H1N1), as well as A/Aichi/2/68 (H3N2), in a dose-dependent manner (**Figure 4**).

Additionally, based on comparison of the structural characteristics among these analogs, a preliminary structure-activity relationship is discussed. Pestalotiopsone F (**14**) exhibited selective inhibitions against the two IAV subtypes

of A/FM-1/1/47 (H1N1) and A/Aichi/2/68 (H3N2) with the IC_{50} values of 6.74 ± 1.26 and 6.17 ± 1.46 μM, respectively. Comparing with the antiviral pestalotiopsones F (**14**) and B (**15**), the co-isolated siblings pestalotiopsones H (**13**) and A (**16**) were inactive toward the three IAV subtypes, which revealed methylation of the carboxyl group at C-1 for the pestalotiopsones with a C_7 aliphatic branch located at C-11, and while ethylation of the carboxyl group at C-1 for the pestalotiopsones with a C_5 aliphatic branch located at C-11, were essential for anti-IAV activities. Notably, among the three xanthones (**25**–**27**), only 3,8-dihydroxy-6-methyl-9-oxo-9*H*-xanthene-1-carboxylate (**26**) demonstrated remarkable inhibitory effects against A/FM-1/1/47 (H1N1), A/Puerto Rico/8/34 H274Y (H1N1), and A/Aichi/2/68 (H3N2) with IC_{50} values of 4.80 ± 1.28, 9.40 ± 1.96, and 5.12 ± 1.49 μM, respectively, which indicated the hydroxyl group at C-3 probably promote the anti-IAV activities toward the three subtypes. By the way, 5-chloroisorotiorin (Luo et al., 2018), a recently reported co-isolated chloroazaphilone derivative obtained with major amount, was also screened for anti-IAV activity, which presented selective inhibition activities against the two IAV subtypes of A/Puerto Rico/8/34 H274Y (H1N1) and A/Aichi/2/68 (H3N2) with the IC_{50} values of 2.52 ± 0.21 and 10.10 ± 1.84 μM, respectively. The remaining ones (**1**–**13**, **16**–**26**, **27**–**28**) showed no obvious inhibition against A/FM-1/1/47 (H1N1), A/Puerto Rico/8/34 H274Y (H1N1), and A/Aichi/2/68 (H3N2).

Characterization of Compounds

Dothiorelone O (**1**): colorless oil; UV (MeOH) λ_{max} (log ε) 302 (3.75), 269 (3.89), 220 (4.16), 204 (4.27) nm; IR (film) ν_{max} 3,356, 2,933, 2,833, 1,732, 1,714, 1,609, 1,591, 1,462, 1,261, 1,163, and 1,028 cm^{-1}; ^1H and ^{13}C NMR data, **Table 1**; HRESIMS *m/z* 365.1607 $[M-H]^-$ (calcd for $C_{19}H_{25}O_7$, 365.1600), 401.1368 $[M+Cl]^-$ (calcd for $C_{19}H_{26}ClO_7$, 401.1367).

(15*R*)-acetoxydothiorelone A (**2**): colorless oil; $[\alpha]_D^{25}$ – 5.8 (*c* 0.10, MeOH); UV (MeOH) λ_{max} (log ε) 303 (3.69), 269 (3.78), 220 (4.14), 204 (4.17) nm; IR (film) ν_{max} 3,358, 2,933, 2,858, 1,732, 1,714, 1,609, 1,558, 1,456, 1,265, 1,249, 1,159, and 1,024 cm^{-1}; ^1H and ^{13}C NMR data, **Table 1**; HRESIMS *m/z* 403.1741 $[M+Na]^+$ (calcd for $C_{20}H_{28}NaO_7$, 403.1733), 419.1470 $[M+K]^+$ (calcd for $C_{20}H_{28}KO_7$, 419.1472), 783.3563 $[2M+Na]^+$ (calcd for $C_{40}H_{56}NaO_{14}$, 783.3568).

Pestalotiopsone H (**13**): colorless oil; UV (MeOH) λ_{max} (log ε) 291 (4.14), 250 (4.31), 242 (4.28), 217 (4.38) nm; IR (film) ν_{max} 3,419, 2,927, 2,856, 1,732, 1,716, 1,645, 1,558, 1,456, 1,375, 1,274, 1,180, 1,161, and 1,028 cm^{-1}; ^1H and ^{13}C NMR data, **Table 1**; HRESIMS *m/z* 317.1403 $[M-H]^-$ (calcd for $C_{18}H_{21}O_5$, 317.1389), 353.1167 $[M+Cl]^-$ (calcd for $C_{18}H_{22}ClO_5$, 353.1156), 635.2860 $[2M-H]^-$ (calcd for $C_{36}H_{43}O_{10}$, 635.2856), 671.2626 $[2M+Cl]^-$ (calcd for $C_{36}H_{44}ClO_{10}$, 671.2623).

(±)-microsphaerophthalide H (**17**): a white solid; $[\alpha]_D^{25}$ – 5 (*c* 0.06, MeOH); UV (MeOH) λ_{max} (log ε) 307 (4.06), 249 (4.05), 220 (4.48) nm; IR (film) ν_{max} 3,419, 2,935, 2,846, 1,747, 1,734, 1,604, 1,558, 1,448, 1,429, 1,375, 1,276, 1,201, 1,159, 1,093, and 1,074 cm^{-1}; ^1H and ^{13}C NMR data, **Table 2**; HRESIMS *m/z* 299.1123 $[M+H]^+$ (calcd for $C_{14}H_{19}O_7$, 299.1131), 321.0954 $[M+Na]^+$ (calcd for $C_{14}H_{18}NaO_7$, 321.0950), 619.2010 $[2M+Na]^+$ (calcd for $C_{28}H_{36}NaO_{14}$, 619.2003).

Microsphaerophthalide I (**18**): colorless needle crystals; $[\alpha]_D^{25}$ = +25 (*c* 0.10, MeOH); UV (MeOH) λ_{max} (log ε) 367 (3.60), 295 (4.07), 245 (4.46), 201 (4.10) nm; ECD (0.15 mg/mL, MeOH) λ_{max} ($\Delta\varepsilon$) 203 (−2.07), 225 (+4.62), 251 (−6.00) nm; IR (film) ν_{max} 3,419, 2,945, 2,885, 1,770, 1,749, 1,668, 1,653, 1,558, 1,489, 1,375, 1,338, 1,286, 1,205, 1,097, and 1,058 cm^{-1}; ^1H and ^{13}C NMR data, **Table 2**; HRESIMS *m/z* 283.0809 $[M+H]^+$ (calcd for $C_{13}H_{15}O_7$, 283.0818), 305.0632 $[M+Na]^+$ (calcd for $C_{13}H_{14}NaO_7$, 305.0637).

Methyl convolvulopyrone (**21**): a white solid; UV (MeOH) λ_{max} (log ε) 343 (4.05), 279 (3.73), 239 (4.51), 205 (4.12) nm; IR (film) ν_{max} 3,446, 2,954, 2,927, 1,681, 1,635, 1,446, 1,355, 1,195, 1,182, 1,139, and 1,039 cm^{-1}; ^1H and ^{13}C NMR data, **Table 2**; HRESIMS *m/z* 239.0917 $[M+H]^+$ (calcd for $C_{12}H_{15}O_5$, 239.0919), 261.0749 $[M+Na]^+$ (calcd for $C_{12}H_{14}NaO_5$, 261.0739), 499.1590 $[2M+Na]^+$ (calcd for $C_{24}H_{28}NaO_{10}$, 499.1580).

CONCLUSIONS

Twenty-eight aromatic polyketides, including two new octaketides (**1**–**2**), one new chromone derivative (**13**), two new highly substituted phthalides (**17**–**18**), and one new α-pyrone derivative (**21**) along with 22 known congeners were isolated from a mangrove-associated fungus *Diaporthe* sp. SCSIO 41011, while methyl (*R*)-2-[2-(7-acetoxyoctanoyl)-3,5-dihydroxyphenyl]acetate (**11**) was isolated as a new natural compound and (±)-microsphaerophthalide H (**17**) was obtained as a racemic mixture. Amongst, pestalotiopsone F (**14**), pestalotiopsone B (**15**), 3,8-dihydroxy-6-methyl-9-oxo-9*H*-xanthene-1-carboxylate (**26**), and 5-chloroisorotiorin displayed pronounced anti-IAV activities against three IAV virus subtypes, including A/Puerto Rico/8/34 H274Y (H1N1), A/FM-1/1/47 (H1N1), and A/Aichi/2/68 (H3N2) with IC_{50} values in the range of 2.52–39.97 μM. This work further enriched secondary metabolites in the genus *Diaporthe* and also expanded the chemical and bioactive diversity of polyketides, such as dothiorelones, cytosporones, phthalides, chromones, etc. Furthermore, our findings provide a basis for further development and utilization of pestalotiopsone, xanthone, and chloroazaphilone derivatives as source of potential anti-IAV chemotherapy agents.

AUTHOR CONTRIBUTIONS

XiaL: designed the experiments and performed the isolation and characterization of all the compounds and wrote the manuscript; JY and FC: performed the antiviral experiment; XiuL: performed the isolation and purification of the fungal strain; CC: contributed to isolation of the compounds; XZ: designed the research work and wrote the manuscript; SL and YL: contributed in project design and manuscript preparation. All authors reviewed the manuscript and approved for submission.

ACKNOWLEDGMENTS

This work was supported by grants from the National Natural Science Foundation of China (81741154, 41476135, 21772210), National Major Scientific and Technological Special Project for Significant New Drugs Development (2018ZX09735001-002-003), the Natural Science Foundation of Guangdong Province (2014A030313765, 2016A030313591), Science and Technology Project of Guangdong Province (2016A020222009), and the Open Project of State Key Laboratory of Organ Failure Research. We thank to Z. Xiao, C. Li and A. Sun, analytical facility center of South China Sea Institute of Oceanology, for recording NMR, and MS data.

SUPPLEMENTARY MATERIAL

The Supplementary Material for this article can be found online at: https://www.frontiersin.org/articles/10.3389/fchem.2018.00282/full#supplementary-material

REFERENCES

Abreu, L. M., Phipps, R. K., Pfenning, L. H., Gotfredsen, C. H., Takahashi, J. A., and Larsen, T. O. (2010). Cytosporones O, P and Q from an endophytic *Cytospora* sp. *Tetrahedron Lett.* 51, 1803–1805. doi: 10.1016/j.tetlet.2010.01.110

Bautista, E., Chorpitayasunondh, T., Gao, Z., Harper, S. A., Shaw, M., Uyeki, T. M., et al. (2010). Medical progress: clinical aspects of pandemic 2009 influenza A (H1N1) virus infection. *New Engl. J. Med.* 362, 1708–1719. doi: 10.1056/NEJMra1000449

Beekman, A. M., and Barrow, R. A. (2015). Syntheses of cytosporones A, C, J, K, and N, metabolites from medicinal fungi. *Aust. J. Chem.* 68, 1583–1592. doi: 10.1071/CH15144

Bracher, F., and Krauss, J. (1998). Total synthesis of secocurvularin, curvulin, and the corresponding carboxylic acids. A convenient application of the enzymatic hydrolysis of acid and base sensitive esters. *Nat. Prod. Lett.* 12, 31–34. doi: 10.1080/10575639808048867

Brady, S. F., Wagenaar, M. M., Singh, M. P., Janso, J. E., and Clardy, J. (2000). The cytosporones, new octaketide antibiotics isolated from an endophytic fungus. *Org. Lett.* 2, 4043–4046. doi: 10.1021/ol006680s

Crawford, J. M., and Townsend, C. A. (2010). New insights into the formation of fungal aromatic polyketides. *Nat. Rev. Microbiol.* 8, 879–889. doi: 10.1038/nrmicro2465

Cui, X., Zhu, G., Liu, H., Jiang, G., Wang, Y., and Zhu, W. (2016). Diversity and function of the Antarctic krill microorganisms from *Euphausia superba*. *Sci. Rep.* 6:36496. doi: 10.1038/srep36496

Egarnes, B., Blanchet, M. R., and Gosselin, J. (2017). Treatment with the NR4A1 agonist cytosporone B controls influenza virus infection and improves pulmonary function in infected mice. *PloS ONE* 12:e0186639. doi: 10.1371/journal.pone.0186639

Fujii, I. (2010). Functional analysis of fungal polyketide biosynthesis genes. *J. Antibiot.* 63, 207–218. doi: 10.1038/ja.2010.17

Hang, L., Liu, N., and Tang, Y. (2016). Coordinated and iterative enzyme catalysis in fungal polyketide biosynthesis. *ACS Catal.* 6, 5935–5945. doi: 10.1021/acscatal.6b01559

Izuchi, Y., Koshino, H., Hongo, Y., Kanomata, N., and Takahashi, S. (2011). Synthesis and structural revision of phomopsin B, a novel polyketide carrying a 10-membered cyclic-ether ring. *Org. Lett.* 13, 3360–3363. doi: 10.1021/ol2011117

Koenigs, P., Rinker, B., Maus, L., Nieger, M., Rheinheimer, J., and Waldvogel, S. R. (2010). Structural revision and synthesis of altechromone A. *J. Nat. Prod.* 73, 2064–2066. doi: 10.1021/np1005604

Kokubun, T., Veitch, N. C., Bridge, P. D., and Simmonds, M. S. J. (2003). Dihydroisocoumarins and a tetralone from *Cytospora eucalypticola*. *Phytochemistry* 62, 779–782. doi: 10.1016/S0031-9422(02)00606-4

Komai, S., Hosoe, T., Itabashi, T., Nozawa, K., Yaguchi, T., Fukushima, K., et al. (2005). New vermistatin derivatives isolated from *Penicillium simplicissimum*. *Heterocycles* 65, 2771–2776. doi: 10.3987/COM-05-10523

Kongprapan, T., Xu, X., Rukachaisirikul, V., Phongpaichit, S., Sakayaroj, J., Chen, J., et al. (2017). Cytosporone derivatives from the endophytic fungus *Phomopsis* sp PSU-H188. *Phytochem. Lett.* 22, 219–223. doi: 10.1016/j.phytol.2017.10.002

Kornsakulkarn, J., Somyong, W., Supothina, S., Boonyuen, N., and Thongpanchang, C. (2015). Bioactive oxygen-bridged cyclooctadienes from endophytic fungus *Phomopsis* sp BCC 45011. *Tetrahedron* 71, 9112–9116. doi: 10.1016/j.tet.2015.10.015

Lai, D., Broetz-Oesterhelt, H., Mueller, W. E., Wray, V., and Proksch, P. (2013). Bioactive polyketides and alkaloids from *Penicillium citrinum*, a fungal endophyte isolated from *Ocimum tenuiflorum*. *Fitoterapia* 91, 100–106. doi: 10.1016/j.fitote.2013.08.017

Li, R., Liu, T., Liu, M., Chen, F., Liu, S., and Yang, J. (2017). Anti-influenza A virus activity of dendrobine and its mechanism of action. *J. Agr Food Chem.* 65, 3665–3674. doi: 10.1021/acs.jafc.7b00276

Liu, M., Chen, F., Liu, T., Chen, F., Liu, S., and Yang, J. (2017). The role of oxidative stress in influenza virus infection. *Microbes Infect.* 19, 580–586. doi: 10.1016/j.micinf.2017.08.008

Liu, Z., Zhao, J., Liang, X., Lv, X., Li, Y., Qu, J., et al. (2018). Dothiorelone derivatives from an endophyte *Diaporthe pseudomangiferaea* inhibit the activation of human lung fibroblasts MRC-5 cells. *Fitoterapia* 127, 7–14. doi: 10.1016/j.fitote.2018.04.009

Luo, X., Lin, X., Tao, H., Wang, J., Li, J., Yang, B., et al. (2018). Isochromophilones A–F, cytotoxic chloroazaphilones from the marine mangrove endophyticfungus *Diaporthe* sp. SCSIO 41011. *J. Nat. Prod.* 81, 934–941. doi: 10.1021/acs.jnatprod.7b01053

Luo, X., Zhou, X., Lin, X., Qin, X., Zhang, T., Wang, J., et al. (2017). Antituberculosis compounds from a deep-sea-derived fungus *Aspergillus* sp. SCSIO Ind09F01. *Nat. Prod. Res.* 31, 1958–1962. doi: 10.1080/14786419.2016.1266353

Medina, R. A., and Garcia-Sastre, A. (2011). Influenza A viruses: new research developments. *Nat. Rev. Microbiol.* 9, 590–603. doi: 10.1038/nrmicro2613

Moghadamtousi, S., Nikzad, S., Kadir, H., Abubakar, S., and Zandi, K. (2015). Potential antiviral agents from marine fungi: an overview. *Mar. Drugs* 13, 4520–4538. doi: 10.3390/md13074520

Nguyen, T. T. N., Tran, H. Q., Kim, K. W., Kim, H. J., Sohn, J. H., Kang, D. G., et al. (2017). Anti-inflammatory effects of secondary metabolites isolated from the marine-derived fungal strain *Penicillium* sp SF-5629. *Arch. Pharm. Res.* 40, 328–337. doi: 10.1007/s12272-017-0890-5

Sommart, U., Rukachaisirikul, V., Tadpetch, K., Sukpondma, Y., Phongpaichit, S., Hutadilok-Towatana, N., et al. (2012). Modiolin and phthalide derivatives from the endophytic fungus *Microsphaeropsis arundinis* PSU-G18. *Tetrahedron* 68, 10005–10010. doi: 10.1016/j.tet.2012.09.043

Song, G., Shen, X., Li, S., Li, Y., Liu, Y., Zheng, Y., et al. (2015). Structure-activity relationships of 3-*O*-beta-chacotriosyl ursolic acid derivatives as novel H5N1 entry inhibitors. *Eur. J. Med. Chem.* 93, 431–442. doi: 10.1016/j.ejmech.2015.02.029

Tan, Q. W., Fang, P. H., Ni, J. C., Gao, F., and Chen, Q. J. (2017). Metabolites produced by an endophytic *Phomopsis* sp and their anti-TMV activity. *Molecules* 22:E2073. doi: 10.3390/molecules22122073

Tan, Y., Yang, B., Lin, X., Luo, X., Pang, X., Tang, L., et al. (2018). Nitrobenzoyl sesquiterpenoids with cytotoxic activities from a marine-derived *Aspergillus ochraceus* Fungus. *J. Nat. Prod.* 81, 92–97. doi: 10.1021/acs.jnatprod.7b00698

Tsantrizos, Y. S., Ogilvie, K. K., and Watson, A. K. (1992). Phytotoxic metabolites of *Pomopsis onvolvulus*, a host-specific pathogen of *Feld bindweed*. *Can. J. Chem.* 70, 2276–2284. doi: 10.1139/v92-286

Von Delius, M., Le, C. M., Ellinger, B., Kuzikov, M., Gul, S., and Dong, V. M. (2017). Synthesis and biological activity of octaketides from the cytosporone family. *Isr. J. Chem.* 57, 975–981. doi: 10.1002/ijch.201700023

Xia, Z., Cao, X., Rico-Bautista, E., Yu, J., Chen, L., Chen, J., et al. (2013). Relative impact of 3-and 5-hydroxyl groups of cytosporone B on cancer cell viability. *Medchemcomm* 4, 332–339. doi: 10.1039/C2MD20243C

Xu, J., Kjer, J., Sendker, J., Wray, V., Guan, H., Edrada, R., et al. (2009a). Chromones from the endophytic fungus *Pestalotiopsis* sp. isolated from the Chinese mangrove plant *Rhizophora mucronata*. *J. Nat. Prod.* 72, 662–665. doi: 10.1021/np800748u

Xu, J., Kjer, J., Sendker, J., Wray, V., Guan, H., Edrada, R., et al. (2009b). Cytosporones, coumarins, and an alkaloid from the endophytic fungus *Pestalotiopsis* sp. isolated from the Chinese mangrove plant *Rhizophora mucronata*. *Bioorgan. Med. Chem.* 17, 7362–7367. doi: 10.1016/j.bmc.2009.08.031

Yang, L. P., Gu, X. L., Chen, J. X., Yang, J., Tan, S. Y., and Duan, W. J. (2018). Chemical constituents from *Canarium album Raeusch* and their anti-influenza A virus activities. *J. Nat. Med.* 72, 808–815 doi: 10.1007/s11418-018-1208-8

Zhan, Y., Du, X., Chen, H., Liu, J., Zhao, B., Huang, D., et al. (2008). Cytosporone B is an agonist for nuclear orphan receptor Nur77. *Nat. Chem. Biol.* 4, 548–556. doi: 10.1038/nchembio.106

Zheng, K., Xie, C., and Hong, R. (2015). Bioinspired iterative synthesis of polyketides. *Front. Chem.* 3:32. doi: 10.3389/fchem.2015.00032

Conflict of Interest Statement: The authors declare that the research was conducted in the absence of any commercial or financial relationships that could be construed as a potential conflict of interest.

frontiers in Chemistry

ORIGINAL RESEARCH
published: 26 July 2018
doi: 10.3389/fchem.2018.00316

The Metabolome of a Cyanobacterial Bloom Visualized by MS/MS-Based Molecular Networking Reveals New Neurotoxic Smenamide Analogs (C, D, and E)

*Christopher W. Via[1], Evgenia Glukhov[2], Samuel Costa[1], Paul V. Zimba[3], Peter D. R. Moeller[4], William H. Gerwick[2] and Matthew J. Bertin[1]**

[1] Department of Biomedical and Pharmaceutical Sciences, College of Pharmacy, University of Rhode Island, Kingston, RI, United States, [2] Center for Marine Biotechnology and Biomedicine, Skaggs School of Pharmacy and Pharmaceutical Sciences, Scripps Institution of Oceanography, University of California at San Diego, La Jolla, CA, United States, [3] Center for Coastal Studies and Department of Life Sciences, Texas A&M Corpus Christi, Corpus Christi, TX, United States, [4] Emerging Toxins Program, Hollings Marine Laboratory, National Ocean Service/NOAA, Charleston, SC, United States

OPEN ACCESS

Edited by:
Xian-Wen Yang,
Third Institute of Oceanography, State Oceanic Administration, China

Reviewed by:
Junfeng Wang,
South China Sea Institute of Oceanology (CAS), China
Tal Luzzatto-Knaan,
University of Haifa, Israel

***Correspondence:**
Matthew J. Bertin
mbertin@uri.edu

Specialty section:
This article was submitted to Medicinal and Pharmaceutical Chemistry, a section of the journal Frontiers in Chemistry

Received: *07 March 2018*
Accepted: *09 July 2018*
Published: *26 July 2018*

Citation:
Via CW, Glukhov E, Costa S, Zimba PV, Moeller PDR, Gerwick WH and Bertin MJ (2018) The Metabolome of a Cyanobacterial Bloom Visualized by MS/MS-Based Molecular Networking Reveals New Neurotoxic Smenamide Analogs (C, D, and E). Front. Chem. 6:316. doi: 10.3389/fchem.2018.00316

Members of the cyanobacterial genus *Trichodesmium* are well known for their substantial impact on nitrogen influx in ocean ecosystems and the enormous surface blooms they form in tropical and subtropical locations. However, the secondary metabolite composition of these complex environmental bloom events is not well known, nor the possibility of the production of potent toxins that have been observed in other bloom-forming marine and freshwater cyanobacteria species. In the present work, we aimed to characterize the metabolome of a *Trichodesmium* bloom utilizing MS/MS-based molecular networking. Furthermore, we integrated cytotoxicity assays in order to identify and ultimately isolate potential cyanotoxins from the bloom. These efforts led to the isolation and identification of several members of the smenamide family, including three new smenamide analogs (**1–3**) as well as the previously reported smenothiazole A-hybrid polyketide-peptide compounds. Two of these new smenamides possessed cytotoxicity to neuro-2A cells (**1** and **3**) and their presence elicits further questions as to their potential ecological roles. HPLC profiling and molecular networking of chromatography fractions from the bloom revealed an elaborate secondary metabolome, generating hypotheses with respect to the environmental role of these metabolites and the consistency of this chemical composition across genera, space and time.

Keywords: *Trichodesmium*, molecular networking, cyanotoxins, harmful algal blooms, metabolomics

INTRODUCTION

Blooms of toxin-producing cyanobacteria (harmful algal blooms, HABs) continue to be a threat to water resources in the U.S. and across the globe (Carmichael and Boyer, 2016). Research surrounding these bloom events with respect to cyanobacteria has generally focused on freshwater planktonic species and a suite of well-characterized toxins, including the anatoxins, saxitoxins and microcystins (Bláha et al., 2009). However, species of cyanobacteria in the marine realm have been

a prolific source of exquisitely potent cytotoxic metabolites (Luesch et al., 2001; Taori et al., 2008; Pereira et al., 2012). Members of the bloom-forming genus *Trichodesmium* are an understudied group of marine cyanobacteria with respect to toxin production and environmental impact. With respect to new natural products, the cyclic peptide trichamide was characterized from a cultured strain of *Trichodesmium erythraeum*, although no significant cytotoxicity was observed against HCT-116 cells and CEM-TART cells when tested at 10 and 50 μg/mL, respectively (Sudek et al., 2006). The lipoamides, credneramides A and B were isolated and characterized from a field-collected benthic cyanobacterium identified as a new species of *Trichodesmium* (Malloy et al., 2012). These metabolites inhibited spontaneous calcium oscillations in murine cerebrocortical neurons (Malloy et al., 2012). Several known cyanotoxins, such as anatoxin, saxitoxin, microcystins and aplysiatoxins have been reported from *Trichodesmium* blooms collected from distinct geographic areas (Ramos et al., 2005; Detoni et al., 2016; Shunmugam et al., 2017).

In the current report, we detail the comprehensive metabolic profiling of a *Trichodesmium* bloom collected from the western Gulf of Mexico utilizing MS/MS-based molecular networking (Watrous et al., 2012; Yang et al., 2013; Wang et al., 2016) and cytotoxicity assays. In our previous work on this *Trichodesmium* bloom, we have utilized cytotoxicity assays, NMR-guided isolation and MS-guided isolation independently to characterize chlorinated polyketides and hybrid polyketide peptides (Bertin et al., 2016, 2017a,b; Belisle et al., 2017). The current report attempts to describe the *Trichodesmium* bloom metabolome more completely, focusing on a networking tool to cluster molecules based on similarities in the MS/MS fragmentation patterns (Watrous et al., 2012). Our efforts ultimately led to the isolation and characterization of three new members of the smenamide family of molecules (**1**–**3**) and the previously reported smenothiazole A (**Figure 1**). Smenamides C and E demonstrated potent neurotoxicity (**1** and **3**).

MATERIALS AND METHODS

General Experimental Procedures

Optical rotations were measured using a Jasco P-2000 polarimeter. UV spectra were measured using a Beckman Coulter DU-800 spectrophotometer. CD spectra were recorded using a Jasco J-1100 CD spectrometer. NMR spectra were collected using a Bruker 800 MHz NMR instrument. Additional NMR spectra were recorded on a Varian 500 MHz NMR instrument. HRESIMS analysis was performed using an AB SCIEX TripleTOF 4600 mass spectrometer with Analyst TF software. LC-MS/MS analysis was carried out using a ThermoFinnigan LCQ AdvantageMax mass spectrometer with an electrospray ionization (ESI) source. Semi-preparative HPLC was carried out using a Dionex UltiMate 3000 HPLC system and Agilent 1100 series system each equipped with a micro vacuum degasser, an autosampler and a diode-array detector.

Collection, Extraction and Fractionation of Bloom Material

Samples from a localized bloom of *Trichodesmium* were collected from Padre Island, Corpus Christi, TX during 9–11 May 2014 as described previously (Bertin et al., 2016, 2017a,b; Belisle et al., 2017). Briefly, bloom material was collected in 5-gallon buckets from *ca*. 0.5-meter water depth and concentrated by gentle filtration through an 18 μm mesh screen. A subsample of the cell mass was examined microscopically and identified using Komárek and Anagnostidis (2005) as being dominated by cyanobacteria of the genus *Trichodesmium*. The material was frozen and shipped for further chemical analysis. The biomass (ca. 14 g dry weight) was repeatedly extracted with 2:1 CH_2Cl_2:CH_3OH and the extracts were combined and evaporated under reduced pressure (3.95 g). The extract was reconstituted in hexanes and applied to silica gel (300 mL) in a wide fritted column with a vacuum attachment. The extract was fractionated using a stepped gradient from 100% hexanes to 100% CH_3OH resulting in nine fractions. Seven of the nine fractions (C-I) were further analyzed by means of cytotoxicity assays and MS/MS-based molecular networking. The first two fractions: 100% hexanes (A) and 90% hexanes in EtOAc (B) were intended to remove hydrocarbons and exceedingly lipophilic substances from the sample and were not analyzed further.

Molecular Networking

Fractions C-I were subjected to LC-MS/MS analysis with data collection in data-dependent acquisition mode on a ThermoFinnigan LCQ AdvantageMax mass spectrometer with an electrospray ionization (ESI) source. A Kinetex 5 μm C18 column (100 × 4.6 mm) was used for separation of analytes. The LC method consisted of a linear gradient from 30 to 99% CH_3CN in water + 0.1% formic acid over 17 minutes, followed by an isocratic period at 99% CH_3CN of 3 minutes. The flow rate was held at 0.6 mL/min. The MS spray voltage was 5 kV with a capillary temperature of 400°C. For the MS/MS component, the CID isolation width was 2.0 and the collision energy was 35.0 eV. The raw data files were converted to mzXML format using MSConvert from the ProteoWizard suite (http://proteowizard.sourceforge.net/tools.shtml)[1]. The molecular network was generated using the online platform at Global Natural Products Social Molecular Networking website (gnps.ucsd.edu) using parameters detailed in Table S5. The network was visualized using the Browser Network Visualizer tool available on the gnps website.

Isolation of 1–3 and Smenothiazole A

Fractions G (100% EtOAc, 104.0 mg) and H (75% EtOAc in CH_3OH, 286.9 mg) were chosen for further purification based on the quantity of network ions in these fractions, the molecular features of these ions (ratio of M^+ and M^{+2} isotope), and cytotoxicity results of the mixed chromatography fractions. Fractions G and H were combined based on similarities in LC-MS/MS profiles and ^1H NMR resonances. The combined

[1]ProteoWizardSoftware Foundation; http://proteowizard.sourceforge.net/tools.shtml

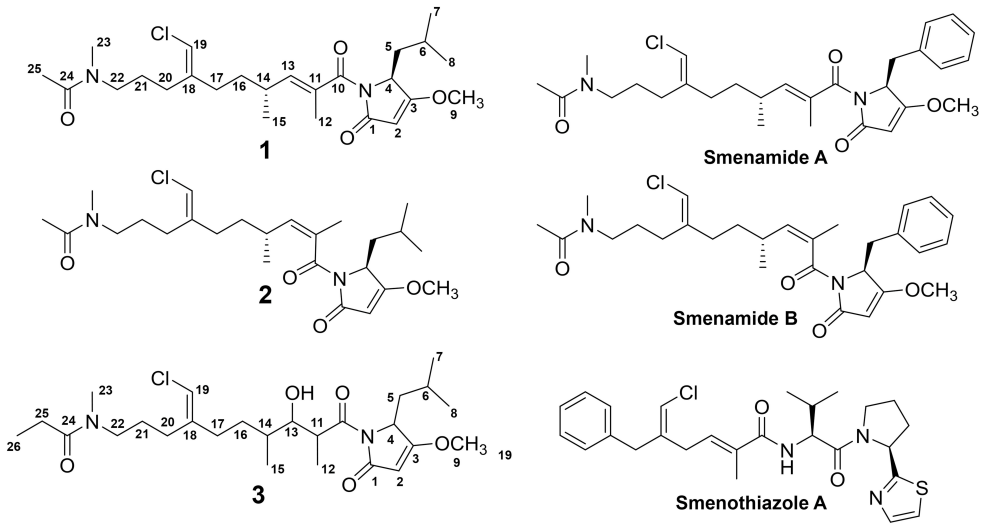

FIGURE 1 | Structures of **1-3**, smenamides A and B and smenothiazole A.

sample was further fractionated over a 2 g C18 SPE column eluting with 50% water in CH_3CN (13.7 mg), 100% CH_3CN (143.2 mg), 100% CH_3OH (74.5 mg) and 100% EtOAc (54.5 mg). The fraction eluting with 100% CH_3CN was subjected to reversed phase HPLC using a YMC 5 μm ODS column (250 × 10 mm); mobile phase: 65% CH_3CN /35% water with 0.05% formic acid added to each solvent, flow 3 mL/min. Fractions were collected based on UV characteristics and HPLC fractions were analyzed by HRESIMS for ions of interest from the molecular network. Further purification was carried out using the YMC column mentioned above; mobile phase: 80% CH_3CN in water with 0.05% formic acid added to each solvent, flow 3 mL/min resulted in the isolation of 7.0 mg of **1** (t_R, 11.5 min). A mobile phase of 65% CH_3CN in water with 0.05% formic acid added to each solvent, flow 3 mL/min was used to isolate 0.6 mg of **2** (t_R, 26.0 min) and 0.3 mg of **3** (t_R, 21.2 min). A final purification was carried out using a YMC 5 μm ODS column (250 × 10 mm); mobile phase: 80% CH_3CN in water with 0.1% formic acid added to each solvent, flow 3 mL/min and 2.0 mg of smenothiazole A was isolated (t_R, 5.0 min).

Smenamide C (**1**): colorless oil; $[\alpha]^{25}_D$ +38.2 (*c* 0.20, CH_3OH); UV (CH_3OH) λ_{max} (log ε) 203 (4.2), 238 (4.0) nm; ^1H NMR (800 MHz, DMSO-d_6) and ^{13}C NMR (200 MHz, DMSO-d_6), see **Table 1**; HRESIMS *m/z* 467.2661 $[M+H]^+$ (calcd for $C_{25}H_{40}N_2O_4Cl$, 467.2677) and *m/z* 489.2486 $[M+Na]^+$ (calcd for $C_{25}H_{39}N_2O_4ClNa$, 489.2496).

Smenamide D (**2**): colorless oil; $[\alpha]^{25}_D$ +16.8 (*c* 0.10, CH_3OH); UV (CH_3OH) λ_{max} (log ε) 203 (3.4), 240 (3.3) nm; ^1H NMR (800 MHz, $CDCl_3$) and ^{13}C NMR (200 MHz, $CDCl_3$), see Table S3; HRESIMS *m/z* 467.2693 $[M+H]^+$ (calcd for $C_{25}H_{40}N_2O_4Cl$, 467.2677) and *m/z* 489.2492 $[M+Na]^+$ (calcd for $C_{25}H_{39}N_2O_4ClNa$, 489.2496).

Smenamide E (**3**): colorless oil; $[\alpha]^{25}_D$ +21.9 (*c* 0.05, CH_3OH); UV (CH_3OH) λ_{max} (log ε) 203 (4.1), 235 (3.8) nm; ^1H NMR (800 MHz, DMSO-d_6) and ^{13}C NMR (200 MHz, DMSO-d_6), see **Table 2**; HRESIMS *m/z* 499.2935 $[M+H]^+$ (calcd for $C_{26}H_{44}N_2O_5Cl$, 499.2939).

Smenothiazole A: colorless oil; $[\alpha]^{23}_D$−5.8 (*c* 0.10, CH_3OH) UV (CH_3OH) λ_{max} (log ε) 202 (3.4) nm; ^1H NMR (800 MHz, DMSO-d_6) and ^{13}C NMR (200 MHz, DMSO-d_6), see Table S4; HRESIMS *m/z* 486.1984 $[M+H]^+$ (calcd for $C_{26}H_{33}ClN_3O_2S$, 486.1982).

Cytotoxicity Assay

Neuro-2A cells and HCT-116 cells were added to assay plates in 100 μl of Eagle's Minimum Essential Media (EMEM) or 100 μl of McCoy's 5A media respectively each supplemented with 10% FBS at a density of 5,000 cells/well. Cells were incubated overnight (37°C, 5% CO_2) and examined microscopically to confirm confluence and adherence. Mixed chromatography fractions (C-I) were dissolved in DMSO (1% v/v) and tested at concentrations of 40 and 4 μg/mL with 10 μM doxorubicin used as a positive control. Compounds **1–3** were dissolved in DMSO (1% v/v) and added to the cells in the range of 100 to 0.1 μM in order to generate EC_{50} curves. Four technical replicates were prepared for each concentration and each assay was performed in triplicate. Doxorubicin was used as a positive control (EC_{50}: 0.043 ± 0.032 μM for neuro-2A cells; EC_{50}: 0.071 ± 0.004 μM for HCT-116 cells) and DMSO (1% v/v) was used as a negative control. Assays were resolved as previously reported (Bertin et al., 2017b) and EC_{50} curves were generated using Graphpad Prism software.

RESULTS

Trichodesmium Bloom-Cytotoxicity of Chromatography Fractions and Molecular Network

Several of the chromatography fractions (D–H) derived from the bloom material showed strong cytotoxicity against neuro-2A cells at 40 μg/mL (Figure S1). Fraction D showed the greatest

TABLE 1 | NMR data for Smenamide C (**1**) *Z*-conformer (800 MHz for ^{1}H NMR; 200 MHz for ^{13}C NMR, DMSO).

Position	δ_C, type	δ_H (*J* in Hz)	HMBC	COSY
1	169.3, qC			
2	93.7, CH	5.28, s	1, 4, 10	
3	180.3, qC			
4	57.6, CH	4.75, t (5.3)	1, 2, 3, 5, 6, 10	5a, 5b
5a	38.6, CH_2	1.72, m	3, 4, 7, 8	4, 5b
5b		1.59, m	3, 4, 7, 8	4, 5a
6	24.2, CH	1.66, m	4, 5, 7, 8	7, 8
7	24.0, CH_3	0.85, d (6.6)	5, 8	6
8	23.3, CH_3	0.87, d (6.6)	5, 7	6
9	59.7, CH_3	3.87, s	3	
10	170.6, qC			
11	131.7, qC			
12	13.9, CH_3	1.77, s	10, 11, 13	
13	141.9, CH	5.59, d (9.8)	10, 11, 12, 14, 15, 16	14
14	32.2, CH	2.45, m	11, 13, 15, 16, 17	13, 15, 16a, 16b
15	20.4, CH_3	0.94, d (6.6)	14, 16, 18	14
16a	34.9, CH_2	1.49, m	17, 18	14, 17a, 17b
16b		1.35, m	17, 18	14, 17a, 17b
17a	32.1, CH_2	2.22, m	14, 16, 18, 19, 20	16a, 16b, 17b
17b		2.10, ovlp[a]	14, 16, 18, 19, 20	16a, 16b, 17a
18	142.8, qC			
19	112.6, CH	6.04, s	17, 18, 20	
20a	27.4, CH_2	2.12, m	17, 18, 19, 21, 22	21
20b		2.07, ovlp	17, 18, 19, 21, 22	21
21	24.8, CH_2	1.56, m	20, 22	20a, 20b, 22
22	46.7, CH_2	3.26, m	20, 21, 23, 24	21
23	35.9. CH_3	2.94, s	22, 24	
24	169.9, qC			
25	22.1, CH_3	1.97, s	23, 24	

[a] *Overlapping signals.*

TABLE 2 | NMR data for Smenamide E *Z/E*-conformers[a] (**3**) (800 MHz for ^{1}H NMR; 200 MHz for ^{13}C NMR, DMSO).

Position	δ_C, type	δ_H (*J* in Hz)	HMBC	COSY
1	170.3, qC			
2	94.2, CH	5.31, s	1, 3, 4	
3	180.8, qC			
4	58.1, CH	4.63, m	1, 2, 3, 5, 6, 10	5
5	39.2, CH_2	1.72, m	3, 4, 6, 7, 8	4
6	24.0, CH	1.76, m	4, 5, 7, 8	7, 8
7	24.3, CH_3	0.84, d	5, 6, 8	6
8	22.9, CH_3	0.86, d	5, 6, 7	6
9	59.5, CH_3	3.86, s	3	
10	175.8, qC			
11	42.7, CH	3.95, m	10, 12, 13	12, 13
12	14.4, CH_3	0.90, d (6.8)	10, 11, 13	11
13	74.3, CH	3.73, m	10, 11, 15	11, OH-13
OH-13		4.40, m	11, 13, 14	13
14	34.3, CH	1.48, ovlp[b]	13, 15	15
15	12.9, CH_3	0.81, d (6.2)	13, 14, 16	14
16a	31.5, CH_2	1.48, ovlp	13, 14, 15, 17	16b, 17a
16b		1.26, m	13, 14, 15, 17	16a, 17b
17a	28.1, CH_2	2.25, m	16, 18, 19	16a, 16b
17b		2.13, m	16, 18, 19	16a, 16b
18	143.0 [142.8], qC			
19	112.3 [112.6], CH	6.04 [6.06], s	17, 18, 20	20
20	31.6 [31.4], CH_2	2.02 [2.07], t (7.5)	18, 19, 21, 22	21
21	25.4 [26.5], CH_2	1.55 [1.63], m	20, 22	20, 22
22	46.9 [48.9], CH_2	3.24 [3.23], m	20, 21, 23, 24	21
23	35.1 [33.2], CH_3	2.94 [2.79], s	22, 24	
24	173.0 [172.7], qC			
25	26.3 [25.7], CH_2	2.27 [2.29], m	24, 26	26
26	9.7 [10.1], CH_3	0.97 [0.98], t (7.4)	24, 25	25

[a] *E-conformer NMR values of **3** in brackets.*
[b] *Overlapping signals.*

potency at 4 μg/mL. Examination of the molecular network showed that compounds from cluster 3 were major ions in fraction D (**Figure 2**). However, these metabolites were not isolable following further purification procedures. The majority of the metabolites in the molecular network were found in fractions F–I. We identified Cluster 2 as a molecular cluster of interest due to the number of ions in the cluster and the M^+ and M^{+2} ratio indicating a single chlorine atom in each of these metabolites (cf. **Figures 2**, **3**). Additionally, fractions G and H showed potent cytotoxicity against neuro-2A cells; thus, our subsequent purification efforts centered on these two fractions. HPLC analysis indicated abundant metabolites in the combined G+H HPLC pre-fraction (Figure S2) and repeated chromatography resulted in the isolation of **1–3** as optically active colorless oils.

Structure Characterization of 1–3

HRESIMS analysis of **1** gave an $[M+H]^+$ of *m/z* 467.2661, suggesting a molecular formula of $C_{25}H_{39}N_2O_4Cl$ and a requirement of 7 degrees of unsaturation. Examination of the ^{1}H NMR spectrum of **1** showed several resonances with split signals in a 1:1 ratio, a phenomenon observed in several cyanobacteria metabolites with methylated tertiary amides such as smenamides A and B and kalkitoxin (Wu et al., 2000; Teta et al., 2013). The split signals were determined to be the result of two conformers in the *E* and *Z* configuration at the tertiary amide functionality in **1**. This phenomenon was observed for all three new metabolites (**1–3**); in the structure characterization for each of these compounds, the data for the *Z* conformer is discussed. NMR data tables in the Supporting Information provide information on the *E* conformer. While the multiple conformers presented difficulties in NMR interpretation, three partial structures of **1** (a–c) were characterized initially based on ^{1}H-^{1}H COSY spin systems followed by HMBC correlation analysis (**Figure 4**). In the first partial structure (a), a moderately deshielded diastereotopic methylene group (H-20a, δ_H 2.12; H-20b, δ_H 2.07) was correlated by COSY to a second methylene group (H_2-21, δ_H 1.56) which itself was correlated by COSY to a third methylene group (H_2-22, δ_H 3.26). This latter deshielded methylene was correlated by HMBC to C-23 (δ_C 35.9) and the C-24 carbonyl (δ_C 169.9). The singlet methyl

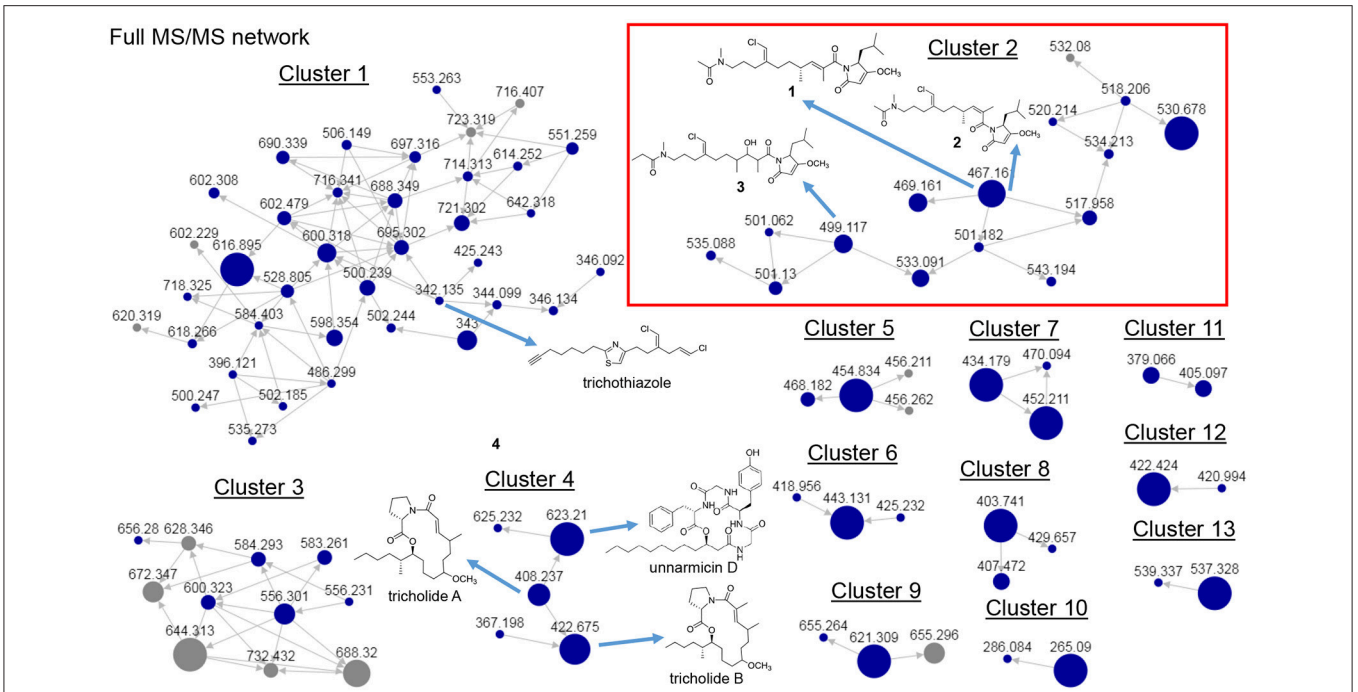

FIGURE 2 | Full MS/MS-based molecular network of *Trichodesmium* bloom. Previously identified molecules trichothiazole, tricholides A and B and unnarmicin D are noted. Cluster 2 (red box) shows new metabolites **1-3** (*m/z* 467.161, 467.161 and 499.117, respectively).

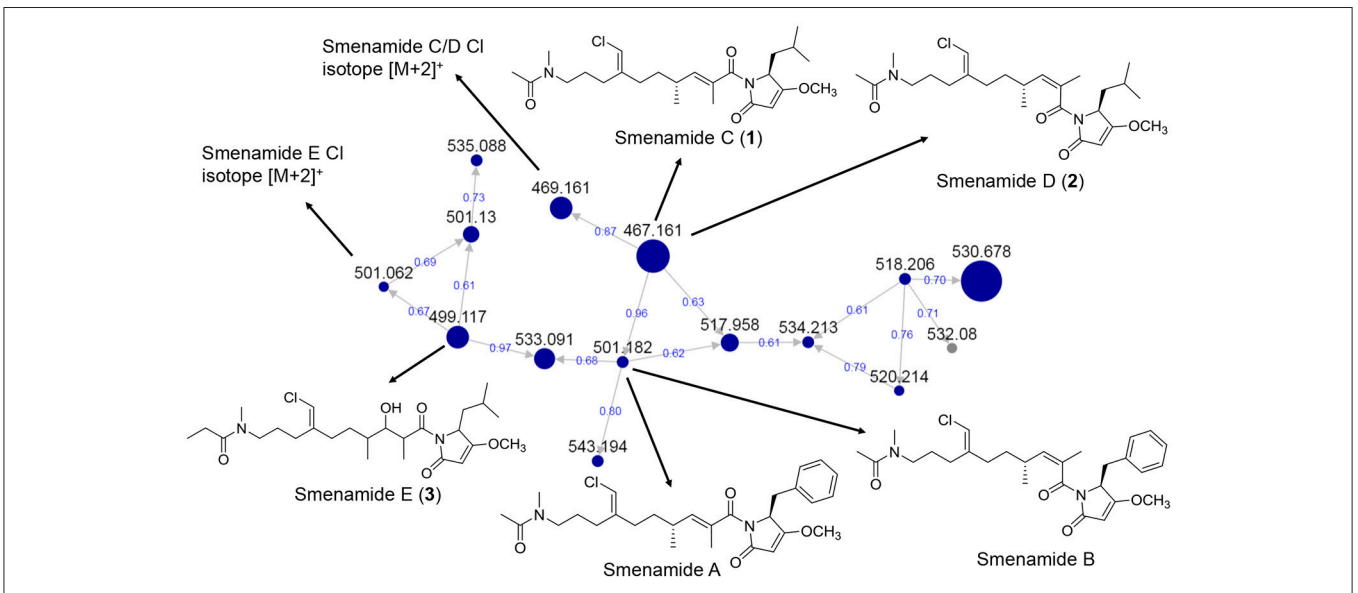

FIGURE 3 | MS/MS-based molecular networking cluster identifying **1–3** and smenamides A or B. Nodes are labeled with parent *m/z* values. Edges are labeled with cosine scores. Node size is relative to ion count.

(H_3-25, δ_H 1.97) showed an HMBC correlation to C-24 and characterized the western half of **1** with an *N*-methyl acetamide functionality. In the second partial structure of **1** (b), another moderately deshielded diastereotopic methylene group (H-17a, δ_H 2.22; H-17b, δ_H 2.10) showed COSY correlations to the H-16 methylene (H-16a, δ_H 1.49; H-16b, δ_H 1.35). H_2-16 showed COSY correlations to the H-14 methine (δ_H 2.45), which itself showed COSY correlations to a doublet methyl (H_3-15, δ_H 0.94) and olefinic proton (H-13, δ_H 5.59). A singlet methyl (H_3-12, δ_H 1.77) and H-13 showed HMBC correlations to a quaternary carbon (C-11, δ_C 131.7) and the C-10 carbonyl (δ_C 170.6) extending the polyketide chain of **1**. The C-11–C-13 olefin was

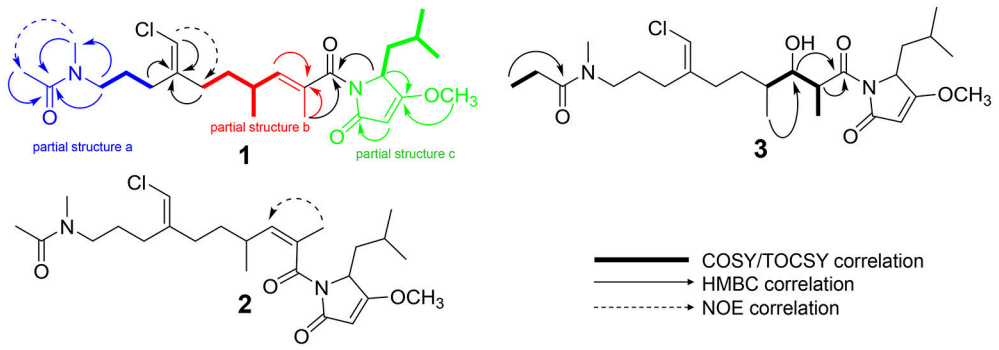

FIGURE 4 | Select 2D NMR correlations of compounds **1–3**.

assigned *E* geometry based on the ^{13}C chemical shift of C-12 (δ_C 13.7) compared to δ_C 20.1 for the *Z* geometry (see below). The two sets of moderately deshielded methylenes (H_2-20 and H_2-17) showed HMBC correlations to the quaternary carbon at C-18 (δ_C 142.8). A deshielded methine singlet (H-19, δ_H 6.04) also showed an HMBC correlation to C-18, supporting an exomethylene vinyl chloride bridge connecting partial structures a and b. The configuration of the vinyl chloride was assigned as *Z* based on NOE correlations from H-19 to H_2-17 and H_2-16. The chemical shift of C-10 was consistent with that of an amide functionality and COSY correlations from H-4 to H-8 supported the assignment of a leucine residue in the third partial structure. However, the chemical shift at C-3 was somewhat deshielded for that of a standard amide or ester carbonyl (δ_C 180.3). An *O*-methyl singlet (H_3-9, δ_H 3.87) was correlated to C-3 by HMBC supporting the presence of a methoxy functionality. Additionally, H-2 (δ_H 5.28) was correlated to C-3 and the C-1 carbonyl by HMBC. HMBC correlations from H-2 and H-4 to C-10 connected the third partial structure to the remainder of the molecule, establishing an isobutyl-methoxypyrrolinone moiety and satisfying the final three degrees of unsaturation required by the molecular formula. The structure of **1** was established as a highly functionalized linear polyketide-peptide of the smenamide family (Teta et al., 2013). While the correlations and chemical shifts described above relate to the *Z* conformer of **1**, NMR data for the *E* conformer were also analyzed, and are listed in Table S1.

The absolute configuration of **1** (4*S*, 14*R*) was determined to be identical to that of smenamide A by comparison of the CD spectrum of **1** to that of naturally occurring smenamide A (Caso et al., 2017). The spectra were nearly identical in sign and magnitude.

HRESIMS analysis of **2** gave an $[M+H]^+$ of *m/z* 467.2693, suggesting a molecular formula of $C_{25}H_{39}N_2O_4Cl$, identical to that of **1**. Examination of ^1H NMR, multiplicity-edited HSQC, and HMBC spectra of **1** and **2** showed that the two molecules were nearly identical (cf. Tables S2 and S3). ^{13}C NMR differences were most pronounced at C-12 (δ_C 13.7 in **1**; δ_C 20.1 in **2**) and C-13 (δ_C 142.7 in **1**; δ_C 135.9 in **2**). These chemical shifts and the NOE correlations between H_3-12 and H-13 in **2** supported the *Z* configuration of the C-11–C-13 olefin in **2** and established **2** as a geometric isomer of **1**. The absolute stereochemistry of **2** is proposed to be identical to that of **1** based on similarity in optical rotation values.

HRESIMS analysis of **3** gave an $[M+H]^+$ of *m/z* 499.2935, suggesting a molecular formula of $C_{26}H_{43}N_2O_5Cl$, and a requirement of 6 degrees of unsaturation. The examination of ^1H and ^{13}C NMR data and the placement of *m/z* 499 in the same molecular network cluster as smenamide C and D (**1** and **2**), suggested that **3** was a close structural analog. The reduction in degrees of unsaturation in **3** compared to **1** was due to the presence of a secondary alcohol at C-13 (H-13, δ_H 3.73; C-13, δ_C 74.3) in **3** and a methine at C-11 (H-11, δ_H 3.95; C-11, δ_C 42.7). The H-11 and H-13 methine protons were correlated by COSY and H-13 also showed a COSY correlation to H-14 (δ_H 1.48). Additionally, the C-25 methyl resonance of the acetyl group in **1** and **2** was not present in **3**. COSY correlations between a methylene at H-25 (δ_H 2.27) and a methyl triplet at H-26 (δ_H 0.97) supported an *N*-methylpropanamide functionality in **3** and completed the planar structure of smenamide E (**3**). The secondary alcohol of **3** was resistant to acylation with Mosher's acid chloride and the configuration of this position could not be determined by chemical derivative formation. Therefore, in the current report, we report only the planar structure for this new metabolite.

During the attempt to isolate the compound with an *m/z* 530 from Cluster 2 in the network (**Figure 3**), we isolated a peptidic compound with spectrometric and spectroscopic characteristics consistent with that of the previously reported cytotoxin smenothiazole A (Esposito et al., 2015). Analysis of NMR data, optical rotation value, and CD spectra (negative Cotton effect at 234 nm, Figure S35) confirmed its identity.

Cytotoxicity of 1–3

Smenamides C and E (**1** and **3**) showed greater cytotoxicity to neuro-2A cells than to the human colon cancer cell line HCT-116. Smenamide E (**3**) showed the greatest potency to neuro-2A cells with an EC_{50} value of 4.8 ± 0.6 μM (EC_{50}: 18.6 ± 1.8 μM against HCT-116 cells). Smenamide C (**1**) showed similar selective potency (EC_{50} neuro-2A: 7.2 ± 3.1 μM; EC_{50} HCT-116: 20.9 ± 2.1 μM). Interestingly, smenamide D (**2**), the geometric isomer of smenamide C (**1**), did not show cytotoxicity against either cell line.

DISCUSSION

In our previous work on *Trichodesmium* blooms and their natural products, we have utilized cytotoxicity assays, NMR-guided isolation, and MS-guided isolation (Bertin et al., 2016, 2017a,b; Belisle et al., 2017). We have previously characterized the cytotoxic polyketide trichophycin A, the polyketides trichotoxins A and B, and the moderately cytotoxic polyketide-peptide trichothiazole (Bertin et al., 2016, 2017b; Belisle et al., 2017). In the current network, we did observe an *m/z* value consistent with trichothiazole (**Figure 2**). The node was in Cluster 1 (*m/z* 342) and showed an identical MS/MS fragmentation pattern to that of trichothiazole. However, we did not observe nodes for trichophycin A or trichotoxins A and B. It should be noted that the macrocyclic polyketide-peptides tricholides A and B and unnarmicin D (Bertin et al., 2017a) also clustered in the network (**Figure 2**, Cluster 4). It may be that some metabolites in the bloom metabolome do not ionize well by ESI+ or give informative fragments during MS/MS acquisition; this represents a limitation in the implementation of MS/MS-based networking to describe bloom metabolomes. Thus, the metabolite information gained in the network may be somewhat biased toward peptides and hybrid polyketide-peptides. Nevertheless, taking into account the limitations of this approach, molecular networking was a remarkable tool for visualizing a complex metabolome rich in metabolites with intriguing structural elements and cytotoxicity to neuro-2A cells. Analyzing fractions C-I using the networking procedure identified 93 nodes that were members of 13 clusters. This approach allowed us to isolate and characterize three new members of the smenamide family (**1–3**). Furthermore, within the smenamide cluster, we tentatively identified the known compound smenamide A or B (double bond isomers of each other at *m/z* 501). This later node in Cluster 2 (**Figure 3**) showed an identical MS/MS fragmentation pattern to that of smenamide A/B from published data and the HRESIMS analysis supported this identification (Figure S36) (Teta et al., 2013). Both of these known metabolites are very potent cytotoxins with IC_{50} values around 50 nM against Calu-1 cells (Teta et al., 2013). Smenamides C and E (**1** and **3**) were less potent cytotoxins than smenamide A and B, possibly due to the replacement of the phenylalanine amino acid unit with leucine (**1**, **3**). Intriguingly, smenamide D (**2**) was not cytotoxic to either the neuro-2A and HCT-116 cell lines and we speculate that the *cis* configuration in the middle of the polyketide chain may affect binding of **2** to its molecular target. Smenothiazole A showed nanomolar levels against multiple cell lines and was previously isolated from a marine sponge; however, the authors indicate a likely cyanobacterial origin (Esposito et al., 2015). This is the first report of smenothiazole A from a bloom of *Trichodesmium*.

Overall, the networking procedure has identified new target molecules for isolation such as those in Cluster 1 (**Figure 2**). A comprehensive characterization of the chemical space within the bloom material is challenging as the metabolic composition of the sub-fractions we have generated are all nearly as complex as that of the sub-fraction from which **1–3** were isolated (Figure S2). The networking tool significantly improves the efficiency of our isolation and characterization workflow.

We did not identify anatoxins, saxitoxins or microcystins during the course of this analysis. This may be due to our focus on lipophilic metabolites, low abundance of these compounds in our samples, or a lack of informative MS/MS fragments. *Trichodesmium* blooms are complex events harboring a diverse array of microorganisms (Capone et al., 1997). Thus, the unequivocal identification of the producing organisms of the toxic metabolites described in this current work and other studies from environmental collections will ultimately require pure cultivation of producing organisms, the identification of biosynthetic gene clusters of toxic molecules, or the localization of metabolites to particular cell types (Simmons et al., 2008). In the original isolation and characterization of smenamides A and B, the authors suggest that a cyanobacterial symbiont is the true producer of the sponge-derived compounds (Teta et al., 2013). The present report supports this observation, as certain structural features such as the exomethylene vinyl chloride moiety are characteristic of cyanobacterial metabolism (Kan et al., 2000; Edwards et al., 2004; Nunnery et al., 2012). To the best of our knowledge, the *N*-methyl propanamide functionality in **3** has not previously been reported in a polyketide-peptide from cyanobacteria, and represents a biosynthetically intriguing unit because these organisms are not known to produce propionate. Conceivably, it may derive from an *S*-adenosylmethionine (SAM)-mediated methylation of an acetate precursor, the proposed first building block in the production of these smenamide-type natural products. This would be a similar biosynthetic transformation to that involved in producing the *t*-butyl group in apratoxin A which employs a combination of two SAM methyl transferases to incorporate these methyl groups (Grindberg et al., 2011; Skiba et al., 2017).

The identification of these neurotoxic metabolites (**1** and **3**) and the other more potent smenamides and smenothiazole A from a *Trichodesmium* bloom raises important questions as to their ecological role during these events. It will be important to characterize these bloom-associated metabolites in a longitudinal sense to evaluate their ongoing contribution to HABs.

AUTHOR CONTRIBUTIONS

MB was responsible for the study design. PZ and PM were involved in sample collection, organism identification and sample storage. CV and MB did the structure characterization of secondary metabolites. CV and SC carried out cytotoxicity studies. EG, WG, and MB did the molecular networking procedure. MB wrote the manuscript with editing help from all co-authors.

FUNDING

Acquisition of certain spectroscopic and spectrometric data in this publication was made possible by the use of equipment and services available through the RI-INBRE Centralized Research

Core Facility at the University of Rhode Island, which is supported by the Institutional Development Award (IDeA) Network for Biomedical Research Excellence from the National Institute of General Medical Sciences of the National Institutes of Health under grant number P20GM103430. Certain NMR experiments were conducted at a research facility at the University of Rhode Island supported in part by the National Science Foundation EPSCoR Cooperative Agreement #EPS-1004057. We gratefully acknowledge the American Society of Pharmacognosy Starter Grant (MB).

ACKNOWLEDGMENTS

We thank Dr. Al Bach at the University of Rhode Island for assistance with certain spectroscopic measurements.

SUPPLEMENTARY MATERIAL

The Supplementary Material for this article can be found online at: https://www.frontiersin.org/articles/10.3389/fchem.2018.00316/full#supplementary-material

REFERENCES

Belisle, R. S., Via, C. W., Schock, T. B., Villareal, T. A., Zimba, P. V., Beauchesne, K. R., et al. (2017). Trichothiazole A, a dichlorinated polyketide containing an embedded thiazole isolated from *Trichodesmium* blooms. *Tetrahedron Lett*. 58, 4066–4068. doi: 10.1016/j.tetlet.2017.09.027

Bertin, M. J., Roduit, A. F., Sun, J., Alves, G., Via, C. W., Gonzalez, M. A., et al. (2017a). Tricholides A and B and unnarmicin D: new hybrid PKS-NRPS macrocycles isolatedfrom an environmental collection of *Trichodesmium thiebautii*. *Mar. Drugs* 15:E206. doi: 10.3390/md15070206

Bertin, M. J., Wahome, P. G., Zimba, P. V., He, H., and Moeller, P. D. R. (2017b). Trichophycin A, a cytotoxic linear polyketide isolated from a *Trichodesmium thiebautii* bloom. *Mar.Drugs* 15:10. doi: 10.3390/md15010010

Bertin, M. J., Zimba, P. V., He, H., and Moeller, P. D. R. (2016). Structure revision of trichotoxin, a chlorinated polyketide isolated from a *Trichodesmium thiebautii* bloom.*Tetrahedron Lett*. 57, 5864–5867. doi: 10.1016/j.tetlet.2016.11.062

Bláha, L., Babica, P., and Maršálek, B. (2009). Toxins produced in cyanobacterial water blooms- toxicity and risks. *Interdiscip. Toxicol*. 2, 36–41. doi: 10.2478/v10102-009-0006-2

Capone, D. G., Zehr, J. P., Paerl, H. W., Bergman, B., and Carpenter, E. J. (1997). *Trichodesmium*, a globally significant marine cyanobacterium. *Science* 276, 1221–1229. doi: 10.1126/science.276.5316.1221

Carmichael, W. W., and Boyer, G. L. (2016). Health impacts from cyanobacteria harmful algaeblooms: implications for the North American Great Lakes. *Harmful Algae* 54, 194–212.doi: 10.1016/j.hal.2016.02.002

Caso, A., Mangoni, A., Piccialli, G., Constantino, V., and Piccialli, V. (2017). Studies toward thesynthesis of smenamide A, an antiproliferative metabolite from *Smenospongia aurea*:total synthesis of *ent*-smenamide A and 16-*epi*-smenamide A. *ACS Omega* 2, 1477–1488. doi: 10.1021/acsomega.7b00095

Detoni, A. M. S., Costa, L. D. F., Pacheco, L. A., and Yunes, J. S. (2016). Toxic *Trichodesmium* bloomoccurrence in the southwestern South Atlantic Ocean. *Toxicon* 110, 51–55.doi: 10.1016/j.toxicon.2015.12.003

Edwards, D. J., Marquez, B. L., Nogle, L. M., McPhail, K., Goeger, D. E., Roberts, M. A., et al.,(2004). Structure and biosynthesis of the jamaicamides, new mixed polyketide-peptideneurotoxins from the marine cyanobacterium *Lyngbya majuscula*. *Chem. Biol*. 11, 817–833. doi: 10.1016/j.chembiol.2004.03.030

Esposito, G., Teta, R., Miceli, R., Ceccarelli, L. S., Sala, G. D., Camerlingo, R., et al. (2015). Isolation and assessment of the in vitro anti-tumor activity of smenothiazole A and B,chlorinated thiazole-containing peptide/polyketides from the Caribbean sponge,*Smenospongia aurea*. *Mar. Drugs* 13, 444–459. doi: 10.3390/md13010444

Grindberg, R. V., Ishoey, T., Brinza, D., Esquenazi, E., Coates, R. C., Liu, W. T., et al. (2011). Single cell genome amplification accelerates natural product pathway characterization from complex microbial assemblages. *PLoS ONE* 6:e18565. doi: 10.1371/journal.pone.0018565

Kan, Y., Sakamoto, B., Fujita, T., and Nagai, H. (2000). New malyngamides from the Hawaiian cyanobacterium *Lyngbya majuscula*. *J. Nat. Prod*. 63, 1599–1602. doi: 10.1021/np000250t

Komárek, J., and Anagnostidis, K. (2005). *Cyanoprokarota* 19 *Part 2: Oscillatoriales*. Munchen: Elsevier.

Luesch, H., Yoshida, W. Y., Moore, R. E., Paul, V. J., and Corbett, T. H. (2001). Total structure determination of apratoxin A, a potent novel cytotoxin from the marine cyanobacterium *Lyngbya majuscula*. *J. Am. Chem. Soc*. 123, 5418–5423. doi: 10.1021/ja010453j

Malloy, K. L., Suyama, T. L., Engene, N., Debonsi, H., Cao, Z., Matainaho, T., et al. (2012). Credneramides, A., and B: neuromodulatory phenethylamine and isopentylamine derivatives of a vinyl chloride-containing fatty acid from cf. *Trichodesmium sp*. nov. *J. Nat. Prod*. 75, 60–66. doi: 10.1021/np200611f

Nunnery, J. K., Engene, N., Byrum, T., Cao, Z., Jabba, S. V., Pereira, A. R., et al. (2012). Biosynthetically intriguing chlorinated lipophilic metabolites from geographically distant tropical marine cyanobacteria. *J. Org. Chem*. 77, 4198–4208. doi: 10.1021/jo300160e

Pereira, A. R., Kale, A. J., Fenley, A. T., Byrum, T., Debonsi, H. M., Gilson, M. K., et al. (2012). The carmaphycins: new proteasomeinhibitors exhibiting an α,β-epoxyketone warhead from a marine cyanobacterium. *Chembiochem*. 13, 810–817. doi: 10.1002/cbic.201200007

Ramos, A. G., Martel, A., Codd, G. A., Soler, E., Coca, J., Redondo, A., et al. (2005). Bloom of the marine diazotrophic cyanobacterium *Trichodesmium erythraeum* in the northwest African upwelling. *Mar Ecol. Prog. Ser*. 301, 303–305. doi: 10.3354/meps301303

Shunmugam, S., Gayathri, M., Prasannabalaji, N., Thajuddin, N., and Muralitharan, G. (2017). Unraveling the presence of multi-class toxins from *Trichodesmium* bloom in the Gulf of Mannar region of the Bay of Bengal. *Toxicon* 135, 43–50. doi: 10.1016/j.toxicon.2017.06.003

Simmons, T. L., Coates, R. C., Clark, B. R., Engene, N., Gonzalez, D., Esquenazi, E., et al.,(2008). Biosynthetic origins of natural products isolatedfrom marine microorganism-invertebrate assemblages. *Proc. Natl. Acad. Sci. U.S.A*. 105, 4587–4594. doi: 10.1073/pnas.0709851105

Skiba, M. A., Sikkema, A. P., Moss, N. A., Tran, C. L., Sturgis, R. M., Gerwick, L., et al. (2017). Mononuclear iron-dependent methyltransferase catalyzes initial steps in assembly of the apratoxin A polyketide starter unit. *ACS Chem. Biol*. 12, 3039–3048. doi: 10.1021/acschembio.7b00746

Sudek, S., Haygood, M. G., Youssef, D. T. A., and Schmidt, E. W. (2006). Structure of trichamide, a cyclic peptide from the bloom-forming cyanobacterium *Trichodesmium erythraeum*, predicted from the genome sequence. *Appl. Environ. Microbiol*. 72, 4382–4387. doi: 10.1128/AEM.00380-06

Taori, K., Paul, V. J., and Luesch, H. (2008). Structure and activity of largazole, a potentantiproliferative agent from the Floridian marine cyanobacterium *Symploca* sp. *J. Am.Chem. Soc*. 130, 1806–1807. doi: 10.1021/ja7110064

Teta, R., Irollo, E., Sala, G. D., Pirozzi, G., Mangoni, A., and Costantino, V. (2013). Smenamides, A., and B, chlorinated peptide/polyketide hybrids containing adolapyrrolidone unit from the Caribbean sponge *Smenospongia aurea*. Evaluation of theirrole as leads in antitumor drug research. *Mar. Drugs* 11, 4451–4463.doi: 10.3390/md11114451

Wang, M., Carver, J. J., Phelan, V. V., Sanchez, L. M., Garg, N., Peng, Y., et al. (2016). Sharing and community curation of mass spectrometry data with global natural products social molecular networking. *Nat. Biotechnol*. 34, 828–837. doi: 10.1038/nbt.3597

Watrous, J., Roach, P., Alexandrov, T., Heath, B. S., Yang, J. Y., Kersten, R. D., et al. (2012). Mass spectral molecular networking of living microbial colonies. *Proc. Natl. Acad. Sci. U.S.A*. 109, E1743–E1752. doi: 10.1073/pnas.1203689109

Wu, M., Okino, T., Nogle, L. M., Marquez, B. L., Williamson, R. T., Sitachitta, N., et al. (2000). Structure, synthesis, and biological properties of kalkitoxin, a novel neurotoxin from themarine cyanobacterium *Lyngbya majuscula*. *J. Am. Chem. Soc*. 122, 12041–12042.doi: 10.1021/ja005526y

Yang, J. Y., Sanchez, L. M., Rath, C. M., Liu, X., Boudreau, P. D., Bruns, N., et al. (2013). Molecular networking as a dereplication strategy. *J. Nat. Prod*. 76, 1686–1699. doi: 10.1021/np400413s

Conflict of Interest Statement: The authors declare that the research was conducted in the absence of any commercial or financial relationships that could be construed as a potential conflict of interest.

frontiers in Chemistry

ORIGINAL RESEARCH
published: 27 July 2018
doi: 10.3389/fchem.2018.00314

Brasilianoids A–F, New Meroterpenoids From the Sponge-Associated Fungus *Penicillium brasilianum*

Jianping Zhang[1], *Bochuan Yuan*[1], *Dong Liu*[1], *Shuang Gao*[2], *Peter Proksch*[3] and *Wenhan Lin*[1]*

[1] State Key Laboratory of Natural and Biomimetic Drugs, Institute of Ocean Research, Peking University, Beijing, China, [2] Institute of Life Sciences, Wenzhou University, Wenzhou, China, [3] Institute für Pharmazeutische Biologie und Biotechnologie, Heinrich-Heine-Universität Düsseldorf, Düsseldorf, Germany

OPEN ACCESS

Edited by:
Simone Brogi,
University of Siena, Italy

Reviewed by:
Roberta Teta,
Università degli Studi di Napoli Federico II, Italy
Edson Roberto Silva,
Universidade de São Paulo, Brazil
Renato Chavez,
Universidad de Santiago de Chile, Chile

***Correspondence:**
Wenhan Lin
whlin@bjmu.edu.cn

Specialty section:
This article was submitted to Medicinal and Pharmaceutical Chemistry, a section of the journal Frontiers in Chemistry

Received: 25 April 2018
Accepted: 09 July 2018
Published: 27 July 2018

Citation:
Zhang J, Yuan B, Liu D, Gao S, Proksch P and Lin W (2018) Brasilianoids A–F, New Meroterpenoids From the Sponge-Associated Fungus Penicillium brasilianum. Front. Chem. 6:314. doi: 10.3389/fchem.2018.00314

3,5-Dimethylorsellinic acid (DMOA) derived meroterpenoids comprise an unique class of natural products with diverse scaffolds and with a broad spectrum of bioactivities. Bioinformatics analysis of the gene clusters in association with the qRT-PCR detection of the amplification of two key genes led to speculate that the sponge associated fungus *Penicillium brasilianum* WZXY-m122-9 is a potential producer of meroterpenoids. Chromatographic separation of the EtOAc extract of this fungal strain on a large-scale fermentation resulted in the isolation of six new DMOA-related meroterpenoids with trivial names of brasilianoids A–F (**1**-**6**), together with preaustinoid D and preaustinoid A2. The structures were determined by extensive analyses of spectroscopic data, including the X-ray diffraction and the ECD data for configurational assignment. Brasilianoids A and F showed an unprecedented skeleton with a γ-lactone in ring A, while brasilianoids B–C featured a 7/6/6/5/5 pentacyclic ring system finding in nature for the first time. The biosynthetic relationship among the isolated compounds was postulated. Compound **1** significantly stimulated the expression of filaggrin and caspase-14 in HaCaT cells in dose-dependent manner, while compounds **2** and **3** showed moderate inhibition against NO production in LPS-induced RAW 264.7 macrophages.

Keywords: sponge-associated fungus, *Penicillium brasilianum*, brasilianoids A–F, stimulation of filaggrin and caspase-14, inhibition of NO production

INTRODUCTION

The fungal meroterpenoids as the fascinating hybrid natural products are widely distributed in marine environments with diverse molecular architectures, that are assembled by terpene moieties with other precursors such as polyketide unit by various biosynthetic pathways (Iida et al., 2008; Silva et al., 2011; Guo et al., 2012; Qi et al., 2017). Among the fungus-derived meroterpenoids, a polyketide-terpenoid biosynthetic pathway that has C-alkylation of 3,5-dimethylorsellinic acid (DMOA) with farnesyl pyrophosphate (FPP) generated more than 100 secondary metabolites with a number of unique scaffolds (Geris and Simpson, 2009; Matsuda and Abe, 2016). The biogenetic pathways of these typical natural products have been extensively investigated, uncovering a series

of synthetic gene clusters and functional enzymes (Lo et al., 2012; Matsuda et al., 2016; Mori et al., 2017). The structure variation of the DMOA-based meroterpenoids was attributed to sequential cyclization, complex oxidative ring rearrangement, and recyclization. Based on the carbocyclic frameworks, the DMOA-FPP derived meroterpenoids can be classified into seven subtypes. Andrastins with a 6,6,6,5-*tetra*-carbocyclic skeleton are the potent inhibitors of RAS proteins, which are important for controlling cell division and the development of cancer (Nielsen et al., 2005). Terretonin-type congeners possessing a δ-lactone in ring D are originated from terrenoid (andrastin-type) by D-ring expansion and unusual rearrangement of the methoxy group (Matsuda et al., 2015). Berkeleyone-type (or protoaustinoid-tyep) derivatives as the caspase-1 inhibitors are the meroterpenoids representing a series of unique and functionalized chemical scaffolds, which are characterized by the presence bicyclo[3.3,1]nonane or its rearranged bicyclo[3,2,1]octane unit in rings C and D. (Stierle et al., 2011), and are derived by the same intermediate as for andrastins with different rearrangement. Austinol and its analogues featured a pentacyclic scaffold with a spiro-δ-lactone in ring A and a γ-lactone in ring E, that were derived from protoaustinoid through oxidation and ring rearrangement (Matsuda et al., 2013). Chrysogenolides are a group of DMOA-based compounds with a unusual seven-numbered ring B, which exhibited the inhibition of nitric oxide production (Qi et al., 2017), while anditomin analogues featured the presence of a unique and highly oxygenated bridged-ring system (Matsuda et al., 2014). Fumigatonin and novofumigatonin are an additional subtype containing highly oxidized and complicatedly condensed ring system (Okuyama et al., 2008; Rank et al., 2008). These meroterpenoids have been reported to possess a range of biological activities (Rank et al., 2008; Zhang et al., 2012). *Penicillium brasilianum* is a remarkable microorganism with great potential to produce secondary metabolite with a variety of carbon skeletons and with interesting biological activities. Fungal strains of *P. brasilianum* are mostly isolated from terrestrial sources. They produced diverse metabolite scaffolds including meroterpenenes, polyketides, alkaloids, and cyclopeptides (Bazioli et al., 2017). In the course of our search for new terpenoids with pharmaceutical bioactivity, a sponge-associated fungal strain, *P. brasilianum* WZXY-m122-9, was selected due to the same fungal species has been reported to produce meroterpenoids with chemical diversity and novelty (Matsuda et al., 2016; Bazioli et al., 2017). Anti-SMASH genome sequence analysis revealed that two gene clusters (clusters A and B) in WZXY-m122-9 are highly identical to the *aus*' clusters (**Figure 1**), that playing key role for the biosynthesis of DMOA-derived meroterpenoids in *P. brasilianum* MG11 (Matsuda et al., 2016). qRT-PCR detection showed that prenyltransferase gene (PM-122-9_1376) and terpene cyclase gene (PM-122-9_1374) in clusters A and B were highly expressed. These findings suggested WZXY-m122-9 strain to be a potential producer of terpenoids. Chromatographic separation of the EtOAc extract of the cultured fungus on a large scale resulted in the isolation of eight meroterpenoids, including six new compounds namely brasilianoids A-F (**1**-**6**) and known analogues preaustinoids D (**7**) and A2 (**8**) (**Figure 2**).

MATERIALS AND METHODS

General Experimental Procedures

Optical rotations were measured with an Autopol III automatic polarimeter. IR spectra were measured with a Thermo Nicolet Nexus 470 FT-IR spectrometer. 1D and 2D NMR spectra were recorded on a Bruker Avance-400/600FT NMR spectrometer using TMS as internal standard. HRESIMS data were acquired on a Bruker APEX IV 70 eV FT-MS spectrometer. ESIMS data were obtained on a Finnigan MAT 95 mass spectrometer. The column chromatographic substrates included silica gel (200–300 mesh) and HF254 silica gel for TLC (Qingdao Marine Chemistry Co. Ltd.), Sephadex LH-20 (18–110 μm; Pharmacia Co., Ltd.); ODS (50 μm; YMC, Milford, MA). Semipreparative HPLC separation was performed with an Alltech instrument (426-HPLC pump) equipped with an UV detector at 210 nm and using a Prevail-C_{18} column (Semipreparative, 5 μm). X-ray data were measured with a Bruker SMART APEX-II DUO instrument.

Fungal Strain and Identification

The fungus *P. brasilianum* WZXY-m122-9 was isolated from an unidentified marine sponge, which was collected in July 2016 from Weizhou Island in the South China Sea, and was identified by microscopic examination and 18S rDNA ITS sequence's BLAST in GenBank (GenBank accession number HM469396). A voucher specimen (WZXY-m122-9) was deposited at the State Key Laboratory of Natural and Biomimetic Drugs, Peking University, China.

Genome Sequencing and Analysis

Genome sequencing of *P. brasilianum* WZXY-m122-9 was performed by Sangon Biotech (Shanghai) Co., Ltd. (Shanghai, China) with an Illumina HiSeq 2000 system. Sequence assembly was performed with SPAdes version 3.5.0 (http://cab.spbu.ru/software/spades/) to yield 1,367 contigs covering approximately 34.7 Mb. Gene prediction was then performed with Prokka (https://github.com/tseemann/prokka). Anti-SMASH (antibiotics and secondary metabolite analysis shell) analysis of genome sequences was performed to detect secondary metabolite gene clusters, and accurate gene cluster alignment was performed manually by comparisons with homologous genes found in the NCBI database. Anti-SMASH of WZXY-m122-9 genome analysis displayed that two gene clusters namely cluster A and cluster B, showed high identity compared with *aus*' clusters that had been reported in *P. brasilianum* MG11 (Matsuda et al., 2016).

Quantitative RT-PCR for Gene Expression

Degenerate primers were designed according to the conserved sequences of prenyltransferase (PM-122-9_1376′) and terpene cyclase (PM-122-9_1374) genes within clusters A and B, and the length of PCR products were 805 bp and 529 bp, respectively. The gene expression levels were detected by qRT-PCR. Total RNA of WZXY-m122-9 was obtained from the rice culture medium,

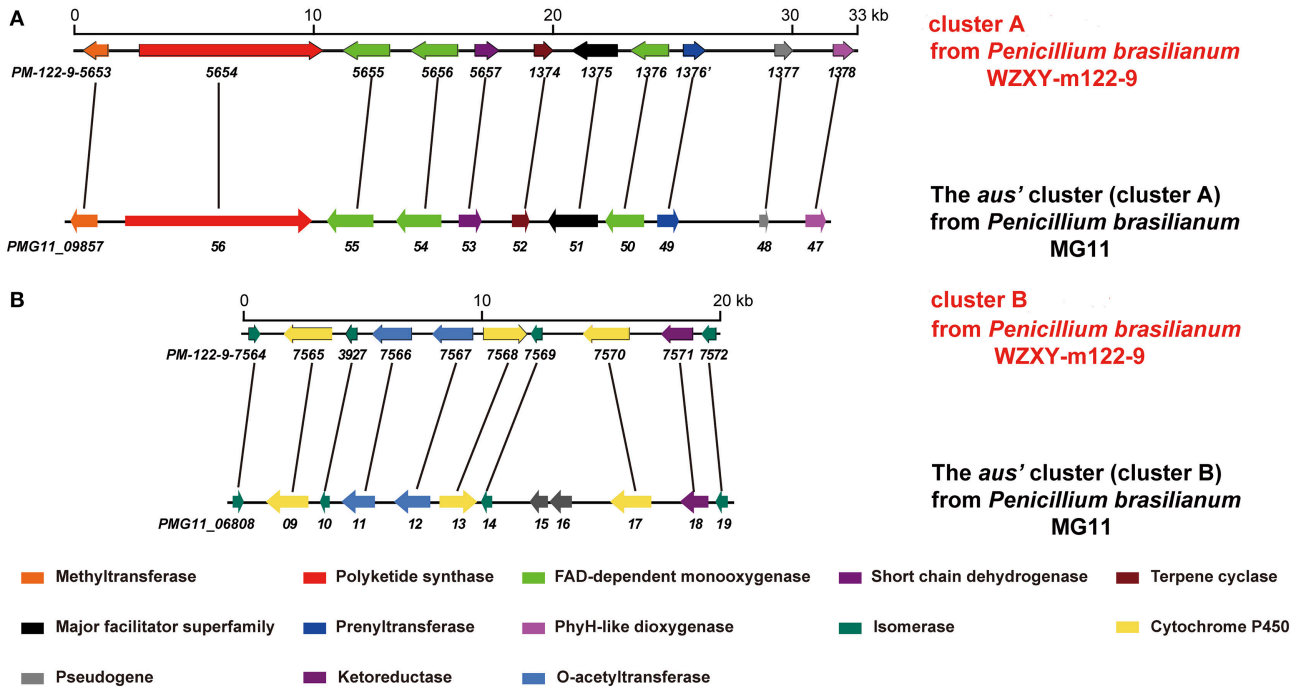

FIGURE 1 | Comparison of the gene clusters between *P. brasilianum* WZXY-m122-9 and *P. brasilianum* MG11. **(A)** Comparison of the genes in cluster A of *P. brasilianum* WZXY-m122-9 with the *aus*'s genes (cluster A) from *P. brasilianum* MG11. The homologous genes between the gene clusters were linked with lines. **(B)** Comparison of the genes in cluster B of *P. brasilianum* WZXY-m122-9 with the *aus*'s genes (cluster B) from *P. brasilianum* MG11. The homologous genes between the gene clusters were linked with lines. *PM-122-9-5653* and others mean the genes in *P. brasilianum* WZXY-m122-9.

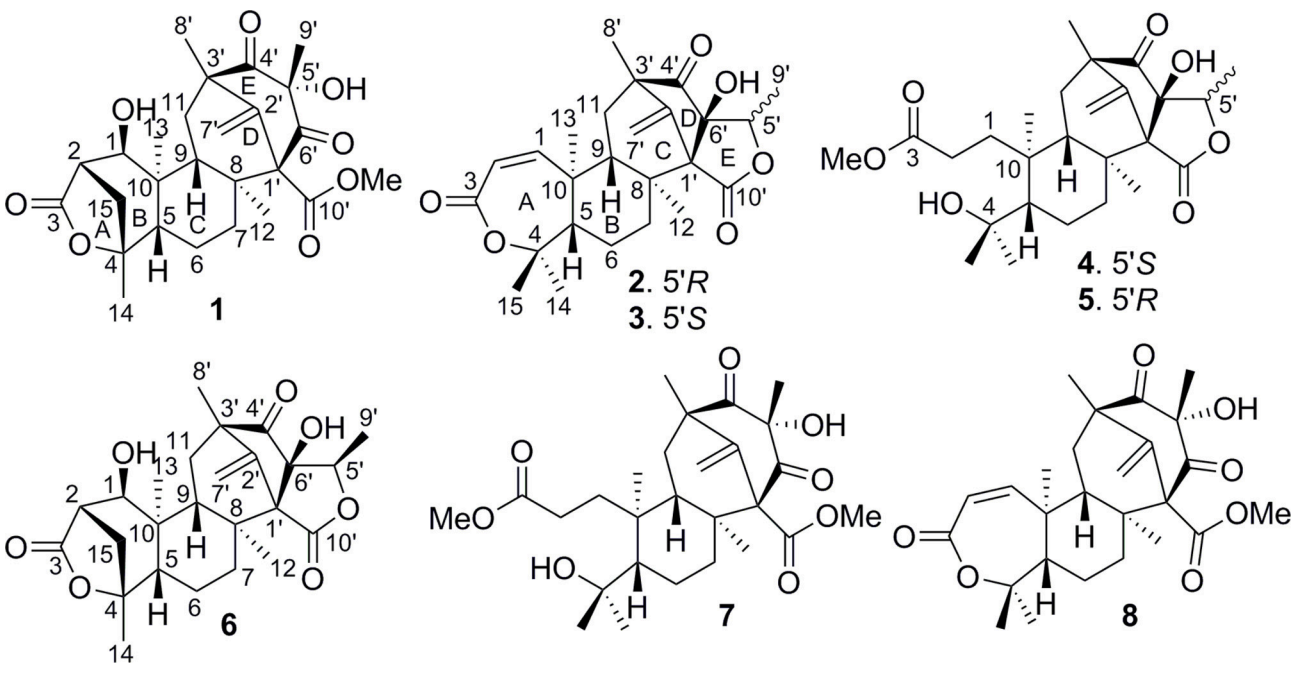

FIGURE 2 | Structures of **1–8**.

and cDNA was synthesized from 1 μg of total RNA in a volume of 20 μL using TransScriptIIAll-in-One first-strand cDNA synthesis super mix (Transgene) according to the manufacturer's instructions. 0.4 μL cDNA, forward primer (10 μM), reverse primer (10 μM) and 10μL 2× TransStart Top Green qPCRSuperMix (Transgene) were used in subsequent RT-PCR reactions with supplement ddH_2O to 20 μL. The specific primers included actin-F (5′-ACCTGCTCTGCGACTACAAC-3′), actin-R (5′-ACACCGCCCTCATAATAAAG-3′), PM-122-9_1376′-F (5′-CCACCAAAGGGGATTACCA-3′), PM-122-9_1376′-R (5′-GAGCAGAAATGTCGCAGGAA-3′), PM-122-9_1374-F (5′-CGGTAGGATGGTCGGTCAAC-3′), PM-122-9_1374-R (5′-ACGGCGGAGTGTAGGAAGAA-3′). Each primer pair gave a single PCR product. The *β-actin* gene was treated as an internal reference gene, optimized PCR conditions were 94°C for 30 s; 45 cycles of 94°C for 5 s; 60°C for 15 s; and 72°C for 10 s; followed by dissociation stage. Three parallel tests for each reaction and recording their respective Ct values. According to amplification curves, every sample was different from no template control (NTC), which indicated that the genes were amplified from cDNA template. Under current culture conditions, the *aus′* gene cluster was expressed in the plasmids of WZXY-m122-9, and the expression level of prenyltransferase (PM-122-9_1376′) and terpene cyclase (PM-122-9_1374) genes was higher than *β-actin* due to Ct_{1376} and Ct_{1374} less than Ct_{actin}.

Fermentation of the Fungus

The fermentation was carried out in 40 Fernbach flasks (500 mL), each containing 80 g of rice. Distilled H_2O (100 mL) was added to each flask, and the contents were soaked overnight before autoclaving at 15 psi for 30 min. After cooling to room temperature, each flask was inoculated with 5.0 mL of the spore inoculum (10^7/mL) and incubated at 25°C for 25 days.

Extraction and Isolation of Metabolites

The fermented material was extracted with EtOAc (3 × 1 L), successively. The EtOAc extract was evaporated to dryness under reduced pressure to afford a crude residue (20.5 g). The crude extract was suspended in 90% MeOH-H_2O and then extracted with petroleum ether (PE) for three times, while the MeOH layer was concentrated under vacuum to obtain MeOH soluble extract (8.0 g). Part of the MeOH fraction (4 g) was then subjected to silica gel (200–300 mesh) vacuum liquid chromatography with gradient elution using PE-EtOAc (from 8:1 to 0:1, v/v) to obtain four fractions (FA-FD). FC (0.9 g) was detected by ^{1}H NMR spectrum, showing the signals featured meroterpenoid analogues, and it was chromatographed over an RP-C_{18} column eluting with MeOH-H_2O (65:35, v/v) to afford six subfractions (FCa–FCf). FCb (60 mg) was separated on a semipreparative RP-C_{18} HPLC column using MeOH-H_2O (50:50, v/v, 2 mL/min) to yield compounds **7** (8 mg) and **1** (4 mg). FCc (110 mg) was purified by a semipreparative RP-C_{18} HPLC column eluting with MeCN-H_2O (40:60, v/v, 2 mL/min) to afford compounds **2** (6 mg), **3** (6 mg) and **6** (2 mg). FCd (70 mg) was separated using a semipreparative RP-C_{18} HPLC column eluting with MeOH-H_2O (55:45, v/v, 2 mL/min) to afford **4** (5.0 mg), **5** (5.0 mg), and **8** (45 mg).

Brasilianoid A (**1**) (methyl (1*R*, 2*S*, 5*R*, 5a*S*, 7a*S*, 8*R*, 10*S*, 12*R*, 13a*R*, 13b*S*)-1, 10-dihydroxy-5,7a,10,12,13b-pentamethyl-14-methylene-3,9,11-trioxotetradecahydro-2,5:8,12-dimethanocycloocta[3,4]benzo[1,2 -c]oxepine-8(5H)-carboxylate). White amorphous powder; $[\alpha]_D^{20}$ −22 (*c* 0.5, MeOH); UV (MeOH) λ_{max} (log ε) 203 nm; IR ν_{max} (KBr) 3,419, 2,985, 2,935, 1,754, 1,720, 1,708, 1,662, 1,227, and 1,025 cm^{-1}. ^{1}H and ^{13}C NMR data, see **Tables 1**, **2**; HRESIMS *m/z* 473.2176 $[M–H]^-$ (calcd for $C_{26}H_{33}O_8$, 473.2175).

Brasilianoid B (**2**) ((5a*S*, 5b*S*, 7*R*, 8a*R*, 9*S*, 11a*R*, 11b*S*, 13a*S*)-8a-hydroxy-1, 1, 5a, 7, 9, 11b-hexamethyl-14-methylene-5a, 5b, 6, 7, 8a, 9, 11b, 12, 13, 13a-decahydro-1H, 11H-7,11a-methanofuro[3″,4″:3′,4′]cyclohepta[1′,2′:3,4]benzo[1,2-c]oxepine-3,8,11-trione). Colorless monoclinic crystals (MeOH-Acetone-H_2O, 5:5:1); m.p. 170–172°C; $[\alpha]_D^{20}$ −40 (*c* 0.5, MeOH); UV (MeOH) λ_{max} (log ε) 206 nm; IR ν_{max} (KBr) 3,420, 2,931, 2,966, 1,754, 1,693, 1,604, 1,384, and 1,043 cm^{-1}. ^{1}H and ^{13}C NMR data, see **Tables 1**, **2**; HRESIMS *m/z* 473.2170 $[M + HCOO]^-$ (cald for $C_{26}H_{33}O_8$, 473.2175).

Brasilianoid C (**3**) ((5a*S*, 5b*S*, 7*R*, 8a*R*, 9*R*, 11a*R*, 11b*S*, 13a*S*)-8a-hydroxy-1, 1, 5a, 7, 9,11b -hexamethyl-14-methylene-5a,5b,6,7,8a,9,11b,12,13,13a-decahydro-1H,11H-7, 11a-methanofuro[3″,4″:3′,4′]cyclohepta[1′,2′:3,4]benzo[1,2-c]oxepine-3,8,11-trione). Colorless monoclinic crystals (MeOH-H_2O, 8:1); m.p. 171–173°C; $[\alpha]_D^{20}$ −40 (*c* 0.5, MeOH); UV (MeOH) λ_{max} (log ε) 208 nm; IR ν_{max} (KBr) 3,420, 2,930, 2,876, 1,760, 1,694, 1,604, 1,385, and 1,027 cm^{-1}. ^{1}H and ^{13}C NMR data, see **Tables 1**, **2**; HRESIMS *m/z* 473.2181 $[M + HCOO]^-$ (cald for $C_{26}H_{33}O_8$, 473.2175).

Brasilianoid D (**4**) (methyl 3-((3*R*, 3a*R*, 5*R*, 6a*S*, 7*S*, 8*S*, 10a*S*, 10b*R*)-3a-hydroxy-8- (2-hydroxypropan-2-yl)-3,5,7,10a-tetramethyl-11-methylene-1,4-dioxodecahydro-1H,3H-5,10b-methanobenzo[3,4]cyclohepta[1,2-c]furan-7-yl)propanoate). Colorless monoclinic crystals; (MeOH-$CHCl_3$, 5:1); m.p. 255–258°C; $[\alpha]_D^{20}$ −60 (*c* 0.5, MeOH); UV (MeOH) λ_{max} (log ε) 202 nm; IR ν_{max} (KBr) 3,420, 2,965, 2,856, 1,750, 1,661, 1,634, 1,384, and 1,072 cm^{-1}. ^{1}H and ^{13}C NMR data, see **Tables 1**, **2**; HRESIMS *m/z* 507.2590 $[M + HCOO]^-$ (calcd for $C_{27}H_{39}O_9$, 507.2594).

Brasilianoid E (**5**) (methyl 3-((3*S*, 3a*R*, 5*R*, 6a*S*, 7*S*, 8*S*, 10a*S*, 10b*R*)-3a-hydroxy-8- (2-hydroxypropan-2-yl)-3,5,7,10a-tetramethyl-11-methylene-1,4-dioxodecahydro-1H,3H-5,10b-methanobenzo[3,4]cyclohepta[1,2-c]furan-7-yl)propanoate). Colorless orthorhombic crystals (MeOH-$CHCl_3$-H_2O, 5:3:1); m.p. 225–228°C; $[\alpha]_D^{20}$ −60 (*c* 0.5, MeOH); UV (MeOH) λ_{max} (log ε) 202 nm; IR ν_{max} (KBr) 3,445, 2,966, 2,939, 1,750, 1,662, 1,607, 1,385, and 1,065 cm^{-1}. ^{1}H and ^{13}C NMR data, see **Tables 1**, **2**; HRESIMS *m/z* 507.2600 $[M + HCOO]^-$ (cald for $C_{27}H_{39}O_9$, 507.2594).

Brasilianoid F (**6**) ((1*R*, 4*S*, 5*R*, 5a*S*, 5b*R*, 7*R*, 8a*R*, 9*R*, 11a*R*, 11b*S*, 13a*S*)-5, 8a-dihydroxy-1,5a,7,9,11b-pentamethyl-14-methylenedodecahydro-1H,11H-1,4:7,11a-dimethanofuro[3″,4″:3′,4′]cyclohepta[1′,2′:3,4]benzo[1,2-c]oxepine-3,8,11-trione). White amorphous powder; $[\alpha]_D^{20}$ −48 (*c* 0.5, MeOH); UV (MeOH) λ_{max} (log ε) 202 nm; IR ν_{max} (KBr) 3,419, 2,986, 2,949, 1,754, 1,720, 1,603, 1,383, and 1,088 cm^{-1}.

^{1}H and ^{13}C NMR data, see **Tables 1**, **2**; HRESIMS *m/z* 443.2077 $[M - H]^-$ (cald for $C_{25}H_{31}O_7$, 443.2070).

ECD Calculation

Conformational searches were carried out by random searching in the Sybyl-X 2.0 using the MMFF94S force field with an energy cutoff of 5.0 kcal/mol. Due to the confirmed NOESY correlations and relatively rigid skeleton, the results showed the lowest energy conformers for (1*R*, 2*S*, 4*R*, 5*S*, 8*S*, 9*R*, 10*S*, 1′*R*, 3′*R*, 5′*S*)-**1′**, 1*R*, 2*S*, 4*R*, 5*S*, 8*S*, 9*R*, 10*S*, 1′*R*, 3′*R*, 5′*R*, 6′*R*-**6′** and for 5*S*, 8*S*, 9*S*, 10*S*, 1′*R*, 3′*R*, 5′*R*, 6′*R*-**7′** within 5.0 kcal/mol. Subsequently, the conformers were re-optimized using DFT at the B3LYP/6-31+G(d) level in gas phase by the GAUSSIAN 09 program. The energies, oscillator strengths, and rotational strengths (velocity) of the first 60 electronic excitations were calculated using the TDDFT methodology at the b3lyp/6-311++g(d, p) level in vacuum. The ECD spectra were simulated by the overlapping Gaussian function (half the bandwidth at 1/e peak height, $\sigma = 0.35$ for **1** and 0.25 for **6**). By comparison of the calculated ECD spectra with the experimental curves, the absolute configuration of **1** and **6** were resolved.

Assay for *in Vitro* Anti-HBV Effects

HepAD38 cells were cultured with DMEM in 48-well plate at 1×10^5 cells/well for 24 h, then treated with 10 μM of each compound for 72 h. After 4 days, the cells were washed with precooled PBS for 2 times. HBV progeny DNA of HepAD38 cells were extracted using QIAamp DNA Blood Mini kit (Biomiga) according to the manufacturer's instruction. Total DNA was reversely transcribed using PrimeScript RT reagent Kit (Takara, Dalian, China). The primers were designed and synthesized by Takara, and the sequences of the primers are indicated in Table S9. PCR amplification was performed on an StepOne Plus real time PCR system (Applied Biosystems, Foster City, CA) using the SYBR Green Master Mix (Applied Biosystems, Foster City, CA). All experiments were performed in triplicate, and the relative levels of assayed HBV DNA were calculated with the delta–delta CT method using lamivudine as a positive control, and normalized to non-treated control.

Assay for Protective Effects on Skin Barrier Functions in *in Vitro*

HaCaT cells were cultured with DMEM in 6-well plate at 1×10^5 cells/well for 24 h, then treated with 20, 10, 5 μM of compounds **1**–**7** for 72 h. Total RNA of HaCaT cells were extracted using RNA Miniprep kit (Biomiga) according to the manufacturer's instruction. Then total RNA was reverse transcribed using PrimeScript RT reagent Kit (Takara, Dalian, China). The primers were designed and synthesized by Takara, the sequences of the primers are indicated in Table S10. PCR amplification was performed on an StepOne Plus real time PCR system (Applied Biosystems, Foster City, CA) using the SYBR Green Master Mix (Applied Biosystems, Foster City, CA). All experiments were performed in triplicate, and the relative levels of assayed mRNAs were calculated with the delta–delta CT method using ACTIN expressions as endogenous control, and normalized to non-treated control.

HaCaT cells were seeded at 5×10^5 cells per well in 6-well plates and incubated under starvation conditions for 24 h using serum-free MEM. HaCaT cells were exposed to UVB irradiation (UVB lamp: SUV-1000, Sigma-China) at a dose of 30 mJ/cm^2. After UVB irradiation, DMEM medium containing **1** (20 μM) or epigallocatechin gallate (20 μM) was added and the cells were incubated for 24 h, and then the MTT assay was performed.

Assay for the Inhibition of Nitric Oxide Production in RAW264.7 Macrophages

All compounds were assayed by measuring the inhibitory effects on NO production induced by LPS in mouse macrophage RAW 264.7 cells. The RAW 264.7 cells were seeded in each well of a 96-well plate at a concentration of 5×10^5 cells/ml in DMEM medium containing 10% fetal bovine serum, 2 mmol/l glutamine, 100 U/ml penicillin, and 100 μg/ml streptomycin. After incubation at 37°C in a humidified atmosphere of 5% CO_2 air for 12 h, cells were treated with LPS (1 μg/ml) and compounds (50 μg/ml for each compound, and compound was dissolved in DMSO to dilute until the final DMSO concentration < 0.1%, v/v), then incubation for 24 h at 37°C. NO production was determined by measuring the quantity of nitrite in the culture medium by the Griess reagent. Aminoguanidine was selected as a positive control. A 50 μl of the supernatant of culture medium was mixed with 100 μl of the Griess reagent. Using nitrite to generate a standard curve, nitrite production was measured by a microplate reader at 540 nm. Cell viability was examined by the MTT method (Wu et al., 2016). The compounds with inhibitory rate more than 50% at a dose of 50 μg/ml were further detected in the gradient concentrations to calculate IC_{50} values.

Statistical Analysis

All quantitative values are given as means ± SEMs. Significant differences among the experimental groups were assessed by one-way ANOVA. Statistical significances were considered at the $^*P < 0.05$ and $^{**}P < 0.01$ levels.

Crystal Structure Analysis

X-ray crystal data of **2**–**5** and **8** were acquired on an Eos CCD with a graphite monochromated Cu Kα radiation ($\lambda = 1.5418$ Å) (Supporting Information). These structures was solved with ShelXT-97 using direct methods and refined with ShelXL using full matrix least-squares on F_2. Crystallographic data for **2**–**5** and **8** have been deposited at the Cambridge Crystallographic Data Center with the numbers of CCDC 1572280 for **2**, CCDC 1572282 for **3**, CCDC 1576933 for **4**, CCDC 1576930 for **5** and CCDC 1583230 for **8**. Crystallographic data are deposited in the Cambridge Crystallographic Data Centre. and are available free of charge via the Internet at www.ccdc.cam.ac.uk/products/csd/request.

RESULTS

Identification of New Compounds

The molecular formula of brasilianoid A (**1**) was determined as $C_{26}H_{34}O_8$ according to the HRESIMS ion at *m/z* 473.2176 [M

– H]$^-$ and the NMR data, requiring ten degrees of unsaturation. The ^{1}H NMR data presented five tertiary methyl singlet at δ_H 0.76 (s), 1.17 (s), 1.29 (s), 1.33 (s), and 1.34 (s), and a methoxy group at δ_H 3.57 (s), one oxygenated methine at δ_H 3.47 (t, $J = 4.2$ Hz), as well as the terminal olefinic methylene protons at δ_H 4.67 (s) and 5.21 (s) (**Table 1**). The ^{13}C NMR and DEPT spectra exhibited a total of 26 carbon resonances (**Table 2**), which were classified into six methyl, five methylene (one olefinic carbon), four methine, and eleven quaternary carbons involving two ketones and two ester carbonyl carbons. Analyses of the 1D and 2D NMR data revealed that **1** is a preaustinoid-related meroterpenoid, while the partial structure regarding rings C/D/E of **1** was corresponded to rings B/C/D of preaustinoid A2 (**8**) (dos Santos and Rodrigues-Fo, 2003) with the exception of ring A. The COSY correlation coupled H-2 (δ_H 2.50, dd, $J = 4.2$, 4.9 Hz) to H-1 (δ_H 3.47) and H_2-15 (δ_H 1.81, 2.24), along with the extension of COSY coupling between H-1 and a D_2O exchangeable proton at δ_H 5.16 (d, $J = 4.2$ Hz), ascertained the location of a hydroxy group at C-1 (δ_C 70.0). A methylene bridge across C-2 (δ_C 48.0) and C-4 (δ_C 86.8) was evident from the HMBC correlations from H_3-14 (δ_H 1.29, s) to C-4, C-5 (δ_C 48.3), and C-15 (δ_C 40.7), and from H_2-15 to C-1, C-2, C-4, and C-5. Additional HMBC correlation from the carbonyl carbon C-3 (δ_C 177.5) to H-1, H-2, and H_2-15 in association with the degrees of molecular unsaturation confirmed the formation of a γ-lactone for ring A.

The relative configuration of **1** was established by the NOE data. As shown in **Figure 3**, the NOE correlations from H-15a (δ_H 2.24) to OH-1 and H-5, and from H-9 (δ_H 1.50) to OH-1, H-5, and H_3-9′, in association with the correlation between H_3-12 (δ_H 1.17) and H_3-13 (δ_H 0.76), clarified *trans* fusion between B/C and C/D rings. When H-1 was arbitrarily assigned to α-orientation, the methylene bridge H_2-15 was ascertained to be in β-orientation. The relative configuration in rings C to E was the same as that of preaustinoid A2, based on the similar NOE relationship. The spatial closure between H_3-9′ and H-9 was recognized by their NOE interaction, while the NOE correlation between H_3-12 and H_2-7′ indicated that the *exo*-vinyl group across C-1′ and C-3′ was α-oriented. In biogenetic consideration, compound **1** was assumed to be derived from preaustinoid A2 by the formation of C-2/C-15 bond. Thus, both compounds were suggested to share the same absolute configuration in rings C-E. Since the absolute configuration of preaustinoid A2 was determined by the single crystal X-ray diffraction analysis using Cu K_α radiation in present work, the stereogenic centers in rings C-E of **1** were supposed to be 8*S*, 9*S*, 10*R*, 3′*R*, 5′*S*, and 7′*R* configurations (Supporting Information). Thus, the absolute configuration in rings A and B was in agreement with 1*R*, 2*R*, 4*S*, and 5*S*, based on the NOE relationships. This assignment was further supported by the ECD data (Stephens and Harada, 2010), of which the Cotton effects of experimental and calculated ECD

TABLE 1 | ^{1}H NMR data of **1**–**6** (DMSO-d_6, δ ppm, J in Hz).

H	1	2	3	4	5	6
1	3.47, t (4.2)	6.30, d (12.6)	6.31, d (12.2)	1.32, m; 2.43, m	1.33, m; 2.43, m	3.50, t (4.5)
2	2.50, dd (4.2, 4.9)	5.76, d (12.6)	5.76, d (12.2)	1.72, m; 2.42, m	1.73, ddd (4.0, 12.5, 15.0) 2.42, m	2.54, ddd (4.5, 5.0, 10.1)
5	1.24, dd (1.7, 11.7)	2.02, br d (12.1)	1.94, dd (2.7, 12.7)	1.29, m	1.29, dd (2.0, 12.0)	1.67, dd (2.0, 12.0)
6	1.43, dt (3.2, 13.0) 1.61, br ddd (1.7, 2.0, 13.0)	1.65, m 1.68, m	1.62, ddd (2.7, 3.0, 13.0) 1.75, ddt (3.0, 12.7, 13.0)	1.49, m; 1.51, m	1.48, m; 1.50, m	1.51, m 1.62, m
7	1.85, dt (3.2, 12.0) 2.07, ddd (2.0, 3.2, 12.0)	1.70, m 2.23, ddd (3.0, 12.0, 12.5)	1.63, dt (3.0, 13.0) 2.30, dt (3.0, 13.0)	1.53, m 2.23, dt (3.0, 12.5)	1.54, m 2.15, dt (4.0, 12.3)	1.63, m 2.16, dt (4.1, 12.7)
9	1.50, dd (3.6, 12.9)	1.99, dd (2.0, 12.5)	2.10, br dd (4.1, 13.7)	2.07, br dd (5.8, 12.1)	1.92, dd (8.9, 13.0)	2.59, dd (3.8, 13.7)
11	1.68, t (12.9) 1.74, dd (3.6, 12.9)	1.84, dd (12.5, 13.0) 1.87, dd (2.0, 13.0)	1.84, t (13.7) 1.89, dd (4.1, 13.7)	1.60, dd (5.8, 13.0) 1.63, dd (12.1, 13.0)	1.48, dd (8.9, 12.0) 1.57, dd (12.0, 13.0)	1.56, dd (11.7, 13.7) 1.93, dd (3.8, 11.7)
12	1.17, s	1.18, s	1.20, s	1.12, s	1.11, s	1.14, s
13	0.76, s	1.08, s	1.08, s	0.87, s	0.88, s	0.78, s
14	1.29, s	1.35, s	1.35, s	1.10, s	1.10, s	1.30, s
15	1.81, br dd (4.9, 11.2) 2.24, d (11.2)	1.30, s	1.31, s	1.13, s	1.13, s	1.87, dd (5.0, 11.1) 2.29, brd (11.1)
5′		4.30, q (6.4)	4.46, q (7.2)	4.42, q (7.2)	4.29, q (6.4)	4.21, q (6.4, 6.4, 6.4)
7′	4.67, s; 5.21, s	4.86, s; 5.09, s	4.93, s; 5.14, s	4.89, s; 5.08, s	4.82, s; 5.04, s	4.81, s; 5.03, s
8′	1.34, s	1.20, s	1.16, s	1.12, s	1.16, s	1.16, s
9′	1.33, s	1.14, d (6.4)	1.03, d (7.2)	1.03, d (7.2)	1.15, d (6.4)	1.15, d (6.4)
OMe	3.57, s			3.57, s	3.57, s	
OH-1	5.16, d (4.2)					5.16, d (4.5)
OH-4′				4.09, s		
OH-5′	6.28, s				6.76, s	
OH-6′		6.95, s	7.09, s	7.04, s		6.68, s

TABLE 2 | ^{13}C NMR data of **1**–**6** (DMSO-d_6, δ ppm).

C	1	2	3	4	5	6
1	70.0	155.0	155.6	34.3	34.3	70.3
2	48.0	119.8	120.1	27.7	27.7	48.3
3	177.5	166.9	167.0	174.3	174.3	177.8
4	86.8	85.1	85.2	74.3	74.3	87.0
5	48.3	55.5	55.7	51.1	51.2	48.2
6	18.6	22.7	23.0	22.5	22.3	19.4
7	32.7	32.6	32.6	32.7	32.7	33.6
8	47.0	41.3	42.1	42.2	41.3	41.5
9	44.0	47.4	47.2	42.5	42.8	43.1
10	42.6	44.2	44.0	41.1	41.1	42.7
11	37.5	39.4	39.7	39.0	38.6	38.2
12	18.1	18.8	18.5	18.5	18.6	20.2
13	17.6	15.7	15.6	20.3	20.4	17.9
14	23.0	26.3	26.5	28.0	27.9	23.3
15	40.7	32.2	32.3	33.9	34.0	41.1
1′	72.6	66.5	65.0	65.7	67.2	66.8
2′	144.1	147.6	148.8	149.4	148.1	148.4
3′	50.5	55.3	55.7	55.6	55.2	55.3
4′	208.0	213.4	215.2	215.9	214.0	213.0
5′	76.9	76.4	83.5	83.3	76.1	76.2
6′	206.0	90.8	90.3	90.3	90.9	90.7
7′	112.3	106.5	107.6	106.8	105.8	105.9
8′	22.0	16.3	15.9	16.0	16.4	16.5
9′	17.5	13.2	18.2	18.3	13.4	13.3
10′	169.8	172.6	172.6	172.8	172.8	172.8
MeO	52.2			51.6	51.6	

for the model molecule of **1** with 1*R*, 2*R*, 4*S*, 5*S*, 8*S*, 9*S*, 10*R*, 3′*R*, 5′*S*, and 7′*R* were comparable (**Figure 4**).

Brasilianoid B (**2**) was isolated as colorless monoclinic crystals. Its molecular formula was determined as $C_{25}H_{32}O_6$ based on the HRESIMS (*m/z* 473.2170 [M + HCOO]$^-$) and NMR data, containing ten degrees of unsaturation. The ^{1}H and ^{13}C NMR data of **2** (**Tables 1**, **2**) regarding rings A-C resembled those of preaustinoid A2, while the distinction was attributed to rings D and E. An exocyclic olefinic group at C-2′ (δ_C 147.6) in ring C was recognized by the HMBC correlations from the olefinic methylene protons H_2-7′ (δ_H 4.86, 5.09) to C-1′ (δ_C 66.5) and C-3′ (δ_C 55.3). Additional HMBC correlations from H_3-8′ (δ_H 1.20, s) to C-2′, C-3′, and a ketone carbon C-4′ (δ_C 213.4), and from OH-6′ (δ_H 6.95, s) to C-4′, C-1′, and C-6′ (δ_C 90.8) established a cyclopentanone unit for ring D. Moreover, the HMBC correlations from H-5′ (δ_H 4.30, q, J = 6.4 Hz) to C-1′, C-4′, C-6′, and a carbonyl carbon C-10′ (δ_C 172.6), in addition to the COSY coupling between H-5′ and H_3-9′ (δ_H 1.14, d, J = 6.4 Hz), deduced a γ-lactone unit for ring E, while a hydroxy group and a methyl group were located at C-6′ and C-5′, respectively.

The relative configuration of **2** in rings A-C was the same as that of preaustinoid A2, based on the similar NOE relationships. The NOE correlations from OH-6′ to H-7a (δ_H 2.23) and H-9 (δ_H 1.99) demonstrated the spatial closure of these protons, suggesting OH-6′ to be in β-orientation. Additional NOE correlations between OH-6′/H_3-9′, H-5′/H_2-7′, H-5′/H_3-8′, and H_2-7′/H_3-12 (**Figure 2**) clarified the relative configuration in rings D and E. Based on the Flack parameters [−0.04(13)] measured by the Cu-Kα X-ray diffraction of the single crystal, the absolute configurations of **2** were finally determined as 5*S*, 8*S*, 9*S*, 10*S*, 1′*R*, 3′*R*, 5′*R*, and 6′*R* (**Figure 5**).

The planar structure of brasilianoid C (**3**) was the same as that of **2**, based on the 1D and 2D NMR data in association with the same molecular formula as determined by the HRESIMS data. The distinction was ascribed to the carbons C-5′ (δ_C 83.5) and C-9′ (δ_C 18.2), which showed more deshielded resonances than the corresponding carbons of **2** (**Table 2**). The NOE data raised from rings A-D were in accordance with those of **2**, indicating that this partial structure in **3** was the same as that of **2**. However, the NOE correlations between OH-6′ (δ_H 7.09, s) and H-5′ (δ_H 4.46, q) and from H_3-9′ (δ_H 1.03, d) to H_2-7′ (δ_H 4.93, 5.14) and H_3-8′ (δ_H 1.16, s) suggested **3** to be an C-5′ epimer of **2**. This assignment was confirmed by the Cu-Kα X-ray diffraction data, that clarified 5′*S* configuration in **3** (**Figure 5**).

Brasilianoid D (**4**) has a molecular formula of $C_{26}H_{38}O_7$ as determined by the HRESIMS and NMR data, bearing nine degrees of unsaturation. Analyses of the 2D NMR (COSY, HMQC, HMBC) data established the partial structure in rings B-E of **4** to be the same as that of **3**. However, the NMR data of **4** presented a methoxy group (δ_H 3.57, δ_C 51.6), and the methoxy protons correlated to a carbonyl carbon C-3 (δ_C 174.3) in the HMBC spectrum to form a methyl ester. The HMBC correlations from H_2-1 (δ_H 1.32, 2.43) and H_2-2 (δ_H 1.72, 2.42) to C-3 and C-10 (δ_C 41.1) demonstrated a methyl propionate unit to be positioned at C-10. In addition, a D_2O exchangeable proton at δ_H 4.09 (s) showed the HMBC correlation with C-4 (δ_C 74.3), C-5 (δ_C 51.1), and two methyl carbons C-14 (δ_C 28.0) and C-15 (δ_C 33.9), and therefore pointed the substitution of a 2-hydroxyisopropane unit at C-5. Thus, compound **4** was likely derived from preaustinoid A1 (Geris dos Santos and Rodrigues-Fo, 2002) by acyclized ring A and the cyclic rearrangement in ring D. The NOE relationship of OH-6′ (δ_H 7.04, s) with H-7a (δ_H 2.23), H-9 (δ_H 2.07), and H-5′ (δ_H 4.42), and from H_3-9′ (δ_H 1.03, d) to H_2-7′ (δ_H 4.89, 5.08), and H_3-8′ (δ_H 1.12, s), deduced the same relative configuration of both **4** and **3**. The absolute configuration of **4** was in agreement with that of **3** according to the Flack parameters of the Cu-Kα X-ray diffraction for the single crystals (**Figure 5**).

The planar structure of brasilianoid E (**5**) was the same as that of **4**, as determined by the HRESIMS data (*m/z* 507.2600 [M + HCOO]$^-$, cald for $C_{27}H_{39}O_9$, 507.2594) and the comparable 1D and 2D NMR data. The distinction was attributed to the NMR resonances at C-5′ (δ_C 76.1) and C-9′ (δ_C 13.4) which shifted 7 and 5 ppm, respectively, to upfield in comparison with those of **4** (**Tables 1**, **2**). As the case of **2**, the NOE correlation between OH-6′ (δ_H 6.76, s) and H-5′ (δ_H 4.29) and between H_3-9′ (δ_H 1.15) and H_2-7′ (δ_H 4.82, 5.04) clarified **5** to be an C-5′ epimer of **4**. The Cu-Kα X-ray crystallographic diffraction of the single crystal using Flack parameters (-0.006(9)) further confirmed the absolute configurations of **5** to be 5*S*, 8*S*, 9*S*, 10*S*, 3′*R*, 5′*R*, 6′*R*, and 7′*R* (**Figure 5**).

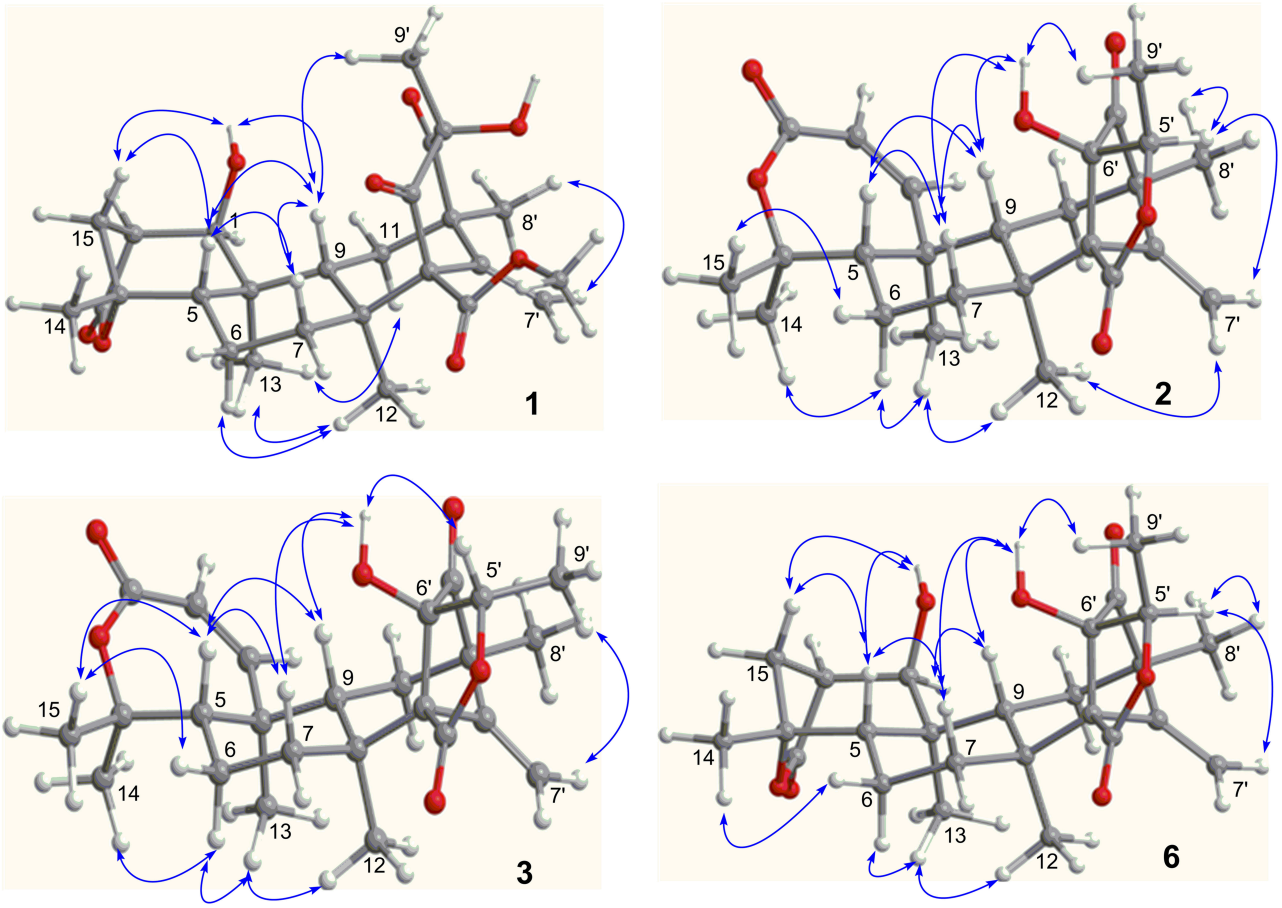

FIGURE 3 | Key NOE correlations of **1–3** and **6**. Arrow line means the NOE correlation from one proton to the other proton.

Brasilianoid F (**6**) has a molecular formula of $C_{25}H_{32}O_6$ as determined by the HRESIMS (*m/z* 443.2077 $[M\text{-}H]^-$, cald for $C_{25}H_{31}O_7$, 443.2070) and NMR data, requiring ten degrees of unsaturation. Analyses of 1D and 2D NMR data indicated that rings A to C are in accordance with those of **1**, as evident from the proton spin systems from OH-1 (δ_H 5.16, d, $J = 4.5$ Hz) to H_2-15 (δ_H 1.87, 2.54) and from H-5 (δ_H 1.67) to H_2-7 (δ_H 1.63, 2.16) in the COSY spectrum, in addition to the key HMBC correlations observed from H_2-15 to C-1, C-2, C-3, C-4 and C-5; H_3-14 to C-4, C-5 and C-15; H_3-12 to C-7, C-8, C-9, and C-1′; H_3-13 to C-1, C-5, C-9, and C-10, and OH-1 to C-1, C-2 and C-10. Moreover, the HMBC and COSY correlations assigned the partial structure of rings D to E to be the same as that of **2**. The similar NOE data, such as the key NOE correlations from OH-1 to H-15b (δ_H 2.54), H-5 and H-9 and between H_3-12 and H_3-13 as observed in the NOESY spectrum of **1** suggested the same relative configuration in rings A-C of both **6** and **1**. The NOE correlations from H-5 to H-15b and H-7b (δ_H 2.16), H-7b to H-9 and OH-6′, and between OH-6′ and H_3-9′ (**Figure 2**) clarified these protons to be cofacial, indicating the same relative configuration in rings C-E of both **6** and **2**. Additional NOE correlations from H-5′ to H_2-7′ and H_3-8′ supported the *exo*-vinyl bridge C-2′ to be in the same orientation as H-5′. In order to assign the absolute configuration, the ECD data of **6** and its enantiomer were calculated at the B31YP/6-311++G(2d, 2p) level in the gas phase using the B3LYP/6-31G(d) optimized geometries after conformational searches via the MMFF94S force field (Ding et al., 2007). Comparison of the experimental ECD data with those calculated for the enantiomers indicated that **6** (**Figure 4**) led to the identification of 1*R*, 2*S*, 4*R*, 5*S*, 8*S*, 9*S*, 10*R*, 3′*R*, 5′*R*, 6′*R*, and 7′*R* configurations.

Analyses of 1D and 2D NMR data established the planar structure of **7** to be identical to preaustinoid D (Duan et al., 2016), while the similar NOE correlation and ECD data clarified both compounds to be identical. However, comparison of the experimental ECD data with that calculated for a model molecule of (5*S*, 8*S*, 9*S*, 10*S*, 3′*R*, 5′*S*, 6′*R*, 7′*R*)-**7** (**Figure 4**) suggested that the structure of preaustinoid D should be revised to its enantiomer. Compound **8** was identical to preaustinoid A2 based on the comparison of its spectroscopic data with these reported in the literature (dos Santos and Rodrigues-Fo, 2003), while the absolute configuration was determined by the Flack parameters of the X-ray diffraction of the single crystals.

The NMR data of the epimers **2**/**3** and **4**/**5** revealed that the chemical shifts for C-5′ and C-9′ in **2** and **5** with 5′ *R* exhibited

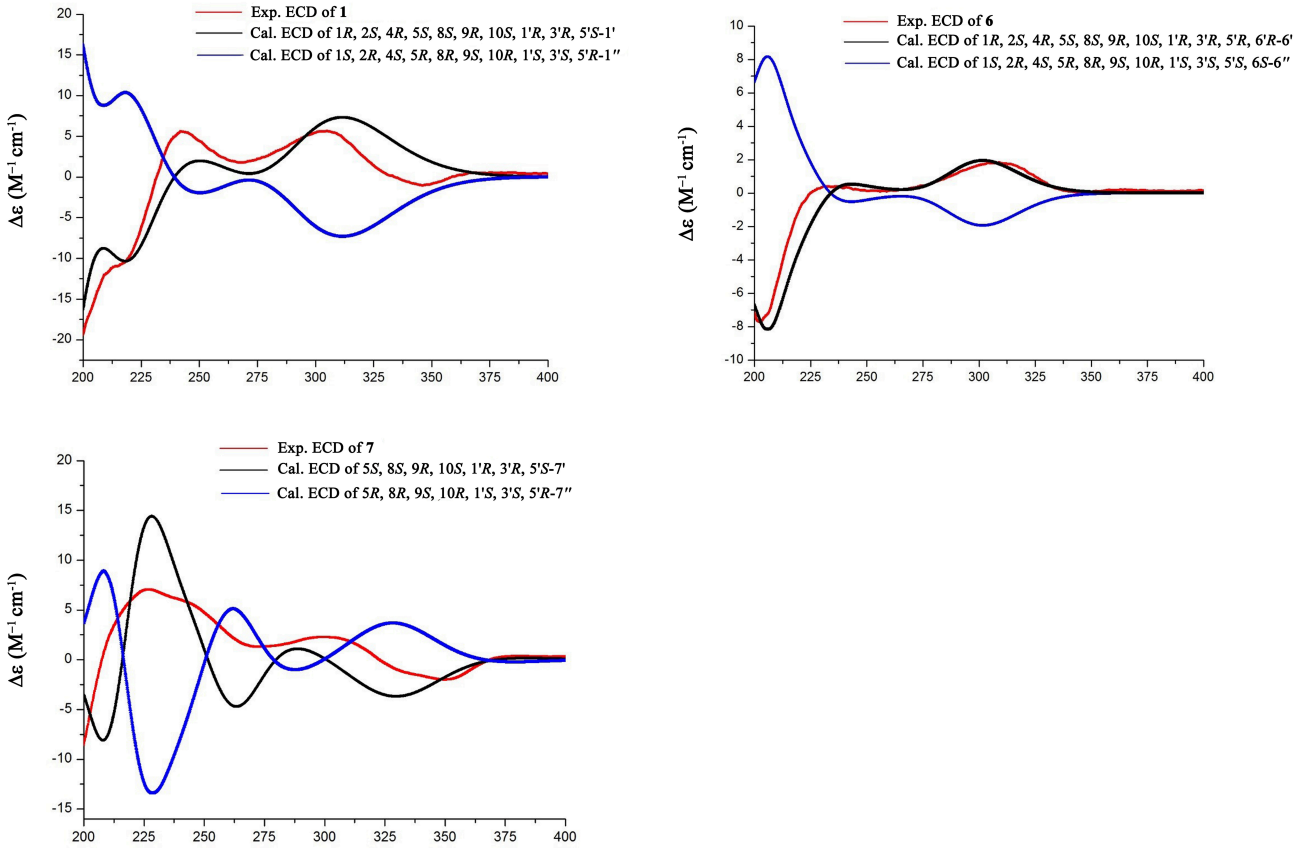

FIGURE 4 | Experimental and calculated ECD of **1, 6**, and **7**.

the resonances at δ_C 76 (C-5′) and δ_C 13 (C-9′), whereas those for 5′*S* isomers (**3**, **4**) showed more deshielded resonances at δ_C 83 (C-5′) and δ_C 18 (C-9′). The similar cases were also found in other analogues reported in literature. These NMR distinction provided the evidence to identify the configuration of C-5′ in austin-related meroterpenoids (Duan et al., 2016; Park et al., 2018). For instance, the chemical shifts of C-5′ (δ_C 76.2) and C-9′ (δ_C 13.3) in **6** and C-5′ (δ_C 78.5) and C-9′ (δ_C 12.2) in **7** implied the same orientation of OH-6′ and H_3-9′.

Biological Activity

Compounds **1–8** showed no cytotoxic activities toward tumor cell lines A549, U937 and SMMC7721 with IC_{50} > 10 μM. However, compound **1** significantly stimulated the expression of filaggrin and caspase-14 in HaCaT cells with a dose dependent manner (**Figure 6**). Filaggrin is a key natural moisturizing factor that maintains the ability to regulate the skin moisture barrier (Rawlings and Harding, 2004), while the mutation of the filaggrin gene resulted in skin losing water to allow the entrance of bacteria, leading to allergies, irritation and infection (Nomura et al., 2007). Caspase-14 deficiency was associated with the accumulation of incompletely degraded filaggrin fragments within the stratum corneum, decreased stratum corneum hydration, increased transepidermal water loss, and sensitivity to UVB photodamage (Eckhart and Tschachler, 2011). To test the skin protective activity against UVB irradiation, the cytotoxicity of **1** against HaCaT cells was measured by the MTT assay. The cell viability was decreased to 70% compared to the normal group after exposure to UVB 30 mJ/cm^2. Treatment of the damaged cells with compound **1** (20 μM) resulted in the cell viability increasing to 77%, while the positive control epigallocatechin gallate increased the cell viability to 75% at the same dose. This finding indicated that compound **1** is able reduce the UVB-induced cell damage.

Compounds **2** and **3** showed moderate inhibition toward NO production in LPS-induced RAW 264.7 macrophages (**Table 3**). In addition, compounds **3–5** (10 μM) inhibited the DNA expression of the HBV virus in HepG2.2.15 cells with the inhibitory rates of 25, 15, and 10%, respectively, whereas lamivudine as a positive control exerted the inhibitory rate of 75% in the same dose (Supporting Information, Figure S8).

DISCUSSION

In present work, we reported *P. brasilianum* WZXY-m122-9 to be obtained from a marine sponge for the first time. It provides a new source to produce austin-related

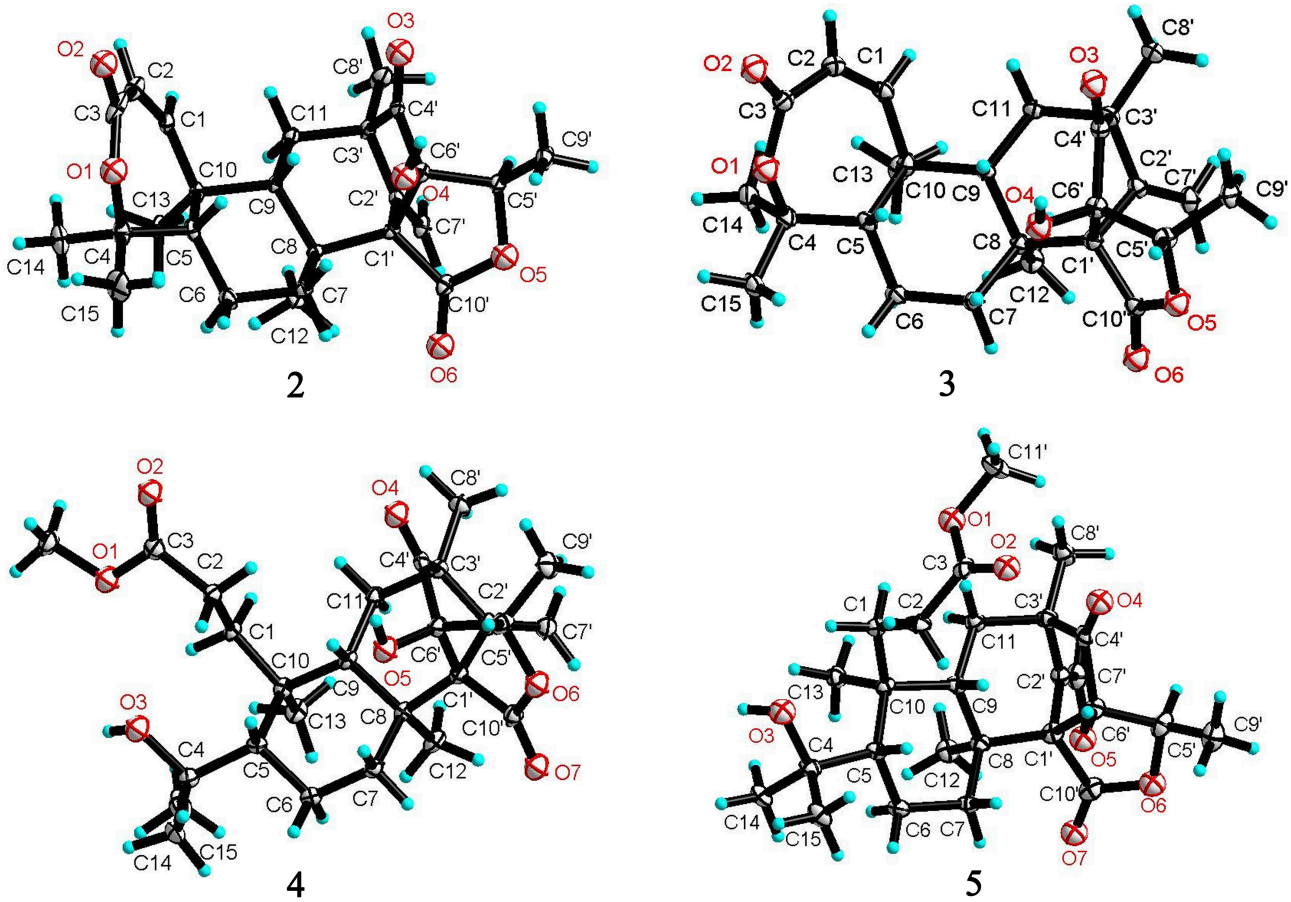

FIGURE 5 | X-ray crystallographic structures of **2-5**.

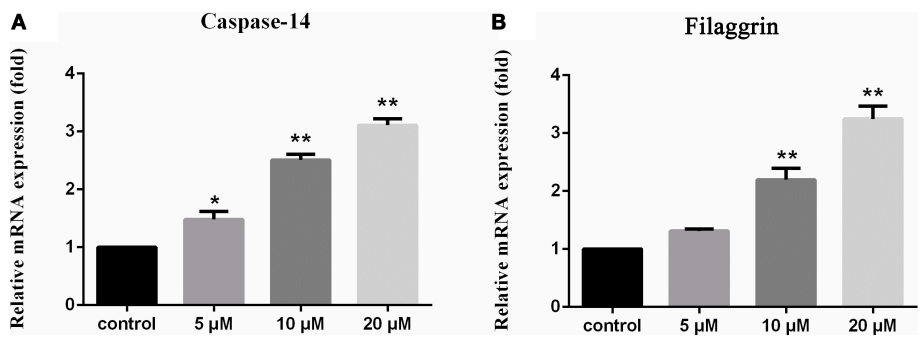

FIGURE 6 | Upregulation of caspase 14 and filaggrin in HaCaT cells induced by **1** 1% DMSO for the dissolution of compounds is used as the control. The vertical axis represents the expression of caspase-14 **(A)** and filaggrin **(B)** in HaCaT cells, and the horizontal axis means the doses of compound **1**. Statistical significances were considered at the $^{*}P < 0.05$ and $^{**}P < 0.01$ levels.

meroterpenenes with the uniquely modified structures, implying the same fungal species from different origins activating distinct biosynthetic pathway or enzyme function. Since austin-related meroterpenenes have been reported to possess insecticide and antibiotic activities, the sponge-associated fungus may generate the relevant metabolites to play chemoecological role in the association with host for the defense of micro- or macro-organism invasion.

The early-stage in the biosynthesis of **1**–**6** was considered to follow the similar pathway of austin (Scott et al., 1986; Ahmed et al., 1989). The PKS synthesizes DMOA, which followed by farnesylation, methylesterification, epoxidation, terpene

cyclization, Baeyer-Villiger oxidation to yield preaustinoid A1 (a product coexisted with **1**–**6** in the fungal strain) (Itoh et al., 2012). The latter compound can be converted to preaustinoid A2 by dehydrogenation. Compounds **1** and **6** presented as unique scaffold with γ-lactone unit in ring A. Both compounds were biogenetically presumed to be converted from preaustinoid A2 by the radical-based pathway, similar to the case for the biotransformation of preandiloid C to andiconin (Matsuda et al., 2014). During the formation of γ-lactone, Me-15 in preaustinoid A2 was catalyzed by a Fe(II)/α-KG-dependent dioxygenase to yield a radical intermediate, which subsequently formed a C-15/C-2 bond with the electron-rich olefin at C-2 to generate an intermediate with a free radical at C-1. The latter carbon was hydroxylated to yield compound **1**. The formation of γ-lactone in **6** was suggested to follow the similar manner as for **1**. Conversion of preaustinoid A2 to **2** and **3** was presumably mediated by the enzymes as the case of the biotransformation from preaustinoid A3 to austinol. Coexistence of C-5′ epimers (**2**, **3**) with equal amount suggested that the stereogenic selection for the reduction of ketone at C-5′ to hydroxy group is unspecific. Compounds **4** and **5** are regarded to be derived from preaustinoid A1, which followed the similar rearrangement as that for the conversion of preaustinoid A2 to **2** and **3**. We isolated a dioxygenase from the fungus, which was identical to AusE (Matsuda et al., 2013; Valiante et al., 2017). The dioxygenase can convert preaustinoid A2 to preaustinoid A3 in vitro experiment. However, The transformation of preaustinoid A2 to **1** or **6** was unsuccessful. This data suggested that the other Fe(II)/α-KG-dependent dioxygenase is required for the generation of the methylene bridge in **1** and **6**. The methyl ester of **4** and **5** is derived by the hydrolysis of the lactone in ring-A to yield a carboxylic acid at the side chain, and then methyl esterification (**Scheme 1**). Although we found **4** and **5** in the HPLC chromatographic profile of EtOAc extract, whether both compounds to be derived by enzymatic step are uncertain.

TABLE 3 | Inhibitory effects against LPS induced NO production in RAW264.7 macrophages.

Compounds	NO inhibition % (50 μM)	IC_{50} (μM)	CC_{50} (μM)
		NO	Cytotoxicity
1	14		>100
2	58	37.69 ± 5.25	>100
3	65	33.76 ± 3.13	>100
4	32		>100
5	36		>100
6	22		>100
7	28		>100
8	14		>100
Aminoguanidine		7.62 ± 0.08	—

IC_{50}, 50% inhibitory concentration; CC_{50}, 50% cytotoxic concentration.

CONCLUSION

In conclusion, compounds **1** and **6** possess unprecedented skeleton featuring the formation of C-2/C-15/C-4 bridge in ring A, while **2** and **3** with 7/6/6/5/5 pentacyclic skeletons of meroterpenoids are found from nature for the first time. The bioassay results indicated that the structural variation directly induced the bioactive spectrum. Compound **1** is the first example of natural products used to promote filaggrin and caspase-14

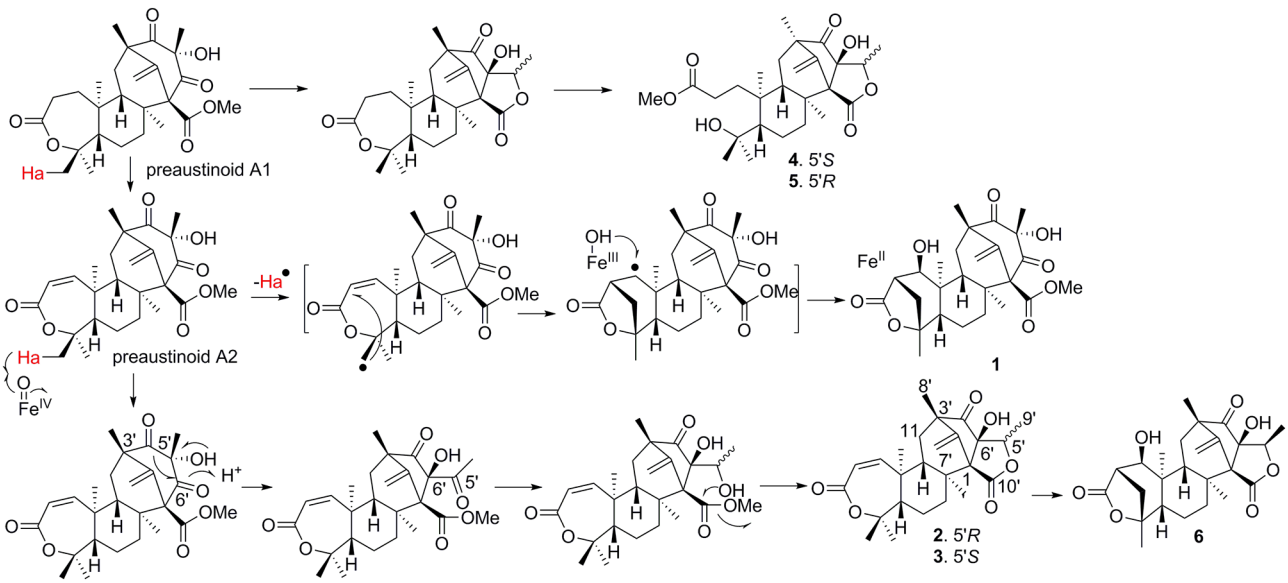

SCHEME 1 | Proposal of putative biosynthetic pathways for the compounds.

expression for the protection of the UVB-induced cell damage, suggesting that it is a promising lead for the treatment of dermatological diseases.

AUTHOR CONTRIBUTIONS

JZ responses for the isolation of compounds. BY performed the biogenetic approach for synthetic gene screening. DL took the antiviral bioassay. SG assayed for the regulation of filaggrin and caspase-14. PP helped to revise the manuscript. WL elucidated the structures and edited the manuscript.

FUNDING

Financial supports from the MOST-973 program (2015CB755906) and the National Natural Science Foundation of China (81630089, 41376127, U1606403) are highly appreciated.

SUPPLEMENTARY MATERIAL

The Supplementary Material for this article can be found online at: https://www.frontiersin.org/articles/10.3389/fchem.2018.00314/full#supplementary-material

REFERENCES

Ahmed, S. A., Scott, F. E., Stenzel, D. J., Simpson, T. J., Moore, R. N., Trimble, L. A., et al. (1989). Studies on te biosynthesis of the mycotoxin austin, a meroterpenoid metabolite of *Aspergillus ustus*. *J. Chem. Soc. Perkin Trans.* 1. 4, 807–816.

Bazioli, M. J., Amaral, L. D. S., Fill, T. P., and Rodrigues-Filho, E. (2017). Insights into *Penicillium brasilianum* secondary metabolism and its biotechnological potential. *Molecules* 22:e858. doi: 10.3390/molecules22060858

Ding, Y., Li, X., and Ferreira, D. (2007). Theoretical calculation of electronic circular dichroism of the rotationally restricted 3,8-biflavonoid morelloflavone. *J. Org. Chem*. 72, 9010–9017. doi: 10.1021/jo071134z

dos Santos, R. M., and Rodrigues-Fo, E. (2003). Further meroterpenes produced by *Penicillium* sp., an endophyte obtained from melia azedarach. *Z. Naturforsch. C* 58, 663–669. doi: 10.1515/znc-2003-9-1012

Duan, R., Zhou, H., Yang, Y., Li, H., Dong, J., Li, X., et al. (2016). Antimicrobial meroterpenoids from the endophytic fungus *Penicillium* sp. T2-8 associated with *Gastrodia elata*. *Phytochem. Lett*. 18, 197–201. doi: 10.1016/j.phytol.2016.10.013

Eckhart, L., and Tschachler, E. (2011). Cuts by caspase-14 control the proteolysis of filaggrin. *J. Invest. Dermatol*. 131, 2173–2175. doi: 10.1038/jid.2011.282

Geris, R., and Simpson, T. J. (2009). Meroterpenoids produced by fungi. *Nat. Prod. Rep*. 26, 1063–1094. doi: 10.1039/b820413f

Geris dos Santos, R. M., and Rodrigues-Fo, E. (2002). Meroterpenes from *Penicillium* sp. found in association with melia azedarach. *Phytochemistry* 61, 907–912. doi: 10.1016/S0031-9422(02)00379-5

Guo, C. J., Knox, B. P., Chiang, Y. M., Lo, H. C., Sanchez, J. F., Lee, K. H., et al. (2012). Molecular genetic characterization of a cluster in A. terreus for biosynthesis of the meroterpenoid terretonin. *Org. Lett*. 14, 5684–5687. doi: 10.1021/ol302682z

Iida, M., Ooi, T., Kito, K., Yoshida, S., Kanoh, K., Shizuri, Y., et al. (2008). Three new polyketide-terpenoid hybrids from *Penicillium* sp. *Org. Lett*. 10, 845–848. doi: 10.1021/ol7029867

Itoh, T., Tokunaga, K., Radhakrishnan, E. K., Fujii, I., Abe, I., Ebizuka, Y., et al. (2012). Identification of a key prenyltransferase involved in biosynthesis of the most abundant fungal meroterpenoids derived from 3,5-dimethylorsellinic acid. *ChemBioChem* 13, 1132–1135. doi: 10.1002/cbic.201200124

Lo, H. C., Entwistle, R., Guo, C. J., Ahuja, M., Szewczyk, E., Hung, J. H., et al. (2012). Two separate gene clusters encode the biosynthetic pathway for the meroterpenoids austinol and dehydroaustinol in *Aspergillus nidulans*. *J. Am. Chem. Soc*. 134, 4709–4720. doi: 10.1021/ja209809t

Matsuda, Y., and Abe, I. (2016). Biosynthesis of fungal meroterpenoids. *Nat. Prod. Rep*. 33, 26–53. doi: 10.1039/C5NP00090D

Matsuda, Y., Awakawa, T., Wakimoto, T., and Abe, I. (2013). Spiro-ring formation is catalyzed by a multifunctional dioxygenase in austinol biosynthesis. *J. Am. Chem. Soc*. 135, 10962–10965. doi: 10.1021/ja405518u

Matsuda, Y., Iwabuchi, T., Fujimoto, T., Awakawa, T., Nakashima, Y., Mori, T., et al. (2016). Discovery of key dioxygenases that diverged the paraherquonin and acetoxydehydroaustin pathways in *Penicillium brasilianum*. *J. Am. Chem. Soc*. 138, 12671–12677. doi: 10.1021/jacs.6b08424

Matsuda, Y., Iwabuchi, T., Wakimoto, T., Awakawa, T., and Abe, I. (2015). Uncovering the unusual D-ring construction in terretonin biosynthesis by collaboration of a multifunctional cytochrome P450 and a unique isomerase. *J. Am. Chem. Soc*. 137, 3393–3401. doi: 10.1021/jacs.5b00570

Matsuda, Y., Wakimoto, W., Mori, T., Awakawa, T., and Abe, I. (2014). Complete biosynthetic pathway of anditomin: nature's sophisticated synthetic route to a complex fungal meroterpenoid. *J. Am. Chem. Soc*. 136, 15326–15336. doi: 10.1021/ja508127q

Mori, T., Iwabuchi, T., Hoshino, S., Wang, H., Matsuda, Y., and Abe, I. (2017). Molecular basis for the unusual ring reconstruction in fungal meroterpenoid biogenesis. *Nature Chem. Biol*. 13, 1066–1073. doi: 10.1038/nchembio.2443

Nielsen, K. F., Dalsgaard, P. W., Smedsgaard, J., and Larsen, T. O. (2005). Andrastins A-D, *Penicillium roqueforti* metabolites consistently produced in blue-mold-ripened cheese. *J. Agric. Food Chem*. 53, 2908–2913. doi: 10.1021/jf047983u

Nomura, T., Sandilands, A., Akiyama, M., Liao, H., Evans, A. T., Sakai, K., et al. (2007). Unique mutations in the filaggrin gene in Japanese patients with ichthyosis vulgaris and atopic dermatitis. *J. Allergy Clin. Immunol*. 119, 434–440. doi: 10.1016/j.jaci.2006.12.646

Okuyama, E., Yamazaki, M., and Katsube, Y. (2008). Funigatonin, a new meroterpenoid from *Aspergillus fumigatus*. *Tetra. Lett*. 25, 3233–3234. doi: 10.1016/S0040-4039(01)91018-4

Park, J. S., Quang, T. H., Yoon, C. S., Kim, H. J., Sohn, J. H., and Oh, H. (2018). Furanoaustinol and 7-acetoxydehydroaustinol: new meroterpenoids from a marine-derived fungal strain *Penicillium* sp. SF–5497. *J. Antibiot*. 71, 557–563. doi: 10.1038/s41429-018-0034-2

Qi, B., Liu, X., Mo, T., Zhu, Z., Li, J., Wang, J., et al. (2017). 3,5-Dimethylorsellinic acid derived meroterpenoids from *Penicillium chrysogenum* MT-12, an endophytic fungus isolated from *Huperzia serrata*. *J. Nat. Prod*. 80, 2699–2707. doi: 10.1021/acs.jnatprod.7b00438

Rank, C., Phipps, R. K., Harris, P., Fristrup, P., Larsen, T. O., and Gotfredsen, C. H. (2008). Novofumigatonin, a new orthoester meroterpenoid from *Aspergillus novofumigatus*. *Org. Lett*. 10, 401–404. doi: 10.1021/ol7026834

Rawlings, A. V., and Harding, C. R. (2004). Moisturization and skin barrier function. *Dermatol. Ther*. 17, 43–48. doi: 10.1111/j.1396-0296.2004.04S1005.x

Scott, F. E., Simpson, T. J., Trimble, L. A., and Vederas, J. C. (1986). Biosynthesis of the meroterpenoid austin, by *Aspergillus ustus*: synthesis and incorporation of carbon-13,oxygen-18-labeled ethyl 3,5-dimethylorsellinate. *J. Chem. Soc. Chem. Commun*. 3, 214–215.

Silva, D. E., Williams, D. E., Jayanetti, D. R., Centko, R. M., Patrick, B. O., Wijesundera, R. L. C., et al. (2011). Dhilirolides A-D, meroterpenoids produced in culture by the fruit-infecting fungus *Penicillium purpurogenum* collected in Sri Lanka. *Org. Lett*. 13, 1174–1177. doi: 10.1021/ol200031t

Stephens, P. J., and Harada, N. (2010). ECD cotton effect approximated by the Gaussian curve and other methods. *Chirality*. 22, 229–233. doi: 10.1002/chir.20733

Stierle, D. B., Stierle, A. A., Patacini, B., McIntyre, K., Girtsman, T., and Bolstad, E. (2011). Berkeleyones and related meroterpenes from a deep water acid mine waste fungus that inhibit the production of interleukin 1-β from induced inflammasomes. *J. Nat. Prod*. 74, 2273–2277. doi: 10.1021/np2003066

Valiante, V., Mattern, D. J., Schüffler, A., Horn, F., Walther, G., Scherlach, K. et al. (2017). Discovery of an extended austinoid biosynthetic pathway in *Aspergillus calidoustus*. *Chem. Biol*. 12, 1227–1234. doi: 10.1021/acschembio.7b00003

Wu, Z., Wang, Y., Liu, D., Proksch, P., Yu, S., and Lin, W. (2016). Antioxidative phenolic compounds from a marine-derived fungus *Aspergillus versicolor*. *Tetrahedron*. 72, 50–57. doi: 10.1016/j.tet.2015.10.038

Zhang, Y., Li, X., Shang, Z., Li, C., Ji, N., and Wang, B. (2012). Meroterpenoid and diphenyl ether derivatives from *Penicillium* sp. MA-37, a fungus isolated from marine mangrove rhizospheric soil. *J. Nat. Prod*. 75, 1888–1895. doi: 10.1021/np300377b

Conflict of Interest Statement: The authors declare that the research was conducted in the absence of any commercial or financial relationships that could be construed as a potential conflict of interest.

frontiers in Chemistry

ORIGINAL RESEARCH
published: 14 August 2018
doi: 10.3389/fchem.2018.00344

Polyketides From the Endophytic Fungus *Cladosporium* sp. Isolated From the Mangrove Plant *Excoecaria agallocha*

Liping Wang[1,2†], *Xiuli Han*[2,3†], *Guoliang Zhu*[2], *Yi Wang*[2], *Arthit Chairoungdua*[4], *Pawinee Piyachaturawat*[4] *and Weiming Zhu*[1,2,5*]

[1] State Key Laboratory of Functions and Applications of Medicinal Plants, Guizhou Medical University, Guiyang, China, [2] Key Laboratory of Marine Drugs, Ministry of Education of China, School of Medicine and Pharmacy, Ocean University of China, Qingdao, China, [3] College of Life Sciences, Shandong University of Technology, Zibo, China, [4] Department of Physiology, Faculty of Science, Mahidol University, Bangkok, Thailand, [5] Laboratory for Marine Drugs and Bioproducts of Qingdao National Laboratory for Marine Science and Technology, Qingdao, China

OPEN ACCESS

Edited by:
Xian-Wen Yang,
Third Institute of Oceanography, State Oceanic Administration, China

Reviewed by:
Massuo Jorge Kato,
Universidade de São Paulo, Brazil
Roberta Teta,
Università degli Studi di Napoli Federico II, Italy

***Correspondence:**
Weiming Zhu
weimingzhu@ouc.edu.cn

[†] These authors have contributed equally to this work

Specialty section:
This article was submitted to Medicinal and Pharmaceutical Chemistry, a section of the journal Frontiers in Chemistry

Received: 08 June 2018
Accepted: 23 July 2018
Published: 14 August 2018

Citation:
Wang L, Han X, Zhu G, Wang Y, Chairoungdua A, Piyachaturawat P and Zhu W (2018) Polyketides From the Endophytic Fungus Cladosporium sp. Isolated From the Mangrove Plant Excoecaria agallocha. Front. Chem. 6:344. doi: 10.3389/fchem.2018.00344

Five new polyketides (**2**–**6**) and ten known compounds (**1** and **7**–**15**) were obtained from the fermentation products of the endophytic fungus *Cladosporium* sp. OUCMDZ-302 with the mangrove plant, *Excoecaria agallocha* (Euphorbiaceae). The new structures of **2**–**6** were established on the basis of ECD, specific rotation and spectroscopic data as well as the chemical calculation. Compound **7** showed cytotoxicity against H1975 cell line with an IC_{50} value of 10.0 μM. Compounds **4** and **8**–**10** showed radical scavenging activity against DPPH with the IC_{50} values of 2.65, 0.24, 5.66, and 6.67 μM, respectively. In addition, the absolute configuration of compound **1** was solidly determined by X-ray and sugar analysis of the acidic hydrolysates for the first time as well as those of compounds **8**–**10** in this paper.

Keywords: *Cladosporium* sp., mangrove fungus, *Excoecaria agallocha*, polyketides, anti-oxidation

INTRODUCTION

Mangrove plants and endophytic fungi are two principal sources of new and bioactive natural products (Zhang et al., 2006; Wu et al., 2008). *Excoecaria agallocha* (Euphorbiaceae), also known as blind-your-eye, is mainly used to treat sores and stings. More than 72 cytotoxic diterpenoids have been identified from *E. agallocha*, structurally belonging to labdane (Konishi et al., 1999, 2003; Anjaneyulu and Rao, 2000; Annam et al., 2015), isopimarane/*ent*-isopimarane (Anjaneyulu et al., 2003; Wang and Guo, 2004; Kang et al., 2005; Wang et al., 2005; Gowri Ponnapalli et al., 2013), atisane/*ent*-atisane (Konishi et al., 2000; Wang et al., 2009), *ent*-kaurane (Anjaneyulu et al., 2002; Li et al., 2010), and beyerane-type (Anjaneyulu et al., 2002).

In our ongoing investigations of new and bioactive compounds from endophytes associated with mangrove plants (Lin et al., 2008; Lu et al., 2009, 2010; Wang et al., 2012; Kong et al., 2014; Zhu et al., 2018), an endogenous fungal strain OUCMDZ-302 identified as *Cladosporium* sp., was isolated from the surface-sterilized stems of *E. agallocha*. The secondary metabolites of the genus *Cladosporium* were mainly reported as polyketides derivatives, such as macrolides (Jadulco et al., 2001; Zhang et al., 2001; Shigemori et al., 2004), α-pyrones (Jadulco et al., 2002), α-pyridone (Ye et al., 2005), and binaphthyl derivatives (Sakagami et al., 1995).

Herein we report five new polyketides (**2**–**6**) (**Figure 1**) isolated from the EtOAc extract of *Cladosporium* sp. OUCMDZ-302, along with the ten known structures (**Figure S36** and **Table S1**), (2*R*)-7-*O*-α-D-ribofuranosyl-5-hydroxy-2-methylchroman-4-one (**1**) (Hu et al., 2017), 7-*O*-α-D-ribosyl-5-hydroxy-2-propylchromone (**7**) (Zhao et al., 2015), 3-(2,3-dihydroxy phenoxy)butanoic acid (**8**) (Dai et al., 2009), (2*S*,4*S*)-4-methoxy-2-methylchroman-5-ol (**9**) (Wu et al., 2010), (2*S*,4*S*)-2-methylchroman-4,5-diol (**10**) (Teles et al., 2005), (±)-5,7-dihydroxy-2-methyl chroman-4-one (**11**) (Rao et al., 1994), (±)-5-hydroxy-2-methylchroman-4-one (**12**) (Dai et al., 2006), 1-(2,6-dihydroxyphenyl) ethanone (**13**) (Dhami and Stothers, 1965), 1-(2,6-dihydroxyphenyl)-1-butanone (**14**) (Huang et al., 2005), and 2-butyryl-3,5-dihydroxycyclohex-2-enone (**15**) (Igarashi et al., 1993). Compound **7** showed inhibitory activity against H1975 cell line with an IC_{50} value of 10.0 μM. Compounds **4** and **8**–**10** exhibited radical scavenging activity against DPPH with IC_{50} values of 2.65, 0.24, 5.66, and 6.67 μM, respectively. In addition, the absolute configurations of compounds **8**–**10** were resolved and that **1** was solidified in this paper.

MATERIALS AND METHODS

General Experimental Procedures

The NMR, ECD, $[\alpha]_D$, UV and IR spectra were recorded on JEOL JNM-ECP 600, JASCO J-810, JASCO P-1020 digital, Beckman DU® 640 and Nicolet NEXUS 470 spectrophotometers, respectively. ESI-MS, EI-MS and GC-MS were measured on Q-TOF ULTIMA GLOBAL GAA076 LC, VG Autospec-3000 and Agilent 6890/5973 spectrometers, respectively. Semipreparative HPLC and chiral separation was performed on a YMC-pack ODS-A column [10 × 250 mm, 5 μm, 4 mL/min] and a CHIRALPAK IA column [20 × 250 mm, 5 μm, 10 mL/min]. TLC was performed on plates precoated with silica gel GF254 (10–40 μm). The column chromatography (CC) was performed over silica gel (200–300 mesh, Qingdao Marine Chemical Factory, Qingdao, China) and Sephadex LH-20 (Amersham Biosciences, Sweden), respectively. The seawater for the cultural medium of *Cladosporium* sp. OUCMDZ-302 was collected from Yellow Sea near Qingdao.

Fungal Material

The strain *Cladosporium* sp. OUCMDZ-302 was isolated from the surface sterilized stems of the mangrove plant *E. agallocha* grown in Wenchang, Hainan, China. Briefly, the stems were washed with tap water and sterile distilled water in sequence. The stems with clean surface were further sterilized in a sequence of 75% ethanol for 2 min, 0.1% of $HgCl_2$ for 3 min, and sterile distilled water. The outer bark was removed, and the inner bark was cut into small pieces that were then placed on a potato dextrose agar (PDA) plate and cultured at 28°C for 3 days. A single colony was transferred to PDA media and was identified according to its morphological characteristics (**Figure S35**) by Prof. Kui Hong, Wuhan University. A voucher specimen is deposited in our laboratory at −80°C. The working strain was prepared on PDA slants and stored at 4°C.

Fermentation and Extraction

The producing fungal strain *Cladosporium* sp. OUCMDZ-302 was inoculated into a 500 mL cylindrical flask containing 100 mL of seawater consisting of 2% maltose, 2% mannitol, 1% glucose, 1% monosodium glutamate, 0.3% yeast extract, 0.1% corn flour, 0.05% KH_2PO_4, 0.03% $MgSO_4 \cdot 7H_2O$ (pH 6.5) and cultured at 28°C for 48 h on a rotary shaker at 120 rpm. The seed culture was transferred into three hundred and fifty 500 mL conical flasks (200 mL/flask) containing the same medium, and performed at 28°C for 7 days on rotary shakers at 160 rpm. The whole fermentation broth (70 L) was filtered through cheese cloth to separate the mycelia from filtrate. The filtrate was concentrated to about one-quarter of the original volume under reduced pressure and then extracted three times with equal volumes of ethyl acetate (EtOAc) and concentrated to dryness. The mycelia were extracted three times with acetone and concentrated to an aqueous solution. The aqueous solution was subsequently extracted three times with equal volumes of EtOAc and concentrated. Both EtOAc extractions were combined to give 45 g of the extract.

Isolation

The extract (45 g) was separated into eight fractions (Fr.1–Fr.8) on a silica gel column (8.5 × 15 cm, 200–300 mesh) using a step gradient elution with $CHCl_3$-petroleum ether (V/V 0:100–100:0, 4 L) and then MeOH–$CHCl_3$ (V/V 0:100–100:0, 16 L). Fr.1 (5.4 g) was separated on a silica gel column (4.5×10 cm, 200–300 mesh) eluted with $CHCl_3$-petroleum ether (V/V, 1: 1, 3L) to give **12** (1g). Fr.3 (0.3 g) was further purified by semipreparative HPLC (60% MeOH/H_2O) to give **10** (7 mg, t_R 4.97 min). Fr.4 (4.3 g) was separated into two subfractions by column chromatography over silica gel (RP-18) eluting with gradient H_2O-MeOH (50–100%). Fr.4-1 (1.4 g) was separated by Sephadex LH-20 (3 × 75 cm, MeOH, 300 mL) to obtain three fractions (130 mL, Fr.4-1-1; 90 mL, Fr.4-1-2; 80 mL, Fr.4-1-3). Fr.4-1-2 (140 mg) was purified by semipreparative HPLC (30% MeOH/H_2O) to yield **5** (1 mg, t_R 8.24 min), **13** (30 mg, t_R 20.20 min), and **15** (5 mg, t_R 18.15 min). Fr.4-1-3 (190 mg) was purified by semipreparative HPLC (30% MeOH/H_2O, 0.15% CF_3CO_2H) to give **4** (15 mg, t_R 16.76 min) and **8** (30 mg, t_R 14.41 min). Fr.4-2 (360 mg) was purified by semipreparative HPLC (50% MeOH/H_2O) to give **6** (10 mg, t_R 12.28 min), and **14** (24 mg, t_R 18.12 min). Fr.5 (1.1 g) was separated into two subfractions by a silica gel column (2.6 × 10 cm, 200–300 mesh) eluted with MeOH–$CHCl_3$ (V/V 1:40, 1L). Fr.5-1 (40 mg) was purified by semipreparative HPLC (25% MeOH/H_2O) to give **3** (3 mg, t_R 6.76 min), and Fr.5-2 (80 mg) was purified by semipreparative HPLC (50% MeOH/H_2O, 0.15% CF_3CO_2H) to give compounds **11** (5 mg, t_R 6.78 min). Fr.6 (2.8 g) was separated into two subfractions by a silica gel column (4.5 × 10 cm, 200–300 mesh) eluted with $CHCl_3$-petroleum ether MeOH–$CHCl_3$ (V/V 1:25, 2L). Fr.6-1 (110 mg) was purified by semipreparative HPLC (60% MeOH/H_2O) to give **9** (10 mg, t_R 10.28 min). Fr.6-2 (340 mg) was purified by semipreparative HPLC (50% MeOH/H_2O) to give **7** (18 mg, t_R 13.55 min) and the mixture of **1** and **2** (70 mg, t_R 5.56 min). The mixture of **1** and **2** were further purified by a chiral column (Chiralpak IA,

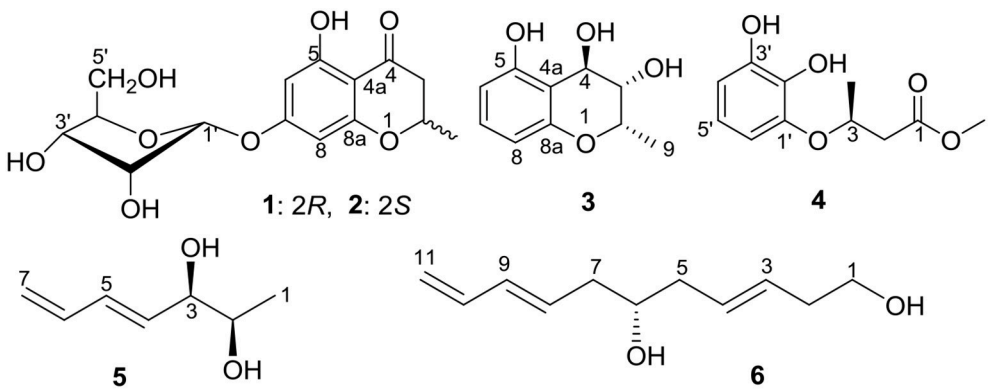

FIGURE 1 | The structure of compounds **1–6**.

MeOH–MeCN–EtOH 40:40:20) to yield compound **1** (35.4 mg, t_R 8.22 min) and **2** (23.7 mg, t_R 4.69 min).

ECD, $[\alpha]_D$ and Coupling Constant Calculation

Calculations for ECD and $[\alpha]_D$ were performed in HyperChem 7.5 and Gaussian 03 (Frisch et al., 2004; Chen et al., 2016; Jin et al., 2018). Karplus formula was used to compute the coupling constant (^3J) from the proton-proton torsion angle (Haasnoot et al., 1980).

Cytotoxic Assays

Cytotoxicities of compounds **1**–**14** against HL-60 and K562 cell lines were assayed by the MTT method (Mosmann, 1983), while those for BEL-7402, A549, HeLa, and H1975 cell lines were tested by SRB (Skehan et al., 1990) methods. Adriamycin was used as the positive control with the IC_{50} values of 0.02, 0.21, 0.48, 1.32, 0.32, and 0.38, respectively.

Anti-oxidant Activities

The anti-oxidant activities of compounds **1**–**14** were evaluated by DPPH assay *in vitro* (Wang et al., 2007). Vitamin C was used as the positive control with an IC_{50} value of 3.29 μM.

Antimicrobial Assays

The antimicrobial activities of compounds **1**–**14** against *E. coli*, *E. aerogenes*, *P. aeruginosa*, *B. subtilis*, and *C. albicans* were evaluated by an agar dilution method (Zaika, 1988). Ciprofloxacin lactate and ketoconazole was used as the positive controls for bacteria and fungi with MIC values of 4.0, 0.5, 32.0, 16.0, 4.1 μg/mL, respectively.

RESULTS AND DISCUSSION

Identification of Compounds

Compounds **1** and **2** were first isolated as an isomeric mixture whose molecular formula was determined to be $C_{15}H_{18}O_8$ by HRESIMS at *m/z* 327.1068 $[M+H]^+$ (calcd 327.1080), indicating seven degrees of unsaturation. An interpretation of the 1D (**Table 1, Figures S1**–**S3**) and 2D NMR (**Figure 2** and **Figures S4**–**S6**) spectra established a pentose moiety and a benzopyrane moiety similar to those of 5,7-dihydroxy-2-methylchroman-4-one (**11**) (Rao et al., 1994). The upfield shift of C-7 (−1.5 ppm) and the key HMBC correlations between the anomeric proton ($\delta_{H-1'}$ 5.66/5.68) and C-7 (δ 165.1/165.0) indicated that **1** and **2** were 7-*O*-pentosides of **11**. Acidic hydrolysis of the mixture of **1** and **2** with 2 *M* HCl yielded (±)-**11** and D-ribose that was identified by GC-MS analysis of the reaction products with L-cysteine methyl ester and Me_3SiCl (**Figures S33**, **S34**) (Deyrup et al., 2007). These data indicated that **1** and **2** are a pair of epimers at C-2. Separation of 2-epimeric mixture of **1** and **2** was achieved on a chiral column using MeOH-MeCN-EtOH as eluent. And then, NMR data of optically-pure **1** (**Figures S7**, **S8**) and **2** (**Figures S9**, **S10**) were obtained. X-ray single crystal diffraction of **1** revealed the α-glycosidic bond and 2*R*-configuration (**Figure 3**). The ECD Cotton effects of compounds **1** and **2** were opposite in sign (**Figure 4**), confirming the opposite configuration of C-2. Thus, the structures of **1** and **2** were unambiguously elucidated as (2*R*)- and (2*S*)-7-*O*-α-D-ribofuranosyl-5-hydroxy-2-methylchroman-4-one, respectively. This is the first time that to solidify the absolute configuration of compound **1**, although it was reported last year (Hu et al., 2017).

The molecular formula of compound **3** was determined to be $C_{10}H_{12}O_4$ based on the HRESIMS peak at *m/z* 195.0659 $[M-H]^-$ (calcd 195.0657), indicating five degrees of unsaturation. The NMR data (**Table 1**, **Figures S11**–**S14**) was similar to those of **10** (Teles et al., 2005), except for the upfield methylene signal at $\delta_{H/C}$ 1.50 & 1.88/38.0 that was replaced by the one of an oxygenated methine at $\delta_{H/C}$ 3.45/69.8. This was further supported by the ^1H-^1H COSY from H-9 (δ 1.31) to H-4 (δ 4.48) through H-2 (δ 4.14) and H-3 (δ 3.45) (**Figure 2** and **Figure S15**), and the key HMBC correlations of H-9 to C-3 (δ 69.8) and H-3 to C-4a (δ 111.2) (**Figure 2** and **Figure S16**). In order to confirm the relative configuration, we calculated the coupling constant of H_2-H_3 and H_3-H_4 for the four possible relative configurations **3A**–**3D** (**Figure 5**). The computational ^3J value of **3A** was most near to the measured result (**Table 3**).

TABLE 1 | ^{1}H (600 MHz) and ^{13}C (150 MHz) NMR Data of Compounds **1**–**4** in DMSO-d_6.

No.	1		2		3		4[a]	
	δ_C	δ_H(*J* in Hz)	δ_C	δ_H(*J* in Hz)	δ_C	δ_H(*J* in Hz)	δ_C	δ_H(*J* in Hz)
2	73.9, CH	4.61(ddq, 12.3, 6.3, 3.1)	74.0, CH	4.61(ddq, 12.3, 6.3, 3.1)	69.0, CH	4.14 dq(6.6, 0.8)	40.7, CH_2	2.79 (dd, 16.5, 8.8) 2.63 (dd, 16.5, 3.3)
3	42.5, CH_2	2.80 (dd,17.2, 12.3) 2.65 (dd, 17.2, 3.1)	42.6, CH_2	2.81 (dd, 17.2,12.3) 2.64 (dd,17.2, 3.1)	69.8, CH	3.45 brs	73.4, CH	4.47 (m)
4	197.3, C		197.3, C		62.6, CH	4.48 (d, 2.2)	19.5, CH_3	1.34 (d, 6.6)
4a	102.9, C		102.9, C		111.2, C			
5	162.6, C		162.7, C		158.3, C			
6	96.6, CH	6.11 (d, 2.2)	96.7, CH	6.11 (d, 2.2)	107.1, CH	6.18(dd, 8.3, 1.1)		
7	165.1, C		165.1, C		128.8, CH	6.91(dd,8.3, 8.2)		
8	95.6, CH	6.10 (d, 2.2)	95.6, CH	6.09 (d, 2.2)	106.8, CH	6.32(dd, 8.2, 1.1)		
8a	162.9, C		162.9, C		156.1, C			
9	20.4, CH_3	1.40 (d, 6.3)	20.4, CH_3	1.40 (d, 6.3)	17.5, CH_3	1.31 (d, 6.6)		
1'	99.9, CH	5.67 (d, 4.5)	99.9, CH	5.65 (d, 4.5)			143.9, C	
2'	71.5, CH	4.07 (m)	71.5, CH	4.07(m)			136.6, C	
3'	69.2, CH	3.91 (dd, 6.3, 3.9)	69.2, CH	3.91 (m)			145.5, C	
4'	86.6, CH	3.94 (dd, 7.6, 3.9)	86.6, CH	3.94 (m)			110.7, CH	6.70 (dd, 7.7, 2.2)
5'	61.4, CH_2	3.47 (m)	61.5, CH_2	3.46(m)			119.0, CH	6.68 (t, 7.7)
6'							113.0, CH	6.52 (dd, 7.7, 2.2)
CH_3O-							52.5, CH_3	3.78 (s)

[a] *Measured in $CDCl_3$ and δ_{C-1} was 174.0.*

The absolute configuration was established by calculation of the specific rotation. The measured $[\alpha]_D$ value of **3** (−53.6) is consistent with the calculated one for (2*S*,3*S*,4*R*)-**3** (−100) and opposite to the calculated one for (2*R*,3*R*,4*S*)-**3** (+102). Thus, the structure of **3** was identified as (2*S*,3*S*,4*R*)-2-methylchroman-3,4,5-triol.

Compound **4** showed the molecular formulae of $C_{11}H_{14}O_5$ based on HRESIMS peaks at *m*/*z* 225.0767 $[M-H]^-$ (calcd 225.0763), indicating five degrees of unsaturation. The 1D (**Figures S17**–**S19**) and HMQC (**Figure S20**) NMR spectra of **4** displayed three sp^2 methines and four sp^2 quaternary carbon signals, one sp^3 oxygenated methine signals, one sp^3 methylene signals and two methyl group (including one methoxy). The 1D NMR data (**Table 1**) of **4** were almost identical to those of **8** [**Figure S1**; (Dai et al., 2009)] except for an additional methoxy ($\delta_{H/C}$ 3.78/52.5) and the upfield shift for carbonyl carbon (−3.5 ppm), indicating that **4** is the methyl ester of **8**. This was confirmed by analysis of ^{1}H-^{1}H COSY correlation (**Figure S21**) and the key HMBC between the methoxy protons at δ_H 3.78 and the carbonyl carbon at δ_{C-1} 174.0 (**Figure 2** and **Figure S22**). The specific rotations of both **4** ($[\alpha]_D$ +14.4) and **8** ($[\alpha]_D$ +8.2) were opposite to the synthetic analog, *R*-3-(3-methoxyphenyloxy)butanoic acid ($[\alpha]_D$ −31.2) (Kawasaki et al., 2008), indicating both **4** and **8** as *S*-configuration. The *S*-configuration of **4** was also backed by the coincidence of experimental and calculated ECD curves (**Figure 6**). Thus, the structure of compounds **4** and **8** were established as methyl (3*S*)-3-(2,3-dihydroxyphenyloxy) butanoate and (3*S*)-3-(2,3-dihydroxyphenyloxy)butanoic acid, respectively.

TABLE 2 | ^{1}H (600 MHz) and ^{13}C (150 MHz) NMR Data of Compounds **5** and **6** in DMSO-d_6.

Position	5		6[a]	
	δ_C	δ_H(*J* in Hz)	δ_C	δ_H(*J* in Hz)
1	19.1, CH_3	1.01 (d, 6.1)	61.9, CH_2	3.65 (dt, 6.0, 2.2)
2	69.7, CH	3.46 (m)	36.0, CH_2	2.31 (m)
3	75.1, CH	3.77 (dd, 6.0, 6.0)	129.4, CH	5.52 (dt, 15.4, 6.6)
4	130.2, CH	5.81 (dd, 15.4, 6.0)	130.2, CH	5.56 (dt, 15.4, 6.6)
5	136.1, CH	6.18 (dd, 15.4, 9.9)	40.1, CH_2	2.15 (ddd, 14.3, 7.7, 6.6); 2.27 (m)
6	137.0, CH	6.34(ddd,17.0, 10.4, 9.9)	70.4, CH	3.69 (m)
7	116.2, CH_2	5.03 (dd, 10.4, 1.7) 5.17 (dd, 17.0, 1.7)	40.2, CH_2	2.24 (ddd,14.3, 7.7, 7.1) 2.31 (m)
8			130.5, CH	5.70 (dt, 14.8, 7.6)
9			134.2, CH	6.14 (dd, 14.8, 10.4)
10			136.9, CH	6.33 (ddd,17.0,10.4,10.4)
11			116.1, CH_2	4.14 (d,17.0) 5.02 (d,10.4)

[a] *Measured in $CDCl_3$.*

The molecular formula of compound **5** was determined as $C_7H_{12}O_2$ based on the HREIMS peak at *m*/*z* 128.0845 $[M]^+$ (calcd 128.0837), corresponding to two degrees of unsaturation. The IR spectrum showed hydroxy groups at 3442 cm^{-1} and double bonds at 3080 and 1646 cm^{-1}. The 1D NMR spectra

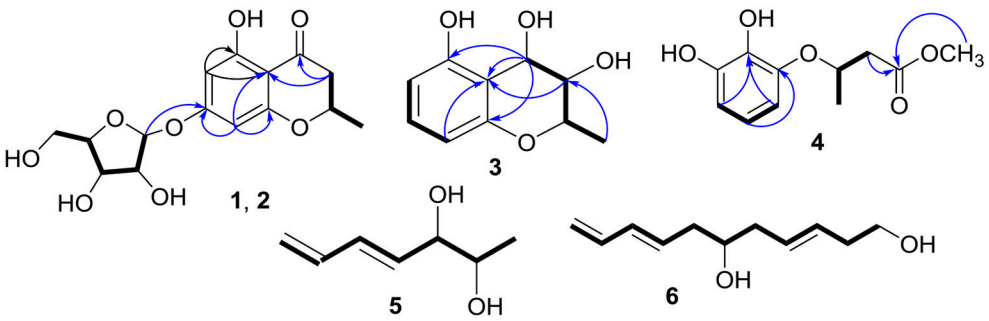

FIGURE 2 | Key HMBC (→) and ^{1}H–^{1}H COSY (–) correlations of **1**–**6**.

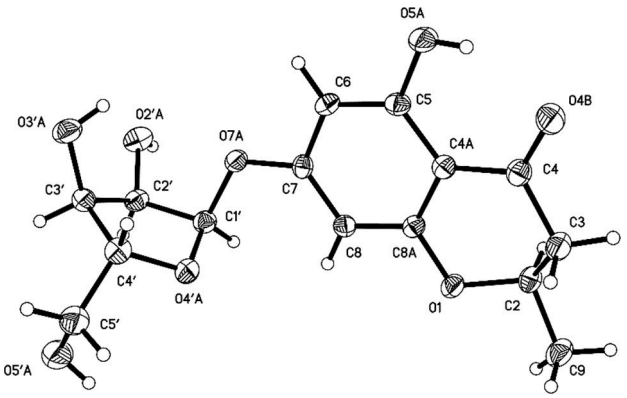

FIGURE 3 | Final X-ray Drawing of compound **1**.

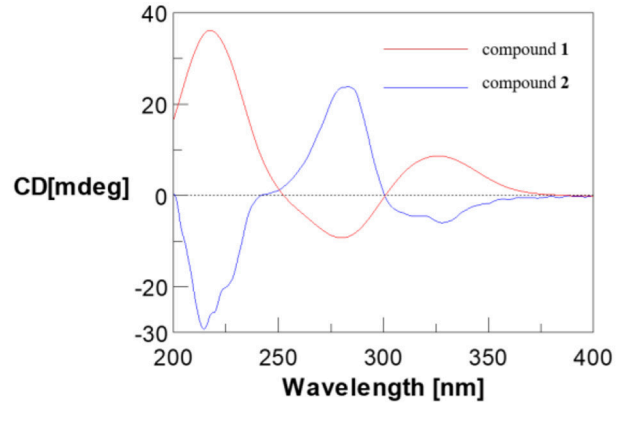

FIGURE 4 | ECD curve of compounds **1** and **2**.

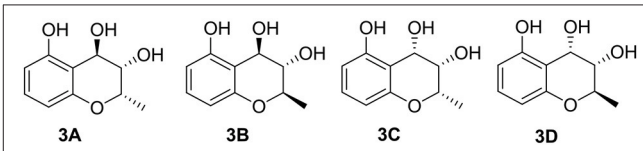

FIGURE 5 | Four possible relative configurations of compound **3**.

TABLE 3 | The calculated $^{3}J_{H-2,H-3}$ and $^{3}J_{H-3,H-4}$ values of compound **3** for the four possible relative configurations.

	H-2, H-3		H-3, H-4	
	Dihedral angle (°)	**^{3}J value (Hz)**	**Dihedral angle (°)**	**^{3}J value (Hz)**
3		0.8		2.2
3A	66.2	3.1	83.8	1.4
3B	173.0	8.0	166.8	7.4
3C	59.2	3.9	42.6	5.8
3D	37.4	6.2	9.0	7.1

(**Table 2**, **Figures S23**–**S25**) of **5** showed two double bonds one of which is terminal, two oxygenated methines and one methyl group (**Table 1**). These groups were connected to the full structure of CH_2 =CH–CH=CH–CH (OH)–CH (OH)–CH_3 on the basis of ^{1}H-^{1}H COSY correlations from the methyl (δ_H 1.01) to the methylene (δ_H 5.03/5.17) through the two oxygenated methines (**Figure 2** and **Figure S26**). The large value of $^{3}J_{H-4,H-5}$ (15.4 Hz) corresponded to *E*-Δ^4 double bond. The large $^{3}J_{H-2,H-3}$ value (6.0 Hz) and the downfield methyl carbon signal (δ_{C-1} 19.1) indicated an *anti*-conformation (Jarvis et al., 1996; Zhang and O'doherty, 2005; Nilewski et al., 2009), corresponding to *threo*-configuration of 2,3-diol (Zheng et al., 2010). In order to confirm the relative configuration of compound **5**, $^{3}J_{H-2,H-3}$ of *threo*-**5** and *erythro*-**5** were computed. The results showed that the predicted $^{3}J_{H-2,H-3}$ values of *threo*-**5** (5.5 Hz) matched with the measured one (6.0 Hz) while the calculated one of *erythro*-**5** (3.8 Hz) was inconsistent, indicating *threo*- configuration. The direction of the specific rotation of **5** ($[\alpha]_D$ −6.8) were similar to the structurally related t-butyl (6*S*,7*S*)-6,7-dihydroxyocta-2,4-dienoate ($[\alpha]_D$ −23) (Zhang and O'doherty, 2005), and opposite to t-butyl (6*R*,7*R*)-6,7-dihydroxyocta-2,4-dienoate ($[\alpha]_D$ +22.9) (Zhang and O'doherty, 2005). The structure of **5** was thus deduced as (2*S*,3*S*,4*E*)-hepta-4,6-diene-2,3-diol.

The molecular formula of compound **6** was determined to be $C_{11}H_{18}O_2$ based on the HREIMS peak at *m*/*z* 182.1305 $[M]^+$ (calcd. 182.1307), indicating three degrees of unsaturation. The EIMS of **6** illustrated in **Figure 7** indicates the existence of

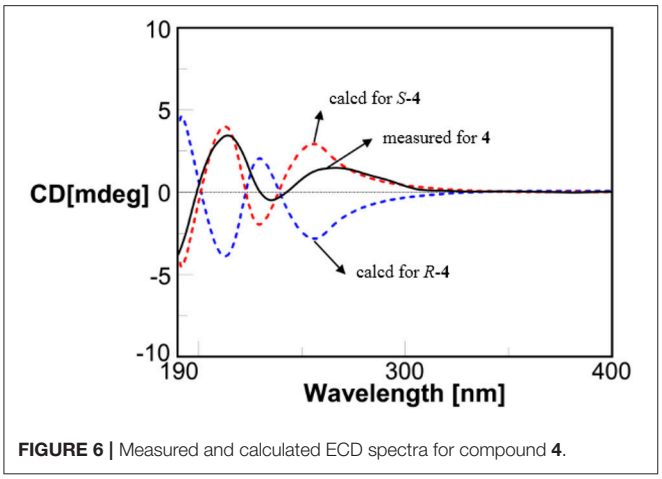

FIGURE 6 | Measured and calcated ECD spectra for compound **4**.

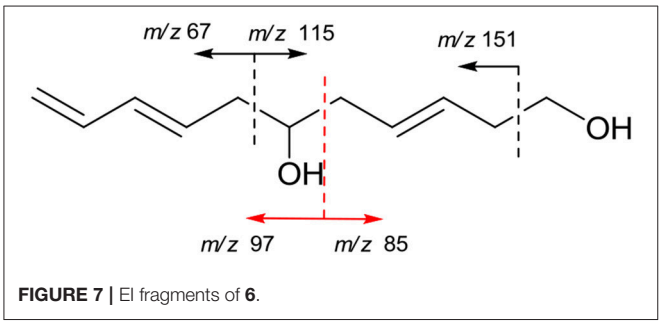

FIGURE 7 | EI fragments of **6**.

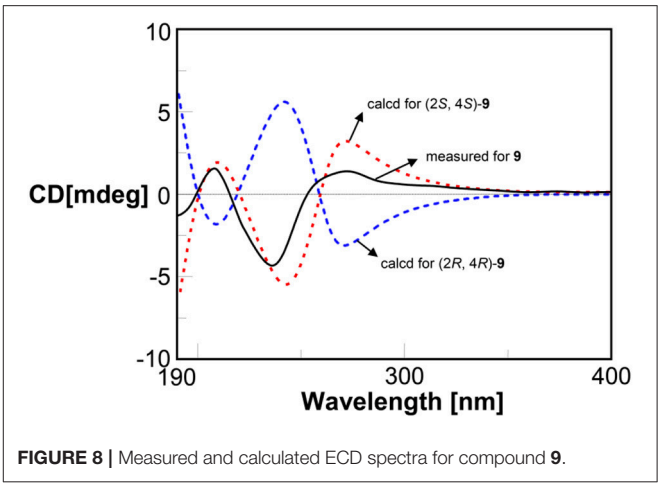

FIGURE 8 | Measured and calcated ECD spectra for compound **9**.

-CH_2OH, -C_6H_9O, and -C_5H_9O moieties. The ^1H (**Figure S27**) and ^{13}C (**Figure S28**) NMR spectra and DEPT (**Figure S29**) and HMQC (**Figure S30**) experiments of **6** revealed 11 signals including three double bonds one of which is terminal, one oxygenated methine, four methylenes one of which is oxygenated. The ^1H-^1H COSY (**Figure S31**) correlations from H-1 (δ 3.65) to H-11 (δ 4.14/5.02) in sequence established the structure, CH_2 =CH–CH=CH–CH_2-CH(OH)–CH_2-CH=CH–CH_2-CH_2OH, which was supported by HMBC correlations (**Figure S32**). The large values of $^3J_{H-3,H-4}$ (15.4 Hz) and $^3J_{H-8,H-9}$ (14.8 Hz) suggested that both Δ^3 and Δ^8 double bonds were *E*-configurations. The direction of specific rotation of **6** ($[\alpha]_D$ +2.0) is similar to that of (*S*)-dodeca-3,5-diene-1,7-diol ($[\alpha]_D$ +56) (Zhang and Kyler, 1989), suggesting *S*-configuration at C-6. Thus, the structure of **6** was deduced as (3*E*,8*E*,6*S*)-undeca-3,8,10-triene-1,6-diol.

The relative configurations of compounds **9** and **10** were determined as (–)-*trans*-4-methoxy-2-methylchroman-5-ol (Wu et al., 2010) and (–)-*trans*-2-methyl chroman-4,5 -diol (Teles et al., 2005), respectively. The absolute configuration of compound **9** was determined by quantum chemical ECD calculation. The measured ECD of **9** was coincident with the calculated ECD of (2*S*,4*S*)-**9** and opposite to ECD of (2*R*,4*R*)-**9** (**Figure 8**). Thus, compound **9** was established to be (2*S*,4*S*)-4-methoxy-2-methyl chroman-5-ol. The similar sign of the specific rotations of **9** and **10** ($[\alpha]_D^{22}$ −2.0 vs. $[\alpha]_D^{22}$ −6.0, MeOH) suggests the same absolute configuration. Therefore, compound **10** was determined to be (2*S*,4*S*)-2-methylchroman-4,5-diol. The absolute configurations of compounds **9** and **10** were determined for the first time in this study.

(2*R*)-7-*O*-α-D-Ribofuranosyl-5-hydroxy-2-methylchroman-4-one (**1**): White amorphous powder; $[\alpha]_D^{23}$ +198.9 (*c* 0.1, MeOH); UV (MeOH) λ_{max} (log ε) 204 (3.62), 278 (3.55), 320 (2.77) nm; ECD (MeOH) λ_{max} ($\Delta\varepsilon$) 211 (+14.21), 284 (−3.51), 327 (+3.42); IR (KBr) ν_{max} 3,416, 1,646, 1,573, 1,354, 1,295, 1,195, 1,155, 1,076, 1,029 cm^{-1}; ^1H and ^{13}C NMR (**Table 1**); HRESIMS *m/z* 327.1068 $[M+H]^+$ (calcd for $C_{15}H_{19}O_8$ 327.1080).

(2*S*)-7-*O*-α-D-Ribofuranosyl-5-hydroxy-2-methylchroman-4-one (**2**): White amorphous powder; $[\alpha]_D^{23}$ +118.6 (*c* 0.1, MeOH); UV (MeOH) λ_{max} (log ε) 204 (3.62), 278 (3.55), 320 (2.77) nm; ECD (MeOH) λ_{max} ($\Delta\varepsilon$) 211 (−10.04), 284 (+9.40), 330 (−2.13); IR (KBr) ν_{max} 3,416, 1,646, 1,573, 1,354, 1,295, 1,195, 1,155, 1,076, 1,029 cm^{-1}; ^1H and ^{13}C NMR (**Table 1**); HRESIMS *m/z* 327.1068 $[M+H]^+$ (calcd for $C_{15}H_{19}O_8$ 327.1080).

(2*S*,3*S*,4*R*)-2-Methylchroman-3,4,5-triol (**3**): Colorless oil; $[\alpha]_D^{23}$ −53.6 (*c* 0.1, MeOH); UV (MeOH) λ_{max} (log ε) 200 (3.25), 270 (2.26) nm; IR (KBr) ν_{max} 3,429, 2,356, 1,627, 1,4,01, 1,090 cm^{-1}; ^1H and ^{13}C NMR (**Table 1**); HRESIMS *m/z* 195.0659 $[M-H]^-$ (calcd. for $C_{10}H_{11}O_4$: 195.0657).

Methyl (3*S*)-3-(2,3-dihydroxyphenyloxy)butanoate (**4**): Colorless oil; $[\alpha]_D^{23}$ +14.4 (*c* 0.1, MeOH); UV (MeOH) λ_{max} (log ε) 200 (3.32), 270 (2.19) nm; IR (KBr) ν_{max} 3,409, 2,356, 1,706, 1,606, 1,481, 1,202, 1,063, 1,010 cm^{-1}; ^1H and ^{13}C NMR (**Table 1**); HRESIMS *m/z* 225.0767 $[M-H]^-$(calcd. for $C_{11}H_{13}O_5$ 225.0763)

(2*S*,3*S*,4*E*)-Hepta-4,6-diene-2,3-diol (**5**): Colorless oil; $[\alpha]_D^{23}$ −6.8 (*c* 0.1, MeOH); UV (MeOH) λ_{max} (log ε) 200 (3.09), 217 (3.38) nm; IR (KBr) ν_{max} 3442, 3080, 1646, 1540, 1023, 446 cm^{-1}; ^1H and ^{13}C NMR (**Table 2**); EIMS *m/z* (%): 129 (45), 256 (8), 111 (26), 97 (51), 83 (69), 82 (38); HREIMS *m/z* 128.0845 $[M]^+$ (calcd. for $C_7H_{12}O_2$ 128.0837).

(3*E*,8*E*,6*S*)-Undeca-3,8,10-trien-1,6-diol (**6**): Colorless oil; $[\alpha]_D^{23}$ +2.0 (*c* 0.1, MeOH); UV (MeOH) λ_{max} (log ε) 200 (2.86), 218 (3.16) nm; IR (KBr) ν_{max} 3,390, 2,927, 1,715, 1,421, 1,047, 973 cm^{-1}; ^1H and ^{13}C NMR (**Table 2**); EIMS *m/z* (%): 181 (8), 164 (9), 151 (14), 129 (17), 115 (16), 97 (31), 85 (28), 71

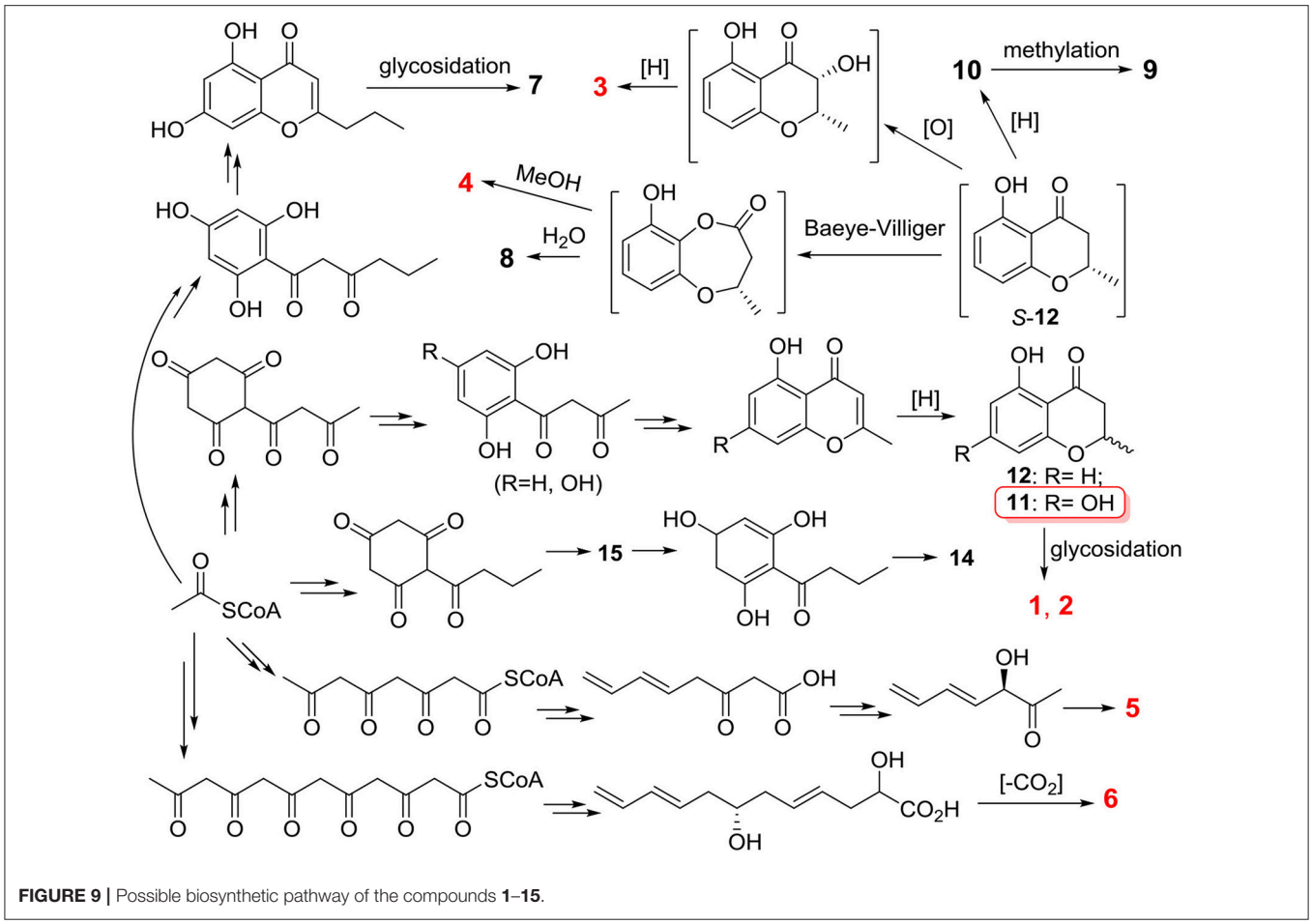

FIGURE 9 | Possible biosynthetic pathway of the compounds **1**–**15**.

(53), 67(88), 53(10); HREIMS *m/z* 182.1305 $[M]^+$ (calcd. for $C_{11}H_{18}O_2$ 182.1307).

X-ray Crystallographic Data of 1

Compound **1** was obtained as a colorless monoclinic crystal with molecular formula of $C_{15}H_{18}O_8$ from MeOH and H_2O. Space group $P2_1$, a = 7.0121(7) Å, b = 10.6659(11) Å, c = 9.8560(8) Å, α = 90.00°, β = 95.3230(10)°, γ = 90.00°, V = 733.95(12) Å^3, Z = 2, D_{calcd} = 1.476 mg/m^3, μ = 0.121 mm^{-1}, $F(000)$ = 344, crystal size 0.42 ×0.30 ×0.21 mm. A total of 3413 unique reflections (2θ<50°= were collected on a CCD area detector diffractometer with graphite monochromated Mo-Ka radiation (λ = 0.71073 Å). The structure was solved by direct methods (SHELXS-97) and expanded using Fourier techniques (SHELXL-97). The final cycle of full-matrix least squares refinement was based on 2053 unique reflections (2θ <50°) and 210 variable parameters and converged with unweighted and weighted agreement factors of R_1 = 0.0421, R_w = 0.0981 and R = 0.0374 for *I>2sigma(I)* data. Crystallographic data (excluding structure factors) for structure **1** in this paper have been deposited in the Cambridge Crystallographic Data Centre as supplementary publication number CCDC 883328 [fax: +44 (0)-1223-336033 or e-mail: deposit@ccdc.cam.ac.uk].

Biogenetic Origin

These compounds were postulated to be biosynthesized by the polyketide pathway from acetyl coenzyme A (**Figure 9**). The acetyl-CoA units underwent condensation, cyclization, dehydration and hydrogenation to produce compounds **11** and **12**. Compound **11** formed compounds **1** and **2** by glycosidation. (*S*)-**12** underwent oxidation and reduction to yield compound **3**. The reduction of (*S*)-**12** produced compound **10** that was transformed to compound **9** followed by methylation. (*S*)-**12** was subjected to Baeyer-Villiger oxidation followed by methanolysis and hydrolysis to yield compounds **4** and **8**, respectively. Compounds **5** and **6** were formed from different lengths of acetyl-CoA units by condensation, reduction, dehydration, and decarboxylation. The condensation of acetyl-CoA units followed by cyclization and reduction formed compound **15** that was transformed to compound **14** after enolization and dehydration.

Biological Activity

Compounds **1**–**14** were tested for cytotoxic effects on the HL-60, BEL-7402, K562, A549, HeLa, and H1975 cell lines, DPPH scavenging activity, and antimicrobial activities against *E. coli*, *E. aerogenes*, *P. aeruginosa*, *B. subtilis*, and *C. albicans*. As the results, compound **6** was cytotoxic to

H1975 cell line with an IC_{50} values of 10.0 μM, while compounds **4** and **8**–**10** showed DPPH radical scavenging activity with the IC_{50} values of 2.65, 0.24, 5.66, and 6.67 μM, respectively. None of the compounds exhibit antimicrobial activities.

CONCLUSIONS

Five new polyketides were isolated and identified from the fermentation of the mangrove fungus *Cladosporium* sp. OUCMDZ-302 with *Excoecaria agallocha*. The new compound **4** showed DPPH radical scavenging activity with an IC_{50} value of 2.65 μM.

AUTHOR CONTRIBUTIONS

All authors listed have made a substantial, direct and intellectual contribution to the work, and approved it for publication.

FUNDING

This research was financially supported by the National Natural Science Foundation of China (NSFC, Nos. 81561148012, U1501221 and 21502034), the 100 Leading Talents of Guizhou Province (fund for W Zhu), the science and technology project of Guizhou (Grant No. QKHT Z-2014-4007), the technology plan of Guizhou (Grant No. QKH YSZ-2015-4009), and by the Thailand Research Fund (TRF) through the International Research Network (IRN-58W0004). The fungus *Cladosporium* sp. OUCMDZ-302 was identified by Prof. Kui Hong, Wuhan University.

SUPPLEMENTARY MATERIAL

The Supplementary Material for this article can be found online at: https://www.frontiersin.org/articles/10.3389/fchem.2018.00344/full#supplementary-material

REFERENCES

Anjaneyulu, A. S., and Rao, V. L. (2000). Five diterpenoids (agallochins A–E) from the mangrove plant *Excoecaria agallocha Linn*. *Phytochemistry* 55, 891–901. doi: 10.1016/S0031-9422(00)00251-X

Anjaneyulu, A. S., Rao, V. L., and Sreedhar, K. (2002). ent-Kaurane and beyerane diterpenoids from *Excoecaria agallocha*. *J. Nat. Prod.* 65, 382–385. doi: 10.1021/np010262u

Anjaneyulu, A. S., Rao, V. L., and Sreedhar, K. (2003). Agallochins J-L, new isopimarane diterpenoids from *Excoecaria agallocha* L. *Nat. Prod. Res.* 17, 27–32. doi: 10.1080/1057563021000027975

Annam, S. Ch., Ankireddy, M., Sura, M. B., Ponnapalli, M. G., Sarma, A. V., and S, JB. (2015). Epimeric excolides from the stems of *Excoecaria agallocha* and structural revision of rhizophorin A. *Org. Lett.* 17, 2840–2843. doi: 10.1021/acs.orglett.5b01257

Chen, Z. B., Hao, J. J., Wang, L. P., Wang, Y., Kong, F. D., and Zhu, W. M. (2016). New α-glucosidase inhibitors from marine algae-derived *Streptomyces* sp. OUCMDZ-3434. *Sci. Rep.* 6:20004. doi: 10.1038/srep20004

Dai, J., Krohn, K., Draeger, S., and Schulz, B. (2009). New naphthalene-chroman coupling products from the endophytic fungus, *Nodulisporium* sp. from Erica arborea. *Eur. J. Org. Chem.* 2009, 1564–1569. doi: 10.1002/ejoc.200801106

Dai, J., Krohn, K., Flörke, U., Draeger, S., Schulz, B., Kiss-Szikszai, A., et al. (2006). Metabolites from the endophytic fungus *Nodulisporium* sp. from Juniperus cedre. *Eur. J. Org. Chem.* 2006, 3498–3506. doi: 10.1002/ejoc.200600261

Deyrup, S. T., Gloer, J. B., O'donnell, K., and Wicklow, D. T. (2007). Kolokosides A–D: triterpenoid glycosides from a Hawaiian isolate of *Xylaria* sp. *J. Nat. Prod.* 70, 378–382. doi: 10.1021/np060546k

Dhami, K. S., and Stothers, J. B. (1965). ^{13}C NMR studies: part iii. carbon-13 nmr spectra of substituted acetophenones. *Can. J. Chem.* 43, 479–497. doi: 10.1139/v65-064

Frisch, M. J., Trucks, G. W., Schlegel, H. B., Scuseria, G. E., Robb, M. A., Cheeseman, J. R., et al. (2004). *Gaussian 03, Revision E.01, 1st Edn*. Wallingford: Gaussian.

Gowri Ponnapalli, M., Ankireddy, M., Rao Annam, S. C. V. A., Ravirala, S., Sukki, S., and Tuniki, V. R. (2013). Unusual ent-isopimarane-type diterpenoids from the wood of *Excoecaria agallocha*. *Tetrahedron Lett.* 54, 2942–2945. doi: 10.1016/j.tetlet.2013.03.105

Haasnoot, C. A. G., De Leeuw, F. A. A. M., and Altona, C. (1980). The relationship between proton-proton NMR coupling constants and substituent electronegativities–I: an empirical generalization of the karplus equation. *Tetrahedron* 36, 2783–2792. doi: 10.1016/0040-4020(80)80155-4

Hu, M., Yang, X. Q., Zhou, Q. Y., Li, S. Q., Wang, B. Y., Ruan, B. H., et al. (2017). Benzopyran derivatives from endophytic *Daldinia eschscholzii* JC-15 in *Dendrobium chrysotoxum* and their bioactivities. *Nat. Prod. Res.* 1–5. doi: 10.1080/14786419.2017.1419236

Huang, H. R., Feng, X. L., She, Z. G., Lin, Y. C., Vrijmoed, L. L. P., and Jones, E. B. G. (2005). 1-(2,6-Dihydroxyphenyl)butanone. *Acta Crys. Sec. E* 61, o282–o283. doi: 10.1107/S160053680500022X

Igarashi, M., Tetsuka, Y., Mimura, Y., Takahashi, A., Tamamura, T., Sato, K., et al. (1993). AB5046 A and B, novel chlorosis-inducing substances from *Nodulisporium* sp. *J. Antibiot.* 46, 1843–1848. doi: 10.7164/antibiotics.46.1843

Jadulco, R., Brauers, G., Edrada, R. A., Ebel, R., Wray, V., Sudarsono, S., et al. (2002). New metabolites from sponge-derived fungi *Curvularia lunata* and *Cladosporium herbarum*. *J. Nat. Prod.* 65, 730–733. doi: 10.1021/np010390i

Jadulco, R., Proksch, P., Wray, V., Sudarsono, Berg, A., and Gräfe, U. (2001). New macrolides and furan carboxylic acid derivative from the sponge-derived fungus *Cladosporium herbarum*. *J. Nat. Prod.* 64, 527–530. doi: 10.1021/np000401s

Jarvis, B. B., Wang, S., and Ammon, H. L. (1996). Trichoverroid stereoisomers. *J. Nat. Prod.* 59, 254–261.doi: 10.1021/np960078m

Jin, Y., Qin, S., Gao, H., Zhu, G., Wang, W., Zhu, W., et al. (2018). An anti-HBV anthraquinone from aciduric fungus *Penicillium* sp. OUCMDZ-4736 under low pH stress. *Extremophiles* 22, 39–45. doi: 10.1007/s00792-017-0975-6

Kang, J., Chen, R. Y., and Yu, D. Q. (2005). A new isopimarane-type diterpene and a new natural atisane-type diterpene from *Excoecaria agallocha*. *J. Asian. Nat. Prod. Res.* 7, 729–734. doi: 10.1080/1028602042000324943

Kawasaki, M., Asano, Y., Katayama, K., Inoue, A., Hiraoka, C., Kakuda, H., et al. (2008). Asymmetric synthesis of 2-substituted 4-chromanones using enzyme-catalyzed reactions. *J. Mol. Catal. B-Enzy.* 54, 93–102. doi: 10.1016/j.molcatb.2007.12.022

Kong, F., Wang, Y., Liu, P., Dong, T., and Zhu, W. (2014). Thiodiketopiperazines from the marine-derived fungus *Phoma* sp. OUCMDZ-1847. *J. Nat. Prod.* 77, 132–137. doi: 10.1021/np400802d

Konishi, T., Konoshima, T., Fujiwara, Y., Kiyosawa, S., Miyahara, K., and Nishi, M. (1999). Stereostructures of new labdane-type diterpenes, excoecarins F, G1, and G2 from the wood of *Excoecaria agallocha*. *Chem. Pharm. Bull.* 47, 456–458. doi: 10.1248/cpb.47.456

Konishi, T., Konoshima, T., Maoka, T., and Fujiwara, Y. (2000). Novel diterpenes, excoecarins M and N from the resinous wood of *Excoecaria agallocha*. *Tetrahedron. Lett.* 41, 3419–3422. doi: 10.1016/S0040-4039(00)00391-9

Konishi, T., Yamazoe, K., Konoshima, T., and Fujiwara, Y. (2003). Seco-labdane type diterpenes from *Excoecaria agallocha*. *Phytochemistry* 64, 835–840. doi: 10.1016/j.phytochem.2003.09.001

Li, Y., Liu, J., Yu, S., Proksch, P., Gu, J., and Lin, W. (2010). TNF-α inhibitory diterpenoids from the chinese mangrove plant *Excoecaria agallocha* L. *Phytochemistry* 71, 2124–2131.doi: 10.1016/j.phytochem.2010.08.011

Lin, Z., Zhu, T., Fang, Y., Gu, Q., and Zhu, W. (2008). Polyketides from *Penicillium* sp. JP-1, an endophytic fungus associated with the mangrove plant *Aegiceras corniculatum*. *Phytochemistry* 69, 1273–1278. doi: 10.1016/j.phytochem.2007.10.030

Lu, Z., Wang, Y., Miao, C., Liu, P., Hong, K., and Zhu, W. (2009). Sesquiterpenoids and benzofuranoids from the marine-derived fungus *Aspergillus ustus* 094102. *J. Nat. Prod.* 72, 1761–1767. doi: 10.1021/np900268z

Lu, Z., Zhu, H., Fu, P., Wang, Y., Zhang, Z., Lin, H., et al. (2010). Cytotoxic polyphenols from the marine-derived fungus *Penicillium expansum*. *J. Nat. Prod.* 73, 911–914. doi: 10.1021/np100059m

Mosmann, T. (1983). Rapid colorimetric assay for cellular growth and survival: application to proliferation and cytotoxicity assays. *J. Immunol. Methods.* 65, 55–63.doi: 10.1016/0022-1759(83)90303-4

Nilewski, C., Geisser, R. W., Ebert, M. O., and Carreira, E. M. (2009). Conformational and configurational analysis in the study and synthesis of chlorinated natural products. *J. Am. Chem. Soc.* 131, 15866–15876. doi: 10.1021/ja906461h

Rao, A. V. R., Gaitonde, A. S., Prakash, K. R. C., and Rao, S. P. (1994). A concise synthesis of chiral 2-methyl chroman-4-ones: stereo selective build-up of the chromanol moiety of anti-HIV agent calanolide A. *Tetrahedron Lett.* 35, 6347–6350.doi: 10.1016/S0040-4039(00)73429-0

Sakagami, Y., Sano, A., Hara, O., Mikawa, T., and Marumo, S. (1995). Cladosporol, β-1, 3-glucan biosynthesis inhibitor, isolated from fungus, *Cladosporium cladosporioides*. *Tetrahedron Lett.* 36, 1469–1472. doi: 10.1016/0040-4039(95)00061-G

Shigemori, H., Kasai, Y., Komatsu, K., Tsuda, M., Mikami, Y., and Kobayashi, J. I. (2004). Sporiolides A and B, new cytotoxic twelve-membered macrolides from a marine-derived fungus *Cladosporium* species. *Marine Drugs* 2, 164–169. doi: 10.3390/md204164

Skehan, P., Storeng, R., Scudiero, D., Monks, A., McMahon, J., Vistica, D., et al. (1990). New colorimetric cytotoxicity assay for anticancer-drug screening. *J. Natl. Cancer. Inst.* 82, 1107–1112. doi: 10.1093/jnci/82.13.1107

Teles, H. L., Silva, G. H., Castro-Gamboa, I., Bolzani Vda S., Pereira, J. O., Costa-Neto, C. M., et al. (2005). Benzopyrans from *Curvularia* sp., an endophytic fungus associated with *Ocotea corymbosa* (Lauraceae). *Phytochemistry* 66, 2363–2367.doi: 10.1016/j.phytochem.2005.04.043

Wang, J. D., and Guo, Y. W. (2004). Agallochaols A and B, two new diterpenes from the Chinese mangrove *Excoecaria agallocha* L. *Hel. Chim. Acta.* 87, 2829–2833. doi: 10.1002/hlca.200490253

Wang, J. D., Li, Z. Y., and Guo, Y. W. (2005). Secoatisane- and isopimarane- type diterpenoids from the Chinese mangrove *Excoecaria agallocha* L. *Hel. Chim. Acta.* 88, 979–985. doi: 10.1002/hlca.2005 90092

Wang, J., Lu, Z., Liu, P., Wang, Y., Li, J., Hong, K., et al. (2012). Cytotoxic polyphenols from the fungus *Penicillium expansum* 091 006 endogenous with the mangrove plant *Excoecaria agallocha*. *Planta. Med.* 78, 1861–1866. doi: 10.1055/s-0032-1315395

Wang, W. L., Zhu, T. J., Tao, H. W., Lu, Z. Y., Fang, Y. C., Gu, Q. Q., et al. (2007). Three novel, structurally unique spirocyclic alkaloids from the halotolerant B-17 fungal strain of *Aspergillus variecolor*. *Chem. Biodivers.* 4, 2913–2919. doi: 10.1002/cbdv.200790240

Wang, Z. C., Lin, Y. M., Feng, D. Q., Ke, C. H., Lin, P., Yan, C. L., et al. (2009). A new atisane-type diterpene from the bark of the mangrove plant *Excoecaria agallocha*. *Molecules* 14:414. doi: 10.3390/molecules14010414

Wu, J., Xiao, Q., Xu, J., Li, M. Y., Pan, J. Y., and Yang, M. H. (2008). Natural products from true mangrove flora: source, chemistry and bioactivities. *Nat. Prod. Rep.* 25, 955–981. doi: 10.1039/b807365a

Wu, Z. C., Li, D. L., Chen, Y. C., and Zhang, W. M. (2010). A new isofuranonaphthalenone and benzopyrans from the endophytic fungus *Nodulisporium* sp. A4 from *Aquilaria sinensis*. *Hel. Chim. Acta* 93, 920–924. doi: 10.1002/hlca.200900307

Ye, Y. H., Zhu, H. L., Song, Y. C., Liu, J. Y., and Tan, R. X. (2005). Structural revision of aspernigrin A, reisolated from *Cladosporium herbarum* IFB-E002. *J. Nat. Prod.* 68, 1106–1108. doi: 10.1021/np050059p

Zaika, L. L. (1988). Spices and herbs: their antimicrobial activity and its determination1. *J. Food Safety* 9, 97–118. doi: 10.1111/j.1745-4565.1988.tb00511.x

Zhang, H. W., Song, Y. C., and Tan, R. X. (2006). Biology and chemistry of endophytes. *Nat. Prod. Rep.* 23, 753–771. doi: 10.1039/b609472b

Zhang, H., Tomoda, H., Tabata, N., Miura, H., Namikoshi, M., Yamaguchi, Y., et al. (2001). Cladospolide D, a new 12-membered macrolide antibiotic produced by *Cladosporium* sp. FT-0012. *J. Antibiot* 54, 635–641. doi: 10.7164/antibiotics.54.635

Zhang, P., and Kyler, K. S. (1989). Enzymic asymmetric hydroxylation of pentadienols using soybean lipoxygenase. *J. Am. Chem. Soc.* 111, 9241–9242. doi: 10.1021/ja00208a024

Zhang, Y., and O'doherty, G. A. (2005). Remote steric effect on the regioselectivity of Sharpless asymmetric dihydroxylation. *Tetrahedron* 61, 6337–6351.doi: 10.1016/j.tet.2005.03.119

Zhao, G. Y., Fan, J. Y., Hua, C. P., Yan, W., Chen, C. J., Lu, Y. H., et al. (2015). Resveratrol improves fungal ribosylation capacity through a unique mechanism. *RSC Adv.* 5, 5657–5663. doi: 10.1039/C4RA12851F

Zheng, J., Xu, Z., Wang, Y., Hong, K., Liu, P., and Zhu, W. (2010). Cyclic tripeptides from the halotolerant fungus *Aspergillus sclerotiorum* PT06-1. *J. Nat. Prod.* 73, 1133–1137. doi: 10.1021/np100198h

Zhu, T., Lu, Z., Fan, J., Wang, L., Zhu, G., Wang, Y., et al. (2018). Ophiobolins from the mangrove fungus *Aspergillus ustus*. *J. Nat. Prod.* 81, 2–9.doi: 10.1021/acs.jnatprod.7b00335

Conflict of Interest Statement: The authors declare that the research was conducted in the absence of any commercial or financial relationships that could be construed as a potential conflict of interest.

frontiers in Chemistry

ORIGINAL RESEARCH
published: 04 September 2018
doi: 10.3389/fchem.2018.00394

Talaropeptides A-D: Structure and Biosynthesis of Extensively *N*-methylated Linear Peptides From an Australian Marine Tunicate-Derived *Talaromyces* sp.

*Pradeep Dewapriya[1], Zeinab G. Khalil[1], Pritesh Prasad[1], Angela A. Salim[1], Pablo Cruz-Morales[2,3], Esteban Marcellin[2] and Robert J. Capon[1]**

[1] Institute for Molecular Bioscience, The University of Queensland, St Lucia, QLD, Australia, [2] Australian Institute for Bioengineering and Nanotechnology, The University of Queensland, St Lucia, QLD, Australia, [3] Joint BioEnergy Institute, Emeryville, CA, United States

OPEN ACCESS

Edited by:
Xian-Wen Yang,
Third Institute of Oceanography, State Oceanic Administration, China

Reviewed by:
Yonghui Zhang,
Huazhong University of Science and Technology, China
Fernando Reyes,
Fundación Centro de Excelencia en Investigación de Medicamentos Innovadores en Andalucía, Spain
Kirk R. Gustafson,
National Cancer Institute (NCI), United States

***Correspondence:**
Robert J. Capon
r.capon@uq.edu.au

Specialty section:
This article was submitted to Medicinal and Pharmaceutical Chemistry, a section of the journal Frontiers in Chemistry

Received: *02 July 2018*
Accepted: *14 August 2018*
Published: *04 September 2018*

Citation:
Dewapriya P, Khalil ZG, Prasad P, Salim AA, Cruz-Morales P, Marcellin E and Capon RJ (2018) Talaropeptides A-D: Structure and Biosynthesis of Extensively N-methylated Linear Peptides From an Australian Marine Tunicate-Derived Talaromyces sp. Front. Chem. 6:394. doi: 10.3389/fchem.2018.00394

An Australian marine tunicate-derived fungus, *Talaromyces* sp. CMB-TU011 was subjected to a program of analytical microbioreactor (MATRIX) cultivations, supported by UHPLC-QTOF profiling, to reveal conditions for producing a new class of extensively *N*-methylated 11-12 residue linear peptides, talaropeptides A-D (**2**-**5**). The structures for **2**-**5**, inclusive of absolute configurations, were determined by a combination of detailed spectroscopic and chemical (e.g., C_3 and C_{18} Marfey's) analyses. We report on the biological properties of **2**-**5**, including plasma stability, as well as antibacterial, antifungal and cell cytotoxicity. The talaropeptide mega non-ribosomal peptide synthetase (NRPS) is described, as second only in size to that for the fungus-derived immunosuppressant cyclosporine (an 11-residue extensively *N*-methylated cyclic peptide).

Keywords: marine-derived, fungus, *Talaromyces*, talaropeptide, NRPS, linear peptide, secondary metabolite, natural product

INTRODUCTION

In an earlier study, we described the structure elucidation of a first-in-class cyclic hexapeptide containing a rare hydroxamate residue, talarolide A (**1**) (**Figure 1**), isolated from an Australian marine tunicate-derived fungus, *Talaromyces* sp. CMB-TU011 (Dewapriya et al., 2017). In an effort to optimize the production of **1**, we now report on a 24-well microbioreactor cultivation analysis (known in-lab as the MATRIX), using a combination of 11 different media and 3 phases (i.e., solid agar, as well as static and shaken broth). *In situ* solvent extraction on individual MATRIX culture wells yielded 33 extracts, which were subjected to UHPLC-DAD and UHPLC-QTOF-MS/MS analysis. While this study successfully revealed optimal conditions for the production of **1**, including new analogs (work-in-progress), it also revealed conditions where talarolide production was fully suppressed in favor of a new class of extensively *N*-methylated linear peptides. This report provides an account of the production, isolation and characterisation of these new peptides, talaropeptides A-D (**2**-**5**), where structure elucidation inclusive of absolute configurations was achieved by a combination of detailed spectroscopic and chemical analyses. We also take the opportunity to report on the biological properties of **2**-**5**, and document the mega non-ribosomal peptide synthetase (NRPS) responsible for the biosynthesis of talaropeptides.

MATERIALS AND METHODS

General Experimental Details

Specific rotations ($[\alpha]_D$) were measured on a JASCO P-1010 polarimeter in a 100 × 2 mm cell at room temperature. NMR spectra were acquired on a Bruker Avance 600 MHz spectrometer with either a 5 mm PASEL ^{1}H/D–^{13}C Z-Gradient probe or 5 mm CPTCI ^{1}H/^{19}F-^{13}C/^{15}N/DZ-Gradient cryoprobe, controlled by TopSpin 2.1 software. In all cases, NMR spectra were acquired at 25°C (unless otherwise specified) in hexadeuterated dimethylsulfoxide (DMSO-d_6) and tetradeuterated methanol (methanol-d_4) with referencing to residual ^{1}H (δ_H 2.50 and δ_H 3.31, respectively) or ^{13}C (δ_C 39.51 and δ_C 49.15, respectively) NMR resonances. HPLC-DAD-ESIMS data were acquired on an Agilent 1100 series separation module equipped with an Agilent 1100 series HPLC/MSD mass detector and Agilent diode array detector. Semi-preparative and preparative HPLCs were performed using Agilent 1100 series HPLC instruments with corresponding detectors, fraction collectors, and software. HRESI(+)MS spectra were obtained on a Bruker micrOTOF mass spectrometer by direct injection in MeCN at 3 μL/min using sodium formate clusters as an internal calibrant. UHPLC-QTOF analysis was performed on UHPLC-QTOF instrument comprising an Agilent 1290 Infinity II UHPLC equipped with a Zorbax C_8 column (2.1 mm × 50 mm, 1.8 μm particles), running with H_2O/MeCN inclusive of 0.1% formic acid coupled to an Agilent 6545 Q-TOF. MS/MS analysis was performed on the same instrument for ions detected in the full scan at an intensity above 1,000 counts at 10 scans/s, with an isolation width of 4 ∼*m/z* using a fixed collision energy and a maximum of 3 selected precursors per cycle. *N*α-(2,4-dinitro-5-fluorophenyl)-L-alaninamide (L-FDAA, synonym 1-fluoro-2-4-dinitrophenyl-5-L-alanine amide) and *N*α-(2,4-dinitro-5-fluorophenyl)-D-alanine amide (D-FDAA, synonym 1-fluoro-2-4-dinitrophenyl-5-D-alanine amide) were purchased from NovaBiochem. Amino acids and standards were purchased from NovaBiochem, BAChem Biosciences, Sigma, Fluka, or Merck.

Fungus Isolation and Taxonomy

Talaromyces sp. CMB-TU011 was isolated from an unidentified tunicate collected near Tweed Heads, NSW, Australia, and taxonomically identified as previously reported (Dewapriya et al., 2017).

Analytical (MATRIX) Cultivation of *Talaromyces* sp. CMB-TU011

Talaromyces sp. CMB-TU011 was cultured in a 24-well microbioreactor plate (Khalil et al., 2014) using a combination of 11 culture media and 3 phases (i.e., solid agar, and liquid static and liquid shaken) known in-lab as the MATRIX (**Table S1**). Briefly, a sterile loop was used to transfer mycelia/spores from an agar plate cultivation to 24-well microbioreactor plate (2.5 mL agar for solid cultures, 1.5 mL of broth for liquid cultures). The microbioreactor plates were sealed with air permeable membranes and incubated at 26.5°C for 10 days (190 rpm for shaken broth). The resulting 33 cultures were extracted *in situ* with EtOAc (2.0 mL/well), with the decanted solvent filtered and dried under N_2. Secondary metabolite production was then analyzed by HPLC-DAD-ESIMS and UHPLC-QTOF.

Scale-Up Cultivation of *Talaromyces* sp. CMB-TU011 and Isolation of 2-5

Agar cubes (∼1 cm^2) recovered from 7 day CMB-TU011 agar plate cultures (3.3% artificial sea salt containing M1 medium) were used to inoculate 10 flasks (500 mL) charged with YES broth (160 mL). Individual flasks were covered with air permeable sterile cotton plugs, and incubated under static conditions for 10 days at 26.5°C, after which the combined broths/mycelia were extracted with EtOAc (4 × 500 mL) to yield a crude extract (1.65 g) which was partitioned between hexane (200 mL) and 1% aqueous MeOH (50 mL) and dried *in vacuo* to yield hexane (495 mg) and MeOH (1.15 g) solubles. The MeOH solubles were further fractionated by gel chromatography (Sephadex® LH-20, MeOH) into 20 fractions, which were selectively combined on the basis of HPLC-DAD-ESIMS analysis (Zorbax SB-C_8 column, analytical gradient 90% H_2O/MeCN – 100% MeCN inclusive of an isocratic 0.05% formic acid) to yield a fraction of interest (49 mg) that was resolved by optimized semi-preparative HPLC (Zorbax SB C_3 column (9.4 mm × 25 cm), 40% MeCN/H_2O elution at 3.0 mL/min inclusive of an isocratic 0.01% TFA modifier) to yield talaropeptide A (**2**) (t_R = 7.11 min, 1.3 mg), talaropeptide B (**3**) (t_R = 8.78 min, 1.3 mg), talaropeptide C (**4**) (t_R = 16.89 min, 1.8 mg), and talaropeptide D (**5**) (t_R = 22.96 min, 2.8 mg) (**Supplementary Scheme S1**).

Talaropeptide A (2): white powder; $[\alpha]_D^{22}$ −135.8 (c 0.04, MeOH); 1D and 2D NMR (600 MHz, DMSO-d_6) see **Table 1** and **Supplementary Material**; HRESI(+)MS *m/z* 1254.8435 [(M+H)$^+$] (calcd for $C_{65}H_{112}N_{11}O_{13}$, 1254.8436).

Talaropeptide B (3): white powder; $[\alpha]_D^{22}$-110.0 (c 0.05, MeOH); 1D and 2D NMR (600 MHz, methanol-d_4) see **Table 2** and **Supplementary Material**; HRESI(+)MS *m/z* 1375.8920 [M+Na]$^+$ (calcd for $C_{70}H_{120}N_{12}O_{14}$Na, 1375.8939).

Talaropeptide C (4): white powder; $[\alpha]_D^{22}$ −151.6 (c 0.05), MeOH); 1D and 2D NMR (600 MHz, methanol-d_4) see **Table 3** and **Supplementary Material**; HRESI(+)MS *m/z* 1318.8376 [(M+Na)$^+$] (calcd for $C_{67}H_{113}N_{11}O_{14}$Na, 1318.8361).

Talaropeptide D (5): white powder; $[\alpha]_D$22 −182.9 (c 0.05), MeOH); 1D and 2D NMR (600 MHz, methanol-d_4) see **Table 4** and **Supplementary Material**; HRESI(+)MS *m/z* 1417.9052 [(M+Na)$^+$] (calcd for $C_{72}H_{122}N_{12}O_{15}$Na, 1417.9045).

Marfey's Analyses

Analyses were carried out following the published method (Vijayasarathy et al., 2016). Briefly, an aliquot (50 μg) of each talaropeptide in 6 M HCl (100 μL) was heated to 100°C in a sealed vial for 12 h, after which the hydrolysate was concentrated to dryness at 40°C under a stream of dry N_2. The hydrolysate was

Abbreviations: UHPLC, ultra-high-performance liquid chromatography; HPLC, high-performance liquid chromatography; QTOF, quadrupole time of flight; ESI, electrospray ionization; SIE, single ion extraction; DAD, diode array detector; NRPS, non-ribosomal peptide synthetase; LSI, Latent semantic indexing; ORFX, orphan protein/enzyme.

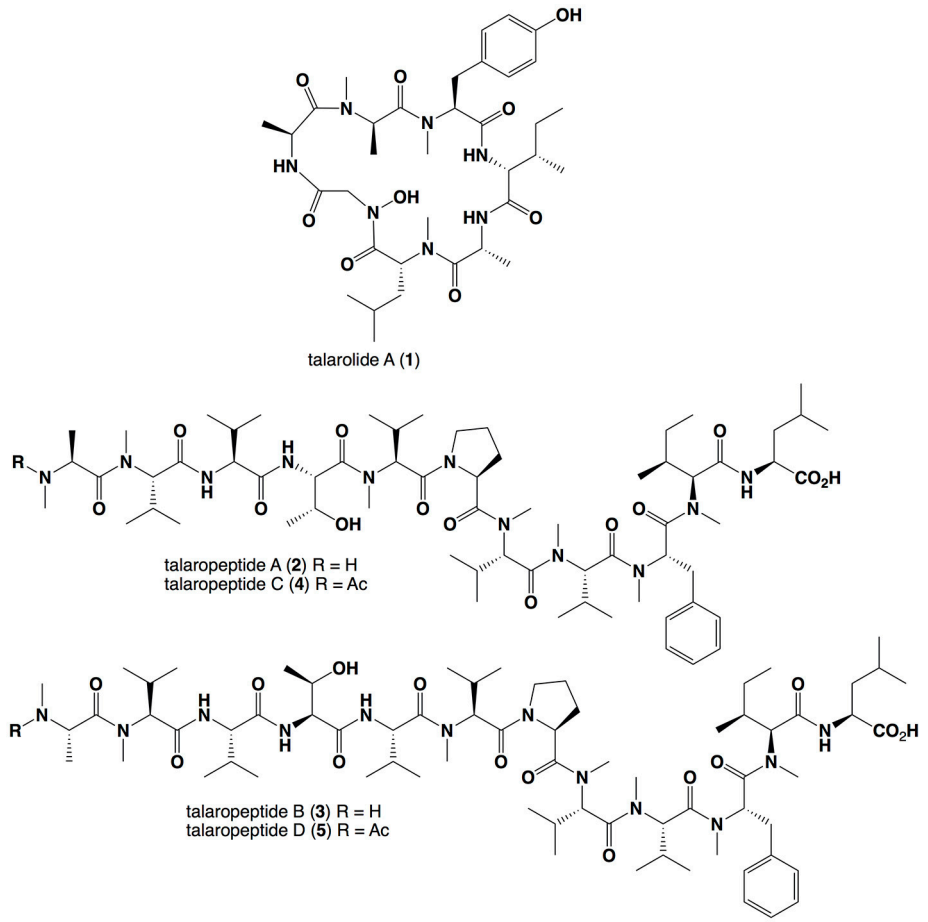

FIGURE 1 | Structures for the *Talaromyces* sp. CMB-TU011 peptides **1**–**5**.

then treated with 1 M $NaHCO_3$ (20 μL) and L-FDAA (1-fluoro-2,4-dinitrophenyl-5-L-alanine amide) as a 1% solution in acetone (40 μL) at 40 °C for 1 h, after which the reaction was neutralized with 1 M HCl (20 μL) and filtered (0.45 μm PTFE) to generate an analyte.

C_3 Marfey's analysis. An aliquot (10 μL) of each analyte was subjected to HPLC-DAD-MS analysis (Agilent Zorbax SB-C_3 column, 5 μm, 4.6 × 150 mm, 50°C, with a 1 mL/min, 55 min linear gradient elution from 15–60% MeOH/H_2O with a 5% isocratic modifier of 1% formic acid in MeCN) with amino acid content assessed by DAD (340 nm) and ESI(±)MS monitoring, supported by SIE (single ion extraction) methodology, with comparison to authentic standards.

C_{18} Marfey's analysis. An aliquot (10 μL) of each analyte was subjected to HPLC-DAD analysis for (Agilent Zorbax SB-C_{18} HPLC column, 5 μm, 4.6 × 150 mm, 50 °C, with a 1 mL/min, 50 min isocratic elution of 21% MeOH/H_2O for *N*-Me-Ala and 34 % MeOH/H_2O for *N*-Me-Phe, with a 5% isocratic modifier of 1% formic acid in MeCN) with amino acid content assessed by DAD (340 nm), with comparison to authentic standards.

Genome Mining of *Talaromyces* sp. CMB-TU011

Genomic DNA from *Talaromyces* sp. CMB-TU011 was extracted using a standard chloroform protocol (Nikodinovic et al., 2003). The extracted DNA was fragmented using a Covaris focused ultrasonicator and the resulting fragments (∼ 1 KB) were used for library construction using a Thrulex DNA-Seq kit (Rubicon Genomics). The library was sequenced using a Next Seq platform in the paired-end (2 × 150) format to yield a total of 6,674,290 reads (1 GB). The raw reads were filtered and trimmed using Trimmomatic v0.36 (Bolger et al., 2014) to yield a total of 5,821,558 high quality reads (0.873 GB), which were assembled using Velvet 1.2.10 (Zerbino and Birney, 2008), Abyss v.2.0.3 (Simpson et al., 2009) and SPAdes v3.11.1 (Bankevich et al., 2012) assemblers with a window of Kmers between 41 and 121, with iterations every 10 units. The best assembly (Velvet with Kmer =51) was annotated for natural products biosynthetic gene clusters using the Fungal implementation of AntiSMASH 4.0 (Blin et al., 2017). The output was manually curated and domain annotation was improved using pFAM (Finn et al., 2016) and the NCBI Conserved Domain Search tool

TABLE 1 | 1D NMR (DMSO-d_6) data for talaropeptide A (**2**).

#	δ_H m (*J* in Hz)	δ_C
***N*-Me-L-Ala[1]**		
1		171.4
2	5.36, m	48.8
3	1.09[a]	14.3
N-Me	2.96, s	30.3[f]
***N*-Me-L-Val[2]**		
1		167.5
2	4.82, m	59.0
3	2.10[b]	27.1
4	0.87[c]	18.9[g]
5	0.71, d (*6.4*)	18.1[h]
N-Me	2.87, s	29.5[i]
L-Val[3]		
1		171.0
2	4.42, m	56.2
3	1.97, m	29.4[i]
4, 5	0.80[d]	18.1[h]
N-H	8.30, d (*8.6*)	
L-Thr[4]		
1		nd
2	4.15, m	55.1
3	3.80, m	66.6
4	1.10[a]	19.3[g]
4-OH	5.84, d (*4.6*)	
N-H	nd	
***N*-Me-L-Val[5]**		
1		nd
2	4.68[e]	61.3
3	2.10[b]	26.3[j]
4	0.87[c]	18.9[g]
5	0.82[d]	19.2[g]
N-Me	3.04, s	30.4[f]
L-Pro[6]		
1		172.1
2	4.69[e]	56.3
3	a 2.09[b]	28.5[k]
	b 1.50, m	
4	a 1.92, m	24.4[l]
	b 1.79, m	
5	a 3.70, m	47.0
	b 3.53, m	
***N*-Me-L-Val[7]**		
1		169.3
2	4.80, m	57.5
3	2.15, m	26.2[j]
4, 5	0.76, m	18.0[h]
N-Me	2.87, s	29.7[i]
***N*-Me-L-Val[8]**		
1		168.5
2	4.91, d (*10.5*)	57.7
3	2.10[b]	26.3[j]
4	0.73, d (*6.5*)	19.1[g]
5	0.56, d (*6.5*)	17.1
N-Me	2.18, s	28.6[k]
***N*-Me-L-Phe[9]**		
1		170.0
2	5.77, t (*7.6*)	53.1
3	2.94, m	34.3
4		137.3
5/9	7.71, m	129.1
6/8	7.22, m	128.0
7	7.17, m	126.3
N-Me	2.85, s	29.9[i]
***N*-Me-L-Ile[10]**		
1		169.7
2	4.69[e]	59.4
3	1.94, m	32.3
4	a 1.20, m	24.3[l]
	b 0.90, m	
5	0.78[d]	10.0
6	0.86[c]	15.1
N-Me	2.94, s	30.4[f]
L-Leu[11]		
1		173.7
2	4.11, m	50.3
3	a 1.56, m	39.2
	b 1.48, m	
4	1.57, m	24.2[l]
5	0.88[c]	22.8
6	0.80[d]	21.3
N-H	8.17, d (*7.4*)	
OH	nd	

[a–e]Assignments with the same superscript are overlapping. [f–l]Assignments with the same superscript may be interchanged. [nd]resonances not detected.

(Marchler-Bauer et al., 2017). Adenylation domain specificity was predicted using the LSI based A-domain functional predictor (Baranašić et al., 2014). Manual sequence curation was done using the Artemis Genome Browser (Rutherford et al., 2000).

Antibacterial Assay

The bacterium to be tested was streaked onto a tryptic soy agar plate and was incubated at 37°C for 24 h. One colony was then transferred to fresh tryptic soy broth (15 mL) and the cell density was adjusted to 10^4-10^5 CFU/mL. The compounds to be tested

TABLE 2 | 1D NMR (methanol-d_4) data for talaropeptide B (**3**).

#	δ_H m (*J* in Hz)	δ_C
***N*-Me-L-Ala[1]**		
1		174.3
2	5.43, m	51.4
3	1.27, d (*6.9*)	14.8
N-Me	3.14, s	31.7[j]
***N*-Me-L-Val[2]**		
1		170.1
2	4.98, d (*10.8*)	61.6
3	2.24[a]	28.6
4	0.97[b]	19.8[k]
5	0.82, d (*6.6*)	19.4[l]
N-Me	3.01, s	31.1[m]
L-Val[3]		
1		173.6[n]
2	4.63, d (*7.6*)	56.2
3	2.05[c]	31.7[j]
4	0.92[d]	18.6[o]
5	0.93[e]	18.9[o]
L-Thr[4]		
1		173.6[n]
2	4.82[f]	56.6
3	4.01, m	68.9
4	1.19, d (*6.3*)	20.3[k]
L-Val*		
1		nd
2	3.50, br s	60.3
3	2.08, m	32.4
4	0.93[e]	19.3[l]
5	0.96[b]	17.9
***N*-Me-L-Val[5]**		
1		171.9
2	4.69, d (*11.0*)	63.6
3	2.23[a]	28.0
4	0.89[g]	19.9[k]
5	0.80, d (*6.5*)	19.2[l]
N-Me	3.22, s	31.9[j]
L-Pro[6]		
1		174.7
2	4.80[f]	58.6
3	a 2.21[h]	30.2[p]
	b 1.66, m	
4	a 2.04[c]	25.8[q]
4	b 1.91, m	
5	3.71, m	49.0
***N*-Me-L-Val[7]**		
1		171.6
2	4.91, d (*10.6*)	60.2
3	2.27, m	28.2
4	0.89[g]	20.5
5	0.86[i]	18.6[o]
N-Me	3.02, s	31.1[m]

(Continued)

TABLE 2 | Continued

#	δ_H m (*J* in Hz)	δ_C
***N*-Me-L-Val[8]**		
1		171.0[r]
2	5.03, d (*10.5*)	60.1
3	2.22[h]	28.4
4	0.83, d (*6.7*)	20.2[k]
5	0.67, d (*6.7*)	18.2
N-Me	2.26, s	30.3[p]
***N*-Me-L-Phe[9]**		
1		172.8
2	5.94, dd (*10.3, 5.4*)	55.4
3	3.04, m	35.9
4		138.3
5/9	7.21, m	130.5
6/8	7.28, m	129.7
7	7.24, m	128.2
N-Me	2.98, s	31.5[j]
***N*-Me-L-Ile[10]**		
1		171.1[r]
2	4.76, d (*11.4*)	62.6
3	2.09, m	33.4
4	a 1.31, m	25.9[q]
	b 1.02, m	
5	0.87[i]	10.7
6	0.94, d (*6.6*)	16.0
N-Me	3.04, s	31.6[j]
L-Leu[11]		
1		nd
2	4.34, br s	54.5
3	a 1.64, m	43.1
	b 1.55, m	
4	1.59, m	26.5
5	0.92[d]	23.8
6	0.91[d]	22.6

[a–i]Assignments with the same superscript are overlapping. [i–r]Assignments with the same superscript may be interchanged. [nd]resonances not detected.

were dissolved in DMSO and diluted with H_2O to give 600 μM stock solution (20% DMSO), which was serially diluted with 20% DMSO to give concentrations from 600 μM to 0.2 μM in 20% DMSO. An aliquot (10 μL) of each dilution was transferred to a 96-well microtiter plate and freshly prepared microbial broth (190 μL) was added to each well to give final concentrations of 30−0.01 μM in 1% DMSO. The plates were incubated at 37°C for 24 h and the optical density of each well was measured spectrophotometrically at 600 nm using POLARstar Omega plate (BMG LABTECH, Offenburg, Germany). Each test compound was screened against the Gram-negative bacteria *Escherichia coli* ATCC 11775 and *Pseudomonas aeruginosa* ATCC 10145 and the Gram-positive bacteria *Staphylococcus aureus* ATCC 25923 and *Bacillus subtilis* ATCC 6051. Rifampicin was used as a positive control (40 μg/mL in 10% DMSO). The IC_{50} value was calculated

TABLE 3 | 1D NMR (methanol-d_4) data for talaropeptide C (**4**).

#	δ_H m (*J* in Hz)	δ_C
***N*-Me-L-Ala[1]**		174.3[h]
1		
2	5.44, m	51.4
3	1.27, d (*6.9*)	14.8
N-Me	3.14, s	31.7[i]
N-$\underline{C}OCH_3$		173.6[j]
N-CO$\underline{C}H_3$	1.99, s	22.3[k]
***N*-Me-L-Val[2]**		170.1
1		
2	4.98, d (*10.9*)	61.5
3	2.24[a]	28.6
4	0.97, d (*6.6*)	19.9[l]
5	0.82, d (*6.6*)	19.3
N-Me	3.01, s	31.1[m]
L-Val[3]		173.7[j]
1		
2	4.63, d (*7.6*)	56.2
3	2.05[b]	31.8[i]
4	0.91[c]	19.9[l]
5	0.93[c]	18.9[n]
L-Thr[4]		174.0
1		
2	4.76[d]	56.6
3	3.99, m	68.9
4	1.17, d (*6.3*)	20.0[l]
***N*-Me-L-Val[5]**		172.0
1		
2	4.69, d (*11.0*)	63.6
3	2.24[a]	28.0
4	0.89[e]	19.9[l]
5	0.82, d (*6.5*)	19.1[n]
N-Me	3.20, s	31.8[i]
L-Pro[6]		174.8
1		
2	4.80, dd (*8.4*, *4.9*)	58.6
3	a 2.21[f]	30.2[o]
	b 1.66, m	
4	a 2.05[b]	25.8[p]
	b 1.92, m	
5	3.71, m	48.9
***N*-Me-L-Val[7]**		171.7
1		
2	4.91, d (*10.6*)	60.2
3	2.28, m	28.2[q]
4	0.90[e]	20.6
5	0.86[g]	18.6
N-Me	3.02, s	31.0[m]
***N*-Me-L-Val[8]**		171.1[r]
1		
2	5.03, d (*10.6*)	60.1
3	2.20[f]	28.3[q]
4	0.84, d (*6.7*)	20.3
5	0.67, d (*6.7*)	18.2
N-Me	2.27, s	30.3[o]
***N*-Me-L-Phe[9]**		172.9
1		
2	5.94, dd (*9.8,5.7*)	55.4
3	3.05, m	35.9
4		138.2
5/9	7.21, m	130.5
6/8	7.28, m	129.7
7	7.24, m	128.2
N-Me	2.98, s	31.5[i]
***N*-Me-L-Ile[10]**		171.1[r]
1		
2	4.75[d]	62.5
3	2.08, m	33.6
4	a 1.32, m	25.9[p]
	b 1.00, m	
5	0.87[g]	10.7
6	0.96, d (*6.6*)	16.0
N-Me	3.05, s	31.7[i]
L-Leu[11]		nd
1		
2	4.36, br s	nd
3	1.62, m	42.4
4	1.61, m	26.5
5	0.93[c]	23.7
6	0.92[c]	22.3[k]

[a–g]Assignments with the same superscript are overlapping. [h–r]Assignments with the same superscript may be interchanged. [nd]resonances not detected.

as the concentration of the compound or antibiotic required for 50% inhibition of the bacterial cells using Prism 7.0 (GraphPad Software Inc., La Jolla, CA).

Antifungal Assay

The fungus *Candida albicans* ATCC 10231 was streaked onto a Sabouraud agar plate and was incubated at 37°C for 48 h. One colony was then transferred to fresh Sabouraud broth (15 mL) and the cell density adjusted to 10^4-10^5 CFU/mL. Test compounds were dissolved in DMSO and diluted with H_2O to give a 600 μM stock solution (20% DMSO), which was serially diluted with 20% DMSO to give concentrations from 600 to 0.2 μM in 20% DMSO. An aliquot (10 μL) of each dilution was transferred to a 96-well microtiter plate and freshly prepared fungal broth (190 μL) was added to each well to give final concentrations of 30–0.01 μM in 1% DMSO. The plates were incubated at 37°C for 24 h and the optical density of each well was measured spectrophotometrically at 600 nm using POLARstar Omega plate (BMG LABTECH, Offenburg, Germany). Amphotericin B was used as a positive control (30 μg/ml in 10% DMSO). Where relevant, IC_{50} value were calculated as the concentration of the compound or antifungal

TABLE 4 | 1D NMR (methanol-d_4) data for talaropeptide D (**5**).

#	δ_H m (*J* in Hz)	δ_C
***N*-Me-L-Ala[1]**		
1		174.3
2	5.45, m	51.3
3	1.27, d (*6.9*)	14.8
N-Me	3.14, s	31.8[g]
N-$\underline{C}OCH_3$		173.6[h]
N-CO$\underline{CH_3}$	1.99, s	22.5[i]
***N*-Me-L-Val[2]**		
1		170.1
2	4.98, d (*10.9*)	61.5
3	2.24, m	28.6
4	0.98, d (*6.5*)	19.9[j]
5	0.82, d (*6.5*)	19.3[k]
N-Me	3.01, s	31.1[l]
L-Val[3]		
1		173.7[h]
2	4.63, d (*7.6*)	56.2
3	2.05[a]	31.8[g]
4	0.92[b]	19.8[j]
5	0.93[b]	18.9[m]
L-Thr[4]		
1		173.7[h]
2	4.80[c]	56.4
3	4.01, m	68.8
4	1.16, d (*6.3*)	20.0[j]
L-Val*		
1		173.9
2	4.21, d (*7.2*)	60.4
3	2.03[a]	31.9[g]
4	0.93[b]	18.8[m]
5	0.92[b]	19.8[j]
***N*-Me-L-Val[5]**		
1		172.0
2	4.69, d (*11.0*)	63.6
3	2.21[d]	28.0
4	0.89, d (*6.5*)	19.8[j]
5	0.80, d (*6.5*)	19.2[k]
N-Me	3.20, s	31.8[g]
L-Pro[6]		
1		174.8
2	4.80[c]	58.6
3	a 2.21[d]	30.2[n]
	b 1.66[e]	
4	a 2.05[a]	25.8[o]
	b 1.92, m	
5	3.71, m	48.9
***N*-Me-L-Val[7]**		
1		171.7
2	4.91, d (*10.6*)	60.2
3	2.28, m	28.2[p]
4	0.90[b]	18.6[m]
5	0.86[f]	20.6
N-Me	3.02, s	31.0[l]
***N*-Me-L-Val[8]**		
1		171.0[q]
2	5.03, d (*10.6*)	60.2
3	2.20[d]	28.3[p]
4	0.83, d (*6.7*)	20.3
5	0.67, d (*6.7*)	18.2
N-Me	2.27, s	30.3[n]
***N*-Me-L-Phe[9]**		
1		172.9
2	5.94, dd (*9.8,5.7*)	55.4
3	3.05, m	35.9
4		138.3
5/9	7.21, m	130.5
6/8	7.28, m	129.7
7	7.24, m	128.2
N-Me	2.98, s	31.6[g]
***N*-Me-L-Ile[10]**		
1		171.1[q]
2	4.76, d (*11.2*)	62.6
3	2.08, m	33.3
4	a 1.32, m	25.9[o]
	b 1.00, m	
5	0.87[f]	10.7
6	0.95, d (*6.5*)	16.0
N-Me	3.05, s	31.7[g]
L-Leu[11]		
1		nd
2	4.32, br s	54.7
3	a 1.65[e]	43.2
	b 1.55, m	
4	1.59, m	26.5
5	0.92[b]	23.8
6	0.91[b]	22.5[i]

[a–f]Assignments with the same superscript are overlapping. [g–q]Assignments with the same superscript may be interchanged. [nd]resonances not detected.

drug required for 50% inhibition of the fungal cells using Prism 7.0 (GraphPad Software Inc., La Jolla, CA).

Cytotoxicity Assay

Adherent cell SW620 (human colorectal carcinoma) and NCI-H460 (human lung carcinoma) cells were cultured in Roswell Park Memorial Institute (RPMI) 1640 medium. All cells were cultured as adherent mono-layers in flasks supplemented with 10% fetal bovine serum, L–glutamine (2 mM), penicillin (100 unit/mL), and streptomycin (100 μg/mL), in a humidified 37°C incubator supplied with 5% CO_2. Briefly, cells were harvested with trypsin and dispensed into 96-well microtiter assay plates at 3,000 cells/well, after which they were incubated for 18 h at

37°C with 5% CO_2 (to allow cells to attach as adherent monolayers). Test compounds were dissolved in 20% DMSO in PBS (v/v) and aliquots (10 μL) applied to cells over a series of final concentrations ranging from 10 nM to 30 μM. After 48 h incubation at 37°C with 5% CO_2 an aliquot (20 μL) of 3-(4,5-dimethylthiazol-2-yl)-2,5-diphenyltetrazolium bromide (MTT) in phosphate buffered saline (PBS, 5 mg/mL) was added to each well (final concentration 0.5 mg/mL), and microtiter plates were incubated for a further 4 h at 37°C with 5% CO_2. After final incubation, the medium was aspirated and precipitated formazan crystals dissolved in DMSO (100 μL/well). The absorbance of each well was measured at 580 nm with a PowerWave XS Microplate Reader from Bio-Tek Instruments Inc. Where relevant, IC_{50} values were calculated using Prism 7.0, as the concentration of analyte required for 50% inhibition of cancer cell growth (compared to negative controls). Negative control was 1% aqueous DMSO, while positive control was doxorubicin (30 μM). All experiments were performed in duplicate.

Plasma Stability Assay

An aliquot of talaropeptide D (**5**) (10 μL, 1 mM in DMSO) was added to rat plasma (190 μL) pooled from >3 different rats, and heated to 37°C in a circulating water bath. Aliquots (20 μL) were taken at time points 0, 60, 120, and 180 min and added to MeCN (80 μL). Samples were centrifuged at 13,000 g for 3 min, and the supernatants concentrated to dryness under N_2. After resuspending in MeOH (30 μL), and aliquot (1 μL) was analyzed by UHPLC-QTOF (MS), to detect and quantify residual talaropeptide D (**5**).

RESULTS

Production and Isolation

UHPLC-QTOF analysis of MATRIX cultivations (i.e., microbioreactor well, **Figure S1**) revealed that YES static broth cultivation was optimum for the production of talaropeptides (**Figures S2**–**S4**). Reversed phase HPLC-DAD-ESIMS analysis of a 10 day YES static broth cultivation of CMB-TU011 revealed complete suppression of talarolide A (**1**) biosynthesis, in favor of four new higher molecular weight *putative* peptides, eluting in the order *m/z* 1254.8 (**2**), 1353.8 (**3**), 1318.8 (**4**), and 1417.9 (**5**) (**Figure S6**). Subsequent studies confirmed the production of **2**–**5** in YES static broth flask cultivations (80 mL broths in 250 mL flasks), with a >10-fold increase in production in flasks sealed with an air permeable cotton plug, as opposed to an air impermeable screw cap (**Figure S5**). Based on these results, scaled up production (160 mL broth in 10 × 500 mL flasks) successfully yielded a crude EtOAc extract (1.65 g), which was subjected to solvent trituration to yield hexane (495 mg) and MeOH (1.15 g) solubles. With analytical HPLC-DAD-ESIMS localizing **2**-**5** in the MeOH solubles, this material was subjected to gel chromatography (Sephadex LH-20, MeOH) followed by semi-preparative reversed phase HPLC chromatography, to yield talaropeptides A (**2**, 1.3 mg), B (**3**, 1.3 mg), C (**4**, 1.8 mg), and D (**5**, 2.8 mg) (**Figure 1**).

Talaropeptide A (2)

HRESI(+)MS analysis of **2** returned a protonated molecular ion attributed to a molecular formula ($C_{65}H_{111}N_{11}O_{13}$, Δmmu−0.1) requiring 16 double bond equivalent (DBEs). Consistent with its *putative* peptide status, C_3 and C_{18} Marfey's analyses (**Figure 2**), together with careful consideration of 1D and 2D NMR (DMSO-d_6) data (**Table 1**, **Figures S8**–**S13**), confirmed the presence of 11 amino acid residues [L-Thr, L-Pro, L-Val, L-Leu, *N*-Me-L-Ala, *N*-Me-L-Val (×4), *N*-Me-L-Phe and *N*-Me-L-Ile]. Whereas the C_3 Marfey's method proved very effective at discriminating most amino acids, and in particular L vs D *N*-Me-Ile and *N*-Me-*allo*-Ile (**Figure 2H**), the C_{18} Marfey's method was needed to discriminate L vs D *N*-Me-Ala (**Figure 2D,** inset). The presence of multiple (×4) *N*-Me-L-Val residues was apparent from the complex array of isopropyl methyl resonances in the ^{1}H NMR data for **2** (**Table 1**). This assessment of the amino acid content in **2** accounted for all DBE and was indicative of a linear undecapeptide. Although overlapping 1D NMR resonances prevented assignment of the complete amino acid sequence, diagnostic 2D NMR HMBC and ROESY correlations did identify a number of partial sequences; (i) *N*-Me-L-Ala^1-*N*-Me-L-Val^2-*N*-H (e.g., an HMBC correlation from *N*-Me-L-Val^2 to C-1 in *N*-Me-L-Ala^1); (ii) L-Thr^4-*N*-Me-L-Val^5 (e.g., a ROESY correlation between H-2 in L-Thr^4 and *N*-Me-L-Val^5); (iii) L-Pro^6-*N*-Me-L-Val^7-*N*-Me-L-Val^8-*N*-Me-L-Phe^9 (e.g., HMBC correlations from H-2 in *N*-Me-L-Val^7 to C-1 in L-Pro^6, from *N*-Me-L-Val^8 to C-1 in *N*-Me-L-Val^7, and from H-2 in *N*-Me-L-Phe^9 to C-1 in *N*-Me-L-Val^8); (iv) *N*-Me-L-Ile^{10}-L-Leu^{11} (e.g., an HMBC correlation from the *N*-H in L-Leu^{11} to C-1 in *N*-Me-L-Ile^{10}) (see **Figure 3**). While the HMBC and ROESY data failed to link fragments (i–iv), or locate L-Val^3, these issues were ultimately resolved by diagnostic UHPLC-QTOF (MS/MS) fragmentation patterns, which identified two consolidated partial sequences; (v) *N*-Me-L-Ala^1-*N*-Me-L-Val^2-L-Val^3-L-Thr^4-*N*-Me-L-Val^5 and (vi) *N*-Me-L-Val^8-*N*-Me-L-Phe^9-*N*-Me-L-Ile^{10}-L-Leu^{11} (**Figure 3**, **Figure S14**). Assembly of the partial sequences i-vi returned the complete structure for talaropeptide A (**2**) as shown (**Figure 1**).

Talaropeptide B (3)

HRESI(+)MS analysis of **3** returned a sodiated molecular ion attributed to a molecular formula ($C_{70}H_{120}N_{12}O_{14}$, Δmmu−1.9) requiring 17 DBEs, suggestive of a Val homolog of **2**. The ^{1}H NMR (DMSO-d_6) spectrum of **3** (**Figure S16**) revealed resonances closely resembling **2**, however, the extra Val residue was not observed in HSQC (DMSO-d_6) spectrum. Therefore, we re-acquired the NMR data in methanol-d_4, which revealed resonances attributed to the additional Val residue (δ_H 3.50, δ_C 60.3) (**Figure S19**). This hypothesis was confirmed by C_3 and C_{18} Marfey's analyses (**Figure S23**) and 1D and 2D NMR (methanol-d_4) data (**Table 2**, **Figures S17**–**S21**), which confirmed the presence of 12 amino acid residues [L-Thr, L-Pro, L-Val (×2), L-Leu, *N*-Me-L-Ala, *N*-Me-L-Val (×4), *N*-Me-L-Phe and *N*-Me-L-Ile], accounting for all DBE and requiring that **3** be a linear dodecapeptide. Diagnostic 2D NMR HMBC and ROESY correlations identified key partial sequences; (i) *N*-Me-L-Ala^1-*N*-Me-L-Val^2 (e.g., an HMBC

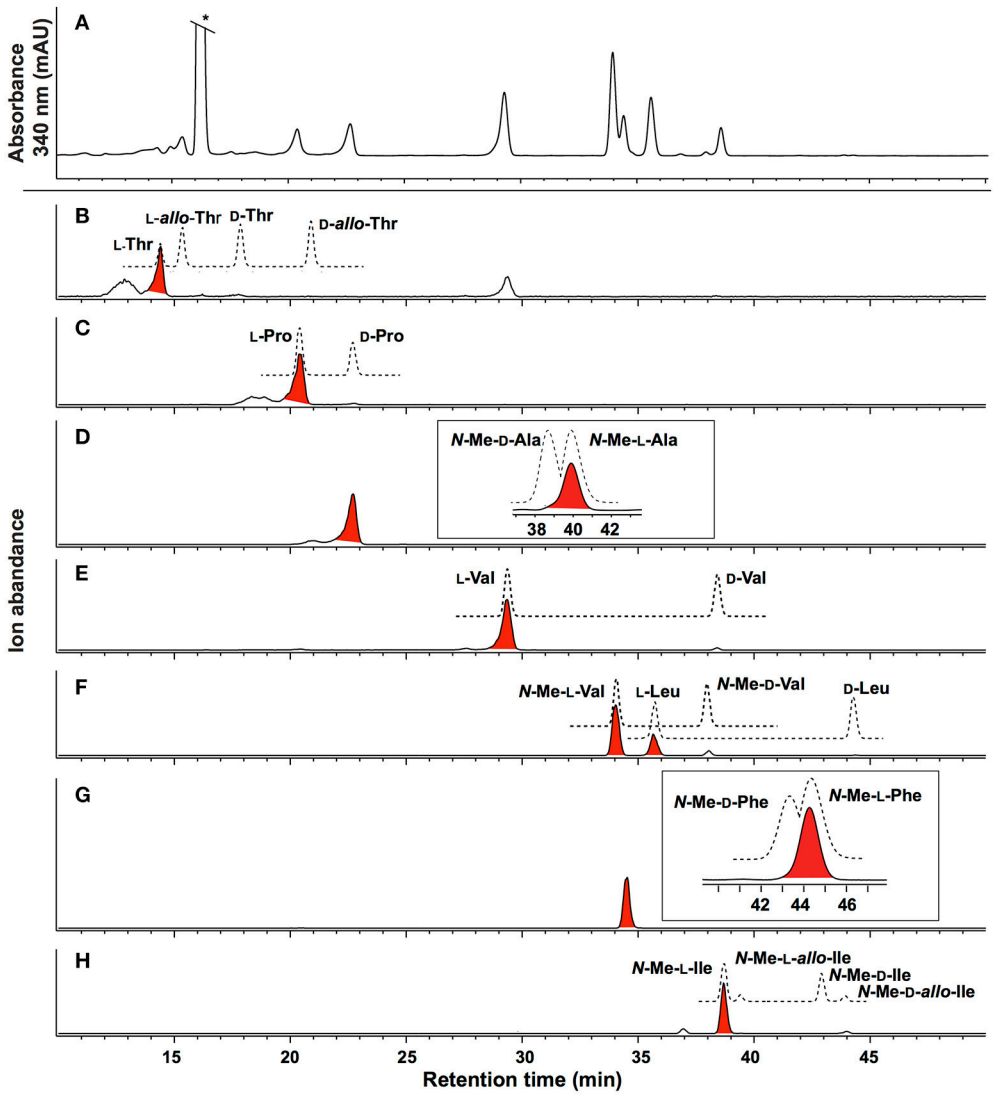

FIGURE 2 | Marfeys analysis for talaropeptide A (**2**). **(A)** C_3 HPLC-DAD (340 nm) chromatogram of L-FDAA derivatised hydrolysate of 2. **(B–H)** C_3 HPLC-MS-SIE chromatograms for selected L-FDAA derivatives of amino acid standards (broken lines) and the acid hydrolysate of 2 (red highlighted peaks). The inset in **(D)** and **(G)** show the C_{18} HPLC-DAD chromatogram. Traces reveal **(B)** L-Thr (SIE *m/z* 372), **(C)** L-Pro (SIE *m/z* 368), **(D)** *N*-Me-L-Ala (SIE *m/z* 356) **(E)** L-Val (SIE *m/z* 370) **(F)** *N*-Me-L-Val and L-Leu (SIE *m/z* 384), **(G)** *N*-Me-L-Phe (SIE *m/z* 432) and **(H)** *N*-Me-L-Ile (SIE *m/z* 398). *Residual Marfey's reagent.

correlation from H-2 in *N*-Me-L-Val[2] to C-1 in *N*-Me-L-Ala[1]); (ii) L-Pro[6]-*N*-Me-L-Val[7]-*N*-Me-L-Val[8]-*N*-Me-L-Phe[9]-*N*-Me-L-Ile[10] (e.g., HMBC correlations from H-2 in *N*-Me-L-Val[7] to C-1 in L-Pro[6], from *N*-Me-L-Val[8] to C-1 in *N*-Me-L-Val[7], from *N*-Me-L-Phe[9] to C-1 in *N*-Me-L-Val[8], and from *N*-Me-L-Ile[10] to C-1 in *N*-Me-L-Phe[9]) (**Figure 4**). Similarly, diagnostic UHPLC-QTOF (MS/MS) fragmentation patterns identified consolidated partial sequence; (iii) *N*-Me-L-Ala[1]-*N*-Me-L-Val[2]-L-Val[3]-L-Thr[4]-L-Val*-*N*-Me-Val[5], and (iv) *N*-Me-L-Val[8]-*N*-Me-L-Phe[9]-*N*-Me-L-Ile[10]-L-Leu[11] (**Figure 4**, **Figure S22**). Assembly of the partial sequences i-iv returned the complete structure for talaropeptide B (**3**) as shown (**Figure 1**), with the following caveat. As *N*-Me-Val[5] and L-Leu[11] are isomeric, their relative position cannot be determined by MS/MS fragmentation (or by way of overlapping 1D NMR resonances). To establish the regiochemistry of these amino acid residues, we draw on biosynthetic comparisons to the co-metabolite **2**, as well as knowledge of the talaropeptide biosynthetic gene cluster (see below).

Talaropeptide C (4)

HRESI(+)MS analysis of **4** returned a sodiated molecular ion attributed to a molecular formula ($C_{67}H_{113}N_{11}O_{14}$, Δmmu +1.5) requiring 17 DBEs, suggestive of an acetylated homolog of **2** (i.e., +42 Da). Comparison of the ^{1}H NMR (methanol-d_6) data for **4** with **2** supported the latter hypothesis, with the only significant difference being the appearance of resonances attributed to an acetyl moiety (δ_H 1.99, δ_C 22.3), with an HMBC correlation from

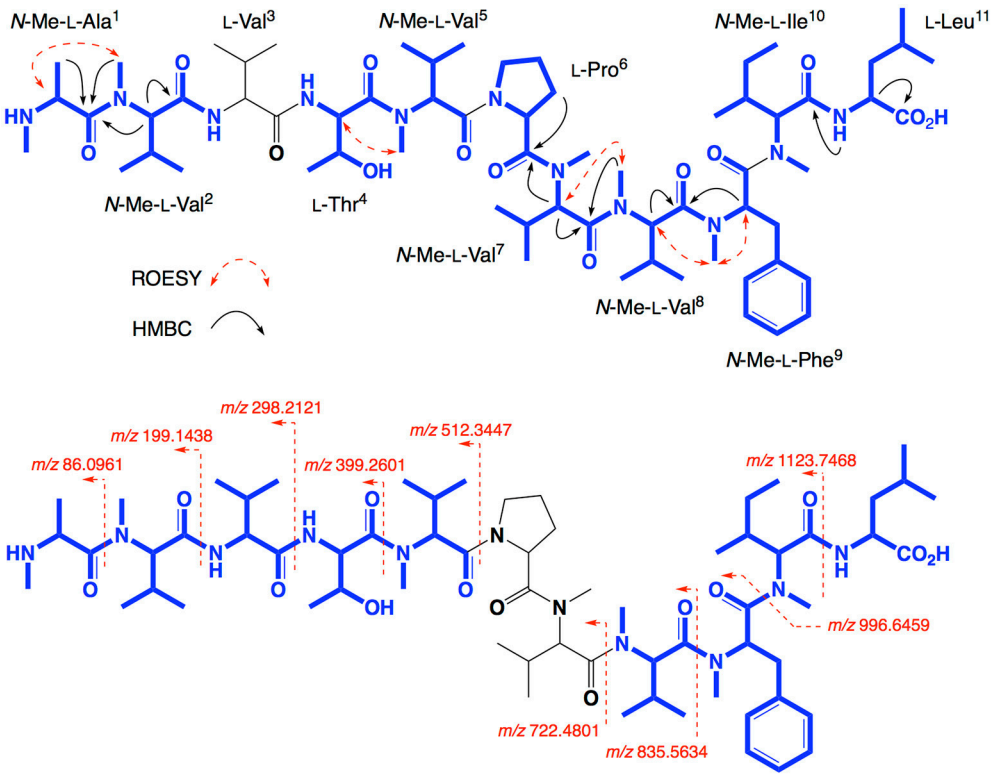

FIGURE 3 | Selected 2D NMR ROESY and HMBC correlations, and MS/MS fragmentations for talaropeptide A (**2**)–partial sequences highlighted in blue.

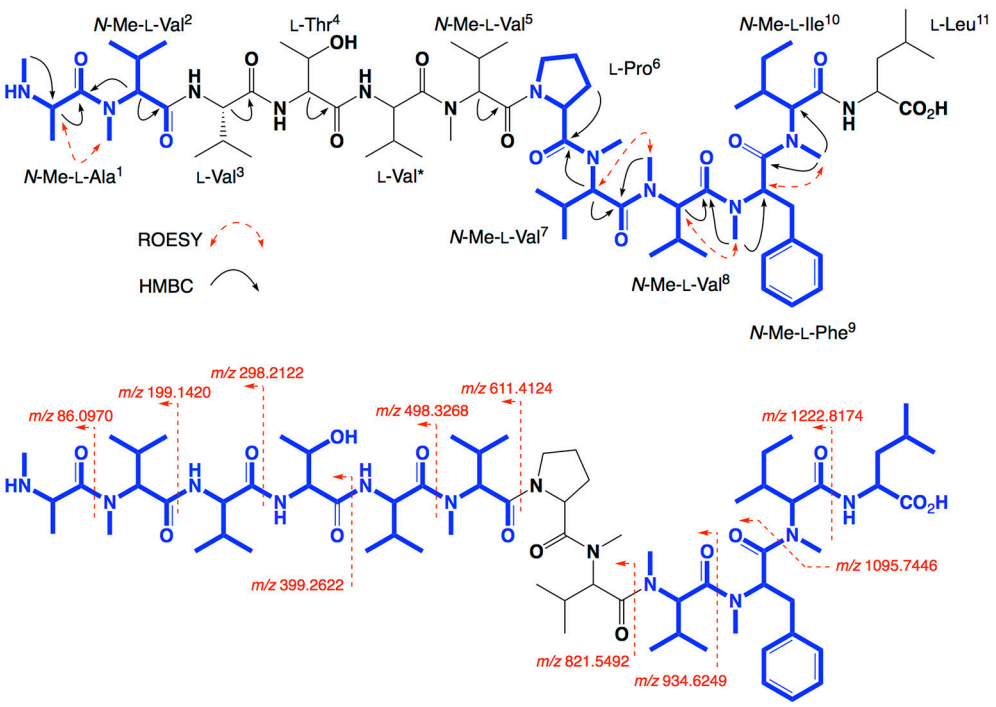

FIGURE 4 | Selected 2D NMR correlations, and MS/MS fragmentations for talaropeptide B (**3**)–partial sequences highlighted in blue.

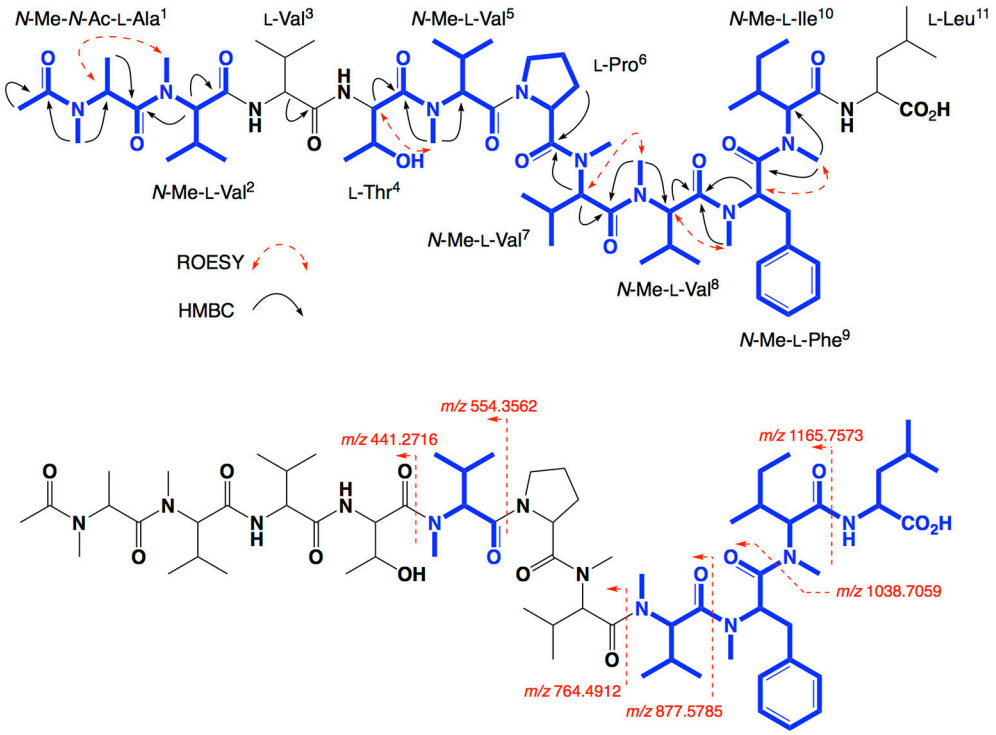

FIGURE 5 | Selected 2D NMR correlations, and MS/MS fragmentations for talaropeptide C (**4**)–partial sequences highlighted in blue.

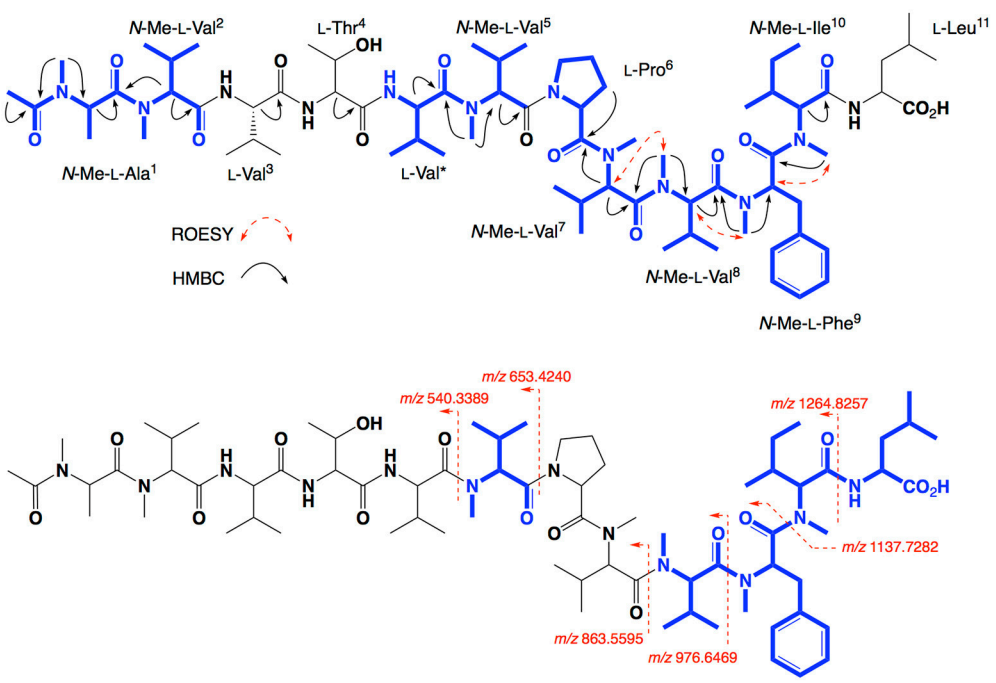

FIGURE 6 | Selected 2D NMR correlations, and MS/MS fragmentations for talaropeptide D (**5**)–partial sequences highlighted in blue.

N-Me-L-Ala[1] to *N*-$COCH_3$ being diagnostic for an *N*-terminal acetamide moiety. C_3 and C_{18} Marfey's analyses (**Figure S31**) together with 1D and 2D NMR (methanol-d_4) data (**Table 3**, **Figures S24–S29**), confirmed the presence of 11 amino acid residues (L-Thr, L-Pro, L-Val, L-Leu, *N*-Me-L-Ala, *N*-Me-L-Val (×4), *N*-Me-L-Phe and *N*-Me-L-Ile), accounting for all DBE and requiring that **4** be a linear undecapeptide. Diagnostic 2D NMR HMBC and ROESY correlations identified key partial sequences; (i) *N*-Me-*N*-Ac-L-Ala[1]-*N*-Me-L-Val[2] (e.g., an HMBC correlation from H-2 in *N*-Me-L-Val[2] to C-1 in *N*-Me-*N*-Ac-L-Ala[1]); (ii) L-Thr[4]-*N*-Me-L-Val[5] (e.g., an HMBC correlation from an *N*-Me-L-Val[5] to C-1 in L-Thr[4]), and (iii) L-Pro[6]-*N*-Me-L-Val[7]-*N*-Me-L-Val[8]-*N*-Me-L-Phe[9]-*N*-Me-L-Ile[10] (e.g., HMBC correlations from H-2 in *N*-Me-L-Val[7] to C-1 in L-Pro[6], and from *N*-Me-L-Val[8] to C-1 in *N*-Me-L-Val[7], and from *N*-Me-L-Phe[9] to C-1 in *N*-Me-L-Val[8], and from *N*-Me-L-Ile[10] to C-1 in *N*-Me-L-Phe[9]) (**Figure 5**). Similarly, diagnostic UHPLC-QTOF (MS/MS) fragmentation patterns identified the consolidated partial sequence (iv) *N*-Me-L-Val[8]-*N*-Me-L-Phe[9]- *N*-Me-L-Ile[10]-L-Leu[11] (**Figure 5**, **Figure S30**). Assembly of the partial sequences i–iv returned the complete structure for talaropeptide C (**4**) as shown (**Figure 1**).

Talaropeptide D (5)

HRESI(+)MS analysis of **5** returned a sodiated molecular ion attributed to a molecular formula ($C_{72}H_{122}N_{12}O_{15}$, Δmmu +0.7) requiring 18 DBEs, suggestive of an acetylated homolog of **3** (i.e., +42 Da). Comparison of the ^{1}H NMR (methanol-d_4) data for **5** with **3** supported the latter hypothesis, with the only significant difference being the appearance of resonances attributed to an acetyl moiety (δ_H 1.99, δ_C 22.5), with HMBC correlations to the *N*-Me-L-Ala[1] position it on the *N*-terminus. C_3 and C_{18} Marfey's analyses (**Figure S38**) and 1D and 2D NMR (methanol-d_6) data (**Table 4**, **Figures S32–S36**), confirmed the presence of 12 amino acid residues [L-Thr, L-Pro, L-Val (×2), L-Leu, *N*-Me-L-Ala, *N*-Me-L-Val (×4), *N*-Me-L-Phe and *N*-Me-L-Ile], accounting for all DBE and requiring that **5** be a linear dodecapeptide. Diagnostic 2D NMR HMBC and ROESY correlations identified key partial sequences; (i) *N*-Me-*N*-Ac-L-Ala[1]-*N*-Me-L-Val[2] (e.g., HMBC correlations from *N*-Me-L-Ala[1] to *N*-$COCH_3$, and from H-2 in *N*-Me-L-Val[2] to C-1 in *N*-Me-L-Ala[1]); (ii) L-Val*-*N*-Me-L-Val[5] (e.g., an HMBC correlation from an *N*-Me-L-Val[5] to C-1 in L-Val*), and (iii) L-Pro[6]-*N*-Me-L-Val[7]-*N*-Me-L-Val[8]-*N*-Me-L-Phe[9]-*N*-Me-L-Ile[10] (e.g., HMBC correlations from H-2 in *N*-Me-L-Val[7] to C-1 in L-Pro[6], and from *N*-Me-L-Val[8] to C-1 in *N*-Me-L-Val[7], and from *N*-Me-L-Phe[9] to C-1 in *N*-Me-L-Val[8], and from an *N*-Me to C-1 in *N*-Me-L-Phe[9]) (see **Figure 6**). Similarly, diagnostic UHPLC-QTOF (MS/MS) fragmentation patterns identified the partial sequence (iv) *N*-Me-L-Val[8]-*N*-Me-L-Phe[9]-*N*-Me-L-Ile[10]-L-Leu[11] (**Figure 6**, **Figure S37**). Assembly of the partial sequences i–iv returned the complete structure for talaropeptide D (**5**) as shown (**Figure 1**), with the following caveat. As the NMR and MS/MS data for **5** could not provide an experimental assignment of relative regiochemistry for the dipeptide fragment comprised of L-Val[3] and L-Thr[4], we draw on biosynthetic comparisons to the co-metabolite **3**, as well as knowledge of the talaropeptide biosynthetic gene cluster (see below).

TABLE 5 | Draft genome sequence of *Talaromyces* sp. CMB-TU011.

Length	27,481,273
GC content	0.47%
Coverage	31X
Contigs	1652
Closest relative (ITS as marker)	*Talaromyces helicus* (99% sequence identity)
Biosynthetic gene clusters	17

Talaropeptide Biosynthesis

A genome sequence of *Talaromyces* sp. CMB-TU011 was obtained, with coverage of 31X length of 27.5 MB, and a GC content of 47 %, consistent with related species (**Table 5**). Natural product genome mining of this sequence identified 17 biosynthetic gene clusters (BGCs, **Table S7**) including three non-ribosomal peptide synthetases (NRPS). A very large intron-less mega synthase that includes 12 modules and 44 domains encoded in a single gene (45,892 bases, 15,297 amino acids) was identified as a plausible talaropeptide NRPS. Of note, this NRPS is only 3.2 kb smaller than the largest NRPS ever reported (49,104 bases, plu2670, 16,367 amino acids), being that documented for the extensively *N*-methylated and commercially important fungal cyclic undecapeptide cyclosporine from *Tolypocladium inflatum* (GenBank accesion: CAA82227, 15281 amino acids) (Weber et al., 1994).

The putative talaropeptide NRPS (**Figure 7**) exhibits an *N*-terminus condensation domain with a similar configuration to that of previously reported C domains associated with peptides incorporating *N*-terminal acyl moieties, consistent with the *N*-terminal *N*-acylation observed in talaropeptides C (**4**) and D (**5**). This domain might have been skipped during the biosynthesis of talaropeptide A (**2**) and B (**3**), or alternatively the *N*-Ac moiety may have been deleted after the biosynthesis (*i.e.* hydrolysed). A total of 12 adenylation domains were detected, in agreement with the number of amino acid residues found in talaropeptides B (**3**) and D (**5**). Predicted amino acid specificities for these domains are largely in agreement with those observed for **3** and **5**, except for modules 1 and 4 (**Table 6**). Seven methyl transferase domains were consistent with *N*-methylation sites in **2**-**5**, with exceptions for *N*-methylation of residues 1 and 2, which may be installed post NRPS assembly. Alternatively, the methyl transferase in module 3 appears to be inactive on its corresponding extension step (i.e., L-Val[3]), and may be responsible for methylation of the first two residues (i.e., *N*-Me-*N*-Ac-L-Ala[1] and *N*-Me-L-Val[2]). The methylation domain at module 5 (L-Val*) appears to be inactive during the biosynthesis of talaropeptides B (**3**) and D (**5**), while the entire module 5 inactive in the biosynthesis of talaropeptides A (**2**) and C (**4**). Finally, a thioesterase domain was detected at the C-terminus of the talaropeptide NRPS, accounting for the release of the peptide product with a C-terminus carboxylic acid.

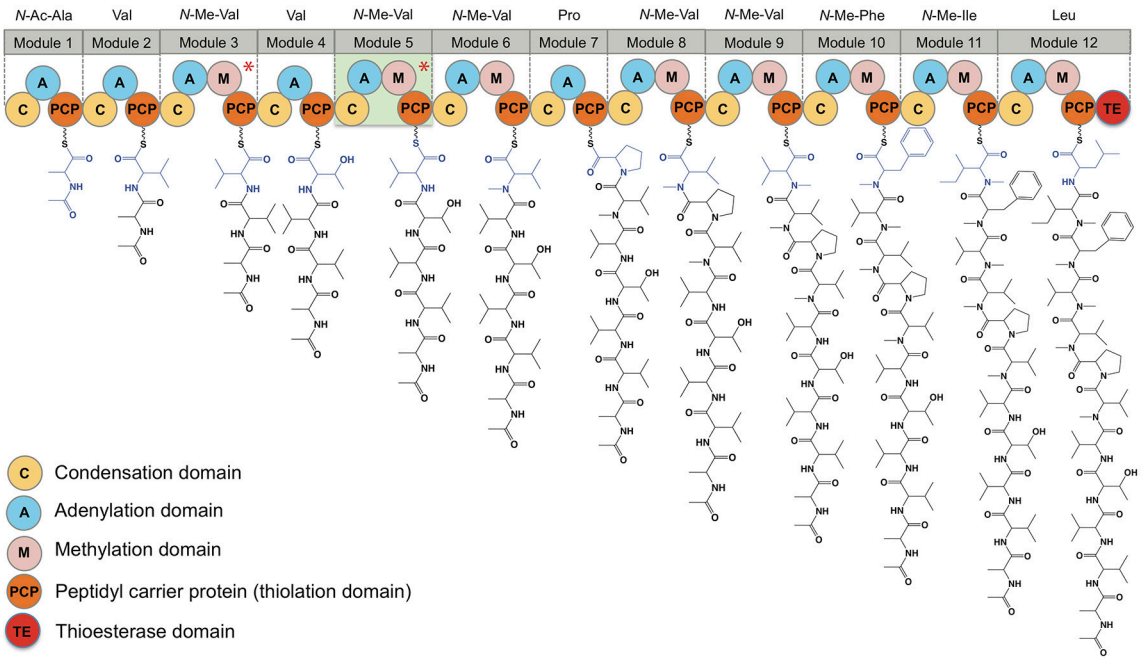

FIGURE 7 | Domain organization of the talaropeptide synthase and biosynthetic logic of the talaropeptides. Biosynthesis of talaropeptide D (**5**) is depicted. Methylation domains marked with an asterisk are skipped during biosynthesis, while module 5 (highlight light green) is skipped during talaropeptides A (**2**) and C (**4**) biosynthesis.

TABLE 6 | Comparison of a predicted product for ORFX (talaropeptide synthase) with structure for talaropeptide D (**5**). Adenylation (A) domain specificity was calculated using the LSI based A-domain functional predictor.

Module	Residue Prediction	Domain LSI score	Residues in 5	Comment
1	*N*-Ac-L-Val	0.585	*N*-Ac-*N*-Me-L-Ala[1]	Adenylation domain promiscuity or new sequence motif. Post-NRPS methylation. Acylation (starter C domain) skipped for talaropeptides A (**2**) and B (**3**).
2	L-Val	0.493	*N*-Me-L-Val[2]	Post-NRPS methylation.
3	*N*-Me-L-Val	0.673	L-Val[3]	Skipped methylation domain.
4	L-Val	0.673	L-Thr[4]	Adenylation domain promiscuity or new sequence motif.
5	*N*-Me- L-Val	0.628	L-Val*	Skipped methylation domain. Module skipped for talaropeptides A (**2**) and C (**4**).
6	*N*-Me-L-Val	0.673	*N*-Me-L-Val[5]	Matched prediction.
7	L-Val/L-Pro	0.49/0.366	L-Pro[6]	Partially matched prediction.
8	*N*-Me-L-Val	0.673	*N*-Me-L-Val[7]	Matched prediction.
9	*N*-Me-L-Val	0.673	*N*-Me-L-Val[8]	Matched prediction.
10	*N*-Me-L-Phe	0.482	*N*-Me-L-Phe[9]	Matched prediction.
11	*N*-Me-L-Ile	0.657	*N*-Me-L-Ile[10]	Matched prediction.
12	L-Leu	0.739	L-Leu[11]	Matched prediction.

Talaropeptide Biological Activity

Talaropeptides A-D (**2**-**5**) exhibited no growth inhibitory activity when tested (up to 30 μM) against human lung (NCI-H460) and colon (SW620) carcinoma cells, or when tested against the Gram-negative bacteria *Escherichia coli* ATCC 11775 and *Pseudomonas aeruginosa* ATCC 10145, the Gram-positive bacteria *Staphylococcus aureus* ATCC 25923 and *S. aureus* ATCC 9144, or the fungus *Candida albicans* ATCC 10231 (**Supplementary Material**). By contrast, talaropeptides A (**2**) and B (**3**) alone exhibited promising growth inhibitory activity (IC_{50} 1.5 and 3.7 μM) against the Gram-positive bacteria *Bacillus subtilis* ATCC 6633 (**Figure S41**). As might be predicted for an extensively *N*-methylated linear peptide, talaropeptide A (**2**) proved stable to rat plasma (i.e., proteases) (**Figure S39**).

DISCUSSION

Although fungi are well-known to produce cyclic peptides, linear peptides > 7 amino acid residues are comparatively rare (Komatsu et al., 2001; Boot et al., 2006). For example, excluding peptaibols such as the recently described trichodermides (Jiao et al., 2018), which are dominated by non-proteinogenic amino acids [e.g., α-aminoisobutyric acid (Aib) and D–isovaline (D–Iva)], only a handful linear peptides of > 7 amino acid residues have been reported from fungi. Interestingly, these reports feature peptides from marine-derived fungi, including the dodecapeptide dictyonamides A and B from a marine red alga-derived fungus (Komatsu et al., 2001), and *N*-methylated octapeptides RHM 1 and RHM 2 from a marine sponge-derived *Acremonium* (Boot et al., 2006). Also of note, no linear peptides have been reported from the genus *Talaromyces*.

The talaropeptides A-D (**2**-**5**) represent a new class of extensively *N*-methylated linear peptide natural product, and at the same time feature peptide amino acid sequences that are unprecedented in the scientific literature. That the talaropeptide pharmacophore lacks mammalian cell cytotoxicity, and exhibits highly selective antibacterial properties (albeit with modest potency), with a clear structure activity relationship requirement built around *N*-terminal acetylation, is intriguing.

From an ecological perspective, the link between antibacterial activity and acetylation suggests that control of *N*-acetylation, perhaps as a post-NRPS modification by hydrolysis of the acetyl group or by an unknown biosynthetic mechanism that lead to domain skipping, may bias production in favor of **2** and **3** as an antibacterial defense, or **4** and **5** as putative antibacterial prodrugs. In an ecological setting rich in microbial competitors, this putative biosynthetic mechanism of control may be mediated by inter-species or even inter-kingdom chemical communication.

The discovery that talaropeptide production was highly culture media and phase dependent (i.e., YES broth, static flask with an air permeable seal) raises the possibility that, the paucity of published fungal linear peptides may be due to a bias for cultivation conditions that disfavor linear peptides. Our application of systematic miniaturized microbioreactor approach to trialing cultivation conditions (i.e., MATRIX) provides a low cost, practical means to access this silent potential.

DATA AVAILABILITY STATEMENT

The raw data supporting the conclusions of this manuscript will be made available by the authors, without undue reservation, to any qualified researcher.

The GeneBank accession; Bankit212474, talarolide_synthase – MH479449.

AUTHOR CONTRIBUTIONS

RC initiated and oversaw all research. PD performed all fungal cultivations, and isolated and characterized talaropeptides. PD, PP, AS, ZK, and RC performed data analysis and talaropeptide structure elucidations. ZK isolated fungal DNA, and together with PD carried out bioassays. PC-M and EM performed all genomic analyses, and identified the talaropeptide NRPS. RC and PD co-drafted the manuscript.

FUNDING

This work was supported in part by The University of Queensland, the Institute for Molecular Bioscience and the Australian Institute for Bioengineering and Nanotechnology.

ACKNOWLEDGMENTS

We thank R Damodar for the original isolation of *Talaromyces* sp. CMB-TU011.

SUPPLEMENTARY MATERIAL

The Supplementary Material for this article can be found online at: https://www.frontiersin.org/articles/10.3389/fchem.2018.00394/full#supplementary-material

Supplementary Material | The includes fungal cultivation trial details, as well as tabulated and annotated 1D and 2D NMR data and spectra, C_3 and C_{18} Marfey's and MS/MS analyses, and biological assay data for **2**–**5**.

REFERENCES

Bankevich, A., Nurk, S., Antipov, D., Gurevich, A. A., Dvorkin, M., Kulikov, A. S., et al. (2012). SPAdes: a new genome assembly algorithm and its applications to single-cell sequencing. *J. Comput. Biol.* 19, 455–477. doi: 10.1089/cmb.2012.0021

Baranašić, D., Zucko, J., Diminic, J., Gacesa, R., Long, P. F., Cullum, J., et al. (2014). Predicting substrate specificity of adenylation domains of nonribosomal peptide synthetases and other protein properties by latent semantic indexing. *J. Ind. Microbiol. Biotechnol.* 41, 461–467. doi: 10.1007/s10295-013-1322-2

Blin, K., Wolf, T., Chevrette, M. G., Lu, X., Schwalen, C. J., Kautsar, S. A., et al. (2017). antiSMASH 4.0-improvements in chemistry prediction and gene cluster boundary identification. *Nucleic Acids Res.* 45, W36–W41. doi: 10.1093/nar/gkx319

Bolger, A. M., Lohse, M., and Usadel, B. (2014). Trimmomatic: a flexible trimmer for Illumina sequence data. *Bioinformatics* 30, 2114–2120. doi: 10.1093/bioinformatics/btu170

Boot, C. M., Tenney, K., Valeriote, F. A., and Crews, P. (2006). Highly N-methylated linear peptides produced by an atypical sponge-derived *Acremonium* sp. *J. Nat. Prod.* 69, 83–92. doi: 10.1021/np0503653

Dewapriya, P., Prasad, P., Damodar, R., Salim, A. A., and Capon, R. J. (2017). Talarolide A, a cyclic heptapeptide hydroxamate from an Australian Marine Tunicate-Associated Fungus, *Talaromyces* sp. (CMB-TU011). *Org. Lett.* 19, 2046–2049. doi: 10.1021/acs.orglett.7b00638

Finn, R. D., Coggill, P., Eberhardt, R. Y., Eddy, S. R., Mistry, J., Mitchell, A. L., et al. (2016). The Pfam protein families database: towards a more sustainable future. *Nucleic Acids Res.* 44, D279–D285. doi: 10.1093/nar/gkv1344

Jiao, W. H., Khalil, Z., Dewapriya, P., Salim, A. A., Lin, H. W., and Capon, R. J. (2018). Trichodermides A–E: new peptaibols isolated from the australian termite nest-derived fungus trichoderma virens CMB-TN16. *J. Nat. Prod.* 81, 976–984. doi: 10.1021/acs.jnatprod.7b01072

Khalil, Z. G., Kalansuriya, P., and Capon, R. J. (2014). Lipopolysaccharide (LPS) stimulation of fungal secondary metabolism. *Mycology* 5, 168–178. doi: 10.1080/21501203.2014.930530

Komatsu, K., Shigemori, H., and Kobayashi, J. (2001). Dictyonamides A and B, new peptides from marine-derived fungus. *J. Org. Chem*. 66, 6189–6192. doi: 10.1021/jo0156767

Marchler-Bauer, A., Bo, Y., Han, L., He, J., Lanczycki, C. J., Lu, S., et al. (2017). CDD/SPARCLE: functional classification of proteins via subfamily domain architectures. *Nucleic Acids Res*. 45, D200–D203. doi: 10.1093/nar/gkw1129

Nikodinovic, J., Barrow, K. D., and Chuck, J. A. (2003). High yield preparation of genomic DNA from Streptomyces. *BioTechniques* 35, 932–936.

Rutherford, K., Parkhill, J., Crook, J., Horsnell, T., Rice, P., Rajandream, M. A., et al. (2000). Artemis: sequence visualization and annotation. *Bioinformatics* 16, 944–945. doi: 10.1093/bioinformatics/16.10.944

Simpson, J. T., Wong, K., Jackman, S. D., Schein, J. E., Jones, S. J. M., and Birol, I. (2009). ABySS: a parallel assembler for short read sequence data. *Genome Res.* 19, 1117–1123. doi: 10.1101/gr.089532.108

Vijayasarathy, S., Prasad, P., Fremlin, L. J., Ratnayake, R., Salim, A. A., Khalil, Z., et al. (2016). C3 and 2D C3 Marfey's methods for amino acid analysis in natural products. *J. Nat. Prod*. 79, 421–427. doi: 10.1021/acs.jnatprod.5b01125

Weber, G., Schörgendorfer, K., Schneider-Scherzer, E., and Leitner, E. (1994). The peptide synthetase catalyzing cyclosporine production in *Tolypocladium niveum* is encoded by a giant 45.8-kilobase open reading frame. *Curr. Genet*. 26, 120–125. doi: 10.1007/BF00313798

Zerbino, D. R., and Birney, E. (2008). Velvet: algorithms for de novo short read assembly using de Bruijn graphs. *Genome Res.* 18, 821–829. doi: 10.1101/gr.074492.107

Conflict of Interest Statement: The authors declare that the research was conducted in the absence of any commercial or financial relationships that could be construed as a potential conflict of interest.

frontiers in Chemistry

ORIGINAL RESEARCH
published: 13 September 2018
doi: 10.3389/fchem.2018.00422

α-Glucosidase Inhibitors From the Coral-Associated Fungus *Aspergillus terreus*

Mengting Liu[1†], Changxing Qi[1†], Weiguang Sun[1†], Ling Shen[1], Jianping Wang[1], Junjun Liu[1], Yongji Lai[2], Yongbo Xue[1], Zhengxi Hu[1] and Yonghui Zhang[1*]*

[1] Hubei Key Laboratory of Natural Medicinal Chemistry and Resource Evaluation, School of Pharmacy, Tongji Medical College, Huazhong University of Science and Technology, Wuhan, China, [2] Department of Pharmacy, the Central Hospital of Wuhan, Wuhan, China

Nine novel butenolide derivatives, including four pairs of enantiomers, named (±)-asperteretones A–D (**1a/1b–4a/4b**), and a racemate, named asperteretone E (**5**), were isolated and identified from the coral-associated fungus *Aspergillus terreus*. All the structures were established based on extensive spectroscopic analyses, including HRESIMS and NMR data. The chiral chromatography analyses allowed the separation of (±)-asperteretones A–D, whose absolute configurations were further confirmed by experimental and calculated electronic circular dichroism (ECD) analysis. Structurally, compounds **2**–**5** represented the first examples of prenylated γ-butenolides bearing 2-phenyl-3-benzyl-4*H*-furan-1-one motifs, and their crucial biogenetically related metabolite, compound **1**, was uniquely defined by an unexpected cleavage of oxygen bridge between C-1 and C-4. Importantly, (±)-asperteretal D and (4*S*)-4-decarboxylflavipesolide C were revised to (±)-asperteretones B (**2a**/**2b**) and D (**4**), respectively. Additionally, compounds **1a/1b–4a/4b** and **5** were evaluated for the α-glucosidase inhibitory activity, and all these compounds exhibited potent inhibitory potency against α-glucosidase, with IC_{50} values ranging from 15.7 ± 1.1 to 53.1 ± 1.4 μM, which was much lower than that of the positive control acarbose (IC_{50} = 154.7 ± 8.1 μM), endowing them as promising leading molecules for the discovery of new α-glucosidase inhibitors for type-2 diabetes mellitus treatment.

Keywords: coral-associated fungus, *Aspergillus terreus*, butenolide derivatives, structure reassignments, α-glucosidase inhibitors

OPEN ACCESS

Edited by:
Xian-Wen Yang,
Third Institute of Oceanography, State Oceanic Administration, China

Reviewed by:
Junfeng Wang,
South China Sea Institute of Oceanology (CAS), China
Valeria Costantino,
Università degli Studi di Napoli Federico II, Italy

***Correspondence:**
Zhengxi Hu
hzx616@126.com
Yonghui Zhang
zhangyh@mails.tjmu.edu.cn

†These authors have contributed equally to this work

Specialty section:
This article was submitted to Medicinal and Pharmaceutical Chemistry, a section of the journal Frontiers in Chemistry

Received: *24 July 2018*
Accepted: *24 August 2018*
Published: *13 September 2018*

Citation:
Liu M, Qi C, Sun W, Shen L, Wang J, Liu J, Lai Y, Xue Y, Hu Z and Zhang Y (2018) α-Glucosidase Inhibitors From the Coral-Associated Fungus Aspergillus terreus. Front. Chem. 6:422. doi: 10.3389/fchem.2018.00422

INTRODUCTION

Diabetes mellitus (DM) is one of the most serious chronic diseases with the ever-increasing incidence rates of obesity and aging of the general population throughout the world (Kopelman, 2000) In 2013, it was estimated that over 382 million people all over the world have DM and this number is predicted to increase up to 500 million in 2030, when this disease will be excepted to be the 7th leading cause of death (Lauritano and Ianora, 2016). Globally, type-2 diabetes (non-insulin-dependent DM) covered 90–95% of all the diabetes cases (Lauritano and Ianora, 2016). Postprandial hyperglycemia is an important factor for the induction of type-2 diabetes and complications related to the diseases, such as micro- and macro-vascular diseases (Baron, 1998). A good strategy to maintain the normal level of postprandial plasma glucose is to medicate in

combination with dietary restriction and an exercise plan (Kim et al., 2008). In type-2 diabetes, delaying glucose absorption after meals by inhibition of α-glucosidase is known to help the therapy (Kim et al., 2008). For diabetic patients, α-glucosidase inhibitors (AGIs) are widely applied either as monotherapy or in combination with other oral hypoglycemic agents or insulin (Hung et al., 2012). However, AGIs-induced serious liver injuries and gastrointestinal side effects restricted the clinical practice (Yin et al., 2014; Kao et al., 2016). In view of the limited number of safe anti-diabetic drugs with low toxicity and ever-increasing number of diabetic patients, the exploration for new α-glucosidase inhibitors, attracted, and still attract great interests from scientific community.

In our continuous search for chemically novel and bioactive secondary metabolites from marine fungi (Hu et al., 2014; Liu et al., 2018a,b; Yang et al., 2018), we focused our attention on a coral-associated fungus *Aspergillus terreus*. A systematic chemical investigation on the ethyl acetate extracts of rice medium of this fungal strain facilitated the isolation and identification of nine novel butenolide derivatives, including four pairs of enantiomers, named (±)-asperteretones A–D **(1a/1b–4a/4b)**, and a racemate, named asperteretone E **(5)**. Structurally, compounds **2–5** represented the first examples of prenylated γ-butenolides bearing 2-phenyl-3-benzyl-4*H*-furan-1-one motifs, and their crucial biogenetically related metabolite, compound **1**, was uniquely defined by an unexpected cleavage of oxygen bridge between C-1 and C-4. Importantly, by an experimental validation method, (±)-asperteretal D and (4*S*)-4-decarboxylflavipesolide C were revised to (±)-asperteretones B **(2a/2b)** and D **(4)**, respectively. Herein, the detailed isolation, structure elucidation, and α-glucosidase inhibitory activity of these compounds (**Figure 1**) are described.

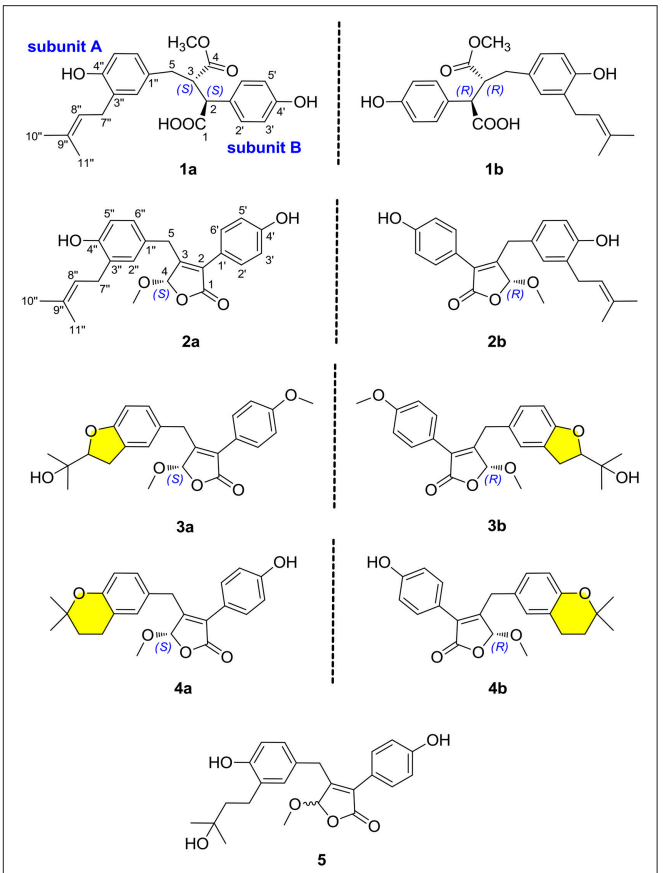

FIGURE 1 | Chemical structures of compounds **1**–**5**.

MATERIALS AND METHODS

General Experimental Procedures

Optical rotations and IR data were collected from a PerkinElmer PE-341 instrument (PerkinElmer, Waltham, MA, USA) and a Bruker Vertex 70 FT-IR spectrophotometer (Bruker, Karlsruhe, Germany) with KBr pellets, respectively. UV and ECD spectra were collected from a Varian Cary 50 UV/vis spectrophotometer (Varian, Salt Lake City, UT, USA) and a JASCO-810 spectrometer, respectively. 1D and 2D NMR spectra were measured by using a Bruker AM-400 NMR spectrometer (Bruker, Karlsruhe, Germany). The solvent or solvent impurity peaks for methanol-d_4 (δ_H 3.31 and δ_C 49.0) and $CDCl_3$ (δ_H 7.24 and δ_C 77.23) were referenced to the ^1H and ^{13}C NMR chemical shifts. High-resolution electrospray ionization mass spectrometry (HRESIMS) were measured by using a Thermo Fisher LTQ XL LC/MS (Thermo Fisher, Palo Alto, CA, USA). Column chromatography (CC) was carried out by using silica gel (200–300 mesh; Qingdao Marine Chemical Inc., China), Sephadex LH-20 (40–70 μm, Amersham Pharmacia Biotech AB, Uppsala, Sweden, Sweden), and octadecylsilyl (ODS, 50 μm, YMC Co. Ltd., Japan). Semi-preparative HPLC separations were carried out on an Agilent 1100 liquid chromatograph with a Zorbax SB-C_{18} (9.4 × 250 mm) and a Daicel IC column (5 μm, 4.6 × 250 mm, Daicel Chiral Technologies Co., Ltd., China) column. Thin-layer chromatography (TLC) was carried out by using silica gel 60 F_{254} (Yantai Chemical Industry Research Institute) and RP-C_{18} F_{254} plates (Merck, Germany).

Fungus Material

The fungus *Aspergillus terreus* was isolated from the soft coral *Sarcophyton subviride*, which was collected from the Xisha Island in the South China Sea. This strain was cultivated on potato dextrose agar (PDA) medium and identified by one of the authors (JW), based on its morphological properties and ITS sequence analysis (GenBank access no. MF972904). The fungal strain was reserved in the culture collection of Tongji Medical College, Huazhong University of Science and Technology.

Cultivation, Extraction, and Isolation

The strain *Aspergillus terreus* was cultivated on PDA (Potato Dextrose Agar) medium at 28°C for 1 week to prepare the seed cultures. Agar plugs were cut into small pieces (approximately 0.5 × 0.5 × 0.5 cm^3) and then was inoculated in 300 × 500 mL Erlenmeyer flasks which were previously sterilized by autoclaving, each containing 200 g rice and 200 mL distilled water. All flasks were incubated at 28°C for 28 days. Then, the whole rice solid medium was extracted seven times in 95% aqueous EtOH at room temperature, and the solvent was

removed under reduced pressure to afford a crude extract, which was partitioned with ethyl acetate against water to obtain the ethyl acetate soluble part (1.5 kg). The organic extract was separated by silica gel CC (100–200 mesh) with a stepwise gradient elution of petroleum ether–ethyl acetate–MeOH (10:1:0, 7:1:0, 5:1:0, 3:1:0, 1:1:0, 2:2:1, 1:1:1) to afford seven fractions (A–G).

Fraction C (75 g) was separated by an RP-C_{18} column using MeOH–H_2O (from 20:80 to 100:0, v/v) to give five main fractions (C1–C5). Fraction C3 (2.3 g) was further purified by Sephadex LH-20 using CH_2Cl_2-MeOH (1:1, v/v) to yield two fractions (C3.1–C3.2). Fraction C3.2 was applied to silica gel CC eluted with petroleum ether–ethyl acetate (stepwise 4:1–1:1) to furnish four additional fractions (C3.2.1–C3.2.4). Repeated purification of fraction C3.2.3 (92 mg) by semi-preparative HPLC with CH_3CN–H_2O (50:50, v/v, 3.0 mL/min) to yield compounds **2** (4.8 mg; t_R 12.5 min) and **4** (4.0 mg; t_R 28.2 min). Afterwards, compound **2** was further purified by chiral HPLC using a Daicel IC column (isopropanol–*n*-hexane, 8:92, v/v, 2.0 mL/min) to give **2a** (2.2 mg; t_R 60.7 min) and **2b** (2.3 mg; t_R 55.2 min). The enantiomers **4a** (1.8 mg; t_R 50.5 min) and **4b** (2.0 mg; t_R 41.8 min) were obtained by chiral HPLC separation of compound **4** using a Daicel IC column eluted with isopropanol–*n*-hexane (8:92, v/v, 2.0 mL/min).

Fraction D (198 g) was subjected to an RP-C_{18} column eluted with MeOH–H_2O (from 20:80 to 100:0, v/v) to yield five fractions (D1–D5). Fraction D4 (2.4 g) was applied to Sephadex LH-20 eluted with CH_2Cl_2-MeOH (1:1, v/v) and further purified by semi-preparative HPLC using CH_3CN–H_2O (60:40, v/v, 3.0 mL/min) to yield a racemic mixture **3** (9.6 mg; t_R 38.2 min). The enantiomers **3a** (1.1 mg; t_R 12.5 min) and **3b** (1.8 mg; t_R 14.8 min) were further purified by chiral HPLC using a Daicel IC column eluted with isopropanol–*n*-hexane (8:92, v/v, 2.0 mL/min).

Fraction E (186 g) was chromatographed on silica gel CC (CH_2Cl_2-MeOH, 1:0–50:1, v/v) to yield five main fractions (E1–E5). Repeated purification of fraction E5 (1.3 g) using Sephadex LH-20 with CH_3OH as eluent and RP-C_{18} column (MeOH–H_2O, from 30:70 to 100:0, v/v) to give three mixtures (E5.1–E5.3). Fractions E5.1 (210 mg) was subjected to semi-preparative HPLC (MeOH–H_2O, 60:40, v/v, 3.0 mL/min) to afford compound **1** (6.7 mg; t_R 43 min). Subsequently, compound **1** was subjected to chiral HPLC using a Daicel IC column (isopropanol–*n*-hexane,

TABLE 1 | ^1H and ^{13}C NMR data for compounds **1** and **3–5** in methanol-d_4 (δ in ppm and *J* in Hz).

No.	1		3		4		5	
	δ_H[a,b]	δ_C[c]	δ_H[a,b]	δ_C[c]	δ_H[a,b]	δ_C[c]	δ_H[a,b]	δ_C[c]
1	–	178.3 C	–	172.7 C	–	172.9 C	–	173.0 C
2	3.61 d (11.5)	55.3 CH	–	130.1 C	–	130.2 C	–	130.0 C
3	3.26 m	52.2 CH	–	158.4 C	–	157.8 C	–	158.1 C
4	–	177.4 C	5.57 s	104.2 CH	5.56 s	104.1 CH	5.55 s	104.2 CH
5	2.38 dd (8.9, 13.7); 2.58 dd (4.0, 13.7)	36.5 CH_2	3.64 d (15.4); 3.96 d (15.4)	32.9 CH_2	3.60 d (15.3); 3.93 d (15.3)	32.7 CH_2	3.60 d (15.3); 3.94 d (15.3)	32.8 CH_2
4-OMe	3.52 s	51.8 CH_3	3.52 s	57.4 CH_3	3.52 s	57.3 CH_3	3.53 s	57.4 CH_3
1'	–	130.4 C	–	122.7 C	–	121.5 C	–	121.5 C
2'	7.21 d (8.4)	130.9 CH	7.44 d (8.9)	131.6 CH	7.34 d (8.7)	131.6 CH	7.36 d (8.7)	131.6 CH
3'	6.79 d (8.4)	116.4 CH	6.99 d (8.9)	115.0 CH	6.85 d (8.7)	116.3 CH	6.86 d (8.7)	116.4 CH
4'	–	157.8 C	–	161.7 C	–	159.5 C	–	159.5 C
5'	6.79 d (8.4)	116.4 CH	6.99 d (8.9)	115.0 CH	6.85 d (8.7)	116.3 CH	6.86 d (8.7)	116.4 CH
6'	7.21 d (8.4)	130.9 CH	7.44 d (8.9)	131.6 CH	7.34 d (8.7)	131.6 CH	7.36 d (8.7)	131.6 CH
4'-OMe	–	–	3.82 s	55.8 CH_3	–	–	–	–
1"	–	130.3 C	–	129.3 C	–	128.6 C	–	128.3 C
2"	6.60 d (2.0)	131.0 CH	6.95 s	126.4 CH	6.84 s	130.9 CH	6.87 d (2.3)	131.4 CH
3"	–	128.8 C	–	129.4 C	–	122.6 C	–	131.0 C
4"	–	154.5 C	–	160.4 C	–	154.3 C	–	155.3 C
5"	6.59 d (8.2)	115.5 CH	6.65 d (8.1)	110.0 CH	6.63 d (9.0)	118.5 CH	6.69 d (8.2)	116.2 CH
6"	6.55 dd (2.0, 8.2)	128.0 CH	6.87 d (8.1)	129.4 CH	6.85 d (9.0)	128.7 CH	6.81 dd (2.3, 8.2)	128.1 CH
7"	3.21 m	29.0 CH_2	3.12 dd (4.2, 9.0)	31.5 CH_2	2.72 t (6.8)	23.3 CH_2	2.61 m	26.2 CH_2
8"	5.27 m	124.1 CH	4.56 t (9.0)	90.6 CH	1.77 t (6.8)	33.7 CH_2	1.68 m	44.9 CH_2
9"	-	132.8 C	–	72.5 C	–	75.3 C	–	71.5 C
10"	1.74 s	26.0 CH_3	1.23 s	25.2 CH_3	1.28 s	27.0 CH_3	1.24 s	29.1 CH_3
11"	1.70 s	17.8 CH_3	1.20 s	25.4 CH_3	1.28 s	27.1 CH_3	1.24 s	29.1 CH_3

[a] *Recorded at 400 MHz.*

[b] *"m" means overlapped or multiplet with other signals.*

[c] *Recorded at 100 MHz.*

7:93, v/v, 2.0 mL/min), resulting in the separation of **1a** (2.7 mg; t_R 12.4 min) and **1b** (2.5 mg; t_R 16.2 min). A racemic mixture **5** (3.2 mg) was isolated by semi-preparative HPLC (MeOH–H_2O, 70:30, v/v, 3.0 mL/min) from fraction E5.2 (54.5 mg).

(±)-Asperteretone A (**1**). White, amorphous powder; $[\alpha]_D^{25}$ 0 (*c* 0.1, MeOH); UV (MeOH) λ_{max} (log ε) = 202 (4.63), 229 (4.06), 279 (3.43) nm; IR ν_{max} = 3435, 2925, 1718, 1623, 1511, 1446, 1381, 1257, 1179, 1047, 829, 573 cm^{-1}; HRESIMS *m/z* 421.1622 $[M + Na]^+$ (calcd for $C_{23}H_{26}O_6Na$, 421.1627); For ^1H NMR and ^{13}C NMR data, see **Table 1**.

(−)-Asperteretone A (**1a**). White, amorphous powder; $[\alpha]_D^{25}$ −34 (*c* 0.1, MeOH); ECD (*c* 0.1, MeOH) = $\Delta\varepsilon_{210}$ −0.85, $\Delta\varepsilon_{227}$ −1.52.

(+)-Asperteretone A (**1b**). White, amorphous powder; $[\alpha]_D^{25}$ +37 (*c* 0.1, MeOH); ECD (*c* 0.1, MeOH) = $\Delta\varepsilon_{209}$ +6.18, $\Delta\varepsilon_{226}$ +5.80.

(±)-Asperteretone B (**2**). White, amorphous powder; $[\alpha]_D^{25}$ 0 (*c* 0.1, MeOH); UV (MeOH) λ_{max} (log ε) = 202 (4.21), 215 (3.85), 285 (3.50) nm; IR ν_{max} = 3425, 2927, 2853, 1747, 1611, 1514, 1440, 1372, 1342, 1269, 1204, 1144, 1113, 1020, 987, 946, 839, 789, 557, 534 cm^{-1}; HRESIMS *m/z* 403.1526 $[M + Na]^+$ (calcd for $C_{23}H_{24}O_5Na$, 403.1521); For ^1H NMR and ^{13}C NMR data, see **Table 2**.

(−)-Asperteretone B (**2a**). White, amorphous powder; $[\alpha]_D^{25}$ −140 (*c* 0.1, MeOH); ECD (*c* 0.1, MeOH) = $\Delta\varepsilon_{207}$−16.99, $\Delta\varepsilon_{232}$−2.90, $\Delta\varepsilon_{282}$−10.57.

(+)-Asperteretone B (**2b**). White, amorphous powder; $[\alpha]_D^{25}$ +136 (*c* 0.1, MeOH); ECD (*c* 0.1, MeOH) = $\Delta\varepsilon_{207}$ +10.92, $\Delta\varepsilon_{232}$ +3.56, $\Delta\varepsilon_{282}$ +8.98.

(±)-Asperteretone C (**3**). White, amorphous powder; $[\alpha]_D^{25}$ 0 (*c* 0.1, MeOH); UV (MeOH) λ_{max} (log ε) = 202 (4.23), 223 (3.77), 285 (3.67) nm; IR ν_{max} = 3483, 2991, 2952, 2878, 1712, 1637, 1453, 1434, 1396, 1351, 1267, 1170, 1133, 1008, 988, 967, 942, 900, 838, 736, 702, 605, 564 cm^{-1}; HRESIMS *m/z* 411.1802 $[M + H]^+$ (calcd for $C_{24}H_{27}O_6$, 411.1808) and *m/z* 433.1635 $[M + Na]^+$ (calcd for $C_{24}H_{26}O_6Na$, 433.1627); For ^1H NMR and ^{13}C NMR data, see **Table 1**.

(−)-Asperteretone C (**3a**). White, amorphous powder; $[\alpha]_D^{25}$ −135 (*c* 0.1, MeOH); ECD (*c* 0.1, MeOH) = $\Delta\varepsilon_{207}$ −9.13, $\Delta\varepsilon_{232}$ −3.29, $\Delta\varepsilon_{282}$ −5.67.

(+)-Asperteretone C (**3b**). White, amorphous powder; $[\alpha]_D^{25}$ +137 (*c* 0.1, MeOH); ECD (*c* 0.1, MeOH) = $\Delta\varepsilon_{208}$ +9.79, $\Delta\varepsilon_{236}$ +1.78, $\Delta\varepsilon_{284}$ +8.67.

(±)-Asperteretone D (**4**). White, amorphous powder; $[\alpha]_D^{25}$ 0 (*c* 0.1, MeOH); UV (MeOH) λ_{max} (log ε) = 202 (4.62), 221 (4.32), 283 (4.05) nm; IR ν_{max} = 3432, 2974, 2930, 2853, 1756, 1616, 1503, 1444, 1374, 1263, 1208, 1158, 1116, 1028, 994, 837, 670 cm^{-1}; HRESIMS *m/z* 381.1692 $[M + H]^+$ (calcd for $C_{23}H_{25}O_5$, 381.1702) and *m/z* 403.1513 $[M + Na]^+$ (calcd for $C_{23}H_{24}O_5Na$, 403.1521); For ^1H NMR and ^{13}C NMR data, see **Table 1**.

(−)-Asperteretone D (**4a**). White, amorphous powder; $[\alpha]_D^{25}$ −120 (*c* 0.1, CH_2Cl_2); ECD (*c* 0.1, MeOH) = $\Delta\varepsilon_{207}$−13.10, $\Delta\varepsilon_{232}$−3.81, $\Delta\varepsilon_{283}$−7.07.

(+)-Asperteretone D (**4b**). White, amorphous powder; $[\alpha]_D^{25}$ +116 (*c* 0.1, CH_2Cl_2); ECD (*c* 0.1, MeOH) = $\Delta\varepsilon_{207}$ +9.95, $\Delta\varepsilon_{232}$ +4.60, $\Delta\varepsilon_{282}$ +9.14.

Asperteretone E (**5**). White, amorphous powder; $[\alpha]_D^{25}$ 0 (*c* 0.1, MeOH); UV (MeOH) λ_{max} (log ε) = 202 (4.55), 218 (4.29), 285 (4.06) nm; IR ν_{max} = 3428, 2965, 2926, 2853, 1750, 1615, 1512, 1441, 1373, 1266, 1207, 1109, 1032, 946, 837, 565 cm^{-1}; HRESIMS *m/z* 421.1626 $[M + Na]^+$ (calcd for $C_{23}H_{26}O_6Na$, 421.1627); For ^1H NMR and ^{13}C NMR data, see **Table 1**.

TABLE 2 | Comparison of the ^1H and ^{13}C NMR data for reported (±)-asperteretal D and **2** in $CDCl_3$ (δ in ppm and *J* in Hz).

No.	(±)-asperteretal D		2	
	δ_H[a,c]	δ_C[d]	δ_H[b,c]	δ_C[e]
1	–	171.4 C	–	171.2 C
2	–	129.3 C	–	129.2 C
3	–	156.3 C	–	156.2 C
4	5.45 s	102.6 CH	5.44 s	102.5 CH
5	3.57 d (15.2); 3.96 d (15.2)	32.0 CH_2	3.57 d (15.2); 3.96 d (15.2)	32.0 CH_2
4-OMe	3.53 s	57.4 CH_3	3.53 s	57.4 CH_3
1'	–	121.6 C	–	121.8 C
2'	7.38 d (8.7)	130.8 CH	7.40 d (8.6)	130.8 CH
3'	6.87 d (8.7)	115.9 CH	6.88 d (8.6)	115.8 CH
4'	–	156.7 C	–	156.6 C
5'	6.87 d (8.7)	115.9 CH	6.88 d (8.6)	115.8 CH
6'	7.38 d (8.7)	130.8 CH	7.40 d (8.6)	130.8 CH
1"	–	128.3 C	–	128.4 C
2"	6.85 m	130.5 CH	6.86 s	130.5 CH
3"	–	127.8 C	–	127.7 C
4"	–	153.6 C	–	153.6 C
5"	6.72 d (8.6)	116.4 CH	6.73 d (7.9)	116.4 CH
6"	6.86 m	127.9 CH	6.87 d (7.9)	127.9 CH
7"	3.30 d (7.1)	29.9 CH_2	3.30 d (7.2)	29.9 CH_2
8"	5.26 t (7.1)	121.6 CH	5.26 t (7.2)	121.6 CH
9"	–	135.3 C	–	135.4 C
10"	1.75 s	26.0 CH_3	1.75 s	26.0 CH_3
11"	1.74 s	18.1 CH_3	1.75 s	18.1 CH_3

[a] *Recorded at 600 MHz.*
[b] *Recorded at 400 MHz.*
[c] *"m" means overlapped or multiplet with other signals.*
[d] *Recorded at 150 MHz.*
[e] *Recorded at 100 MHz.*

ECD Calculations

The theoretical calculations of compounds **1a**/**1b** and **2a**/**2b** were performed using Gaussian 09 and figured using GaussView 5.0 (He et al., 2017a,b,c; Hu et al., 2017). Conformation search using molecular mechanics calculations was performed in the Discovery Studio 3.5 Client with MMFF force field with 20 kcal mol^{-1} upper energy limit (Smith and Goodman, 2010). The optimized conformation geometries and thermodynamic parameters of all selected conformations were provided. The predominant conformers were optimized at B3LYP/6-31G(d,p) level. The theoretical calculation of ECD was performed using time dependent Density Functional Theory (TDDFT) at the

B3LYP/6-31G(d,p) level in MeOH with PCM model (Miertus et al., 1981). The ECD spectra of compounds **1a**/**1b** and **2a**/**2b** were obtained by weighing the Boltzmann distribution rate of each geometric conformation (Tähtinen et al., 2003).

The ECD spectra were simulated by overlapping Gaussian functions for each transition according to:

$$\triangle \varepsilon(E) = \frac{1}{2.297 \times 10^{-39}} \times \frac{1}{\sqrt{2\pi}\sigma} \sum_{i}^{A} \triangle E_i R_i e^{-[(E-E_i)/(2\sigma)]^2}$$

The σ represented the width of the band at $1/e$ height, and ΔE_i and R_i were the excitation energies and rotational strengths for transition i, respectively. R_{vel} had been used in this work.

α-Glucosidase Inhibitory Assay

The α-glucosidase enzyme from *Saccharomyces cerevisiae* (Sigma Aldrich, USA) solution (1.5 U/mL) was prepared by dissolving the α-glucosidase in 200 M phosphate buffer (pH 6.8). The α-glucosidase enzyme solution (20 μL), test compounds (10 μL) and buffer (40 μL) were pipetted and mixed in a 96 well microtiter plate. The mixture was incubated at 37°C for 10 min. After incubation, *p*-nitrophenyl-α-D-glucopyranoside (PNP-G) substrate solution (10 μL, in 20 mM phosphate buffer) was added. The increment of absorbance due to the hydrolysis of PNP-G by α-glucosidase was measured at the wavelength of 410 nm with a microplate reader (Thermo Scientific, Waltham, MA). Acarbose was used as a positive control and averages of three replicates were calculated. The α-glucosidase inhibitory activity was expressed as percentage inhibition and was calculated using the following formula: inhibition (%) = $[1-(OD_{sample}/OD_{blank})] \times 100$. The half-maximal inhibitory concentration (IC_{50}) was calculated as the compound concentration that is required for 50% inhibition, and the IC_{50} value of the acarbose was 154.7 ± 8.1 μM.

Molecular Docking Simulation

The virtual docking was implemented in the Surflex-Dock module of the FlexX/Sybyl software, which is a fast docking method that allows sufficient flexibility of ligands and keeps the target protein rigid. Molecules were built with Chemdraw and optimized at molecular mechanical and semiempirical level by using Open Babel GUI. The crystallographic ligands were extracted from the active site and the designed ligands were modeled. All the hydrogen atoms were added to define the correct ionization and tautomeric states, and the carboxylate, phosphonate and sulphonate groups were considered in their charged form. In the docking calculation, the default FlexX scoring function was used for exhaustive searching, solid body optimizing and interaction scoring. Finally, the ligands with the lowest-energy and the most favorable orientation were selected.

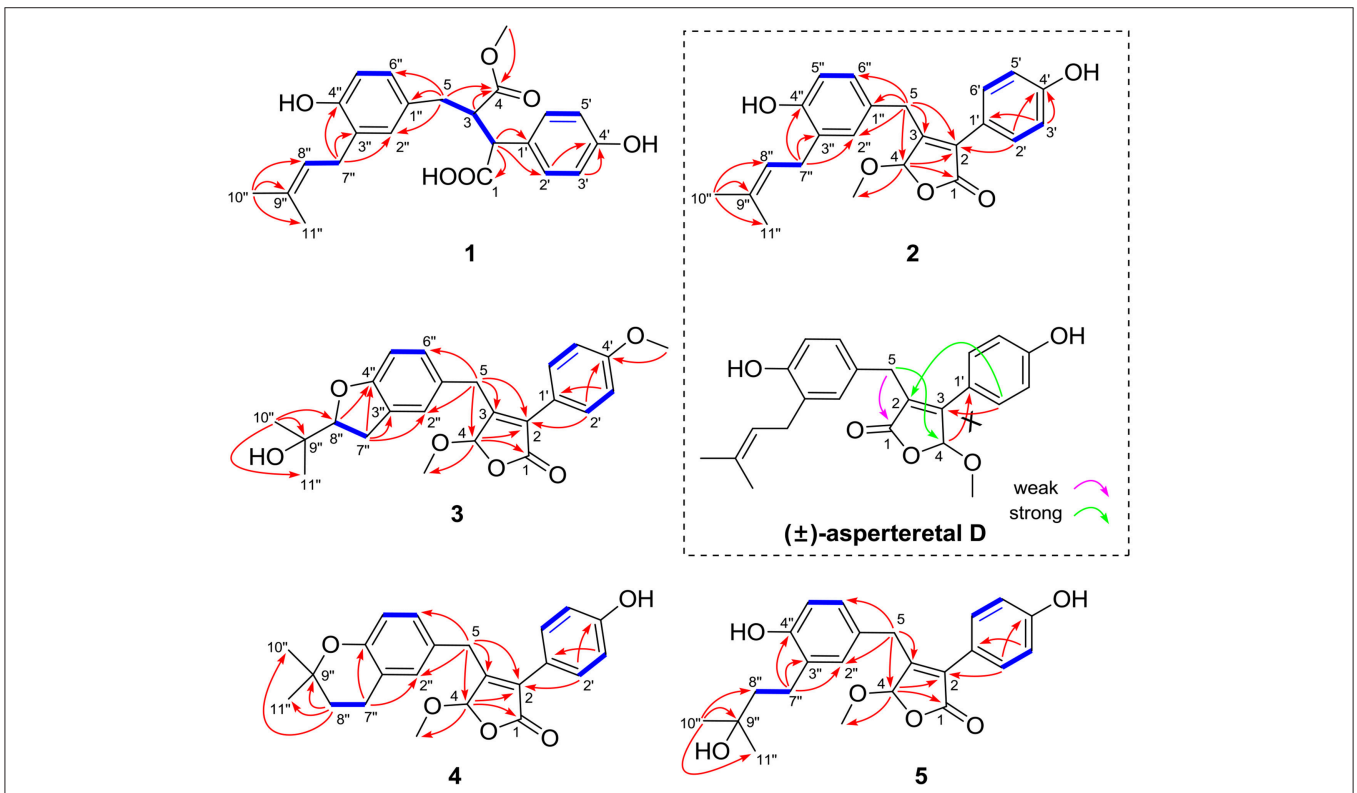

FIGURE 2 | Selected ^{1}H–^{1}H COZY (blue bold lines) and HMBC (single arrows) correlations of compounds **1**–**5** and key HMBC analysis in original structure (±)-asperteretal D.

RESULTS AND DISCUSSION

(±)-Asperteretone A (**1a**/**1b**) were obtained as white, amorphous powders. The molecular formula $C_{23}H_{26}O_6$ was deduced from the HRESIMS data at *m/z* 421.1622 $[M + Na]^+$ (calcd for $C_{23}H_{26}O_6Na$, 421.1627), requiring 11 degrees of unsaturation. Its IR spectrum displayed intense absorption bands for hydroxyl (3,435 cm^{-1}), carbonyl (1,718 cm^{-1}), and aromatic ring (1,623 and 1,511 cm^{-1}). The ^1H NMR spectrum (**Table 1**) of **1** showed characterized signals for a *para*-disubstituted phenyl group at δ_H 7.21 (d, J = 8.4 Hz, H-2', 6') and 6.79 (d, J = 8.4 Hz, H-3', 5'), a 1,3,4-trisubstituted phenyl group at δ_H 6.60 (d, J = 2.0 Hz, H-2"), 6.59 (d, J = 8.2 Hz, H-5"), and 6.55 (dd, J = 2.0, 8.2 Hz, H-6"), a prenyl group at δ_H 3.21 (m, H_2-7"), 5.27 (m, H-8"), 1.74 (s, H_3-10"), and 1.70 (s, H_3-11"), a methoxy group at δ_H 3.52 (s, OMe-4), two methines at δ_H 3.61 (d, J = 11.5 Hz, H-2) and 3.26 (m, H-3), and a methylene at δ_H 2.38 (dd, J = 8.9, 13.7 Hz, H-5) and 2.58 (dd, J = 4.0, 13.7 Hz, H-5). The ^{13}C NMR and DEPT spectra (**Table 1**) of **1** showed 23 carbon resonances categorized as two methyls, two methylenes, ten methines (including eight olefinic), eight nonprotonated carbons (including six olefinic, one carboxyl, and one ester carbonyl), and one methoxyl. The diagnostic data above indicated that compound **1** was a butenolide derivative.

The protons and protonated carbon resonances in the NMR spectra were unambiguously assigned through the HSQC experiment. In the HMBC experiment (**Figure 2**), the correlations from H_3-10" to C-8", C-9", and C-11" and from H_2-7" to C-2", C-3", and C-4", as well as the ^1H–^1H COZY correlations (**Figure 2**) of H_2-7"/H-8" and H-5"/H-6", confirmed the presence of the 1,3,4-trisubstituted phenyl group (subunit A)

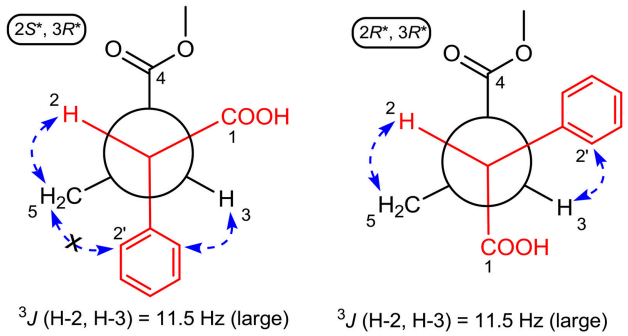

FIGURE 4 | ROESY correlations (dashed blue arrows) and coupling constant were used to determine the relative configuration of **1** by optimized conformation analysis for C-2 to C-3.

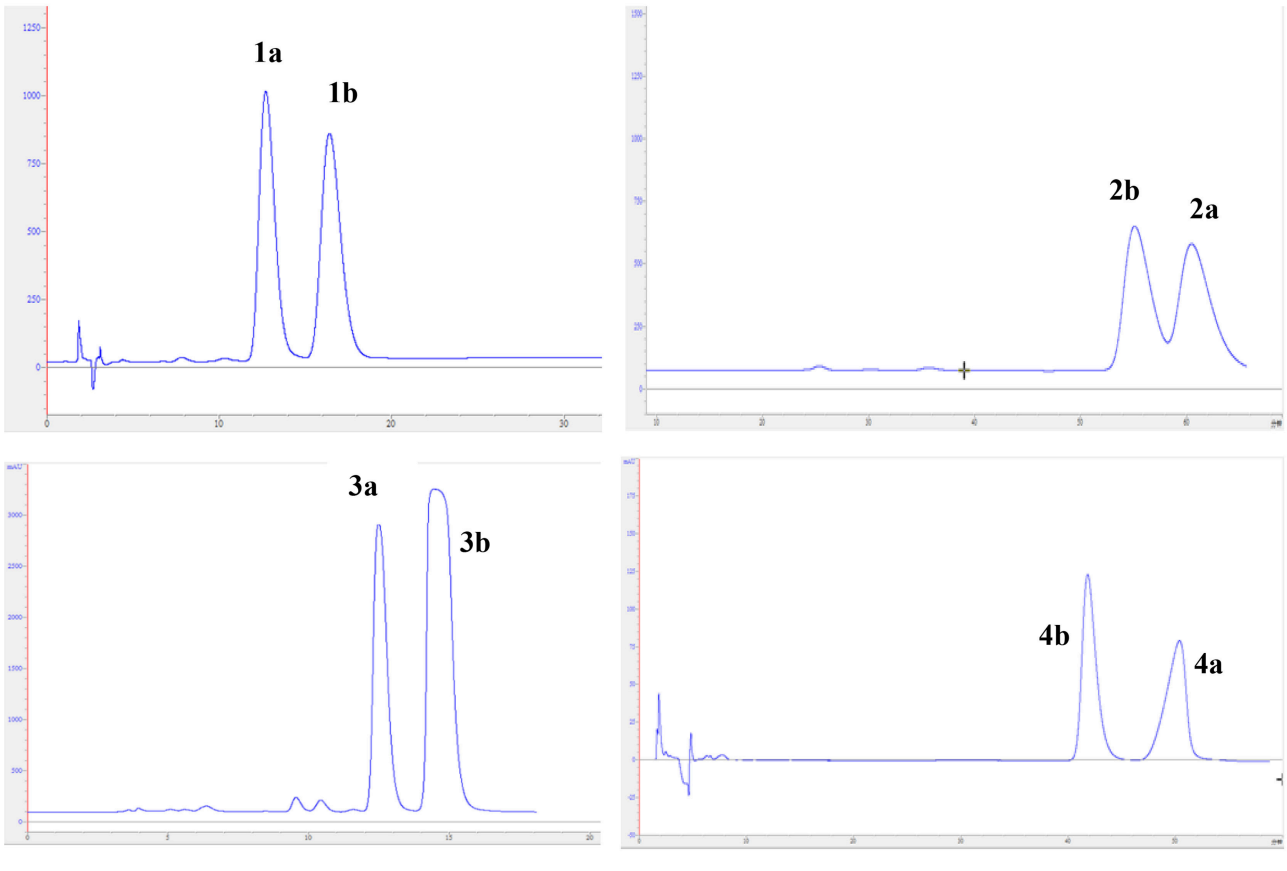

FIGURE 3 | Chiral HPLC separation profiles of compounds **1a**/**1b**–**4a**/**4b**.

with a hydroxyl and a prenyl motif attached at C-4" and C-3", respectively. Besides, the ^{1}H–^{1}H COZY correlations of H-2'/H-3' and H-5'/H-6' and HMBC correlations from both H-2' and H-3' to C-4' (δ_C 157.8) confirmed the presence of the *para*-disubstituted phenyl group (subunit B) with a hydroxyl motif attached at C-4'. Subunits A and B were connected through a "-CH_2(5)-CH(3)-CH(2)-" group, as confirmed by the ^{1}H–^{1}H COZY correlations of H-2/H-3/H_2-5 and HMBC correlations from H_2-5 to C-1", C-2", and C-6" and from H-2 to C-1', C-2', and C-6'. In addition, the key HMBC correlations from H-3,

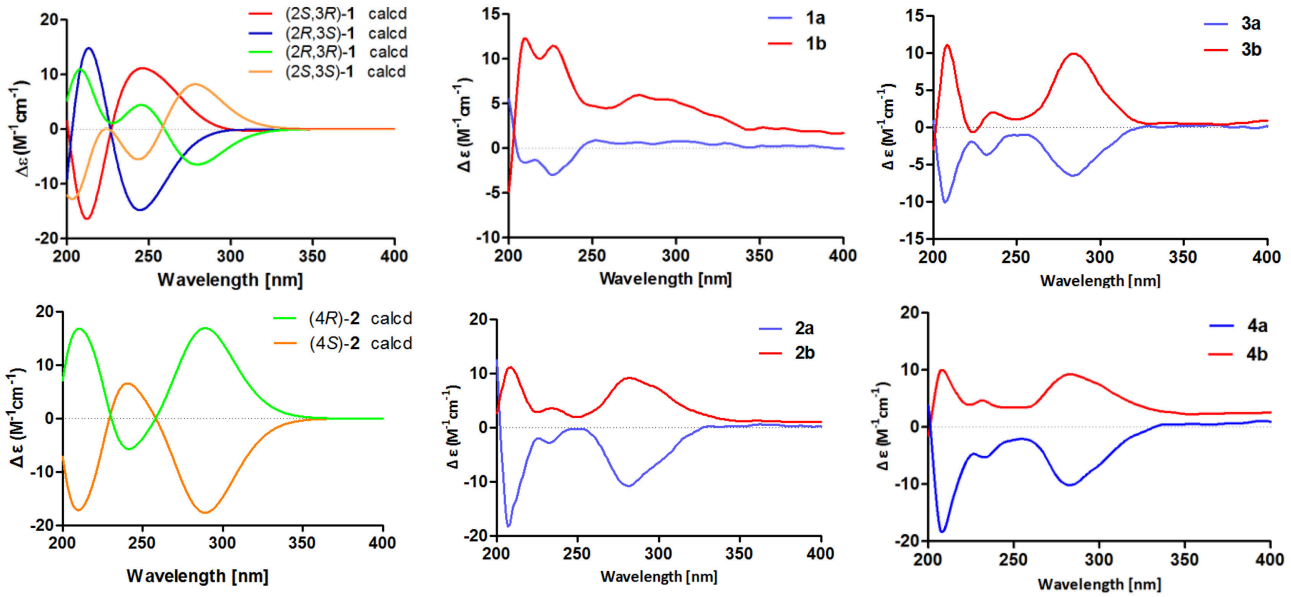

FIGURE 5 | Calculated ECD spectra of (2*S*,3*R*)-**1**, (2*R*,3*S*)-**1**, (2*R*,3*R*)-**1**, (2*S*,3*S*)-**1**, (4*R*)-**2**, and (4*S*)-**2** and experimental ECD spectra of **1a**/**1b**–**4a**/**4b**.

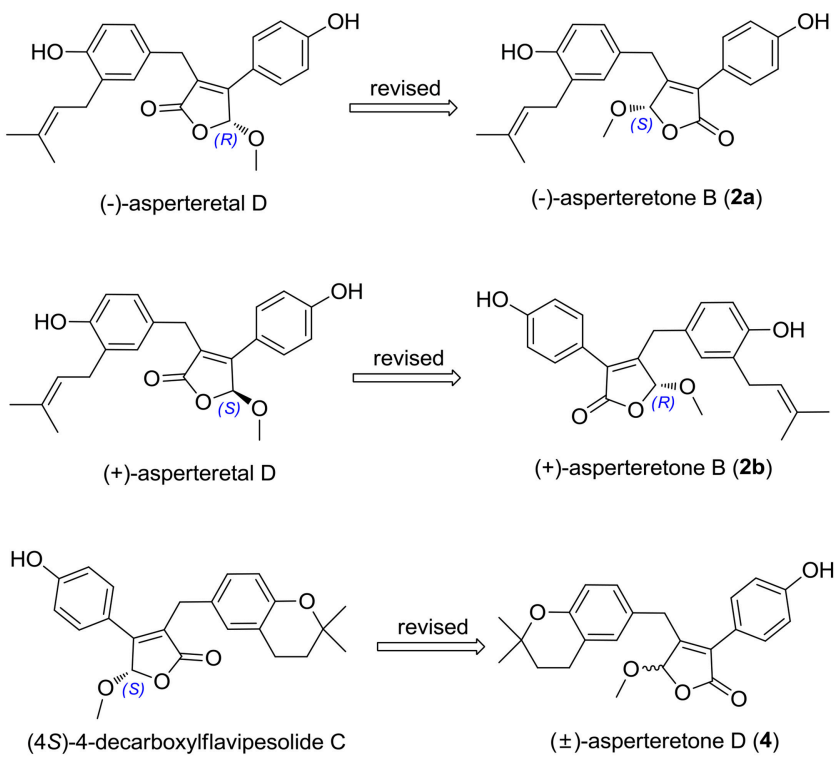

FIGURE 6 | Structure reassignments of 2-benzyl-3-phenyl-type (±)-asperteretal D and (4*S*)-4-decarboxylflavipesolide C to 2-phenyl-3-benzyl-type (±)-asperteretones B (**2a**/**2b**) and D (**4**), respectively.

H_2-5, and OMe-4 to C-4 (δ_C 177.4) and H-2 to C-1 (δ_C 178.3) indicated that a methyl ester and a carboxyl group were attached at C-3 and C-2, respectively. Thus, the planar structure of **1** was determined.

The experimental electronic circular dichroic (ECD) spectrum was measured in MeOH. Surprisingly, no apparent ECD Cotton effects were observed, suggesting that compound **1** was racemic, which adhered well to its lack of optical rotation. Subsequently, compound **1** was separated into two optically pure enantiomers, (−)-asperteretone A (**1a**, $[\alpha]_D^{25}$ −34) and (+)-asperteretone A (**1b**, $[\alpha]_D^{25}$ +37) using high performance liquid chromatography (HPLC) on a Daicel IC column (**Figure 3**).

The large coupling constant (J = 11.5 Hz) suggested the *trans*-relationship of H-2 and H-3, thus two possible optimal conformations existed for its conformation analysis (**Figure 4**). When the relative configuration of **1** was 2*S**,3*R**, despite there were obvious NOE correlations of H-2/H_2-5 and H-3/H-6' (or H-2'), the diagnostic NOE correlation of H_2-5/H-2' (or H-6') was not observed in the NOESY spectrum, indicating that the assumption for 2*S**,3*R**-configuration should be wrong. Thus, the relative configuration of **1** was deduced to be 2*R**,3*R**, which was completely supported by the NOE correlations of H-2/H_2-5 and H-3/H-2' (or H-6'). Accordingly, the relative configuration of **1** was determined to be 2*R**,3*R**.

To further confirm the above conclusion and determine the absolute configurations of **1a** and **1b**, a time-dependent density functional theory (TDDFT) method at the at B3LYP/6-31G(d,p) level in MeOH with PCM model was performed for (2*S*,3*R*)-**1**, (2*R*,3*S*)-**1**, (2*S*,3*S*)-**1**, and (2*R*,3*R*)-**1** (**Figure 5**), of which the DFT-calculated ECD spectra of (2*S*,3*S*)-**1** and (2*R*,3*R*)-**1** showed close similarities to the experimental ECD spectra of **1a** and **1b**, suggesting that the absolute structures of **1a** and **1b** should be assigned as (2*S*,3*S*)- and (2*R*,3*R*)-configuration, respectively.

(±)-Asperteretone B (**2a**/**2b**) were also obtained as white, amorphous powders and assigned the molecular formula $C_{23}H_{24}O_5$, as determined from the HRESIMS analysis at *m/z* 403.1526 $[M + Na]^+$ (calcd for $C_{23}H_{24}O_5Na$, 403.1521) and ^{13}C NMR data. The 1D (**Table 2**) and 2D NMR spectra of **2** were completely identical to that of the reported (±)-asperteretal D (Sun Y. et al., 2018), which drove us to believe that they shared the same structures. The 1,3,4-trisubstituted phenyl group with a C-4" hydroxyl and a C-3" prenyl motif and *para*-disubstituted phenyl group with a C-4' hydroxyl motif were explicitly confirmed by detailed analysis of the 2D NMR data (**Figure 2**) of **2**. However, a strong four-bond HMBC correlation from H_2-5 to C-4 made us confused about the correctness of (±)-asperteretal D. After careful examination of the HMBC spectrum (**Figure 2**) of (±)-asperteretal D, key correlations from H-2' to C-3 and from H-4 to C-1' were not observed in the HMBC spectrum; on the contrary, two four-bond HMBC correlations from H-2' to C-2 and from H_2-5 to C-4 were observed, which were also found in the HMBC spectrum of **2**. These data above suggested that (±)-asperteretal D should be structurally revised from 2-benzyl-3-phenyl-type to 2-phenyl-3-benzyl-type.

The chiral resolution (**Figure 3**) of **2** afforded a pair of enantiomers, (±)-asperteretone B (**2a**/**2b**). To determine their absolute configurations, the ECD spectra of (4*S*)-**2** and (4*R*)-**2** were calculated by the TDDFT methodology, which matched well with those of (−)-asperteretone B (**2a**) and (+)-asperteretone B (**2b**), respectively, indicating that the absolute stereochemistry of **2a** and **2b** should be 4*S*- and 4*R*-configuration, respectively. Furthermore, by comparison of their experimental ECD spectra (**Figure 5**) and similar specific rotation values, the structures of (−)-asperteretal D and (+)-asperteretal D were revised to **2a** and **2b** (**Figure 6**), respectively.

(±)-Asperteretone C (**3a**/**3b**), obtained as white, amorphous powders, were determined to have the molecular formula

TABLE 3 | α-Glucosidase inhibitory activity of **1a/1b**−**4a/4b** and **5**.

Compound	α-glucosidase inhibitory activity (IC_{50}, μM)
1a	45.4 ± 3.8
1b	53.1 ± 1.4
2a	17.3 ± 2.4
2b	19.2 ± 1.9
3a	52.2 ± 4.6
3b	49.8 ± 5.7
4a	15.7 ± 1.1
4b	18.9 ± 2.3
5	48.9 ± 7.3
acarbose	154.7 ± 8.1

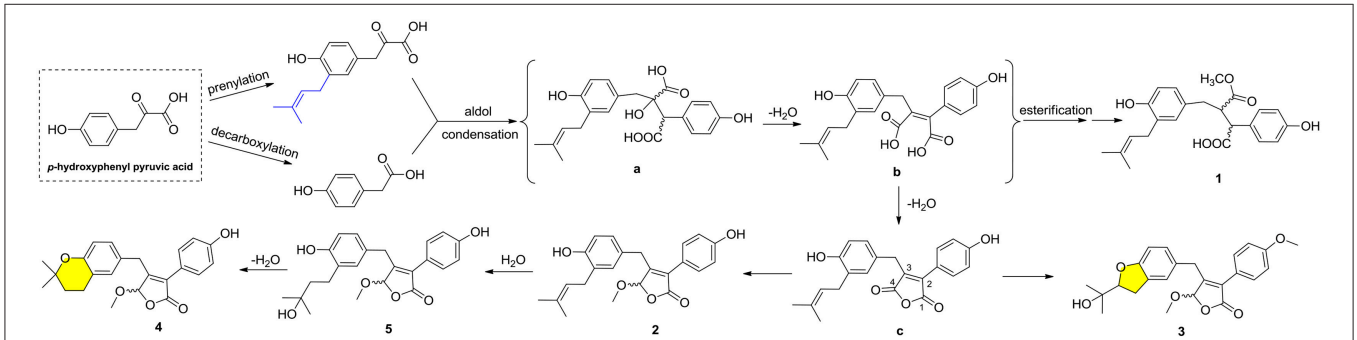

SCHEME 1 | Plausible biogenetic pathways for compounds **1**–**5**.

$C_{24}H_{26}O_6$, as deduced from the HRESIMS data at *m/z* 411.1802 $[M + H]^+$ (calcd for $C_{24}H_{27}O_6$, 411.1808) and *m/z* 433.1635 $[M + Na]^+$ (calcd for $C_{24}H_{26}O_6Na$, 433.1627), which was indicative of twelve degrees of unsaturation. Its high similarities of NMR data (**Table 1**) with those of **2** suggested that **3** was also a butenolide derivative, with the differences that the *para*-disubstituted phenyl group was attached with a C-4' methoxy motif in **3** rather than a C-4' hydroxyl motif in **2**, and the 1,3,4-trisubstituted phenyl group attached with a C-4" hydroxyl and a C-3" prenyl motif in **2** was replaced by a 2-(2,3-dihydrobenzofuran-2-yl)propan-2-ol motif in **3**, as supported by the 2D NMR spectra (**Figure 2**), including HMBC and ^1H–^1H COZY correlations. Thus, the structure of **3** was determined.

Considering the similar structural features of **2** and **3**, we deduced that compound **3** was likely a racemic mixture. As expected, by chiral HPLC resolution (**Figure 3**), two isolates were obtained. Since no apparent Cotton effects were decisive for the absolute stereochemistry of C-8", the experimental ECD spectra (**Figure 5**) of **3a** and **3b** were closely similar to those of (−)-asperteretone B (**2a**) and (+)-asperteretone B (**2b**), respectively, indicating that compounds **3a** and **3b** possessed the 4*S*- and 4*R*-configuration, respectively. Regrettably, the configuration of C-8" was difficult to be determined (Liu et al., 2018b).

(±)-Asperteretone D (**4a/4b**) gave the molecular formula $C_{23}H_{24}O_5$, as determined by the HRESIMS analysis at *m/z* 381.1692 $[M + H]^+$ (calcd for $C_{23}H_{25}O_5$, 381.1702) and *m/z* 403.1513 $[M + Na]^+$ (calcd for $C_{23}H_{24}O_5Na$, 403.1521), corresponding to twelve degrees of unsaturation. Detailed analysis of the ^1H and ^{13}C NMR data (**Tables 1**, **2**) of **4** and **2** suggested that they shared the similar structural features, differing in that the 1,3,4-trisubstituted phenyl group attached with a C-4" hydroxyl and a C-3" prenyl motif in **2** was replaced by the 1,3,4-trisubstituted phenyl with the fusion of gem-dimethyl substituted tetrahydropyrane ring, as supported by the HMBC correlations from H_2-8" to C-9", C-10", and C-11" and from H_2-7" to C-2" and C-4", as well as the ^1H–^1H COZY correlation of H_2-7"/H_2-8". Thus, the planar structure of **4** was determined.

The lack of optical rotation and no obviously observed Cotton effects in the experimental ECD spectrum suggested that compound **4** was also a racemic mixture, which was then subjected to the Daicel IC column by chiral HPLC resolution (**Figure 3**), thus affording a pair of enantiomers, (±)-asperteretone D (**4a/4b**). The ECD spectra of (−)-asperteretone D (**4a**) and (+)-asperteretone D (**4b**) matched well with those of (−)-asperteretone B (**2a**) and (+)-asperteretone B (**2b**) (**Figure 5**), respectively, indicating that the absolute structures of **4a** and **4b** should be 4*S*- and 4*R*-configuration, respectively.

Most importantly, the ^1H and ^{13}C NMR data in $CDCl_3$ (**Supplementary Materials**, **Figures S39**, **S40**) of **4** were identical to those of (4*S*)-4-decarboxylflavipesolide C (Sun K. et al., 2018), indicating that (4*S*)-4-decarboxylflavipesolide C should be revised to **4** (**Figure 6**), as supported by the strong correlations from H_2-5 (δ_H 3.58 and 3.99) to C-4 (δ_C 102.2) and from H-2' (δ_H 7.43) to C-2 (δ_C 128.9) in the HMBC spectrum of (4*S*)-4-decarboxylflavipesolide C, whose situation was just the same as that of (±)-asperteretal D (Sun Y. et al., 2018). The minor specific rotation value $\{[\alpha]_D^{25}$ −18 (*c* 0.1, $CH_2Cl_2)\}$ of (4*S*)-4-decarboxylflavipesolide C was obviously different from those of **4a** $\{[\alpha]_D^{25}$ −120 (*c* 0.1, $CH_2Cl_2)\}$ and **4b** $\{[\alpha]_D^{25}$ +116 (*c* 0.1, $CH_2Cl_2)\}$, indicating that (4*S*)-4-decarboxylflavipesolide C should be a racemic mixture with unsymmetrical amounts rather than a pure substance.

Asperteretone E (**5**), obtained as a white, amorphous powder, was found to have a molecular formula of $C_{23}H_{26}O_6$ with 11 degrees of unsaturation, as deduced from the HRESIMS analysis at *m/z* 421.1626 $[M + Na]^+$ (calcd for $C_{23}H_{26}O_6Na$, 421.1627). Side-by-side comparison of the ^1H and ^{13}C NMR data (**Tables 1**, **2**) of **5** with those of **2**, suggesting that they shared the same core skeleton, with the only difference being that the $\Delta^{8'',9''}$ double bond in **2** was replaced by a methylene (δ_C 44.9, C-8") and an oxygenated tertiary carbon (δ_C 71.5, C-9") in **5**, as supported by the HMBC correlations (**Figure 2**) from H_3-10" to C-8", C-9", and C-11". Thus, the structure of compound **5** was determined.

The optical rotation of zero in MeOH and inapparent Cotton effects in the ECD curve highlighted that **5** was racemic. Unluckily, despite for many attempts for several chiral columns using various mobile phase systems, we still failed to obtain the enantiomers of **5**, which might own to that the rapid interconversion of these two enantiomers in the solvents prevented the separation on chiral columns.

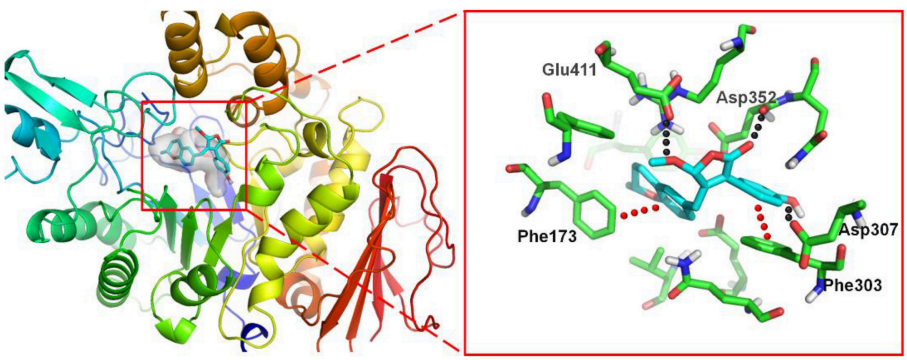

FIGURE 7 | 3D docking pose shows the interaction of **4a** in the binding site of the enzyme from *Saccharomyces cerevisiae* (PDB ID: 3A4A): the left side shows the global view of the enzyme; the right side shows an expanded view of **4a** in the binding site.

Compounds **1–5** represented two special classes of 7,8-dimeric phenylpropanoids with unexpected architectures, and their plausible biogenetic pathways were proposed as follows (**Scheme 1**): two molecules, *p*-hydroxyphenyl pyruvic acid, underwent prenylation and decarboxylation reactions, respectively, followed by aldol condensation and dehydration reactions to create intermediate **b**. Alternatively, a further dehydration reaction of **b** could generate an acid anhydride-containing intermediate **c**, which could furnish **2–5** through a series of reduction, cyclization, esterification, and so on. Meanwhile, the esterification at C-4 and reduction of $\Delta^{2,3}$ double bond could from **1**, which was identified as a crucial biogenetically related metabolite, was the first report of 2,3-disubstituted butenolide derivatives with an unexpected cleavage of oxygen bridge between C-1 and C-4. This finding would greatly expand the chemical space and biosynthesis study for butenolide derivatives.

Biological Evaluation of Compounds 1a/1b–4a/4b and 5

Compounds **1a/1b–4a/4b** and **5** were evaluated for the α-glucosidase inhibitory activity. As shown in **Table 3**, all the compounds exhibited potent inhibitory potency against α-glucosidase, with IC_{50} values ranging from 15.7 ± 1.1 to 53.1 ± 1.4 μM, which was much lower than that of the positive control acarbose (IC_{50} = 154.7 ± 8.1 μM). All enantiomers displayed nearly horizontal IC_{50} values against α-glucosidase inhibitory activity, indicating that the difference of chirality might have a negligible impact on the activity. Most importantly, compounds **1a/1b–4a/4b** and **5** may provide novel chemical scaffolds for the discovery of new α-glucosidase inhibitors.

To investigate the binding mode of these compounds with α-glucosidase, molecular docking study was carried out by using the SYBYL 2.0 software. Due to the unavailable of crystal structure of α-glucosidase from *Saccharomyces cerevisiae*, the crystal structure of isomaltase (PDB ID: 3A4A) from *S. cerevisiae*, which is 84% similar to that of *S. cerevisiae* α-glucosidase, was conducted as docking model (Shen et al., 2015). The theoretical binding mode between **4a** and the enzyme was shown in **Figure 7**. Compound **4a** adopted a "V-shaped" conformation in the pocket. Detailed analysis showed that the phenolic group and benzopyran group of **4a** formed π-π stacking interaction with the residue Phe303 and Phe173, respectively. It was also shown that the residue Asp307, Asp352, and Glu411 formed key hydrogen bonds with **4a**, which were the main interactions between **4a** and the enzyme. All these interactions helped **4a** to anchor in the binding site of the enzyme.

CONCLUSIONS

In conclusion, nine novel butenolide derivatives belonging to two undescribed structural types, including four pairs of enantiomers (**1a/1b–4a/4b**) and a racemate (**5**), were isolated from the coral-associated fungus *Aspergillus terreus*. More importantly, (±)-asperteretal D and (4*S*)-4-decarboxylflavipesolide C were structurally revised to **2a**/**2b** and **4**, respectively. This study further enriched secondary metabolites in the *Aspergillus* species and was also a strong structural supplement to the new class of γ-butenolides. In addition, bioactivity evaluation results showed that all the isolates exhibited potent α-glucosidase inhibitory activity with IC_{50} values ranging from 15.7 ± 1.1 to 53.1 ± 1.4 μM. On the background that DM is becoming a global public health problem and more new effective therapeutic agents are in the urgent need, our findings provide a basis for further development and utilization of butenolide derivatives as source of potential α-glucosidase inhibitors as therapeutic agents for type-2 diabetes mellitus.

AUTHOR CONTRIBUTIONS

ML and CQ contributed to the extraction, isolation, identification, and manuscript preparation. WS contributed to the α-glucosidase inhibitory activity test. LS contributed to the fungal isolation and fermentation. JW advised and assisted Liu's experiments. JL contributed to the ECD calculations. YL contributed to the molecular docking experiment. YX contributed to the structure identification of isolated compounds. ZH guided Liu's experiments and wrote the manuscript. YZ designed the experiments and revised the manuscript.

FUNDING

We greatly acknowledge the financial support from the National Science Fund for Distinguished Young Scholars (No. 81725021), the Innovative Research Groups of the National Natural Science Foundation of China (No. 81721005), the Program for Changjiang Scholars of Ministry of Education of the People's Republic of China (No. T2016088), the National Natural Science Foundation of China (Nos. 21702067, 81573316, 81703580, and 81502943), the China Postdoctoral Science Foundation Funded Project (Nos. 2017M610479 and 2018T110777), the Academic Frontier Youth Team of HUST, and the Integrated Innovative Team for Major Human Diseases Program of Tongji Medical College (HUST).

ACKNOWLEDGMENTS

We are also thankful to the Analytical and Testing Center at Huazhong University of Science and Technology for assistance in measuring the CD and IR data.

SUPPLEMENTARY MATERIAL

The Supplementary Material for this article can be found online at: https://www.frontiersin.org/articles/10.3389/fchem.2018.00422/full#supplementary-material

REFERENCES

Baron, A. D. (1998). Postprandial hyperglycaemia and α-glucosidase inhibitors. *Diabetes Res. Clin. Pr.* 40, 51–55. doi: 10.1016/S0168-8227(98)00043-6

He, Y., Hu, Z., Li, Q., Huang, J., Li, X. N., Zhu, H., et al. (2017a). Bioassay-guided isolation of antibacterial metabolites from *Emericella* sp. TJ29. *J. Nat. Prod.* 80, 2399–2405. doi: 10.1021/acs.jnatprod.7b00077

He, Y., Hu, Z., Sun, W., Li, Q., Li, X. N., Zhu, H., et al. (2017b). Spiroaspertrione A, a Bridged Spirocyclic meroterpenoid, as a potent potentiator of oxacillin against methicillin-resistant *Staphylococcus aureus* from *Aspergillus* sp. TJ23. *J. Org. Chem.* 82, 3125–3131. doi: 10.1021/acs.joc.7b00056

He, Y., Zheng, M., Li, Q., Hu, Z., Zhu, H., Liu, J., et al. (2017c). Asperspiropene A, a novel fungal metabolite as an inhibitor of cancer-associated mutant isocitrate dehydrogenase 1. *Org. Chem. Front.* 4, 1137–1144. doi: 10.1039/c6qo00847j

Hu, Z., Wu, Y., Xie, S., Sun, W., Guo, Y., Li, X. N., et al. (2017). Phomopsterones A and B, two functionalized ergostane-type steroids from the endophytic fungus *Phomopsis* sp. TJ507A. *Org. Lett.* 19, 258–261. doi: 10.1021/acs.orglett.6b03557

Hu, Z. X., Xue, Y. B., Bi, X. B., Zhang, J. W., Luo, Z. W., Li, X. N., et al. (2014). Five new secondary metabolites produced by a marine-associated fungus, *Daldinia eschscholzii*. *Mar. Drugs* 12, 5563–5575. doi: 10.3390/md12115563

Hung, H. Y., Qian, K., Morris-Natschke, S. L., Hsu, C. S., and Lee, K. H. (2012). Recent discovery of plant-derived anti-diabetic natural products. *Nat. Prod. Rep.* 29, 580–606. doi: 10.1039/C2NP00074A

Kao, C. C., Wu, P. C., Wu, C. H., Chen, L. K., Chen, H. H., Wu, M. S., et al. (2016). Risk of liver injury after α-glucosidase inhibitor therapy in advanced chronic kidney disease patients. *Sci. Rep.* 6:18996. doi: 10.1038/srep18996

Kim, K. Y., Nam, K. A., Kurihara, H., and Kim, S. M. (2008). Potent α-glucosidase inhibitors purified from the red alga *Grateloupia elliptica*. *Phytochemistry* 69, 2820–2825. doi: 10.1016/j.phytochem.2008.09.007

Kopelman, P. G. (2000). Obesity as a medical problem. *Nature* 404, 635–643. doi: 10.1038/35007508

Lauritano, C., and Ianora, A. (2016). Marine organisms with anti-diabetes properties. *Mar. Drugs* 14:220. doi: 10.3390/md14120220

Liu, M., Sun, W., Wang, J., He, Y., Zhang, J., Li, F., et al. (2018a). Bioactive secondary metabolites from the marine-associated fungus *Aspergillus terreus*. *Bioorg. Chem.* 80, 525–530. doi: 10.1016/j.bioorg.2018.06.029

Liu, M., Zhou, Q., Wang, J., Liu, J., Qi, C., Lai, Y., et al. (2018b). Anti-inflammatory butenolide derivatives from the coral-derived fungus *Aspergillus terreus* and structure revisions of aspernolides D and G, butyrolactone VI and 4',8"-diacetoxy butyrolactone VI. *RSC Adv.* 8, 13040–13047. doi: 10.1039/c8ra01840e

Miertus, S., Scrocc, E., and Tomasi, J. (1981). Electrostatic interaction of a solute with a continuum. A direct utilizaion of AB initio molecular potentials for the prevision of solvent effects. *J. Chem. Phys.* 55, 117–129. doi: 10.1016/0301-0104(81)85090-2

Shen, X., Saburi, W., Gai, Z., Kato, K., Ojima-Kato, T., Yu, J., et al. (2015). Structural analysis of the α-glucosidase HaG provides new insights into substrate specificity and catalytic mechanism. *Acta Cryst.* 71, 1382–1391. doi: 10.1107/S139900471500721X

Smith, S. G., and Goodman, J. M. (2010). Assigning stereochemistry to single diastereoisomers by GIAO NMR calculation: the DP4 probability. *J. Am. Chem. Soc.* 132, 12946–12959. doi: 10.1021/ja105035r

Sun, K., Zhu, G., Hao, J., Wang, Y., and Zhu, W. (2018). Chemical-epigenetic method to enhance the chemodiversity of the marine algicolous fungus, *Aspergillus terreus* OUCMDZ-2739. *Tetrahedron* 74, 83–87. doi: 10.1016/j.tet.2017.11.039

Sun, Y., Liu, J., Li, L., Gong, C., Wang, S., Yang, F., et al. (2018). New butenolide derivatives from the marine sponge-derived fungus *Aspergillus terreus*. *Bioorg. Med. Chem. Lett.* 28, 315–318. doi: 10.1016/j.bmcl.2017.12.049

Tähtinen, P., Bagno, A., Klika, K. D., and Pihlaja, K. (2003). Modeling NMR parameters by DFT methods as an aid to the conformational analysis of cis-fused 7a(8a)-methyl octa(hexa)hydrocyclopenta[*d*][1,3]oxazines and [3,1]benzoxazines. *J. Am. Chem. Soc.* 125, 4609–4618. doi: 10.1021/ja021237t

Yang, B., Sun, W., Wang, J., Lin, S., Li, X. N., Zhu, H., et al. (2018). A new breviane spiroditerpenoid from the marine-derived fungus *Penicillium* sp. TJ403-1. *Mar. Drugs* 16:110. doi: 10.3390/md16040110

Yin, Z., Zhang, W., Feng, F., Zhang, Y., and Kang, W. (2014). α-glucosidase inhibitors isolated from medicinal plants. *Food Sci. Hum. Wellness* 3, 136–174. doi: 10.1016/j.fshw.2014.11.003

Conflict of Interest Statement: The authors declare that the research was conducted in the absence of any commercial or financial relationships that could be construed as a potential conflict of interest.

frontiers in Chemistry

ORIGINAL RESEARCH
published: 18 October 2018
doi: 10.3389/fchem.2018.00498

Coculture of Marine *Streptomyces* sp. With *Bacillus* sp. Produces a New Piperazic Acid-Bearing Cyclic Peptide

*Daniel Shin, Woong Sub Byun, Kyuho Moon, Yun Kwon, Munhyung Bae, Soohyun Um, Sang Kook Lee and Dong-Chan Oh**

Natural Products Research Institute, College of Pharmacy, Seoul National University, Seoul, South Korea

Microbial culture conditions in the laboratory, which conventionally involve the cultivation of one strain in one culture vessel, are vastly different from natural microbial environments. Even though perfectly mimicking natural microbial interactions is virtually impossible, the cocultivation of multiple microbial strains is a reasonable strategy to induce the production of secondary metabolites, which enables the discovery of new bioactive natural products. Our coculture of marine *Streptomyces* and *Bacillus* strains isolated together from an intertidal mudflat led to discover a new metabolite, dentigerumycin E (**1**). Dentigerumycin E was determined to be a new cyclic hexapeptide incorporating three piperazic acids, *N*-OH-Thr, *N*-OH-Gly, β-OH-Leu, and a pyran-bearing polyketide acyl chain mainly by analysis of its NMR and MS spectroscopic data. The putative PKS-NRPS biosynthetic gene cluster for dentigerumycin E was found in the *Streptomyces* strain, providing clear evidence that this cyclic peptide is produced by the *Streptomyces* strain. The absolute configuration of dentigerumycin E was established based on the advanced Marfey's method, ROESY NMR correlations, and analysis of the amino acid sequence of the ketoreductase domain in the biosynthetic gene cluster. In biological evaluation of dentigerumycin E (**1**) and its chemical derivatives [2-*N*,16-*N*-deoxydenteigerumycin E (**2**) and dentigerumycin methyl ester (**3**)], only dentigerumycin E exhibited antiproliferative and antimetastatic activities against human cancer cells, indicating that *N*-OH and carboxylic acid functional groups are essential for the biological activity.

Keywords: marine microorganism, coculture, natural product, dentigerumycin, cyclic peptide

OPEN ACCESS

Edited by:
Xian-Wen Yang,
Third Institute of Oceanography, State Oceanic Administration, China

Reviewed by:
Xuefeng Zhou,
South China Sea Institute of Oceanology (CAS), China
Xingyun Chai,
Beijing University of Chinese Medicine, China
Kyo Bin Kang,
Sookmyung Women's University, South Korea

****Correspondence:***
Dong-Chan Oh
dongchanoh@snu.ac.kr

Specialty section:
This article was submitted to Medicinal and Pharmaceutical Chemistry, a section of the journal Frontiers in Chemistry

Received: *06 August 2018*
Accepted: *01 October 2018*
Published: *18 October 2018*

Citation:
Shin D, Byun WS, Moon K, Kwon Y, Bae M, Um S, Lee SK and Oh D-C (2018) Coculture of Marine Streptomyces sp. With Bacillus sp. Produces a New Piperazic Acid-Bearing Cyclic Peptide. Front. Chem. 6:498. doi: 10.3389/fchem.2018.00498

INTRODUCTION

Genomic analysis of microbes strongly suggests that microorganisms have more potential gene clusters that would allow them to produce more secondary metabolites than are currently known (Omura et al., 2001). Even if it is poorly understood, microorganisms are presumed to communicate with each other physically or/and chemically (Hogan and Kolter, 2002; Straight et al., 2006). Coculturing has been shown to alter individual cellular physiology and induce the production of microbial secondary metabolites that are genetically encoded but not produced under conventional laboratory culture conditions (Ueda and Beppu, 2017). In this context, coculturing different microbes to elicit the production of bioactive microbial compounds not previously observed when microbes are cultured independently could be a promising strategy to access microbial

chemical diversity. A thorough literature search indicated that chemical studies of cocultures initially focused on mixed cultures of fungi and bacteria. The first new natural product from a coculture, pestalone, was discovered by cocultivation of the marine fungus *Pestalotia* sp. and the marine bacterium *Thalassospira* sp. (Cueto et al., 2001). A subsequent coculture experiment with the *Thalassospira* strain with the marine fungus *Libertella* sp. resulted in the production of new pimarane-type diterpenoids (Oh et al., 2005). In addition, the interaction between the fungus *Aspergillus fumigatus* and the bacterium *Sphingomonas* afforded glionitrin A (Park et al., 2009). Relatively recently, cocultures of two different bacterial strains have also successfully contributed to the discovery of new bioactive natural products. Cocultivating various *Streptomyces* strains with *Tsukamurella pulmonis* elicited the production of new butanolides (Hoshino et al., 2015). Ecologically relevant cocultures of marine invertebrate-associated *Rhodococcus* and *Micromonospora* strains produced the antibiotic bis-nitroglycosylated anthracycline (Adnani et al., 2017). As part of our efforts to discover new bioactive molecules from marine bacteria, we adopted the coculture strategy. Chemical analysis of a coculture of two marine bacterial strains isolated together from an intertidal mudflat in Wando, Republic of Korea, showed the induction of the formation of a bacterial metabolite. This result prompted us to scale up the coculture and subsequently characterize the metabolite. Here, we report the production, structure elucidation, putative biosynthetic gene cluster (BGC), and biological activity of the new bacterial metabolite, dentigerumycin E (**1**).

MATERIALS AND METHODS

General Experimental Procedures

Specific rotations were obtained using a JASCO P-2000 polarimeter with a 1-cm cell at 25°C. UV spectra were obtained using an Applied Photophysics Chirascan^{TM}-plus spectrometer with a 1-cm quartz cell at 25°C. IR spectral data were obtained using a JASCO FT/IR-4200 spectrometer. NMR spectra were recorded on an 800 MHz Bunker Avance III HD spectrometer with a 5-mm TCI cryoprobe and a Bunker Avance 600 MHz spectrometer at the National Center for Inter-university Research Facilities (NCIRF). LC-MS and low-resolution electrospray ionization mass spectroscopic (LR-ESI-MS) data were obtained using an Agilent Technologies 1200 series high performance liquid chromatography (HPLC) coupled with an Agilent Technologies 6130 quadrupole MS. High-resolution fast atom bombardment MS (HR-FAB-MS) data were obtained using a JEOL JMS-700 high-resolution MS at NCIRF.

Bacterial Isolation

A mud sample was collected from the intertidal mudflat in Wando (34°18′55.5″N 126°45′21.8″E), Republic of Korea in September 2014. For bacterial isolation from the sample, 1 g of the mud sample was diluted in 10 mL of sterilized artificial seawater, and the mixture was spread onto A4 medium, actinomycete isolation agar medium, starch casein medium, chitin-based medium, Czapek-Dox agar medium, Bennet's agar medium, YPM agar medium, YPG agar medium, and K agar medium (all agar media were made with artificial seawater and 100 mg/L cycloheximide). These isolation agar plates were incubated at 25°C for 3 weeks. The actinobacterial strain JB5 and the *Bacillus* strain GN1 were isolated on the same plate together from actinomycete isolation agar medium. The strain JB5 was identified as *Streptomyces* sp. (99% identical to *Streptomyces albogriseolus* strain B24) on the basis of 16S rRNA gene sequence analysis (GenBank accession No. MH656702). The strain GN1 was identified as *Bacillus* sp. (99% identical to *Bacillus cereus*) by 16S rRNA gene sequence analysis (GenBank accession No. MH656703).

Coculture Experiment

Streptomyces sp. strain JB5 and various strains in different phyla were cultivated separately in 50 mL of YEME liquid medium (4 g of yeast extract, 10 g of malt extract, and 4 g of glucose as a 40% solution in 1 L of artificial seawater) in a 125-mL Erlenmeyer flask. After 4 days of cultivation in a rotary shaker at 200 rpm at 30°C, equal volumes of the liquid cultures of JB5 and other strains were mixed (10 mL to 10 mL) and inoculated into a 500-mL baffled Erlenmeyer flask containing 200 mL of YEME liquid medium. Mixed strains were cocultivated over 8 days in a rotary shaker at 200 rpm at 30°C, and the chemical profiles of the cocultures were monitored by LC-MS every 2 days. The strains cocultivated with JB5 were *Bacillus* sp. (GN1), *Streptomyces* sp. (SD53; isolated from the gut of *Bombyx mori*), *Paenibacillus* sp. (CC2; isolated from the gut of *Meloe proscarabaeus*), *Brevibacillus* sp. (PTH23; isolated from the excreta of *Onthophagus lenzii*), *Streptomyces* sp. (UTZ13; isolated from the *Nicrophorus concolor* parasitic mites), *Mycobacterium* sp. (Myc06; isolated from the vegetable mold formed by *Oligochaeta*), *Hafnia* sp. (CF1; isolated from the *Meloe proscarabaeus*), and *Bacillus* sp. (HR1; isolated from the gut of *Pseudopyrochroa rufula*).

Genome Sequencing and Analysis

The genome of the JB5 strain was constructed de novo using Pacbio sequencing data. Genome sequencing of the JB5 strain was performed using the PacBio RS II by Chunlab, Inc. (Seoul, Republic of Korea), and sequencing data were assembled with PacBio SMRT Analysis 2.3.0 using the HGAP2 protocol (Pacific Biosciences, USA). Nucleotide sequences with 122.76-fold coverage of the *Streptomyces* sp. JB5 genome (∼7.72 Mbp) were generated. Gene prediction was performed using Prodigal 2.6.2, and sequences were annotated with ChunLab's in-house pipeline with EggNOG 4.5, Swissprot, KEGG, and SEED as references. The dentigerumycin E BGC was identified using antiSMASH (Medema et al., 2011; Weber et al., 2015).

Production and Extraction of Dentigerumycin E

JB5 and GN1 strains were cultivated separately in 50 mL of YEME liquid medium in 125-mL Erlenmeyer flasks. After 4 days of cultivation in a rotary shaker at 200 rpm at 30°C, 10 mL of the JB5 culture and 1 mL of the GN1 culture (based on a serial dilution, approximately 4.9×10^7 cells were estimated to be in 1 mL of

Bacillus sp. GN1 culture) were inoculated together into a 500-mL baffled Erlenmeyer flask containing 200 mL of YEME liquid medium. The *Streptomyces* sp. JB5 and *Bacillus* sp. GN1 were cocultivated for 6 days in a rotary shaker at 200 rpm at 30°C. A total of 120 L of the coculture was extracted twice with 180 L of EtOAc by using a separation funnel. The EtOAc layer was separated from the aqueous phase, and the residual water in the organic layer was removed by adding anhydrous sodium sulfate.

Isolation of Dentigerumycin E

The crude extract was filtered through a 25HP045AN syringe filter unit and directly injected onto a semipreparative reversed-phase HPLC column (YMC-Pack ODS-A, 250 × 10 mm, C_{18}, 5 μm) and was separated with a gradient solvent system (flow rate: 2 mL/min; UV detection: 210 nm; 35% to 50% CH_3CN/H_2O with 0.1% formic acid over 50 min). Dentigerumycin E (**1**) eluted at a retention time of 27 min and was further purified by semipreparative HPLC using gradient solvent conditions (column: YMC-Pack ODS-A, 250 × 10 mm, C_{18}, 5 μm, flow rate: 2 mL/min; UV detection: 230 nm; 66 to 88% gradient MeOH/H_2O with 0.1% formic acid over 20 min). Pure dentigerumycin E (34 mg) was obtained at a retention time of 38 min under the final purification conditions.

Dentigerumycin E (**1**): white, amorphous powder; $[\alpha]_D^{25} = -3.1$ (c 0.01, MeOH); UV (MeOH) λ_{max} (log ε) 204 (3.36) nm; IR (neat) ν_{max} 3401, 2929, 1741, 1644, 1507, 1445, 1248, 1196 cm^{-1}; HR-FAB-MS $[M+Na]^+$ *m/z* 936.4290 (calcd for $C_{39}H_{63}N_9O_{16}Na$, 936.4290); For ^1H and ^{13}C NMR spectral data, **Table 1**.

Reduction of *N*-OHs in Dentigerumycin E

Dentigerumycin E (**1**, 10 mg) was dissolved in 4 mL of THF (tetrahydrofuran). Aqueous ammonium acetate (2 mL, 4.5 M) and 1 mL of 12% $TiCl_3$ solution in 20-30 wt. % HCl were added to the solution. The mixture was stirred at room temperature for 2 h, and the product was extracted with 20 mL of EtOAc. The organic layer was concentrated *in vacuo*, and the reaction product (2-*N*,16-*N*-deoxydentigerumycin E, **2**) was purified by reversed-phase HPLC (YMC-Pack ODS-A, 250 × 10 mm, C_{18}, 5 μm) with an isocratic solvent system (flow rate: 2 mL/min; UV detection: 210 nm; 36% CH_3CN/H_2O with 0.1% formic acid). 2-*N*,16-*N*-deoxydentigerumycin E (**2**, 3.1 mg) eluted at 38.2 min, and its molecular formula was confirmed as $C_{39}H_{63}N_9O_{14}$ by HR-FAB mass spectroscopic analysis. The ^1H and ^{13}C NMR chemical shifts of 2-*N*,16-*N*-deoxydentigerumycin E (**2**) were assigned based on ^1H NMR, HSQC, COSY, HMBC, ROESY, and TOCSY analyses.

2-N,16-N-deoxydentigerumycin E (**2**): white, amorphous powder; $[\alpha]_D^{25} = -2.6$ (c 0.01, MeOH); UV (MeOH) λ_{max} (log ε) 200 (3.31) nm; IR (neat) ν_{max} 3385, 2935, 1745, 1640, 1511, 1314, 1246, 1201 cm^{-1}; HR-FAB-MS $[M+Na]^+$ *m/z* 904.4399 (calcd for $C_{39}H_{63}N_9O_{16}Na$, 904.4392); For ^1H and ^{13}C NMR spectral data, **Table S1**.

Application of Advanced Marfey's Method

Dentigerumycin E (**1**, 0.6 mg) was hydrolyzed in 0.5 mL of 6 N HCl at 115°C for 1 h with stirring, and the reaction was quenched by cooling in an ice bath for 3 min. The HCl was evaporated *in vacuo*. Then, 0.5 mL of water was added to the dry material and dried *in vacuo* three times to remove the residual HCl. The hydrolysate was lyophilized for 24 h to ensure complete removal of the acid. The hydrolysate containing free amino acids was divided into two vials. Each hydrolysate was dissolved in 200 μL of 1 N $NaHCO_3$, and 100 μL of L-FDAA (1-fluoro-2,4,dinitrophenyl-5-L-alanine amide) or D-FDAA in acetone (10 mg/mL) was added to each vial. Both vials were incubated at 80°C for 3 min, and 100 μL of 2 N HCl was added to neutralize the reactions. Each reaction mixture was diluted with 300 μL of 50% CH_3CN/H_2O solution, and 20-μL aliquots of each reaction product were analyzed by LC-MS using a gradient solvent system (flow rate: 0.7 mL/min; UV detection: 340 nm; 10 to 60% CH_3CN/H_2O with 0.1% formic acid over 40 min) with a reversed-phase column (Phenomenex Luna $C_{18}(2)$, 100 × 4.6 mm, C_{18}, 5 μm). To determine the stereochemistry of *N*-OH Thr, the reduction product (**2**, 1.5 mg) was hydrolyzed with 6 N HCl at 115°C for 1 h with stirring. The hydrolysate of **2** was derivatized with Marfey reagents (L-FDAA and D-FDAA), and the FDAA-adducts were analyzed by LC-MS in the same manner as described above.

GITC (2,3,4,6-Tetra-*O*-Acetyl-β-D-Glucopyranosyl Isothiocyanate) Derivatization

Authentic standards of L-*allo*-Thr and L-Thr (0.5 mg) along with the hydrolysate of the reduction product (**2**) were dissolved in 200 μL of water in 4-mL vials. Then, 200 μL of 6% trimethylamine and 1% GITC (2,3,4,6-tetra-*O*-acetyl-β-D-glucopyranosyl isothiocyanate) in acetone were added to each vial. The reaction mixtures were stirred at 25°C for 15 min, and the derivatization was quenched by adding 100 μL of 5% acetic acid. Aliquots of each reaction mixture (40 μL) were analyzed by LC-MS under gradient HPLC conditions (flow rate: 0.7 mL/min; UV detection: 254 nm; 10 to 100% CH_3CN/H_2O with 0.1% formic acid over 50 min, column: Phenomenex Luna $C_{18}(2)$, 100 × 4.6 mm, 5 μm).

Methylation of Dentigerumycin E

Dentigerumycin E (**1**, 10 mg) was dissolved in 3 mL of anhydrous MeOH. AcCl (2.5 μL) was added to the solution, and the mixture was stirred at room temperature for 9 h with LC-MS monitoring of the reaction progress. The reaction mixture was concentrated *in vacuo* and purified by reversed-phase HPLC (YMC-Pack ODS-A, 250 × 10 mm, C_{18}, 5 μm) with an isocratic solvent system (flow rate: 2 mL/min; UV detection: 210 nm; 38% CH_3CN/H_2O with 0.1% formic acid). Dentigerumycin E methyl ester (**3**, 1.5 mg) eluted at 41.5 min under these HPLC conditions. Its molecular formula was confirmed as $C_{40}H_{65}N_9O_{16}$ by HR-FAB mass spectroscopic analysis. The ^1H and ^{13}C NMR chemical shifts of dentigerumycin E methyl ester (**3**) were assigned by ^1H NMR, HSQC, COSY, HMBC, ROESY, and TOCSY spectral analyses.

Dentigerumycin E methyl ester (**3**): white, amorphous powder; $[\alpha]_D^{25} = -1.3$ (c 0.012, MeOH); UV (MeOH) λ_{max} (log ε) 205

TABLE 1 | ^{1}H and ^{13}C NMR spectral data of dentigerumycin E (**1**) in pyridine-d_5[a].

Position	δ_C	Type	δ_H	mult (*J* in Hz)	Position	δ_C	Type	δ_H	mult (*J* in Hz)
1	170.6	C			20a	21.3	CH_2	1.68	m
2	66.9	CH	4.19	d (10.0)	20b			1.37	m
2-N-OH			n.d.		21a	47.4	CH_2	3.11	m
3	68.8	CH	6.0	m	21b			2.95	br. d (15.5)
3-OH			n.d.		21-NH			5.69	br. d (13.0)
4	19.0	CH_3	1.89	d (6.5)	22	169.3	C		
5	169.6	C			23	57.0	CH	5.83	dd (10.0, 10.0)
6	52.7	CH	5.44	dd (5.5, 1.5)	23-NH			9.13	d (10.0)
7a	24.4	CH_2	2.25	br. d (14.0)	24	77.8	CH	5.95	dd (10.0, 1.0)
7b			1.62	m	25	30.6	CH	2.46	m
8a	22.0	CH_2	1.21	m	26	15.5	CH_3	1.35	d (7.0)
8b			1.06	br. d (13.0)	27	20.4	CH_3	1.25	d (7.0)
9a	47.3	CH_2	3.03	br. d (13.0)	28	178.2	C		
9b			2.69	m	29	77.8	C		
9-NH			4.90	br. d (13.0)	29-OH			6.97	s
10	176.3	C			30	100.0	C		
11	43.7	CH	6.55	br. d (6.5)	30-OH			7.03	s
12a	25.2	CH_2	1.84	br. d (13.0)	31a	28.3	CH_2	2.26	m
12b			1.68	m	31b			2.06	m
13a	20.4	CH_2	2.02	m	32a	26.0	CH_2	2.10	m
13b			1.26	m	32b			2.05	m
14a	47.6	CH_2	2.93	br. d (14.5)	33	36.9	CH	2.17	m
14b			2.59	m	34	75.2	CH	4.03	m
14-NH			5.59	dd (12.5, 1.0)	35	22.7	CH_3	1.75	s
15	167.4	C			36a	38.0	CH_2	2.62	dd (15.0, 4.5)
16a	52.6	CH_2	5.21	d (17.5)	36b			2.28	dd (15.0, 8.5)
16b			4.82	d (17.5)	37	175.2	C		
16-N-OH			n.d.		37-OH			n.d.	
17	174.1	C			38a	25.7	CH_2	1.72	m
18	48.7	CH	6.22	br. d (6.5)	38b			1.45	m
19a	25.8	CH_2	2.42	br. d (13.5)	39	9.7	CH_3	0.98	t (7.5)
19b			1.92	m					

[a] *H and ^{13}C NMR data were recorded at 800 and 200 MHz, respectively.*

(3.65) nm; IR (neat) ν_{max} 3263, 2935, 1738, 1643, 1508, 1442, 1355, 1247, 1195 cm^{-1}; HR-FAB-MS $[M+Na]^+$ *m/z* 950.4442 (calcd for $C_{40}H_{65}N_9O_{16}Na$, 950.4447); For ^{1}H and ^{13}C NMR spectral data, **Table S1**.

Cell Culture

Human cancer cells (A549, HCT116, MDA-MB-231, SK-HEP-1) and human breast epithelial cell (MCF-10A) were obtained from the American Type Culture Collection (Manassas, VA, USA) and a stomach cancer cell (SNU-638) was obtained from the Korean Cell Line Bank (Seoul, Korea). The cells were cultured in an appropriate medium (Dulbecco's modified Eagle's medium for MDA-MB-231 and SK-HEP-1; Roswell Park Memorial Institute 1640 for A549, HCT116 and SNU-638 cells; Dulbecco's modified Eagle's medium: Nutrient Mixture F-12 for MCF-10A) supplemented with antibiotics-antimycotics (PSF: 100 units/mL sodium penicillin G, 100 μg/mL streptomycin, and 250 ng/mL amphotericin B) and 10% fetal bovine serum (FBS) in an incubator containing 5% CO_2 at 37°C. All reagents were purchased from Gibco® Invitrogen Corp. (Grand Island, NY, USA).

Cell Proliferation Assay

Cell proliferation was measured by a sulforhodamine B (SRB) assay. Briefly, cells were seeded in 96-well plates and incubated for 30 min (for zero day controls) or treated with **1**-**3** for the indicated times. After incubation, the cells were fixed, dried and stained with 0.4% SRB in 1% acetic acid. Unbound dye was removed by washing, and the stained cells were suspended in 10 mM Tris (pH 10.0). The absorbance was measured at 515 nm, and the cell proliferation was determined. IC_{50} values were calculated by nonlinear regression analysis using TableCurve 2D v5.01 software (Systant Software Inc., Richmond, CA, USA). All reagents were purchased from Sigma-Aldrich.

Wound Healing Assay

MDA-MB-231 cells were grown to 80–90% confluence in a 6-well plate. A confluent monolayer of MDA-MB-231 cells was artificially wounded with a 200 μL pipette tip, and the detached cells were washed with phosphate-buffered saline (PBS, Invitrogen Corp.) and then incubated with 1% FBS in medium containing various concentrations of **1**–**3** for 24 h. The wounds were photographed at 0 and 24 h using an inverted microscope (Olympus, Tokyo, Japan). The wound area was quantified using ImageJ Software (National Institutes of Health) and presented as wound healing (%) relative to the area of the wound at 0 h.

Cell Invasion Assay

Twenty-four-well transwell membrane inserts 6.5-mm in diameter with 8 μm pores (Corning, Tewksbury, MA, USA) were coated with 10 μL of type I collagen (0.5 mg/mL, BD Biosciences, San Diego, CA, USA) and 20 μL of a 1:20 mixture of Matrigel (BD Biosciences)/PBS. After treatment with the test compounds for 24 h, MDA-MB-231 cells were harvested, resuspended in serum-free medium, and plated (1×10^6 cells/chamber) in the upper chamber of the Matrigel-coated transwell insert. Medium containing 30% FBS was used as the chemoattractant in the lower chambers. After 24 h of incubation, the cells that had invaded the outer surface of the lower chambers were fixed and stained using a Diff-Quik Staining Kit (Sysmex, Kobe, Japan) and imaged. Representative images from 3 separate experiments are shown, and the number of invaded cells was counted in 5 randomly selected microscopic fields (200× magnification) (Kim et al., 2018).

RESULTS AND DISCUSSION

Coculture Experiments for the Production of Dentigerumycin E

The marine *Streptomyces* sp. JB5, isolated from an intertidal mudflat in Wando, Republic of Korea, was cocultivated with the marine *Bacillus* sp. GN1, which was associated with the *Streptomyces* strain JB5 (**Figure S1**). The production of secondary metabolites was monitored by LC-MS every 2 days. the coculture with marine *Bacillus* sp. GN1, which was isolated from the intertidal mudflat along with *Streptomyces* sp. JB5, displayed a significantly different chemical profile compared with those of the pure cultures of the strains JB5 and GN1. In particular, on the sixth day cocultivation, LC-MS analysis of the coculture of JB5 and GN1 showed a newly produced metabolite at a retention time of 12.8 min that was not virtually detected in the cultures of the individual strains (**Figure 1**, **Figure S2**). The observed compound, later identified as a new cyclic depsipeptide, dentigerumycin E (**1**), showed a UV absorption maximum at 204 nm and a molecular ion $[M+H]^+$ at *m*/*z* 914. To optimize the production of dentigerumycin E, the two bacterial strains were mixed in various ratios. After 4 days of individual cultivation, the two pure cultures of JB5 and GN1 were mixed in ratios of 1:1, 2:1, 5:1, and 10:1. LC-MS analysis of the cocultures indicated that a 10:1 ratio of JB5/GN1 provides the best yield of dentigerumycin E (**1**).

The *Streptomyces* sp. JB5 was also cocultivated with phylogenetically diverse but ecologically irrelevant bacterial strains including *Bacillus* sp. HR1, *Paenibacillus* sp. CC2, *Brevibacillus* sp. PTH23, *Streptomyces* sp. SD53, *Streptomyces* sp. UTZ13, *Hafnia* sp. CF1, and *Mycobacterium* sp. Myc06. Most of the cocultures of *Streptomyces* sp. JB5 with these bacterial strains did not show the production of dentigerumycin E or the induction of other metabolites, the coculture with *Bacillus* sp. HR1, which is phylogenetically close to *Bacillus* sp. GN1, produced dentigerumycin E (**Figure S3**). Although the mechanism triggering the biosynthesis of dentigerumycin E by *Bacillus* strains remains unclear, these coculture experiment results implied that *Bacillus* strains, which are most closely related to *B. cereus*, possibly have common ability to induce the production of dentigerumycin E from *Streptomyces* sp. JB5.

Structure Elucidation of Dentigerumycin E

Dentigerumycin E (**1**) was isolated as an amorphous white power with a molecular formula of $C_{39}H_{63}N_9O_{16}$ based on HR-FAB-MS analysis (obsd. $[M+Na]^+$ at *m*/*z* 936.4290, calcd. 936.4290). The molecular formula indicated that this molecule possesses 13 degrees of unsaturation. The ^{13}C NMR spectrum of **1** indicated eight carbonyl carbons (δ_C: 178.2, 176.3, 175.2, 174.1, 170.6, 169.4, 169.3, and 167.4), one dioxygenated carbon (δ_C: 100.0), 13 N/O-bound carbons (δ_C: 77.8, 77.8, 75.2, 68.8, 66.9, 57.0, 52.7, 52.6, 48.7, 47.6, 47.4, 47.3, and 43.7), and 18 alkyl carbons (δ_C: 38.0 ∼ 9.7) (**Table 1**). The ^1H and HSQC NMR spectra of **1** indicated six exchangeable protons (δ_H: 9.13, 7.03, 6.97, 5.69, 5.59, and 4.90), three oxygenated methines (δ_C/δ_H: 77.8/5.95, 75.2/4.03, and 68.8/6.00), five methines at the α-positions of amino acids (δ_C/δ_H: 66.9/4.19, 57.0/5.83, 52.7/5.44, 48.7/6.22, and 43.7/6.55), four nitrogenous methylenes (δ_C/δ_H: 52.6–5.21 and 4.82, 47.6/2.93 and 2.59, 47.4/3.11 and 2.95, and 47.3/3.03 and 2.69), two alkyl methines, 10 alkyl methylenes, one singlet methyl (δ_C/δ_H: 22.71.75), three doublet methyls (δ_C/δ_H: 20.4/1.25, 19.0/1.89, and 15.5/1.35), and one triplet methyl (δ_C/δ_H: 9.7/0.98) (**Table 1**).

The COSY, TOCSY, and HMBC NMR spectra indicated that dentigerumycin E (**1**) possesses six unusual amino acid residues and one polyketide-derived substructure (**Figure 2**, **Figures S4–S10**). First, an array of COSY/TOCSY correlations constructed a spin system from H-6 to 9-NH. The HMBC correlation from H-6 to the C-5 carbonyl carbon and from 9-NH to C-6 demonstrated that this spin system includes a piperazic acid (Pip-1). Two additional piperazic acid units (Pip-2 and Pip-3) were similarly assigned based on the corresponding COSY, TOCSY, and HMBC correlations. Further analysis of COSY and TOCSY spectroscopic data revealed another discrete spin system from 23-NH to two doublet methyl groups (H_3-26 and H_3-27). The α-amino proton H-23 displayed an HMBC correlation with the carbonyl carbon at C-22, indicative of a β-hydroxy leucine (β-OH-Leu). In addition, a *N*-hydroxy threonine unit (*N*-OH-Thr) was proposed based on the COSY/TOCSY correlations among H-2, H-3, and H_3-4. An independent α-amino methylene signal correlated with the C-15 carbonyl carbon in the HMBC NMR spectrum indicated the presence of *N*-hydroxy glycine (*N*-OH-Gly).

The final structural fragment was assigned as a pyran-bearing polyketide-derived moiety. A terminal triplet methyl group (C-39) was connected to C-38 by the H_3-39/H_2-38 COSY

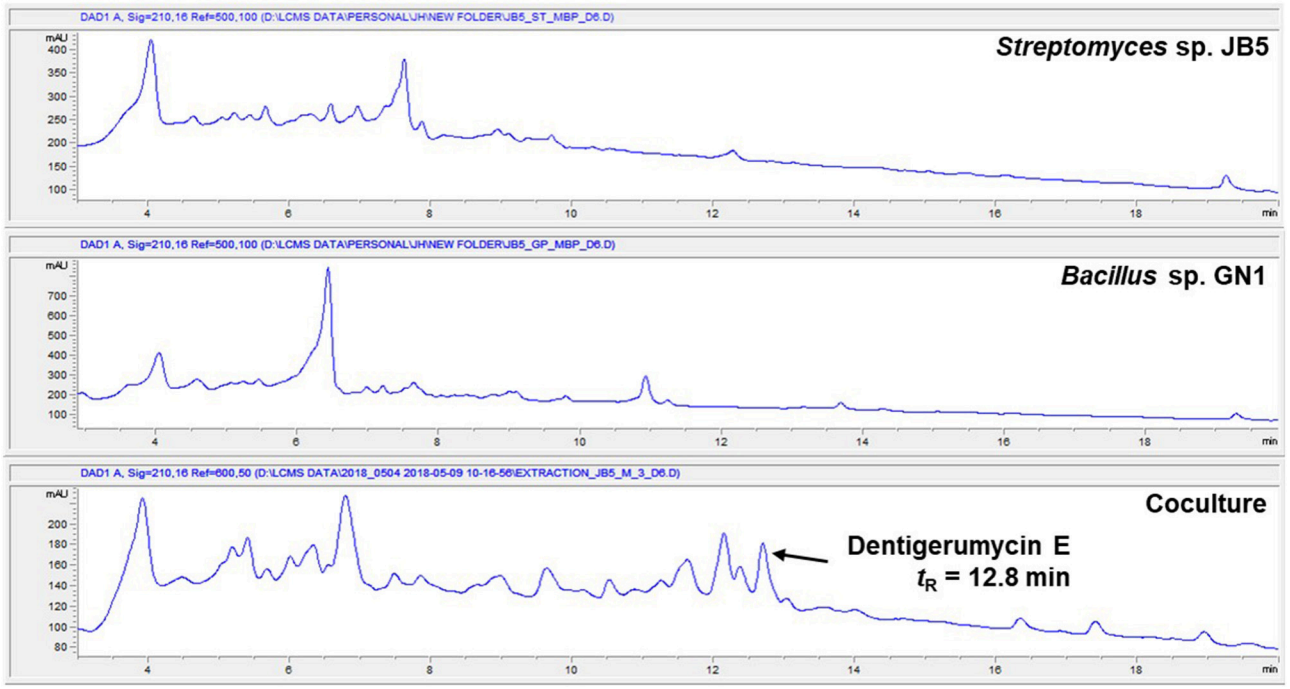

FIGURE 1 | HPLC profiles of the single culture of *Streptomyces* sp. JB5, the single culture of *Bacillus* sp. GN1, and their coculture.

correlation. The 3-bond ^{1}H-^{1}H couplings between H_2-38 and H-34 placed the C-39-C-38 ethyl group next to C-34. Subsequently, the COSY and TOCSY correlations among H-34, H-33, H_2-32, and H_2-31 constructed an alkyl chain spin system from C-39 to C-31. H_2-36 displayed a COSY coupling with H-33, indicating C-33 was a branch point. The 3-bond ^{1}H-^{13}C correlations from H_2-36 to the C-37 carbonyl carbon connected C-37 to C-36. The alkyl chain was further extended from C-31 to C-30, a dioxygenated carbon, based on the H_2-31/C-30 HMBC correlation. A singlet methyl signal (H_3-35) exhibited strong HMBC correlations to C-30, C-29, and C-28, which finally constructed a C_9 backbone chain with a C_2 branch and a branch methyl group. 29-OH and 30-OH, which were visible in the ^{1}H NMR spectrum, were assigned at C-29 and C-30, respectively, based on their HMBC correlations. Further analysis of the HMBC spectrum revealed the presence of a pyran ring by the H-34/C-30 3-bond correlation. Therefore, the polyketide-derived partial structure was determined to be a C_{12} alkyl moiety bearing a pyran ring and a branching C_2 chain and a branch methyl group (**Figure 3**).

The six amino acids and the polyketide-derived acyl chain were assembled by analysis of the HMBC spectrum. *N*-OH-Thr was located adjacent to Pip-1 based on the H-2/C-5 and H_2-7/C-5 ^{1}H-^{13}C correlations. The HMBC correlations from H-6 and H-12 to C-10 connected Pip-1 and Pip-2. The sequence from Pip-2 to *N*-OH-Gly was established by heteronuclear couplings from 14-NH and H_2-16 to C-15. H_2-16 also displayed an HMBC correlation to C-17. The connectivity between *N*-OH-Gly and Pip-3 was supported by the H_2-19/C-17 HMBC coupling. β-OH-Leu was located next to Pip-3 based on the 3-bond correlations from 21-NH and H-23 to C-22. The polyketide-derived moiety was connected to β-OH-Leu by the 28-NH/C-28 HMBC correlation. Therefore, the sequence of the partial structures of **1** was determined to be *N*-OH-Thr-Pip-1-Pip-2-*N*-OH-Gly-Pip-3-β-OH-Leu-polyketide-derived acyl chain (**Figure 3**).

The carbonyl groups explained 8 of the 13 double bond equivalents, indicating that dentigerumycin E (**1**) must be a pentacyclic compound. The three piperazic acids and pyran ring accounted for another four of the double bond equivalents. Thus, dentigerumycin E must possess an additional ring. The 3-bond HMBC correlation between H-24 and C-1 constructed a macrocycle (**Figure 3**). After elucidating most of the structure of **1**, the C-37 carbonyl carbon was proposed to be a carboxylic acid based on the molecular formula, which allowed the planar structure of dentigerumycin E (**1**) to be proposed as shown.

The uncertainty in the planar structure of **1** due to the invisibility of the *N*-OH and carboxylic OH moieties in the ^{1}H NMR spectrum was further clarified by utilizing chemical reactions and NMR spectroscopic analyses of the products. To confirm the presence of two *N*-OH groups, the *N*-OHs were converted to NHs using $TiCl_3$ (Pennings et al., 1983). The structure of the reduction product (2-*N*,16-*N*-deoxydentigerumycin E, **2**) (**Figure 2**) was elucidated based on the ^{1}H NMR, COSY, HMBC, HSQC, TOCSY, and ROESY spectra (**Table S1**, **Figures S11**–**S16**) and HRMS data, confirming the presence of the *N*-OH groups of *N*-OH-Thr and *N*-OH-Gly in dentigerumycin E (**1**). On the other hand, the only HMBC correlation to the C-37 carbonyl carbon (δ_C 175.2) was from H_2-36, not fully proving the proposed

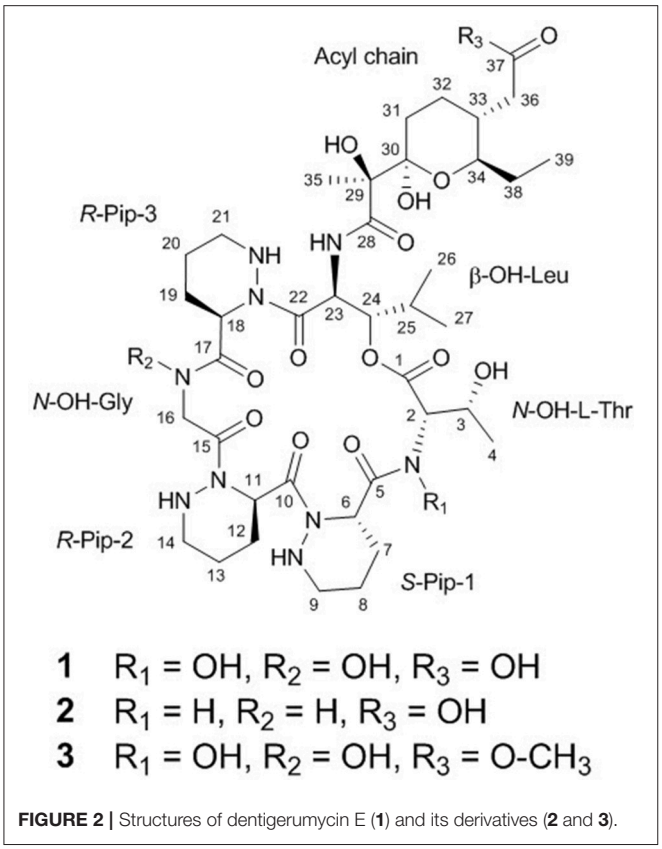

FIGURE 2 | Structures of dentigerumycin E (**1**) and its derivatives (**2** and **3**).

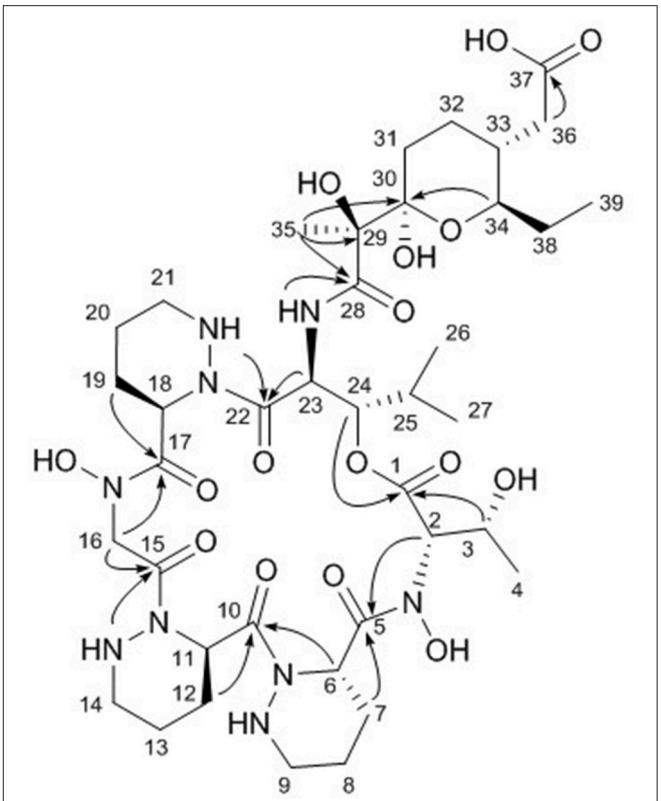

FIGURE 3 | Key HMBC correlations (arrows) in dentigerumycin E (**1**).

carboxylic acid functionality. To validate the presence of the carboxylic acid group in the acyl side chain, we performed an AcCl-mediated methylation and confirmed the structure of the methylated product (dentigerumycin E methyl ester, **3**) (**Figure 2**) by ^{1}H NMR, COSY, HMBC, HSQC, TOCSY, and ROESY (**Table S1**, **Figures S17**–**S22**) as well as HRMS analysis. The protons of the methoxy group displayed a clear HMBC correlation to the carbonyl carbon in **3**, confirming the carboxylic acid functionality in **1**. Therefore, the planar structure of dentigerumycin E (**1**) was unequivocally elucidated.

The relative configuration of the two congruent stereogenic centers in β-hydroxy leucine were established through *J*-based configuration analysis (**Figure 4A**). The large ^{1}H-^{1}H coupling between H-23 and H-24 (J_{H23H24} = 10.0 Hz) indicated that these two protons have *anti*-relationship. Further ROESY correlations allowed the assignment of 23*S** and 24*S** (Matsumori et al., 1999). The relative configuration of the pyran ring in the acyl side chain was determined by ROESY correlations (**Figure 4B**).

To establish the absolute configuration of dentigerumycin E (**1**), acid hydrolysis was performed using 6 N HCl at 115°C for 1 h. The hydrolysate was then derivatized with Marfey's reagents (L-FDAA and D-FDAA) and analyzed by LC-MS (Fujii et al., 1997). The L-FDAA and D-FDAA derivatives of β-hydroxy leucine were detected at retention times of 15.2 min and 18.2 min, determining its L(*S*)-configuration at the α-amino position (**Figure S23**). Based on the advanced Marfey method and the previously determined relative stereochemistries, the

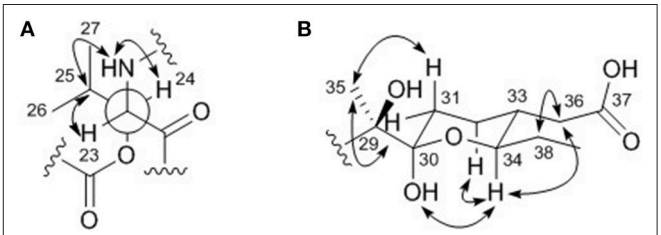

FIGURE 4 | Key ROESY correlations (double headed arrows) for determining the relative configurations of **(A)** the β-hydroxy leucine and **(B)** the acyl chain in dentigerumycin E (**1**).

absolute configuration of the chiral centers in the β-hydroxy leucine were determined to be 23*S* and 24*S*. The L-FDAA and D-FDAA derivatives of the three piperazic acid units eluted at retention times of 11.9 min and 14.1 min in a ratio of 2:1. Based on Marfey analysis of synthetic (*S*)- and (*R*)-piperazic acids, the L-FDAA derivative of piperazic acid elutes faster than the D-FDAA derivative when piperazic acid has an *R*-configuration (Oh et al., 2009). Therefore, dentigerumycin E contains two *R*-Pip and one *S*-Pip units.

Because the free *N*-OH-Thr does not react with Marfey's reagents, 2-*N*,16-*N*-deoxydentigerumycin E (**2**), which possesses Thr converted from *N*-OH-Thr, was hydrolyzed and derivatized with Marfey's reagents. In the LC-MS analysis of the derivatives,

the L-FDAA and D-FDAA derivatives of threonine eluted at 18.2 min and 21.4 min, respectively, indicating the α-position of threonine was in the L (*S*) configuration (**Figure S23**). Due to the presence of the additional stereogenic center at the *β*-carbon in threonine, GITC (2,3,4,6-tetra-*O*-acetyl-*β*-D-glucopyranosyl isothiocyanate) derivatization was performed (Hess et al., 2004). The retention times of the GITC derivatives of **2** and authentic standards of L-*allo*-Thr and L-Thr were compared. The GITC derivatives of L-*allo*-Thr, L-Thr, and Thr in **2** eluted at retention times of 14.7 min, 15.1 min, and 15.1 min, respectively (**Figure S24**). Therefore, the *N*-hydroxy threonine of dentigerumycin E (**1**) was determined to be *N*-OH-L-Thr, and thus the absolute configurations of its stereogenic centers were determined to be 2*S* and 3*R*.

Analysis of the Putative Biosynthetic Pathway of Dentigerumycin E for Stereochemical Assignment

Complete assignment of the sequence of the two *R*- and one *S*-piperazic acid moieties was accomplished through analysis of the putative biosynthetic gene cluster (BGC) (**Table S2**). Full genome sequencing of *Streptomyces* sp. JB5 allowed the identification of the BGC of dentigerumycin E (**1**). Even though its origin was reasonably inferred as *Streptomyces* sp. JB5 based on previous reports of dentigerumycin class compounds (Oh et al., 2009; Wyche et al., 2017), identifying the BGC added clearer evidence of its *Streptomyces* origin because sometimes the same class of compounds can be discovered together from phylogenetically diverse bacteria (Blodgett et al., 2010). As predicted based

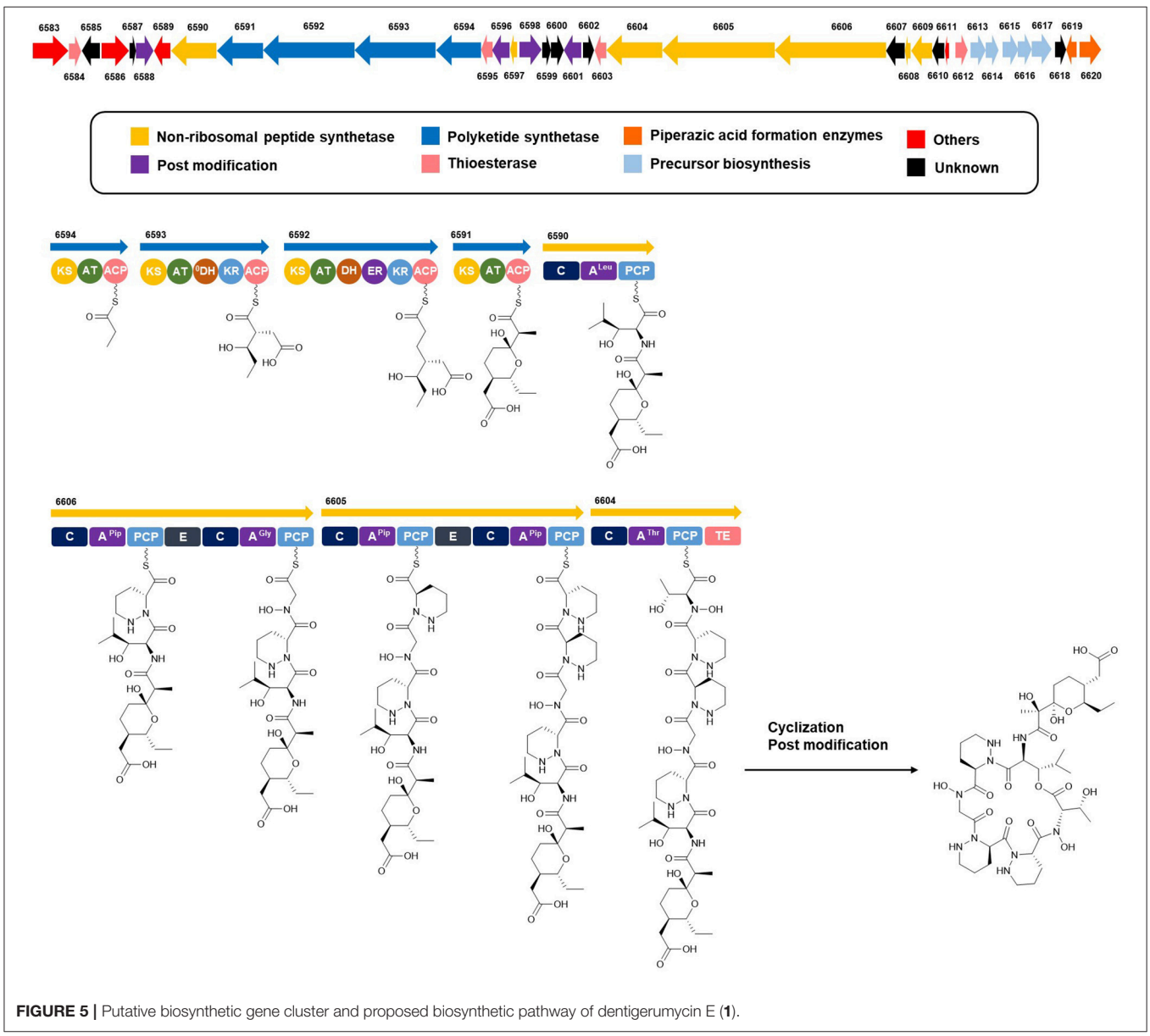

FIGURE 5 | Putative biosynthetic gene cluster and proposed biosynthetic pathway of dentigerumycin E (**1**).

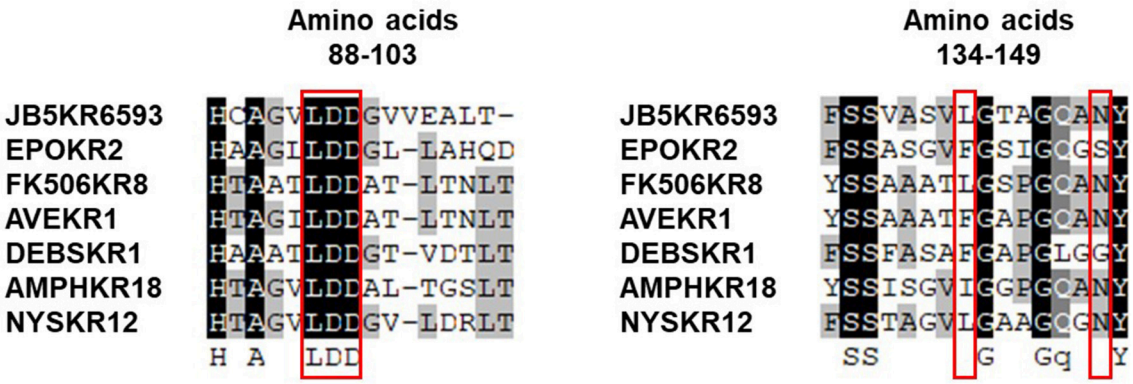

FIGURE 6 | Sequence alignment of KR domains in the biosynthetic gene cluster of dentigerumycin E (JB5KR6593) and various other PKSs reported by Caffrey (2003).

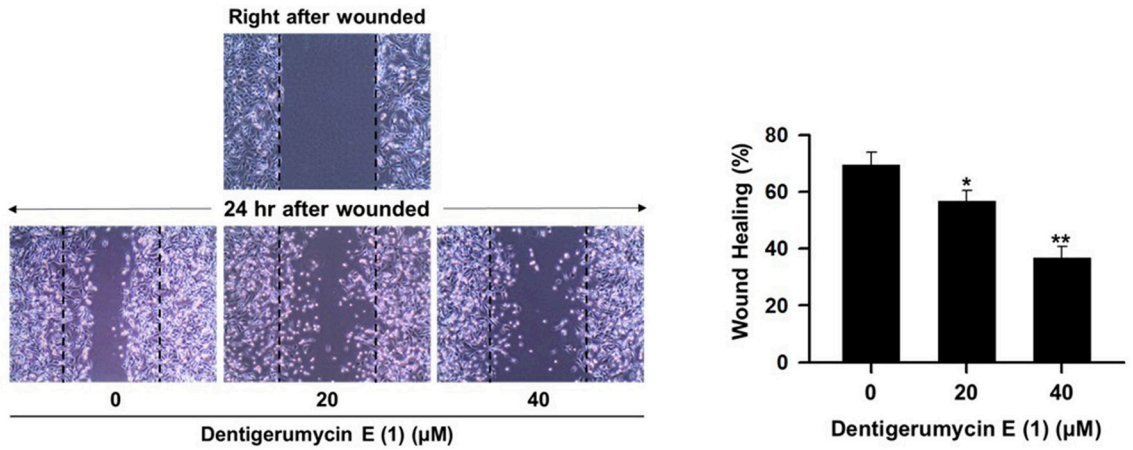

FIGURE 7 | Dentigerumycin E (**1**) suppresses cell migration of the metastatic human breast cancer cell line (MDA-MB-231) in the wound healing assay. The data are represented as the means ± SD from three independent experiments: $^{*}p < 0.05$, $^{**}p < 0.01$.

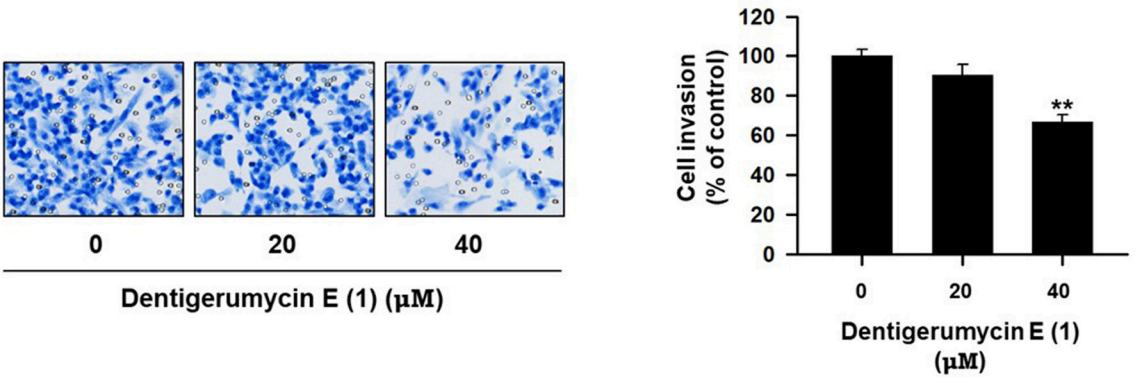

FIGURE 8 | Dentigerumycin E suppresses cell invasion of the human breast cancer cell line (MDA-MB-231) in the cell invasion assay. The data are represented as the means ± SD from three independent experiments: $^{**}p < 0.01$.

on the structure, the BGC was composed of a multimodular hybrid polyketide synthase (PKS) and a nonribosomal peptide synthetase (NRPS) (**Figure 5**). The feature of NRPS involving six modules in the four open reading frames (ORFs 6590, 6606, 6605, and 6604) showed high degree similarity to that of dentigerumycins B-D (Wyche et al., 2017). Based on the antiSMASH analysis, these modules produce a cyclic peptide with the sequence Leu-Pip-3-Gly-Pip-2-Pip-1-Thr, which is

consistent with the structure elucidated by spectroscopic analysis. Epimerase domains, which determine the absolute configurations of the amino acid residues in NRPS, were incorporated in the modules for Pip-3 and Pip-2 but not Pip-1. The 2:1 ratio of *R*- and *S*-piperazic acids determined by advanced Marfey's analysis (*vide supra*) established that the absolute configuration of the three piperazic acids is 6*S*, 11*R*, and 18*R* (*S*-Pip-1, *R*-Pip-2, and *R*-Pip-3) (**Figure 5**).

The absolute configuration of the acyl side chain was also assigned through analysis of the BGC. Within the BGC of dentigerumycin E, four type I PKS modules (ORFs 6594, 6593, 6592, and 6591) were involved in the biosynthesis of the C_{12} acyl side chain (**Figure 5**). Both module 6594 and 6591 are composed of a ketosynthase (KS), an acyltransferase (AT), and an acyl carrier protein (ACP). Because the KS of 6594 was identified as KS_Q with the active site cysteine (C) being replaced by glutamine (Q) (Kuhstoss et al., 1996), 6594 was identified as the loading module of dentigerumycin E BGC (**Figure S25**). Module 6593 involves KS, AT, dehydratase (DH), ketoreductase (KR), and ACP. In modular polyketide synthase (PKS), certain amino acid motifs in the KR domain are correlated with the stereochemistry of the hydroxyl groups in the product (Caffrey, 2003; Reid et al., 2003). KR domains lead to A-type alcohol stereochemistry (3*S* when C-2 has higher priority than C-4 and 3*R* when C-4 has higher priority than C-2) if amino acid residue 141 is tryptophan (W) and B-type alcohol stereochemistry (3*R* when C-2 has higher priority than C-4 and 3*S* when C-4 has higher priority than C-2) if an LDD motif is present in the region between 88 and 103. In addition, B-type KR domains typically contain proline (P) or/and asparagine (N) at residue 144 and 148, respectively. During the reaction with PKS, it was hypothesized that the tryptophan motif guides the polyketide into the active site of A-type KRs, while the LDD motif guides polyketides into the active site of B-type KRs (Zheng et al., 2010). The KR domain of module 6593, which determines the absolute configuration of C-34 hydroxy group, was aligned with other KR domains reported by Caffrey (2003), and the residues were compared. Based on the LDD motif, the KR domain of module 6593 was identified as B-type, indicating the product should have a 34*R* configuration (**Figure 6**). *R*-configuration is also supported by the evidence that residue 141 was not a tryptophan and the presence of asparagine at residue 148. Based on the relative configuration previously determined by ROESY correlations, the absolute configuration of the stereogenic centers in the acyl side chain should be 29*S*, 30*R*, 33*R*, and 34*R* (**Figure 2**).

On the other hand, because the hydroxy group at C-34 was preserved rather than eliminated, the DH domain in module 6593 is assumed to be nonfunctional, similar to what is seen with polyoxypeptin A (Du et al., 2014), which has a BGC that closely resembles that of the dentigerumycin class of compounds. Although this DH domain of dentigerumycin E has all three key amino acids residues of the conserved motif HxxxGxxxxP, the motif is not always universally conserved (Joshi and Smith, 1993). In addition, the two tyrosine (Y) residues in the GYxYGPxF motif were altered to phenylalanine (F) and histidine (H), respectively. Such a significant alteration in these conserved motifs could cause the domain to be nonfunctional (Keatinge-Clay, 2008), and these alterations in the GYxYGPxF motif could explain the nonfunctional DH in module 6593. (**Figure S26**).

Biological Activity of Dentigerumycin E and Its Derivatives

To explore the biological activities of dentigerumycin E (**1**) and its derivatives (**2** and **3**), cytotoxicity was evaluated against various human cancer cells. Dentigerumycin E (**1**) showed moderate cytotoxicity against the tested cancer cell lines including A549 (lung cancer), HCT116 (colorectal cancer), MDA-MB-231 (breast cancer), SK-HEP-1 (liver cancer), and SNU638 (stomach cancer) whereas 2*N*,16*N*-deoxydentigerumycin E (**2**) and dentigerumycin E methyl ester (**3**) did not inhibit the proliferation of these cancer cell lines (**Table S3**). To determine the cancer cell-specific cytotoxicity, cytotoxicity of **1**-**3** against a normal human breast epithelial cell line (MCF-10A) was also evaluated. As shown in **Table S3**, in comparison to cancer cell lines, dentigerumycin E (**1**) did not demonstrated a significant cytotoxicity against normal epithelial cells with IC_{50} value of over 50 μM. Furthermore, the antimetastatic activity of dentigerumycin E was evaluated with metastatic breast cancer cells (MDA-MB-231) by wound healing and cell invasion assays. For each assay, cells were treated with 20 μM or 40 μM dentigerumycin E for 24 h. Compared to the vehicle-treated group, dentigerumycin E inhibited cell migration in the wound healing assay by 20 and 48% at 20 and 40 μM, respectively (**Figure 7**). In the cell invasion assay, dentigerumycin E exhibited inhibitory activity by 10 and 34% at 20 and 40 μM, respectively (**Figure 8**). These results indicated the antimetastatic potential of dentigerumycin E (**1**) against breast cancer cells. However, 2*N*,16*N*-deoxydentigerumycin E (**2**) and dentigerumycin E methyl ester (**3**) displayed no significant activity in the wound healing and cell invasion assays (**Figures S27, S28**), suggesting that 2-*N*-OH, 16-*N*-OH, and 37-OH (carboxylic acid) in **1** are essential for its antiproliferative and antimetastatic activities.

CONCLUSION

A new cyclic peptide, dentigerumycin E (**1**), was discovered from a coculture of marine *Streptomyces* sp. JB5 and *Bacillus* sp. GN1 strains isolated from an intertidal mudflat. Cocultivating *Streptomyces* sp. JB5 and a *Bacillus* strain (either GN1 or HR1), most closely related *B. cereus*, was required because dentigerumycin E was virtually detectable only in cocultures of these bacterial strains, not in single cultures of these bacteria. Dentigerumycin E was determined to be a new member of the dentigerumycin nonribosomal peptide class with three piperazic acid units and an acyl chain of PKS origin (Oh et al., 2009). Dentigerumycin E (**1**) is most similar to dentigerumycin B, previously reported from the *Pseudonocardia* symbiont of a fungus-growing ant (Wyche et al., 2017), but the *N*-hydroxy threonine moiety in **1** has a different configuration from that in dentigerumycin B (L-Thr for dentigerumycin E whereas L-*allo*-Thr for dentigerumycin B). Moreover, the polyketide-derived acyl chain of **1** has a carboxylic acid group in the

branched C_2 chain, which has not been reported in the other dentigerumycin-type compounds. Our biological evaluation of the antiproliferative and antimetastatic activities revealed that the 2-*N*-OH, 16-*N*-OH, and 37-OH groups are essential for the activities of dentigerumycin E. Genomic analysis of the *Streptomyces* sp. JB5 strain allowed the identification of the putative BGC of dentigerumycin E (**1**) and thus confirmed that **1** was produced by the *Streptomyces* strain. In conjunction with chemical derivatizations, comprehensive analysis of the biosynthetic modules allowed the absolute configurations of the piperazic acid residues and PKS-derived acyl chain to be proposed. Induction of dentigerumycin E production by a couple of phylogenetically close *Bacillus* strains raised an interesting question about the mechanism activating the biosynthetic gene cluster for dentigerumycin E in *Streptomyces* sp. JB5, which might lead a more comprehensive mechanism study. The discovery of dentigerumycin E (**1**) in the marine bacterial coculture highlights that marine microorganisms are prolific chemical sources of bioactive natural products and that the coculture strategy could be a promising method for exploring hidden microbial chemical diversity.

AUTHOR CONTRIBUTIONS

DS, WB, KM, YK, MB, SU, SL, and D-CO designed the experiments. YK and MB collected intertidal mud samples. KM isolated the bacterial strains. DS performed the coculture experiments, chemical experiments, and analyzed the data. WB and SL performed the bioassay. DS, WB, KM, SU, SL, and D-CO wrote the manuscript.

ACKNOWLEDGMENTS

This work was supported by a National Research Foundation (NRF) of Korea grant funded by the Korean Government Ministry of Science and ICT (No. 2009-0083533 and 2018R1A4A1021703).

SUPPLEMENTARY MATERIAL

The Supplementary Material for this article can be found online at: https://www.frontiersin.org/articles/10.3389/fchem.2018.00498/full#supplementary-material

REFERENCES

Adnani, N., Chevrette, M. G., Adibhatla, S. N., Zhang, F., Yu, Q., Braun, D. R., et al. (2017). Coculture of marine invertebrate-associated bacteria and interdisciplinary technologies enable biosynthesis and discovery of a new antibiotic, keyicin. *ACS Chem. Biol.* 12, 3093–3102. doi: 10.1021/acschembio.7b00688

Blodgett, J. A. V., Oh, D.-C., Cao, S., Currie, C. R., Kolter, R., and Clardy, J. (2010). Common biosynthesis origins of polycyclic tetramate macrolactams from phylogenetically diverse bacteria. *Proc. Natl. Acd. Sci. U.S.A.* 107, 11692–11697. doi: 10.1073/pnas.1001513107

Caffrey, P. (2003). Conserved amino acid residues correlating with ketoreductase stereospecificity in modular polyketide synthases. *ChemBioChem* 4, 649–662. doi: 10.1002/cbic.200300581

Cueto, M., Jensen, P. R., Kauffman, C., Fenical, W., Lobkovsky, E., and Clardy, J. (2001). Pestalone, a new antibiotic produced by a marine fungus in response to bacterial challenge. *J. Nat. Prod.* 64, 1444–1446. doi: 10.1021/np0102713

Du, Y., Wang, Y., Huang, T., Tao, M., Deng, Z., and Lin, S. (2014). Identification and characterization of the biosynthetic gene cluster of polyoxypeptin A, a potent apoptosis inducer. *BMC Microbiol.* 14:30. doi: 10.1186/1471-2180-14-30

Fujii, K., Ikai, Y., Oka, H., Suzuki, M., and Harada, K. (1997). A nonempirical method using LC/MS for determination of the absolute configuration of constituent amino acids in a peptide: combination of Marfey's method with mass spectrometry and its practical application. *Anal. Chem.* 69, 5146–5151. doi: 10.1021/ac970289b

Hess, S., Gustafson, K. R., Milanowski, D. J., Alvira, E., Lipton, M. A., and Pannell, L. K. (2004). Chirality determination of unusual amino acids using precolumn derivatization and liquid chromatography-electrospray ionization mass spectrometry. *J. Chromatogr. A* 1035, 211–219. doi: 10.1016/j.chroma.2004.02.068

Hogan, D. A., and Kolter, R. (2002). *Pseudomonas-Candida* interactions: an ecological role for virulence factors. *Science* 296, 2229–2232. doi: 10.1126/science.1070784

Hoshino, S., Wakimoto, T., Onaka, H., and Abe, I. (2015). Chojalactones A–C, cytotoxic butanolides isolated from *Streptomyces* sp. cultivated with mycolic acid containing bacterium. *Org. Lett.* 17, 1501–1504. doi: 10.1021/acs.orglett.5b00385

Joshi, A. K., and Smith, S. (1993). Construction, expression, and characterization of a mutated animal fatty acid synthase deficient in the dehydrase function. *J. Biol. Chem.* 268, 22508–22513.

Keatinge-Clay, A. T. (2008). Crystal structure of the erythromycin polyketide synthase dehydratase. *J. Mol. Biol.* 384, 941–953. doi: 10.1016/j.jmb.2008.09.084

Kim, W. K., Byun, W. S., Chung, H.-J., Oh, J., Park, H. J., Choi, J. S., et al. (2018). Esculetin suppresses tumor growth and metastasis by targeting Axin2/E-cadherin axis in colorectal cancer. *Biochem. Pharmacol.* 152, 71–83. doi: 10.1016/j.bcp.2018.03.009

Kuhstoss, S., Huber, M., Turner, J. R., Paschal, J. W., and Rao, R. N. (1996). Production of a novel polyketide through the construction of a hybrid polyketide synthase. *Gene* 183, 231–236. doi: 10.1016/S0378-1119(96)00565-3

Matsumori, N., Kaneno, D., Murata, M., Nakamura, H., and Tachibana, K. (1999). Stereochemical determination of acyclic structures based on carbon-proton spin-coupling constants. A method of configuration analysis for natural products. *J. Org. Chem.* 64, 866–876. doi: 10.1021/jo981810k

Medema, M. H., Blin, K., Cimermancic, P., de Jager, V., Zakrzewski, P., Fischbach, M. A., et al. (2011). antiSMASH: rapid identification, annotation and analysis of secondary metabolite biosynthesis gene clusters in bacterial and fungal genome sequences. *Nucleic Acids Res.* 39, W339–W346. doi: 10.1093/nar/gkr466

Oh, D.-C., Jensen, P. R., Kauffman, C. A., and Fenical, W. (2005). Libertellenones A–D: induction of cytotoxic diterpenoid biosynthesis by marine microbial competition. *Bioorg. Med. Chem.* 13, 5267–5273. doi: 10.1016/j.bmc.2005.05.068

Oh, D.-C., Poulsen, M., Currie, C. R., and Clardy, J. (2009). Dentigerumycin: a bacterial mediator of an ant-fungus symbiosis. *Nat. Chem. Biol.* 5, 391–393. doi: 10.1038/nchembio.159

Omura, S., Ikeda, H., Ishikawa, J., Hanamoto, A., Takahashi, C., Shinose, Y., et al. (2001). Genome sequence of an industrial microorganism *Streptomyces avermitilis*: deducing the ability of producing secondary metabolites. *Proc. Natl. Acad. Sci. U.S.A.* 98, 12215–12220. doi: 10.1073/pnas.211433198

Park, H. B., Kwon, H. C., Lee, C. H., and Yang, H. O. (2009). Glionitrin A an antibiotic-antitumor metabolite derived from competitive interaction between abandoned mine microbes. *J. Nat. Prod.* 72, 248–252. doi: 10.1021/np800606e

Pennings, M. L. M., Reinhoudt, D. N., Harkema, S., and van Hummel, G. J. (1983). Chemistry of four-membered cyclic nitrones. 4. Reaction with electrophilic reagents and conversion into β-lactam derivatives. *J. Org. Chem.* 48, 486–491. doi: 10.1021/jo00152a015

Reid, R., Piagentini, M., Rodriguez, E., Ashley, G., Viswanathan, N., Carney, J., et al. (2003). A model of structure and catalysis for ketoreductase domains in modular polyketide synthases. *Biochemistry* 42, 72–79. doi: 10.1021/bi0268706

Straight, P. D., Willey, J. M., and Kolter, R. (2006). Interactions between *Streptomyces coelicolor* and *Bacillus subtilis*: role of surfactants in raising aerial structures. *J. Bacteriol.* 188, 4918–4925. doi: 10.1128/JB.00162-06

Ueda, K., and Beppu, T. (2017). Antibiotics in microbial coculture. *J. Antibiot*. 70, 361–365. doi: 10.1038/ja.2016.127

Weber, T., Blin, K., Duddela, S., Krug, D., Kim, H. U., Bruccoleri, R., et al. (2015). antiSMASH 3.0-a comprehensive resource for the genome mining of biosynthetic gene clusters. *Nucleic Acids Res.* 43, W237–W243. doi: 10.1093/nar/gkv437

Wyche, T. P., Ruzzini, A. C., Beemelmanns, C., Kim, K. H., Klassen, J. L., Cao, S., et al. (2017). Linear peptides are the major products of a biosynthetic pathway that encodes for cyclic depsipeptides. *Org. Lett.* 19, 1772–1775. doi: 10.1021/acs.orglett.7b00545

Zheng, J., Taylor, C. A., Piasecki, S. K., and Keatinge-Clay, A. T. (2010). Structural and functional analysis of A-type ketoreductase from amphotericin modular polyketide synthase. *Structure* 18, 913–922. doi: 10.1016/j.str.2010.04.015

Conflict of Interest Statement: The authors declare that the research was conducted in the absence of any commercial or financial relationships that could be construed as a potential conflict of interest.

frontiers in Chemistry

ORIGINAL RESEARCH
published: 30 October 2018
doi: 10.3389/fchem.2018.00528

Marine Bacterial Aromatic Polyketides From Host-Dependent Heterologous Expression and Fungal Mode of Cyclization

Chunshuai Huang[1,2], *Chunfang Yang*[1], *Yiguang Zhu*[1]*, *Wenjun Zhang*[1], *Chengshan Yuan*[1] *and Changsheng Zhang*[1,2]*

[1] CAS Key Laboratory of Tropical Marine Bio-resources and Ecology, Guangdong Key Laboratory of Marine Materia Medica, South China Sea Institute of Oceanology, RNAM Center for Marine Microbiology, Chinese Academy of Sciences, Guangzhou, China, [2] University of Chinese Academy of Sciences, Beijing, China

The structure diversity of type II polyketide synthases-derived bacterial aromatic polyketides is often enhanced by enzyme controlled or spontaneous cyclizations. Here we report the discovery of bacterial aromatic polyketides generated from 5 different cyclization modes and pathway crosstalk between the host and the heterologous fluostatin biosynthetic gene cluster derived from a marine bacterium. The discovery of new compound SEK43F (**2**) represents an unusual carbon skeleton resulting from a pathway crosstalk, in which a pyrrole-like moiety derived from the host *Streptomyces albus* J1074 is fused to an aromatic polyketide SEK43 generated from the heterologous fluostatin type II PKSs. The occurrence of a new congener, fluoquinone (**3**), highlights a bacterial aromatic polyketide that is exceptionally derived from a characteristic fungal F-mode first-ring cyclization. This study expands our knowledge on the power of bacterial type II PKSs in diversifying aromatic polyketides.

Keywords: heterologous expression, aromatic polyketides, type II polyketide synthase, cyclization modes, pathway crosstalk

OPEN ACCESS

Edited by:
Xian-Wen Yang,
Third Institute of Oceanography, State Oceanic Administration, China

Reviewed by:
Shuangjun Lin,
Shanghai Jiao Tong University, China
Steven Gary Van Lanen,
University of Kentucky, United States

***Correspondence:**
Yiguang Zhu
ygzhu@scsio.ac.cn
Changsheng Zhang
czhang2006@gmail.com

Specialty section:
This article was submitted to Medicinal and Pharmaceutical Chemistry, a section of the journal Frontiers in Chemistry

Received: *04 September 2018*
Accepted: *11 October 2018*
Published: *30 October 2018*

Citation:
Huang C, Yang C, Zhu Y, Zhang W, Yuan C and Zhang C (2018) Marine Bacterial Aromatic Polyketides From Host-Dependent Heterologous Expression and Fungal Mode of Cyclization. Front. Chem. 6:528. doi: 10.3389/fchem.2018.00528

INTRODUCTION

Aromatic polyketides (APKs) comprise a rich class of natural products with diverse structures and exhibit antimicrobial, antitumor, antiparasitic, antiviral, and other activities (Shen, 2000; Hertweck et al., 2007; Das and Khosla, 2009; Zhou et al., 2010; Zhang Z. et al., 2017). Most bacterial APKs are synthesized by type II polyketide synthases (PKSs). The "minimal" type II PKSs consist of a set of iteratively used enzymes including two ketosynthase units (KS_α and KS_β) and an acyl-carrier protein (ACP) (Shen, 2000; Hertweck et al., 2007; Das and Khosla, 2009; Zhou et al., 2010; Zhang Z. et al., 2017). The KS_α unit catalyzes iterative decarboxylative condensations of ACP-tethered malonyl to generate a linear poly-β-ketone chain, the length of which is controlled by the KS_β unit (also known as chain-length factor, CLF). The poly-β-ketone chains are converted into diverse APKs by enzymatic tailoring modifications such as cyclization, oxidation, glycosylation, and methylation. In many cases, shunt products are also produced from the reactive poly-β-ketone chains by spontaneous and aberrant cyclization to further enhance the structural diversity of APKs (Shen, 2000; Hertweck et al., 2007; Das and Khosla, 2009; Zhou et al., 2010; Zhang Z. et al., 2017).

Fluostatins (FSTs) are a growing family of atypical angucycline-type APKs and display antibacterial, antitumor and peptidase inhibition activities (Akiyama et al., 1998a,b; Baur et al., 2006; Feng et al., 2010; Zhang et al., 2012; Yang et al., 2015; Jiang et al., 2017; Zhang W. et al., 2017; Huang et al., 2018; Jin et al., 2018). Recently, heterologous expression of the type II PKS gene cluster (*fls*) of FSTs from South China Sea-derived *Micromonospora rosaria* SCSIO N160 in *Streptomyces coelicolor* YF11 (Zhou et al., 2012) enabled the production of new FST derivatives (Yang et al., 2015). Intriguingly, introduction of the *fls*-gene cluster in *Streptomyces albus* J1074 led to production of diverse C–C and C–N coupled dimeric FSTs (Huang et al., 2018). Herein we report the discovery of APKs derived from different chain lengths and cyclization patterns in the heterologous host *S. albus* J1074.

MATERIALS AND METHODS

General Experimental Procedures

Optical rotation was determined on a 341 polarimeter (Perkin Elmer, Inc.). UV spectrum was recorded with a U-2900 spectrophotometer (Hitachi). IR spectrum was obtained using a Nicolet*6700 FT-IR spectrometer (Thermo Scientific). ^{1}H, ^{13}C, and 2D NMR spectra were recorded on Bruker 700 spectrometer with tetramethylsilane (TMS) as the internal standard. Low-resolution mass spectrometric data were determined using an amaZon SL ion trap mass spectrometer. High-resolution electrospray ionization mass spectrometric (HRESIMS) data were measured on a MaXis 4G UHR-TOFMS spectrometer (Bruker Daltonics Inc.). Column chromatography (CC) was performed with silica gel (100–200 mesh, Jiangyou Silica Gel Development, Inc., Yantai, P. R. China). Thin layer chromatography (TLC, 0.1–0.2 or 0.3–0.4 mm) was conducted with precoated silica gel GF254 (10–40 nm, Yantai) glass plates. Preparative TLC (pTLC) was conducted with precoated glass plates (silica gel GF254, 10–40 nm). Sephadex LH-20 (40–70 μm; Amersham Pharmacia Biotech AB, Uppsala, Sweden), and YMC*gel ODS-A (12 nm S-50 μm; Japan). MCI gel CHP-20P (75–150 μm, Mitsubishi Chemical Corp., Tokyo, Japan). Medium pressure liquid chromatography (MPLC) was performed on automatic flash chromatography (Cheetahtmmp 200, Bonna-Agela Technologies Co., Ltd.) with the monitoring wavelength at 220 nm and the collecting wavelength at 254 nm. Semi-preparative HPLC was carried out on a Hitachi-L2130 HPLC (equipped with a Hitachi L-2455 diode array detector) using a Phenomenex Luna C18 column (250 × 10 mm, 5 μm). Analytical HPLC was performed on an Agilent 1260 Infinity series instrument (equipped with a quaternary pump, a vacuum degasser, an autosampler, a thermostatic column compartment, and a DAD detector) using an Agilent ZORBAX SB-C18 column (150 × 4.6 mm, 5 μm) under the following program: solvent system (solvent A, 10% acetonitrile in water supplementing with 0.08% formic acid; solvent B, 90% acetonitrile in water); 5% B to 80% B (linear gradient, 0–20 min), 80% B to 100% B (20–21 min),100% B (isocratic elution, 21–24 min), 100% B to 5% B (24–25 min), 5% B (isocratic elution, 25–30 min) with the monitoring wavelength at 400 nm. Small scale production process was performed in a compact sterilizable-in-place fermentation system BioFlo 510 fermentator (Eppendorf AG, German).

Bacterial Material

The recombinant strain *S. albus* J1074/pCSG5033 has been previously described (Huang et al., 2018).

Fermentation, Extraction, and Isolation

The recombinant strain *S. albus* J1074/pCSG5033 was cultured in the seed medium (3% tryptic soya broth, pH 7.0) and carried on a rotary shaker (200 rpm) at 28°C for 1–3 days. A 20 L scale fermentation was performed by inoculating 1.5 L of the seed culture into a 40 L fermentator (stirring rate:120–230 rpm; dissolved oxygen: 30%; ventilation volume: 15–20 L min^{-1}; pH: 7.2–7.4; pressure: 3 psi; fermentation temperature: 28°C) containing 20 L of the production medium (0.1% peptone fish, 1% starch soluble, 0.6% corn powder, 0.2% bacterial peptone, 0.5% glycerol, 0.2% $CaCO_3$, 3% sea salt), and cultured at 28°C for 3–5 days. A total of 20 L fermentation cultures were harvested and centrifuged to supernatants and mycelium. The supernatants and mycelium were extracted 3 times with equal volume of butanone and acetone, respectively. And then both were evaporated to dryness under reduced pressure and combined to obtain the crude extract (10.0 g).

The crude extract was subjected to normal phase silica gel (100–200 mesh) column chromatography eluted with a gradient solvent system of chloroform/methanol (from 100:0 to 0:100, v/v) to give four fractions (Fr.1–Fr.4) on the basis of initial assessment by thin-layer chromatography (TLC). Fr.1 was subjected to Sephadex LH-20 column chromatography, eluting with $CHCl_3$/MeOH (1:1) to afford four subfractions (Fr.1.L1–Fr.1.L4). Subfraction Fr.1.L3 was further purified using C18 reversed phase MPLC [40 × 2.5 cm ID, eluting with a linear gradient of H_2O/CH_3CN (100:0 → 0:100, 15 mL min^{-1}, 200 min)], Sephadex LH-20 column chromatography, and reversed-phase semi-preparative HPLC (H_2O/CH_3CN) successively, to yield **3** (7.0 mg), **4** (1.4 mg), **5** (9.6 mg), and **6** (7.0 mg). Subfraction Fr.2 was further separated with MCI gel column (CH_3CN/H_2O, from 0:100 to 100:0) to give five fractions Fr.2.M1-Fr.2.M5. SEK43F (**2**, 4.0 mg) was obtained from Fr.2.M3 by Sephadex LH-20 column chromatography and pTLC (petroleum ether/acetone 50:50), successively. FST C (**1**, 56.0 mg) was obtained from subfraction Fr.4.

SEK43F (2)

Yellow-green powder; UV (MeOH) λ_{max} (log ε) 452 (4.21), 296 (3.65), 257 (3.37), 205 (4.07) nm; IR ν_{max} 3,273, 1,593, 1,435, 1,287 cm^{-1}; ^{1}H and ^{13}C NMR spectroscopic data, **Table 1**; HRESIMS *m/z* 486.1557 [M - H]$^{-}$ (calcd for $C_{28}H_{24}NO_7$, 486.1558).

Fluoquinone (3)

Yellow powder; [α] + 1.6 (*c* 0.22, $CHCl_3$); UV (MeOH) λ_{max} (log ε) 414 (2.49), 275 (3.02), 253 (3.00), 227 (3.19), 203 (3.30) nm;

IR ν_{max} 2,922, 1,686, 802 cm^{-1}; ^1H and ^{13}C NMR spectroscopic data, **Table 1**; HRESIMS *m/z* 365.0672 [M - H]$^-$ (calcd for $C_{20}H_{13}O_7$, 365.0667).

Biological Assays

Antimicrobial activities were measured against seven indicator strains, *Staphylococcus aureus* ATCC 29213, *Enterococcus faecalis* ATCC 29212, *Escherichia coli* ATCC 25922, *Acinetobacter baumannii* ATCC 19606, *Bacillus subtilis* SCSIO BS01, *Micrococcus luteus* SCSIO ML01, and methicillin resistant *S. aureus* ATCC 43300, by previously described broth microdilution method (Yang et al., 2015). MCF7 (human breast adenocarcinoma cell line), NCI-H460 (human non-small cell lung cancer cell line), HepG2 (Human hepatocellular liver carcinoma cell line), and SF268 (human glioma cell line) were kindly used for cytotoxic activities assay *in vitro* according to the previously established protocols (Mosmann, 1983).

TABLE 1 | ^1H (700 MHz) and ^{13}C NMR (176 MHz) data for **2** and **3** in DMSO-d_6 (δ in ppm).

2			3		
Position	**δ_C, type**	**δ_H, mult. (*J* in Hz)**	**Position**	**δ_C, type**	**δ_H, mult. (*J* in Hz)**
1	165.5, C		1	166.8, C	
2	104.8, C		3	74.0, CH	5.02, m
3	180.8, C		4	31.8, CH_2	4.12, dd (2.9, 18.1)
4	109.0, CH	5.59, s			3.31, dd (11.8, 18.2)
5	164.5, C				
6	36.9, CH_2	3.58, s			
7	132.7, C		4a	146.8, C	
8	121.6, CH	6.83, d (8.2)	5	114.6†, CH	7.61, s
9	130.6, CH	7.24, dd (8.2, 8.8)	5a	139.3, C	
10	115.2, CH	6.82, d (8.8)	6	181.9, C	
11	154.3, C		6a	132.8, C	
12	131.3, C		7	118.9, CH	7.70, d (7.3)
13	200.3, C		8	136.6, CH	7.79, dd (7.3, 8.3)
14	116.1, C		9	124.9, CH	7.40, d (8.3)
15	165.6, C		10	161.7, C	
16	101.2, CH	6.11, d (2.3)	10a	117.2, C	
17	163.7, C		11	188.6, C	
18	112.1, CH	6.07, d (2.3)	11a	114.9, C	
19	143.5, C		12	165.0†, C	
20	22.0, CH_3	1.86, s	12a	121.0†, C	
1'	134.9, CH	7.84, s	13	47.4, CH_2	3.09, dd (5.0, 17.4)
2'	130.9, C				3.13, dd (7.4, 17.4)
3'	140.6, C				
4'	126.3, C				
5'	149.6, C		14	205.4, C	
7'	10.3, CH_3	2.23, s	15	30.4, CH_3	2.20, s
8'	9.4, CH_3	2.00, s	10-OH		12.60, s
9'	13.5, CH_3	2.42, s			
11-OH		9.84, s			
15-OH		12.69, s			
17-OH		10.40, brs			
NH-6'		14.65, s			

†*Chemical shift observed in HSQC or HMBC spectra.*

RESULTS AND DISCUSSION

Isolation and Structure Elucidation

Upon a large scale fermentation of *S. albus* J1074/pCSG5033 (containing the intact *fls* gene cluster (Yang et al., 2015; **Supplementary Figure 1**) in a 40-L fermentator and the subsequent isolation with various chromatographic methods, FST C (**1**) was obtained as the major product, along with several new dimeric FSTs derived from non-enzymatic reactions (Huang et al., 2018). In addition, two new decaketide derivatives SEK43F (**2**) and fluoquinone (**3**), two known non-aketide-derived anthraquinones 2-acetylchrysophanol (**4**) (Abdelfattah, 2009) and 4-acetylchrysophanol (**5**) (Shaaban et al., 2007), and a previously synthesized compound 3,3′,4,4′,5,5′-hexamethyl-2,2′-dipyrrolylmethene (**6**) (**Figure 1**), were also isolated (Guseva et al., 2008; Lund and Thompson, 2014).

SEK43F (**2**) was isolated as a yellow-green solid. The molecular formula of **2** was established to be $C_{28}H_{25}NO_7$ (*m/z* 486.1557 [M - H]$^-$, calcd for 486.1558) by high-resolution electrospray ionization mass spectroscopy (HRESIMS), suggesting 17 degrees of unsaturation. The NMR data of **2** (**Table 1**, **Supplementary Figure 2**) revealed the presence of four methyls, one methylene, seven sp^2 methines, and 16 sp^2 quaternary carbons. HMBC correlations from H_3-7′ to C2′/C3′/C4′, H_3-8′ to C3′/C4′/C5′, H_3-9′ to C4′/C5′, and NH-6′ to C3′/C4′/C5′ revealed the presence of a 1,2,3,4-tetrasubstituted pyrrole moiety (unit A, **Figure 2**). The remaining NMR data of **2** (unit B, **Figure 2**) were highly similar to those for SEK43 (Meurer et al., 1997), including a characteristic 1,2,3-trisubstituted phenyl fragment (δ_H 6.82, 1H, d, $J = 8.8$ Hz; 7.24, 1H, dd, $J = 8.2$, 8.8 Hz; δ_H 6.83, 1H, d, $J = 8.2$ Hz; **Table 1**) and *meta* couplings spin system of H16 (δ_H 6.11, 1H, d, $J = 2.3$ Hz) and H18 (δ_H 6.07, 1H, d, $J = 2.3$ Hz) (**Figure 2**, **Table 1**). In addition, presence of the β-oxo-δ-lactone moiety was supported by HMBC correlations from H4 (δ_H 5.59) to C2/C3/C5, and from H1′ (δ_H 7.84) to C1/C2/C3 (**Figure 2**, **Supplementary Figure 2**). Finally, the two units A and B were linked by C2–C1′, which was supported by HMBC correlations (**Figure 2**, **Supplementary Figure 2**) from H1′ (δ_H 7.84) to C3′ and C1/C2/C3. However, the *Z*/*E* configuration of $\Delta^{2,1'}$ in **2** couldn't be determined solely by NMR data. Similar phenomena were observed for hybrubins (Zhao et al., 2016).

The molecular formula of fluoquinone (**3**) was determined to be $C_{20}H_{14}O_7$ (*m/z* 365.0672 [M - H]$^-$, calcd for 365.0667) by HRESIMS, requiring 14 degrees of unsaturation. The ^1H, ^{13}C, and HSQC NMR data for **3** displayed a singlet methyl, two sp^3 methylenes, one sp^3 methine, four sp^2 methines, and 12 sp^2

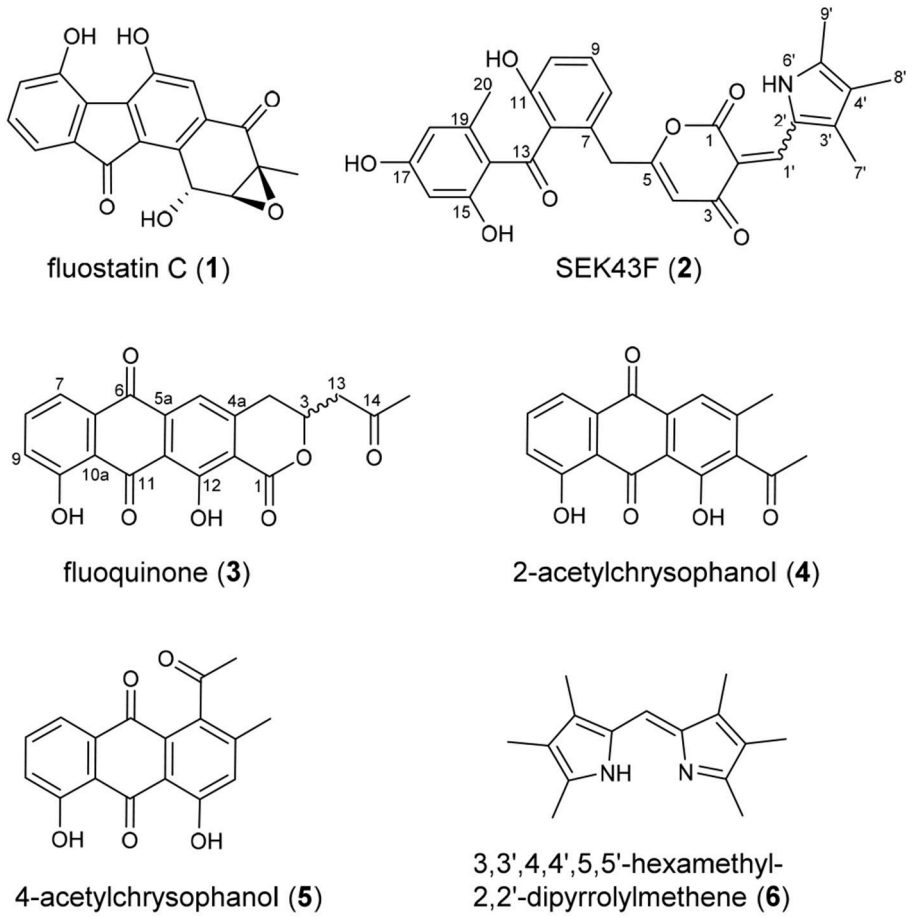

FIGURE 1 | Chemical structures of compounds **1**–**6**.

quaternary carbons (**Table 1**, **Supplementary Figure 3**). The ^{1}H-^{1}H COSY spectrum of **3** (**Figure 2**, **Supplementary Figure 3**, **Table 1**) showed a characteristic aromatic ABC spin system (δ_H 7.70/7.79/7.40) and a CH_2-CH(O)-CH_2 fragment (δ_H 3.31/4.12/5.02 and 3.09/3.13/5.02). HMBC correlations (**Figure 2**, **Supplementary Figure 3**) from H5/H7 to C6, from H8 to C10, together with four-bond HMBC correlations (**Figure 2**, **Supplementary Figure 3**) from H5/H7/H9 to C11, and from H5 to C12 supported the presence of a 1,8-dihydroxyanthraquinone moiety, highly similar to that of the fungal metabolite dermolactone (Gill and Gimenez, 1990; Cotterill et al., 1995). Comparison of NMR data revealed that **3** was different from dermolactone by the absence of a methoxy group at C8 (COSY correlations between H7/H8/H9 in **3**) and the presence of an additional acetyl group at C13 (HMBC correlations from H_3-15 to C14/C13 in **3**). Thus, the planar structure of **3** was determined as shown in **Figure 1**. The optical rotation value of **3** ([α]25 D + 1.6, $CHCl_3$; *c* 0.22) was quite different from that of the synthesized (*S*)-(+)-dermolactone ([α]22 D + 169.3, *c* 0.21) (Cotterill et al., 1995), but comparable to that of the naturally isolated dermolactone ([α]22 D + 22.0, $CHCl_3$; *c* 0.07) (Gill and Gimenez, 1990). Natural dermolactone had been confirmed as a mixture of the (*S*)-(+)- and (*R*)-(-)-enantiomers (Cotterill et al., 1995). It was thus deduced that fluoquinone (**3**) should also contain a pair of racemic (*S*)-(+)- and (*R*)-(-)-enantiomers (almost in a ration of 1:1) due to its negligible optical rotation. Analysis of the ^{1}H NMR and ^{13}C NMR data of compounds **4**–**6** revealed that they were identical to 2-acetylchrysophanol (**4**) (**Supplementary Figure 4**, **Supplementary Table 1**) (Abdelfattah, 2009), 4-acetylchrysophanol (**5**) (**Supplementary Figure 5**, **Supplementary Table 1**) (Shaaban et al., 2007), and 3,3′,4,4′,5,5′-hexamethyl-2,2′-dipyrrolylmethene (**6**) (**Supplementary Figure 6**, **Supplementary Table 1**) (Guseva et al., 2008; Lund and Thompson, 2014).

The Biological Evaluation

Compounds **1**–**6** exhibited negligible antibacterial activity against seven indicator strains: *S. aureus* ATCC 29213, *E. faecalis* ATCC 29212, *E. coli* ATCC 25922, *A. baumannii* ATCC 19606, *B. subtilis* SCSIO BS01, *Micrococcus Luteus* SCSIO ML01, and methicillin resistant *S. aureus* ATCC 43300. Compound **2** showed weak cytotoxic activities against four human cancer cell lines (SF-268,

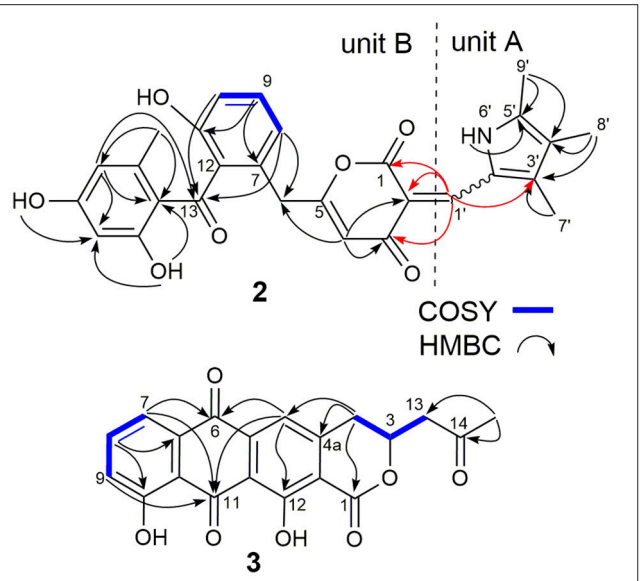

FIGURE 2 | Selected key COSY and HMBC correlations of SEK43F (**2**) and fluoquinone (**3**). Key HMBC correlations connecting units A and B of **2** are in red.

TABLE 2 | Cytotoxic activities of SEK43F (**2**).

	IC_{50} (μM)			
	SF-268	**MCF-7**	**NCI-H460**	**HepG-2**
2	56.46 ± 0.87	35.73 ± 1.45	44.62 ± 2.49	39.22 ± 3.00
Cisplatin	2.37 ± 0.17	2.94 ± 0.05	2.33 ± 0.17	1.39 ± 0.18

MCF-7, NCI-H460, and HepG-2) with IC_{50} values at the range of 36–57 μM (**Table 2**).

Plausible Biosynthetic Pathway

The heterologous expression of the intact *fls*-gene cluster from *M. rosaria* SCSIO N160 in *S. albus* J1074 afforded a set of APKs **1**–**5**. These aromatic compounds should be derived from the *fls* gene cluster-encoded enzymes because that the host *S. albus* J1074 is known for the absence of type II PKS gene clusters (Olano et al., 2014). Previously, a biosynthetic pathway of fluostatins has been proposed (Yang et al., 2015). Briefly, the type II PKS enzymes FlsA (the KS_α unit), FlsB (the KS_β unit) and FlsC (the dissociated ACP) assemble one unit of acetyl-CoA and 9 units of malonyl-CoA to generate a linear decaketide, which undergoes the FlsE-catalyzed C9 ketoreduction to give **M1** (**Figure 3A**). Subsequently, the aromatic cyclase FlsD catalyzes the "norm" C7/C12 first-ring cyclization to convert **M1** to **M2**. The downstream enzymes FlsI (a second cyclase analogous to JadI in jadomycin biosynthesis; Kulowski et al., 1999) and FlsO3 (oxygenases) converted **M2** to prejadomycin (**cyclization pattern I**: C7/C12, C5/C14, C4/C17, C2/C19), an established precursor to undergo oxidative modifications to produce diverse FST derivatives (e.g., **1**, **Figure 3A**) (Huang et al., 2018). Alternatively, **M2** could undergo spontaneous cyclization (**pattern II**: C7/C12, C14/C19, C1-OH/C5) to produce SEK43 (a shunt product often encountered in bacterial type II PKS pathways) (McDaniel et al., 1995; Hertweck et al., 2007), which is a key precursor leading to SEK43F (**2**). The tri-methylated pyrrole unit in **2**, which is also present in **6**, should be biosynthesized by the host strain, because that the production of **6** was also observed in *S. albus* J1074 harboring the void vector pSET152 (**Supplementary Figure 1**). We propose that **6** is produced by the coupling of two putative subunits **6a** and **6b** (**Figure 3B**), through a condensation reaction similar to RedH catalysis in the biosynthesis of undecylprodigiosin and hybrubins (Williamson et al., 2005; Zhao et al., 2016). The formation of **2** should be produced from a "pathway crosstalk" event via a condensation reaction by connecting C2 of SEK43 (generated by the heterologous *fls* type II PKS) and the aldehyde group of **6b** (produced by the host), either spontaneously or catalyzed by a host-derived RedH-like enzyme (**Figures 3A,B**) (Zhao et al., 2016).

It is intriguing to discover the anthraquinone derivative **3** in a bacterium. It was speculated that fundamentally different cyclization strategies were employed by bacterial and fungal type II PKSs to biosynthesize structurally similar APKs with fused-rings (Thomas, 2001, 2016). The first-ring cyclization modes were classified into F-mode for fungi to contain two intact acetate units, and S-mode for bacteria to contain three intact acetate units in the first cyclized phenol ring (**Supplementary Figure 7**) (Thomas, 2001, 2016; Zhou et al., 2010). This fundamental difference was reinforced by the discovery of three divergent first-ring cyclization strategies to converge in generating the same metabolite chrysophanol, namely F-mode (C6/C11) in fungi and plants (Bringmann et al., 2006), and S-mode (C5/C10) or S′-mode (C7/C12) in bacteria (Bringmann et al., 2006, 2009). Several bacterial fused-ring APKs were found as exceptions to be putatively derived from fungal F-mode cyclizations, such as TW93f and Tw93g (Shen et al., 1999), piloquinone (Polonsky and Lederer, 1963), murayaquinone (Gould et al., 1997), and haloquinone (Krone et al., 1981). However, it was recently discussed that evidence should be provided for these exceptions to either validate the structures (TW93f and Tw93g), or confirm the folding pattern by detailed labeling studies (Thomas, 2016). In contrast, the presence of the six-membered lactone ring in fluoquinone (**3**) strongly suggested that **3** should be derived from the first-ring cyclization via C6/C11 (**cyclization pattern III**: C6/C11, C4/C13, C2/C15, C17-OH/C1, **Figure 3C**). The fungal natural product dermolactone, highly similar to **3**, was confirmed to be derived from the F-mode of first ring cyclization (**Figure 3D**) (Gill and Gimenez, 1990). Thus, fluoquinone (**3**) represents an exception as a bacterial F-mode (fungal mode) to the F and S biosynthetic classifications of fused ring APKs (Thomas, 2001, 2016).

Compounds **4** and **5** were proposed to be derived from a common non-aketide, which was putatively assembled by FlsABC from one unit of acetyl-CoA and eight units of malonyl-CoA (**Figures 3E,F**). The discovery of **4** and **5** indicated that the CLF enzyme FlsB should exhibit a loose control in the chain length, allowing the formation of both decaketides (**Figures 3A,C**) and non-aketides (**Figure 3E**). The promiscuous

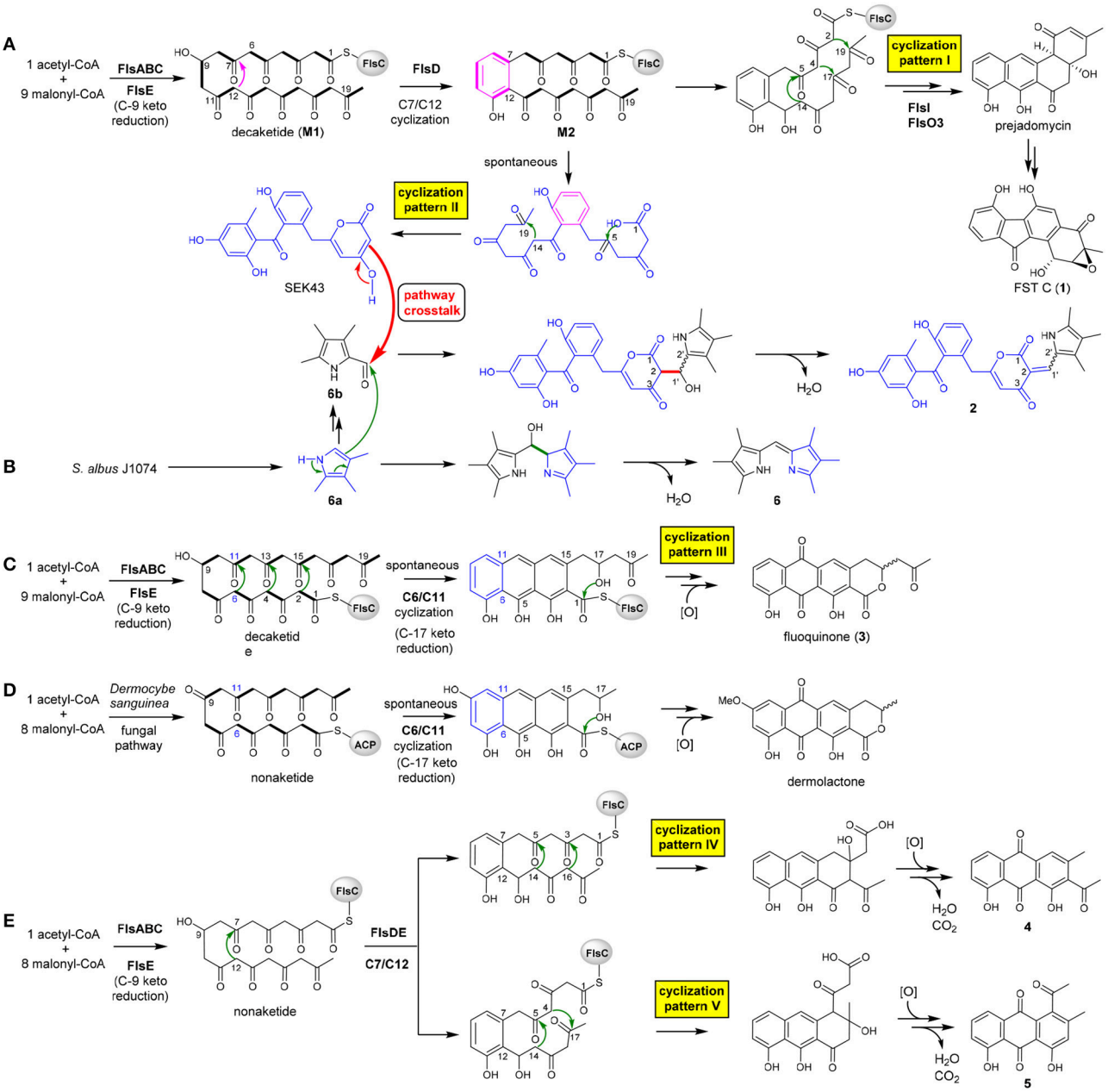

FIGURE 3 | Proposed biosynthesis scheme leading to diversified APKs by taking 5 different cyclization strategies **(A–E)** and a pathway crosstalk between the host *S. albus* and the heterologous *fls* gene cluster **(A,B)**.

chain length control has been reported for native type II PKS enzymes (McDaniel et al., 1993; Meurer et al., 1997; Shen et al., 1999), or can be altered by enzyme engineering (Burson and Khosla, 2000; Tang et al., 2003). Subsequently, the non-aketide was divergent in the third ring cyclization to provide two products **4** (**cyclization pattern IV**: C7/C12, C5/C14, C3/C16) and **5** (**cyclization pattern V**: C7/C12, C5/C14, C4/C17).

Although there are different cyclization patterns involved in the formation of **1**–**5**, the cyclization mechanisms are quite common and well-known in type II PKS biosynthesis: (i) enzyme-catalyzed or spontaneous cyclization via aldol condensation (Shen et al., 1999; Zhou et al., 2010), e.g., C7/C12, C6/C11, C5/C14, C4/C17, C4/C13, C3/C16, C2/C15, C2/C19, and C14/C19 (**Figure 3**); (ii) spontaneous cyclization via lactonization (Meurer et al., 1997), e.g., C1-OH/C5, C17-OH/C1 (**Figure 3**).

CONCLUSION

This study expands our knowledge on the power of type II PKSs in diversifying APKs with the occurrence of five

different cyclization patterns by a single set of type II PKSs. SEK43F (**2**) represents an unusual carbon skeleton resulting from a pathway crosstalk, in which a pyrrole-like moiety derived from the host *S. albus* J1074 is fused to an APK SEK43 generated from the heterologous *fls* type II PKSs. The occurrence of **3** highlights a bacterial APK that is exceptionally derived from a fungal F-mode first-ring cyclization.

AUTHOR CONTRIBUTIONS

CZ and YZ designed the study protocol and directed the research. CH, WZ, and CheY performed compound isolation and structure determination. CH carried out the biological assays. ChuY conducted the *in vivo* genetic studies. CH, YZ, and CZ analyzed the data and wrote the manuscript.

FUNDING

This work is supported in part by the National Natural Science Foundation of China (31820103003, 41676165, 31700042), Guangdong Province (GDME-2018C005, 2015A030308013), the Chinese Academy of Sciences (QYZDJ-SSW-DQC004).

ACKNOWLEDGMENTS

We are grateful to Y. Gao, Z. Xiao, A. Sun, C. Li, and Y. Zhang in the analytical facilities of SCSIO.

SUPPLEMENTARY MATERIAL

The Supplementary Material for this article can be found online at: https://www.frontiersin.org/articles/10.3389/fchem.2018.00528/full#supplementary-material

REFERENCES

Abdelfattah, M. S. (2009). Mansoquinone: isolation and structure elucidation of new antibacterial aromatic polyketides from terrestrial *Streptomyces* Sp. Eg5. *Nat. Prod. Res.* 23, 212–218. doi: 10.1080/14786410801961550

Akiyama, T., Harada, S., Kojima, F., Takahashi, Y., Imada, C., Okami, Y., et al. (1998a). Fluostatins, A., and B, new inhibitors of dipeptidyl peptidase III, produced by *Streptomyces* sp. TA-3391-I. Taxonomy of producing strain, production, isolation, physico-chemical properties and biological properties. *J. Antibiot.* 51, 553–559.

Akiyama, T., Nakamura, K. T., Takahashi, Y., Naganawa, H., Muraoka, Y., Aoyagi, T., et al. (1998b). Fluostatins, A., and B, new inhibitors of dipeptidyl peptidase III, produced by *Streptomyces* sp. TA-3391-II. Structure determination. *J. Antibiot.* 51, 586–588.

Baur, S., Niehaus, J., Karagouni, A. D., Katsifas, E. A., Chalkou, K., Meintanis, C., et al. (2006). Fluostatins C∼E, novel members of the fluostatin family produced by *Streptomyces* strain Acta 1383. *J. Antibiot.* 59, 293–297. doi: 10.1038/ja.2006.41

Bringmann, G., Gulder, T. A. M., Hamm, A., Goodfellow, M., and Fiedler, H. P. (2009). Multiple convergence in polyketide biosynthesis: a third folding mode to the anthraquinonechrysophanol. *Chem. Commun.* 6810–6812. doi: 10.1039/b910501h

Bringmann, G., Noll, T. F., Gulder, T. A., Grune, M., Dreyer, M., Wilde, C., et al. (2006). Different polyketide folding modes converge to an identical molecular architecture. *Nat. Chem. Biol.* 2, 429–433. doi: 10.1038/nchembio805

Burson, K. K., and Khosla, C. (2000). Dissecting the chain length specificity in bacterial aromatic polyketide synthases using chimeric genes. *Tetrahedron* 56, 9401–9408. doi: 10.1016/S0040-4020(00)00824-3

Cotterill, A. S., Gill, M., and Milanovic, N. M. (1995). Pigments of Fungi. 41. Synthesis of (*S*)-(+)-dermolactone and (+/-)-dermolactone: stereochemistry of dermolactone from the Australian fungus *Dermocybe sanguinea* (Wulf. *Ex Fr.) Wunsche sensu* Cleland. *J. Chem. Soc. Perkin Trans.* 1, 1215–1223.

Das, A., and Khosla, C. (2009). Biosynthesis of aromatic polyketides in bacteria. *Acc. Chem. Res.* 42, 631–639. doi: 10.1021/ar8002249

Feng, Z., Kim, J. H., and Brady, S. F. (2010). Fluostatins produced by the heterologous expression of a TAR reassembled environmental DNA derived type II PKS gene cluster. *J. Am. Chem. Soc.* 132, 11902–11903. doi: 10.1021/ja104550p

Gill, M., and Gimenez, A. (1990). Pigments of fungi. Part 17. (*S*)-(+)-dermochrysone, (+)-dermolactone, dermoquinone, and related pigments; new nonaketides from the fungus *Dermocybe sanguinea* (sensu Cleland). *J. Chem. Soc. Perkin Trans.* 1, 2585–2591.

Gould, S. J., Melville, C. R., and Chen, J. (1997). The biosynthesis of murayaquinone, a rearranged polyketide. *Tetrahedron* 53, 4561–4568. doi: 10.1016/S0040-4020(97)00226-3

Guseva, G. B., Antina, E. V., V'yugin, A. I., and Loginova, A. E. (2008). Complex formation of Cu(II), Ni(II), Zn(II), Co(II), and Cd(II) acetates with 3,3',4,4',5,5'-hexamethyldipyrrolylmethene. *R. J. Coord. Chem.* 34, 599–605. doi: 10.1134/S1070328408080071

Hertweck, C., Luzhetskyy, A., Rebets, Y., and Bechthold, A. (2007). Type II polyketide synthases: gaining a deeper insight into enzymatic teamwork. *Nat. Prod. Rep.* 24, 162–190. doi: 10.1039/B507395M

Huang, C., Yang, C., Zhang, W., Zhang, L., De, B. C., Zhu, Y., et al. (2018). Molecular basis of dimer formation during the biosynthesis of benzofluorene-containing atypical angucyclines. *Nat. Commun.* 9:2088. doi: 10.1038/s41467-018-04487-z

Jiang, X., Zhang, Q., Zhu, Y., Nie, F., Wu, Z., Yang, C., et al. (2017). Isolation, structure elucidation and biosynthesis of benzo[*b*]fluorene nenestatin A from deep-sea derived *Micromonospora echinospora* SCSIO 04089. *Tetrahedron* 73, 3585–3590. doi: 10.1016/j.tet.2017.03.054

Jin, J., Yang, X., Liu, T., Xiao, H., Wang, G., Zhou, M., et al. (2018). Fluostatins M–Q featuring a 6-5-6-6 ring skeleton and high oxidized A-rings from marine *Streptomyces* sp. PKU-MA00045. *Mar. Drugs* 16, 87–100. doi: 10.3390/md16030087

Krone, B., Hinrichs, A., and Zeeck, A. (1981). Metabolic products of microorganisms. 208. Haloquinone, a new antibiotic active against halobacteria. 2. Chemical-structure and derivatives. *J. Antibiot.* 34, 1538–1543. doi: 10.7164/antibiotics.34.1538

Kulowski, K., Wendt-Pienkowski, E., Han, L., Yang, K., Vining, L. C., and Hutchinson, C. R. (1999). Functional characterization of the *jadI* gene as a cyclase forming angucyclinones. *J. Am. Chem. Soc.* 121, 1786–1794. doi: 10.1021/ja982707f

Lund, K. L. A. R., and Thompson, A. (2014). Synthesis of symmetric *meso*-H-dipyrrin hydrobromides from 2-formylpyrroles. *Synlett* 25, 1142–1144. doi: 10.1055/s-0033-1341066

McDaniel, R., Ebertkhosla, S., Hopwood, D. A., and Khosla, C. (1993). Engineered biosynthesis of novel polyketides: manipulation and analysis of an aromatic polyketide synthase with unproved catalytic specificities. *J. Am. Chem. Soc.* 115, 11671–11675. doi: 10.1021/ja00078a002

McDaniel, R., Ebertkhosla, S., Hopwood, D. A., and Khosla, C. (1995). Rational design of aromatic polyketide natural-products by recombinant assembly of enzymatic subunits. *Nature* 375, 549–554. doi: 10.1038/375549a0

Meurer, G., Gerlitz, M., WendtPienkowski, E., Vining, L. C., Rohr, J., and Hutchinson, C. R. (1997). Iterative type II polyketide synthases,

cyclases and ketoreductases exhibit context-dependent behavior in the biosynthesis of linear and angular decapolyketides. *Chem. Biol.* 4, 433–443. doi: 10.1016/S1074-5521(97)90195-2

Mosmann, T. (1983). Rapid colorimetric assay for cellular growth and survival: application to proliferation and cytotoxicity assays. *J. Immunol. Methods* 65, 55–63. doi: 10.1016/0022-1759(83)90303-4

Olano, C., Garcia, I., Gonzalez, A., Rodriguez, M., Rozas, D., Rubio, J., et al. (2014). Activation and identification of five clusters for secondary metabolites in *Streptomyces albus* J1074. *Microb. Biotechnol.* 7, 242–256. doi: 10.1111/1751-7915.12116

Polonsky, J., and Lederer, E. (1963). Piloquinone: a new phenanthrene-*o*-quinone isolated from mycelium of *Streptomyces pilosus*. *Nature* 199, 285–286. doi: 10.1038/199285a0

Shaaban, K. A., Shaaban, M., Grün-Wollny, I., Maier, A., Fiebig, H. H., and Laatsch, H. (2007). Julichrome Q_6 glucuronide, a monomeric subunit of the julimycin B-I complex from a terrestrial *Streptomyces* sp. *J. Nat. Prod.* 70, 1545–1550. doi: 10.1021/np070196h

Shen, B. (2000). Biosynthesis of aromatic polyketides. *Top. Curr. Chem.* 209, 1–51. doi: 10.1007/3-540-48146-X_1

Shen, Y. M., Yoon, P., Yu, T. W., Floss, H. G., Hopwood, D., and Moore, B. S. (1999). Ectopic expression of the minimal *whiE* polyketide synthase generates a library of aromatic polyketides of diverse sizes and shapes. *Proc. Natl. Acad. Sci. U.S.A.* 96, 3622–3627. doi: 10.1073/pnas.96.7.3622

Tang, Y., Tsai, S. C., and Khosla, C. (2003). Polyketide chain length control by chain length factor. *J. Am. Chem. Soc.* 125, 12708–12709. doi: 10.1021/ja0378759

Thomas, R. (2001). A biosynthetic classification of fungal and *Streptomycete* fused-ring aromatic polyketides. *ChemBioChem* 2, 612–627. doi: 10.1002/1439-7633(20010903)2:9<612::AID-CBIC612>3.0.CO;2-Z

Thomas, R. (2016). Examination of potential exceptions to the F and S biosynthetic classification of fused-ring aromatic polyketides. *ChemBioChem* 17, 2208–2215. doi: 10.1002/cbic.201600315

Williamson, N. R., Simonsen, H. T., Ahmed, R. A., Goldet, G., Slater, H., Woodley, L., et al. (2005). Biosynthesis of the red antibiotic, prodigiosin, in *Serratia*: identification of a novel 2-methyl-3-n-amyl-pyrrole (MAP) assembly pathway, definition of the terminal condensing enzyme, and implications for undecylprodigiosin biosynthesis in *Streptomyces*. *Mol. Microbiol.* 56, 971–989. doi: 10.1111/j.1365-2958.2005.04602.x

Yang, C., Huang, C., Zhang, W., Zhu, Y., and Zhang, C. (2015). Heterologous expression of fluostatin gene cluster leads to a bioactive heterodimer. *Org. Lett.* 17, 5324–5327. doi: 10.1021/acs.orglett.5b02683

Zhang, W., Liu, Z., Li, S., Lu, Y., Chen, Y., Zhang, H., et al. (2012). Fluostatins I-K from the South China Sea-derived *Micromonospora rosaria* SCSIO N160. *J. Nat. Prod.* 75, 1937–1943. doi: 10.1021/np300505y

Zhang, W., Yang, C., Huang, C., Zhang, L., Zhang, H., Zhang, Q., et al. (2017). Pyrazolofluostatins A–C, pyrazole-fused benzo[*a*]fluorenes from South China Sea-derived *Micromonospora rosaria* SCSIO N160. *Org. Lett.* 19, 592–595. doi: 10.1021/acs.orglett.6b03745

Zhang, Z., Pan, H. X., and Tang, G. L. (2017). New insights into bacterial type II polyketide biosynthesis. *F1000Research* 6:172. doi: 10.12688/f1000research.10466.1

Zhao, Z., Shi, T., Xu, M., Brock, N. L., Zhao, Y.-L., Wang, Y., et al. (2016). Hybrubins: bipyrrole tetramic acids obtained by crosstalk between a truncated undecylprodigiosin pathway and heterologous tetramic acid biosynthetic genes. *Org. Lett.* 18, 572–575. doi: 10.1021/acs.orglett.5b03609

Zhou, H., Li, Y., and Tang, Y. (2010). Cyclization of aromatic polyketides from bacteria and fungi. *Nat. Prod. Rep.* 27, 839–868. doi: 10.1039/b911518h

Zhou, H., Wang, Y., Yu, Y., Bai, T., Chen, L., Liu, P., et al. (2012). A non-restricting and non-methylating *Escherichia coli* strain for DNA cloning and high-throughput conjugation to *Streptomyces coelicolor*. *Curr. Microbiol.* 64, 185–190. doi: 10.1007/s00284-011-0048-5

Conflict of Interest Statement: The authors declare that the research was conducted in the absence of any commercial or financial relationships that could be construed as a potential conflict of interest.

frontiers in Chemistry

ORIGINAL RESEARCH
published: 01 November 2018
doi: 10.3389/fchem.2018.00536

Phenol Derivatives From the Sponge-Derived Fungus *Didymellaceae* sp. SCSIO F46

Yongqi Tian[1,2], *Xiuping Lin*[2], *Xuefeng Zhou*[2]* and *Yonghong Liu*[2,3]*

[1] College of Biological Science and Technology, Fuzhou University, Fuzhou, China, [2] CAS Key Laboratory of Tropical Marine Bio-resources and Ecology, Guangdong Key Laboratory of Marine Materia Medica, South China Sea Institute of Oceanology, Chinese Academy of Sciences, Guangzhou, China, [3] University of Chinese Academy of Sciences, Beijing, China

Seven new phenol derivatives named coleophomones E and F (**1**, **2**), diorcinols L and M (**3**, **4**), 1-hydroxy-6-methyl-11-methoxy-8-hydroxymethylxanthone (**5**), porric acid E (**6**), and 7-(2-hydroxyphenyl) butane-7,8,9-triol (**7**), were isolated from the EtOAc extract of the marine sponge-derived fungus *Didymellaceae* sp. SCSIO F46, together with 10 known compounds. Their structures were determined by spectroscopic analyses, including NMR, MS, X-ray diffraction, and theoretical calculations. Each of **1** and **2** contains an unusual spiro [cyclohexane-1,2′-inden] moiety, which is relatively seldom in nature products. Cytotoxic and COX-2 inhibitory activities of all purified compounds were tested and evaluated. Compound **3** displayed obvious cytotoxicities against Huh-7, HeLa, DU145 and HL60 cells (IC_{50} values 5.7–9.6 μM) and weak activities against other five cell lines, while **8** showed weak cytotoxicities against HeLa and HL7702 cells. Compound **6** displayed COX-2 inhibitory activity with IC_{50} value of 3.3 μM.

Keywords: sponge-derived fungus, *Didymellaceae* sp., Phenol derivatives, cytotoxic, COX-2 inhibitory

OPEN ACCESS

Edited by:
Xian-Wen Yang,
Third Institute of Oceanography, State Oceanic Administration, China

Reviewed by:
José Carlos Menéndez,
Complutense University of Madrid, Spain
Shan He,
Ningbo University, China

***Correspondence:**
Xuefeng Zhou
xfzhou@scsio.ac.cn
Yonghong Liu
yonghongliu@scsio.ac.cn

Specialty section:
This article was submitted to Medicinal and Pharmaceutical Chemistry, a section of the journal Frontiers in Chemistry

Received: *09 August 2018*
Accepted: *16 October 2018*
Published: *01 November 2018*

Citation:
Tian Y, Lin X, Zhou X and Liu Y (2018) Phenol Derivatives From the Sponge-Derived Fungus Didymellaceae sp. SCSIO F46. Front. Chem. 6:536. doi: 10.3389/fchem.2018.00536

INTRODUCTION

Natural products are still irreplaceable and continuing sources of novel drug leads, especially in the anti-infective area (Newman and Cragg, 2016). The marine ecosystem is one of the most complex and largest aquatic systems on earth, and host a huge microbial biodiversity (Agrawal et al., 2017; Corinaldesi et al., 2017). The unique and extreme characteristics of marine systems have driven a variety of biological adaptations, leading to the production of a large number of novel molecules for the treatment of many diseases (Gerwick and Fenner, 2013; Blunt et al., 2017). Marine sponges, a kind of precious marine organisms for new drug discovery, are hosts for a large community of microbes (up to 50–60% of the biomass of the sponge host) (Bergmann and Burke, 1955; Wang, 2006; Zhang et al., 2017). It was indicated that the symbiotic microbes of marine sponges might be the true producers of bioactive chemical defense substance of the sponge ecosystem (Richelle-Maurer et al., 2003; Thomas et al., 2010).

Sponge-derived fungi have been proven to be a treasure trove of novel biomolecules (Indraningrat et al., 2016; Blunt et al., 2017). During an ongoing search for new bioactive metabolites from the sponge-derived fungi (Tian et al., 2015a, 2018a,b), a strain of *Didymellaceae* sp. (SCSIO F46) isolated from a sponge *Callyspongia* sp. was subjected to chemical study. The EtOAc extract of rice fermentation of F46 showed toxicity against brine shrimp. Further isolation yielded seven new phenol derivatives, coleophomones E, F (**1**, **2**), diorcinols L, M (**3**,**4**), 1-hydroxy-6-methyl-11-methoxy-8-hydroxymethylxanthone (**5**), porric acid E (**6**), and 7-(2-hydroxyphenyl)

butane-7,8,9-triol (**7**), together with ten known compounds (**Figure 1**). The cytotoxic and COX-2 inhibitory activities of all compounds were evaluated. Details of the isolation structure elucidation, and bioactivity screening of these metabolites are reported herein.

MATERIALS AND METHODS

General Experimental Procedures

The NMR spectra were recorded on a Bruker AC 500 NMR (Bruker, Fällanden, Switzerland) spectrometer with TMS as an internal standard. HRESIMS data were measured on a Bruker micro TOF-QII mass spectrometer (Bruker, Fällanden, Switzerland). UV spectra were recorded on a Shimadzu UV-2600 UV-Vis spectrophotometer (Shimadzu, Kyoto, Japan). ECD spectra were performed on a Chirascan circular dichroism spectrometer (Applied Photophysics). X-ray diffraction intensity data were collected on a CrysAlis PRO charge-coupled device (CCD) area detector diffractometer with graphite monochromated Cu Kα radiation ($\lambda = 1.54178$ Å). Semi-preparative reversed-phase HPLC (RP-HPLC) was performed on a YMC-Pack Pro C_{18} *RS* column (5 μm, 250 × 10 mm id; YMC, Kyoto, Japan) with a Agilent 1260 separation module equipped with a Photodiode Array (PDA) detector. Silica gel GF254 used for TLC were supplied by the Qingdao Marine Chemical Factory, Qingdao, China. Sephadex LH-20 gel (GE Healthcare, Uppsala, Sweden) was used. Spots were detected on TLC under UV light or by heating by spraying with 12% H_2SO_4 in H_2O.

Fungal Material

The fungal strain SCSIO F46 was isolated from a sponge *Callyspongia* sp., collected from the sea area near Xuwen County, Guangdong Province, China, during August 2013. The isolate was stored on MB agar (malt extract 15 g, sea salt 10 g, agar 15 g) slants at 4°C and then deposited at CAS Key Laboratory of Tropical Marine Bio-resources and Ecology. The fungus was identified using a molecular biological protocol by DNA amplification and sequencing of the ITS region. The nucleotide sequence of the ITS region reported in this article was assigned the GenBank accession number KU361223.

Extraction and Isolation

Didymellaceae sp. SCSIO F46 was cultured on MB-agar plates at 25°C for 7 days. The seed medium (malt extract 15 g, sea salt 10 g, distilled water 1,000 mL, pH 7.4–7.8) was inoculated with strain F46 and incubated at 25°C for 72 h on a rotating shaker (170 rpm). Mass scale fermentation of F46 was carried out using solid rice medium in 1,000 mL flasks (rice 200 g, sea salt 2.5 g, distilled water 200 mL), and inoculated with 10 mL of seed solution. Flasks were incubated at 25°C under normal day night cycle. After 30 days, cultures from 30 flasks were harvested. The culture of solid rice medium was soaked in acetone and cut into small pieces and kept for 1 day. The content was filtered and evaporated under vacuum and extracted with EtOAc thrice. The extract was partitioned between petroleum ether, and 90% aqueous MeOH to obtain the crude extract (43.0 g). The crude extract was subjected to silica gel column chromatography (CC) eluted with petroleum

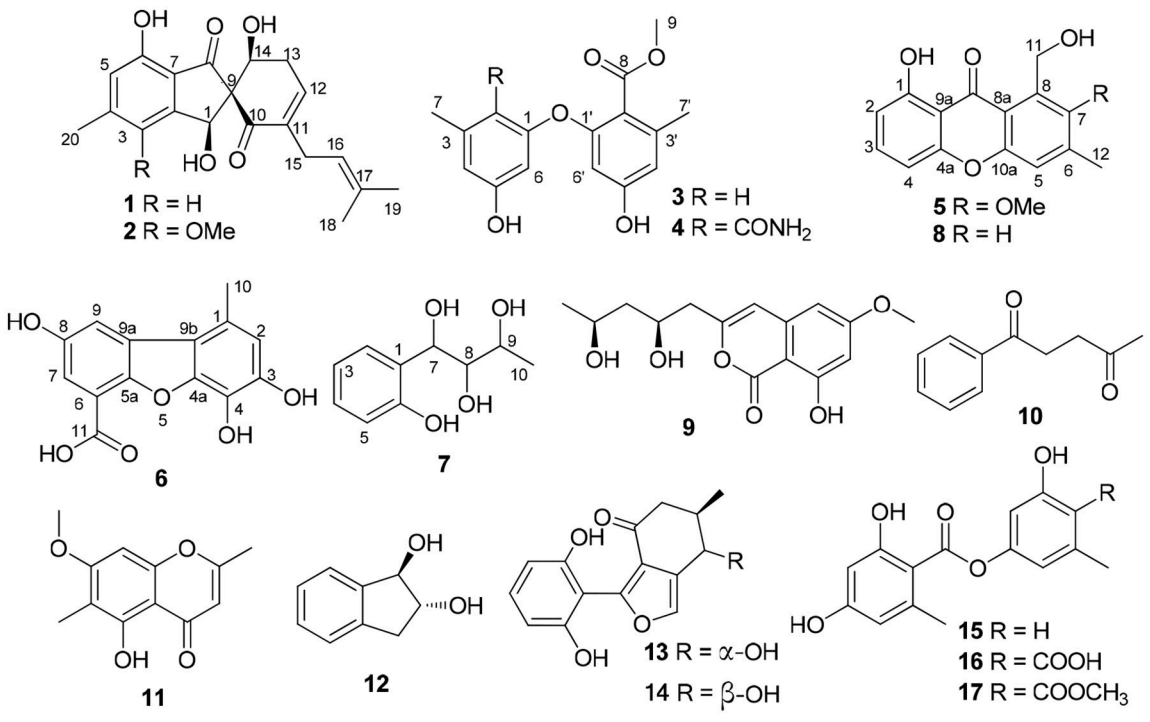

FIGURE 1 | Structures of **1**–**17**.

ether/EtOAc in a gradient eluent (v/v, 50:1, 30:1, 20:1, 10:1, 5:1, 1:1, 0:1) to obtain 8 fractions (fractions 1–8). Fr. 2 was subjected to ODS CC eluted with MeOH/H_2O in a gradient eluent (1:9, 2:3, 3:2, 4;1, 9:1), to give 3 sub fractions (fr. 2.1–2.3). Fr. 2.2 was further purified by HPLC eluting with MeOH/H_2O (60:40) to afford **9** (5.5 mg), **10** (4.7 mg), and **11** (3.8 mg). Fr. 3 was purified by Sephadex LH-20 (CH_3Cl/MeOH, 1:1) to give 3 sub fractions (fr. 3.1–3.3). Fr. 3.2 was further purified by silica gel CC eluted with petroleum ether/EtOAc in a gradient eluent (v/v, 10:1) to obtain **5** (20.1 mg) and **8** (10.3 mg). Fr. 4 was subjected to an ODS column (MeOH/H_2O: 10–100%) to give 4 sub fractions (fr. 4.1–4.4). Fr. 4.2 was further purified by HPLC eluting with MeOH/H_2O (50:50, 1‰TFA) to afford **3** (20.8 mg). Compounds **16** (20.3 mg) and **17** (43.2 mg) were purified from Fr. 4.4 by HPLC (35% MeCN, 1‰ TFA). Fr.5 was purified by ODS CC (MeOH/H_2O: 10–100%) and HPLC (35% MeCN, 1‰ TFA) to afford **1** (7.4 mg), **2** (4.3 mg) and **6** (5.5 mg). Compound **12** (2.3 mg) was isolated from Fr.6 by an ODS CC and followed by HPLC using 10% MeCN. Fr.7 was subjected to Sephadex LH-20 CC (CH_3Cl/MeOH, 1:1) to provide 4 subfractions (Frs.7.1–7.4). Fr. 7.1 was further purified on HPLC by 25% MeCN (2.5 mL/min) to give **13** (32.3 mg), **14** (43.7 mg). Fr. 7.2 was purified on HPLC by 10% MeCN to give **7** (15 mg). Finally, compounds **15** (4.4 mg) and **4** (3.5 mg) were isolated from Fr.7.3 and Fr. 7.4 by HPLC using 25% MeCN and 30% MeCN, respectively.

Coleophomone E (**1**): Yellow amorphous solid; [α]25 D+14.1 (*c* 0.31, MeOH); UV (MeOH) λ_{max} (log ε) 266 (3.16), 322 (2.25) nm, HRESIMS *m/z* 343.1541 $[M + H]^+$ (calcd for $C_{20}H_{23}O_5$, 343.1541); ^1H and ^{13}C NMR data, **Table 1**.

Coleophomone F (**2**): Yellow amorphous solid; [α]25 D+13.2 (*c* 0.46, MeOH); UV (MeOH) λ_{max} 220 (3.85), 266 (3.20), 313 (2.43) nm, HRESIMS *m/z* 373.1638 $[M + H]^+$ (calcd for $C_{21}H_{25}O_6$, 373.1646); ^1H and ^{13}C NMR data, **Table 1**.

Diorcinol L (**3**): Yellow amorphous solid; HRESIMS *m/z* 289.1070 $[M + H]^+$ (calcd for $C_{16}H_{17}O_5$, 289.1071); ^1H and ^{13}C NMR data, **Table 1**; The structure of **3** have been deposited in the Cambridge Crystallographic Data Centre as supplementary publication number CCDC 1502322.

Diorcinol M (**4**): Yellow amorphous solid; HRESIMS *m/z* 332.1127 $[M + H]^+$ (calcd for $C_{17}H_{18}NO_6$, 332.1129). ^1H and ^{13}C NMR data, **Table 1**.

1-Hydroxy-6-methyl-11-methoxy-8-hydroxymethylxanthone (**5**): Yellow needle crystals; HRESIMS *m/z* 287.0913 $[M + H]^+$ (calcd for $C_{16}H_{15}O_5$, 287.0919); ^1H and ^{13}C NMR data, **Table 2**.

Porric acid E (**6**): Colorless needle crystals; HRESIMS *m/z* 275.0544 $[M + H]^+$ (calcd for $C_{14}H_{11}O_6$, 275.0550); ^1H and ^{13}C NMR data, **Table 2.**

7-(2-Hydroxyphenyl) butane-7,8,9-triol (**7**): Yellow oil; HRESIMS *m/z* 221.0781 $[M + Na]^+$ (calcd for $C_{10}H_{14}NaO_4$, 221.0784); ^1H and ^{13}C NMR data, **Table 2.**

ECD Calculation

The eight possible stereoisomers (**a**-**h**) of **1** were initially performed using Confab (O'Boyle et al., 2011) with systematic search at MMFF94 force field. Room-temperature equilibrium

TABLE 1 | ^1H, ^{13}C NMR data of **1**–**4** (500/125 MHz, in DMSO-d_6, δ ppm, and *J* in Hz).

No.	1		2		No.	3		4	
	δ_H	δc, type	δ_H	δc, type		δ_H	δc, type	δ_H	δc, type
1	5.50, s	67.7, CH	5.70, s	66.3, CH	1		158.0, C		155.7, C
2		154.7, C		146.2, C	2	6.22, s	110.3, CH		120.9, C
3	6.84, s	116.8, CH		148.5, C	3		140.6, C		137.4, C
4		147.4, C		141.0, C	4	6.35, s	111.9, CH	6.27, d (1.5)	110.3, CH
5	6.63, s	115.6, CH	6.68, s	118.0, CH	5		158.9, C		157.2, C
6		157.2, C		150.7, C	6	6.14, s	103.2, CH	6.22, d (1.5)	102.7, CH
7		121.7, C		123.1, C	7	2.18, s	21.5, CH_3	2.20, s	19.5, CH_3
8		200.1, C		201.2, C	8		167.7, C		167.1, C
9		71.8, C		71.6, C	9	3.67, s	52.2, CH_3	3.69, s	51.9, CH_3
10		196.9, C		196.6, C	10	-	-		169.2, C
11		138.4, C		138.3, C	1′		155.8, C		154.5, C
12	6.63, d (5.5)	141.9, CH	6.62, d (5.5)	141.8, CH	2′		117.1, C		116.9, C
13	2.61, m	32.4, CH_2	2.66, m	32.3, CH_2	3′		138.9, C		138.6, C
14	4.39, dd (9.2, 5.9)	67.4, CH	4.34, dd (9.5, 5.0)	67.8, CH	4′	6.41, s	112.8, CH	6.47, d (2.0)	112.9, CH
15	2.72, m	27.3, CH_2	2.72, m	27.3, CH_2	5′		159.7, C		159.4, C
16	5.03, t (6.8)	121.3, CH	5.06, t (7.0)	121.3, CH	6′	6.14, s	103.9, CH	6.16, d (2.0)	104.0, CH
17		132.2, C		132.3, C	7′	2.20, s	19.9, CH_3	2.22, s	19.5, CH_3
18	1.54, s	17.5, CH_3	1.55, s	17.5, CH_3	5OH	9.95, br.s		10.02, br.s	
19	1.65, s	25.5, CH_3	1.66, s	25.5, CH_3	5'OH	9.50, br.s		9.93, br.s	
20	2.31, s	21.7, CH_3	2.22, s	16.2, CH_3	NH_2			7.45, 7.35, br.s	
21			3.72, s	60.6, CH_3					

populations were calculated according to Boltzmann distribution law. The conformers with Boltzmann-population of over 1% were chosen were chosen for ECD calculations using Gaussian 09 (Frisch et al., 2009) software, and the stable conformers were initially optimized at the B3LYP/6-311G(d,p) in methanol using the IEFPCM model. Vibrational frequency analysis confirmed the stable structures. Under the same condition, the ECD calculation was conducted using Time-dependent Density functional theory (TD-DFT). Rotatory strengths for a total of 30 excited states were calculated. The ECD spectrum was simulated in SpecDis (University of Würzburg) with a half-bandwidth of 0.3–0.4 eV, according to the Boltzmann-calculated contribution of each conformer after UV correction.

NMR Calculation

The two stereoisomers **1e** and **1f** were delivered to geometry optimization at B3LYP/6-31+G(d,p) in gas phase. The theoretical calculation of NMR was conducted using the Gauge-Independent Atomic Orbitals (GIAO) method at mPW1PW91/6-311+G(2d,p) in methanol by the IEFPCM model. Finally, the TMS-corrected NMR chemical shift values were averaged according to Boltzmann distribution for each conformer and fitting to the experimental values by linear regression. The calculated ^{13}C-NMR chemical shift values of TMS in methanol were 0 ppm.

Cytotoxicity Assay

The cytotoxic activities of **1**-**17** were screened against the growth panel of 10 tumor cell lines (K562, MCF-7, A549, Huh-7, H1975, HeLa, HL7702, HL60, MOLT-4, and DU145) (Bergeron et al., 1994) (**Supplementary Material**).

COX-2 Inhibitory Activity Assay

According to the manufacturer's instructions. The test compounds were dissolved in DMSO and the final concentration was set as 10 μM. The percentage inhibition has been calculated

TABLE 2 | ^{1}H, ^{13}C NMR data of **5**–**7** (500/125 MHz, in $CDCl_3$, δ ppm, *J* in Hz).

No.	5		No.	6		No.	7	
	δ_H	δc, type		δ_H	δc, type		δ_H	δc, type
1		161.7, C	1		126.5, C	1		154.3, C
2	6.71, d (8.0)	110.4, CH	2	6.71, s	116.9, CH	2	6.72, d (8.0)	114.9, CH
3	7.49, t (8.0)	136.7, CH	3		146.9, C	3	7.04, td (8.0, 2.0)	127.4, CH
4	6.80, d (8.0)	106.5, CH	4		131.2, C	4	6.77, t (7.5)	118.6, CH
4a		155.4, C	4a		141.6, C	5	7.29, dd (7.5, 1.0)	128.7,CH
5	7.18, s	119.5, CH	5a		164.7, C	6		129.8, C
6		142.4, C	6		97.3, C	7	5.01, d (3.5)	67.5, CH
7		153.5, C	7	6.36, d (1.5)	101.0, CH	8	3.32, dd (6.0, 3.5)	78.0, CH
8		133.9, C	8		165.5, C	9	3.58, dq (6.0, 6.0)	66.8, CH
8a		117.8, C	9	7.21, d (1.5)	104.5, CH	10	1.11, d (6.0)	19.7, CH_3
9		184.2, C	9a		138.8, C	6-OH	9.33, br.s	
9a		108.9, C	9b		109.4, C			
10a		153.8, C	10	2.60, s	24.8, CH_3			
11	4.99, s	56.7, CH_2	11		164.2, C			
12	2.40, s	17.2, CH_3	COO*H*	11.84, s				
13	3.81, s	62.6, CH_3						
1-OH	12.53, s							
11-OH	4.37, br.s							

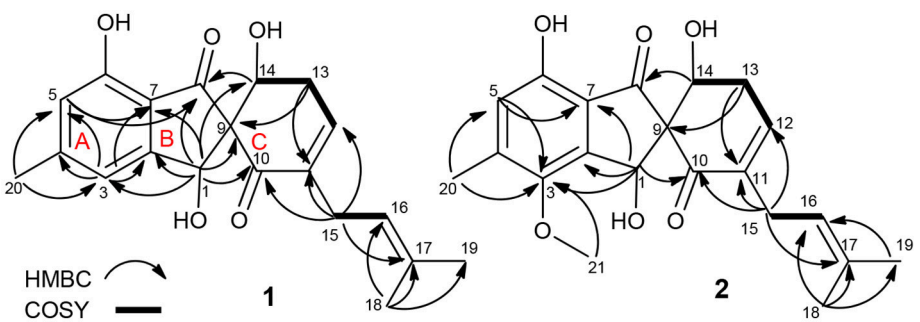

FIGURE 2 | Key COSY and HMBC correlations of **1** and **2**.

by comparison with control incubations (Tian et al., 2015b) (**Supplementary Material**).

RESULTS AND DISCUSSION

Compound **1** was assigned a molecular formula of $C_{20}H_{22}O_5$ (10 degrees of unsaturation) by HRESIMS (*m/z* 343.1541 $[M + H]^+$). Its NMR spectra showed resonances for three methyls, two methylenes, two oxygenated sp^3 methine, one sp^3 quaternary carbon, four sp^2 methine, six sp^2 quaternary carbon, and two ketocarbonyl carbons (δ_C 200.1 and 196.9) (**Table 1**). These data suggested a tricyclic skeleton of **1**. The ^1H NMR spectrum exhibited aromatic signals at δ_H 6.84 (s, H-3), 6.63 (s, H-5) indicating the presence of a tetrasubstituted aromatic ring. The HMBC correlations of H-3/C-2, C-4, C-5, C-7, and C-20, H_3-20 (δ_H 2.31, s)/C-4, and C-5, and H-5/C-6, and C-7 suggested a methyl (C-20) and a hydroxy at C-4 and C-6, respectively. The HMBC correlations of H-1 (δ_H 5.50, s)/C-2, C-3, C-4, C-6, C-7, C-8 (δ_C 200.1) and C-9 (δ_C 71.8), and H-5/C-8 indicated linkage of ring B and the connection of C-1 to C-2 and C-7 to C-8. The COSY cross-peaks of H-13 (δ_H 2.61, m) /H-14 (δ_H 4.39, dd, J = 9.2, 5.9 Hz), and H-12 (δ_H 6.33, d, J = 5.9 Hz) delineated the spin system C_{12}-C_{13}-C_{14}. Moreover, the HMBC correlations of H-12/C-10 and C-14, H-13/C-9, C-11, and C-12, and H-14/C-1, C-8 and C-9 indicated the presence of a α,β-unsaturated ketone (ring C) and rings B/C are connected by C-9. Finally, a 2-methyl-2 butene group was attached to C-11 (δ_C 138.4) by the evidence of the HMBC correlations of H_3-18 (δ_H 1.54, s)/C-16 (δ_C 121.3), C-17 (δ_C 132.2), and C-19 and H_2-15 (δ_H 2.72, s)/C-10, C-11, C-12, C-13, C-16, and C-17.

NOESY correlations and Mosher method were failure to determine the configurations of **1**, so theoretical calculations were used to solve it. There are eight possible stereoisomers (**a-h**) of **1,** as shown in **Figure 3A**. Computational studies of electron circular dichroism (ECD) were carried out. All stereoisomers (**a–h**) were selected for theoretical calculations using time dependent density functional theory (TDDFT) B3LYP/6-311G (d,p) level with the IEFPCM model in MeOH (**Tables S1**, **2**, **4**). A comparison of the experimental spectrum of **1** with the calculated ECD spectra of eight possible stereoisomers (**a**-**h**) were presented

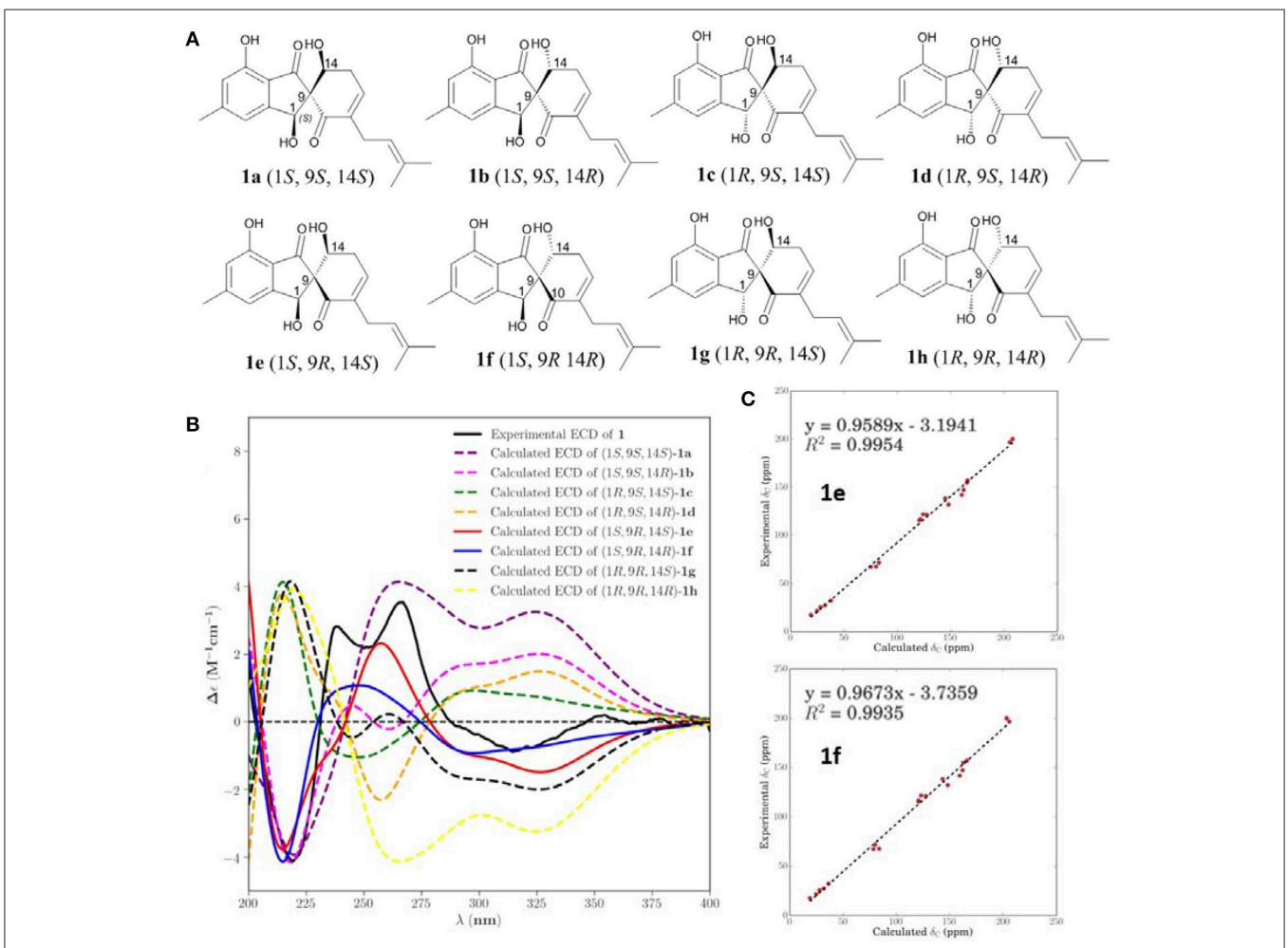

FIGURE 3 | Calculated ECD and NMR studies of **1**. **(A)** Eight possible stereoisomers **(a-h)** of **1**. **(B)** Calculated ECD spectra of configurations **a**-**h** were compared with the experimental ECD spectra. **(C)** Linear regression fitting of calculated ^{13}C-NMR chemical shifts of **1e** and **1f** with experimental values.

in **Figure 3B**. The measured ECD curve exhibits two negative Cotton effects (CEs) at 219 and 315 nm, and two positive cotton effects at 238 and 267 nm, matching well with the calculated ECD curve of **1e** (1*S*, 9*R*, 14*S*) and **1f** (1*S*, 9*R*, 14*R*). Then, computed ^{13}C-NMR chemical shifts was carried out to define the stereochemistry of C-14. Computed ^{13}C-NMR chemical shifts of each conformer were first Boltzmann-weighted averaged, and then fitted to experimental values by Ordinary Least Squares (OLS) Linear Regression method in order to remove systematic error that results from the conformational search and random error from experimental conditions (**Tables S3**, **5**). As a result, the computed chemical shift for C-14 of **1e** is δ_C = 68.7 ppm, with only a deviation of 1.3 ppm from the experimental value (δ_C = 67.4 ppm) (**Table S8**). All in all, the computed chemical shifts of **1e** showed good agreement with the experimental values and has the higher R^2 and R^2_{adj} values than that of **1f**, which suggesting that **1e** (1*S*, 9*R*, 14*S*) be the true isomer of **1** (**Figure 3C**, **Table S7**).

The molecular formula of **2** was determined as $C_{21}H_{24}O_6$ by its HRESIMS (*m/z* 373.1638 $[M + H]^+$), corresponding to 10 units of unsaturation. Its UV and NMR date were similar to those of **1**, except for the presence of a methoxy (δ_H 3.72, δ_C 60.6) in **2** (**Table 1**). The extra methoxy (C-21) was located at C-3 by HMBC correlations from H_3-21 to C-3 (δ_C 148.5) (**Figure 2**). The absolute configuration of **2** was suggested as (1*S*,9*R*,14*S*), as its chemical shift, coupling constant, optical rotation and CD effect (**Table 1**, **Figure S20**) almost the same as those of **1**.

The molecular formula of **3** was assigned as $C_{16}H_{16}O_5$ by its HRESIMS ion peak at *m/z* 289.1070 $[M + H]^+$ and NMR date. The ^{1}H NMR spectrum of **3** exhibited two hydroxyl proton at δ_H 9.95 and 9.50, five aromatic signals at δ_H 6.41, 6.35, 6.22, and 6.14×2, one *O*-methyl at δ_H 3.67, and two single methyls at δ_H 2.18 and 2.20 (**Table 2**). Analysis of the ^{13}C and DEPT-135 NMR spectra of **3** indicated the presence of 16 carbons, including one carbonyl carbon (δ_C 167.7), 12 aromatic carbons (four oxygenated ones at δ_C 159.7, 158.9, 158.0 and 155.8), one methoxy and two methyls. These spectra of **3** were similar to those of diorcinol (Tian et al., 2015b), except for the presence of a metheyl formate group (one carbonyl carbon at δ_C 167.7 and one methoxy at δ_H 3.67/δ_C 52.2). However, relying solely on the NMR date, the location of metheyl formate was more difficult to determine. In order to determine location of metheyl formate of **3**, a single-crystal X-ray diffraction pattern was obtained using the anomalous scattering of Cu Kα radiation shows an ORTEP drawing (**Figure 4**, **Table S9**) and unambiguously determined metheyl formate at C-2′. Thus, the structure of **3** was determined, and named as diorcinol L.

Compound **4** was obtained as brown powder. The molecular formula of was determined as $C_{17}H_{17}NO_6$ by its HRESIMS (*m/z* 332.1131 $[M + H]^+$), which corresponded to ten units of unsaturation. The ^{1}H and ^{13}C NMR data of **4** were similar to those of **3**, except for the presence of one amide [δ_C 169.2 ($CONH_2$)/ δ_H 7.45, 7.35 ($CONH_2$)] (**Table 1**). The extra amide was determined at C-2 by the HMBC correlations of H-4, H-6/C-2, as well as H_3-7/C-2, C-3, C-4, and C-10 (**Figure 5**). Hence, the structure of was elucidated and the trivial name diorcinol M was assigned.

Compound **5** was isolated as pale yellow needle-like crystals. Its molecular formula was determined to be $C_{16}H_{14}O_5$, by HR-ESI-MS, indicating 10 degrees of unsaturation. The 1D NMR data (**Table 3**) of **5** contained resonances for one carbonyl carbon, eight sp^2 quarternary carbons, four sp^2 methines, one sp^3 methylene, two sp^3 methys. Comparison of UV-vis and NMR data with those of 1-Hydroxy-6-methyl-8-hydroxy-methylxanthone (**8**) revealed a high degree of similarity skeleton, where the only obvious differences is in the presence of one methoxy (δ_H 3.81; δ_C 62.6) and low-field chemical shift of C-7 (from δ_C 127.2 in **8** to 153.5 in **1**). Meanwhile, this difference can also be ascribed by the HMBC correlations (**Figure 5**) of δ_H (3.81,

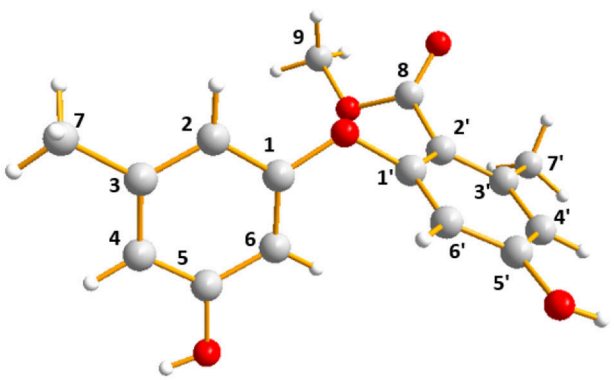

FIGURE 4 | X-ray crystallographic structure of **3**.

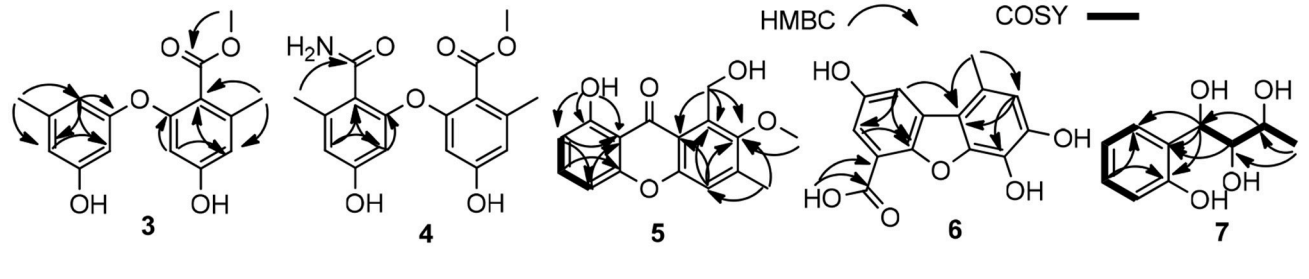

FIGURE 5 | Key COSY and HMBC correlations of **3**–**7**.

TABLE 3 | Cytotoxic results of the compounds (IC_{50}, μM).

Comp.	K562	MCF-7	A549	Huh-7	H1975	HeLa	HL7702	HL60	MOLT-4	DU145
3	43.5	10.5	17.7	5.7	15.3	7.1	68.2	9.6	NA	9.1
8	NA	141.0	128.0	122.0	NA	14.3	33.8	NA	NA	NA
TSA	0.1	0.7	0.3	0.08	0.09	0.08	0.09	0.04	0.03	0.04

NA, No active (IC_{50} > 200 μM).

s, H-13) with δ_C (153.5, C-7) and requirements of HRESIMS spectrum. Thus, the structure of **5** was determined and named as 1-hydroxy-6-methyl-11-methoxy-8-hydroxymethylxanthone.

Compound **6** showed a molecular ion peak at *m/z* 275.0544 $[M + H]^+$ in the HR-ESI-MS, in accordance with the molecular formula $C_{14}H_{10}O_6$, which was also supported by NMR data. The ^{1}H NMR data displayed one sharp hydroxy proton singlet (11.84, s, COO*H*), two aromatic protons at δ_H 7.21 (1H, d, J = 1.5 Hz), 6.71 (1H, s), 6.36 (1H, d, J = 1.5 Hz), and a singlet methyl at δ_H 2.60 (3H, s). The ^{13}C and DEPT-135 NMR spectra (**Table 2**) showed 14 carbons, including one carboxyl group (δ_C 164.2), three aromatic methine carbons (δ_C 116.9, 104.5, 101.0), 11 aromatic quaternary carbons (δ_C 165.5, 164.7, 146.9, 141.6, 138.8, 131.2, 126.5, 109.4, 97.3), and one methyl (δ_C 24.8). The aforementioned NMR data showed **1** was closely related structurally to the porric acid C (Carotenuto et al., 1998). The only difference was the substituent of C-4, the chemical shift to low field of C-4 (δ_C 131.2 in **4**; δ_C 101.0 in porric acid C), the HMBC correlation (**Figure 5**, **Table 2**) from H-2 (δ_H 6.71, s) to C-3 (δ_C 146.9) and C-4 (δ_C 131.2) requirements of HRESIMS spectrum suggested that a hydroxy proton group was connected to C-4. Thus, the structure of **6** was determined and named porric acid E.

Compound **7** was obtained as a yellow oil. Its HRESIMS gave the molecular formula $C_{10}H_{14}O_4$, requiring four degrees of unsaturation. The ^{1}H NMR spectrum (**Table 2**) exhibited aromatic signals at δ_H 7.29 (dd, J = 7.5, 1.0 Hz, H-5), 7.04 (td, J = 8.0, 2.0 Hz, H-3), 6.77 (t, J = 8.0, Hz, H-4), and 6.72 (d, J = 8.0 Hz, H-2), indicating the presence of a disubstituted aromatic ring. The substitutions of a trihydroxybutyl group (C-7—C-10) and a hydroxy (δ_H 9.33, br.s, OH-6) at C-1 (δ_C 154.3) and C-6 (δ_C 129.8), were assigned by the COSY and HMBC interactions (**Figure 5**, **Table 2**).

Biological Activity

Cytotoxic activities of the isolated compounds **1**–**17** and trichostatin A (TSA, positive control) against 10 tumor cell lines (K562, MCF-7, A549, Huh-7, H1975, HeLa, HL7702, HL60, MOLT-4, and DU145) were tested. Among all of them, **3** displayed a wide range of cytotoxicities with IC_{50} values in the range of 5.7–68.2 μM, and **8** showed weak selective cytotoxicities against HeLa and HL7702 cells (**Table 3**). Furthermore, compound **6** displayed COX-2 inhibitory activity with the prominent IC_{50} values of 3.3 μM. Celecoxib was used as the positive control with IC_{50} values of 0.01 μM.

CONCLUSION

In conclusion, 17 phenol derivatives were isolated from the EtOAc extract of a marine sponge-derived fungus *Didymellaceae* sp. SCSIO F46. Coleophomones E and F (**1** and **2**) possess unprecedented spiro [cyclohexane-1,2′-inden] moiety, which is relatively seldom in natural products. Other new compounds **3**-**7** represent common types of phenol derivatives, which are widely found in fungal metabolites. Amongst, compounds **3** and **8** displayed a wide range of cytotoxicities against several tumor cell lines. In addition, **6** displayed significant COX-2 inhibitory activity with the prominent IC_{50} value of 3.3 μM.

AUTHOR CONTRIBUTIONS

YT designed the experiments and performed the isolation and characterization of all the compounds and wrote the manuscript. XL performed the isolation and purification of the fungal strain. XZ designed the research work and revised the manuscript. YL contributed in project design and manuscript preparation. All authors reviewed the manuscript and approved for submission.

ACKNOWLEDGMENTS

This work was supported by the National Natural Science Foundation of China (Nos. 21502204, 31270402, 21172230, 81741154 and 41476135), the Foundation for Scholars of Fuzhou University (No. XRC-1672, 2017T022), the Scientific and Technological Project of Fuzhou City of Fujian Province (No. 2017-G-39), the Natural Science Foundation of Fujian Provincial Department of Education (No. JAT170077), Project from Department of Ocean and Fishery of Guangdong Province (GDME-2018C010), and the Open Project of CAS Key Laboratory of Tropical Marine Bio-resources and Ecology (2018011009) and Guangdong Key Laboratory of Marine Materia Medica (LMM2018-3).

SUPPLEMENTARY MATERIAL

The Supplementary Material for this article can be found online at: https://www.frontiersin.org/articles/10.3389/fchem.2018.00536/full#supplementary-material

REFERENCES

Agrawal, S., Acharya, D., Adholeya, A., Barrow, C. J., and Deshmukh, S. K. (2017). Nonribosomal peptides from marine microbes and their antimicrobial and anticancer potential. *Front. Pharmacol.* 8:828. doi: 10.3389/fphar.2017.00828

Bergeron, J. J., Brenner, M. B., Thomas, D. Y., and Williams, D. B. (1994). Calnexin: a membrane bound chaperone of the endoplasmic reticulum. *Trends Biochem. Sci.* 19, 124–128.

Bergmann, W. B., and Burke, D. C. (1955). Contributions to the study of marineproducts. XXXIX. The nucleosides of sponges. III. Spongothymidine and spongouridine. *J. Org. Chem.* 20, 1501–1507.

Blunt, J. W., Carroll, A. R., Copp, B. R., Davis, R. A., Keyzers, R. A., and Prinsep, M. R. (2017). Marine natural products. *Nat. Pro. Rep.* 34, 235–294. doi: 10.1039/c7np00052a

Carotenuto, A., Fattorusso, E., Lanzotti, V., and Magno, S. (1998). Porric acids A-C—new antifungal dibenzofurans from the Bulbs of *Allium porrum* L. *Eur. J. Org. Chem*. 29, 661–663.

Corinaldesi, C., Barone, G., Marcellini, F., Dell'Anno, A., and Danovaro, R. (2017). Marine microbial-derived molecules and their potential use in cosmeceutical and cosmetic products. *Mar Drugs* 15:118. doi: 10.3390/md15040118

Frisch, M. J., Trucks, G. W., Schlegel, H. B., Scuseria, G. E., Robb, M. A., Cheeseman, J. R., et al. (2009). *Gaussian 09*. (Wallingford, CT: Gaussian. Inc).

Gerwick, W. H., and Fenner, A. M. (2013). Drug discovery from marine microbes. *Microb Ecol*. 65, 800–806. doi: 10.1007/s00248-012-0169-9

Indraningrat, A. A., Smidt, H., and Sipkema, D. (2016). Bioprospecting sponge-associated microbes for antimicrobial compounds. *Mar Drugs*. 14:87. doi: 10.3390/md14050087

Newman, D. J., and Cragg, G., M. (2016). Natural products as sources of new drugs from 1981 to 2014. *J. Nat. Prod.* 79, 629–661. doi: 10.1021/acs.jnatprod.5b01055

O'Boyle, N. M., Vandermeersch, T., Flynn, C. J., Maguire, A. R., and Hutchison, G. R. (2011). Confab-systematic generation of diverse low-energy conformers. *J. Cheminformatics* 3, 1–9. doi: 10.1186/1758-2946-3-8

Richelle-Maurer, E. G., Gomez, R., Braekman, J. C., van de Vyver, G., van Soest, R. W., and Devijver, C. (2003). Primary cultures from the marine sponge *Xestospongia* muta (petrosiidae, haplosclerida). *J. Biotechnol*. 100, 169–176. doi: 10.1016/S0168-1656(02)00251-1

Thomas, T., Rusch, D., DeMaere, M. Z., Yung, P. Y., Lewis, M., Halpern, A., et al. (2010). Functional genomic signatures of sponge bacteria reveal unique and shared features of symbiosis. *ISME J*. 4, 1557–1567. doi: 10.1038/ismej.2010.74

Tian, Y., Qin, X., Lin, X., Kaliyaperumal, K., Zhou, X., Liu, J., et al. (2015b). Sydoxanthone C and acremolin B produced by deep-sea-derived fungus *Aspergillus* sp. SCSIO Ind09F01. *J. Antibiot*. 68, 703–706. doi: 10.1038/ja.2015.55

Tian, Y. Q., Lin, S. N., Kaliyaperumal, K., Zhou, H., Wang, S. Y., and Liu, Y. H. (2018b). Polyketide-derived metabolites from the sponge-derived fungus *Aspergillus* sp. F40. *Phytochem Lett*. 27, 74–77. doi: 10.1016/j.phytol.2018.06.009

Tian, Y. Q., Lin, S. N., Zhou, H., Lin, S. T., Wang, S. Y., and Liu, Y. H. (2018a). Protuboxepin C and protuboxepin D from the sponge-derived fungus *Aspergillus* sp SCSIO XWS02F40. *Nat. Prod. Res*. 32, 2510–2515. doi: 10.1080/14786419.2017.1423303

Tian, Y. Q., Lin, X. P., Wang, Z., Zhou, X. F., Qin, X. C., Kaliyaperumal, K., et al. (2015a). Asteltoxins with antiviral activities from the marine sponge-derived fungus *Aspergillus* sp. SCSIOXWS02F40. *Molecules* 21:E34. doi: 10.3390/molecules21010034

Wang, G. (2006). Diversity and biotechnological potential of the sponge-associated microbial consortia. *J. Ind. Microbiol. Biotechnol.* 33, 545–551. doi: 10.1007/s10295-006-0123-2

Zhang, H., Zhao, Z., and Wang, H. (2017). Cytotoxic natural products from marine sponge-derived microorganisms. *Mar. Drugs* 15:68. doi: 10.3390/md15030068

Conflict of Interest Statement: The authors declare that the research was conducted in the absence of any commercial or financial relationships that could be construed as a potential conflict of interest.

frontiers in Chemistry

ORIGINAL RESEARCH
published: 15 November 2018
doi: 10.3389/fchem.2018.00538

New Pim-1 Kinase Inhibitor From the Co-culture of Two Sponge-Associated Actinomycetes

Seham S. El-Hawary[1], Ahmed M. Sayed[2,3], Rabab Mohammed[2], Mohammad A. Khanfar[4,5], Mostafa E. Rateb[2,6,7], Tarek A. Mohammed[8], Dina Hajjar[9], Hossam M. Hassan[2,3], Tobias A. M. Gulder[10,11] and Usama Ramadan Abdelmohsen[12]**

[1] Pharmacognosy Department, Faculty of Pharmacy, Cairo University, Cairo, Egypt, [2] Pharmacognosy Department, Faculty of Pharmacy, Beni-Suef University, Beni-Suef, Egypt, [3] Pharmacognosy Department, Faculty of Pharmacy, Nahda University, Beni-Suef, Egypt, [4] Faculty of Pharmacy, The University of Jordan, Amman, Jordan, [5] College of Pharmacy, Alfaisal University, Riyadh, Saudi Arabia, [6] School of Computing, Engineering and Physical Sciences, University of the West of Scotland, Paisley, United Kingdom, [7] Marine Biodiscovery Centre, University of Aberdeen, Aberdeen, United Kingdom, [8] Marine Invertebrates, National Institute of Oceanography and Fisheries, Red Sea Branch, Hurghada, Egypt, [9] Department of Biochemistry, Faculty of Science, Center for Science and Medical Research, University of Jeddah, Jeddah, Saudi Arabia, [10] Department of Chemistry and Center for Integrated Protein Science Munich (CIPSM), Biosystems Chemistry, Technical University of Munich, Garching, Germany, [11] Chair of Technical Biochemistry, Technische Universität Dresden, Dresden, Germany, [12] Department of Pharmacognosy, Faculty of Pharmacy, Minia University, Minia, Egypt

OPEN ACCESS

Edited by:
Peter Proksch, Heinrich Heine Universität Düsseldorf, Germany

Reviewed by:
Margherita Brindisi, Università degli Studi di Siena, Italy
Diego Brancaccio, Università degli Studi di Napoli Federico II, Italy

***Correspondence:**
Tobias A. M. Gulder
tobias.gulder@ch.tum.de
Usama Ramadan Abdelmohsen
usama.ramadan@mu.edu.eg

Specialty section:
This article was submitted to Medicinal and Pharmaceutical Chemistry, a section of the journal Frontiers in Chemistry

Received: *04 June 2018*
Accepted: *16 October 2018*
Published: *15 November 2018*

Citation:
El-Hawary SS, Sayed AM, Mohammed R, Khanfar MA, Rateb ME, Mohammed TA, Hajjar D, Hassan HM, Gulder TAM and Abdelmohsen UR (2018) New Pim-1 Kinase Inhibitor From the Co-culture of Two Sponge-Associated Actinomycetes. Front. Chem. 6:538. doi: 10.3389/fchem.2018.00538

Saccharomonospora sp. UR22 and *Dietzia* sp. UR66, two actinomycetes derived from the Red Sea sponge *Callyspongia siphonella*, were co-cultured and the induced metabolites were monitored by HPLC-DAD and TLC. Saccharomonosporine A (**1**), a novel brominated oxo-indole alkaloid, convolutamydine F (**2**) along with other three known induced metabolites (**3-5**) were isolated from the EtOAc extract of *Saccharomonospora* sp. UR22 and *Dietzia* sp. UR66 co-culture. Additionally, axenic culture of *Saccharomonospora* sp. UR22 led to isolation of six known microbial metabolites (**6-11**). A kinase inhibition assay results showed that compounds **1** and **3** were potent Pim-1 kinase inhibitors with an IC_{50} value of 0.3 ± 0.02 and 0.95 ± 0.01 μM, respectively. Docking studies revealed the binding mode of compounds **1** and **3** in the ATP pocket of Pim-1 kinase. Testing of compounds **1** and **3** displayed significant antiproliferative activity against the human colon adenocarcinoma HT-29, (IC_{50} 3.6 and 3.7 μM, respectively) and the human promyelocytic leukemia HL-60, (IC_{50} 2.8 and 4.2 μM, respectively). These results suggested that compounds **1** and **3** act as potential Pim-1 kinase inhibitors that mediate the tumor cell growth inhibitory effect. This study highlighted the co-cultivation approach as an effective strategy to increase the chemical diversity of the secondary metabolites hidden in the genomes of the marine actinomycetes.

Keywords: *Saccharomonospora* sp., *Dietzia* sp., actinomycetes, Saccharomonosporine A, convolutamydine F, docking, Pim-1 kinase, co-cultivation

INTRODUCTION

Marine sponge-associated microorganisms have been proved an essential source of biologically active natural products (Thomas et al., 2010; Roue et al., 2012; Abdelmohsen et al., 2014a). Large numbers of secondary metabolites with novel molecular scaffolds and diverse biological activities including antimicrobial (Hentschel et al., 2001; Eltamany et al., 2014), anti-parasitic (Abdelmohsen et al., 2014b; Viegelmann et al., 2014), immunomodulatory (Tabares et al., 2011), and anticancer (Simmons et al., 2011; Yi-Lei et al., 2014) effects have been isolated from sponge-associated actinomycetes. For example, salinosporamide A, a potent inhibitor of the 20S proteasome that has been isolated from a *Salinospora* species (Feling et al., 2003; Gulder and Moore, 2010), entered clinical trials for multiple myeloma treatment, only three years after its discovery (Fenical et al., 2009). Due to the continuous discovery of bioactive natural products from marine microbes, re-isolation of known microbial secondary metabolites has become a real challenge (Hong et al., 2009). However, microbial genome sequencing has confirmed the presence of a large number of silent biosynthetic gene clusters that encode for secondary metabolites which are not produced under normal laboratory conditions (Dashti et al., 2014). Microbial competition for nutrition and other resources is considered one of the most important factors for induction of novel bioactive secondary metabolites (Oh et al., 2005). Crosstalk between microbes inhabiting the same environment induces the unexpressed biosynthetic pathways leading to production of unusual secondary metabolites (Pettit, 2009; Schroeckh et al., 2009; Zuck et al., 2011). Co-cultivation of two different microbial strains together in one culture allows direct interaction between them, which may lead to the induction of new cryptic secondary metabolites not previously detected in the axenic cultures (Rateb et al., 2013). Examples of the production of induced new natural products by co-fermentation of marine derived microorganisms include a rare class of pseurotins, 11-O-methylpseurotin A_2 derived from mixed fermentation of *Streptomyces bullii* and the fungus *Aspergillus fumigatus* MBC-F1-10 (Rateb et al., 2013), the cyclic depsipeptides emericellamides A and B isolated from a co-culture of marine-derived fungus *Emericella* sp. (CNL-878) and the marine bacterium *Salinispora arenicola* (Oh et al., 2007), the diterpenoids libertellenones A–D isolated from mixed fermentation of the marine α-proteobacterium strain CNJ-328 with the fungus and *Libertella* sp. CNL-52 (Oh et al., 2005) and a chlorinated benzophenone pestalone sourced from a co-culture of the same bacterial strain CNJ-328 with *Pestalotia* sp. strain (Cueto et al., 2001). Recently, co-culture has also proved that both strains affect each other and induce new fungal and bacterial metabolites which were not detected in axenic cultures (Wakefield et al., 2017). In this study, we report on the induction of new bioactive secondary metabolites (**Figure 1**) saccharomonosporine A (**1**) and convolutamydine F (**2**) along with other three known metabolites **3-5** in response to microbial co-cultivation of two marine actinomycetes, *Saccharomonospora* sp. UR22 and *Dietzia* sp. UR66, derived from the Red Sea sponge *Callyspongia siphonella*. The HPLC and TLC chromatograms of the axenic cultures together with the co-culture derived extracts showed that compounds **1-5** were produced only during co-fermentation of both microbes. On the other hand, fermentation of *Saccharomonospora* sp. UR22 alone led to the isolation of a set of known microbial metabolites (**6-11**). Performing *in vitro* assay and docking studies on the isolated compounds revealed the potential of Pim-1 kinase as a promising target for only compound **1** and **3**. Cytotoxicity evaluation of the isolated compounds showed that compound **1** and **3** have significant antiproliferative activities against HT-29 and HL-60 cell lines. These results coincide with the enzyme inhibition assay ones.

MATERIAL AND METHODS

General Apparatus and Chemicals

Ultra violet (UV) spectra were acquired on a ultra-violet visible (UV-vis) spectrometer (Shimadzu UV 1800 spectro, Japan). Optical rotation values were acquired at Bellingham + Stanley ADP600 Series Polarimeter at the sodium D line (589 nm) and 25°C. IR spectra were recorded as KBr disks on a IR spectrophotometer (Shimadzu S8400, Japan) High performance liquid chromatography (HPLC) analysis was performed by Thermofisher dionex ultimate 3000 with PDA detector and Xterra (Waters) C_{18} RP analytical HPLC column (5 μm, 4.6 × 250 mm). High resolution mass spectrometric data were obtained using a Thermo Instruments MS system (LTQ XL/LTQ Orbitrap Discovery) coupled to a Thermo Instruments HPLC system (Accela PDA detector, Accela PDA autosampler, and Accela pump). 1D and 2D NMR spectra were recorded on Bruker Avance III 400 MHz (Bruker AG, Switzerland) with BBFO Smart Probe and Bruker 400 AEON Nitrogen-Free Magnet. Data were analyzed using Topspin 3.1 Software. Each sample was dissolved in suitable deuterated solvent. Chemical shifts were recorded and expressed in ppm related to the TMS signal at 0.00 ppm as internal reference. All solvent used for preparing extracts were of technical grade (ADWIC; El-Nasr Pharmaceutical Chemicals Co., Egypt); and reagents used for preparing samples were of analytical grade (E-Merck, Darmstadt, Germany). Silica gel (60–120 mesh, 50 g, Fluka®) was used for chromatographic isolation and purification. TLC analysis was performed using Merck 9385 pre-coated aluminum plate silica gel (Kieselgel 60) with F254 indicator thin layer plates.

Isolation and Cultivation of the Actinomycetes

Callyspongia siphonella was collected at a depth of 10 m in the Red Sea (Hurghada, Egypt) in November 2015. A voucher specimen was reserved at the National Institute of Oceanography and Fisheries, Red Sea Branch, Invertebrates Department. Sponge biomass was transferred to plastic bag containing seawater and transported to the laboratory. Sponge specimens were rinsed in sterile seawater, cut into pieces of ca. 1 cm^3, and then thoroughly homogenized in a sterile mortar with 10 volumes of sterile seawater. The supernatant was diluted in ten-fold series (10^{-1}, 10^{-2}, 10^{-3}) and subsequently plated out on agar plates. Five different media M1 (Mincer et al., 2002), ISP2 medium (Shirling and Gottlieb, 1966), oligotrophic medium (OLIGO) (Olson et al., 2000), actinomycete

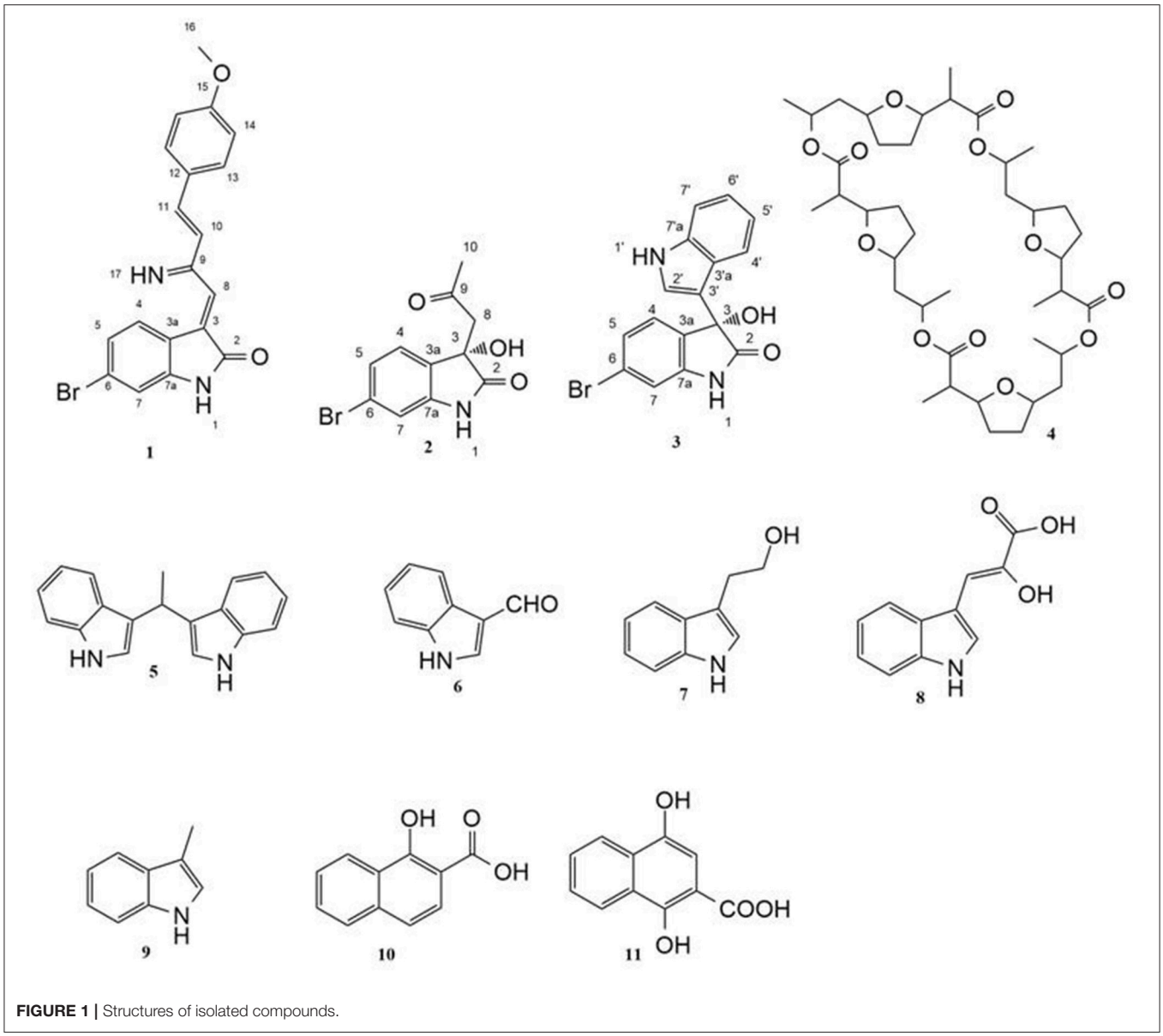

FIGURE 1 | Structures of isolated compounds.

isolation agar (AIA) (Lechevalier and Lechevalier, 1975) and marine agar (MA) (Weiner et al., 1985) were used for the isolation of actinomycetes. All media were supplemented with 0.2 μm pore size filtered cycloheximide (100 μg/mL), nystatin (25 μg/mL), and nalidixic acid (25 μg/mL) to facilitate the isolation of slow-growing actinomycetes. Cycloheximide and nystatin inhibit fungal growth, while nalidixic acid inhibits many fast-growing Gram-negative bacteria. All media contained DifcoBacto agar (18 g/L) and were prepared in 1 L artificial sea water (NaCl 234.7 g, $MgCl_2$.6 H_2O 106.4 g, Na_2SO_4 39.2 g, $CaCl_2$ 11.0 g, $NaHCO_3$ 1.92 g, KCl 6.64 g, KBr 0.96 g, H_3BO_3 0.26 g, $SrCl_2$ 0,24 g, NaF 0.03 g, and ddH_2O to 10.0 L) (Lyman and Fleming, 1940). The inoculated plates were incubated at 30°C for 6–8 weeks. Distinct colony morphotypes were picked and re-streaked until visually free of contaminants. *Saccharomonospora* sp. UR22 and *Dietzia* sp. UR66 were cultivated on ISP2 medium. The isolates were maintained on plates for short-term storage and long-term strain collections were set up in medium supplemented with 30% glycerol at −80°C.

Molecular Identification

16S rRNA gene amplification, cloning and sequencing were performed according to Hentschel et al. using the universal primers 27F and 1492R (Lane, 1991). Chimeric sequences were identified by using the Pintail program (Ashelford et al., 2005). The genus-level affiliation of the sequence was validated using the Ribosomal Database Project Classifier. The genus-level identification of all the sequences was done with RDP Classifier (-g 16srrna, -f allrank) and validated with the SILVA Incremental Aligner (SINA) (search and classify option) (Pruesse et al., 2012). An alignment was calculated again using the

SINA web aligner (variability profile: bacteria). Gap-only position were removed with trimAL (-noallgaps). For phylogenetic tree construction, the best fitting model was estimated initially with Model Generator. RAxML (-f a -m GTRGAMMA –x 12345 –p 12345 –# 1000) and the estimated model was used with 1,000 bootstrap resamples to generate the maximum-likelihood tree. Visualization was done with Interactive Tree of Life (ITOL).

Fermentation, Extraction, and Isolation

Each strain was fermented in 10 Erlenmeyer flasks (2 L), each containing 1 L of ISP 2 (International Streptomyces Project) medium in artificial sea water and incubated at 30°C for 14 days with shaking at 150 rpm. For co-cultivation experiment, 10 mL of 5-day-old culture of *Saccharomonospora* sp. UR22 was inoculated into 15 Erlenmeyer flasks (2 L), each containing 1 L of ISP 2 medium inoculated with 10 mL of 5-day-old culture of

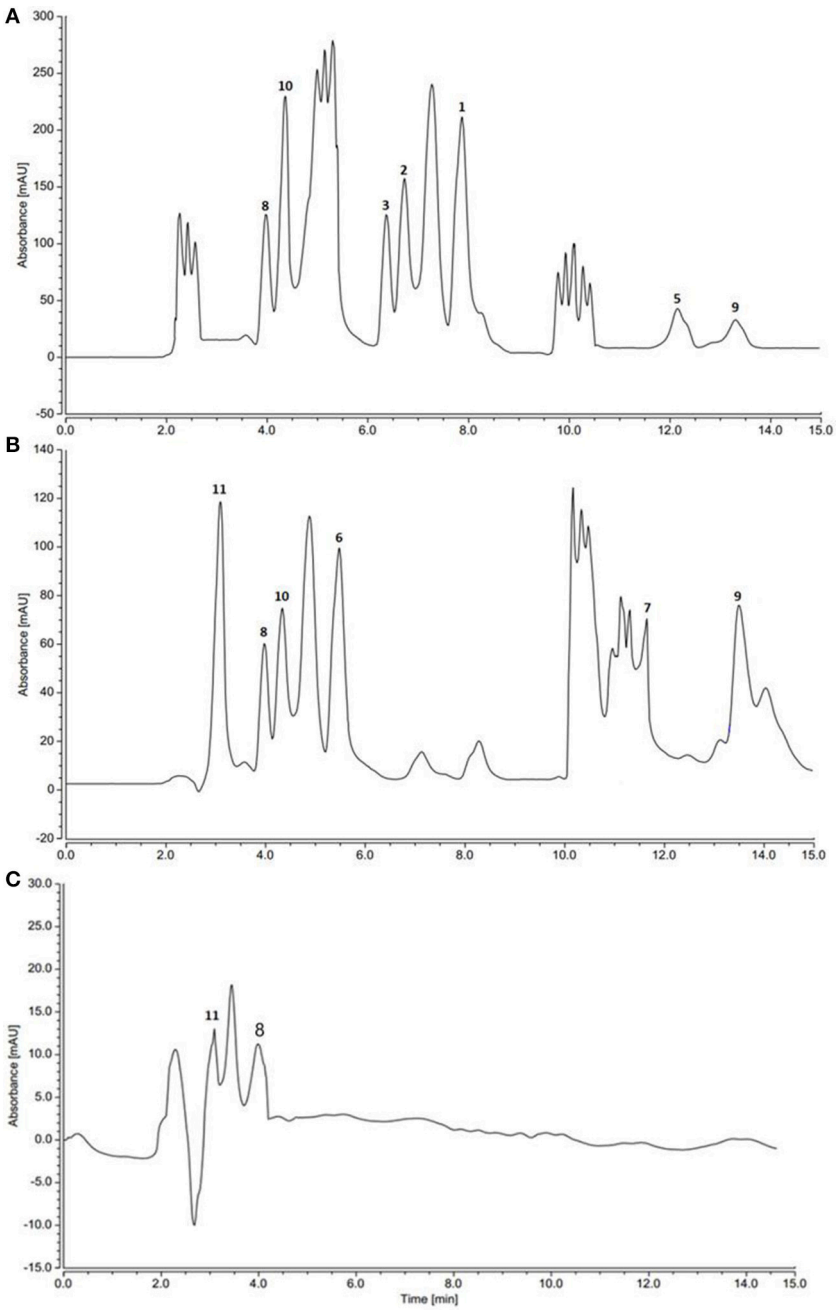

FIGURE 2 | HPLC profiles of actinomycetes extracts. **(A)** *Saccharomonospora* sp. UR22 and *Dietzia* sp. UR66 co-culture **(B)** *Saccharomonospora* sp. UR22 mono-culture **(C)** *Dietzia* sp. UR66 mono-culture.

*Dietzia*sp. UR66. After fermentation of single cultures and co-culture, filtration was done, and the supernatant was extracted with ethyl acetate (3 × 500 mL) to give the ethyl acetate extracts. These extracts (400 mg for *Saccharomonospora* sp. UR22, 950 mg for co-culture) were fractionated on a Sephadex LH20 (32-64 μm, 100 x 25 mm, Fluka®) column eluting with MeOH/H_2O (90:10%), to yield six fractions. Fraction Nr. 2 (from co-culture) was subjected to C18 reversed-phase column chromatography (0.04–0.063 mm, 50 × 10 mm, Merck®) with an isocratic elution using acetonitrile/water (40:60) to give five crude compounds **1-5**. Further purification was performed by preparative TLC on a (20 cm × 20 cm) silica gel plates that developed in CH_2Cl_2/MeOH/NH_3 (7:4:0.5, v/v) solvent system. Fraction Nr. 4 (from *Saccharomonospora* sp. UR22) was treated in the same manner to obtain six known compounds **6-11** (**Figure 1**).

HPLC Analysis

All actinomycete-derived extracts were analyzed by HPLC-DAD. Fifty micro liters (1 mg/mL in acetonitrile) of bacterial crude extracts was injected. Then, isocratic elution was performed with 50% aqueous acetonitrile containing 0.1% trifluoroacetic as amobile phase over 15 min at a flow rate of 1 mL/min and UV detection at different wavelengths (210, 254, 270, and 300 nm).

Pim-1 Kinase Assay

The kinase activity was measured following the manufacturer's instructions (HTScan Kinase Assays from Cell Signaling Technology) using staurosporine as a positive control. Different concentrations of test compounds were incubated with 50 ng of Pim-1 kinase enzyme in the reaction buffer [25 mM Tris–HCl pH 7.5, 10 mM $MgCl_2$, 0.1 mM Na_3VO_4, 5 mM–glycerophosphate, 2 mM dithiothreitol (DTT)] and the ATP/substrate cocktail [200 μM ATP + 1.5 μM biotinylated BAD Ser112 peptide] at room temperature for 30 min. The reaction was stopped by the addition of stop buffer (50 mM EDTA, pH 8) and transferred to a streptavidincoated 96-well plate. After incubation for 1 h at room temperature, the wells were washed three times with phosphate-buffered saline Tween-20 (PBST) buffer. After incubation with anti BADSer112 antibody for 2 h, the wells were washed three times with 1 × PBST and incubated with the peroxidase-conjugated secondary antibody for 30 min. Following three washes with 1 × PBST, the substrate (3,3,5,5-tetramethylbenzidine) was added and the samples were incubated at room temperature for 15 min. The reaction was stopped by the addition of 2 N HCl and the absorbance was measured with a spectrophotometer at 450 nm. The assay was performed in triplicate.

TABLE 1 | ^{1}H (400 MHz) and ^{13}C NMR (100 MHz) data for saccharomonosporine A (1) in DMSO-d_6.

Position	δ_H, mult. (*J* in Hz)	δ_C	Type	COSY	HMBC	NOESY
1-NH	7.98, br s				C-3a, C-2	
2		168.8	C			
3		143	C			
3a		122.6	C			
4	8.12, d, (8.8)	127.9	CH	H-5	C-6, C-3, C-7a	H-17
5	7.75, dd, (8.8, 2)	130	CH	H-4	C-6	
6		123.7	C			
7	8.2, d, (2)	131.1	CH			
7a		149.3	C			
8	7.96, s	118.2	CH		C-3a, C-9, C-2	H-10
9		157.4	C			
10	7.37, d, (16.4)	126	CH	H-11	C-8, C-12, C-9	H-13, H-8
11	7.88, d, (16.4)	136	CH	H-10	C-13, C-9	
12		129	C			
13	7.73, d, (8.8)	129.5	CH	H-14	C-11, C-15	H-10
14	7.03, d, (8.8)	114.9	CH	H-13	C-13, C-15, C-12	H-16
15		160.6	C			
16	3.81, s	55.7	CH_3		C-15	H-14
17-NH	8.3, br s					H-4

Docking Studies

The crystal structure of Pim-1 of PDB code 3umw was used. Docking experiments were conducted employing LigandFit docking engine. This docking software considers the ligand as flexible and the receptor as rigid structure. The binding site was generated from the "Find sites as volume of selected ligands" option in Discovery Studio 2.5. The number of trials of Monte Carlo search parameters = 30,000; and search step for torsions with polar hydrogens = 30.0°. The root mean square threshold for ligand-to-binding-site shape matching was set to 2.0 Å, employing a maximum of 1.0 binding-site partitions. The interaction energies were assessed employing the CFF force field (v.1.02) with a non-bonded cutoff distance of 10.0 Å and distance-dependent dielectric. An energy grid extending 5.0 Å from the binding site was implemented. The interaction energy was estimated with a trilinear interpolation value using soft potential energy approximations. Rigid body ligand minimization parameters: 40 steepest descent iterations followed by the 80 Broyden–Fletcher–Goldfarb–Shannon minimization iterations were applied to every orientation of the docked ligand. The proposed inhibitors were further energy minimized within the binding site by implementing the "Smart Minimization" option for a maximum of 1,000 iterations (Khanfar and Taha, 2013).

MTT Assay

Cell proliferation was evaluated in cell lines by the MTT assay in triplicates. 10^4 cells were plated in a 96-well microtiter plate in a final volume of 100 μl of culture medium. Cells were treated for 24 h with test compound at 37 °C with 5% CO_2. After treatment, the cells were immediately incubated with 10 μl MTT (5.0 mg/mL) for 4 h at 37°C. The cells were then lysed in 100 μl of lysis buffer (isopropanol, conc. HCl and Triton X-100) for 10 min at room temperature and 300 rpm/min shaking. The enzymatic reduction of MTT to formazan crystals that dissolved in DMSO was quantified by photometry at 570 nm.

Dose-response curves were generated and the IC_{50} values were define d as the concentration of compound required to inhibit cell proliferation by 50%. 5-Flurouracil was used as a positive control.

RESULTS AND DISCUSSION

Mono and Co-culture HPLC Profiles

HPLC and TLC analysis of EtOAc extracts obtained from axenic fermentation of each actinomycete compared to that from mixed fermentation indicated a very different chemical profiles (**Figure 2**). The co-culture derived extract showed a higher metabolic diversity than extracts from mono cultures. Exclusive detection of metabolites **1-5** in the co-culture illustrated that they are produced only upon co-fermentation of the two microbes.

Isolation and Structural Characterization

Guided by HPLC-DAD, the EtOAc extracts from the liquid cultures of the axenic fermentations and mixed fermentation were subjected to Sephadex LH-20 column chromatography followed by C_{18} reversed-phase column chromatography and final preparative TLC purification to target the isolation of the new metabolites **1** and **2** together with the other nine known metabolites **3-11**. Compound **1** was isolated as yellow amorphous powder. The molecular formula $C_{19}H_{15}O_2N_2Br$ was suggested on the basis of positive HRESIMS ion at *m/z* 383.0392 $[M+H]^+$, indicating 13 degrees of unsaturation. Furthermore, the presence of a bromine atom was confirmed by its characteristic isotope cluster (**Figure S1**). ^1H NMR spectral data of **1** (**Figure S2**) (**Table 1**) in DMSO-d_6 suggested the presence of a methyl singlet at δ_H 3.81 (3H, s, H-16) and two exchangeable protons (δ_H 8.32, 7.98) due to NH. The splitting pattern of resonances at δ_H 8.20 (H-7), 8.12 (H-4), and 7.75 (H-5) together with the COSY correlation (**Figure S5**) between (H-4) and (H-5) suggested the presence of a 1,3,4-trisubstituted benzene ring. On the other hand, the signals at δ_H 7.73 (H-13), 7.03 (H-14) and the ^1H-^1H COSY correlation between them indicated

TABLE 2 | ^1H (400 MHz) and ^{13}C NMR (100 MHz) data for 2 in DMSO-d_6.

Position	δ_H, mult. (*J* in Hz)	δ_C	Type	COSY	HMBC
1-NH	10.37, br s	-			C-2, C-3a
2	-	178.0	C		
3	-	72.3	C		
3a	-	131.0	C		
4	7.19, d, (9)	125.5	CH	H-5	C-6, C-3, C-3a
5	7.09, dd, (9, 2)	123.8	CH	H-4	
6	-	121.6	C		
7	6.93, d, (2)	112.3	CH		
7a	-	144.4	C		
8	3.05, d, (18)	50.0	CH_2		C-9, C-3a, C-2
	3.33, d, (18)				
9	-	205.3	C		
10	2.0, s	30.4	CH_3		C-9, C-8
11-OH	6.07, br s	-			

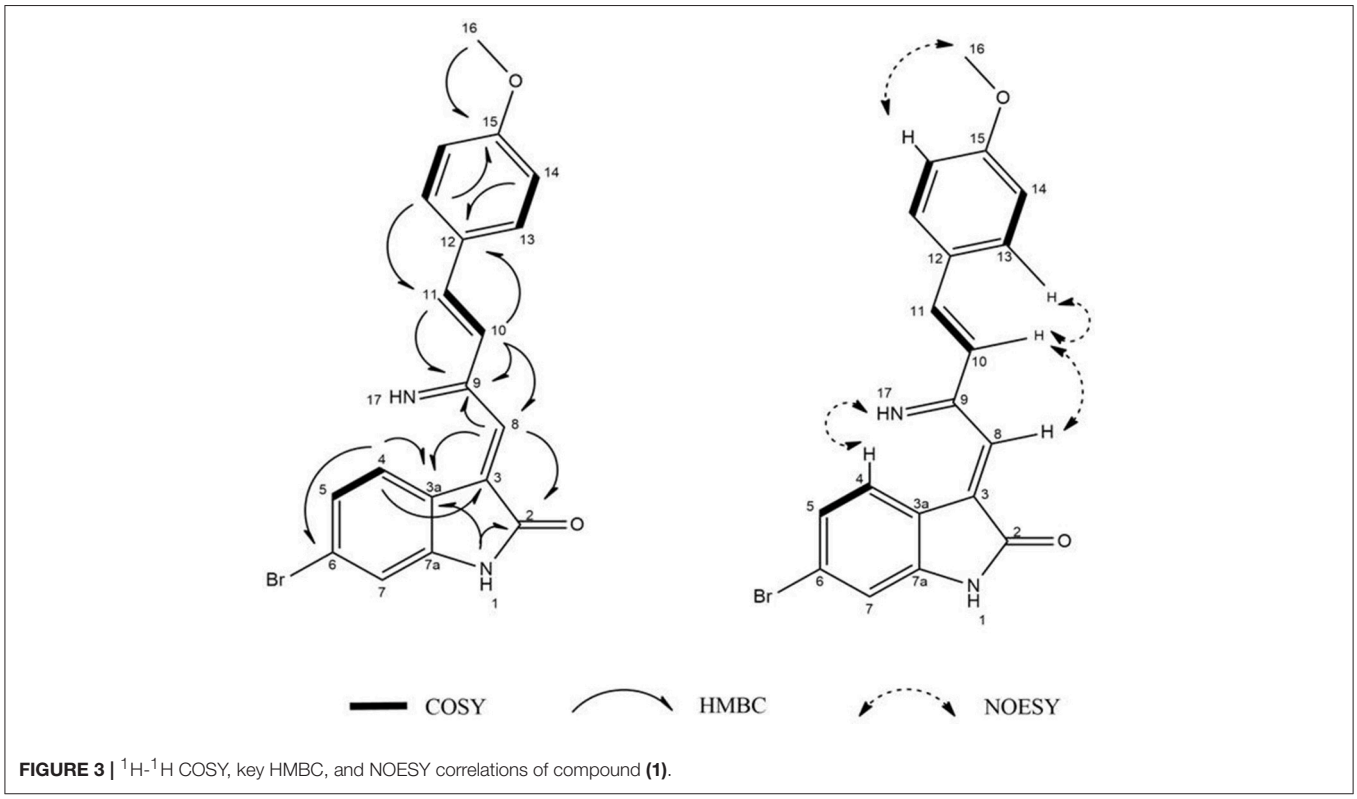

FIGURE 3 | ^1H-^1H COSY, key HMBC, and NOESY correlations of compound **(1)**.

the presence of 1,4 disubstituted benzene ring. The DEPTQ spectrum (**Figure S3**) (**Table 1**) displayed seventeen signals, with eight sp^2 aromatic carbons including eight CH groups and six quaternary carbons, and one sp^3 aliphatic carbon (CH_3 group). The spectra also revealed an aminocarbonyl at δ_C168.8 (C-2), an imino carbon at δ_C 157.4 (C-9) and one oxygenated carbon at δ_C 55.7 (C-16). The assignment of protonated carbons was achieved by the HSQC data (**Figure S4**). The key HMBC correlations (**Figure S6**) from H-4 (δ_H 8.12) to C-3 (δ_C 143), and from the exchangeable proton H-1(δ_H 7.98) to the carbonyl carbons C-2 (δ_C 168.8) and C-3a (δ_C 122.6) together with the previous reported data (Guo et al., 2010) suggested the presence of brominated indolin-2-one skeleton at C-6 (δ_C 123.7). The sub-structure of a methoxyphenyl group was deduced from the HMBC correlation between the methyl protons H-16 (δ_H 3.81) and C-15 (δ_C 160.6). ^{1}H-^{1}H COSY correlation between H-11 (δ_H 7.88) and H-10 (δ_H 7.37) together with HMBC correlations from H-11 to C-10 (δ_C 126) and C-9 (δ_C 157.4), from H-10 to C-9 and C-8 (δ_C 118.2) indicated the presence of an imino butenylidene moiety. The *E* configuration of H-11 (δ_H 7.88, d) and H-10 (δ_H 7.37, d) was deduced from the *J*-values extracted from the ^{1}H NMR spectrum (J = 16.4 H_z). The connection of the imino butenylidene moiety to the methoxyphenyl group was established through the HMBC correlation from H-13 (δ_H 7.73) to C-11 (δ_C 136). Moreover, the HMBC correlations (**Figure 3**) from H-8 (δ_H 7.96) to C-2 (δ_C 168.8) and C-3a (δ_C 122.6) connected this moiety to the indolin-2-one skeleton at C-3. The chemical shifts of H-8 at δ_H 7.96 and H-4 at δ_H 8.12 are very characteristic for *E* configuration at the double bond between C-3 and C-9 (Faita et al., 1994). Furthermore, NOESY correlation (**Figures S7, S8**) between the NH proton H-17 and H-4, and absence of NOESY cross-peak between H-8 and H-4, also pointed to the *E* configuration at the C-3/C-8 double bond. On that basis, the structure of **1** was established as (*E*)-6-bromo-3-((*E*)-2-imino-4-(4-methoxyphenyl)but-3-en-1-ylidene)indolin-2-one,

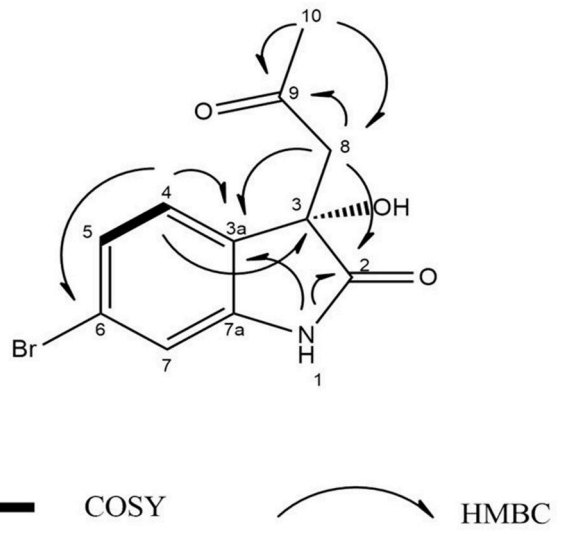

FIGURE 4 | ^{1}H-^{1}H COSY, key HMBC, and NOESY correlations of compound **(2)**.

a new secondary metabolite to which were named as **Saccharomonosporine A.**

Compound **2** was isolated as white crystals, the molecular formula $C_{11}H_{10}O_3NBr$ was suggested on the basis of positive HRESIMS ion at *m/z* 283.9899 $[M+H]^+$, indicating seven degrees of unsaturation. Furthermore, the presence of a bromine atom was confirmed by its characteristic isotope cluster (**Figure S9**). Similar to compound **1**, the ^{1}H and ^{13}C NMR spectra (**Figures S10**, **S11**) of **2** (**Table 2**) also revealed an aminocarbonyl at δ_C178.0 and one oxygenated carbon at δ_C 72.3 (C-3). The key HMBC correlations (**Figure 4** and **Figure S14**) from H-4 (δ_H 7.19) to C-3 (δ_C 72.3), and from the exchangeable proton H-1(δ_H 10.37) to the carbonyl carbons C-2 (δ_C 178) and C-3a (δ_C 131) together with the previous reported data (Guo et al., 2010) suggested the presence of brominated indolin-2-one skeleton. A 2-oxopropyl unit was deduced from the HMBC cross-peaks of H-8 (δ_H 3.05) to C-9 (δ_C 205.3), H-10 (δ_H 2.0) to C-8 (δ_C 50), and H-10 to C-9 and was indicated to be attached at C-3 (δ_C 72.3) through the HMBC correlation of H-8 to C-3. These spectroscopic data together with the optical rotation value $[\alpha]_D^{25}$ –13.8 (*c* 0.85, MeOH), revealed that this compound is the previously unreported (*S*) enantiomer of (*R*)-6-Bromo-3-hydroxy-3-(2 oxopropyl)indolin-2-one, a synthetic 3-hydroxyoxindole derivative (Guo et al., 2010). Several 3-hydroxyoxindole derivatives have been reported from natural marine sources (Kamano et al., 1995; Zhang et al., 1995). For example, convolutamydine A, a brominated (*R*) enantiomer of **2** (Kamano et al., 1995), so the name **convolutamydine F** was suggested to compound **2**.

Compound **3** was isolated as white crystals. HRESIMS, 1D and 2D NMR spectral data (**Table S1**, **Figures S15–S20**) revealed that compound **3** has a planer structure identical to compound 3f, a previously reported synthetic intermediate (Wang and Ji, 2006), which obtained as a racemic mixture. Compound **3** had a negative optical rotation of $[\alpha]_D^{25}$ −8.7 (*c* 0.3, MeOH), in contrast to previous reports on similar optically active compounds that showed a positive optical rotations for the (*R*) enantiomers (Deng et al., 2010; Guo et al., 2010). On this basis compound **3** was identified as (*S*) 6-bromo-3-hydroxy-3-(1H-indol-3-yl)

TABLE 3 | *In-vitro* Pim-1 kinase inhibitory activity of isolated metabolites.

Tested Compound	IC_{50} ± S.D. (μM)[a]
1	0.3 ± 0.02
2	>20
3	0.97 ± 0.01
4	>20
5	>20
6	>20
7	>20
8	>20
9	>20
10	>20
11	>20
Staurosporine	0.04 ± 0.01

[a] *Values are a mean of 3 independent experiments.*

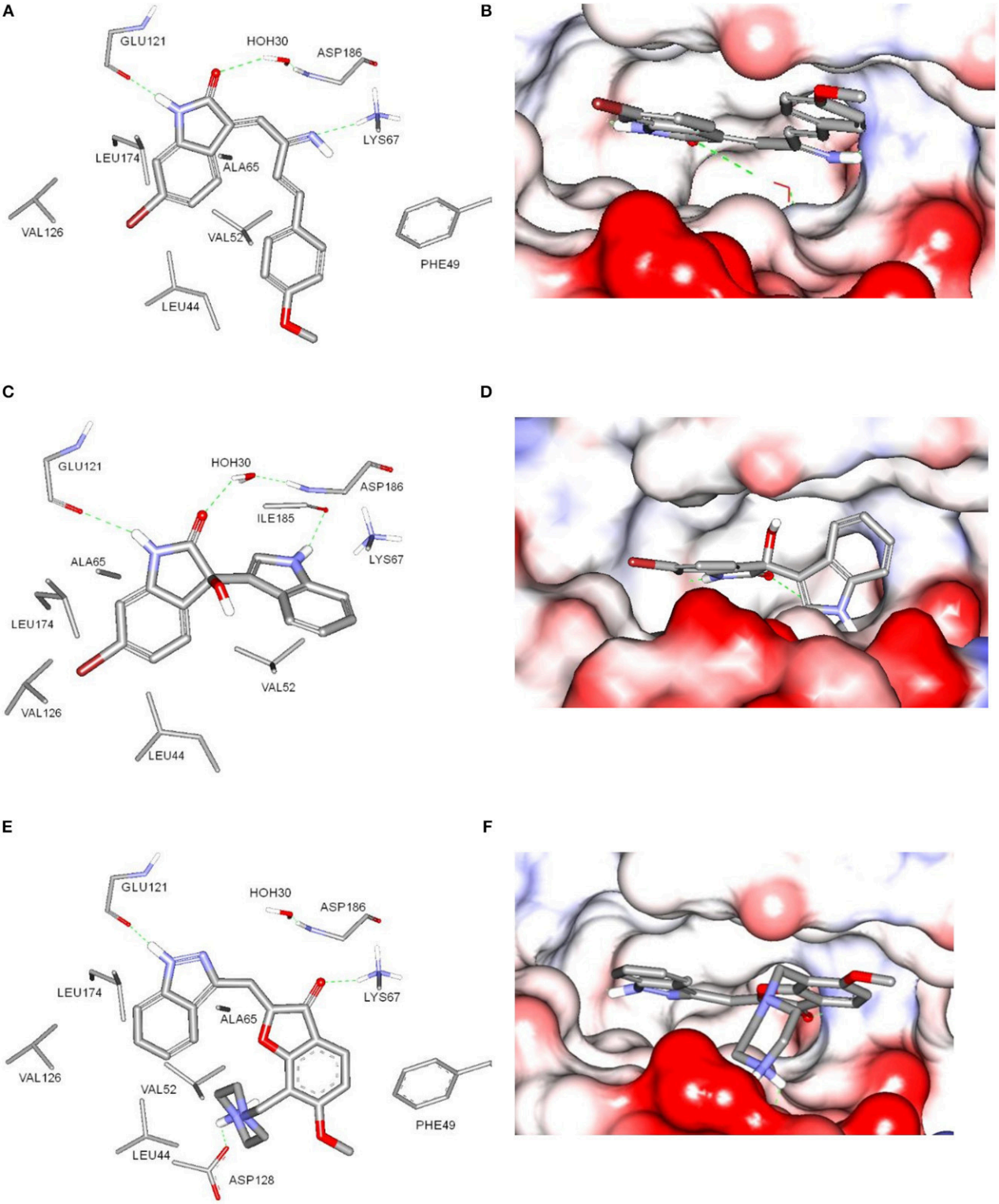

FIGURE 5 | Docking of compounds **1 (A,B)** and **3 (C,D)** within the ATP-binding site of Pim-1 kinase (PDB code 3umw). **(E,F)** The key binding interactions of Pim-1 co-crystallized ligand. The amino acid side chains were depicted in **(A,C,E)** for clarification.

indolin-2-one. To the best of our knowledge, compounds **2** and **3** are considered the first (*S*) 3-hydroxyoxindole derivatives reported from natural sources. Nonactin (**4**) (Wu and Sun, 2006) and vibrindole (**5**) (Ronit et al., 1994) were also isolated from the co-culture of *Saccharomonospora* sp. UR22 and *Dietzia* sp. UR66. In addition, indole-3-carbaldehyde (**6**) (Ashour et al., 2007), tryptophol (**7**) (Gore et al., 2012), indole-3-pyruvic acid (**8**) (Wishart et al., 2007), skatole (**9**) (Chen et al., 2015), 1-hydroxy-2-naphthoic acid (**10**) (Kauko and Lajunen, 1978) and 1,4 dihydroxy-2-naphthoic acid (**11**) (Isawa et al., 2002) were isolated from the axenic culture of *Saccharomonospora* sp. UR22. All isolated known metabolites were identified based on their accurate mass analyses and comparison of their NMR spectroscopic data (**Figures S21–S28**) with those reported in the literature.

Pim-1 Kinase Assay

Pim-1 kinase is a well-established oncoprotein in several tumor entities, e.g., myeloid leukemia, prostate cancer, colorectal cancer, or pancreatic cancer (Weirauch et al., 2013). In addition, over expression of Pim-1 kinase has been described in both human colon adenocarcinoma HT-29 cell (Weirauch et al., 2013) and human promyelocytic leukemia HL-60 (Fan et al., 2016) cell lines. Treatment of the aforementioned cell lines with Pim-1 kinase inhibitors resulted in a potent growth inhibitory activity (Weirauch et al., 2013; Fan et al., 2016). Furthermore, previous compounds structurally similar to compounds **1** and **3** showed potent and selective Pim-1 kinase inhibitory activity (Nakano et al., 2012; Sun et al., 2015). In order to investigate Pim-1 kinase as a potential target that mediates tumor cell growth inhibitory effect, all isolated compounds were evaluated for their efficacy to inhibit the *in vitro* enzymatic activity of Pim-1 kinase (**Table 3**). Compounds **1** and **3** exhibited significant inhibitory effects on Pim-1 enzyme activity with an IC_{50} value of 0.3 ± 0.02 and 0.95 ± 0.01 μM, respectively.

Docking of the Active Compounds

The potential binding mode of compounds **1** and **3** with Pim-1 kinase was analyzed by docking in the ATP-binding site of Pim-1. The protein data bank (PDB) contains several Pim-1 crystallographic proteins, however, Pim-1 of PDB code (3umw) was selected for docking experiments since it has optimum resolution (2.08 Å) and is co-crystalized with Pim-1 inhibitor that is structurally similar to compound **1** and **3** (Nakano et al., 2012). The sphere surrounding the co-crystallized inhibitor was selected as an active site for docking. Both compounds **1** and **3** showed similar docking poses (**Figure 5**) and comparable to the co-crystalized inhibitor (Nakano et al., 2012). The bromobenzene moiety of compound **1** is impeded within a hydrophobic pocket of ALA65, LEU44, VAL126, and LEU175. The oxindole proton of amidic group is interacted with the hinge region through hydrogen bonding to the main chain carbonyl of GLU121. Hydrogen bonding of this nature was reported with several Pim-1 inhibitors (Nakano et al., 2012). Moreover, the oxindole carbonyl oxygen is hydrogen bonded to the peptidic proton of ASP186 bridged through the conserved water molecule (HOH30). The imine nitrogen of compound **1** is hydrogen bonded to the terminal amino moiety of LYS67. The phenoxy ring is sandwiched between two hydrophobic surfaces of PHE49 and VAL52 (**Figure 5A**). Alternatively, compound **3** share similar interactions as in compound **1** within the hydrophobic pocket of ALA65, LEU44, VAL126, and LEU175, and hydrogen bonding interaction with GLU121 and ASP186. Moreover, the indole nitrogen is hydrogen bonded with peptidic oxygen of ILE185. However, the interaction with LYS67 is a π-cation interaction with the indole ring of compound **3** (**Figure 5C**). The binding interactions of compounds **1** and **3** showed high resemblance with the binding mode of the co-crystalized ligand (PDB code: 3umw) within the ATP-binding site of Pim-1 (Nakano et al., 2012). The co-crystalized structure forms similar hydrogen bonding interactions (with GLU121 and LYS67), hydrophobic interactions (with LEU174, VAL126, LEU44, VAL52, and ALA65), and π-stacking (with PHE49) as with compounds **1** and **3** (**Figure 5E**). However, the co-crystalized ligand forms additional electrostatically-enforced hydrogen bonding interaction with ASP128. Such interaction can explain the superior activity of the co-crystalized ligand (IC_{50} = 3 nM) over compounds **1** and **3**. Therefore, the electrostatic interaction with ASP128 should be taking into consideration for future designing of more active analogs of compounds **1** and **3**.

Antiproliferative Activity

The antiproliferative properties of the nine isolated compounds were evaluated against lung adenocarcinoma H1650, the human promyelocytic leukemia HL-60 and the human colon adenocarcinoma HT-29 cell lines (**Table 4**). Compounds **1** and **3** displayed potent antiproliferative activity against HL-60 and HT-29 cells (IC_{50} 2.8, 3.6 and 4.2, 3.7 μM, respectively). The other compounds did not exhibit any cytotoxicity at the tested concentrations. These results came in great accordance with the Pim-1 kinase assay results.

Data for Saccharomonosporine A (1)

Yellow powder (18 mg); UV (MeOH) λ_{max} (log ε) 343 (4.22), 425 (3.16); IR (KBr) ν_{max} 3165, 1716, 1605, 1570, cm^{-1}; ^{1}H-NMR

TABLE 4 | Antiproliferative activity of isolated metabolites against H1650, HL-60, and HT-29 cancer cells.

Tested Compounds	IC_{50} ± S.D. (μM)[a]		
	H1650	HL-6	HT-29
1	>100	2.8 ± 0.74	3.6 ± 0.55
2	>100	>100	>100
3	>100	4.2 ± 0.23	3.7 ± 0.31
4	>100	>100	>100
5	>100	>100	>100
6	>100	>100	>100
7	>100	>100	>100
8	>100	>100	>100
9	>100	>100	>100
10	>100	>100	>100
11	>100	>100	>100
5-Flurouracil	0.5 ± 0.67	0.2 ± 0.43	0.3 ± 0.35

[a] *Values are a mean of 3 independent experiments.*

(DMSO-d_6, 400 MHz); and ^{13}C-NMR (DMSO-d_6, 100 MHz) data, see **Table 1**; HRESIMS *m/z* 383.0392 $[M + H]^+$ (calcd for $C_{19}H_{15}O_2N_2Br$).

Data for Convolutamydine F (2)

White crystals (10 mg); UV (MeOH) λ_{max} (log ε) 323 (3.18), 408 (2.83); $[\alpha]_D^{25}$ –13.8 (*c* 0.85, MeOH), IR (KBr) ν_{max} 3331, 1742, 1714 cm^{-1}; ^{1}H-NMR (DMSO-d_6, 400 MHz) and ^{13}C-NMR (DMSO-d_6, 100 MHz) data, see **Table 2**; HRESIMS *m/z* 283.9899 $[M + H]^+$ (calcd for $C_{11}H_{10}O_3NBr$).

CONCLUSION

In this study, two sponge-derived actinomycetes, *Saccharomonospora* sp. UR22 and *Dietzia* sp. UR66, were co-fermented in liquid media. The presence of induced metabolites was studied by comparison of the HPLC-DAD and TLC chromatograms of the crude extracts of the two axenic cultures and the co-culture. Co-cultivation of *Saccharomonospora* sp. UR22 and *Dietzia* sp. UR66 induced the biosynthesis of novel oxindole alkaloid saccharomonosporine A (**1**), convolutamydine F (**2**) along with other three induced metabolites (**3-5**) which were not detected in either microorganism in a single culture. Axenic culture of *Saccharomonospora* sp. UR22 led to isolation of common known microbial metabolites **6-11**. Compounds **1** and **3** exhibited potent antiproliferative activities toward HL-60 and HT-29. Based on previous reports on similar compounds, Pim-1 inhibitory assay results and docking studies in the ATP-binding site of Pim-1 kinase, we suggested that both compounds **1** and **3** mediated their cytotoxicity by inhibiting the well-known oncoprotein Pim-1 kinase. These findings highlighted the co-cultivation approach as an effective strategy to enhance the chemical diversity of the secondary metabolites hidden in the genomes of the marine actinomycetes.

AUTHOR CONTRIBUTIONS

SE, RM, and HH designed the experiments. TM collected and identified the marine sponge. AS, HH, and UA performed the experiments and isolated the compounds. AS and MR performed data acquisition and structure elucidation. DH and TG performed the biological assays. MK performed the docking study. UA, RM, MR, TG, AS and MK drafted and revised the manuscript.

FUNDING

Research in the TAMG lab is generously funded by the DFB (GU 1233/1-1, CIPSM). This work was supported by the German Research Foundation (DFG) and the Technical University of Munich (TUM) in the framework of the Open Access Publishing Program.

ACKNOWLEDGMENTS

We would also like to thank Dr. Mohammed E. Deraz for his support in the HPLC analysis work.

SUPPLEMENTARY MATERIAL

The Supplementary Material for this article can be found online at: https://www.frontiersin.org/articles/10.3389/fchem.2018.00538/full#supplementary-material

REFERENCES

Abdelmohsen, U. R., Bayer, K., and Hentschel, U. (2014a). Diversity, abundance and natural products of marine sponge-associated actinomycetes. *Nat. Prod. Rep.* 31, 381–399. doi: 10.1039/c3np70111e

Abdelmohsen, U. R., Cheng, C., Viegelmann, C., Zhang, T., Grkovic, T., Ahmed, S., et al. (2014b). Dereplication strategies for targeted isolation of new antitrypanosomal actinosporins A and B from a marine sponge associated-*Actinokineospora* sp. EG49. *Mar. Drugs* 12, 1220–1244. doi: 10.3390/md12031220

Ashelford, K. E., Chuzhanova, N. A., Fry, J. C., Jones, A. J., and Weightman, A. J. (2005). At least 1 in 20 16S rRNA sequence records currently held in public repositories is estimated to contain substantial anomalies. *Appl. Environ. Microbiol.* 71, 7724–7736. doi: 10.1128/AEM.71.12.7724-7736.2005

Ashour, M. A., Elkhayat, E. S., Ebel, R., Edrada, R., and Proksch, P. (2007). Indole alkaloid from the Red Sea sponge *Hyrtios erectus*. *ARKIVOC* 2007, 225–231. doi: 10.3998/ark.5550190.0008.f22

Chen, S., Lu, G. P., and Cai, C. (2015). Iridium-catalyzed methylation of indoles and pyrroles using methanol as feedstock. *RSC Adv.* 86, 70329–70332. doi: 10.1039/C5RA15822B

Cueto, M., Jensen, P. R., Kauffman, C., Fenical, W., Lobkovsky, E., and Clardy, J. (2001). Pestalone, a new antibiotic produced by a marine fungus in response to bacterial challenge. *J. Nat. Prod.* 64, 1444–1446. doi: 10.1021/np0102713

Dashti, Y., Grkovic, T., Abdelmohsen, U. R., Hentschel, U., and Quinn, R. J. (2014). Production of induced secondary metabolites by a co-culture of sponge-associated actinomycetes, *Actinokineospora* sp. EG49 and *Nocardiopsis* sp. RV163. *Mar. Drugs* 12, 3046–3059. doi: 10.3390/md12053046

Deng, J., Zhang, S., Ding, P., Jiang, H., Wang, W., and Li, J. (2010). Facile creation of 3-indolyl-3-hydroxy-2-oxindoles by an organocatalytic enantioselective Friedel–Crafts reaction of indoles with isatins. *Adv. Synth. Catal.* 352, 833–838. doi: 10.1002/adsc.200900851

Eltamany, E. E., Abdelmohsen, U. R., Ibrahim, A. K., Hassanean, H. A., Hentschel, U., and Ahmed, S. A. (2014). New antibacterial xanthone from the marine sponge-derived *Micrococcus* sp. EG45. *Bioorg. Med. Chem. Lett.* 24, 4939–4942. doi: 10.1016/j.bmcl.2014.09.040

Faita, G., Mella, M., Righetti, P. P., and Tacconi, G. (1994). An easy lewis acid-mediated isomerization from (E)-to (Z)-oxoindolin-3-ylidene ketones. *Tetrahedron* 37, 10955–10962. doi: 10.1016/S0040-4020(01)85706-9

Fan, Y. B., Huang, M., Cao, Y., Gong, P., Liu, W. B., Jin, S. Y., et al. (2016). Usnic acid is a novel Pim-1 inhibitor with the abilities of inhibiting growth and inducing apoptosis in human myeloid leukemia cells. *RSC Adv.* 6, 24091–24096. doi: 10.1039/C6RA01159D

Feling, R. H., Buchanan, G. O., Mincer, T. J., Kauffman, C. A., Jensen, P. R., and Fenical, W. (2003). Salinosporamide A: a highly cytotoxic proteasome inhibitor from a novel microbial source, a marine bacterium of the new genus *Salinospora*. *Angew. Chem. Int. Ed.* 42, 355–357. doi: 10.1002/anie.200390115

Fenical, W., Jensen, P. R., Palladino, M. A., Lam, K. S., Lloyd, G. K., and Potts, B. C. (2009). Discovery and development of the anticancer agent salinosporamide A (NPI-0052). *Bioorg. Med. Chem.* 17, 2175–2180. doi: 10.1016/j.bmc.2008.10.075

Gore, S., Baskaran, S., and König, B. (2012). Fischer indole synthesis in low melting mixtures. *Org. Lett.* 17, 4568–4571. doi: 10.1021/ol302034r

Gulder, T. A. M., and Moore, B. S. (2010). The salinosporamide natural product family: potent 20S proteasome inhibitors as potential cancer chemotherapeutics. *Angew. Chem. Int. Ed.* 49, 9346–9367. doi: 10.1002/anie.201000728

Guo, Q., Bhanushali, M., and Zhao, C.G. (2010). Quinidine thiourea-catalyzed aldol reaction of unactivated ketones: highly enantioselective synthesis of 3-alkyl-3-hydroxyindolin-2-ones. *Angew. Chem. Int. Ed.* 49, 9460–9464. doi: 10.1002/anie.201004161

Hentschel, U., Schmid, M., Wagner, M., Fieseler, L., Gernert, C., and Hacker, J. (2001). Isolation and phylogenetic analysis of bacteria with antimicrobial activities from the mediterranean sponges *Aplysina aerophoba* and *Aplysina cavernicola*. *FEMS Microbiol. Ecol.* 35, 305–312. doi: 10.1111/j.1574-6941.2001.tb00816.x

Hong, K., Gao, A. H., Xie, Q. Y., Gao, H. G., Zhuang, L., Lin, H. P., et al. (2009). Actinomycetes for marine drug discovery isolated from mangrove soils and plants in China. *Mar. Drugs* 7, 24–44. doi: 10.3390/md7010024

Isawa, K., Hojo, K., Yoda, N., , Kamiyama, T., Makino, S, Saito, M., et al. (2002). Isolation and identification of a new bifidogenic growth stimulator produced by *Propionibacterium freudenreichii* ET-3. *Biosci. Biotech. Biochem.* 3, 679–681. doi: 10.1271/bbb.66.679

Kamano, Y., Zhang, H. P., Ichihara, Y., Kizu, H., Komiyama, K., and Pettit, G.R. (1995). Convolutamydine A, a novel bioactive hydroxyoxindole alkaloid from marine bryozoan *Amathia convoluta*. *Tetrahedron Lett.* 36, 2783–2784. doi: 10.1016/0040-4039(95)00395-S

Kauko, R., and Lajunen, L. H. J. (1978). NMR Studies on aromatic compounds I-13C NMR spectra of some mono- and disulphonato-substituted hydroxynaphthoic acids in DMSO-&water solution. *Mag. Res. Chem.* 11, 12–15. doi: 10.1002/mrc.1270110104

Khanfar, M., and Taha, M. (2013). Elaborate ligand-based modeling coupled with multiple linear regression and K nearest neighbor QSAR analyses unveiled new nanomolar mTOR inhibitors. *J. Chem. Inform. Model.* 53, 2587–2612. doi: 10.1021/ci4003798

Lane, D. J. (1991). "16S/23S rRNA sequencing," in *Nucleic Acid Techniques in Bacterial Systematics*, eds. E. Stackebrandt, and M. Goodfellow (Chichester: John Wiley and Sons), 115–175.

Lechevalier, M. P., and Lechevalier, H.A. (1975). Actinoplanete with cylindrical sporangia, actinoplanes-*Rectilineatus* sp. nov. *Int. J. Syst. Bacteriol.* 25, 371–376. doi: 10.1099/00207713-25-4-371

Lyman, J., and Fleming, R. (1940). Composition of seawater. *J. Mar. Res.* 3, 134–146.

Mincer, T. J., Jensen, P. R., Kauffman, C. A., and Fenical, W. (2002). Widespread and persistent populations of a major new marine actinomycete taxon in ocean sediments. *Appl. Environ. Microbiol.* 68, 5005–5011. doi: 10.1128/AEM.68.10.5005-5011.2002

Nakano, H., Saito, N., Parker, L., Tada, Y., Abe, M., Tsuganezawa, K., et al. (2012). Rational evolution of a novel type of potent and selective proviral integration site in moloney murine leukemia virus kinase 1 (PIM1) inhibitor from a screening-hit compound. *J. Med. Chem.* 55, 5151–5164. doi: 10.1021/jm3001289

Oh, D. C., Jensen, P. R., Kauffman, C. A., and Fenical, W. (2005). Libertellenones A–D: induction of cytotoxic diterpenoid biosynthesis by marine microbial competition. *Bioorg. Med. Chem.* 13, 5267–5273. doi: 10.1016/j.bmc.2005.05.068

Oh, D. C., Kauffman, C. A., Jensen, P. R., and Fenical, W. (2007). Induced production of emericellamides A and B from the marine-derived fungus *Emericella* sp. in competing co-culture. *J. Nat. Prod.* 70, 515–520. doi: 10.1021/np060381f

Olson, J. B., Lord, C. C., and McCarthy, P. J. (2000). Improved recoverability of microbial colonies from marine sponge samples. *Microb. Ecol.* 40, 139–147. doi: 10.1007/s002480000058

Pettit, R.K. (2009). Mixed fermentation for natural product drug discovery. *Appl. Microbiol. Biotechnol.* 83, 19–25. doi: 10.1007/s00253-009-1916-9

Pruesse, E., Peplies, J., and Glockner, F.O. (2012). SINA: accurate high-throughput multiple sequence alignment of ribosomal RNA genes. *Bioinformatics* 28, 1823–1829. doi: 10.1093/bioinformatics/bts252

Rateb, M. E., , Hallyburton, I., Houssen, W. E., , Bull, A. T., Goodfellow, M., Santhanam, R., et al. (2013). Induction of diverse secondary metabolites in *Aspergillus fumigatus* by microbial co-culture. *RSC Adv.* 3, 14444–14450. doi: 10.1039/c3ra42378f

Ronit, B., Carmeli, S., and Sar, N. (1994). Vibrindole A, a metabolite of the marine bacterium, *Vibrio parahaemolyticus*, isolated from the toxic mucus of the boxfish *Ostracion cubicus*. *J. Nat. Prod.* 11, 1587–1590.

Roue, M., Quevrain, E., Domart-Coulon, I., and Bourguet-Kondracki, M. L. (2012). Assessing calcareous sponges and their associated bacteria for the discovery of new bioactive natural products. *Nat. Prod. Rep.* 29, 739–751. doi: 10.1039/c2np20040f

Schroeckh, V., Scherlach, K., Nutzmann, H. W., Shelest, E., Schmidt-Heck, W., Schuemann, J., et al. (2009). Intimate bacterial–fungal interaction triggers biosynthesis of archetypal polyketides in *Aspergillus* nidulans. *Proc. Natl. Acad. Sci.* 106, 14558–14563. doi: 10.1073/pnas.0901870106

Shirling, E., and Gottlieb, D. (1966). Methods for characterization of *Streptomyces* species. *Int. J. Syst. Bacteriol.* 16, 317–327. doi: 10.1099/00207713-16-3-313

Simmons, L., Kaufmann, K., Garcia, R., Schwar, G., Huch, V., and Muller, R. (2011). Bendigoles D–F, bioactive sterols from the marine sponge-derived *Actinomadura* sp. SBMs009. *Bioorg. Med. Chem.* 19, 6570–6575. doi: 10.1016/j.bmc.2011.05.044

Sun, H. B., Wang, X. Y., Li, G. B., Zhang, L. D., Liu, J., and Zhao, L. F. (2015). Design, synthesis and biological evaluation of novel C3-functionalized oxindoles as potential Pim-1 kinase inhibitors. *RSC Adv.* 5, 29456–29466. doi: 10.1039/C5RA00177C

Tabares, P., Pimentel-Elardo, S. M., Schirmeister, T., Hunig, T., and Hentschel, U. (2011). Anti-protease and immunomodulatory activities of bacteria associated with Caribbean sponges. *Mar. Biotechnol.* 13, 883–892. doi: 10.1007/s10126-010-9349-0

Thomas, T. R., Kavlekar, D. P., and LokaBharathi, P. A. (2010). Marine drugs from sponge-microbe association—A review. *Mar. Drugs* 8, 1417–1468. doi: 10.3390/md8041417

Viegelmann, C., Parker, J., Ooi, T., Clements, C., Abbott, G., Young, L., et al. (2014). Isolation and identification of antitrypanosomal and antimycobacterial active steroids from the sponge *Haliclona simulans*. *Mar. Drugs* 12, 2937–2952. doi: 10.3390/md12052937

Wakefield, J., Hassan, H. M., Jaspars, M., Ebel, R., and Rateb, M. E. (2017). Dual induction of new microbial secondary metabolites by fungal bacterial co-cultivation. *Front. Microbiol.* 8:1284. doi: 10.3389/fmicb.2017.01284

Wang, S. Y., and Ji, S. J. (2006). Facile synthesis of 3,3-di (heteroaryl) indolin-2-one derivatives catalyzed by ceric ammonium nitrate (CAN) under ultrasound irradiation. *Tetrahedron* 62, 1527–1535. doi: 10.1016/j.tet.2005.11.011

Weiner, R. M., Segall, A. M., and Colwell, R. R. (1985). Characterization of a marine bacterium associated with *Crassostrea Virginica* (the Eastern Oyster). *Appl. Environ. Microbiol.* 49, 83–90.

Weirauch, U., Beckmann, N., Thomas, M., Grünweller, A., Huber, K., Bracher, F., et al. (2013). Functional role and therapeutic potential of the pim-1 kinase in colon carcinoma. *Neoplasia* 15, 783–794. doi: 10.1593/neo.13172

Wishart, D. S., Tzur, D., Knox, C., et al. (2007). HMDB: the human metabolome database. *Nucleic Acids Res.* 35, D521–D526. doi: 10.1093/nar/gkl923

Wu, Y., and Sun, Y.P. (2006). Synthesis of nonactin and the proposed structure of trilactone. *Org. Lett.* 13, 2831–2834. doi: 10.1021/ol0609661

Yi-Lei, N., Yun-Dan, W., Chuan-Xi, W., Ru, L., Yang, X., Dong-Sheng, F., et al. (2014). Compounds from marine-derived *Verrucosispora* sp. FIM06054 and their potential antitumour activities *Nat. Prod. Res.* 28, 2134–2139. doi: 10.1080/14786419.2014.926350

Zhang, H. P., Kamano, Y., Ichihara, Y., Kizu, H., Komiyama, K., Itokawa, H., et al. (1995). Isolation and structure of convolutamydines B∼D from marine bryozoan *Amathia convoluta*. *Tetrahedron* 51, 5523–5528. doi: 10.1016/0040-4020(95)00241-Y

Zuck, K. M., Shipley, S., and Newman, D. J. (2011). Induced production of *N*-formyl alkaloids from *Aspergillus fumigatus* by co-culture with *Streptomyces peucetius*. *J. Nat. Prod.* 74, 1653–1657. doi: 10.1021/np200255f

Conflict of Interest Statement: The authors declare that the research was conducted in the absence of any commercial or financial relationships that could be construed as a potential conflict of interest.

frontiers in Chemistry

ORIGINAL RESEARCH
published: 07 December 2018
doi: 10.3389/fchem.2018.00605

(±)-Peniorthoesters A and B, Two Pairs of Novel Spiro-Orthoester en-antiomers With an Unusual 1,4,6-Trioxaspi-ro[4.5]decane-7-One Unit From *Penicillium minioluteum*

Xiaorui Liu†, Chunmei Chen†, Yinyu Zheng, Mi Zhang, Qingyi Tong, Junjun Liu, Qun Zhou, Jianping Wang, Zengwei Luo, Hucheng Zhu and Yonghui Zhang**

Hubei Key Laboratory of Natural Medicinal Chemistry and Resource Evaluation, School of Pharmacy, Tongji Medical College, Huazhong University of Science and Technology, Wuhan, China

OPEN ACCESS

Edited by:
Bin-Gui Wang,
Institute of Oceanology (CAS), China

Reviewed by:
Dipesh Dhakal,
Sun Moon University, South Korea
Christophe Salome,
SpiroChem AG, Switzerland

***Correspondence:**
Hucheng Zhu
zhuhucheng@hust.edu.cn
Yonghui Zhang
zhangyh@mails.tjmu.edu.cn

†These authors have contributed equally to this work

Specialty section:
This article was submitted to Medicinal and Pharmaceutical Chemistry, a section of the journal Frontiers in Chemistry

Received: *02 August 2018*
Accepted: *26 November 2018*
Published: *07 December 2018*

Citation:
Liu X, Chen C, Zheng Y, Zhang M, Tong Q, Liu J, Zhou Q, Wang J, Luo Z, Zhu H and Zhang Y (2018) (±)-Peniorthoesters A and B, Two Pairs of Novel Spiro-Orthoester en-antiomers With an Unusual 1,4,6-Trioxaspi-ro[4.5]decane-7-One Unit From Penicillium minioluteum. Front. Chem. 6:605. doi: 10.3389/fchem.2018.00605

(±)-Peniorthoesters A and B (±**1** and ±**2**), two pairs of unprecedented spiro-orthoester enantiomers with a 1,4,6-trioxaspiro[4. 5]decane-7-one unit, were obtained from *Penicillium minioluteum*. Their structures were determined by spectroscopic methods, X-ray diffraction analyses, and ECD calculations. (±)-Peniorthoesters A and B are the first examples of spiro-orthoester enantiomers, and they represent the first spiro-orthoesters originating from fungi. All compounds showed potential inhibitory activities comparable to dexamethasone against NO production with IC_{50} values ranging from 14.2 to 34.5 μM.

Keywords: peniorthoesters, *Penicillium minioluteum*, spiro-orthoester, enantiomers, NO production inhibition activity

INTRODUCTION

Orthoesters, a special functional group characterized by three alkoxy groups attached to a single carbon atom, are unusual structural subunits in natural products (Liao et al., 2009). Natural occurring orthoesters include several major types, such as daphnane diterpenoid orthoesters (He et al., 2002), limonoid orthoesters (Roy and Saraf, 2006), steroid orthoesters (Steyn and van Heerden, 1998), and coumarinoid orthoesters (Santana et al., 2004). In our previous study on the plant Wikstroemia chamaedaphne, three new daphnane type diterpenoids with orthoester group were isolated (Guo et al., 2015). A literature investigation revealed that most of these orthoesters originate from plants, and only a few originate from fungi, such as novofumigatonin, a meroterpenoid orthoester from *Aspergillus novofumigatus* (Rank et al., 2008). As a special class of natural products, orthoesters have attracted great attention due to their diverse structures and biological properties (Liao et al., 2009; Bourjot et al., 2014; Li et al., 2015; Liu et al., 2017).

Fungi have historically played an important role in drug discovery. The genus *Penicillium* has been shown to be a rich source of structurally unique and biologically active secondary metabolites (Meng et al., 2016; Sun et al., 2016; Luo et al., 2017) and many metabolites from *Penicillium* are clinically used drugs with penicillin as a representative compound. Previous studies on the secondary metabolites of *Penicillium minioluteum* have resulted in the identification of scores of bioactive metabolites, including isomeric furanones with cytotoxic activities against HeLa cell lines (Tang et al., 2015), sesquiterpene-conjugated amino acids with cytotoxic activities against HepG2 cells (Ngokpol et al., 2015), and hybrid polyketide-terpenoids (Iida et al., 2008). This fungus

was also used to produce clovane derivatives, which are the raw materials for the synthesis of rumphellclovane A (Gontijo de Souza et al., 2012), and an enzyme from this fungus was used in the bioconversion (Kmiecik and Zymanczyk-Duda, 2017). During our ongoing search for structurally unique and biologically interesting constituents from fungi (Zhu et al., 2015; Chen et al., 2017; Zhou et al., 2017), *P. minioluteum*, obtained from China General Micro-biological Culture Collection Center (CGMCC), was phytochemically investigated, and two pairs of new orthoesters (**Figure 1**, compounds ±**1** and ±**2**) were isolated along with their biosynthetic intermediate, sclerotinin A (**3**) (Xiao et al., 2009). The structures and absolute configurations of (±)-**1** and (±)-**2** were determined by a combination of spectroscopic methods, X-ray diffraction analyses, and ECD calculations. (±)-Penicorthoesters A (±**1**) and B (±**2**) are the first examples of spiro-orthoester enantiomers and represent the first spiro-orthoesters originating from fungi.

MATERIALS AND METHODS

General Experimental Procedures

Optical rotations were determined in acetonitrile and dichloromethane on a PerkinElmer 341 polarimeter. UV spectra were obtained on Varian Cary 50 spectrometer. ECD spectra were obtained with a JASCO J-810 spectrometer. IR spectra were acquired on a Bruker Vertex 70 instrument. NMR spectra were recorded on Bruker AM-400 spectrometers, and the ^{1}H and ^{13}C NMR chemical shifts were referenced to the solvent or solvent impurity peaks for CD_3Cl at δ_H 7.26 and δ_C 77.20. HRESIMS data were acquired in the positive-ion mode on a Thermo Fisher LC-LTQ-Orbitrap XL spectrometer. The crystallographic experiments were performed on a Bruker APEX DUO diffractometer equipped with graphite-monochromated Cu Kα radiation (λ = 1.541 78 Å). Semi-preparative HPLC was carried out on an instrument consisting of an Agilent 1,220 controller, an Agilent 1,220 pump, an Agilent UV detector, with a reversed-phased C18 column (5 μm, 10 × 250 mm, Welch Ultimate XB-C18), an Ultimate SiO_2 column (5 μm, 10 × 250 mm, Welch Materials, Inc.), and a Chiralpak IC column (5 μm, 4.6 × 250 mm, Daicel Chiral Technologies Co., Ltd., China). Chromatography coloums (CC) were performed on silica gel (200–300 mesh; Qingdao Marine Chemical, Inc., Qingdao, China), Sephadex LH-20 (40–70 μm, Amersham Pharmacia Biotech AB, Uppsala, Sweden), and ODS (50 μm, Merck, Germany). Thin-layer chromatographies (TLC) was performed with RP-C_{18} F_{254} plates (Merck, Germany) and silica gel 60 F_{254} (Yantai Chemical Industry Research Institute).

Fungal Material and Fermentation

The strain in this work was bought from China General Micro-biological Culture Collection Center (CGMCC). A voucher Specimen was preserved in the herbarium of Huazhong University of Science and Technology, China. The fungal strain was cultured on potato dextrose agar (PDA) at 28°C for 8 days to prepare the seed culture. Then the strain was inoculated into 200 Erlenmeyer flasks (1 L each) which had previously been sterilized by autoclaving. Each flask contained 250 g rice and 200 mL distilled water. The flasks were incubated at 20°C for 26 days.

Extraction and Isolation

The fermented rice substrate was extracted six times in 95% aqueous EtOH at room temperature. The 95% aqueous EtOH extracts were concentrated under vacuum to afford a residue (1.5 kg). The residue was suspended in H_2O and successively partitioned with petroleum ether and EtOAc. The EtOAc partition fraction (630.0 g) was subjected to a silica gel chromatograph column (CC) using petroleum ether–EtOAc and EtOAc–MeOH gradient elution to give five fractions. Fraction 2 (20.0 g) was chromatographed on C18 reversed phase (RP-18) silica gel CC (gradient elution of MeOH–H_2O, 20:80–100:0) to give seven subfractions, named Fr. 2A−2G. Fr.2F was successively separated via Sephadex LH-20 CC (CH_2Cl_2-MeOH, 1:1) and further purified by RP-C_{18} HPLC to afford compounds **1** and **2** (MeCN–H_2O, 45:55, 3.5 ml/min, **1** at t_R 53.2 min, 6.0 mg; **2** at t_R 56.7 min, 5.1 mg). Subsequently, the separation of **1** by chiral HPLC using a Daicel IC column eluting with isopropanol–n-hexane (5:95) afforded (+)-**1** (t_R 28.0 min, 2.1 mg) and (−)-**1** (t_R 30.1 min, 2.0 mg). The enantiomers (+)-**2** (t_R 8.2 min, 1.6 mg) and (−)-**2** (t_R 11.1 min, 2.7 mg) were also obtained by chiral HPLC using a Daicel IC column eluting with isopropanol–*n*-hexane (10:90).

*Compounds (±)-**1***: white powder; [α] ±0 (c 0.4, MeCN); UV (MeCN) λ_{max} (log ε) 216 (4.50), 259 (4.23), 329 (4.04) nm; IR (KBr) ν_{max} 3,435, 2,982, 2,936, 1,661, 1,612, 1,456, 1,420, 1,383, 1,341, 921, 883, 809, 753 cm^{-1}; ^{1}H NMR ($CDCl_3$, 400 MHz) and ^{13}C NMR ($CDCl_3$, 100 MHz) data, see **Table 1**; HRESIMS *m/z* 307.1538 $[M + H]^+$ (calcd for $C_{17}H_{23}O_5$, 307.1545).

*(+)-**1***: white amorphous powder; $[\alpha]_D^{25}$ +37 (c 0.1, CH_2Cl_2); ECD (MeCN) 229 (Δε +1.63), 254 (Δε +4.75), 325 (Δε −0.99) nm.

*(−)-**1***: white amorphous powder; $[\alpha]_D^{25}$ −36 (c 0.1, CH_2Cl_2); ECD (MeCN) 229 (Δε −1.66), 254 (Δε −4.34), 325 (Δε +1.23) nm.

*Compounds (±)-**2***: white powder; $[\alpha]_D^{25}$ ±0 (c 0.3, MeCN); UV (MeCN) λ_{max} (log ε) 216 (4.60), 259 (3.99), 329 (3.71) nm; IR (KBr) ν_{max} 3,435, 2,980, 2,932, 1,669, 1,612, 1,456, 1,421, 1,379, 1,339, 920, 881, 810, 763 cm^{-1}; ^{1}H NMR ($CDCl_3$, 400 MHz) and ^{13}C NMR ($CDCl_3$, 100MHz) data, see **Table 1**; HRESIMS *m/z* 307.1534 $[M + H]^+$ (calcd for $C_{17}H_{23}O_5$, 307.1545).

*(+)-**2***: white amorphous powder; $[\alpha]_D^{25}$ +30 (c 0.1, CH_2Cl_2); ECD (MeCN) 224 (Δε +2.37), 258 (Δε +4.64), 319 (Δε −0.84) nm.

*(−)-**2***: white amorphous powder; $[\alpha]_D^{25}$ −30 (c 0.1, CH_2Cl_2); ECD (MeCN) 224 (Δε −2.42), 258 (Δε −6.58), 319 (Δε +1.60) nm.

Computational Details

The crystal structure of 9*R*,10*S*,11*S*-**1,** and 9*R*,10*R*,11*R*-**2** were optimized at the B3LYP/6-31G(d) level in acetonitrile with the IEFPCM solvation model using Gaussian 09 program. The harmonic vibrational frequencies were calculated to confirm the stability of the optimized structure. The electronic

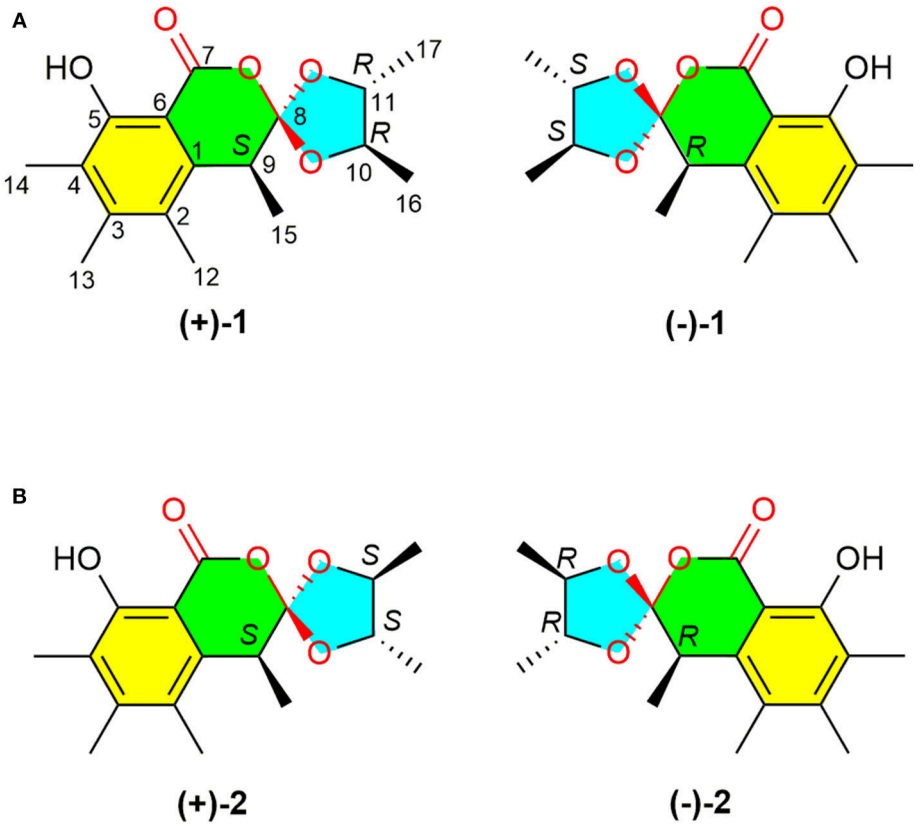

FIGURE 1 | Structures of (±)-peniorthoesters A (±**1**) and B (±**2**).

circular dichroism (ECD) spectrum were calculated using the TDDFT methodology at the LC-wPBE/6-311++G(d,p) level with acetonitrile as solvent by the IEFPCM solvation model implemented in Gaussian 09 program. The ECD spectra was simulated using a Gaussian function with a bandwidth σ of 0.3 eV. The UV correction was applied to generate the final spectra (Zhu, 2015).

Single-Crystal X-ray Diffraction Analysis and Crystallographic Data

Crystallographic data of compound **1** (CCDC 1840165): $C_{17}H_{22}O_5$, $M = 306.34$, monoclinic, $T = 297(2)$ K, $\lambda = 1.54178$ Å, colorless platelet (crystallized from distilled water at room temperature), size 0.12 × 0.10 × 0.10 mm3, $a = 11.7937(4)$ Å, $b = 32.5593(12)$ Å, $c = 8.1659(3)$ Å, $\alpha = 90.00°$, $\beta = 91.95(2)°$, $\gamma = 90.00°$, $V = 3{,}133.84(19)$ Å3, space group $P21/c$, $Z = 8$, $Dc = 1.299$ g/cm^3, μ(CuKα) = 0.782 mm^{-1}, $F_{(000)} = 1312$, 48082 reflections and 5,729 independent reflections ($R_{int} = 0.0528$) were collected in the θ range of $2.71° \leq \theta \leq 69.99°$ with index ranges of $h(-14/14)$, $k(-39/39)$, $l(-9/9)$, completeness θmax = 98%, data/restraints/parameters 5,729/0/412. Largest difference peak and hole = 0.257 and −0.184 e Å−3. The final R_1 values were 0.0489 ($I > 2\sigma(I)$). The final $wR(F^2)$ values were 0.1364 ($I > 2\sigma(I)$). The final R_1 values were 0.0521 (all data). The final $wR(F^2)$ values were 0.1381 (all data). The goodness of fit on F^2 was 1.045.

Crystallographic data of compound **2** (CCDC 1840166): $C_{17}H_{22}O_5$, $M = 306.34$, monoclinic, $T = 297(2)$ K, $\lambda = 1.54178$ Å, colorless platelet (crystallized from distilled water at room temperature), size 0.12 × 0.10 × 0.10 mm3, $a = 7.4709(2)$ Å, $b = 8.9377(12)$ Å, $c = 13.5720(3)$ Å, $\alpha = 92.43°$, $\beta = 100.25(2)°$, $\gamma = 113.76°$, $V = 809.60(19)$ Å3, space group P-1, $Z = 2$, $Dc = 1.257$ g/cm^3, μ(CuKα) = 0.757 mm^{-1}, $F_{(000)} = 328$, 14,855 reflections and 2,814 independent reflections ($R_{int} = 0.0374$) were collected in the θ range of $5.45° \leq \theta \leq 70.86°$ with index ranges of $h(-8/7)$, $k(-10/10)$, $l(-16/16)$, completeness θmax = 95%, data/restraints/parameters 2,814/0/207. Largest difference peak and hole = 0.232 and −0.241 e Å−3. The final R_1 values were 0.0588 ($I > 2\sigma(I)$). The final $wR(F^2)$ values were 0.1750 ($I > 2\sigma(I)$). The final R_1 values were 0.0647 (all data). The final $wR(F^2)$ values were 0.1855 (all data). The goodness of fit on F^2 was 1.076.

Determination of No Production

RAW 264.7 cells were obtained from the Boster Biological Technology Co., Ltd (Wuhan, China) and maintained in DMEM containing 10% heat-inactived fetal bovine serum (FBS) (Gibco BRL Co, Grand Island, NY, United States) at 37°C in humidified incubator containing 5% CO_2. All tested compounds were dissolved in DMSO (the final concentration of DMSO was

TABLE 1 | ^{1}H and ^{13}C NMR Spectroscopic Data for **1** and **2** (in $CDCl_3$).

No.	1			2		
	δ_C	type	δ_H (mult., *J* in Hz)	δ_C	type	δ_H (mult., *J* in Hz)
1	137.8	C		137.6	C	
2	123.5	C		123.6	C	
3	145.7	C		145.7	C	
4	123.7	C		123.8	C	
5	158.8	C		158.7	C	
6	103.5	C		103.7	C	
7	170.3	C		170.2	C	
8	124.0	C		124.0	C	
9	38.4	CH	3.31 q (7.1)	38.5	CH	3.33 q (7.0)
10	81.7[a]	CH	3.91 dq (8.5, 6.1)[a]	81.1[a]	CH	3.84 dq (8.1, 6.2)[a]
11	79.3[a]	CH	4.18 dq (8.5, 6.1)[a]	79.8[a]	CH	4.36 dq (8.1, 6.2)[a]
12	14.7	CH_3	2.17 s	14.6	CH_3	2.17 s
13	17.5	CH_3	2.25 s	17.4	CH_3	2.24 s
14	11.9	CH_3	2.20 s	11.9	CH_3	2.20 s
15	16.9	CH_3	1.30 d (7.1)	17.2	CH_3	1.30 brd (6.3)
16	16.7[a]	CH_3	1.47 d (6.1)[a]	16.7[a]	CH_3	1.30 brd (6.1)[a]
17	18.4[a]	CH_3	1.25 d (6.1)[a]	18.6[a]	CH_3	1.39 d (6.1)[a]
HO-5			11.41 s			11.41 s

[a]*Interchangeable assignments between the two $CHCH_3$ groups.*

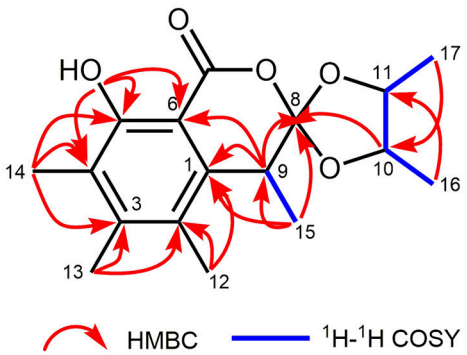

FIGURE 2 | Key 1H−1H COSY and HMBC correlations of **1**.

<0.25% in assay). RAW 264.7 cells were seeded into 48-well plates (1×10^5cells/well) for 24 h and then pretreated with different concentrations (1–40 μM) of test compounds. After being incubated for 3 h, the cells were stimulated with 100 ng/ml LPS (final concentration) for another 24 h. Dexamethasone was used as the positive control in the experiment. NO content in the supernatant was measured using Griess reagent. The absorbance at 540 nm was measured on a microplate reader. All the experiments were performed in three independent replicates.

Cytotoxic Activity

Cell lines were cultured in RPMI-1640 or DMEM medium (HyClone, USA), supplemented with 10% fetal bovine serum (HyClone, USA) at 37°C in a humidified atmosphere with 5% CO_2. For cell viability assay, cells were plated into 96-well plates in 50 μl of medium and then compounds were serially diluted in medium and delivered to the cells as 2 × solutions in 50 μl of medium. After 48 h, cell viability was detected by a CCK-8 Kit (Dojindo,Japan) according to the instruction. Growth relative to untreated cells was calculated (positive control, anticancer drug VP16), and this data was used for the dose-response curve, the IC_{50} (50% inhibiting concentration) of compounds to each cell lines were calculated by SPSS.

RESULTS AND DISCUSSIONS

Compound **1** was isolated as a white powder. Its UV spectrum exhibited absorption maxima at 216 and 260 nm. Its IR spectrum indicated the presence of an OH functionality (3,435 cm^{-1}), a conjugated carbonyl group (1,661 cm^{-1}), and an aromatic ring (1,612 and 1,456 cm^{-1}). The molecular formula of **1** was determined to be $C_{17}H_{22}O_5$ by HRESIMS with an $[M + H]^+$ ion peak at *m/z* 307.1538 (calcd for $C_{17}H_{23}O_5$, 307.1545), implying seven degrees of unsaturation. The ^{1}H NMR spectroscopic data of **1** (**Table 1**) revealed the presence of two oxygenated methines [δ_H 4.18 (1H, dq, $J = 8.5$, 6.1 Hz, H-11) and 3.91 (1H, dq, $J = 8.5$, 6.1 Hz, H-10)], one sp^3 methine [δ_H 3.31, 1H, q, $J = 7.1$ Hz, H-9], and six methyl groups [δ_H 1.47 (d, $J = 6.1$ Hz, H_3-16), 1.30 (d, $J = 7.1$ Hz, H_3-15), 1.25 (d, $J = 6.1$ Hz, H_3-17), 2.17 (s, H_3-12), 2.20 (s, H_3-14), and 2.25 (s, H_3-13)]. The ^{13}C NMR spectrum of **1** exhibited signals assignable to a conjugated carbonyl (δ_C 170.3), a hexa-substituted benzene ring [δ_C 158.8, 145.7, 137.8,

123.7, 123.5, and 103.5], one oxygenated quaternary carbon (δ_C 124.0), six methyl groups and three methines (including two oxygenated ones). The above analyses confirmed the presence of an ester carbonyl group and a hexa-substituted benzene ring, which account for five degrees of unsaturation, indicating the presence of two additional rings. With the aid of the HSQC spectrum, all protons were unambiguously assigned to their respective carbons.

The planar structure of **1** was elucidated on the basis of ^{1}H–^{1}H COSY and HMBC experiments (**Figure 2**). The HMBC spectrum of **1** displayed correlations from H_3-14 to C-3, C-4, and C-5; from H_3-13 to C-2, C-3, and C-4; from H_3-12 to C-1, C-2, and C-3; and from H-9 to C-1, and C-6, which together with the HMBC correlations from the OH to C-4, C-5, and C-6 constructed the hexa-substituted benzene ring. In addition, two spin systems of H_3-17/H-11/H-10/H_3-16 and H-9/H_3-15 were established from the ^{1}H–^{1}H COSY spectrum. Therefore, the HMBC correlations from H-9 to C-1, C-6, and C-8 and from H_3-15 to C-1, C-8, and C-9 suggested the C-15/C-9/C-8 fragment was connected to the benzene ring via C-9. Moreover, the ester carbonyl (δ_C 170.3) was connected to C-6 based on the chemical shifts of C-6 (δ_C 103.5), C-1 (δ_C 137.8), and C-3 (δ_C 145.7). Combined with the chemical shifts of C-10 (δ_C 81.7) and C-11 (δ_C 79.3), the C-17/C-11/C-10/C-16 fragment was proposed to be a 2,3-butanediol unit, which should be linked with C-8 and form a 4,5-dimethyl-1,3-dioxolane moiety. Finally, a lactone ring was proposed between C-7 and C-8 to satisfy the above deduced tricyclic ring system as well as the chemical shift of C-8 (δ_C 124.0). This planar structure satisfied all of the correlations observed in the 2D NMR spectra and the chemical shifts in the 1D NMR spectra.

A NOESY experiment was performed on **1**, but no interactions useful for determining the relative configuration were observed. Unfortunately, the relative configuration of H-10 and H-11 could also not be determined from their coupling constants because they were located on a five-membered ring. To confidently assign the configuration of **1**, we tried to crystallize it so we could use X-ray single-crystal analysis. After a number of attempts, a high-quality single-crystal of **1** was finally obtained from a mixture of methyl alcohol and water. The X-ray crystallography data (CCDC 1840165) obtained with Cu Kα radiation confirmed the structure of **1** (**Figure 3**). However, because it has a centrosymmetric monoclinic space group of chiral $P2_1/c$, indicating the crystal is racemic, the absolute configuration of **1** could not be determined. After analyses by using various types of chiral columns, the racemic nature of this solution was further confirmed by the presence of two peaks in the HPLC chromatogram acquired using a chiral Daicel IC column (**Figure 4**). Finally, compounds (+)-**1** and (−)-**1** were successfully obtained, and they showed specific rotations with opposite signs {(+)-**1**: $[\alpha]_D^{20}$+37 (c 0.1, CH_2Cl_2); (−)-**1**: $[\alpha]_D^{20}$-36 (c 0.1, CH_2Cl_2)}. In addition, the ECD spectra of (+)-**1** and (−)-**1** displayed similar signal intensities but mirror-image Cotton effects (**Figure 5**).

The absolute configurations of the two enantiomers of (±)-**1** were further determined by comparing their experimental ECD spectra with those predicted by time-dependent density functional theory (TDDFT) calculations at the B3LYP/6-31G(d) level. As shown in **Figure 5**, the calculated ECD curve of 9*R*,10*S*,11*S*-**1** displayed good agreement with the experimental

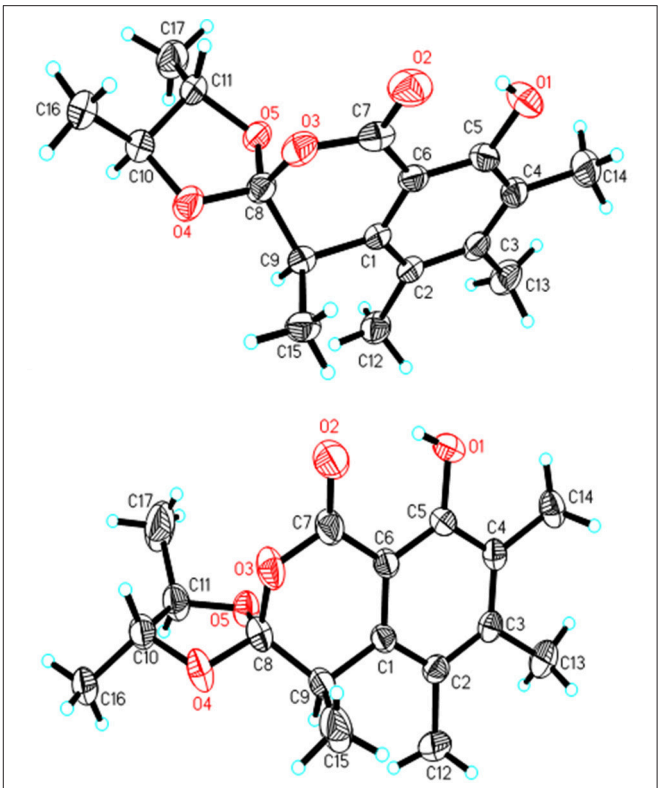

FIGURE 3 | X-ray structures of **1** and **2**.

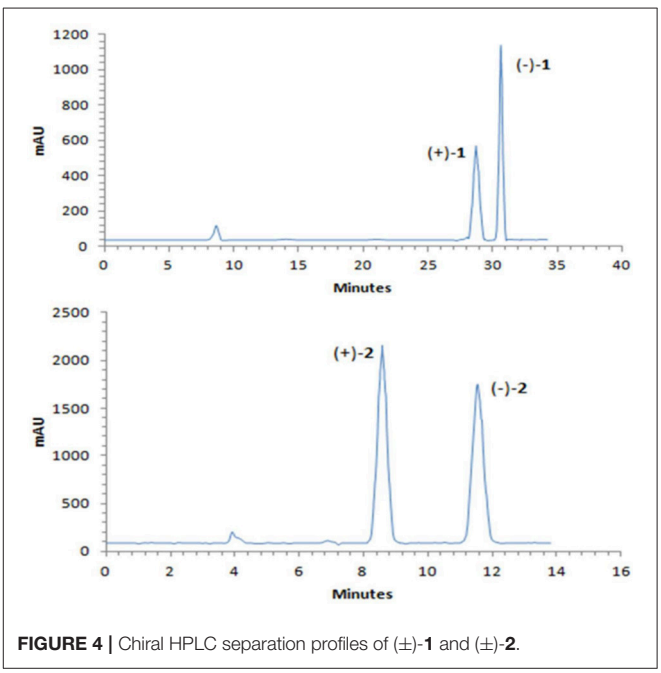

FIGURE 4 | Chiral HPLC separation profiles of (±)-**1** and (±)-**2**.

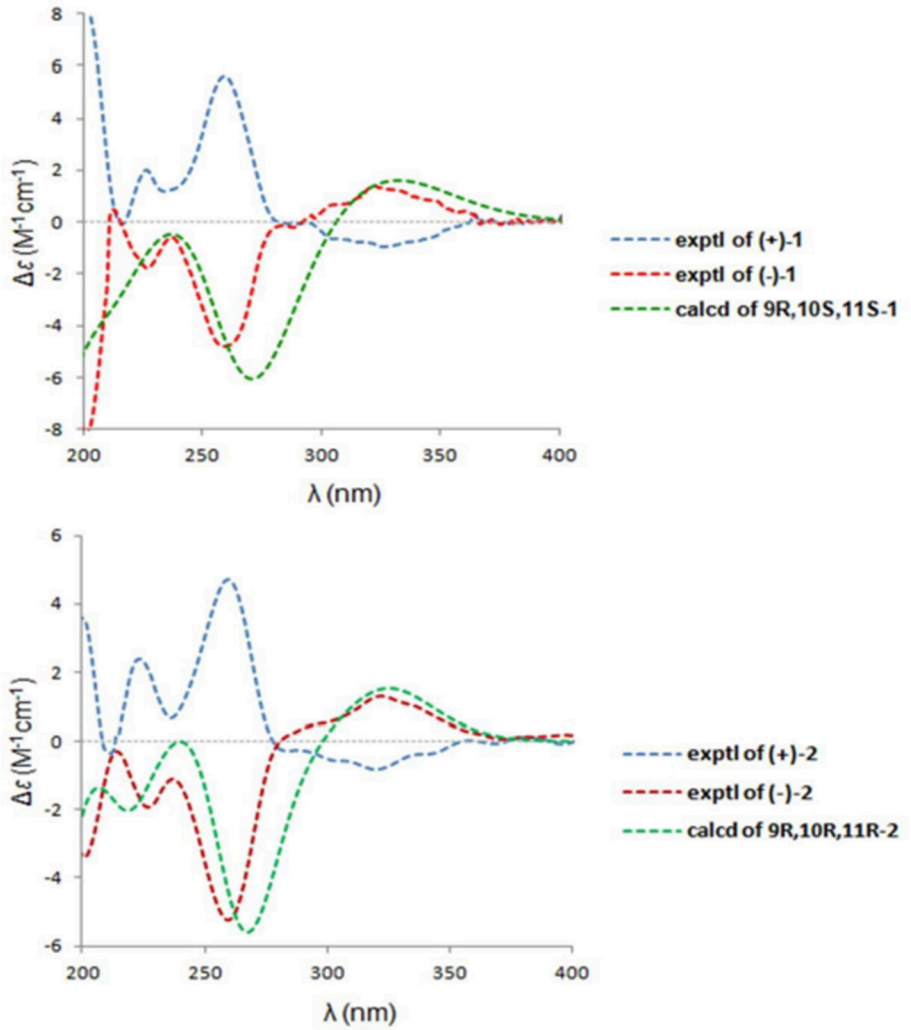

FIGURE 5 | The experimental ECD spectra of (±)-**1** and (±)-**2** and the cal-culated ECD curves.

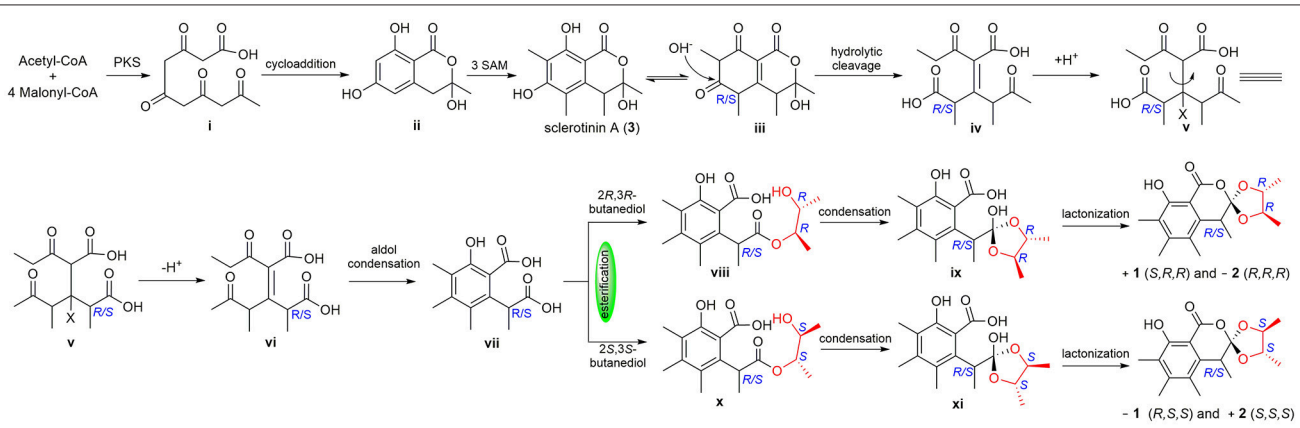

FIGURE 6 | Proposed biosynthetic pathway of **1** and **2**.

curve of (–)-**1**. Therefore, the absolute configurations of (+)-**1** and (–)-**1** were elucidated as 9*S*,10*R*,11*R* and 9*R*,10*S*,11*S*, respectively.

Compound **2**, obtained as a white powder, possesses the same molecular formula ($C_{17}H_{22}O_5$) as that of compound **1** based on its HRESIMS data with an $[M + H]^+$ ion peak at *m/z* 307.1534 (calcd for $C_{17}H_{23}O_5$, 307.1545). A detailed comparison of its NMR spectroscopic data with those of **1** indicated that the main differences between **1** and **2** were tiny changes in the chemical shifts of C-10 and C-11 as well as their protons [δ_C 81.1 (C-10), 79.8 (C-11); δ_H 3.84 (1H, dq, J = 8.1, 6.2 Hz, H-10), 4.36 (1H, dq, J = 8.1, 6.2 Hz, H-11) in **2**; δ_C 81.7 (C-10), 79.3(C-11); δ_H 3.91 (1H, dq, J = 8.5, 6.1 Hz, H-10), 4.18 (1H, dq, J = 8.5, 6.1 Hz, H-11) in **1**]. These findings, combined with the 2D NMR data, implied that **2** has the same planar structure as **1**, and it should be a stereoisomer of **1**. The planar structure of **2** was further confirmed by analyses of its ^{1}H–^{1}H COSY and HMBC spectra. Unfortunately, the NOESY experiment of **2** also did not show any NOESY correlations useful in for the elucidation of the relative configuration of compound **2**.

Similarly, after many attempts, we finally determined the relative configuration of compound **2** by X-ray crystallography analysis with Cu Kα radiation (**Figure 3**, CCDC 1840166). This single-crystal is triclinic with space group of chiral P-1, also indicating it is racemic. Compound **2** was then separated into a pair of enantiomers by a method similar to what was used for compound **1** (**Figure 4**), and the enantiomers showed opposite optical rotations {(+)-**2**: $[\alpha]_D^{20}$+30 (c 0.1, CH_2Cl_2); (–)-**2**: $[\alpha]_D^{20}$-30 (c 0.1, CH_2Cl_2)} and mirror image ECD curves (**Figure 5**). The absolute configurations of the two enantiomers of **2** were further determined by ECD calculations. As shown in **Figure 5**, the calculated ECD curve of 9*R*,10*R*,11*R*-**2** closely resembled the experimental curve of (–)-**2**, and the absolute configurations of (+)-**2** and (–)-**2** were elucidated as 9*S*,10*S*,11*S* and 9*R*,10*R*,11*R*, respectively.

To the best of our knowledge, (±)-**1** and (±)-**2** are the first examples of spiro-orthoester enantiomers with an unusual 1,4,6-trioxaspiro[4.5]decane-7-one unit, and they represent the first spiro-orthoesters originating from fungi. The proposed biosynthetic pathway of **1** and **2** was outlined in **Figure 6**. First, the condensation of acetyl-CoA and four molecules of malonyl-CoA by a polyketide synthase formed **i**, which underwent cycloaddition and methylations to form precursor sclerotinin A (**3**). Then, sclerotinin A underwent isomerization and hydrolytic cleavage to afford **iv**, which further formed **vi** by a H^+ mediated double bond isomerization. After that, intermediate **vii** was produced by an aldol condensation, which further generated the key intermediates **viii** and **x** via an esterification reaction with 2*R*,3*R*-butanediol and 2*S*,3*S*-butanediol (Ji et al., 2011), respectively. Finally, compounds (±)-**1** and (±)-**2** were formed via condensation and lactonization reactions.

Compounds (±)-**1** and (±)-**2** were tested for their inhibitory activities against NO production in lipopolysaccharide (LPS)-induced RAW264.7 cells. The results revealed that (+)-**1**, (–)-**1**, (+)-**2**, and (–)-**2** exhibited potential inhibitory activities with IC_{50} values of 34.5, 29.6, 23.5, and 15.2 μM, respectively (**Table 2**). Interestingly, for both pairs of enantiomers, the levorotatory compounds (–**1** and –**2**) showed better inhibitory effects than the dextrorotatory compounds (+**1** and +**2**). Moreover, both (+)-**2** and (–)-**2** showed better inhibitory effects than those of (+)-**1** and (–)-**1** as well as the positive control, dexamethasone. We also tested cytotoxicity of these compounds, but even at the concentration of 40 μM, none of them showed cytotoxicity activity.

TABLE 2 | Inhibition of LPS-Induced NO Production.

Compound	IC_{50} (μM)
(+)-1	34.5
(–)-1	29.6
(+)-2	23.5
(–)-2	14.2
Dexamethasone	27.1

CONCLUSION

In conclusion, two pairs of new spiro-orthoester enantiomers, (±)-peniorthoesters A and B (±**1** and ±**2**), were isolated from *P. minioluteum*. These compounds, characterized by an unexpected 1,4,6-trioxaspi-ro[4.5]decane-7-one unit, are the first examples of spiro-orthoester enantiomers, and they represent the first spiro-orthoesters originating from fungi. All of them showed potential inhibitory activities against NO production in activated macrophages with IC_{50} values ranging from 14.2 to 34.5 μM, which are comparable to the positive control, dexamethasone. Their highly functionalized structures and promising biological activities will attract considerable attention from the pharmacological, synthetic, and biosynthetic communities.

DATA AVAILABILITY STATEMENT

The raw data supporting the conclusions of this manuscript will be made available by the authors, without undue reservation, to any qualified researcher.

AUTHOR CONTRIBUTIONS

XL and CC conducted the main experiments and wrote the manuscript. YiZ, MZ, and QZ carried out bioassays. JL did the ECD calculations. JW and ZL analyzed the spectroscopic data. HZ and YoZ initiated and oversaw all research. All authors reviewed the manuscript.

ACKNOWLEDGMENTS

This work was financially supported by the Program for Changjiang Scholars of Ministry of Education of the People's Republic of China (No. T2016088); the National Natural

Science Foundation for Distinguished Young Scholars (No. 81725021); Innovative Research Groups of the National Natural Science Foundation of China (81721005); the Academic Frontier Youth Team of HUST; and the Integrated Innovative Team for Major Human Diseases Program of Tongji Medical College (HUST). We thank the Analytical and Testing Center at Huazhong University of Science and Technology for assistance in the acquisition of the ECD, UV, and IR spectra.

SUPPLEMENTARY MATERIAL

The Supplementary Material for this article can be found online at: https://www.frontiersin.org/articles/10.3389/fchem.2018.00605/full#supplementary-material

The Supplementary Material includes Full NMR, HRESIMS, UV, and IR spectra of 1 and 2; detailed of the ECD calculations of 1 and 2; X-ray data of 1 and 2 (PDF); and crystallographic data (CIF).

REFERENCES

Bourjot, M., Leyssen, P., Neyts, J., Dumontet, V., and Litaudon, M. (2014). Trigocherrierin A, a potent inhibitor of chikungunya virus replication. *Molecules* 19, 3617–3627. doi: 10.3390/molecules19033617

Chen, K., Zhang, X., Sun, W., Liu, J., Yang, J., Chen, C., et al. (2017). Manginoids A–G: seven monoterpene–shikimate-conjugated meroterpenoids with a spiro ring system from *Guignardia mangiferae*. *Org. Lett.* 19, 5956–5959. doi: 10.1021/acs.orglett.7b02955

Gontijo de Souza, G., Oliveira, T. S., Takahashi, J. A., Collado, I. G., Macias-Sanchez, A. J., and Hernandez-Galan, R. (2012). Biotransformation of clovane derivatives. Whole cell fungi mediated domino synthesis of *rumphellclovane A*. *Org. Biomol. Chem.* 10, 3315–3320. doi: 10.1039/C2OB07114B

Guo, J., Tian, J., Yao, G., Zhu, H., Xue, Y., Luo, Z., et al. (2015). Three new 1α-alkyldaphnane-type diterpenoids from the ?ower buds of *Wikstroemia chamaedaphne*. *Fitoterapia* 106, 242–246. doi: 10.1016/j.fitote.2015.09.017

He, W., Cik, M., Appendino, G., Puyvelde, L. V., Leysen, J. E., and De Kimpe, N. (2002). Daphnane-type deterpene orthoesters and their biological activities. *Mini. Rev. Med. Chem.* 2, 185–200. doi: 10.2174/1389557024605492

Iida, M., Ooi, T., Kito, K., Yoshida, S., Kanoh, K., Shizuri, Y., et al. (2008). Three New polyketide–terpenoid hybrids from *Penicillium* sp. *Org. Lett.* 10, 845–848. doi: 10.1021/ol7029867

Ji, X. J., Huang, H., and Ouyang, P. K. (2011). Microbial 2,3-butanediol production: a state-of-the-art review. *Biotechnol. Adv.* 29, 351–364. doi: 10.1016/j.biotechadv.2011.01.007

Kmiecik, N., and Zymanczyk-Duda, E. (2017). Enantio convergent biotransformation of O,O-dimethyl-4-oxoazetidin-2-ylphosphonate using fungal cells of *Penicillium minioluteum* and purified enzymes. *Bioorg. Chem.* 71, 81–85. doi: 10.1016/j.bioorg.2017.01.014

Li, L., Knickelbein, K., Zhang, L., Wang, J., Obrinske, M., Ma, G. Z., et al. (2015). Amphiphilic sugar poly (orthoesters) as pH-responsive nanoscopic assemblies for acidity-enhanced drug delivery and cell killing. *Chem. Commun.* 51, 13078–13081. doi: 10.1039/C5CC04078G

Liao, G. S., Chen, H. D., and Yue, J.-M. (2009). Plant orthoesters. *Chem. Rev.* 109, 1092–1140. doi: 10.1021/cr0782832

Liu, F., Yang, X., Ma, J., Yang, Y., Xie, C., Tuerhong, M., et al. (2017). Nitric oxide inhibitory daphnane diterpenoids as potential anti-neuroinflammatory agents for AD from the twigs of *Trigonostemon thyrsoideus*. *Bioorg. Chem.* 75, 149–156. doi: 10.1016/j.bioorg.2017.09.007

Luo, M., Cui, Z., Huang, H., Song, X., Sun, A., Dang, Y., et al. (2017). Amino acid conjugated anthraquinones from the marine-derived fungus *Penicillium* sp. SCSIO sof101. *J. Nat. Prod.* 80, 1668–1673. doi: 10.1021/acs.jnatprod.7b00269

Meng, L. H., Wang, C. Y., Mandi, A., Li, X. M., Hu, X. Y., Kassack, M. U., et al. (2016). Three Diketopiperazine alkaloids with spirocyclic skeletons and one bisthiodiketopiperazine derivative from the mangrove-derived endophytic fungus *Penicillium brocae* MA-231 *Org. Lett.* 18, 5304–5307. doi: 10.1021/acs.orglett.6b02620

Ngokpol, S., Suwakulsiri, W., Sureram, S., Lirdprapamongkol, K., Aree, T., Wiyakrutta, S., et al. (2015). Drimane sesquiterpene-conjugated amino acids from a marine isolate of the fungus *Talaromyces minioluteus* (*Penicillium Minioluteum*). *Mar. Drugs* 13, 3567–3580. doi: 10.3390/md13063567

Rank, C., Phipps, R. K., Harris, P., Fristrup, P., Larsen, T. O., and Gotfredsen, C. H. (2008). N ovofumigatonin, a new orthoester meroterpenoid from *Aspergillus novofumigatus*. *Org. Lett.* 10, 401–404. doi: 10.1021/ol7026834

Roy, A., and Saraf, S. (2006). Limonoids: overview of significant bioactive triterpenes distributed in plants kingdom. *Biol. Pharm. Bull.* 29, 191–201. doi: 10.1248/bpb.29.191

Santana, L., Uriarte, E., Roleira, F., Milhazes, N., and Borges, F. (2004). Furocoumarins in medicinal chemistry. Synthesis, natural occurrence and biological activity. *Curr. Med. Chem.* 11, 3239–3261. doi: 10.2174/0929867043363721

Steyn, P. S., and van Heerden, F. R. (1998). Bufadienolides of plant and animal origin. *Nat. Prod. Rep.* 15, 397–413. doi: 10.1039/A815397Y

Sun, J., Zhu, Z. X., Song, Y. L., Dong, D., Zheng, J., Liu, T., et al. (2016). Nitric Oxide Inhibitory Meroterpenoids from the Fungus *Penicillium purpurogenum* MHZ 111. *J. Nat. Prod.* 79, 1415–1422. doi: 10.1021/acs.jnatprod.6b00160

Tang, H. Y., Zhang, Q., Gao, Y. Q., Zhang, A. I., and Gao, J. M. (2015). Miniolins A–C, novel isomeric furanones induced by epigenetic manipulation of *Penicillium minioluteum*. *RSC Adv.* 5, 2185–2190. doi: 10.1039/C4RA11712C

Xiao, N., Gao, J., Cai, X., and She, Z. (2009). Secondary metabolites of mangrove endophytic fungus SK5 in the South China Sea. *Zhongyaocai* 32, 1843–1845. doi: 10.3321/j.issn:1001-4454.2009.12.017

Zhou, P., Wu, Z., Tan, D., Yang, J., Zhou, Q., Zeng, F., et al. (2017). Atrichodermones A–C, three new secondary metabolites from the solid culture of an endophytic fungal strain, *Trichoderma atroviride*. *Fitoterapia* 123, 18–22. doi: 10.1016/j.fitote.2017.09.012

Zhu, H., Chen, C., Xue, Y., Tong, Q., Li, X. N., Chen, X., et al. (2015). *Asperchalasine* A, a cytochalasan dimer with an unprecedented decacyclic ring system, from *Aspergillus flavipes*. *Angew. Chem. Int. Ed.* 54, 13374–13378. doi: 10.1002/anie.201506264

Zhu, H. J. (2015). *Organic Stereochemistry: Experimental and Computational Methods*. Weinheim: Wiley-VCH Verlag GmbH and Co. KGaA.

Conflict of Interest Statement: The authors declare that the research was conducted in the absence of any commercial or financial relationships that could be construed as a potential conflict of interest.

frontiers in Chemistry

ORIGINAL RESEARCH
published: 15 February 2019
doi: 10.3389/fchem.2019.00080

Anti-*Vibrio* Indole-Diterpenoids and C-25 Epimeric Steroids From the Marine-Derived Fungus *Penicillium janthinellum*

Xing-Chen Guo[1†], *Lan-Lan Xu*[1†], *Rui-Yun Yang*[2], *Meng-Yue Yang*[1], *Lian-Dong Hu*[1], *Hua-Jie Zhu*[1*] and *Fei Cao*[1*]

[1] Key Laboratory of Pharmaceutical Quality Control of Hebei Province, Key Laboratory of Medicinal Chemistry and Molecular Diagnostics of Education Ministry of China, College of Pharmaceutical Sciences, Hebei University, Baoding, China, [2] State Key Laboratory for Chemistry and Molecular Engineering of Medicinal Resources, College of Chemistry and Pharmaceutical Sciences, Guangxi Normal University, Guilin, China

OPEN ACCESS

Edited by:
Bin-Gui Wang,
Institute of Oceanology (CAS), China

Reviewed by:
Kyeongsoon Park,
Chung-Ang University, South Korea
Dehai Li,
Ocean University of China, China

***Correspondence:**
Hua-Jie Zhu
hjzhu2017@163.com
Fei Cao
caofei542927001@163.com

[†]These authors have contributed equally to this work

Specialty section:
This article was submitted to Medicinal and Pharmaceutical Chemistry, a section of the journal Frontiers in Chemistry

Received: 17 May 2018
Accepted: 29 January 2019
Published: 15 February 2019

Citation:
Guo X-C, Xu L-L, Yang R-Y, Yang M-Y, Hu L-D, Zhu H-J and Cao F (2019) Anti-Vibrio Indole-Diterpenoids and C-25 Epimeric Steroids From the Marine-Derived Fungus Penicillium janthinellum. Front. Chem. 7:80. doi: 10.3389/fchem.2019.00080

A systematic chemical exploration of the marine-derived fungus *Penicillium janthinellum* led to the isolation of four indole-diterpenoid derivatives (**1**–**4**), including new penijanthines C and D (**1** and **2**), and a pair of new steroidal epimers, penijanthoids A and B (**5** and **6**). The calculated ECD spectra and Snatzke's method for the new compound **1** were carried out to determine its absolute configuration. The absolute configuration of **3** was established by X-ray diffraction and calculated ECD methods for the first time. DP4plus approach was used to elucidate the absolute configurations of the C-25 epimeric steroids **5** and **6**. 25-Epimeric **5** and **6** represent the first examples of steroids forming a five-membered lactone between C-23 and C-27 from marine fungi. Compounds **1**, **2**, **5**, and **6** displayed significant anti-*Vibrio* activity (Minimum inhibitory concentration, MIC values ranging from 3.1 to 50.0 μM) against three pathogenic *Vibrio* spp.

Keywords: *Penicillium janthinellum*, indole-diterpenoid, steroid, absolute configuration, anti-*Vibrio* activity

INTRODUCTION

Vibrio spp., such as *Vibrio anguillarum*, *Vibrio parahemolyticus*, and *Vibrio alginolyticus*, is a class of Gram-negative halophilic bacteria that occurs usually in marine and coastal environments throughout the world, which could lead vibriosis in crustaceans and cause serious damage to mariculture production (Vezzulli et al., 2015; Moreno et al., 2017). However, there was no effective vaccine to prevent vibriosis due to lacking adaptive immunity in crustacean species (Buchmann, 2014). In the past few decades, searching for marine-derived bioactive substances as anti-*Vibrio* agents has drawn the attention of chemists and pharmacologists (Meng et al., 2015; Wang et al., 2015). In our continuing efforts to explore anti-*Vibrio* natural products from marine-derived fungi (Xu et al., 2017; Yang et al., 2018), the Bohai Sea fungus *Penicillium janthinellum* was selected for further chemical exploration due to the anti-*Vibrio* activity of its EtOAc extract. As a result, two new indole-diterpenoids, penijanthines C and D (**1** and **2**), and two known analogs, PC-M6 (**3**) (Yamaguchi et al., 1993), 7-hydroxy-13-dehydroxypaxilline (**4**) (Mantle and Weedon, 1994), along with two new steroids, penijanthoids A and B (**5** and **6**), were obtained (**Figure 1**). Compounds **1**–**6** displayed anti-*Vibrio* activity against three pathogenic *V. anguillarum*, *V. parahemolyticus*, and *V. alginolyticus*.

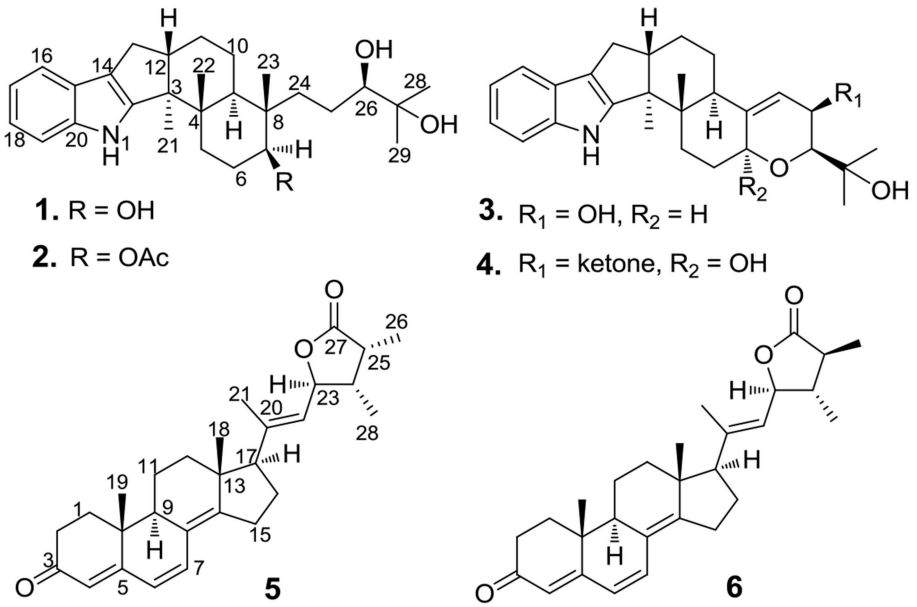

FIGURE 1 | Chemical structures of **1**–**6**.

MATERIALS AND METHODS

General Experimental Procedures

Optical rotations (OR) values of the new compounds were determined using a JASCO-1020 polarimeter. Electronic circular dichroism (ECD) experiments, including $Mo_2(AcO)_4$ ICD experiments, were carried out on a JASCO J-815 circular dichroism spectrometer. Ultraviolet–visible (UV) data were provided in MeOH by a Perkin-Elmer model 241 spectrophotometer. Infrared radiation (IR) data of the new compounds (using KBr pellets) were measured on a Nicolet NEXUS 470 spectrophotometer. 1D NMR (^{1}H NMR and ^{13}C NMR) and 2D NMR (HSQC, ^{1}H-^{1}H COZY, HMBC and NOESY) data were recorded on a Bruker AV-600 spectrometer. HR-ESI-MS spectra were performed with a Thermo Scientific LTQ Orbitrap XL spectrometer. Semi-preparation HPLC, which had the Shimadzu LC-20AT system with a SPD-M20A detector and a Waters RP-18 column, was used for chemical separation. Further chromatographic separation was taken on 200–300 mesh silica gel and 18–110 μm Sephadex LH-20 columns.

Isolation of the Fungal Material

The strain in our research, which was derived from the marine sediment collected from the Bohai Sea in June 2016, was deposited at Hebei University, China. According to its 16S rRNA amplification and sequencing of the ITS region, the strain was identified as *Penicillium janthinellum* (Gene Bank KY979507). The fungus *Penicillium janthinellum* was cultivated using solid medium in forty Erlenmeyer flasks (80 g raw rice, 60 mL H_2O, 2.0 g sea salt in each Erlenmeyer flask) at 28°C for 4 weeks. Mixed solvent of CH_2Cl_2-MeOH (v/v = 1:1) was used to extract fermented rice, and the solution was evaporated to give the crude extract, which was dissolved and extracted with EtOAc for five times to provide the EtOAc extract (12.0 g). The EtOAc extract, which was eluted with EtOAc-petroleum ether (PE) on the silica gel column chromatography (CC), was separated into different fractions ranged from Fr.1 to Fr.8. Fr.2 (1.46 g), which was eluted with 40% EtOAc in PE, was applied on a Sephadex LH-20 and waters RP-18 (XBridge OBD, 5 μm, 10 × 250 mm, 70%-MeOH in water) columns to produce **5** (10.5 mg) and **6** (7.6 mg). Fr.4 (4.34 g, 60% EtOAc in PE) was separated by repeatedly silica gel CC and HPLC to provide **1** (20.5 mg), **2** (5.8 mg), **3** (16.4 mg), and **4** (8.2 mg).

Penijanthine C (**1**)

Yellow powder; $[\alpha]_D^{20}$ −80.0 (*c* 0.20, CH_2Cl_2); UV (MeOH) λ_{max} (log ε) 230 (2.60), 280 (0.85) nm; CD (MeOH) λ_{max} ($\Delta\varepsilon$) 230 (13.1), 291 (−1.2) nm; IR (KBr) ν_{max} 3,473, 2,945, 1,628, 1,302, 1,240, 1,054, 931, 820 cm^{-1}; ^{1}H and ^{13}C NMR data, see **Table 1**; HRESIMS *m/z* 440.3163 $[M + H]^+$ (calcd. for $C_{28}H_{42}O_3N$, 440.3159).

Penijanthine D (**2**)

Yellow powder; $[\alpha]_D^{20}$ −27.0 (*c* 0.20, CH_2Cl_2); UV (MeOH) λ_{max} (log ε) 240 (3.50), 280 (3.20) nm; CD (MeOH) λ_{max} ($\Delta\varepsilon$) 230 (11.4), 291 (−1.7) nm; IR (KBr) ν_{max} 3,435, 2,943, 1,641, 1,629, 1,312, 1,233, 1,054, 930, 819 cm^{-1}; ^{1}H and ^{13}C NMR data, see **Table 1**; HRESIMS *m/z* 504.3072 $[M + Na]^+$(calcd. for $C_{30}H_{43}O_4NNa$, 504.3084).

Penijanthoid A (**5**)

Colorless powder; $[\alpha]_D^{25}$ +424 (*c* 3.0, CH_2Cl_2); UV (MeOH) λ_{max} (log ε) 350 (1.50) nm; CD (MeOH) λ_{max} ($\Delta\varepsilon$) 223 (7.1), 247 (3.4), 363 (24.3) nm; IR (KBr) ν_{max} 2,932, 2,249, 1,725, 1,650, 1,600, 1,468, 1,395, 1,176 cm^{-1}; ^{1}H and ^{13}C NMR data, see **Table 2**; HRESIMS *m/z* 421.2732 $[M + H]^+$ (calcd. for $C_{28}H_{36}O_3$, 421.2737) (**Figure S24**).

TABLE 1 | ^{1}H (600 MHz) and ^{13}C (150 MHz) NMR Data for **1** and **2** (DMSO-d_6).

Position	1		2	
	δ_H, mult. (*J* in Hz)	δ_C, type	δ_H, mult. (*J* in Hz)	δ_C, type
1	10.56, s		10.55, s	
2		151.3, C		151.0, C
3		52.6, C		52.5, C
4		38.6, C		38.5, C
5	1.86, m	32.1, CH_2	1.89, m	31.6, CH_2
	1.70, m		1.69, m	
6	1.70, m	27.2, CH_2	1.69, m	23.5, CH_2
	1.64, t (12.6)			
7	3.34, m	71.4, CH	4.56, m	75.4, CH
8		48.6, C		39.9, C
9	1.64, t (12.6)	40.8, CH	1.66, m	40.1, CH
10	1.53, m	22.3, CH_2	1.50, m	22.0, CH_2
	1.35, dt (12.6, 12.0)		1.33, m	
11	1.69, m	25.0, CH_2	1.69, m	24.9, CH_2
	1.53, m		1.50, m	
12	2.63, m	48.5, CH	2.60, m	48.5, CH
13	2.56, dd (12.6, 6.0)	27.1, CH_2	2.51, dd (12.6, 6.6)	27.0, CH_2
	2.24, dd (12.6, 11.2)		2.20, dd (12.6, 11.2)	
14		115.8, C		115.9, C
15		124.4, C		124.4, C
16	7.27, d (7.8)	117.5, CH	7.21, d (7.8)	117.6, CH
17	6.89, dd (7.8, 7.2)	118.3, CH	6.84, dd (7.8, 7.2)	118.4, CH
18	6.94, dd (7.8, 7.2)	119.2, CH	6.88, dd (7.8, 7.2)	119.3, CH
19	7.27, d (7.8)	111.8, CH	7.21, d (7.8)	111.8, CH
20		140.2, C		140.2, C
21	0.94, s	14.7, CH_3	0.91, s	14.6, CH_3
22	1.02, s	18.6, CH_3	1.00, s	18.6, CH_3
23	0.75, s	17.1, CH_3	0.83, s	17.5, CH_3
24	1.85, m	34.8, CH_2	1.50, m	35.2, CH_2
	1.06, m		1.08, m	
25	1.44, t (11.8)	23.6, CH_2	1.67, m	23.8, CH_2
	1.15, m		1.36, m	
26	3.00, t (7.2)	78.6, CH	2.90, m	78.0, CH
27		71.7, C		71.6, C
28	1.03, s	24.6, CH_3	0.94, s	24.6, CH_3
29	1.08, s	26.4, CH_3	0.99, s	26.4, CH_3
-OAc			1.94, s	21.0, CH_3
				169.9, C
7-OH	4.26, s			
26-OH	4.21, s		4.12, s	
27-OH	4.10, s		4.04, s	

Penijanthoid B (**6**)

Colorless powder; $[\alpha]_D^{25}$ +263 (*c* 3.0, CH_2Cl_2); UV (MeOH) λ_{max} (log ε) 350 (0.86) nm; CD (MeOH) λ_{max} ($\Delta\varepsilon$) 213 (1.4), 223 (−1.9), 230 (−2.3), 247 (−14.6), 283 (1.6), 358 (13.6) nm; IR (KBr) ν_{max} 2,932, 2,249, 1,725, 1,650, 1,600, 1,468, 1,395, 1,176 cm^{-1}; ^{1}H and ^{13}C NMR data, see **Table 2**; HRESIMS *m/z* 421.2732 $[M + H]^+$ (calcd. for $C_{28}H_{36}O_3$, 421.2737) (**Figure S31**).

Computational Section

Conformational search of the new compounds **1**, **5**, and **6** for quantum calculations was taken using MMFF94S force field with low energetics from 0–10.0 kcal/mol. Optimization for these geometries were carried out in the gas phase at the B3LYP/6-311+G(d) level. The optimized conformations with the relative energy between 0 and 2.5 kcal/mol was selected for ECD calculations, which were computed at the B3LYP/6-311++G(2d,p) level (gas phase) (Zhu, 2009, 2015; Zhu et al., 2014). For the DP4plus applications of **5** and **6**, unshielding tensor values of the optimized conformers were computed at the mPW1PW91/6-311+G(d,p)//mPW1PW91/6-311+G(d,p) level in the gas phase. All of the quantum chemical calculations were performed using Gaussian 09 package (Frisch et al., 2009).

X-Ray Crystallographic Study of PC-M6 (3)

The crystal of **3** was acquired from a mixed solvent of methanol and dichlorine in a refrigerator for 14 days. The detail X-ray diffraction data of single-crystal **3** were collected by Bruker Smart APEXII with the crystal system of Mo target. The wavelength of radiation is 0.71073 Å. The block crystals of **3** are monoclinic, space group C2 with cell dimensions $a = 19.2301(8)$ Å, $b = 7.0166(3)$ Å, $c = 17.2255(8)$ Å, $V = 2322.67(18)$ Å^3, $Z = 4$, $F_{(000)} = 912$, and goodness of fit on $F^2 = 1.042$. The Final R indices [$I > 2\sigma(I)$] were $R1 = 0.0390$, $wR2 = 0.0871$. R indices (all data) were $R1 = 0.0524$, $wR2 = 0.0951$. The detail data of the crystal for **3** has been uploaded to the Cambridge Crystallographic Data Center. The relevant single crystal data can be viewed in the database and copies can be downloaded free of charge. The CCDC number for supplementary publication is NO. CCDC 1839742. CCDC's mailing address is as follows, 12 Union Road, Cambridge CB2 1EZ, U.K. (Fax, + 44(0)-1223–336033; email, deposit@ccdc.cam.ac.uk).

Anti-*Vibrio* Activity Assays

The conventional broth dilution assay described by on the related literature (Appendio et al., 2008) was used to test the anti-*Vibrio* activity of these compounds. Three pathogenic *Vibrio* strains, *Vibrio anguillarum*, *Vibrio parahemolyticus* and *Vibrio alginolyticus* were incubated about 16–18 h at 37°C as the tested strains. The overnight cultures were used to prepare the turbidity of the bacterial suspensions, which had a concentration of 10^5-10^6 colony formingunits/mL and had the absorbance of 0.4–0.6 at 600 nm. The 96-well plates, which contained 2 μL of test solutions/positive control ciprofloxacin and 198 μL of bacterial culture, were used to test the minimum inhibitory concentration (MIC) of anti-*Vibrio* activity for these compounds. Finally, the different concentrations of tested compounds from 25.0 to 0.195 μM were prepared and incubated overnight for 24 h at 37°C to measure the MIC values of anti-*Vibrio* activity. Ciprofloxacin had the MIC values of 0.078, 0.312, and 0.625, respectively, against *V. anguillarum*, *V. parahemolyticus,* and *V. alginolyticus*.

RESULTS AND DISCUSSION

Penijanthine C (**1**) was isolated as a yellow amorphous powder. The molecular formula of $C_{28}H_{41}NO_3$ for **1** was determined

TABLE 2 | ^{1}H (600 MHz) and ^{13}C (150 MHz) NMR Data for **5** and **6** ($CDCl_3$).

Position	5		6	
	δ_H, mult. (*J* in Hz)	δ_C, type	δ_H, mult. (*J* in Hz)	δ_C, type
1	2.03, m 1.81, m	34.1, CH_2	2.03, m 1.81, m	34.1, CH_2
2	2.54, m	34.1, CH_2	2.55, m	34.1, CH_2
3		199.4, C		199.4, C
4	5.75, s	123.4, CH	5.75, s	123.4, CH
5		164.0, C		164.0, C
6	6.06, d (9.5)	125.0, CH	6.06, d (9.5)	125.0, CH
7	6.60, d (9.5)	133.5, CH	6.61, d (9.5)	133.5, CH
8		125.4, C		125.4, C
9	2.18, m	44.6, CH	2.18, m	44.6, CH
10		36.8, C		36.8, C
11	1.60, m 1.55, m	19.0, CH_2	1.58, m	19.1, CH_2
12	1.93, m 1.91, m	35.0, CH_2	1.94, m 1.92, m	35.0, CH_2
13		44.8, C		44.7, C
14		153.6, C		153.6, C
15	2.54, m	25.3, CH_2	2.55, m	25.3, CH_2
16	2.12, m 2.01, m	25.0, CH_2	2.14, m 2.03, m	25.0, CH_2
17	2.14, m	58.1, CH	2.14, m	58.2, CH
18	0.84, s	19.7, CH_3	0.85, s	19.7, CH_3
19	1.00, s	16.6, CH_3	1.00, s	16.6, CH_3
20		141.5, C		142.2, C
21	1.81, s	18.8, CH_3	1.83, s	18.9, CH_3
22	5.32, d (8.4)	124.1, CH	5.27, d (8.7)	123.6, CH
23	4.87, dd (8.4, 7.7)	81.4, CH	4.72, dd (8.7, 9.3)	81.1, CH
24	2.33, m	40.8, CH	1.80, m	46.1, CH
25	2.73, m	38.7, CH	2.21, m	43.0, CH
26	1.20, d (7.6)	10.4, CH_3	1.24, d (7.0)	13.0, CH_3
27		179.9, C		178.9, C
28	1.03, d (7.0)	12.2, CH_3	1.10, d (6.5)	14.4, CH_3

by high resolution mass spectrometry m/z = 440.3163 $[M + H]^+$ (calcd. 440.3159) (**Figure S10**), suggesting nine degrees of unsaturation in **1**. In the ^{13}C NMR spectroscopic data (**Table 1**) of **1**, 28 carbon signals which contain five methyls, seven methylenes, eight methines including four olefinic carbons, and two oxygen-bearing carbons, and eight quaternary carbons with four sp^2 and two oxygenated sp^3 were observed. The above ^{13}C NMR signals agreed well with the ^{1}H NMR spectroscopic data (**Table 1**) of **1**, which displayed a 1,2-disubstituted aromatic unit [δ_H 7.27 (2H, d, J = 7.8 Hz, H-16 and H-19), 6.94 (1H, dd, J = 7.8, 7.2 Hz, H-18), and 6.89 (1H, dd, J = 7.8, 7.2 Hz, H-17)], two oxymethine protons [δ_H 3.34 (1H, m, H-7) and 3.00 (1H, t, J = 7.2 Hz, H-26)], and five methyls [δ_H 1.08 (3H, s, H-29), 1.03 (3H, s, H-28), 1.02 (3H, s, H-22), 0.94 (3H, s, H-21), and 0.75 (3H, s, H-23)]. The above characteristic ^{1}H and ^{13}C NMR data of **1** suggested an indole-diterpenoid framework for **1**. In fact, **1** could be identified as an indole-diterpenoid analog of emindole SB, which was previously isolated from the fungus

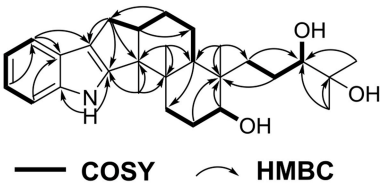

FIGURE 2 | COZY and key HMBC correlations for **1**.

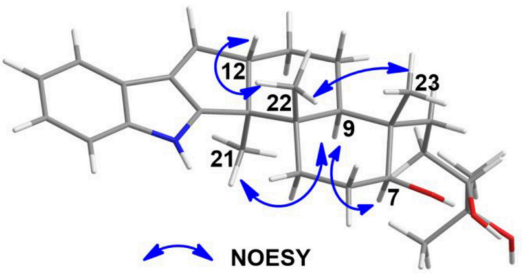

FIGURE 3 | Selected NOESY correlations for **1**.

Penicillium camemberti (Fan et al., 2013), by careful comparison of their 1D NMR data. The structural difference between them was that the 26,27-trisubstituted double bond in emindole SB was replaced by a *vic*-diol moiety [δ_H 3.00 (1H, t, J = 7.2 Hz, H-26); δ_C 78.6 (CH, C-26) and 71.7 (C, C-27)] in **1** (**Figures S4**, **S5**). The long-range couplings of H_3-28/C-26, H_3-28/C-27, H_3-29/C-26, H_3-29/C-27, and H_2-24/C-26 in the HMBC spectrum of **1**, as well as the proton spin system of H_2-25/H-26 from the ^{1}H-^{1}H COZY spectrum in **1**, supported the above deduction (**Figure 2**). The assignment of the planar structure for **1** was consequently confirmed by the 2D NMR data of HSQC, ^{1}H-^{1}H COZY, and HMBC in **1** (**Figures S6–S8**).

The analysis of the NOESY data allowed the relative configuration of the five rings for the indole-diterpenoid nuclei in **1**. The NOESY cross-peaks between the H-12 and H_3-22, H_3-22, and H_3-23 as well as H-9 had NOE with both H_3-21 and H-7 were observed in the NOESY experiment of **1**, suggesting that H-12, H_3-22, and H_3-23 were place on the opposite direction to H-7, H-9, and H_3-21 in the molecule of **1** (**Figure 3**). However, the NOESY experiment was unable to conclusively determine the configuration at C-26 in **1** (**Figure S9**).

To assign the stereochemistry of 26-stereogenic carbon in **1**, induced circular dichroism (ICD) procedure (Snatzke's method) was applied (Frelek et al., 1997; Di Bari et al., 2001). The Mo-complexes of compound **1** (0.5 mg) and $Mo_2(OAc)_4$ (dimolybdenum tetraacetate) was prepared to measure the its ICD spectrum. Compared with the ICD spectrum of the reference Mo_2 complex (Frelek et al., 1997; Di Bari et al., 2001), the Cotton effect bands II (near 400 nm) and IV (around 312 nm) in the ICD data of Mo-complexes of **1** were negative (**Figure 4**), suggesting the 26*R* absolute configuration for **1**. The absolute configuration of the five rings in the indole-diterpenoid nuclei of **1** was investigated by quantum chemical calculation. Based

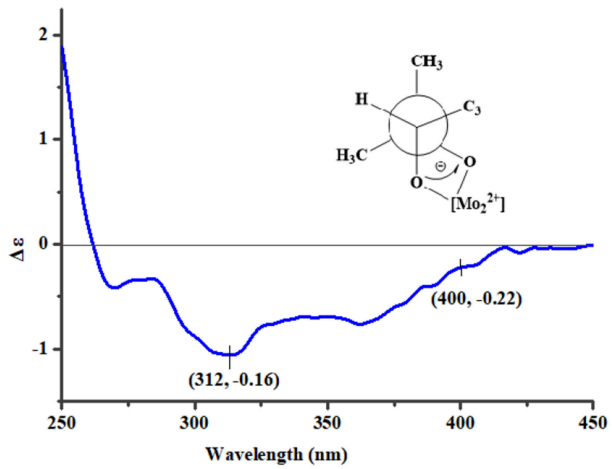

FIGURE 4 | The ICD spectrum of Mo-complexes of **1**.

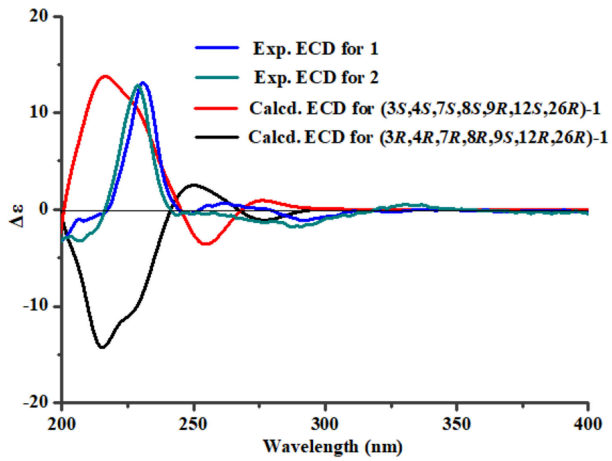

FIGURE 5 | The predicted ECD spectra of **1** and the experimental ECD spectra of **1** and **2**.

on the relative configuration of **1**, two possible structures of (3*S*,4*S*,7*S*,8*S*,9*R*,12*S*,26*R*)-**1** and (3*R*,4*R*,7*R*,8*R*,9*S*,12*R*,26*R*)-**1** of **1** were used for ECD calculations. Time-dependent density functional theory/electronic circular dichroism (TDDFT-ECD) method at the B3LYP/6-311++G(2d,p)//B3LYP/6-311+G(d) level in the gas phase was taken. ECD simulations were calculated by Boltzmann statistics for the structures of (3*S*,4*S*,7*S*,8*S*,9*R*,12*S*,26*R*)-**1** and (3*R*,4*R*,7*R*,8*R*,9*S*,12*R*,26*R*)-**1** with a standard deviation of σ 0.2 eV. The calculated ECD curve of (3*S*,4*S*,7*S*,8*S*,9*R*,12*S*,26*R*)-**1** agreed better with the experimental ECD data of **1** (**Figure 5**), indicating an obvious assignment of 3*S*,4*S*,7*S*,8*S*,9*R*,12*S*,26*R* absolute configuration for **1**.

Penijanthine D (**2**) had the molecular formula of $C_{30}H_{43}NO_4$, which was determined by the high resolution mass data *m/z* = 504.3072 $[M + H]^+$ (calcd. 504.3084) of **2** (**Figure S17**). Compound **2** was also defined as an indole-diterpenoid analog by the strikingly similar NMR data of **2** (**Figures S11–S15**) compared with those of **1** (**Table 1**), with the appearance of the

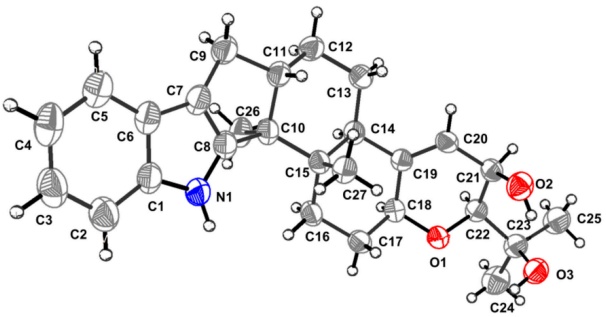

FIGURE 6 | Perspective ORTEP drawing for **3**.

additional acetoxy signals [δ_H 1.94 (3H, s); δ_C 169.9 and 21.0] in **2**. This additional acetoxy group was connected at C-7 in **2** was through the key HMBC correlation between H-7 and C-$COCH_3$. The NOESY (**Figure S16**) and ECD (**Figure 5**) experiments of **2** indicated the stereochemistry of **2** was the same as **1**. Therefore, compound **2** was assigned as the 7-acetylation derivative of **1**.

The known PC-M6 (**3**) (Yamaguchi et al., 1993) and 7-hydroxy-13-dehydroxypaxilline (**4**) (Mantle and Weedon, 1994) were determined by comparing their ^1H, ^{13}C NMR and positive Mass data with the corresponding data in the literature. The stereochemistry of PC-M6 (**3**) was further verified by the data of X-ray diffraction (**Figure 6**) and calculated ECD (**Figure S1**) for the first time. The present work affords four indole-diterpenoids (**1**–**4**), which consist of a common cyclic diterpene backbone and an indole moiety. According to the literature, over 100 indole-diterpenoids with unique chemical scaffolds were produced by various fungal sources (Li et al., 2002; Zhao et al., 2018). The complexity of these intriguing structures may encourage further investigations on the chemistry and biological activity of this cluster of metabolites.

Penijanthoid A (**5**), which had the molecular formula of $C_{28}H_{36}O_3$, was also isolated as a colorless powder. According to the ^1H NMR spectrum of **5** (**Table 2**), the downfield region gave four olefinic protons [δ_H 6.60 (1H, d, J = 9.5 Hz, H-7), 6.06 (1H, d, J = 9.5 Hz, H-6), 5.75 (1H, s, H-4), and 5.32 (1H, d, J = 8.4 Hz, H-22)], the highfield region displayed five CH_3 signals [δ_H 1.81 (1H, s, H-21), 1.20 (1H, d, J = 7.6 Hz, H-26), 1.03 (1H, d, J = 7.0 Hz, H-28), 1.00 (1H, s, H-19), and 0.84 (1H, s, H-18)] and numerous CH_2 and CH signals in the range of δ_H 2.80–1.25 ppm. The above spectroscopic features suggested that **5** was a steroidal derivative, which was structural similar to the known steroid (22*E*)-ergosta-4,6,8(14),22-tetraen-3-one (Chen et al., 2015). In fact, the main difference between compound **5** and (22*E*)-ergosta-4,6,8(14),22-tetraen-3-one was located on the side chains of them. Then, a five-membered lactone ring was proven to be present in the side chain of **5** by the HMBC correlations from H-23 (δ_H 4.87) and H_3-26 (δ_H 1.20) to C-27 (δ_C 179.9), C-24 (δ_C 40.8), C-25 (δ_C 38.7), and from H_3-28 (δ_H 1.03) to C-23 (δ_C 81.4), and the COSY (**Figures S18–S22**) cross-peaks of H-22/H-23/H-24/H-25/H_3-26 in **5** (**Figure 7**).

Further, NOESY experiment of **5** (**Figure 8**) was used to define its relative configuration. The NOE correlation between H_3-21 and H-23 in the NOESY spectrum of **5** indicated the

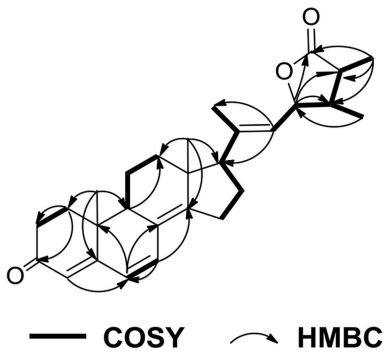

FIGURE 7 | COZY and key HMBC correlations for **5**.

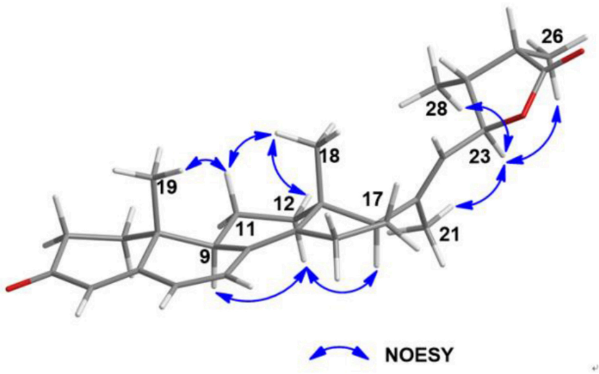

FIGURE 8 | Selected NOESY correlations for **5**.

E orientational double bond between C-20 and C-22 in **5**. The NOESY cross-peaks of H-11α/H_3-18, H-11α/H_3-19, H-12β/H_3-18, H-12α/H-9, and H-12α/H-17 suggested that **5** had the same relative configuration in tetracyclic nucleus as that of the compound (22*E*)-ergosta-4,6,8(14),22-tetraen-3-one in the literature (Chen et al., 2015). Furthermore, the NOE interactions of H-23/H_3-26 and H-23/H_3-28 indicated the same orientation of these protons (**Figure S23**). Besides, the carbonyl of cyclohexanone mainly contributed to the positive ECD effect at 363 nm ($\Delta\varepsilon$ + 24.3) (**Figure S2**) of **5**. By applying octant rule to cyclohexanones (Ochi et al., 1991), the absolute configuration of tetracyclic nucleus in **5** could be assigned as 9*R*,10*R*,13*R*,17*R*. In order to further determine the absolute configuration of five-membered lactone ring in **5**, two possible absolute configurations of **5**, [(9*R*,10*R*,13*R*,17*R*,23*S*,24*S*,25*R*)-**5** and (9*R*,10*R*,13*R*,17*R*,23*R*,24*R*,25*S*)-**5**], were used for GIAO NMR shift calculations at the mPW1PW91/6-311+G(d,p) level in the gas phase. When the parameter of DP4plus probability was used (Grimblat et al., 2015), the configuration of (9*R*,10*R*,13*R*,17*R*,23*S*,24*S*,25*R*)-**5** was more likely than (9*R*,10*R*,13*R*,17*R*,23*R*,24*R*,25*S*)-**5** (97.6 *vs.* 2.4% in both the unscaled shift data and shielding tensor data) (**Figure S32**). Therefore, the absolute configuration of **5** was suggested to be (9*R*,10*R*,13*R*,17*R*,23*S*,24*S*,25*R*).

Penijanthoid B (**6**) was also obtained with the same molecular formula of $C_{28}H_{36}O_3$ as **5**, indicating that **5** and **6** may be a pair of epimers. The above deduction was further confirmed by the fact that the NMR data of **6** were almost the same as **5** (**Table 2**) and the detailed analysis of the HSQC, ^{1}H-^{1}H COZY and HMBC spectra of **6** (**Figures S25–S29**). The NOESY (**Figure S30**) correlations between H-23 and H_3-21/H-25/H_3-28 demonstrated that **6** was the C-25 epimer of **5**. The absolute configuration (9*R*,10*R*,13*R*,17*R*,23*S*,24*S*,25*S*) of **6** was also assigned by ECD spectrum (**Figure S3**) and DP4plus (**Figure S33**) approaches. Among the various classes of biologically active natural produces obtained from marine-derived fungi, a large number of steroidal compounds have been described (Gautschi et al., 2004; Zhang et al., 2007; Wang et al., 2008; Qiao et al., 2010). However, **5** and **6** represent the first examples of steroids forming a five-membered lactone between C-23 and C-27 from marine fungi.

Vibriosis, which is also known as bacterial canker, is one of the bacterial diseases which cause serious damage and great losses to mariculture production (Vezzulli et al., 2015; Moreno et al., 2017). Research and development of effective anti-*Vibrio* drugs for controlling vibriosis is needed for mariculture. Thus, the anti-*Vibrio* activities against *V. anguillarum*, *V. parahemolyticus,* and *V. alginolyticus* of the new compounds **1**, **2**, **5**, **6** were carried out. Compound **1** displayed strongest anti-*Vibrio* activity against *V. Anguillarum* (MIC = 3.1 μM), *V. parahemolyticus* (MIC = 6.3 μM), and *V. Alginolyticus* (MIC = 3.1 μM), respectively. Compound **2** showed moderate anti-*Vibrio* activity against three pathogenic *Vibrio* spp. with the same MIC values of 12.5 μM, suggesting that the presence of an acetoxy group at C-7 in **2** may decrease the anti-*Vibrio* activity. A literature survey showed that the other known indole diterpenoid analogs, such as 6-hydroxylpaspalinine, paspalitrem C, emindole SB and so on, were also showed anti-*Vibrio* activity against three pathogenic *Vibrio* spp. (Hu et al., 2017). These finding suggested that it was worth ongoing to seek new anti-*Vibrio* compunds from indole diterpenoid derivatives. However, compounds **5** and **6** only exhibited weak anti-*Vibrio* activity against three pathogenic *Vibrio* spp. (MICs, 25.0–50.0 μM).

CONCLUSION

Four indole-diterpenoids and two steroidal epimers were isolated from the marine-derived fungus *Penicillium janthinellum*. Snatzke's, X-ray diffraction, and calculated ECD methods were used to assign the absolute configurations of these compounds.. The absolute configurations of steroidal epimers were suggested by DP4plus approach. Compounds **1** and **2** exhibited potential anti-*Vibrio* activity and represented a promising new class of anti-*Vibrio* agents.

AUTHOR CONTRIBUTIONS

L-LX and R-YY: contribute to fermentation, extraction, and isolation. X-CG: contribute to manuscript preparation. M-YY and L-DH: contribute to quantum chemistry calculation and

bioactivities test. H-JZ and FC: were the project leaders organizing and guiding the experiments and manuscript writing.

FUNDING

This work was supported by the National Natural Science Foundation of China (Nos. 41606174; 21877025), the project of State Key Laboratory for Chemistry and Molecular Engineering of Medicinal Resources (Guangxi Normal University) (CMEMR 2017-B07) the Scientific Research Foundation of Hebei Educational Committee (QN2016177; ZD2017004), the Natural Science Foundation of Hebei Province of China (No. B2017201059), the Top Young Talents Program of Hebei Province, National Training Program of Innovation and Entrepreneurship for Undergraduates (No. 201810075023), and the High Performance Computer Center of Hebei University.

SUPPLEMENTARY MATERIAL

The Supplementary Material for this article can be found online at: https://www.frontiersin.org/articles/10.3389/fchem.2019.00080/full#supplementary-material

REFERENCES

Appendio, G., Gibbons, S., Giana, A., Pagani, A., Grassi, G., Stavri, M., et al. (2008). Antibacterial cannabinoids from *Cannabis sativa*: a structure-activity study. *J. Nat. Prod.* 71, 1427–1430. doi: 10.1021/np8002673

Buchmann, K. (2014). Evolution of innate immunity: clues from invertebrates via fish to mammals. *Front. Immunol.* 5:459. doi: 10.3389/fimmu.2014.00459

Chen, M., Wang, K. L., Liu, M., She, Z. G., and Wang, C. Y. (2015). Bioactive steroid derivatives and butyrolactone derivatives from a gorgonian-derived *Aspergillus* sp. *fungus. Chem. Biodivers.* 47, 1398–1406. doi: 10.1002/cbdv.201400321

Di Bari, B. L., Pescitelli, G., Pratelli, C., Pini, D., and Salvadori, P. (2001). Determination of absolute configuration of acyclic 1,2-diols with $Mo_2(OAc)_4$. 1. Snatzke's method revisited. *J. Org. Chem.* 66, 4819–4825. doi: 10.1021/jo010136v

Fan, Y., Wang, Y., Liu, P., Fu, P., Zhu, T., Wang, W., et al. (2013). Indole-diterpenoids with anti-H1N1 activity from the aciduric fungus *Penicillium camemberti* OUCMDZ-1492. *J. Nat. Prod.* 76, 1328–1336. doi: 10.1021/np400304q

Frelek, J., Ikekawa, N., Takatsuto, S., and Snatzke, G. (1997). Application of $[Mo_2(OAc)_4]$ for determination of absolute configuration of brassinosteroid vic-diols by circular dichroism. *Chirality* 9, 578–582. doi: 10.1002/(SICI)1520-636X(1997)9:5/6<;578::AID-CHIR27>;3.0.CO;2-K

Frisch, M. J., Trucks, G. W., Schlegel, H. B., Scuseria, G. E., Robb, M. A., Cheeseman, J. R., et al. (2009). Wallingford. CT: Gaussian Inc.

Gautschi, J. T., Amagata, T., Amagata, A., Valeriote, F. A., Mooberry, S. L., and Crews, P. (2004). Expanding the strategies in natural product studies of marine-derived fungi: a chemical investigation of *penicillium* obtained from deep water sediment. *J. Nat. Prod.* 67, 362–367. doi: 10.1021/np030388m

Grimblat, N., Zanardi, M., and Sarotti, A. (2015). Beyond DP4: an improved probability for the stereochemical assignment of isomeric compounds using quantum chemical calculations of NMR shifts. *J. Organ. Chem.* 80, 12526–12534. doi: 10.1021/acs.joc.5b02396

Hu, X. Y., Meng, L. H., Li, X., Yang, S. Q., Li, X. M., and Wang, B. G. (2017). Three new indole diterpenoids from the Sea-anemone-derived fungus *Penicillium* sp. AS-79. *Mar. Drugs* 15:137. doi: 10.3390/md15050137

Li, C., Gloer, J. B., Wicklow, D. T., and Dowd, P. F. (2002). Thiersinines A and B: novel antiinsectan indole diterpenoids from a new fungicolous *Penicillium* species (NRRL 28147). *Org. Lett.* 4, 3095–3098. doi: 10.1021/ol026424a

Mantle, P. G., and Weedon, C. M. (1994). Biosynthesis and transformation of tremorgenic indolediterpenoids by *Penicillium paxilli* and *Acremonium lolii*. *Phytochemistry* 36, 1209–1217. doi: 10.1016/S0031-9422(00)89639-9

Meng, L. H., Liu, Y., Li, X. M., Xu, G. M., Ji, N. Y., and Wang, B. G. (2015). Citrifelins A and B, citrinin adducts with a tetracyclic framework from cocultures of marine-derived isolates of *Penicillium citrinum* and *Beauveria felina*. *J. Nat. Prod.* 78, 2301–2305. doi: 10.1021/acs.jnatprod.5b00450

Moreno, E., Parks, M., Pinnell, L. J., Tallman, J. J., and Turner, J. W. (2017). Draft genome sequence of a *Vibrio harveyi* strain associated with vibriosis in Pacific white shrimp (*Litopenaeus vannamei*). *Genome Announcements* 5, e01662–e01616. doi: 10.1128/genomeA.01662-16

Ochi, M., Yamada, K., Kotsuki, H., and Shibata, K. (1991). Calicoferols A and B, two novel secosterols possessing brine-shrimp lethality from the gorgonian *Calicogorgia* sp. *Chem. Lett.* 20, 427–430. doi: 10.1246/cl.1991.427

Qiao, M. F., Ji, N. Y., Liu, X. H., Li, F., and Xue, Q. Z. (2010). Asporyergosterol, a new steroid from an algicolous isolate of *Aspergillus oryzae*. *Nat. Prod. Commun.* 5, 1575–1578.

Vezzulli, L., Pezzati, E., Brettar, I., Höfle, M., and Pruzzo, C. (2015). Effects of global warming on *Vibrio* ecology. *Microbiol. Spectrum* 3, VE-0004–2014. doi: 10.1128/microbiolspec.VE-0004-2014

Wang, F., Fang, Y., Zhang, M., Lin, A., Zhu, T., Gu, Q., et al. (2008). Six new ergosterols from the marine-derived fungus *Rhizopus* sp. *Steroids* 73, 19–26. doi: 10.1016/j.steroids.2007.08.008

Wang, H., Hong, J., Yin, J., Moon, H. R., Liu, Y., Wei, X., et al. (2015). Dimeric octaketide spiroketals from the jellyfish-derived fungus *Paecilomyces variotii* J08NF-1. *J. Nat. Prod.* 78, 2832–2836. doi: 10.1021/acs.jnatprod.5b00594

Xu, L. L., Zhang, C. C., Zhu, X. Y., Cao, F., and Zhu, H. J. (2017). Bioactive phenyl ether derivatives from the marine-derived fungus *Aspergillus carneus*. *Nat. Prod. Res.* 31, 1875–1879. doi: 10.1080/14786419.2016.1263848

Yamaguchi, T., Nozawa, K., Hosoe, T., Nakajima, S., and Kawai, K. I. (1993). Indoloditerpenes related to tremorgenic mycotoxins, penitrems, from *Penicillium crustosum*. *Phytochemistry* 32, 1177–1181. doi: 10.1016/S0031-9422(00)95087-8

Yang, J. K., Zhang, B., Gao, T., Yang, M. Y., Zhao, G. Z., Zhu, H. J., et al. (2018). A pair of enantiomeric 5-oxabicyclic[4.3.0]lactam derivatives and one new polyketide from the marine-derived fungus *Penicillium griseofulvum*. *Nat. Prod. Res.* 32, 1–4. doi: 10.1080/14786419.2017.1410815

Zhang, Y., Li, X. M., Proksch, P., and Wang, B. G. (2007). Ergosterimide, a new natural diels-alder adduct of a steroid and maleimide in the fungus *Aspergillus niger*. *Steroids* 72, 723–727. doi: 10.1016/j.steroids.2007.05.009

Zhao, J. C., Wang, Y. L., Zhang, T. Y., Chen, Z. J., Yang, T. M., Wu, Y. Y., et al. (2018). Indole diterpenoids from the endophytic fungus *Drechmeria* sp. *as natural antimicrobial agents. Phytochemistry* 148, 21–28. doi: 10.1016/j.phytochem.2018.01.010

Zhu, H. J. (2009). *Current Organic Stereochemistry*. Beijing: Science Presses of China.

Zhu, H. J. (2015). *Organic Stereochemistry—Experimental and Computational Methods*. Weinheim: Wiley-VCH Verlag GmbH and Co.; KGaA.

Zhu, H. J., Li, W. X., Hu, D. B., and Wen, M. L. (2014). Discussion of absolute configuration for bioactive Griseusins by comparing computed optical rotations and electronic circular dichroism with the experimental results. *Tetrahedron* 70, 8236–8243. doi: 10.1016/j.tet.2014.09.032

Conflict of Interest Statement: The authors declare that the research was conducted in the absence of any commercial or financial relationships that could be construed as a potential conflict of interest.

Advantages of publishing in Frontiers

OPEN ACCESS
Articles are free to read for greatest visibility and readership

FAST PUBLICATION
Around 90 days from submission to decision

HIGH QUALITY PEER-REVIEW
Rigorous, collaborative, and constructive peer-review

TRANSPARENT PEER-REVIEW
Editors and reviewers acknowledged by name on published articles

Frontiers
Avenue du Tribunal-Fédéral 34
1005 Lausanne | Switzerland

Visit us: www.frontiersin.org
Contact us: info@frontiersin.org | +41 21 510 17 00

REPRODUCIBILITY OF RESEARCH
Support open data and methods to enhance research reproducibility

DIGITAL PUBLISHING
Articles designed for optimal readership across devices

FOLLOW US
@frontiersin

IMPACT METRICS
Advanced article metrics track visibility across digital media

EXTENSIVE PROMOTION
Marketing and promotion of impactful research

LOOP RESEARCH NETWORK
Our network increases your article's readership